SAND--96-1117

SAND96-1117
Unlimited Release
Printed December 1996

Proceedings of US/Japan Workshop, Q219

on

High Heat Flux Components and Plasma Surface Interactions for Next Fusion Devices

Colorado Springs, Colorado
January 9-11, 1996

Edited by M. A. Ulrickson, P. L. Stevens, Sandia National Laboratories
T. Hino and Y. Hirohata, Hokkaido University

Sandia National Laboratories
Albuquerque, New Mexico

Table of Contents

Workshop Summary

T. Hino and M. Ulrickson

Summary of Q219
Jan. 9-11, 1996

T. Hino

37 participants

46 presentations

PFC in devices:	7
HHFC:	14
PFM:	7
Tritium:	4
Material damage:	5
Session summaries:	6
General:	3

PFC in Devices

- Tore Supra
  Numerous HHFCs be developed

- TRIAM-IM
  Suitable for PSI studies

- LHD
  Construction be on schedule
  Conditioning be needed for wall with $T \leq 100°$ C
  LID experiments in CHS be promising

- JT-60 U
  New boronization
  New divertor experiment

HHFC

- Silverless Be/Cu and W/Cu be developed
- Thermal fatigue tests for numerous Be
- Many works for manufacturing and testing
- CFC (ID)/Cu brazed material
  → normal operation of ITER

PFM

- Systematic data of H retention
  (SiC, Be, W, B and C, doped material)
- Erosion study requires surface contamination effect

Tritium

- First T retention experiment in JAERI
- TFTR: T recycling and D GDC
- T inventory vs. Radiation damage

Material Damage

- Disruption studies modeling & diagnostics

Present data discussed are very useful for next devices in terms of

Heat & particle control,

Reliability of In-vessel comp.,

Improvement of confinement,

Safety.

SPECIAL THANKS TO:

Mike Ulrickson

Peggy Stevens

and

Yuko Hirohata

JAERI

Welcome to JAERI

Next Workshop will be held at JAERI-Naka.

- Place: JAERI-Naka
- Date: December 9-13, 1996
  or
  December 16-20, 1996
  (depending on TAC meeting)
- Local Host: M. Akiba

Special Thanks

to

Tomoaki Hino
Yuko Hirohata
Pat Hubbard
Peggy Stevens
Stephanie Willis

and to the following companies for their significant contributions which made the complimentary dinner and reception possible:

Brush Wellman
General Atomics
McDonnell Douglas
Sandia National Laboratories
and
Lockheed Martin

Session I

Welcome, Organization and Overviews

Chaired by: T. Hino and M. Ulrickson

Opening Remarks

by

Professor T. Hino
Hokkaido University

US-J Workshop Q219
Jan. 9-11, 1996, Colorad Springs
Opening Talk

US-Japan Workshop on PFC/PSI

○Most important workshop as exchange program

○Histrical workshop

⇩

○Very important to continue

Q1/HINO

Fusion Engineering Studies in Japan

JAERI ITER/EDA

- ○Superconducting magnet
- ○Rector structure/Remote handling
- ○Heating/Current drive
- ○Plasma facing components
- ○Blanket/Neutronics
- ○Tritium fuel cycle
- ○Structure material
- ○Diagnostics

MOE/Universities

○Basic studies have been conducted in numerous fields, independently so far.

⇩

○NIFS:Head quarter

⇩

○The project, Systematization and Promotion of Fusion Research, has been organized since 1991.

Q2/HINO

「Systematization and Promotion of Fusion Research」 Project

Leader : A.Iiyoshi
Members : ～50
Period : 1991-1995

Purpose
- Pick up important R&D
- Promotion of fusion research in universities
- Construction of network system

Group
- Fusion Engineering (T.Yamashina)
- Fusion Science (T.Tanabe)

  Magnetic & inetia conferment

- Plasma Science (H.Nishida)
- Basic plasma study

Q3/HINO

Fusion Engineering Group

Number of Researchers

Approximately 1000 (including graduate students)

Major fields (3 working groups/10 fields)

(1) Material /Fuel Group

PSI/PFC	• Control of recycling, impurity and heat &particle flow • HHFC • High Z material • Tritium inventory • Reduction of heat flux
Structure Material	• Material damage • Material behavior under irradiation
Blanket	• Blanket system and safety • Breeding material
Tritium Science	• Tritium handling system • Tritium material interaction • Recovering and disposal

Q4/HINO

(2) Reactor System/Safety Group

Tritium Biology	• Risk to human • Behavior in environment
Heat and Structure	• Heat removal • Energy conversion • Material strength • Remote control
Reactor Design and Safety	• Problems in several devices • Helical reactor
Fusion Neutron	• Particle transport • Experiment in high intensity • neutron source • Plasma Diagnostics

(3) Magnet and Electromagnetic Structure

Magnet	• Super conductor • Electromagnetic properties • Safety and protection
Electromagnetic structure	• Electromagnetic behavior and structure design

Q5/HINO

Research Target

Near Term (LHD, ITER)

PSI/PFC
Magnet

Long Term (Demo, Reactor)

Structure Material

Both

All fields (except Structure Material Field)

Q6/HINO

Network of PSI/PFC Field

Headquarter :NIFS (both for R&D and information)
2-3Major Sites :Collaborative experiments

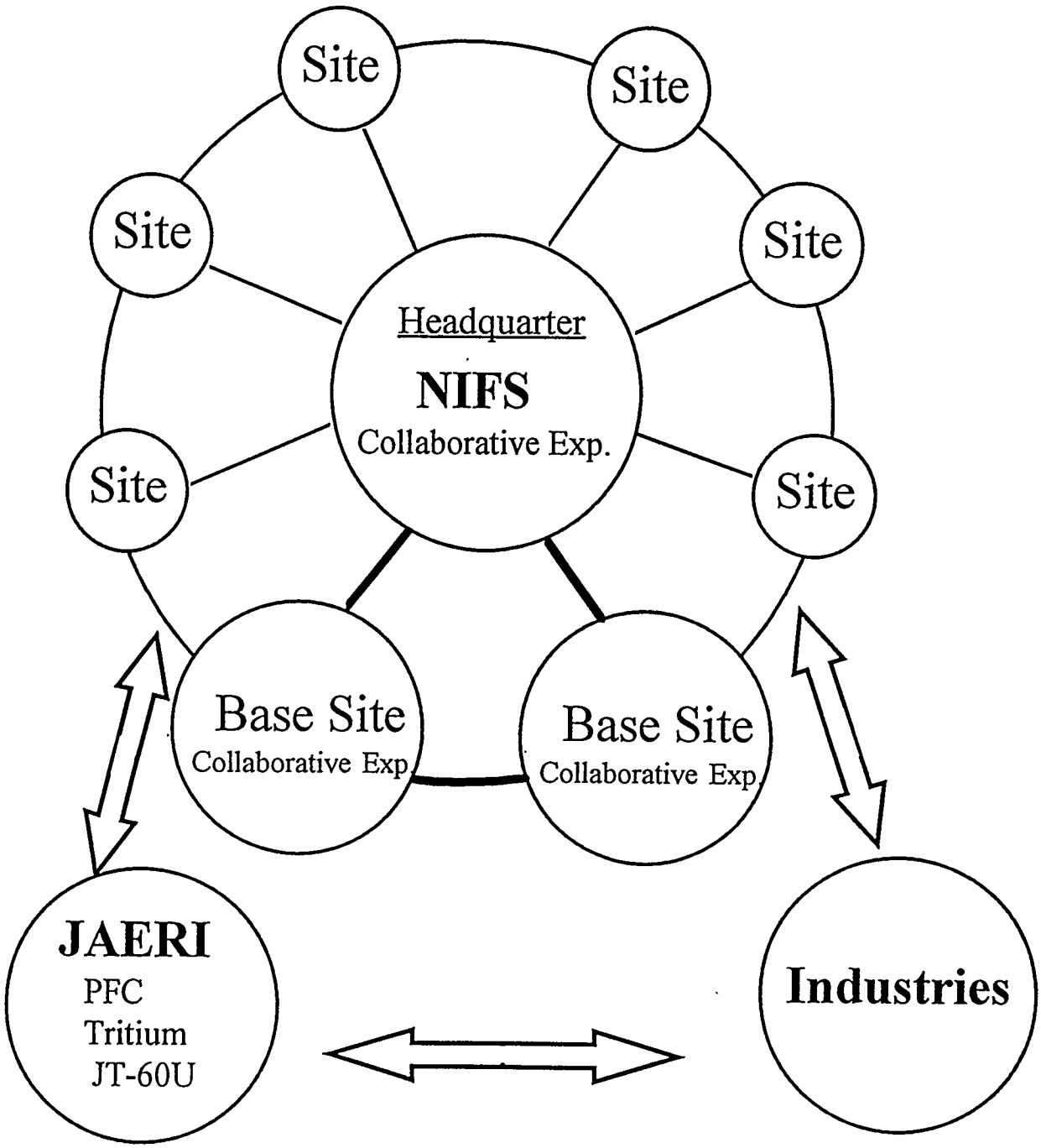

Q7/HINO

Present Meeting in PSI/PFC Field

- **Evaluation of LHD Plasma Facing Wall**
  (NIFS Collaborative Study, T.Yamashina)
  ~70 Members
- **Evaluation of Plasma Facing Materials**
  (Future Energy Institute, N.Yoshida)
  ~80 Members
- **PSI in Burning Plasma State**
  (Atomic Energy Society of Japan, T.Hino)
  ~40 Members
- **First Wall Engineering for Heat & Particle Control**
  (Japan Society of Plasma Science and Nuclear Fusion Research)
  ~30 Members
- **R&D Project for LHD LID**
  (NIFS, T.Yamashina & O.Motojima)
  ~20 Members
- **JAERI PFC Meeting**
  (JAERI, M.Akiba)
  ~60 Members

Q8/HINO

US-J Workshop Q219
Jan.9-11,1996, Colorad Springs
Overview Talk

Japanese Activities for PFC/PSI

T.Hino
Hokkaido University

Contents

R1/HINO

1.Meetings After Workshop P243

(1) First PFC/PSI Meeting

NIFS (Toki Site)

June 16, 1995

Topics: Brazed mater, Disruption erosion,
PSI in JT-60U, TRIAM-1M and CHS

(2) Second PFC/PSI Meeting

JAERI (Naka)

Oct.16, 1995

Topics: LHD/JT-60U/ TRIAM-1M/ TEXTOR,
PFC for TEXTOR and LHD, JFT-2M divertor,
Li, Mater. damage, Tritium

(3) Third PFC/PSI Meeting

Kyushu Univ.

Feb.15-16, 1996

R2/HINO

2.PFC/PSI in Devices

JT-60U

○ Reduction of H content (B -film)

- He discharge+decaborane($B_{10}H_{12}$) →H: 10-14 %
- (D_2+He) discharge+decaborane →H: 2-4 %

↓

Effect of H disappeared

○ Tritium measurement for tiles (1991-Oct.1993)

- Total inventory of all tiles: 50 % of produced T (3.2×10^{10} Bq)
- Low at striking point and high at tile edge (co-deposited region)

○ Plan for divertor modification

- Reduction of heat flux
- Closed divertor configuration with low T and high n

R3/HINO

Divertor Modifications of JT-60U and Other Tokamaks

JT-60U及び他のトカマク装置のダイバータ改造計画

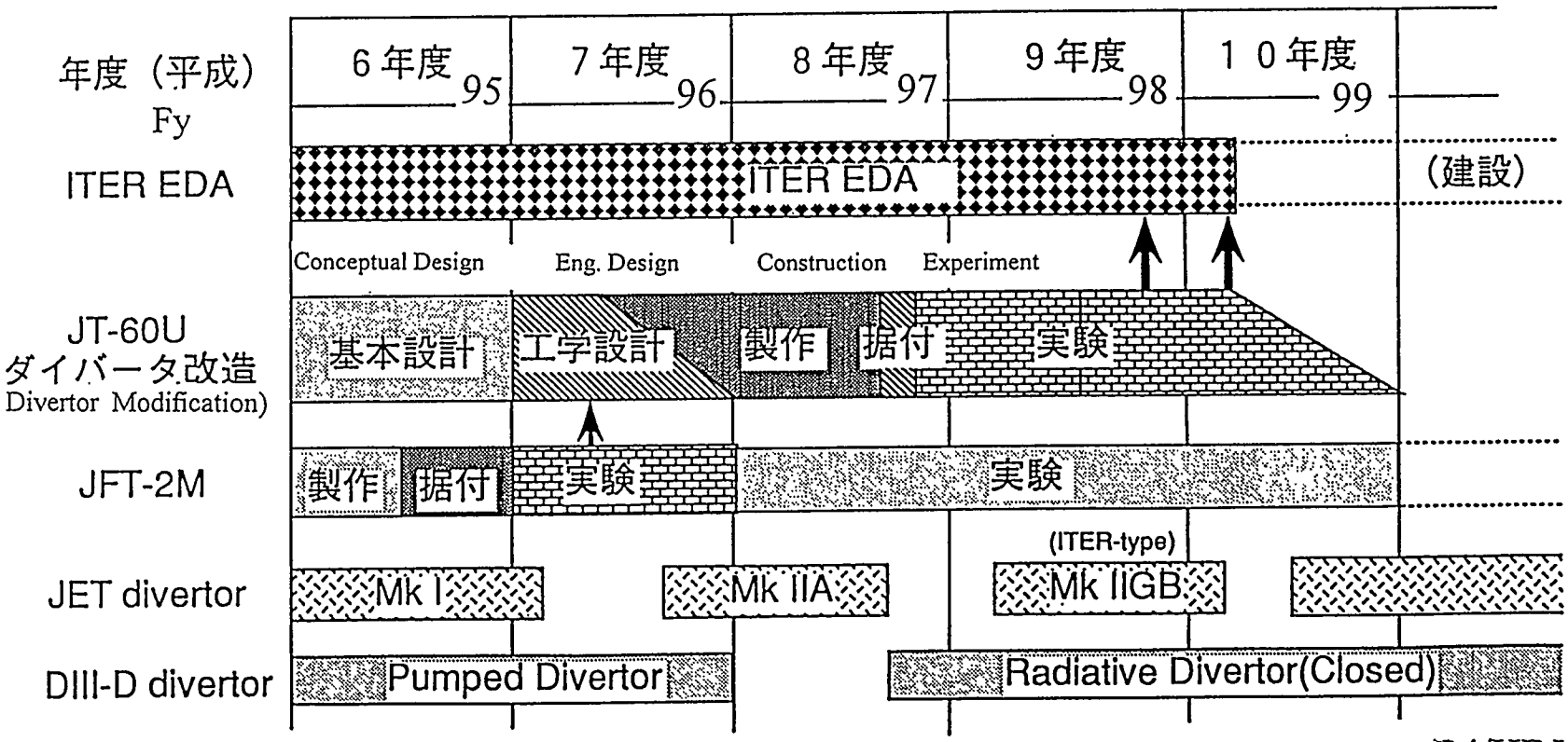

R4/HINC

Designed Divertor Shape

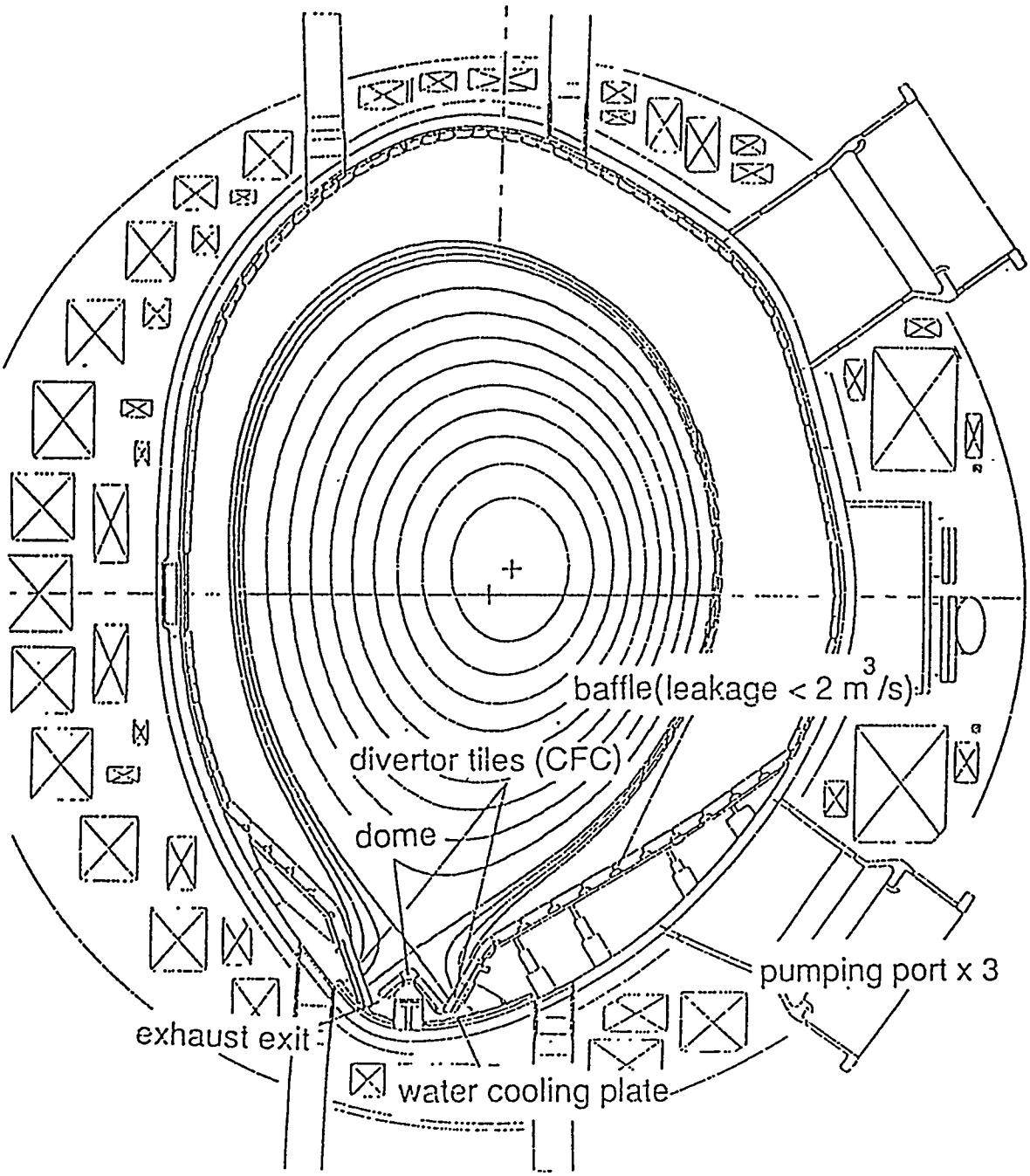

R5/HINO

LHD

GOAL OF LHD PROJECT

1, PHYSICS EXPERIMENT EXTRAPOLATABLE TO FUSION CONDITION

HIGH $n \tau T$ > 10^{20} $keVm^{-3}s$ ($Q \sim 0.35$)

HIGH T > 10 keV

HIGH β > 5 %

2, CURRENTLESS STEADY PLASMA PRODUCTION

DIVERTOR EXPERIMENT

3, COMPLEMENTARY TOROIDAL DEVICE TO TOKAMAK APPROACH

R6/HINO

Construction schedule for LHD

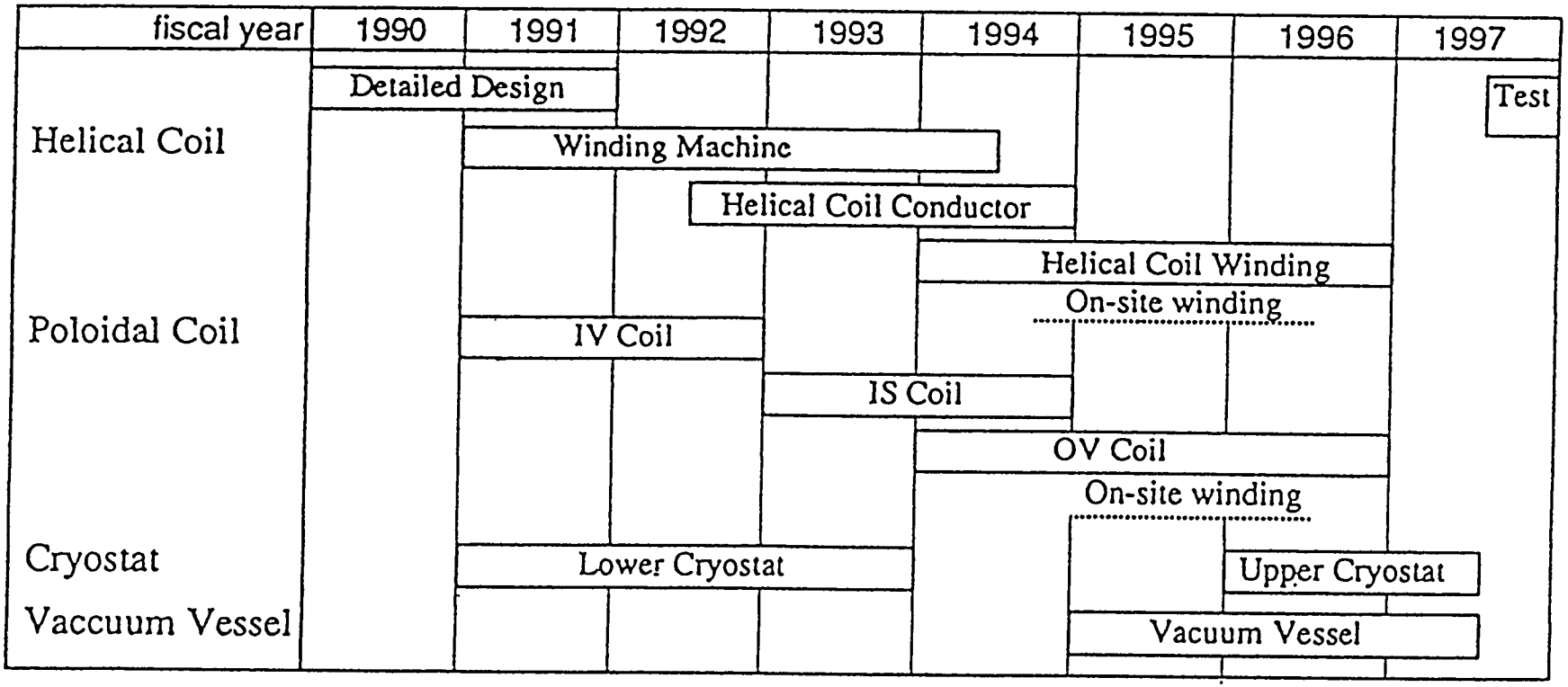

R7/HINO

Discharge types

10s discharge →10 MW/m^2

Steady state → 0.75 MW/m^2

Divertor in early operation phase (LID)

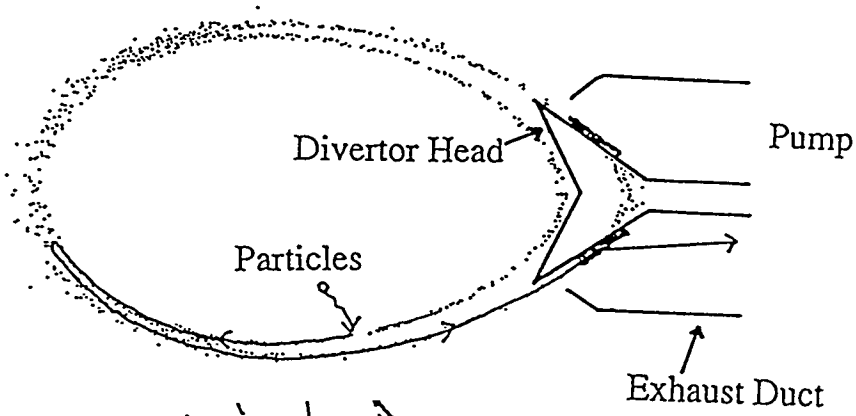

Pumping
Efficiency ~30%

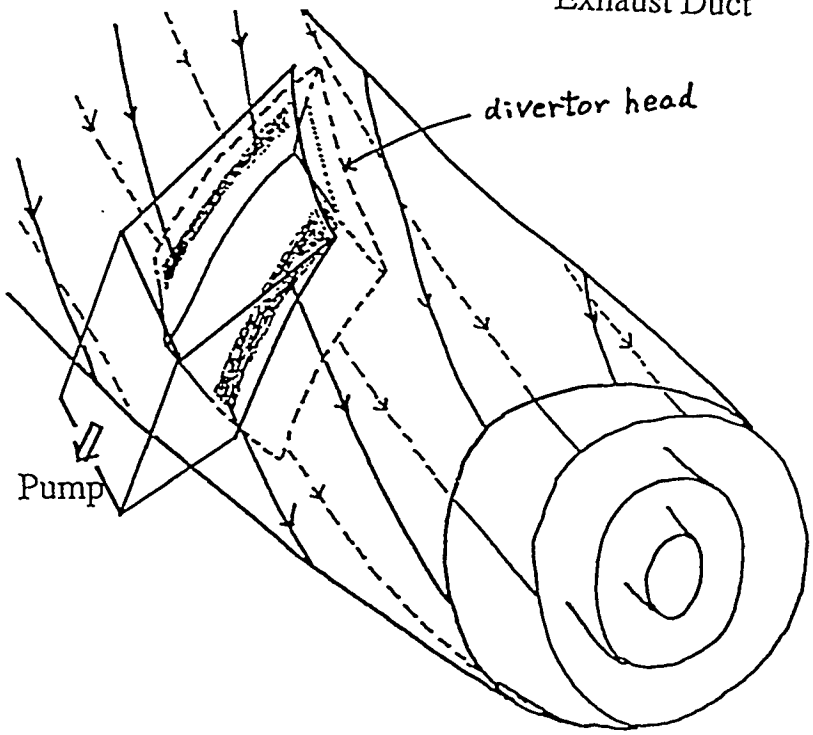

Heat flux
~10 MW/m^2

Prototype LID experiment →CHS

R8/HINO

TRIAM-1M

○ Material damage study

- Surface →Al, Cu, SS, Mo, W
- TEM, EPS, AES →Damage, Blistering, Impurity deposition

TEXTOR

○ High Z limiter experiment (W, Mo)

- Local shielding around at limiter
- Density limit for radiation to be enhanced (OH discharge)

○ RF bias experiment (positive potential)

- Reduction of ion saturation current
- Heat flow not changed

R9/HINO

3.PFC Development

JAERI

Disruption erosion

- ○ Weight loss of CFC → reduced with increase of thermal conductivity
- ○ CVD-W → loss erosion than Powder Metal W or Monocrystal W

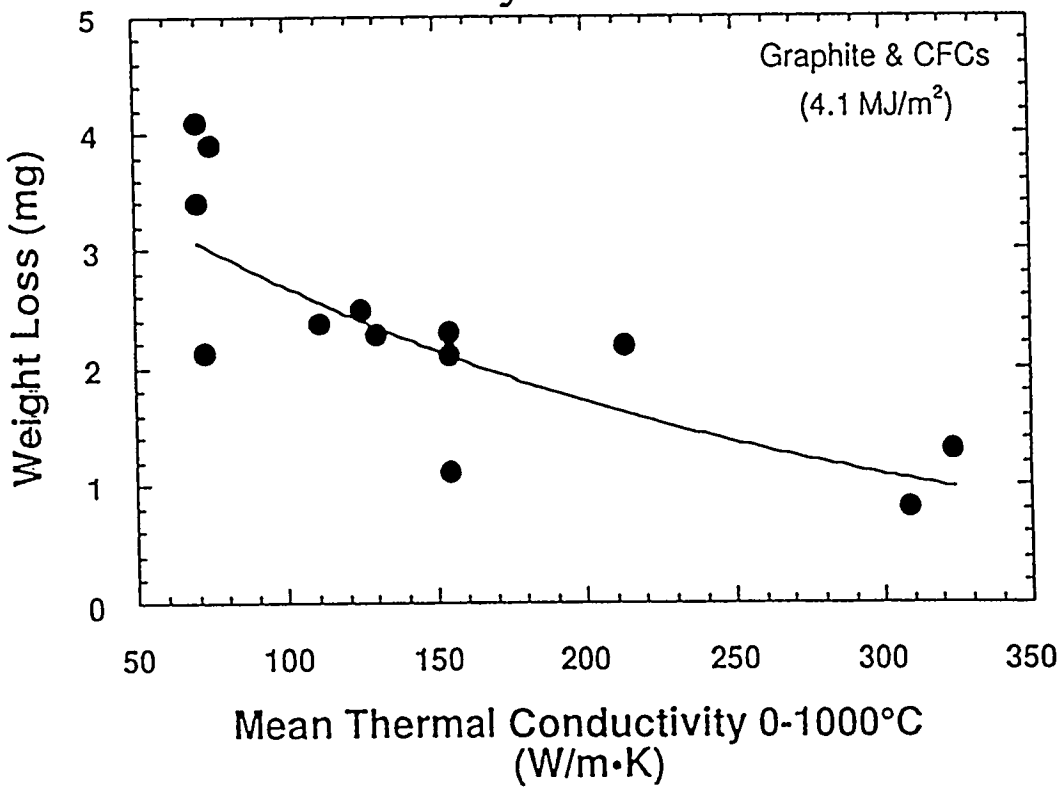

Be/OFHC-Copper mock-up

- ○ Shear stress measurement

R10/HINO

1m-long divertor mock-up

-Saddle Type: MFC-1+ OFHC Cu
-Armor: MFC-1 (1D CFC)
(min. 10 mm thick, 25 mmW ×25 mmL)
-Cooling Tube: Swirl Tube (twisted ratio = 3)
-Support: Fully rigid, OFHC Cu
-Braze: Silver Braze

↓

25 MW/m^2, 1000 Cycles (30s Pulse)
30 MW/m^2, 900 Cycles (30s Pulse)・・・cracked

Hot cell electron beam facility (OHBIS)

50 KW power
Thermal response of irradiated brazed material
Disruption erosion measurement

R11/HINO

Screw Tube Test

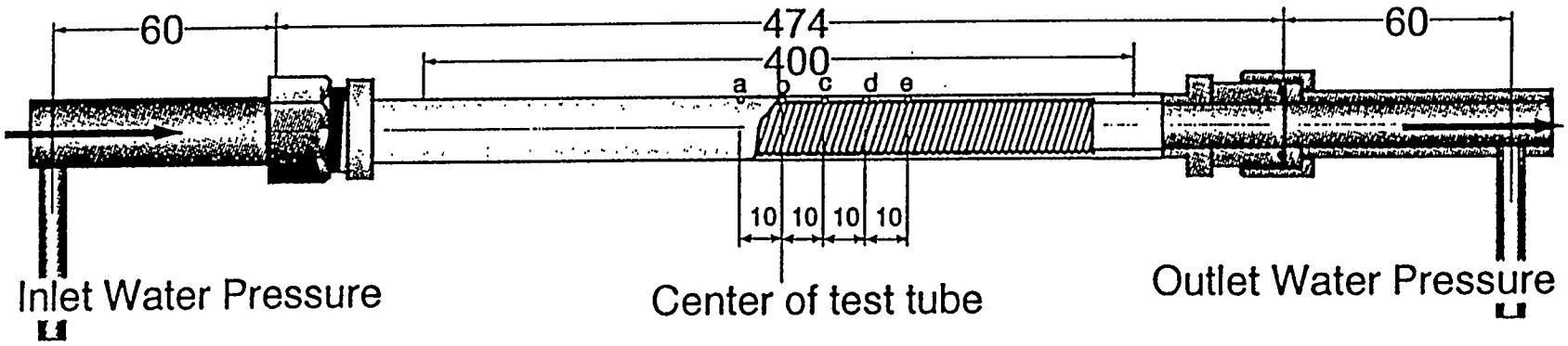

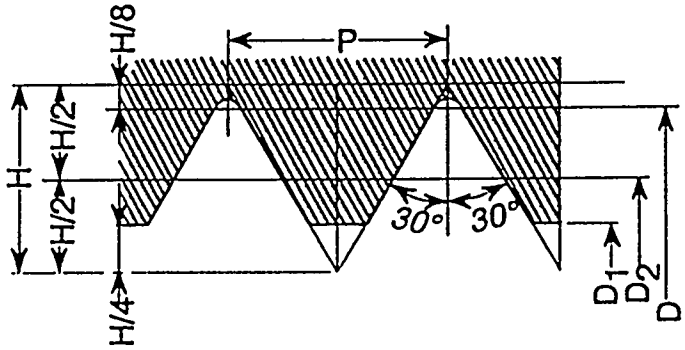

○ One-side heating test

↓

○ Critical heat flux → Comparable with swirl tube

R12/HINO

NIFS

Divertor →Helical divertor (helical running array)
LID
CFC or Graphite/Cu brazed material
(Flat plate, Saddle, Monoblock)
↓
10 MW/m^2, 5000 cycles (30s Pulse)

Mechanical joint type

Bolt structure
Carbon sheet (0.1-0.2 mm)

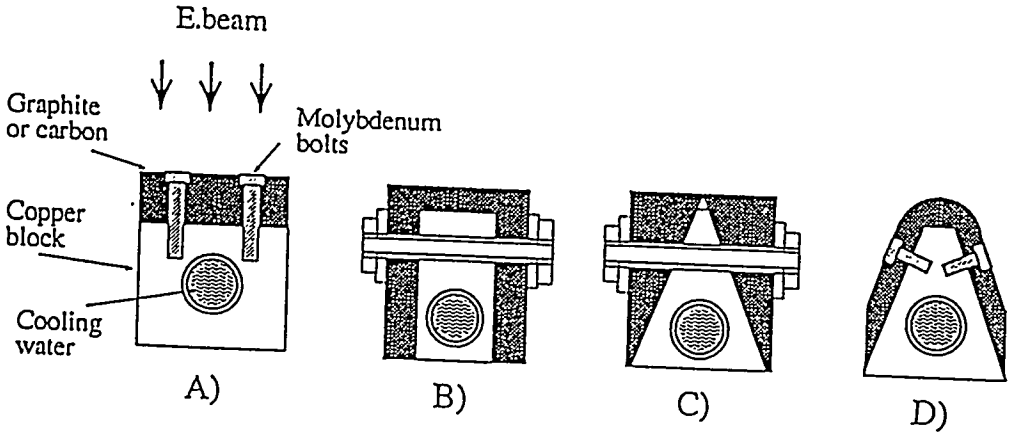

↓
5-7 MW/m^2
2100 Cycles

↓
Best result
13 MW/m^2

R13/HINO

4.Evaluation of PFM

Gettering of Li

- o Li deposited wall → reactive with O_2, H_2O, CO, CH_4
- o Oxygen gettering → O/Li= 1/2 (Li_2O)
- o H_2 gas → no reactive
- o H atom or ion → reactive, H/Li= 1 at T< 200 °C
  (Most H desorbs at T~200 °C)

Hydrogen Retention

- o Retained amounts

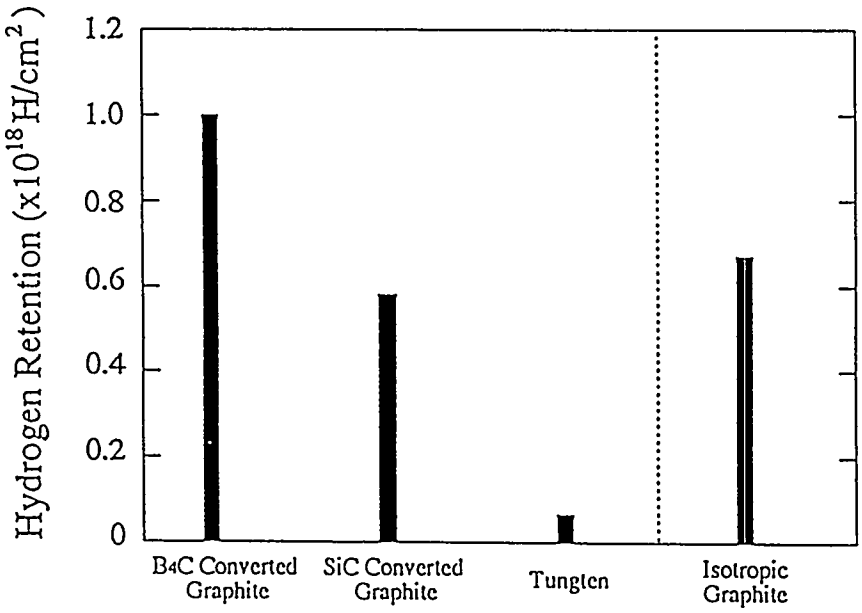

R14/HINO

○Temperature dependence

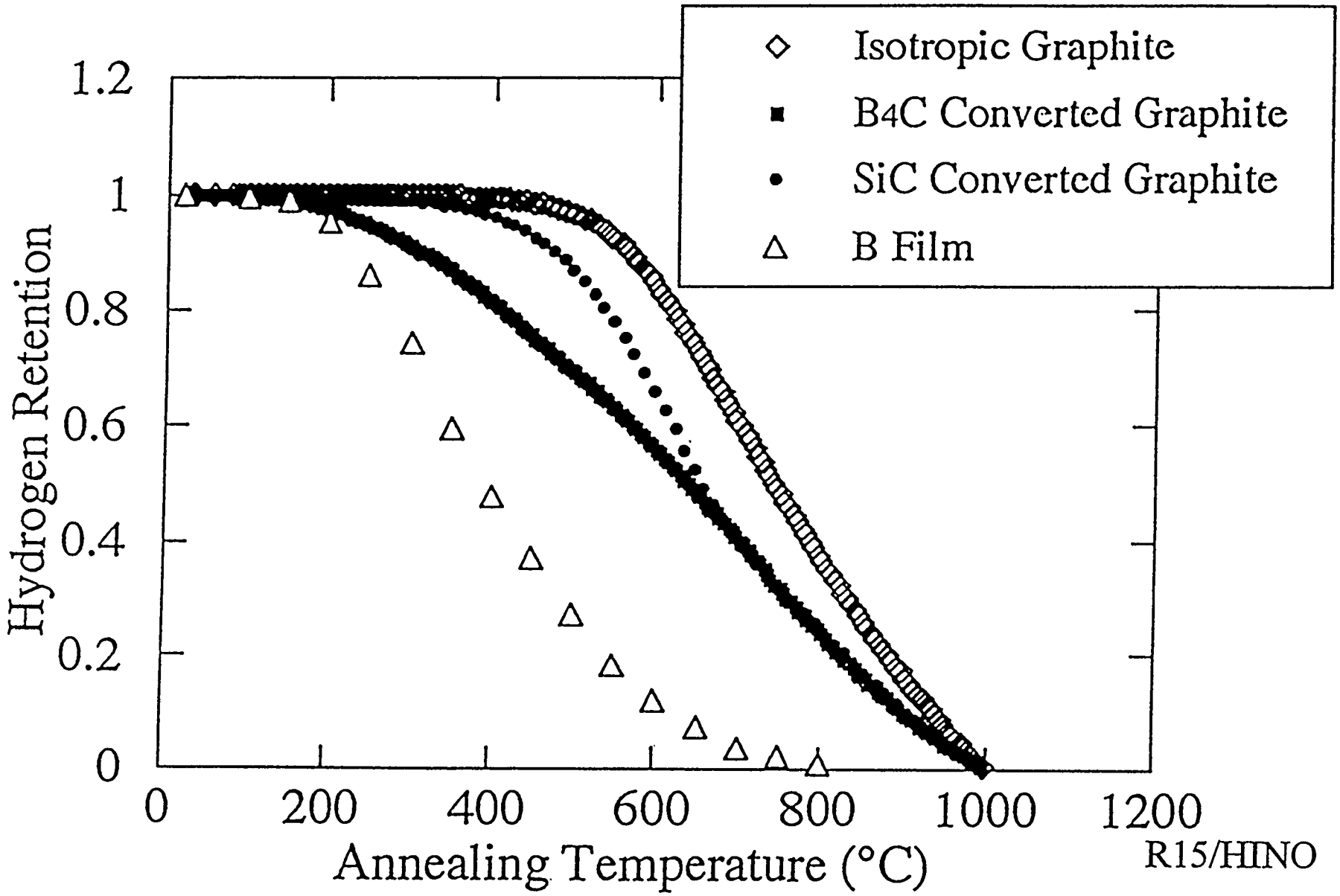

R15/HINO

Deuterium Desorption of Be

8 KeV-D_2^+
1×10^{21} D/cm^2
TDS: 1K/s

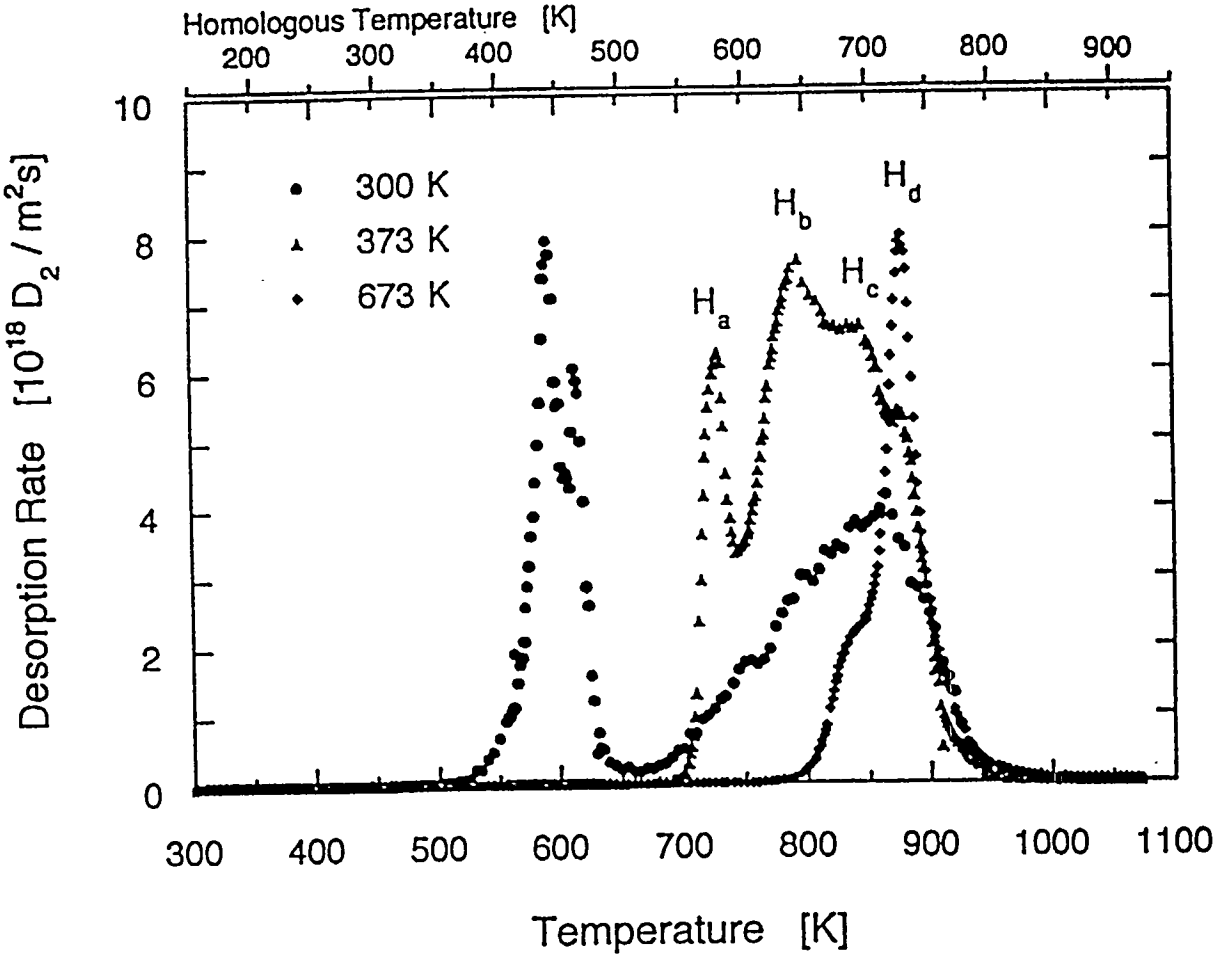

Desorption peaks : 600 K, 900 K
Trapped amount : 1 order higher than metal

R16/HINO

Boronized CFC (High Conductivity) ・・・CXB-400L

B_4C Powder mixing → fixed by PyG
B conc. = 15 at % at surface
$\rho = 1.4 g/cm^3$
k = 200 W/mK (RT)

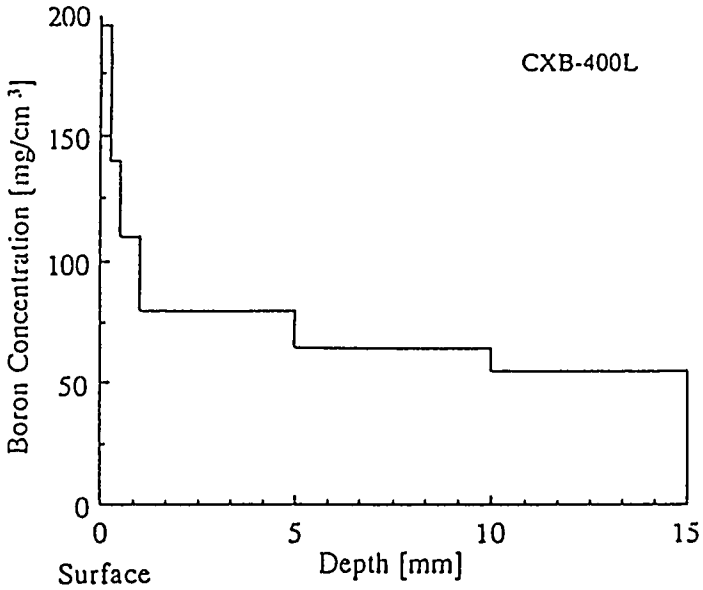

Depth profile of boron concentration of boron-mixed CFC

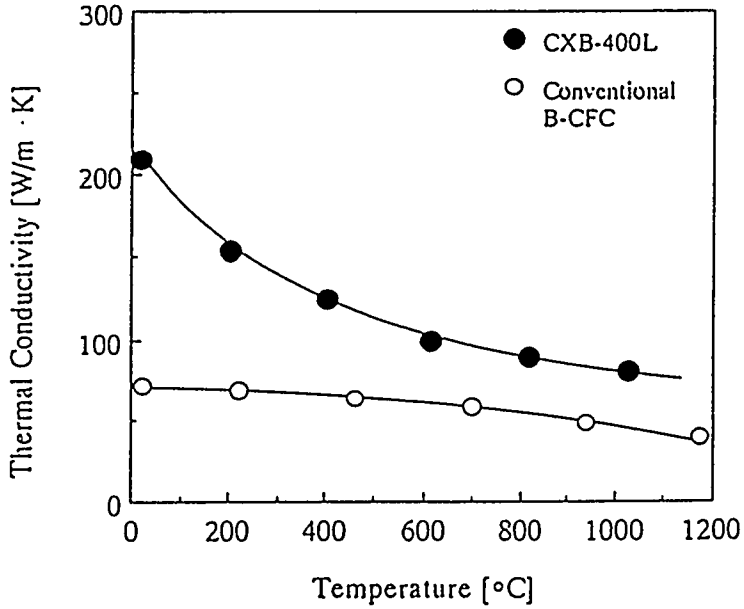

Temperature dependences of thermal coductivities for Boron-mixed CFC (CXB-400L) and conventional B-CFC.

R17/HI

Acknowledgments

M.Saidoh (JAERI)
N.Hosonaga (JAERI)
O.Motojima (NIFS)
N.Noda (NIFS)
Y.Kubota (NIFS)
A.Komori (NIFS)
A.Sagara (NIFS)
N.Yoshida (kyushu Univ.)
M.Araki (JAERI)
K.Nakamura (JAERI)
H.Sugai (Nagoya Univ.)
T.Sogabe (Toyo Tanso)

R18/HINO

An Overview of US Activities

M. Ulrickson

Presented at the US-Japan Workshop
January 9-11, 1996

Activities

- Development of thermally compliant silver free joints between Be and Cu, and W and Cu
- Critical heat flux experiments with long heated lengths
- Design and scale-up to full size divertor components
- Tritium retention, inventory, and permeation with duplex structures
- Erosion studies of Be and mixed materials
- Measurement of erosion in the divertor region

Activities

- Modeling of disruption and erosion measurements
- Measurements of the characteristics of disruption induced erosion
- Plasma edge modeling

Sandia National Laboratories

MAU

Critical Issues

- Heat removal in steady state with low activation materials
  - Heat sink materials
  - Coolants
  - Joints
- Neutron irradiation effects
  - Strengthening
  - Embrittlement
  - Diffusion of materials
  - Tritium generation and trapping
- Mixed materials effects

Sandia National Laboratories

MAU

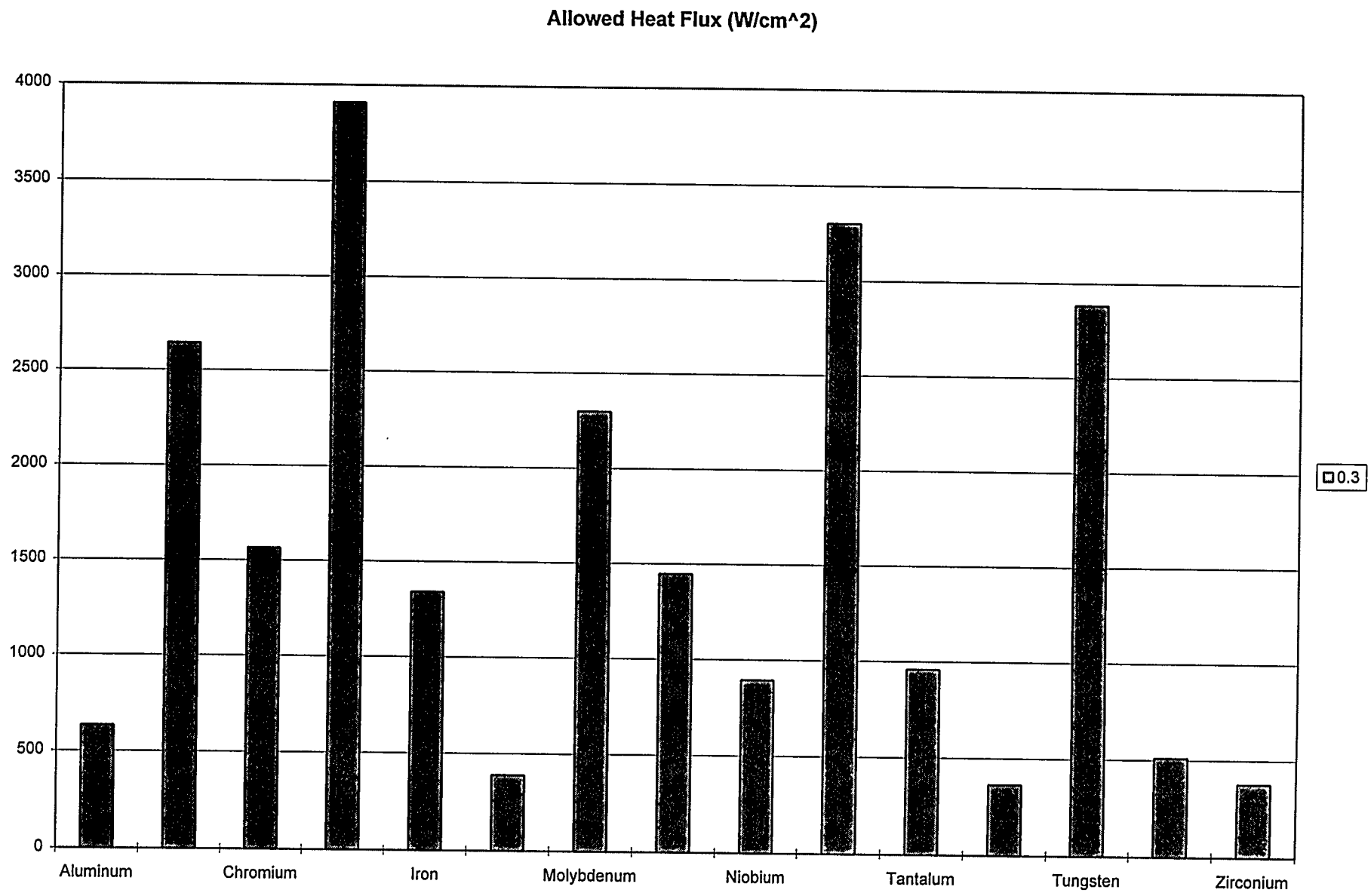
Allowed Heat Flux (W/cm^2)
4000
3500
3000
2500
2000
1500
1000
500
0
Aluminum
Chromium
Iron
Molybdenum
Niobium
Tantalum
Tungsten
Zirconium
0.3

Session II

PFC/PSI in Tokamak and Helical Devices

Chaired by: *R. Nygren and N. Yoshida*

II.1	**Yoshida**	PSI Under Long Pulse Operation in TRIAM-1M
II.2	**Komori**/Motojima	LID Experiments on CHS
II.3	**Masuzaki**/Motojima	Study of Impurity Transport in LID Configuration in CHS
II.4	**Morisaki**/Motojima	LID Design for LHD
II.5	**Sagara**/Noda	Wall Conditioning Scenario in LHD
II.6	**Saidoh**	PFC/PSI Studies in JT-60U
II.7	**Nygren**	Experience with the Tore Supra Phase III Outboard Pump Limiter

US-Japan Workshop Q-219(1996.1.9-11, Colorado Springs)

PSI UNDER LONG PULSE OPERATION IN TRIAM-1M

N. Yoshida, T. Hirai, K. Tokunaga, S. Itoh and TRIAM-Group

Research Institute for Applied Mechanics, Kyushu University

Contents

Configuration of TRIAM-1M

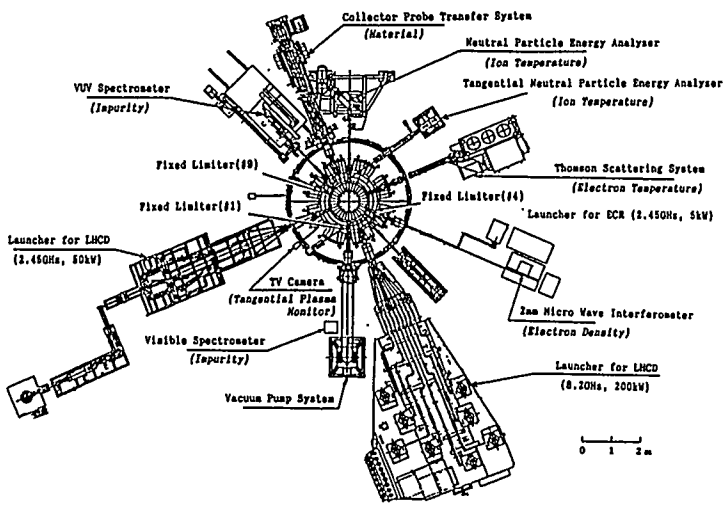

Background and Objectives

Effect of Particles from Plasma on Plasma Facing Materials

- Boundary Plasma
  low energy but very high flux ·····*erosion by sputtering*, heating (studied extensively)
- Core Plasma
  high energy neutrals, low flux·····*displacement damage* (expected) (limited number of experiments)
- Impurity atoms and ions····· *formation of new surface*

Present work

- Collector probe experiments at TRIAM-1M
  (very long pulse discharge·····suitable for material test)
- Simulation H^+ Irrad. (link of ion gun-TEM·····in-situ observation)

↓

Understanding of radiation damage of PFM in a plasma confinement device and effects of impurity deposition on surface property change

Main Parameters of TRIAM−1M

Middle size tokamak with supper conducting toroidal coils (Nb_3Sn)

Major Radius	0.8 m
Minor Radius	0.12 m x 0.18 m
Elongation	1.6
Toroidal Field (plasma center)	8 T
Plasma Current	0.5 MA
Discharge Duration (OH)	0.5 s
Discharge Duration (LHCD)	>4000 s
Outer Vessel Diameter	~4 m
Outer Vessel Hight	~4 m
Total Weight	95 ton

Collector Probe and Specimen Position

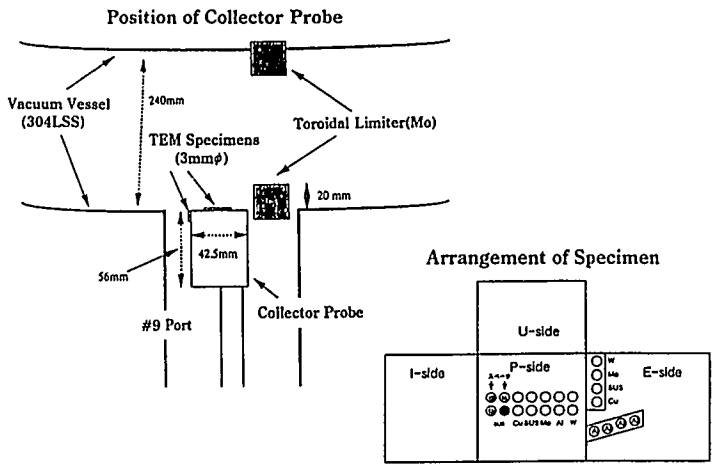

Damage Formed by Long Pulse Plasma at TRIAM-1M

TR-10, I_p=20kA, $\langle n_e \rangle = 2\times10^{12}/m^3$, t_j=78.4min (5 shots)

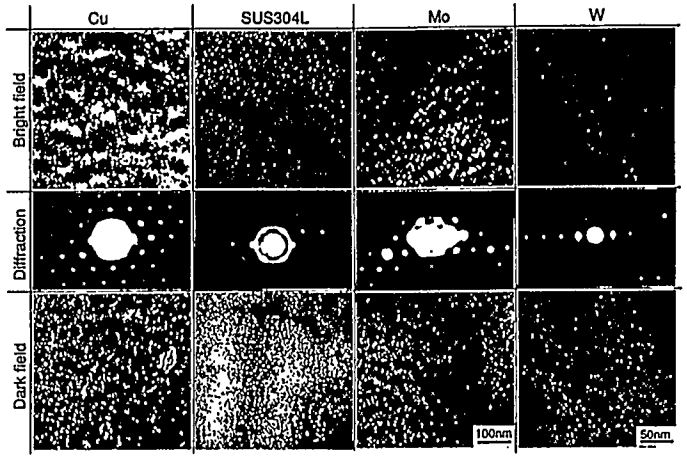

Identification of Particles Causing Displacement Damage in TRIAM-1M

Charge Exchanged Hydrogen Neutrals from core plasma
cause displacement damage

- Energy : 0.5-3keV
- Flux : $1.5\text{-}3\times10^{18} H/m^2s$
  (on the plasma facing side at the wall position)

⇩

full damage at the sub-surface region
by the operation for several hours

Energy Distribution of Neutral H in TRIAM-1M

I_p=23kA, $\langle n_e \rangle = 2\times10^{18}/m^3$

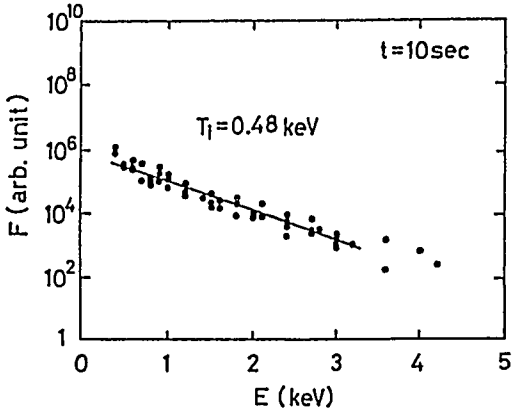

Damage Evolution in Mo at 300K under H^+ Irradiation

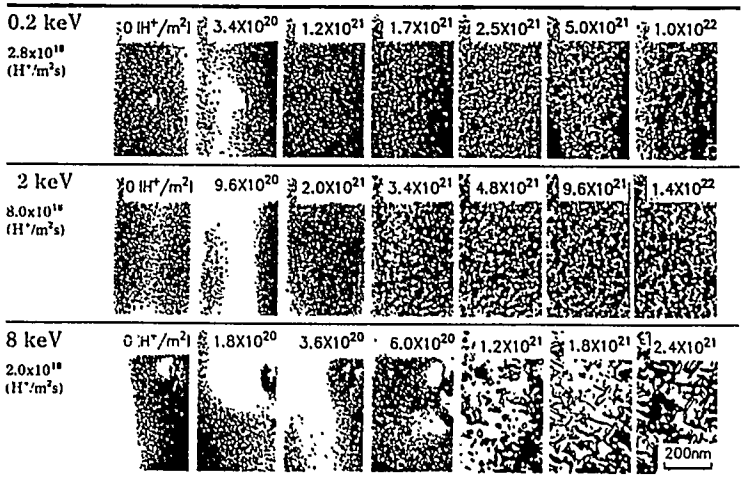

Hardening of Mo by H^+ Irradiation at R. Temp.

- 5keV H^+
- projected range = 45nm
- damage peak depth = 25nm

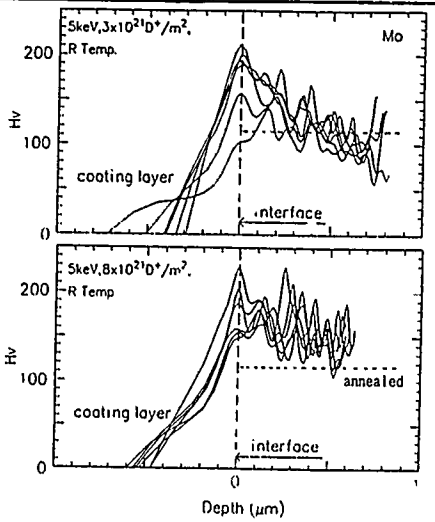

Degradation of SS304 Limiter of TRIAM-1M

- Exfoliation & Hardening (3 times)
- Hydrogen induced α' martensite formation

Recovery of Damage in W formed by D^+ and He^+ Irradiation

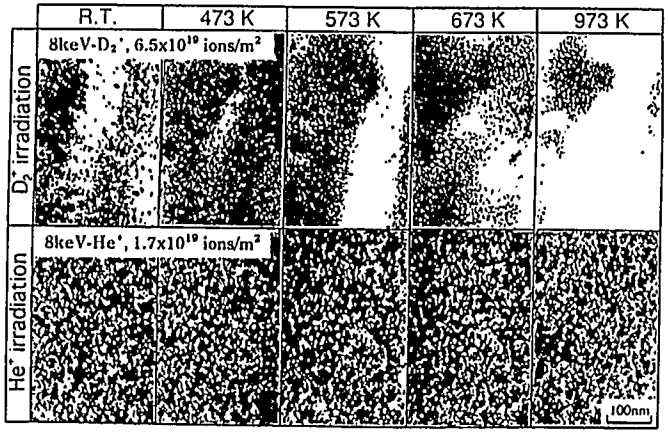

Re-deposited Impurity Layer on Al Foil at P-side

TR-10, I_p=20kA, $<n_e>$=2x10^{18}/m^3, t_j=78.4min (5 shots), Al(P-side)

- blistering & exfoliation ➡ new impurity source

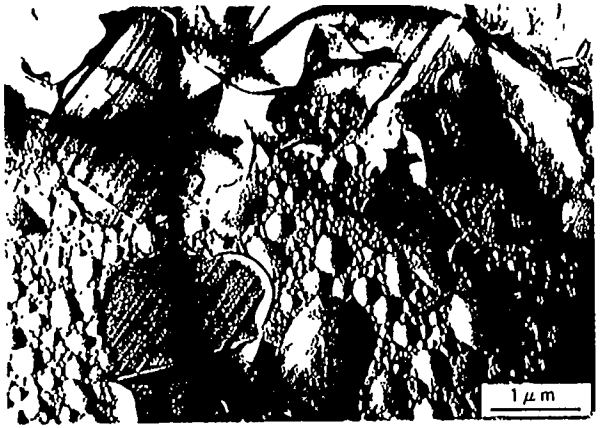

AES Analysis of Impurity Layer

TR-10, I_p=20kA, $<n_e>$=2x10^{18}/m^3, t_j=78.4min (5 shots) , Al(P-side)

- Co-deposition of Mo(limiter), Fe, Cr(vac. vessel), C and O

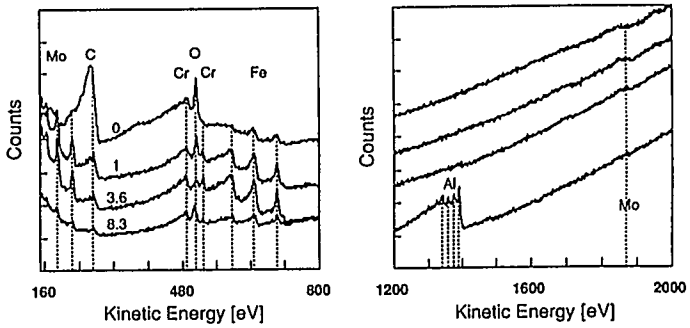

Quantitative EDS Analysis of Impurity Layer

TR-10, I_p=20kA, $<n_e>$=2x10^{18}/m^3, t_j=78.4min (5 shots) , Cu(P-side)

EDS Spectrum at Position A

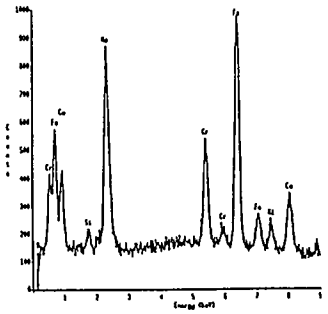

Cross Section of Specimen

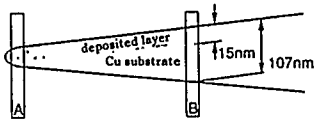

Content of Elements (at%)
(excepting light elements)

	A	B
Cr	14.8 (16.4)	2.30 (15.9)
Fe	35.0 (38.8)	6.15 (42.5)
Ni	3.41 (3.31)	0 06 (0.00)
Mo	37.4 (41.5)	6.02 (41.7)
Cu	9.41	85 5

( ): value without Cu

Crystal Structure of Impurity Layer

TR-10, I_p=20kA, $<n_e>$=2x10^{18}/m^3, t_j=78.4min (5 shots)

- very fine grains of FCC structure ⇒ effects of co-deposited oxygen atoms

Deposited layer of TRIAM-1M

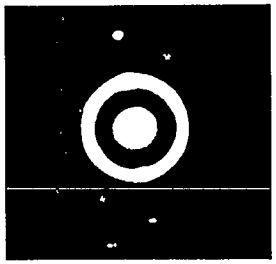

Vacuum deposited Fe film

(a) 2x10^{-4}Torr(O_2) (b) 5x10^{-5}Torr(air)

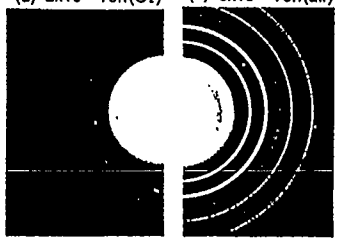

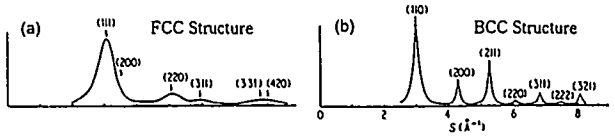

TEM Micrograph of Impurity Layer

TR-10, I_p=20kA, $<n_e>$=2x10^{18}/m^3, t_j=78.4min (5 shots), Cu(P-side)

- new materials of very fine grain < 1nm (Fe, Mo, Cr, Ni, O, C)

  ↓

  Change PSI
  - *H-recycling*
  - *H-retention*
  - *impurity source*

- element content and structure depend on the position in the Tokamak and operation conditions

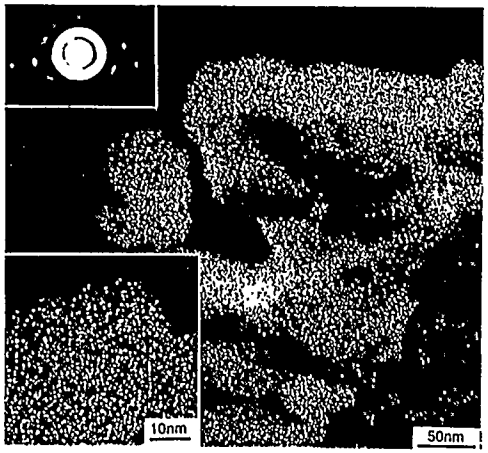

Summary

- In the case of LHCD discharge of TRIAM-1M, *charge exchanged energetic neutral hydrogen atoms emitted from the core plasma cause remarkable displacement damage in PFM.*
- The energy and the flux of the neutrals responsible for displacement damage are about *0.5-3keV* and *1.5-3x10^{18}H/m^{2}s.*
- It is estimated that the energetic neutrals will cause severe degradation of material properties at the sub-surface region by using about 10 hours (*~10^{22}H/m^2*) and will *change bulk properties after using long.*
- Co-deposited impurity atoms form completely different material on the plasma facing surface. In the present case, very fine grain FCC alloy of Fe, Mo, Cr, Ni, C and O is formed on the collector probe at the wall position. It is expected that element contents and crystal structure will depend on the position in a vacuum chamber and discharge condition.
- Combined use of different type of materials to PFM may lead to formation of unexpected materials on the PFS, and this may change PSI.

LID EXPERIMENTS ON CHS

A. Komori, N. Ohyabu, S. Masuzaki, T. Morisaki,
H. Suzuki, C. Takahashi, S. Sakakibara, K. Watanabe,
T. Watanabe, T. Minami, S. Morita, K. Tanaka,
S. Ohdachi, S. Kubo, N. Inoue, H. Yamada, K. Nishimura,
S. Okamura, K. Matsuoka, O. Motojima, and M. Fujiwara

National Institute for Fusion Sience
Nagoya 464-01, Japan

C. C. Klepper, A. C. England, J. A. Rome, and J. F. Lyon

Oak Ridge National Laboratory
Oak Ridge, TN 37831-8072, USA

Contents

(1) Status of LHD construction

The construction of the eight year project is going almost on schedule.

(a)Helical coil
Completed 600 turns out of 900 turns in total.
Winding accuracy is as good as 2mm.

(b)Poloidal coil
Lower OV coil winding was completed.
Upper OV coil winding started.

(c)Recently, LHD vacuum pumping system has been ordered to a fabricator, which will be completed ~~next~~ this March.

(d)LHD vacuum vessel system has been also ordered to a fabricator, which will be completed in 1997.

(e)The National Diet passed the bill of the second supplementary budget at the end of October 1995, and a capital budget was approved to construct an LID system for the LHD. In this fiscal year, we will fabricate 20 copper coils that generate resonant perturbation fields, and 3 electric power supplies that provide the electric currents into the coils.

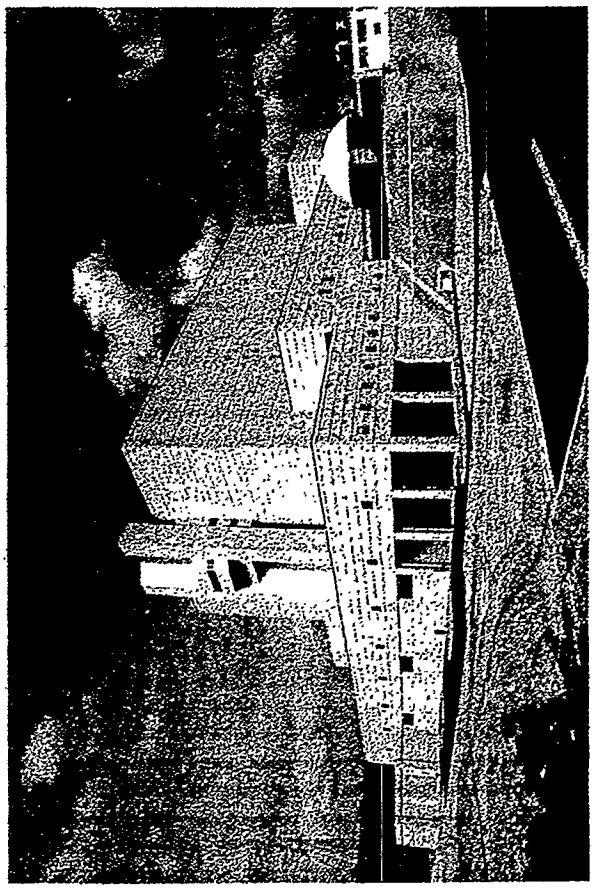

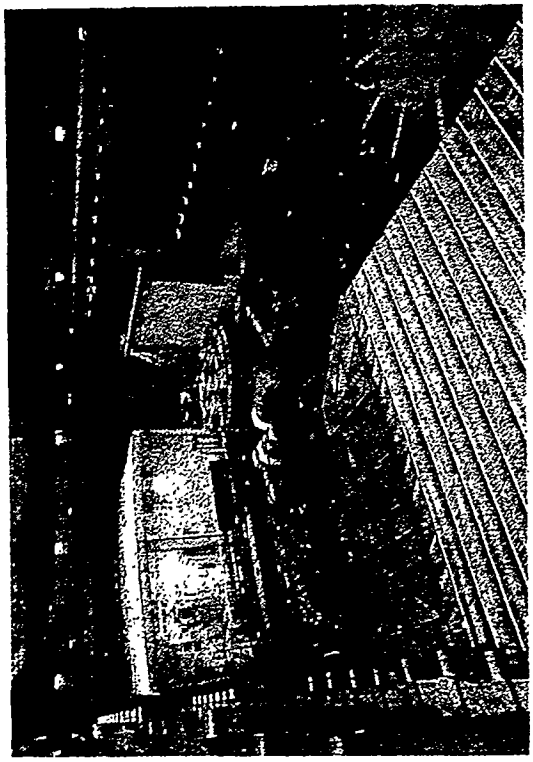

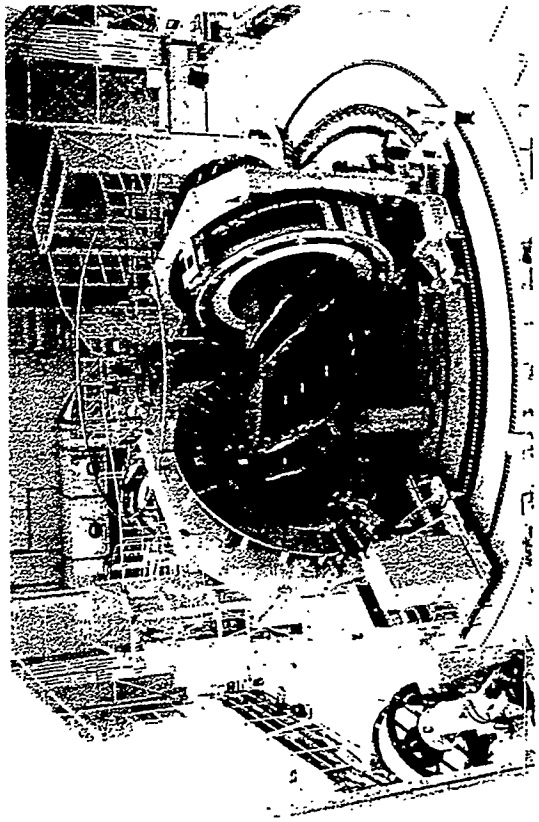

(2) Helical coil winding

The helical coil is wound in a helical coil can made of a thick stainless steel case. The case is used as a bobbin as well as a liquid helium bath. The helical coils have 450 turns for each and the total length is 37 km. Ground insulation is pasted directly on the can and cured by auto-cleave method. The winding of helical coils on site has started at the beginning of 1995 and will be completed by the summer of 1996.

Table 1 Major parameters of helical coil

Items	Phase I	Phase II
Coil temperature	4.4 K	1.8 K
Current	13.0 kA	17.3 kA
Current density	40 A/mm^2	53 A/mm^2
Maximum field	6.9 T	9.2 T
Magnetic stored energy	0.92 GJ	1.64 GJ
Turn number	450 (150 x 3)	
Spacer factor	30%-70%	
Spacer pitch	49.2 mm-64.3 mm	
Positioning error	< 2 mm	
Stress on the conductor	< 290 MPa	
Average gap between layers	< 65 mm	

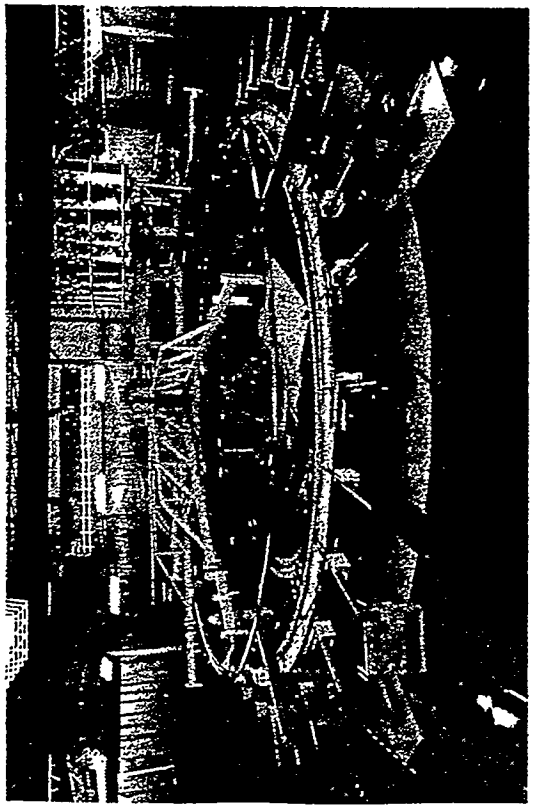

(3) Fabrication of poloidal coils

The poloidal coils are made of forced flow type conductors which are called Cable-in-Conduit Conductor (CICC). Fabrication of two pairs of poloidal coils: an inner vertical field coil (IV) and an inner shaping field coils (IS) have been completed. The largest poloidal coils, the outer vertical coils, are being constructed in the LHD experimental hall. The coil is composed of eight double pancakes with a nominal current of 30 kA. The major radius of the coil is 5.5m and its thickness is 0.54m. The specification of the coils are listed in the Table 3 & 4.

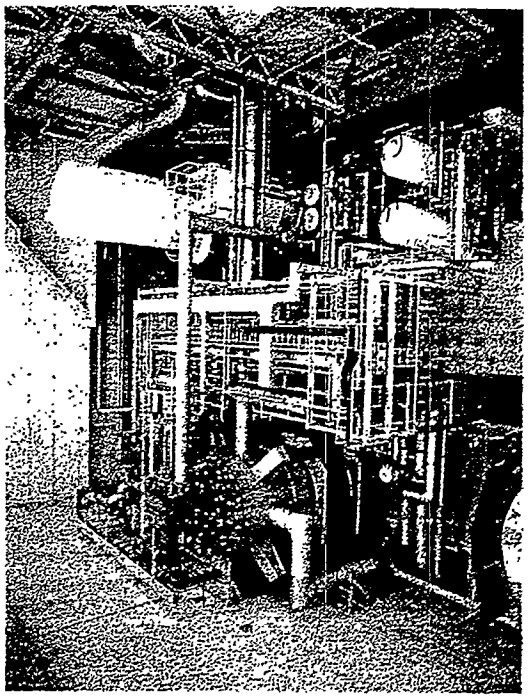

(4) Experiment of a single IV coil (EXSIV)

The initial cool down of the IV-L coil has been carried out successfully. It took about 250 hours to cool down the coil from room temperature to 4.4K. To prevent thermal stresses within the coil, the coil was cooled with less than 50K temperature gradient between the inlet and the outlet. Fundamental tests for checking the electrical insulation and the joint between the conductors, were performed with energizing the coil at 2.2 kA. The final test which energizes the IV-L coil with 20.8kA current, was conducted in December 1995.

(5) Activity of the Plasma Heating Division

I. The development of high current negative ion beam

1) A 1/3 model of the real LHD ion source was used to extract the current of 16.3 A with a current density of 30 mA/cm^2.
2) The working gas pressure was reduced down to 0.5 Pa.
3) The extracted negative ion beam was accelerated up to 125 keV.
4) The beam current density already satisfies the specification required for LHD neutral beam injector.
5) Based on the success of the beam acceleration and physical study of the beam penetration, the design value of the beam energy was raised to 180keV for hydrogen.

II. Test of the ICRF power source

1) The test of the ICRF power source is progressing rapidly after improvements were made on the dummy load and on the cooling of the cavity of the final amplifier.
2) Long pulse operations, 1.5MW/1hour and 1.9MW/10sec, has been conducted successfully. The former is regarded as a steady state operation.
3) Since the power source consists of two such tetrodes, this result suggests a capability of 3MW ICRF power injection in steady state.

4) R&D of water cooled antenna and transmission line is going on.

III. ECH gyrotron and transmission line development

1) 84GHz gyrotron (NIFS/Varian) was tested successfully on the test bench in Toki site with following records: 400KW/10sec, 500kW/2.2sec
2) Reflection from the dummy load was reduced carefully prior to the high power test. This is essential for development of steady state gyrotrons.
3) Development of transmission system including quasi-optical launcher has been mostly finished: a)Sufficiently low transmission loss of the corrugated wave guide was demonstrated by use of 62 meter long test wave guide (b) A systematic method to design 3D quasi-optical transmission system was established, and (c) it has been examined in CHS supporting experiments in various aspects.
4) Development of windows needs to be continued.

Local Island Divertor

O Utilizes a magnetic island (m/n=1/1) as a divertor magnetic configuration, which can be generated by an additional set of small island control coils.

O Has two operational modes with a closed system, as well as helical divertor.

- Low recycling operation by high pumping efficiency
  " High temperature and low density"

  High efficient pumping
  ↓
  High edge temperature
  ↓
  A significant enhancement in the core energy confinement
  (deep fueling such as NBI or pellet fueling is needed.)

- High recycling operation by high plasma plugging efficiency
  "Low temperature and High density"

  Impurity trapping in the edge by plasma flow
  ↓
  Radiative cooling

O Realizes localized recycling.
- Easier pumping → Modest cost
- Plasma heating power up to
  3 MW (steady state) on LHD
  1.5 MW (150 msec) on CHS

O Has the following properties.
- No leading edge problem
- Efficient discharge cleaning

Principle of LID

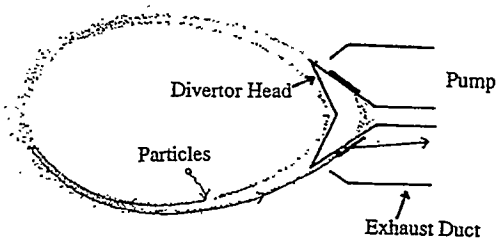

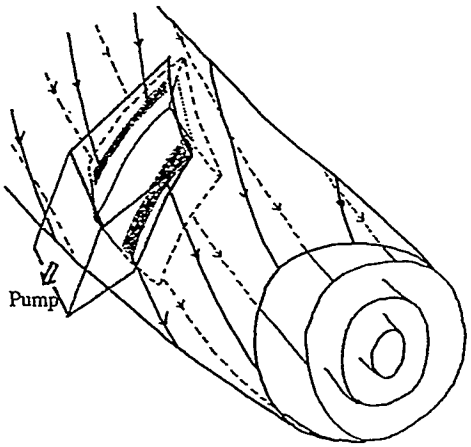

Motivation & Rationale of LID Project

○ Closed full helical divertor will not be completed in the early experimental phase, because of high fabrication and installation costs.

↓

We decided to construct the LID for the LHD edge plasma control in the early experimental phase.

- Information about edge plasma behavior, obtained with LID, will be utilized for optimizing the design of the closed full helical divertor.
- It is a good test bed for high heat flux component system.
- The LID experiment will provide insights into the relation between edge and core plasma confinement, and will motivate exploration of advanced divertor concepts.

○ The principle of LID should be demonstrated experimentally.

↓

LID experiments on CHS

Compact Helical System

Poloidal mode number	= 2
Toroidal mode number	= 8
Major radius	= 1 m
Averaged plasma minor radius	~ 0.2 m
Magnetic field	≦ 2 T
Microwave power	= 150 kW at 53.2GHz
NBI power	= 1.5 MW with 40 keV

Design of the LID Head

Magnetic field = 1 T

Currents of island control coils = 10 ~ 11 kAT

- Island full size ~ 4 cm
- Width of the divertor head ~ 49 cm
- Length of the divertor head ~ 21 cm

Pumping System

- Geometrical shapes of the divertor head and pumping duct are designed to form a closed divertor configuration.
- The particles recycled on the divertor head are pumped out by a cryogenic pump with pumping speed of 21,000 l/s.

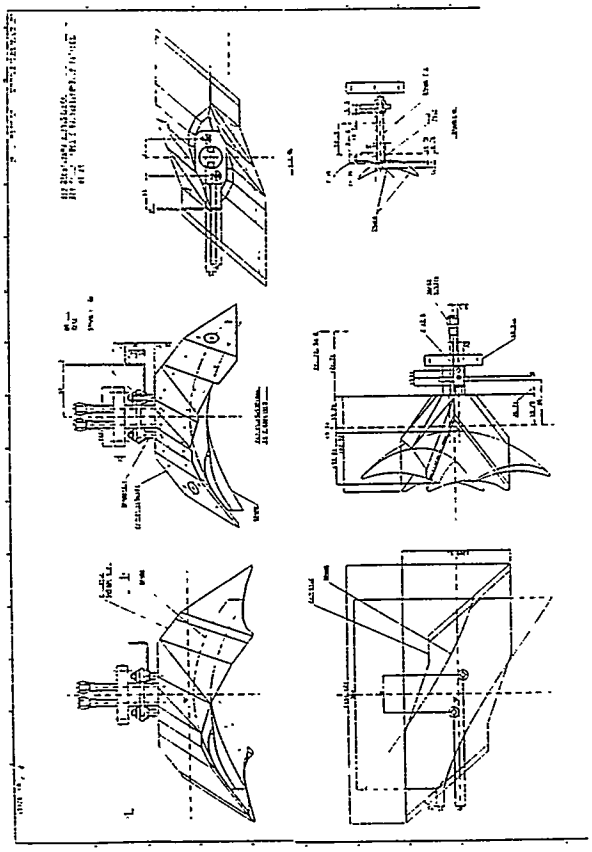

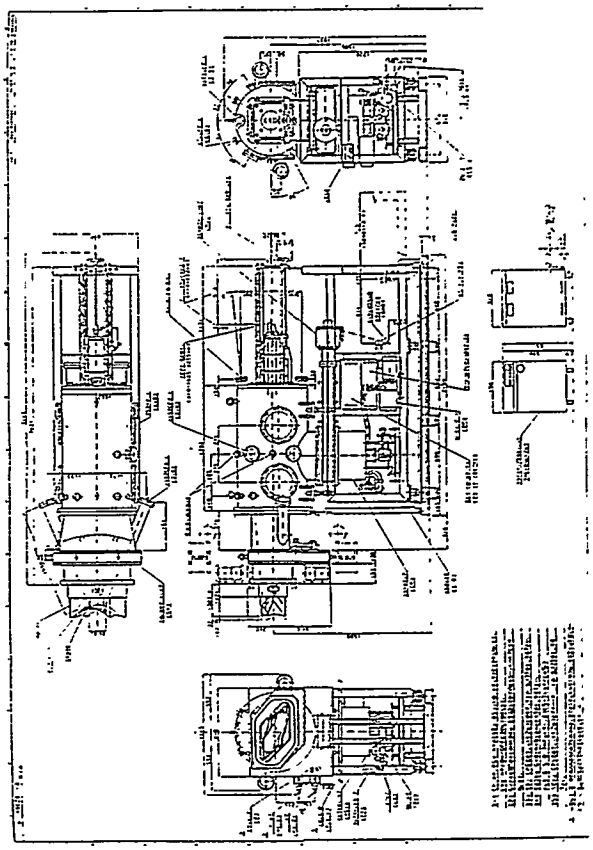

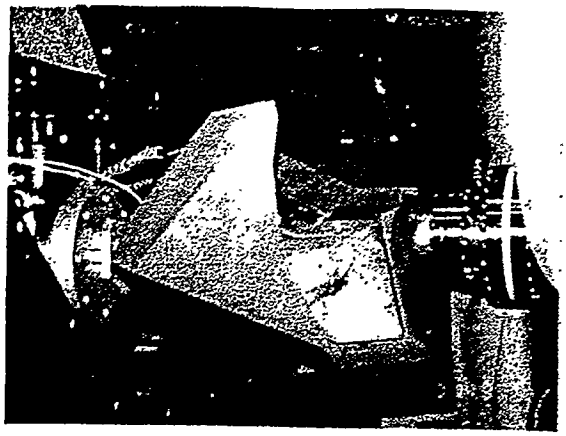

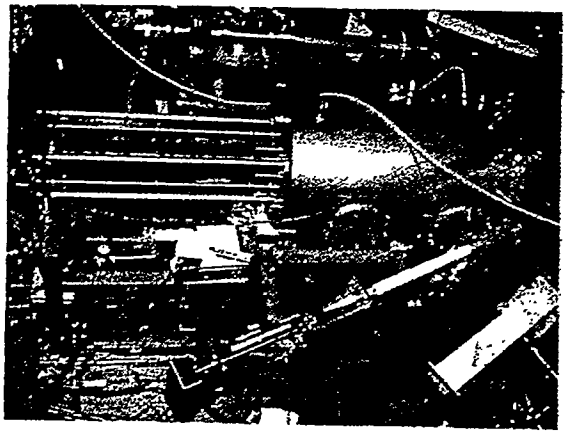

Fundamental LID Functions

- The outward heat and particle fluxes are guided to the back side of the divertor head by the island magnetic field structure.
- The particles which strike upon the back side of the divertor head are pumped out with high pumping efficiency.
- The leading edge of the divertor head is protected from the high outward heat flux from the core, because it is situated inside the island.

Expected Effects of LID on CHS Plasma Parameters

High efficient pumping
↓
High edge temperature
↓
A significant enhancement in the core energy confinement

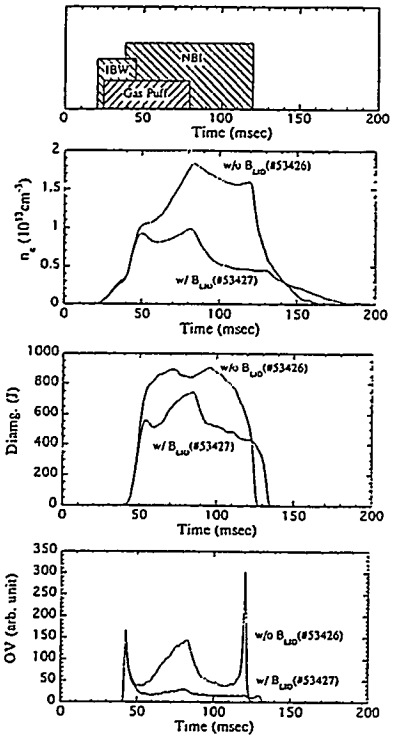

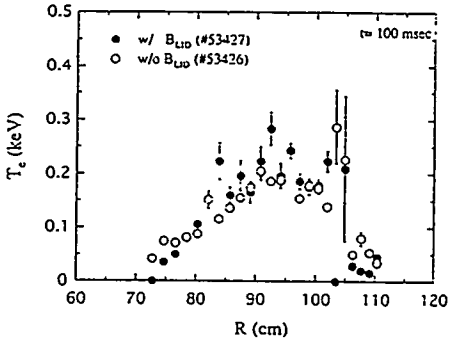

LHD scaling

$$\tau_E = 0.047 \times a^{2.0} R^{0.75} B_t^{0.84} n_e^{0.09} P_{tot}^{-0.58}$$

a : averaged plasma radius
R : major radius
B_t : toroidal magnetic field
n_e : electron density
P_{tot} : total input power

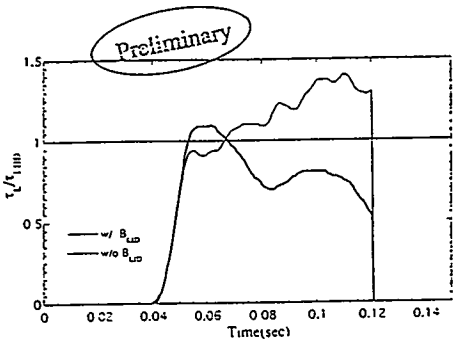

Summary

- LID experiment on CHS has just started.
- Plasma parameters were found to change when the island was formed.
- With the perturbation field on and at fixed gas puffing, line average electron density decreases, compared with discharges without the perturbation field. On the other hand, stored energy decreases a little, being accompanied by an increase in electron temperature.
- A comparison of the stored energy at the fixed line average density shows that the stored energies in discharges with the perturbation field are about 20% higher than those without the perturbation field, indicating a modest improvement of energy confinement.

The experimental data shown here are still preliminary and further experimental study is needed. But the results so far are encouraging in terms of the effectiveness of the LID. The LID experiment will be continued untill the end of March 1996.

NIFS

Study of Impurity Transport in LID Configuration in CHS

S.Masuzaki, A.Komori, N.Ohyabu, T.Morisaki, H.Suzuki, C.Takahashi, S.Sakakibara, K.Watanabe, T.Watanabe, T.Minami, S.Morita, K.Tanaka, S.Ohdachi, S.Kubo, N.Inoue, H.Yamada, K.Nishimura, S.Okamura, O.Motojima, and M.Fujiwara

National Institute for Fusion Science
Nagoya, Japan

C.C.Klepper, A.C.England, J.A.Rome, and J.F.Lyon

Oak Ridge National Laboratory,
Oak Ridge, TN 37831-8072, USA

NIFS

OUTLINE

1. Experimental Results indicating fundamental LID Function
   (1) Experimental Set-up
   (2) Experimental Results
   (3) Summary

2. Impurity Transport in LID Configuration
   (1) Experimental Results
   (2) Plan to Study Impurity Transport in LID Configuration

Experimental Set-up (1)

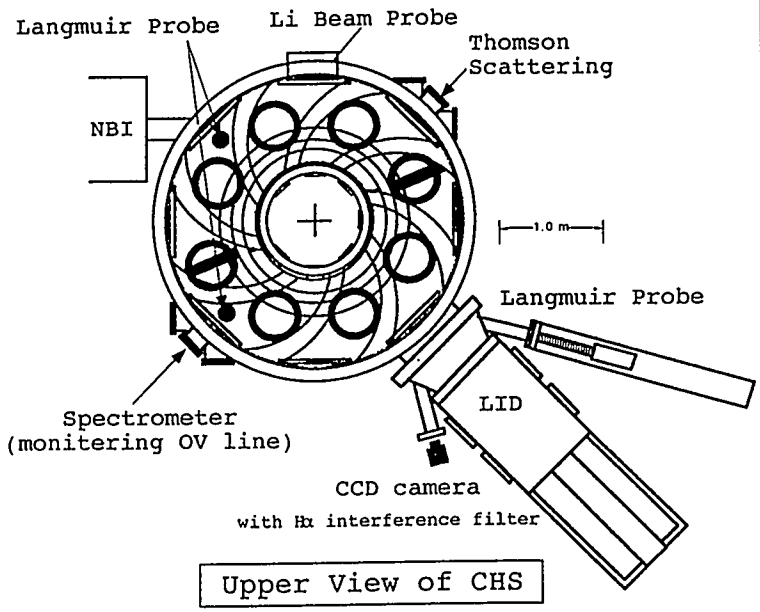

Upper View of CHS

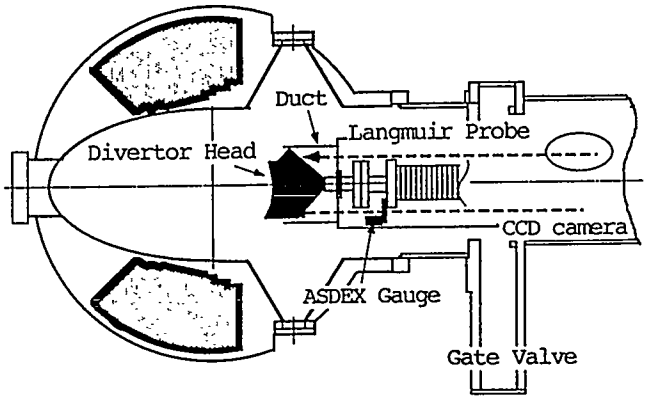

poroidal cross section

Experimental Set-up (2)

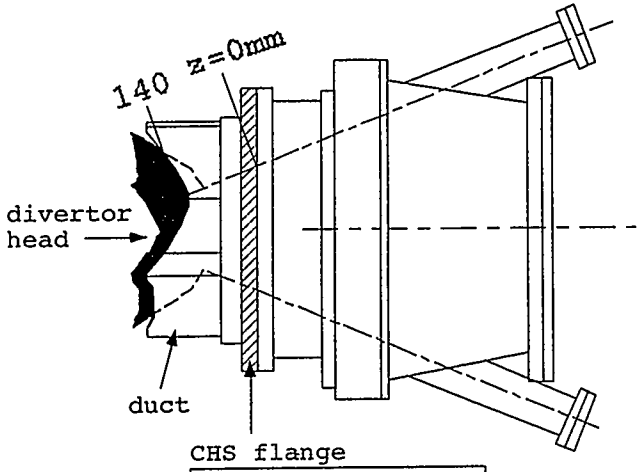

upper view of LID

Langmuir probe measures plasma parameters behind divertor head.

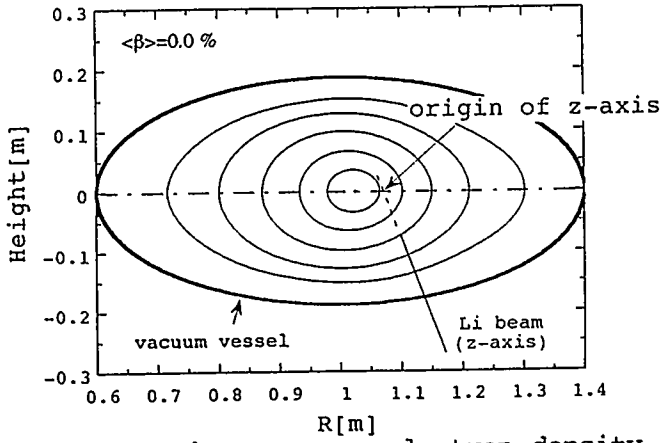

Li beam probe measures electron density.

Time Development of n_e

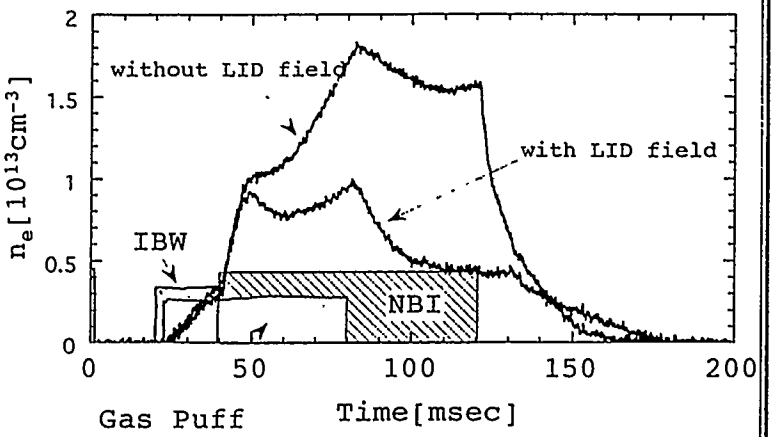

- With LID field, averaged density is smaller than that without LID field.
- After gas puffing, n_e decreases rapidly in the case of LID configuration. although n_e is almost kept in the case of without LID field.

ASDEX Gauge Results

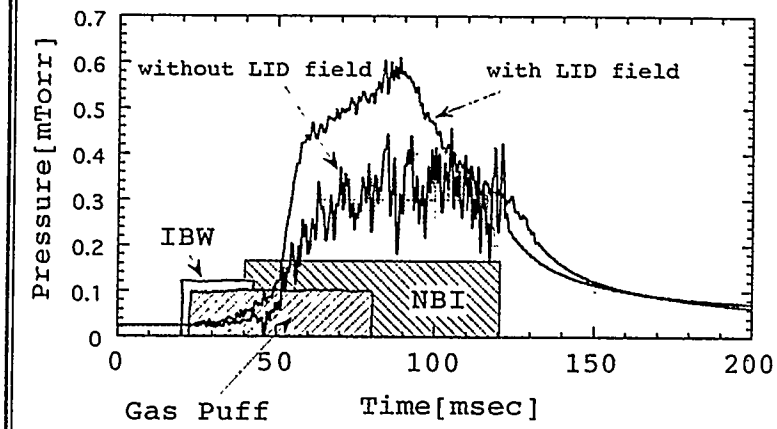

- Neutral pressure in the duct rises with plasma density.
- With LID field, the peak pressure is about two times larger than that without LID field.
- After gas puffing, neutral pressure decreases rapidly in the case of LID configuration. On the other hand, neutral pressure is kept constant after gas puffing in the case of no LID field.

Langmuir Probe measurement (1)

NIFS

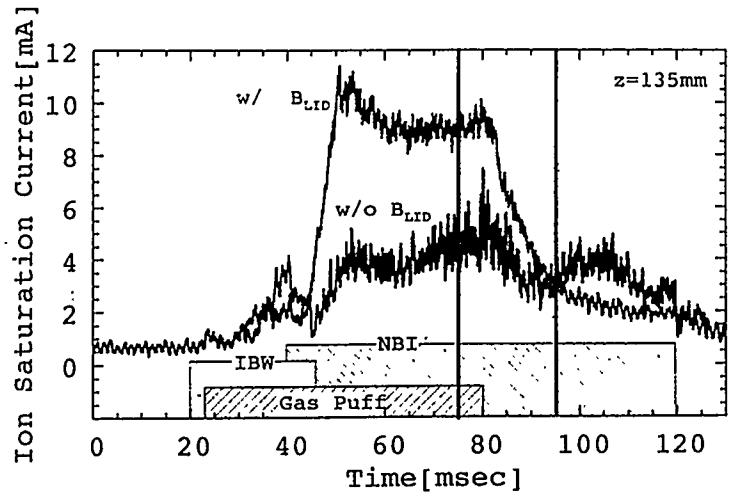

Ion saturation current time development behind divertor head

- In LID configuraiton, ion saturation current decreases rapidly after gas puffing, although that is almost kept in the case of without LID field.

Langmuir Probe measurement (2)

NIFS

Electron density and temperature profiles behind divertor head

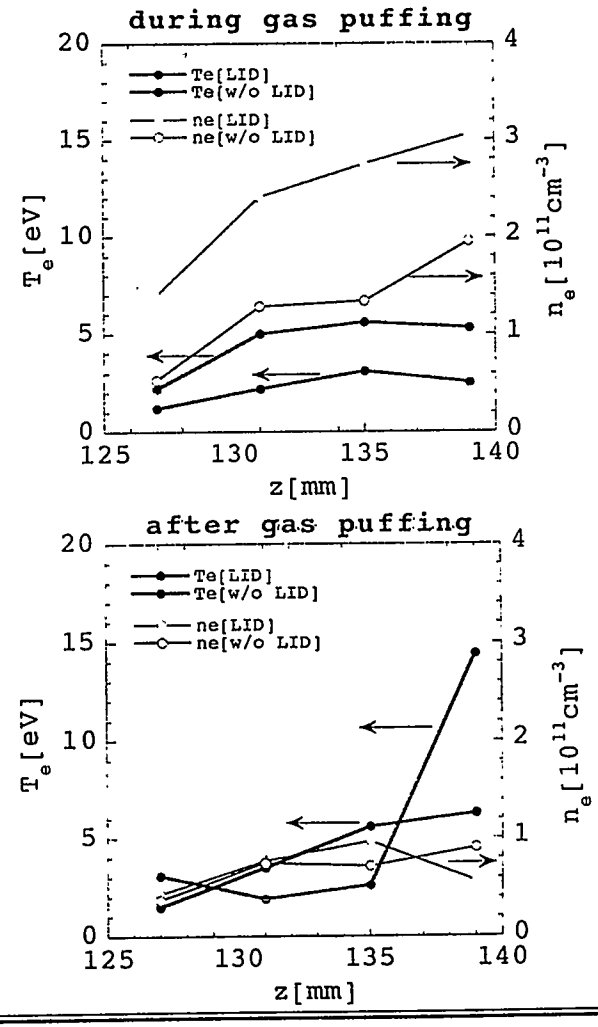

Li Beam Probe Results

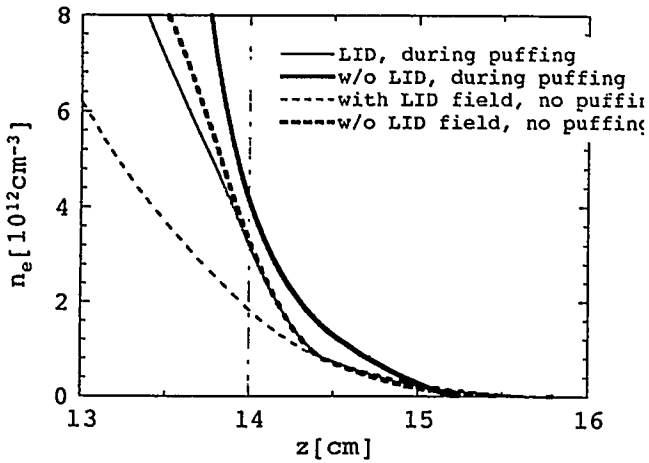

Li beam probe measures near X-point

- After gas puffing, electron density decreases in the case of LID configuration.

Summary

Fundamental LID functions are indicated experimentally.

- By the LID magnetic field configuration, the outward particle flux is lead to divertor head.

  <= ASDEX gauge, Langmuir probe

- The particles striking on divertor head are pumped out with effective pumping using cryopump.

  <= Langmuir probe, Li beam probe, $\overline{n}_e$

OV line intensity behaviour (1)

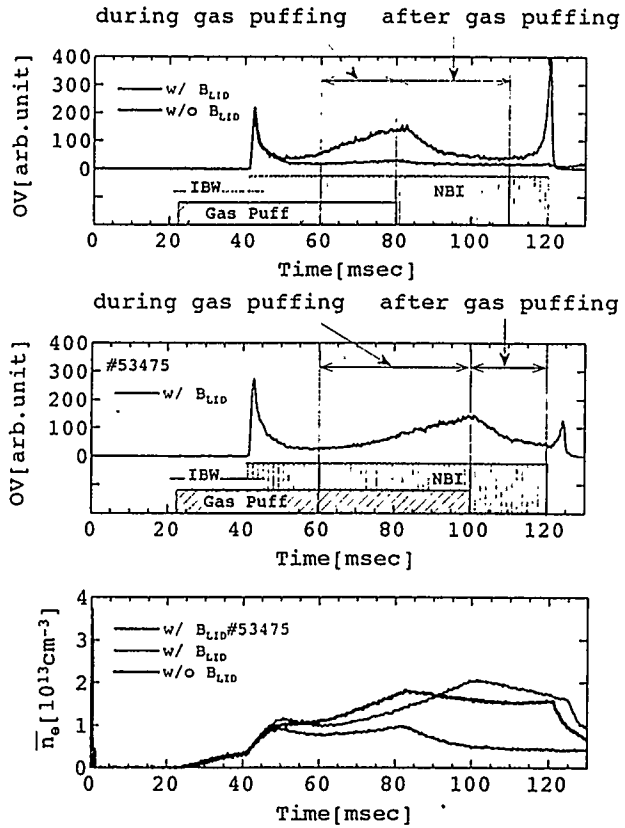

Gas puffing amount was increased and time was extended respectively, to obtain high density discharge with LID field.

OV line intensity behaviour (2)

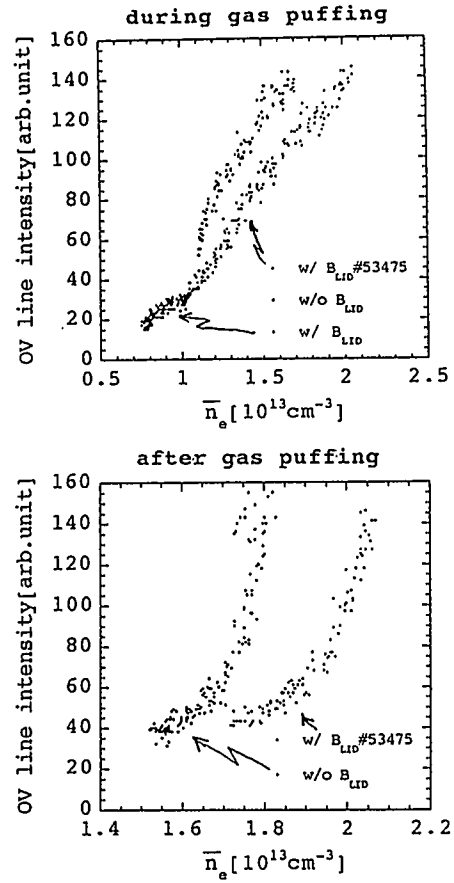

Temperature dependence of rate coefficient is not considered.

Plan to Study Impurity Transport in LID Configuration

NIFS

GOALS

(1)Confirm the effect of LID configuration on impurity transport

(2)Count the energy barance in LID configuration

EXPERIMENTAL METHODS

(1)Ar gas puffing for tracer gas

(2)Spectroscopic diagnostics measure the toroidal and radial distribution of Ar line intensity.

NIFS

LID Design for LHD

T. Morisaki, A. Komori, N. Ohyabu, S. Masuzaki
H. Suzuki, K. Watanabe, T. Watanabe, Y. Kubota,
N. Noda, O. Motojima and M. Fujiwara

National Institute for Fusion Science
Nogoya 464-01, Japan

Contents

Schematic of LID Concept

NIFS

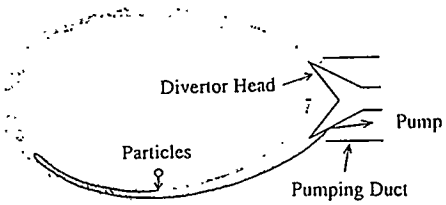

Since the core region is surrounded by the separatrix of the island, the outward heat and particle fluxes cross the island separatrix, and flow along the field lines to the back side of the island, where target plates are placed on a divertor head to receive the heat and particle loads.

Perturbation Coils

NIFS

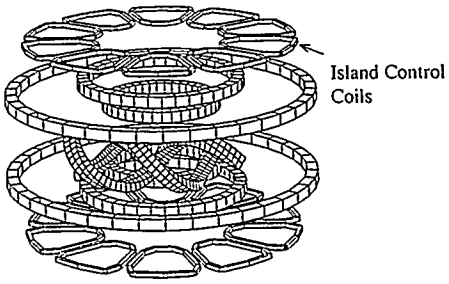

Application of Perturbation Field

NIFS

(a)

Application of m/n=1/1 component. m/n = 2/1 island is also produced by toroidal coupling.

(b)

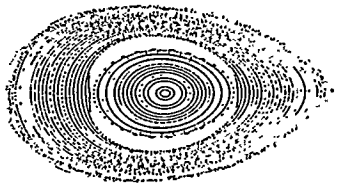

Application of m/n=2/1 component.

(c)

Complete elimination of m/n=2/1 island by adding (b) to (a)

Final Design of LID Coil

NIFS

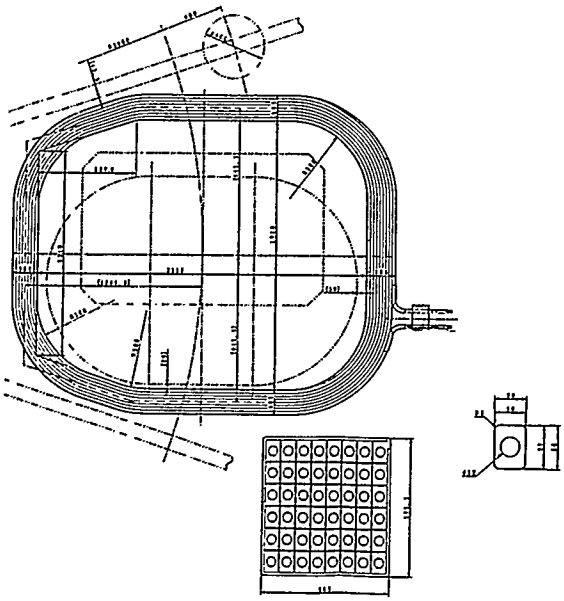

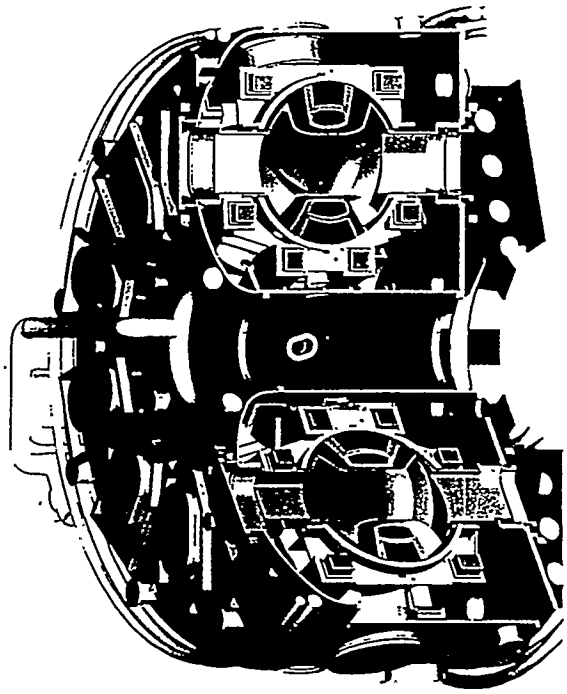

LID Installed in LHD

NIFS

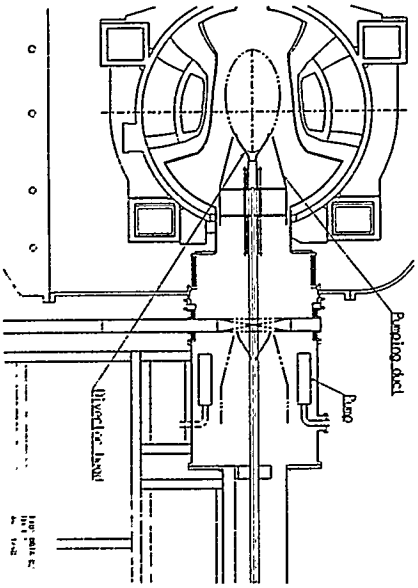

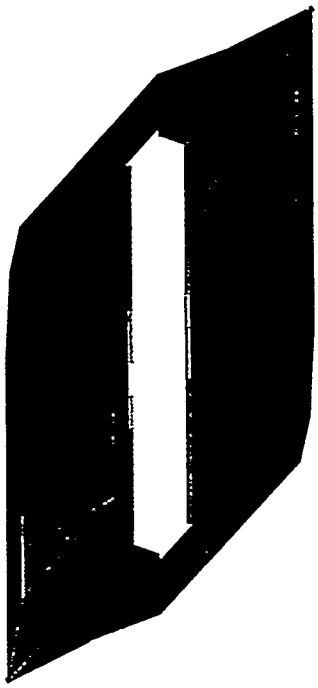

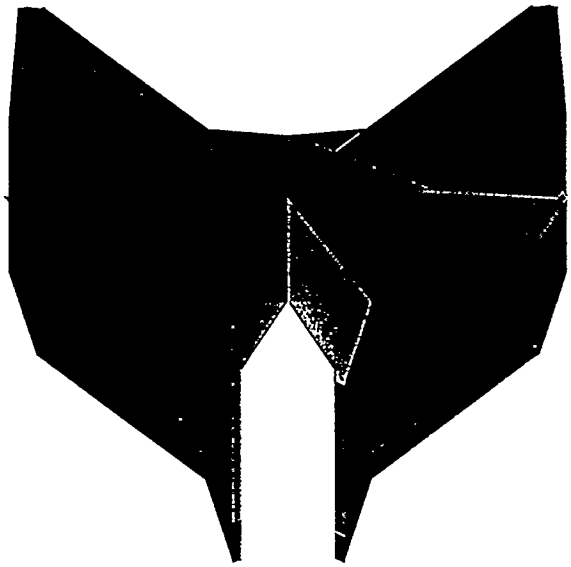

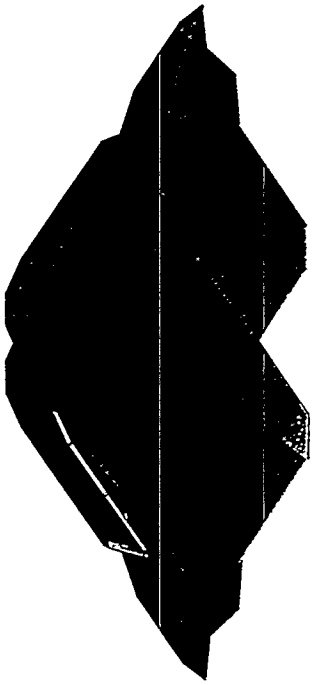

NIFS-P0045

LID Installed in LHD

NIFS

Leading-edge Problem

NIFS

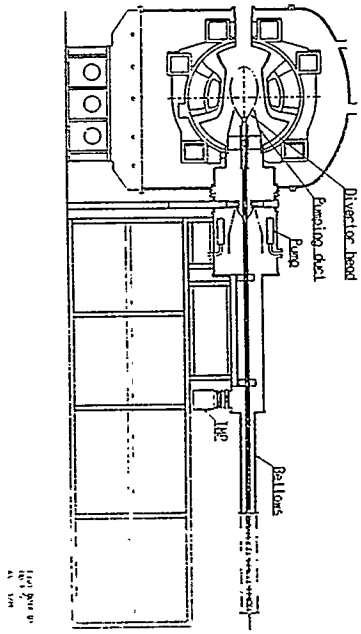

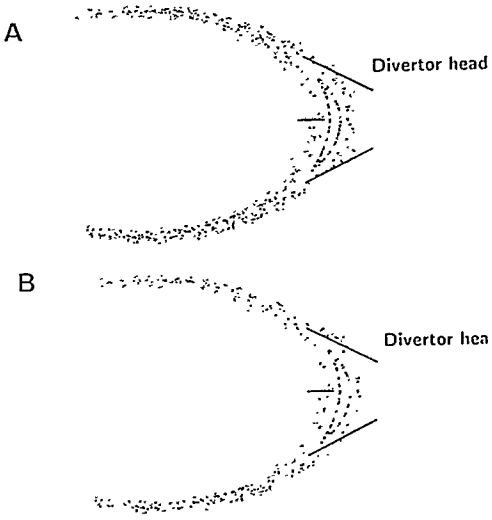

Viewing Area of IR Camera

NIFS

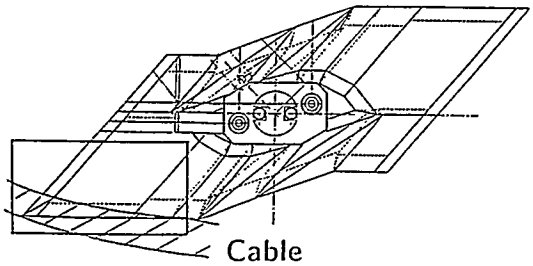

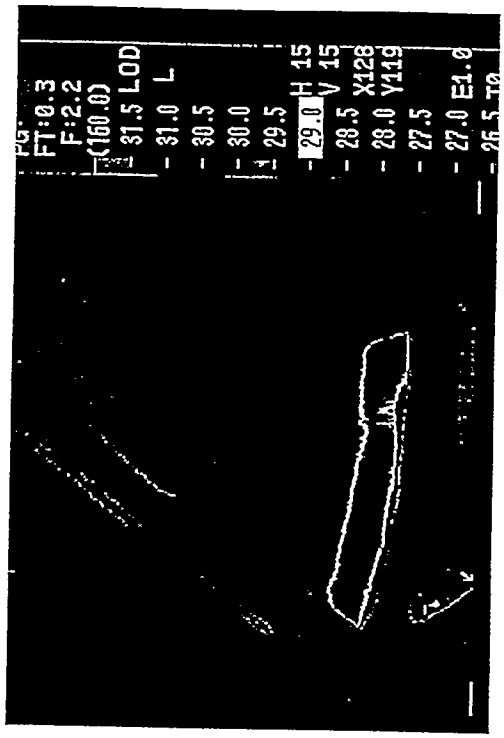

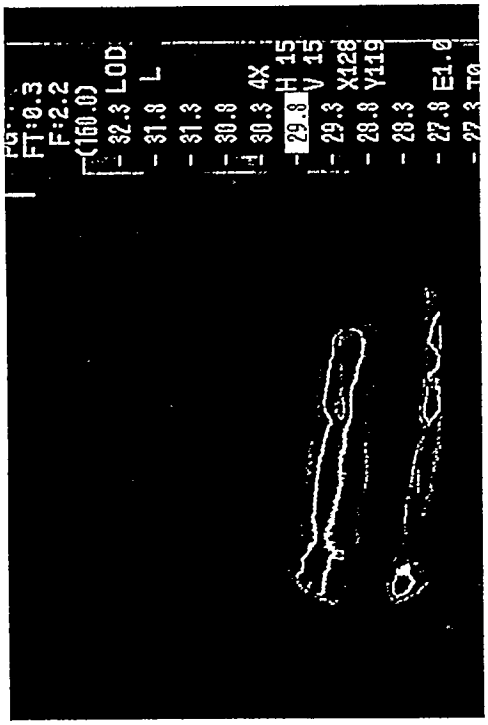

Material and Structure of Divertor Head

NIFS

Heat Load to the Tile

Heating Power in Steady State	3MW
Power to Divertor Head	1.5MW
Head Surface Area	0.4m^2

↓

4MW/m^2 (6MW/m^2 in max.)

↓

Surface Plate	C/C or Graphite
Brazing	
Back Plate (Water Cooled)	Cu

Thermal Responses of Brazed Material

NIFS

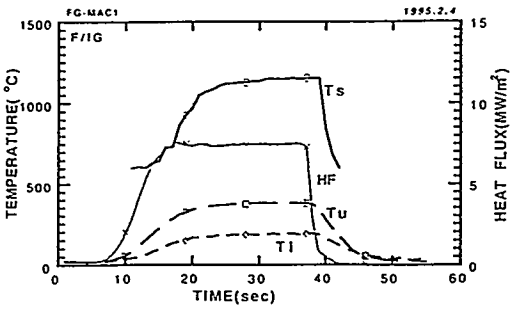

Typical thermal responses and heat load(HF) of brazed material during heat loading test.Ts,Tu,Tl are temperatures at surface of tile, at upper brazing region, at lower brazing region, respectively

Divertor Head Cooling

NIFS

Necessary Water Flow

Divertor Head consists of ~32 segments.

↓

Heat Load ~ 47 kW/segment

↓

$\Delta T = T_{outlet} - T_{inlet} = 50\ °C$

↓

Water Flow ~ 14 ℓ /min

Water Tube

Diameter	1 cm
Length	~ 100 cm
ΔP =	$P_{outlet} - P_{inlet}$
=	0.15 kgf/cm^2

> ~ 14 ℓ /min

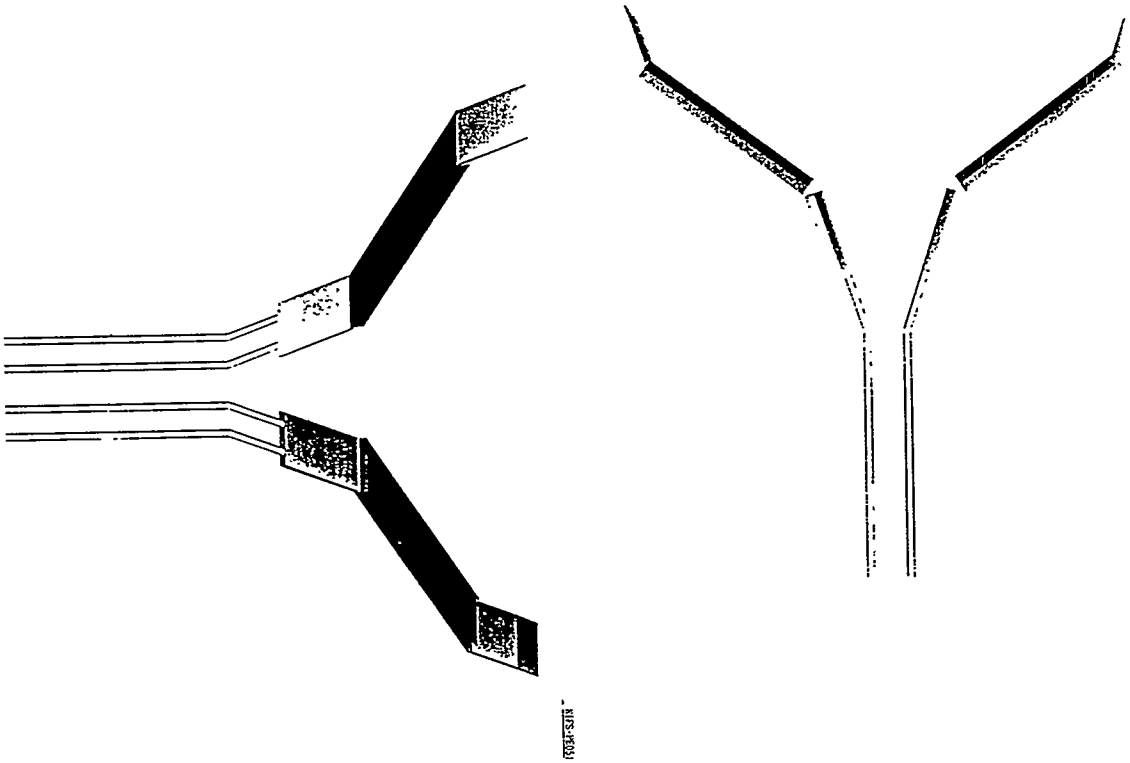

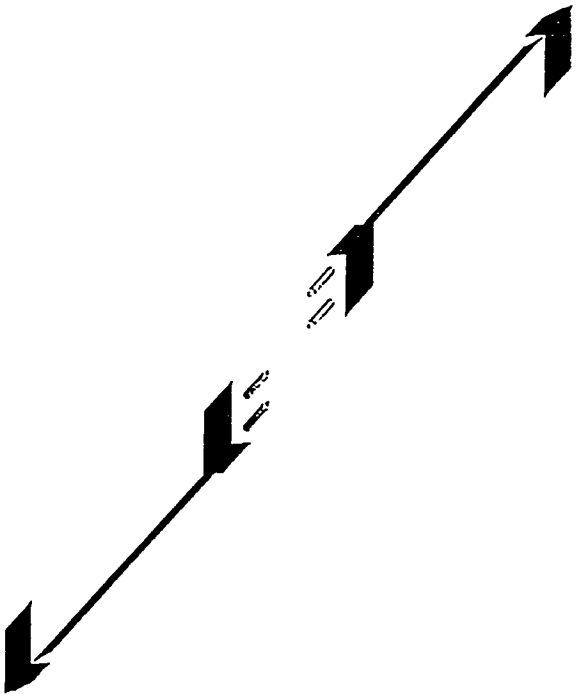

Principle of Superpermeable Membrane Pump

NIFS

THE PERMEATION PROBABILITY APPROACHES TO ~1 (SUPERPERMEATIO

Energetic hydrogen atoms pass through a superpermeable membrane ONLY ONE DIRECTION.

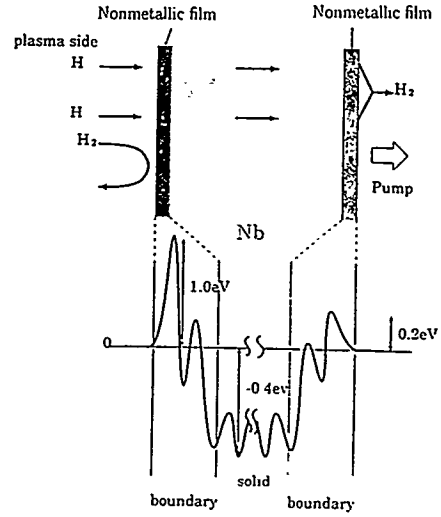

Experimental Results

NIFS

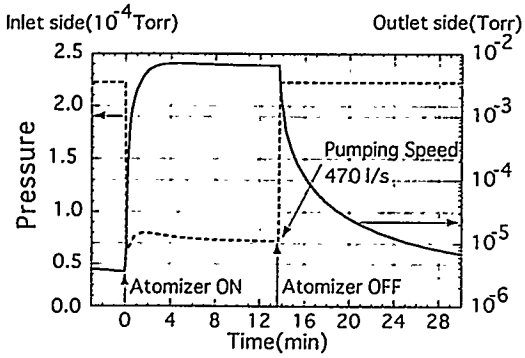

- Atomizer area : 125cm^2 (2 section)
- Atomizer temperature : 1870K
  (Atomization probability ~0.12)
- Membrane area : 1000cm^2
- Membrane temperature : ~850K

Performance of the Membrane Pump

NIFS

Maximum pumping speed

~1000 ℓ/s (P < 10^{-3}Torr)

400 ℓ/s (P=10^{-2}Torr)

Maximum permeation flux

7×10^{16} H/cm^{2}s (s=1000 ℓ/s)

3×10^{17} H/cm^{2}s (s=400 ℓ/s)

(Preliminary result. Still in progress)

Advantage of the Superpermeable Membrane Pump

NIFS

- Highly efficient hydrogen pumping
- No mechanical parts. It may operate in high magnetic field.
- No cold parts. The acceptable temperature for operation is 500~1000°C.
- Continuous operation
- Easy to make any shape.
- Low tritium inventory
- Separation of D/T mixture from He and any impurities. Only hydrogen isotops permeates

Superpermeable Membrane Pump is suitable for pumping hydrogen in plasma devices.

Summary

NIFS

1) LID coil design was presented.

2) Heat load measurement of the divertor head was performed on CHS with IR camera, and it was demonstrated that there is no leading-edge problem in LID configuration.

3) Precise design of Divertor head was presented.
   * Divertor head consists of ~32 segments.
   * Materials of surface tile and back plate are C/C (or graphite) and Cu, respectively.
   *Cooling system was designed, and the cooling tube with a diameter of 1cm can supply enough water fo cooling the tile.

4) Pumping system for LID was presented, i.e., cryogenic pump and metal membrane pump.

Wall Conditioning Scenario in LHD

A. Sagara
N. Noda, N. Ohyabu, O. Motojima

1. Standard stage

[w/o high magnetic field]

(1) Baking
  a) Temp.< 100°C due to SC

(2) Coating & Gettering
  a) Boronization
  b) Ti flashing(arrangements)

(3) Low power DC
  a) Glow 10kW
  b) ECH 20kW (2.45GHz)
  c) ICH(?)

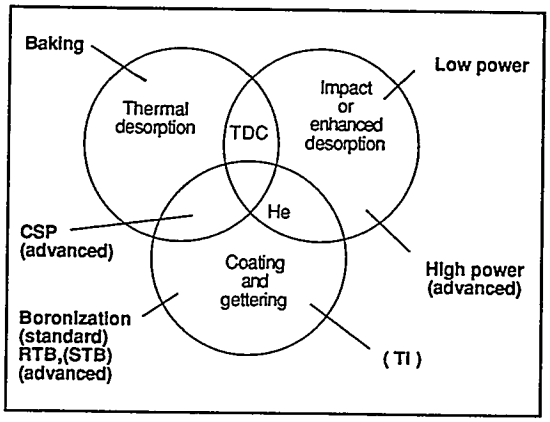

2. Advanced stage

[with high magnetic field of 1.5 - 4 T between shots]

(4) High power discharge cleaning

Phase	Scheme	Duration	Cycle	Pump	Power	Control
I	A	1 - 2sec	1/60Hz	main	ECH : 0.5 - 2 MW	H
I	(B1)	1 - 2 sec	1/60Hz	limiter	ECH : 0.5 - 2 MW	H
I	B2	1 -10sec	1/60Hz	LID	ECH : 0.5 - 2 MW	H
II	B3	- 4 min		LID	ECH : 0.5 - 3 MW	H
I	C	CW -2h		LID *	ECH : 0.5 MW	O (H)

* *High Efficient Oxygen Removal Using LID*
*(**within ~ 1 h << 1 month**)*
[main points]
[a] Active use of magnetic field
[b] H_2 gas puffing to release O
[c] CO production on graphite
[d] Efficient removal of CO & H_2

----> R&D required in real machines

cf. A. Sagara et al, Trans. of Fusion Technology, 27 (1995) 523 (6th ITC).

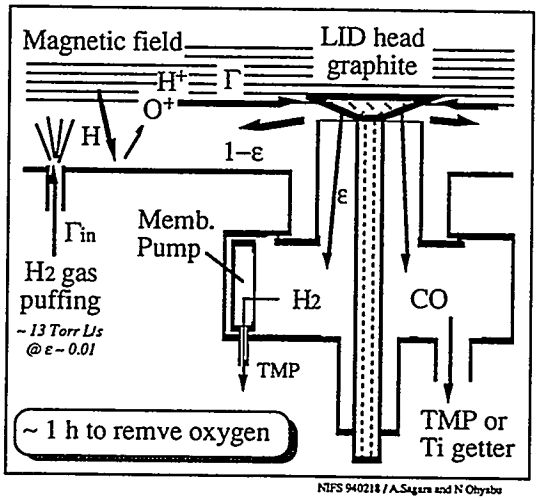

(5) Carbon Sheet Pump
  a) Usable as a local heater

cf. A. Sagara et al, J. Nucl. Mater., 220-222 (1995) 627 (11th PSI).
H. Suzuki et al, Trans. of Fusion Technology, 27 (1995) 523 (6th ITC).

3. Scenario for long-time operations :

with mode-changes on heating , magnetic field, etc.

(a) Purpose

1. Density control : thermal desorption of H_2,
   particularly from divertor graphite plates
   (at 400 ~ 600°C)
2. Impurity control : accumulation in core plasma, e.g. oxygen.

(b) Methods

1. Pre-conditioning
2. Divertor pumping :
   LID -- under R&D in CHS
3. Real Time Boronization (RTB):(submitted to the 12th PSI)
   <u>good results in CHS by puffing $B_{10}H_{14}$</u>
   - efficient reduction of O up to higher density plasma
   - with only a small amount of B used (~ 1% of non-RTB)
     , resulting in low density operations even after RTB.

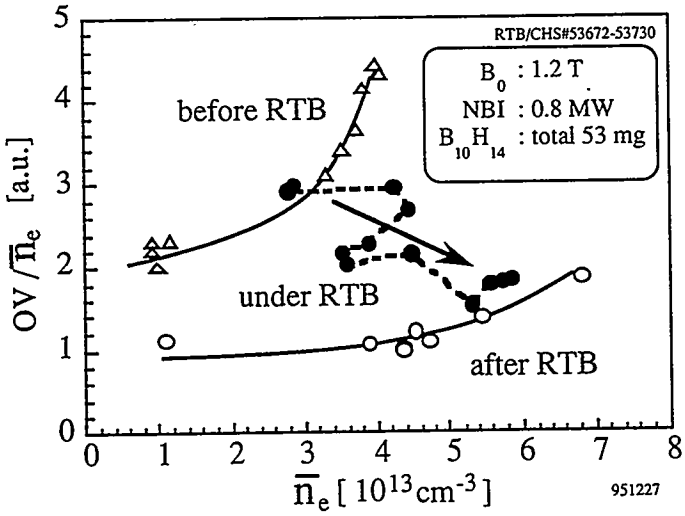

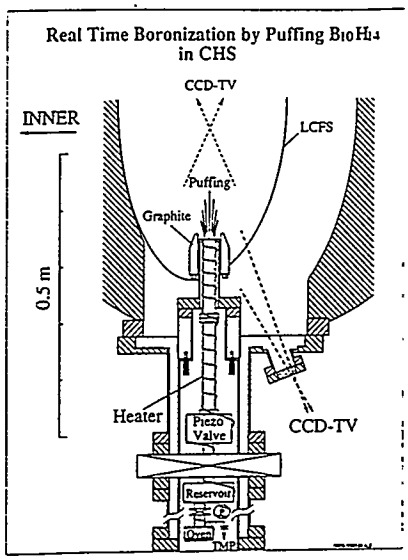

Wall Conditioning Scenario in LHD

A. Sagara
N. Noda, N. Ohyabu, O. Motojima

NIFS, Japan

1. Standard Stage : **w/o high magnetic field**
   (1) Baking
   a) Temp.< 100°C due to SC helical coiles

   (2) Coating & Gettering
   a) Boronization
   b) Ti flashing(?, but making arrangements)

   (3) Low power discharge cleaning
   a) Glow 10kW
   b) ECH 20kW (2.45GHz)
   c) ICH(?)

2. Advanced stage :

with high magnetic field between shots

(1.5 - 4 T)

(4) High power discharge cleaning

Phase	Scheme	Duration	Cycle	Pump	Power	Control
I	A	1 - 2sec	1/60Hz	main	ECH : 0.5 - 2 MW	H
I	(B1)	1 - 2 sec	1/60Hz	limiter	ECH : 0.5 - 2 MW	H
I	B2	1 -10sec	1/60Hz	LID	ECH : 0.5 - 2 MW	H
II	B3	- 4 min		LID	ECH : 0.5 - 3 MW	H
I	C	CW -2h		LID *	ECH : 0.5 MW	O (H)

**High Efficient Oxygen Removal Using LID*

*High Efficient Oxygen Removal Using LID
(**within ~ 1 h << 1 month**)

[1] Active use of magnetic field
[2] H_2 gas puffing to release O
[3] CO production on graphite
[4] Efficient removal of CO & H_2

------> R&D required
in real machines

cf. A. Sagara et al, Trans. of Fusion Technology, 27 (1995) 523 (6th ITC).

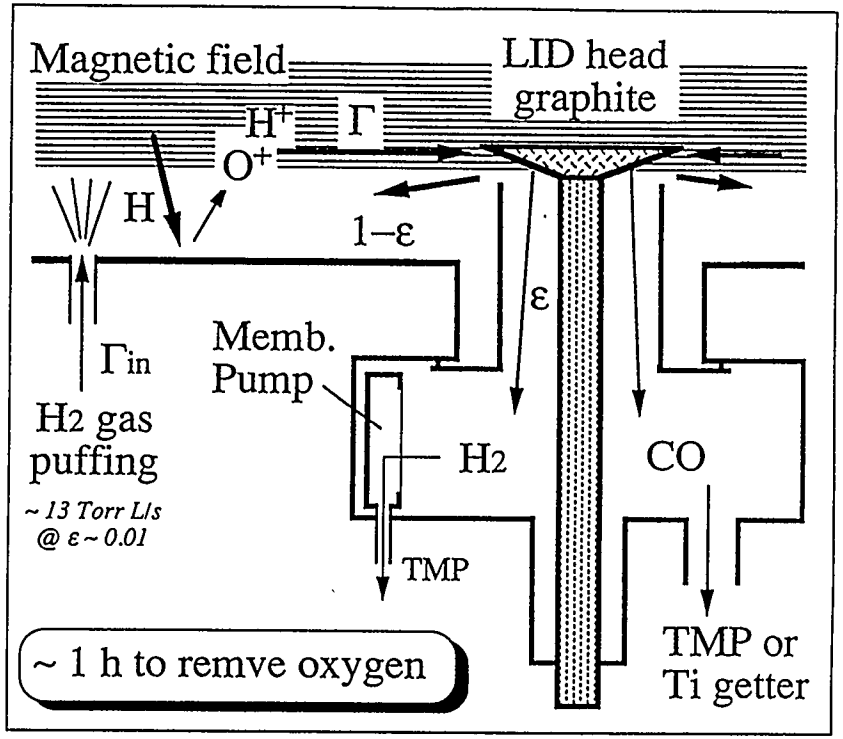

NIFS 940218 / A.Sagara and N.Ohyabu

(5) Carbon Sheet Pump
a) Usable as a local heater

cf. A. Sagara et al, J. Nucl. Mater., 220-222 (1995) 627 (11th PSI).
H. Suzuki et al, Trans. of Fusion Technology, 27 (1995) 523 (6th ITC).

3. Scenario for long-time operations :
with mode-changes on heating, magnetic field, etc.

(a) Purpose

1. Density control : thermal desorption of H_2, particularly from graphite plates (at 400 ~ 600°C)
2. Impurity control : accumulation in core plasma, e.g. oxygen.

(b) Methods

1. Pre-conditioning : Boronization, etc.
2. Divertor pumping : LID -- under R&D in CHS
3. Real Time Boronization (RTB):
   good results in CHS by puffing $B_{10}H_{14}$
   - efficient reduction of O up to higher density plasma
   - with a small amount of B used (~1% of non-RTB)
   , resulting in low density operations even after RTB.
   (submitted to the 12th PSI)

Real Time Boronization by Puffing $B_{10}H_{14}$ in CHS

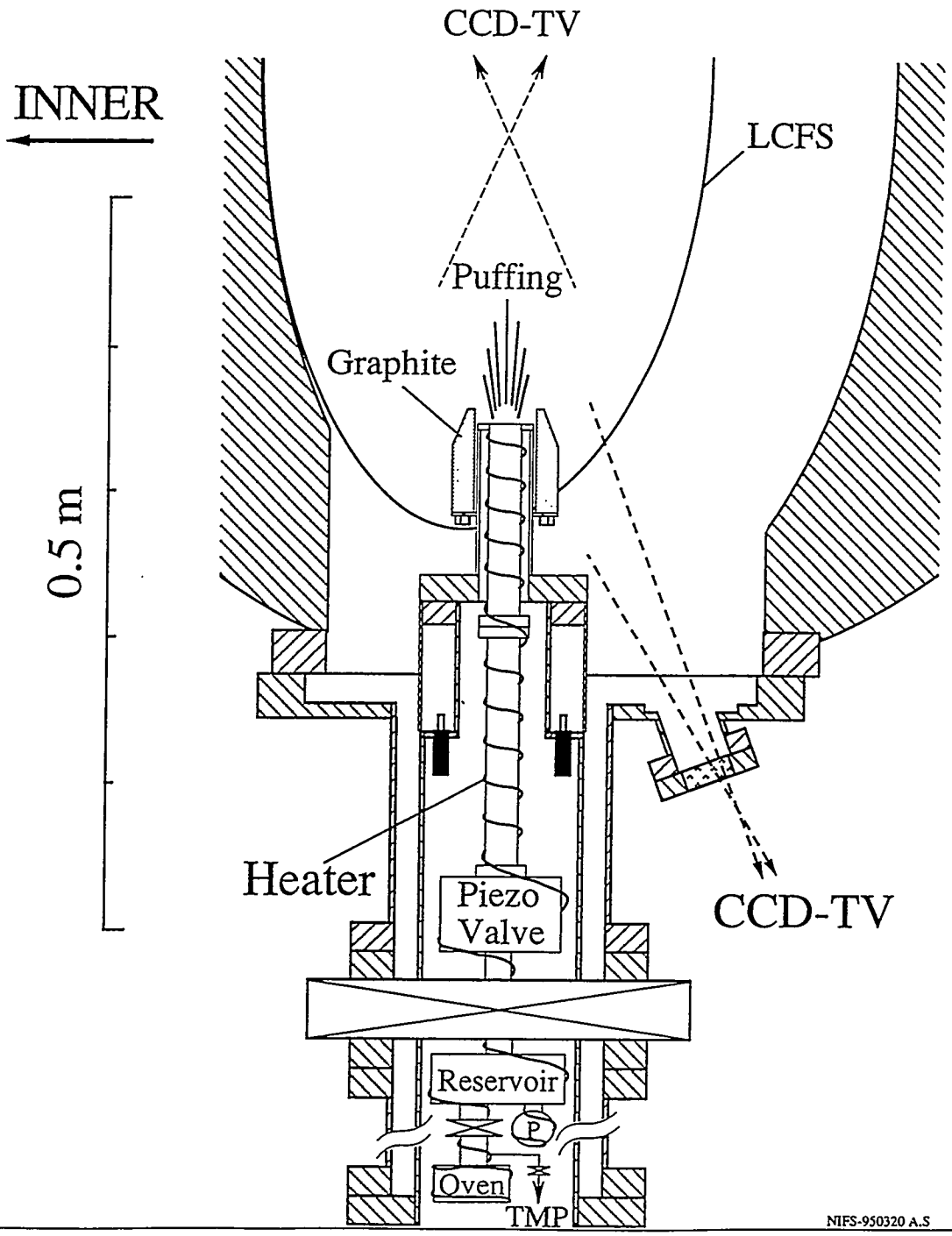

Good results in CHS by puffing $B_{10}H_{14}$

- Efficient reduction of O up to higher density plasma
- with only a small amount of B used (~1% of non-RTB) , resulting in low density operations even after RTB.

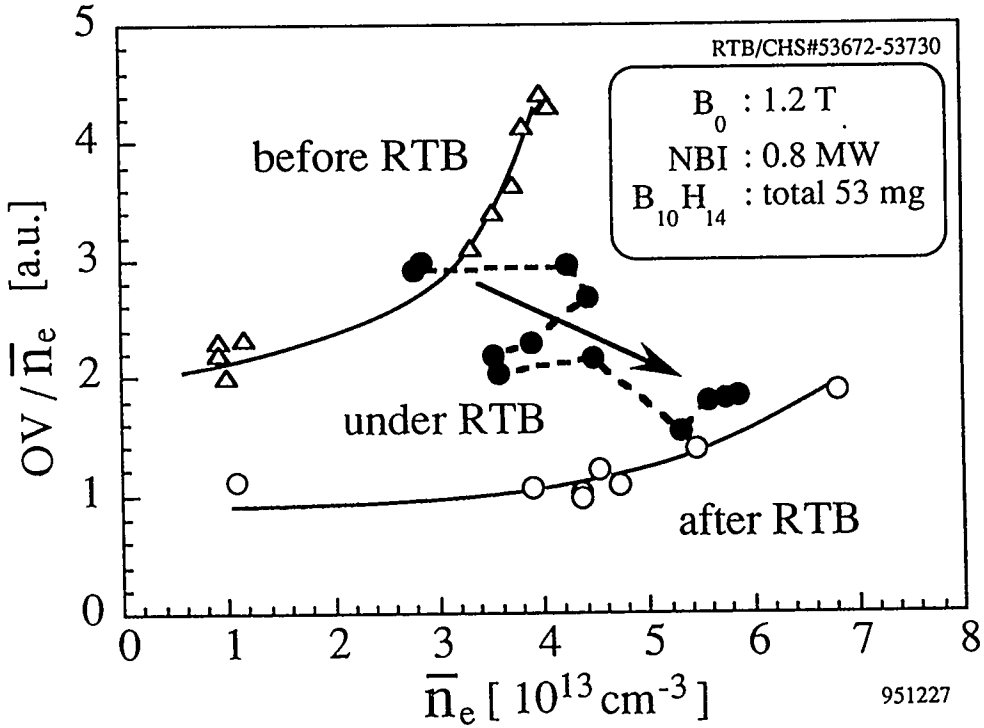

SUMMARY

" LHD has many cards for conditioning "

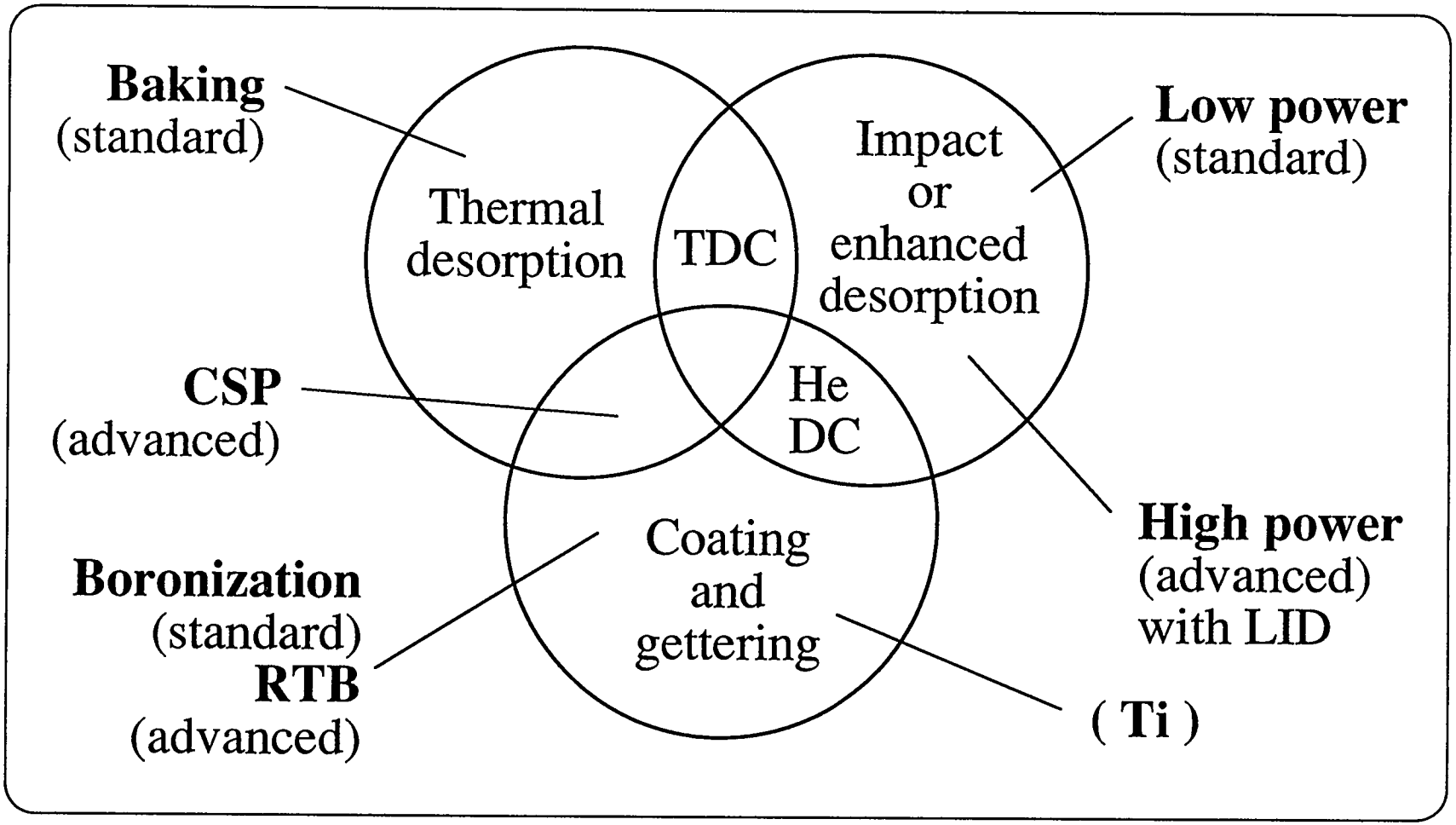

US-Japan Workshop Q219 on High Heat Flux Components and Plasma Surface Interactions for Next Devices, Colorado Springs, Colorado USA, 9-11 January 1996

PFC/PSI Studies in JT-60U

M. Saidoh
Department of Fusion Facility
JAERI

Collaborator: K. Kodama
K. Masaki
J. Yagyu
T. Arai
H. Hiratsuka
N. Hosogane

Contents

Wall conditioning in JT-60U

○ Baking

up to 300 ℃ : Vacuum Vessel

up to 150 ℃ : NBI ports, Diagnostic ports etc.

○ Discharge cleaning (DC)

Taylor DC (TDC)---during shots

Glow DC (GDC)---lunch/dinner time and during night

DC using Tokamak discharge

○ Boronization

Plasma-assisted Chemical Vapor Deposition(CVD) using Decaborane ($B_{10}H_{14}$) since July 1992

Decaborane (~100g)

→ 300 nm deposited boron film in average thickness

Deposited boron film is well characterized.

Deuterated boronization has been carried out on March 1995.

Solid Target Boronization (STB) since January 1994---real time boronization

Plasma impact on B_4C-converted CFC divertor tiles (row-e) causes B_4C evaporation.

Operation History and major attainment in JT-60U

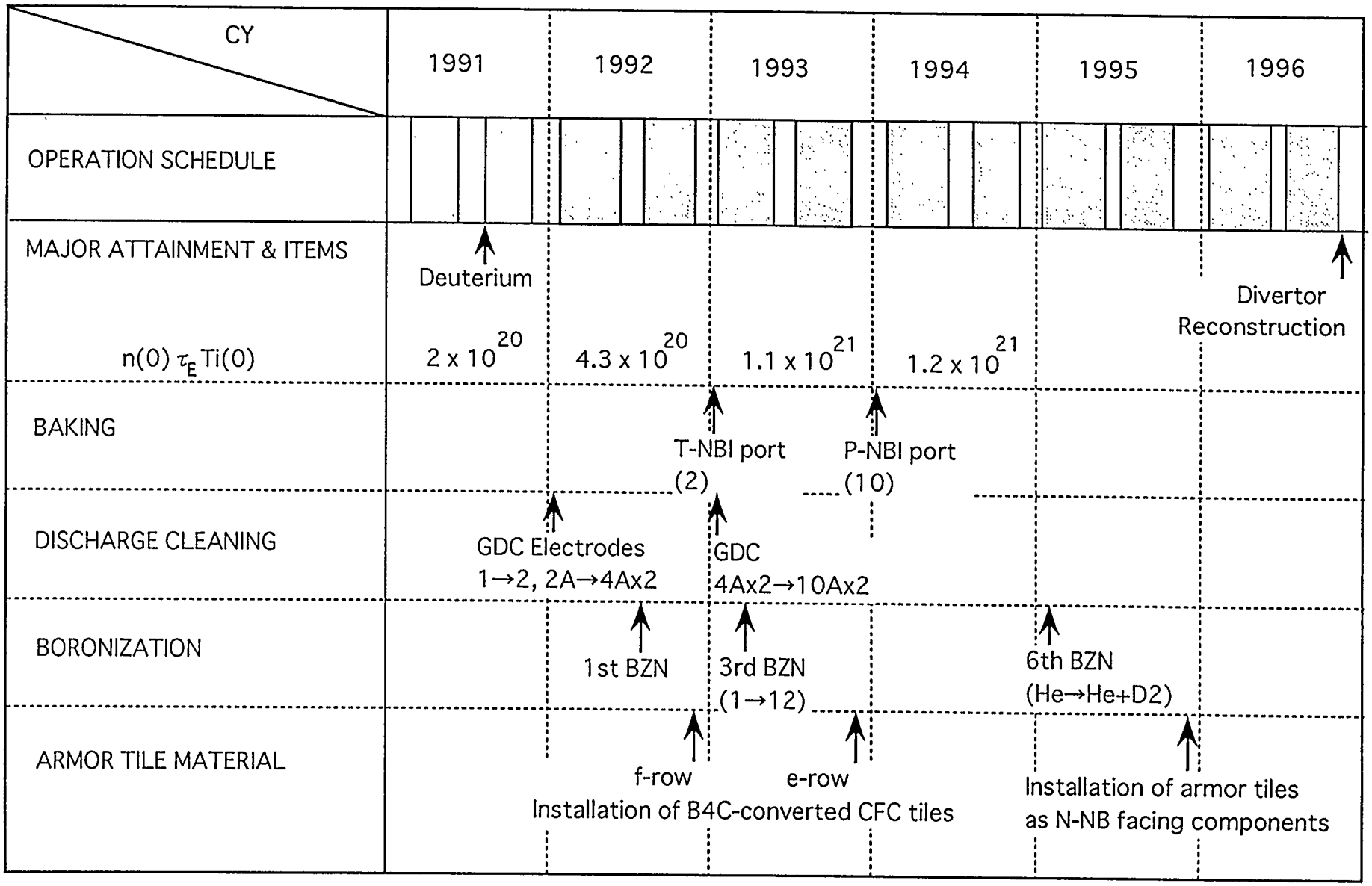

The 6th (deuterated) Boronization

(March 1995)

Objective

Reduction of hydrogen content in deposited boron due to H-D exchange during boronization using mixed dilution gas of He and D_2

Dilution gas

Up to 5th boronization: He + decaborane($B_{10}H_{14}$)

6th boronization: He(62%) + D_2(38%) + decaborane

Results

Hydrogen/deuterium content in deposited boron

1) Reduction of hydrogen content → 1/4 (12%→3%)

2) Increase of total content (D_2 + H_2)→3 (12%→32%)

Effects on plasma performance

1) Remarkable reduction of H/D ratio

($\sim 10 \rightarrow < 0.3$)

2) Low recycling as the same as previous ones

3) Oxygen reduction even for NB-heated plasma, which is the first time after boronizations

3') Remarkable reduction of re-ionization loss of neutral beam from NBI

H/D ratio after 5th and 6th Boronization

○ After 6th boronization, H/D ratio was extremely low (below 0.3) compared with the 5th one (～10).

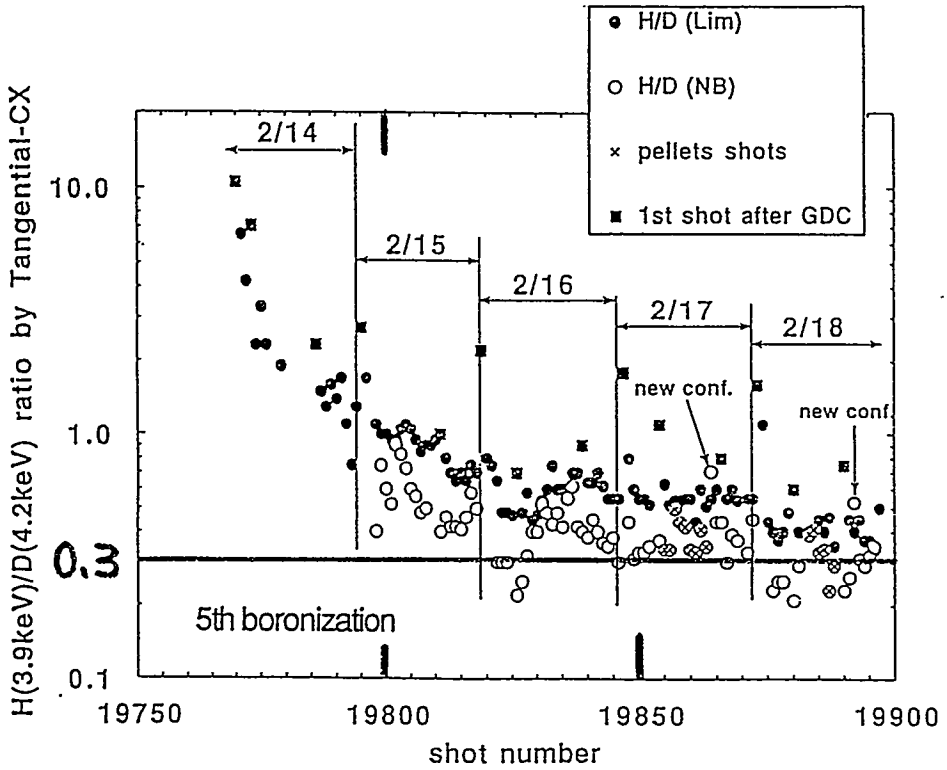

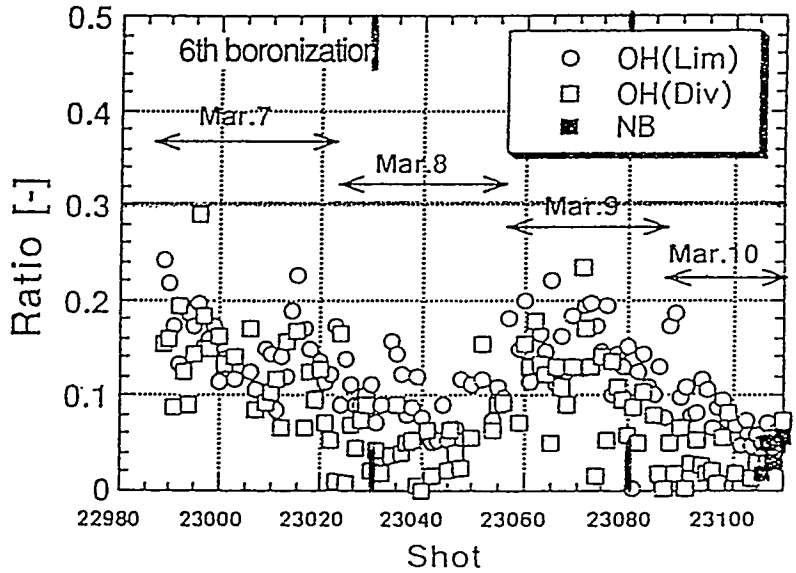

Recycling after 6th boronization

○ Recycling is very low and the same as those obtained in the previous boronization.

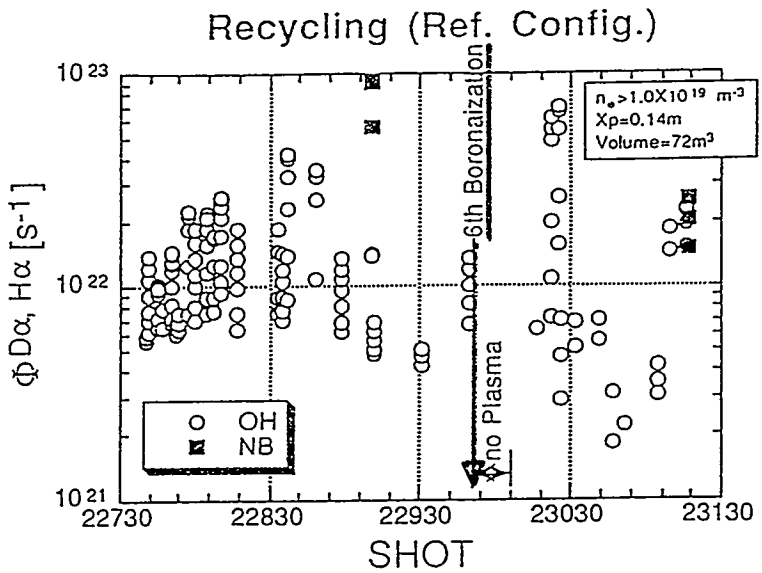

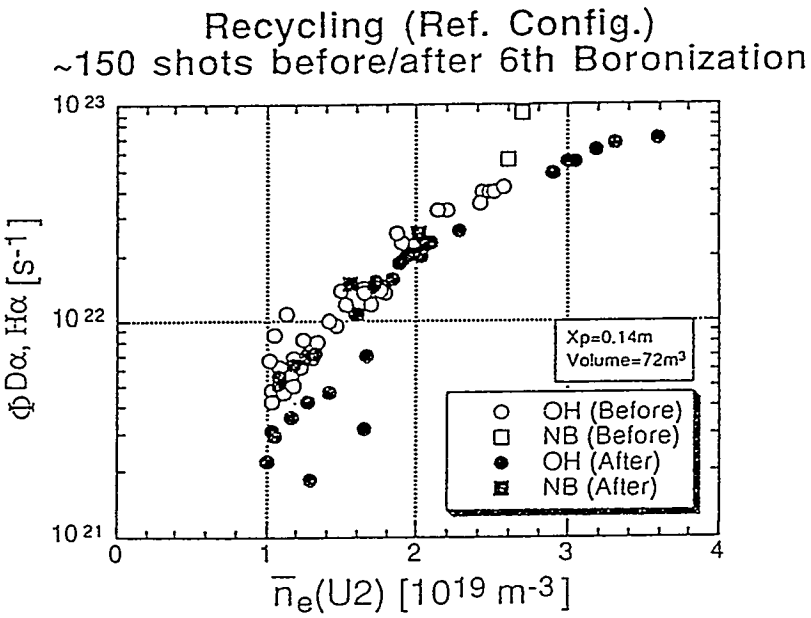

Impurity reduction effects after 6th boronization

- ○ Zeff values are the same as those in the previous five boronizations.
- ○ Oxygen is reduced even in the NB-heated plasma, which is the first time after boronizations.

~150 shots before/after 6th Boronization

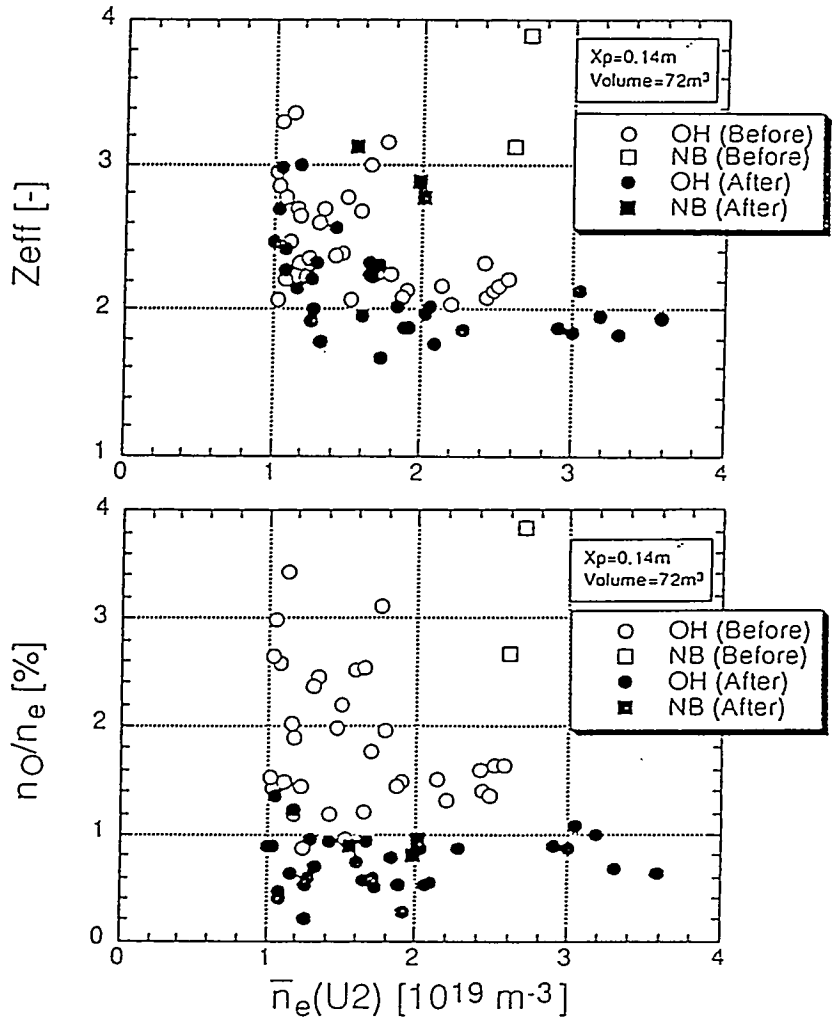

Operation History of JT-60U

Operation Phases	I	II	III	IV	V
No. of Discharges	1293	1880	2335	2766	2568
No. of NBI Discharges	629	1085	1305	1653	1649
NBI Power (MW)	≤ 20	≤ 27	≤ 36	≤32	≤33
Integrated Time of TDC	221H45m	186H19m	63H43m	19H57m	30H50m
Integrated Time of GDC	222H01m	548H26m	643H13m	535H29m	472H13m

I : Mar.-Oct. 1991 *July 1991: Start of D-D Discharge Operation

II : Jan.-Oct. 1992 *July 1992: 1st Boronization

III : Jan.-Oct. 1993 *December 1992: Increase of Gas Inlet (1 → 12)
Installation of B_4C-converted CFC (row-f of divertor tiles)
*February 1993: 3rd Boronization

IV : Jan.-Oct. 1994 *December 1993: Installation of B_4C-converted CFC (row-e of divertor tiles)
*February 1994: 5th Boronization

V : Jan.-Oct. 1995 *March 1995: 6th Boronization (mixed gases of D_2 and He)

Tritium measurement of the inner wall tiles in JT-60U

Objectives

Retention of tritium generated D-D fusion in the tiles and their poloidal distribution

Comparison with tritium inventory in the tiles estimated from tritium concentration measurement in exhaust gases

Samples and procedure

Long term exposed tiles from July 1991 to October 1993 (generated tritium ~32GBq)

Conbustion in dry air

→ Tritiated water (oxidation of tritium)

→ Scintillation counting of HTO in the collected water

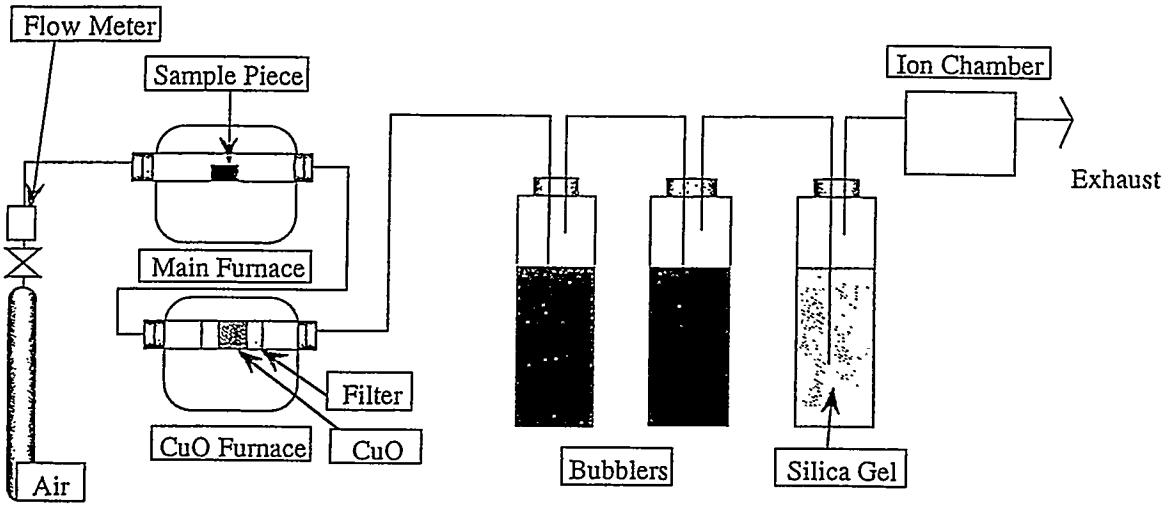

Tritium inventory in the inner wall tiles

Tritium poloidal distribution

1) Tritium concentration in the divertor tiles was higher than that in the first wall tiles.
2) The highest tritium concentration was in the divertor tile faced to the private zone.
3) The lowest tritium concentration was in the strike point on the divertor.

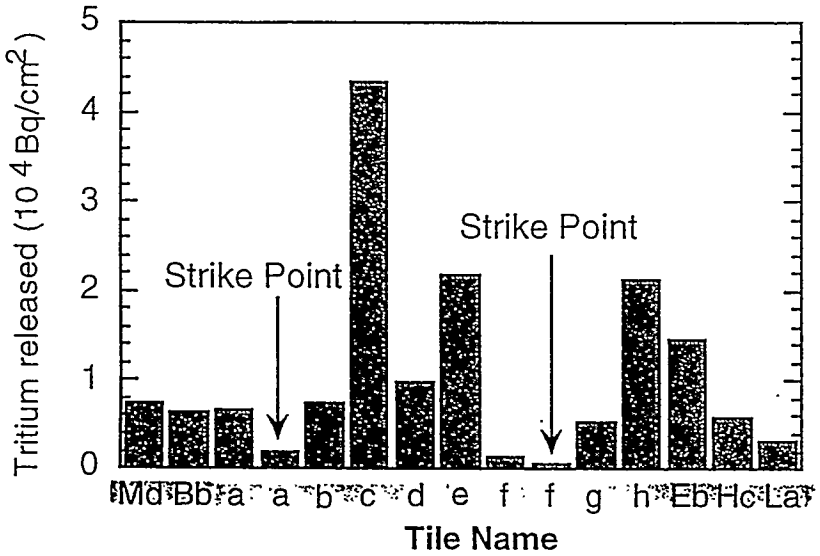

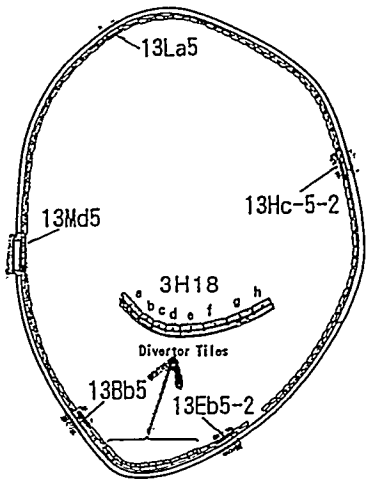

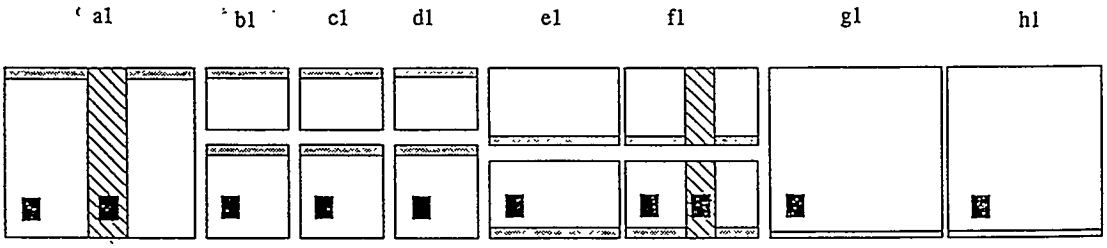

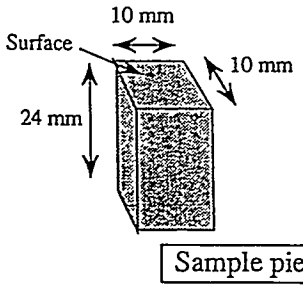

Inboard ⟷ Outboard

Poloidal Direction

Eroded Area

Sample Pieces

Strike Point

Tritium inventory in the inner wall tiles

Tritium toroidal distribution

1) The highest tritium concentration was in the sample piece which had severe erosion area. This value was about 3 times larger than those of the other sample pieces.

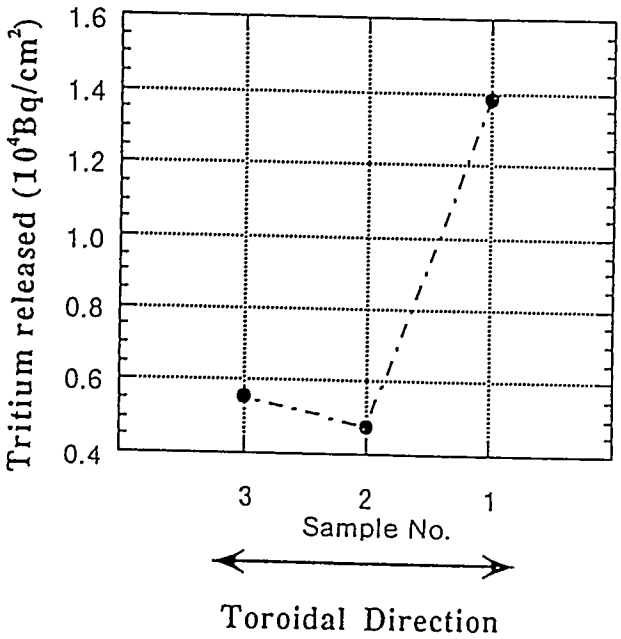

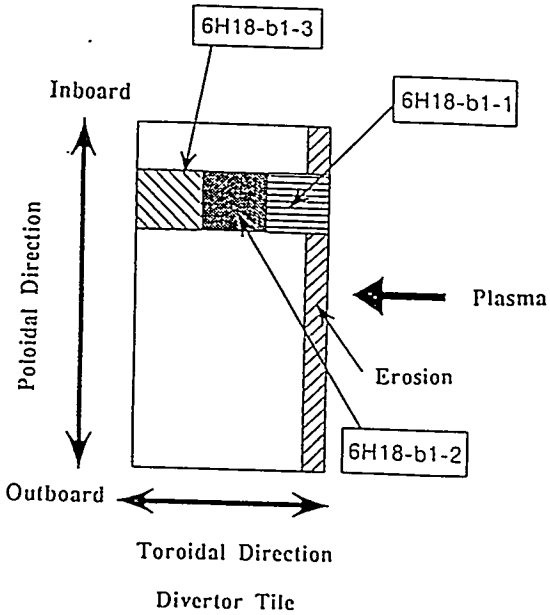

Tritium inventory in the inner wall tiles

1) From both poloidal and toroidal distribution total tritium inventory was estimated to be 1.6 x 10^{10}Bq, which corresponds to approximately 50% (10% in divertor tiles and 40% in first wall tiles) of the tritium generated from July 1991 to October 1993.

(K. Masaki et al., Accepted for publication in Fusion Eng. & Des.)

Objectives of Divertor Modification

1. Divertor study as R&D for designing ITER and JT-60SU

ITER Physics R&D Issues:

- 2.20 Target Geometry
- 2.21 Baffle Geometry
- 2.22 Pulses and Geometry
- 2.23 Pumping Locations
- 2.24 Impurities + Geometry
- 2.25 Helium and Geometry

2. Improved performance of JT-60U plasmas

- compatibility of good confinement with high density divertor---> ITER, JT-60SU

- divertor compatible with relatively low density plasmas;
  1) high β_p plasmas
  2) ELMy H-mode
  3) Steady tokamak operations by NBCD with N-NBI + bootstrap current

A New JT-60U Divertor

1. W-type geometry with central dome

   - capability of forming high recycling state
   - dome for separating inner, private and outer divertor regions, and for baffling the influx of impurity gases to the x-point region.

2. Pumping by NB cryo-pumps:

   - S_{eff} =35 m^3/s(0.1 Pa) - 72 m^3/s(1 Pa)
   - D/He/(D+He) pumping with/without Ar frost
   - two pumping regions: 1) only the inner region, 2) both the inner and outer regions.
   - control of pumping speed during a shot.

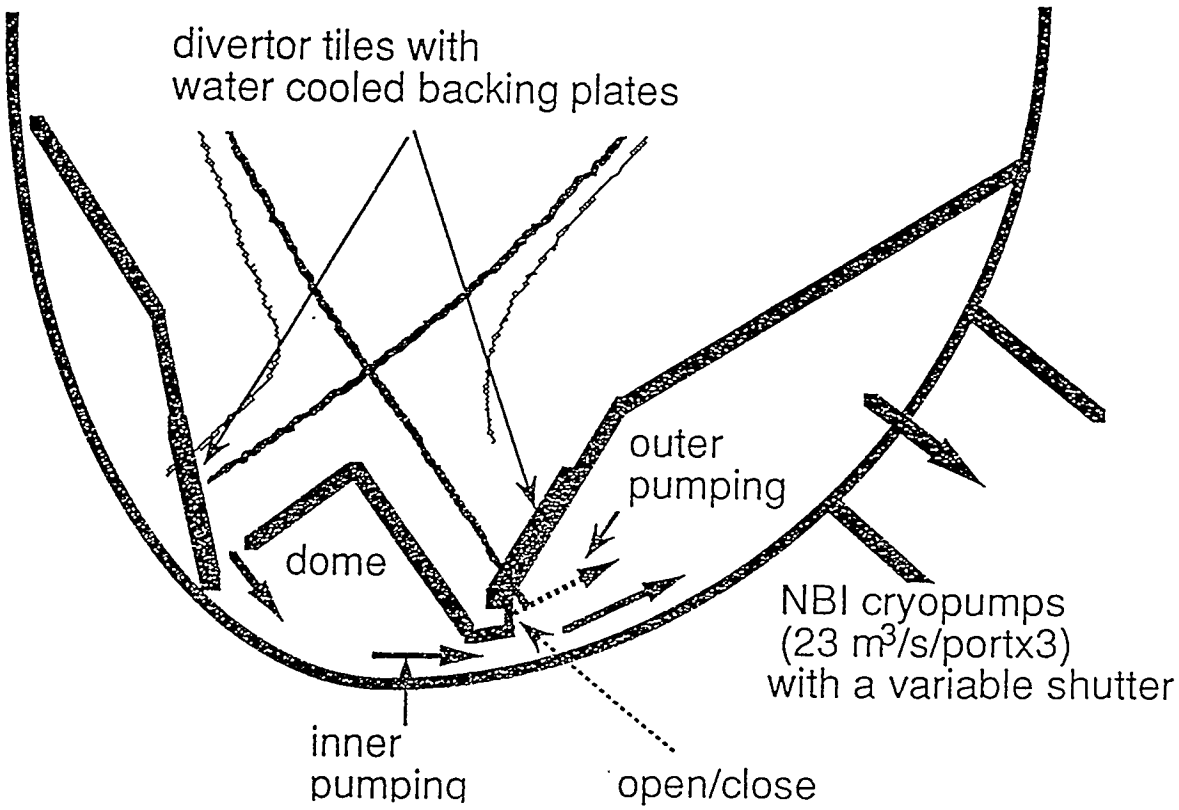

Discharge Parameters

1. Plasma size

   R=3.32, a=1.1,
   κ=1.4(1.2)-1.7, δ=0-0.2(0.4)
   ( )--> high triangularity coil configuration

2. Heating power

   positive ion based NBI
   perpendicular injection < 18 MW
   tangential injection = 10 MW
   negative ion based NBI
   tangential injection = 10 MW

3. Plasma current $\leqq$ 3 MA

4. Toroidal magnetic field $\leqq$ 4 T

5. Duration time of
   divertor configurations $\leqq$ 8 s for 3 MA

Designed Divertor Shape

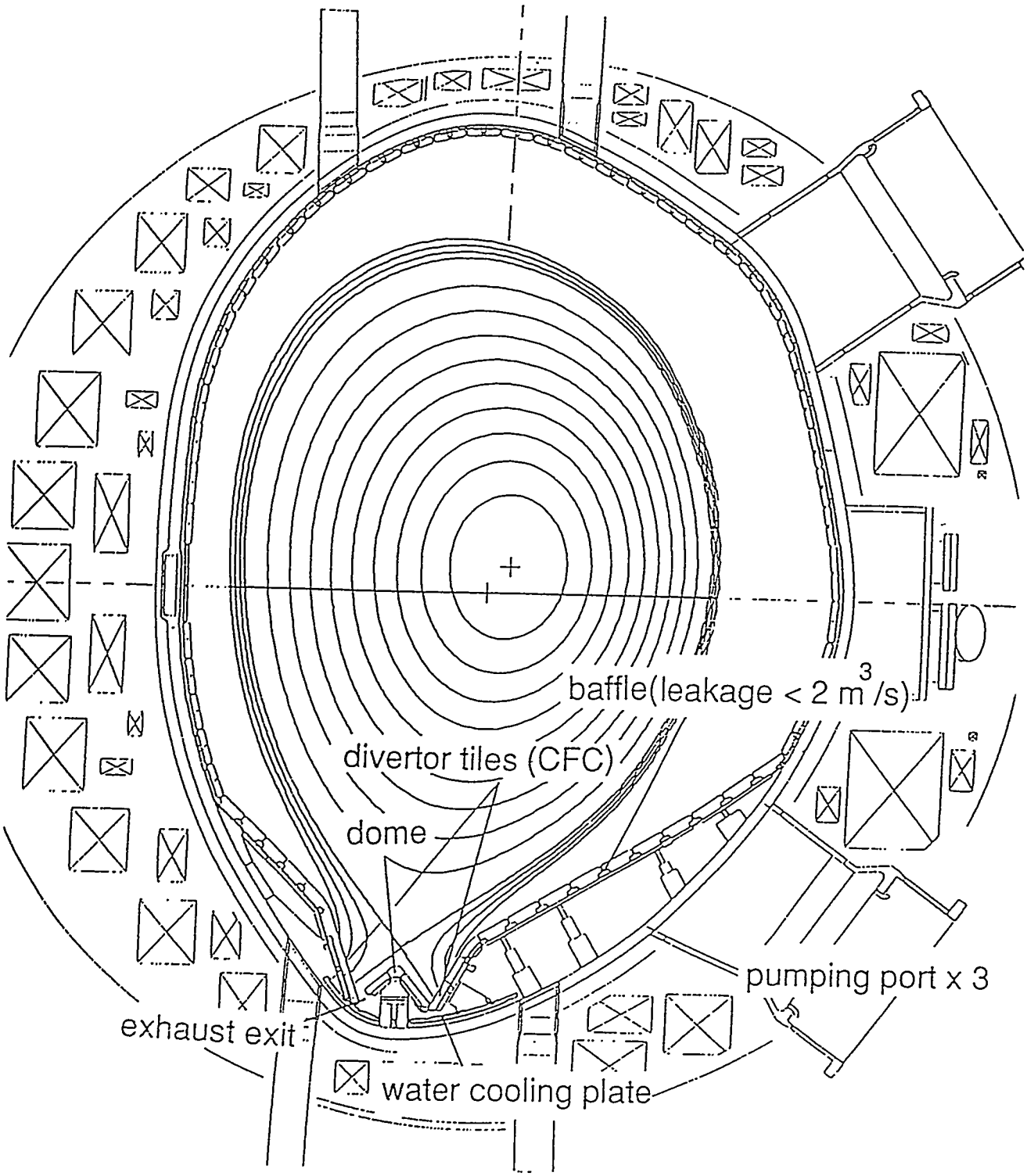

Schedule of Divertor Modification

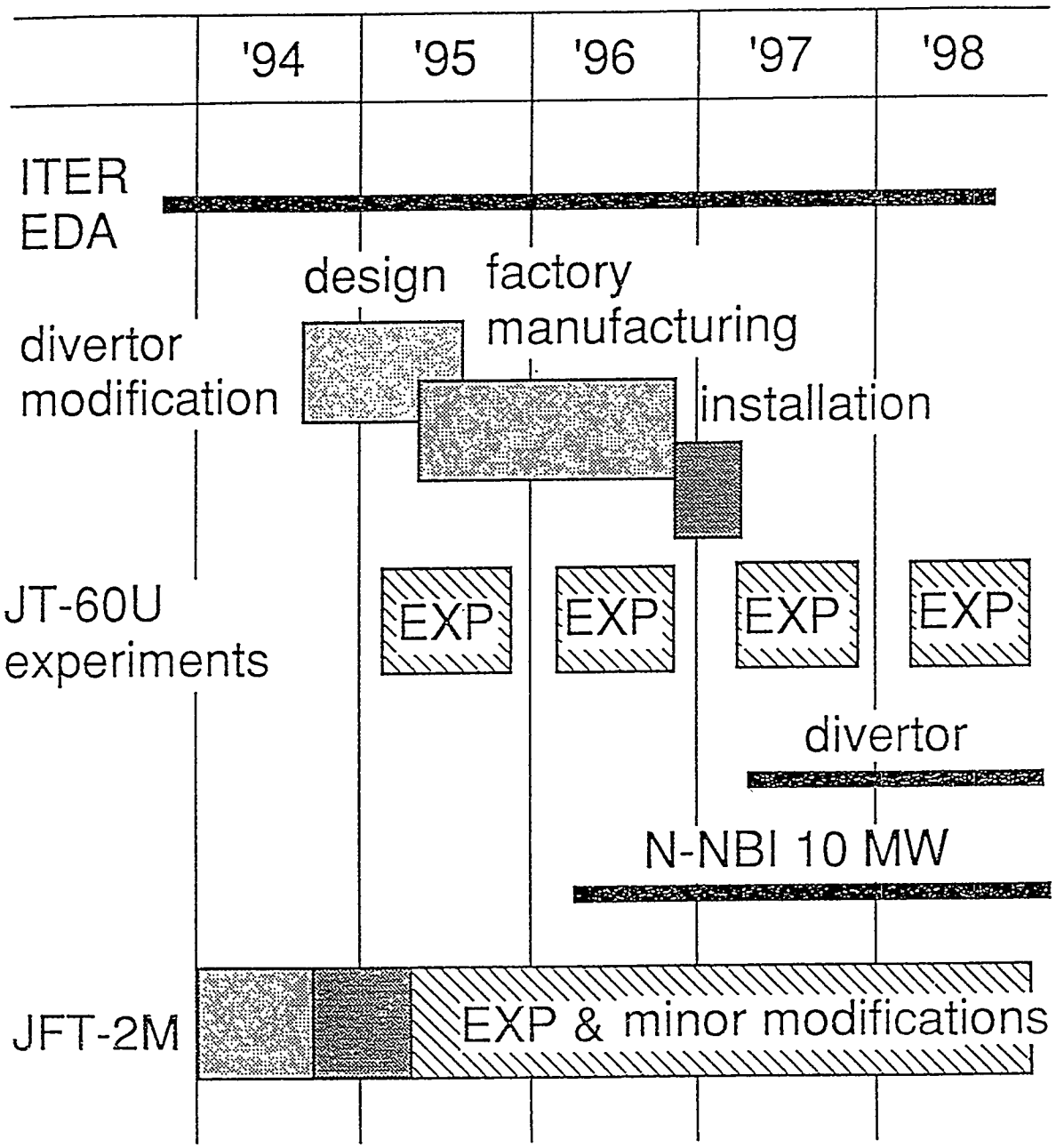

Summary

- Deuterated decaborane-based boronization has been successfully carried out on March 1995 using a mixed gas of He and D_2.

- Measurement of tritium retention has been made by scintillation counting of HTO in the collected water, results of which showed that 50% of tritium generated from July 1991 to October 1993 retained in the inner wall tiles (10% in divertor tiles and 40% in first wall tiles).

- JT-60U new divertor plan is presented.

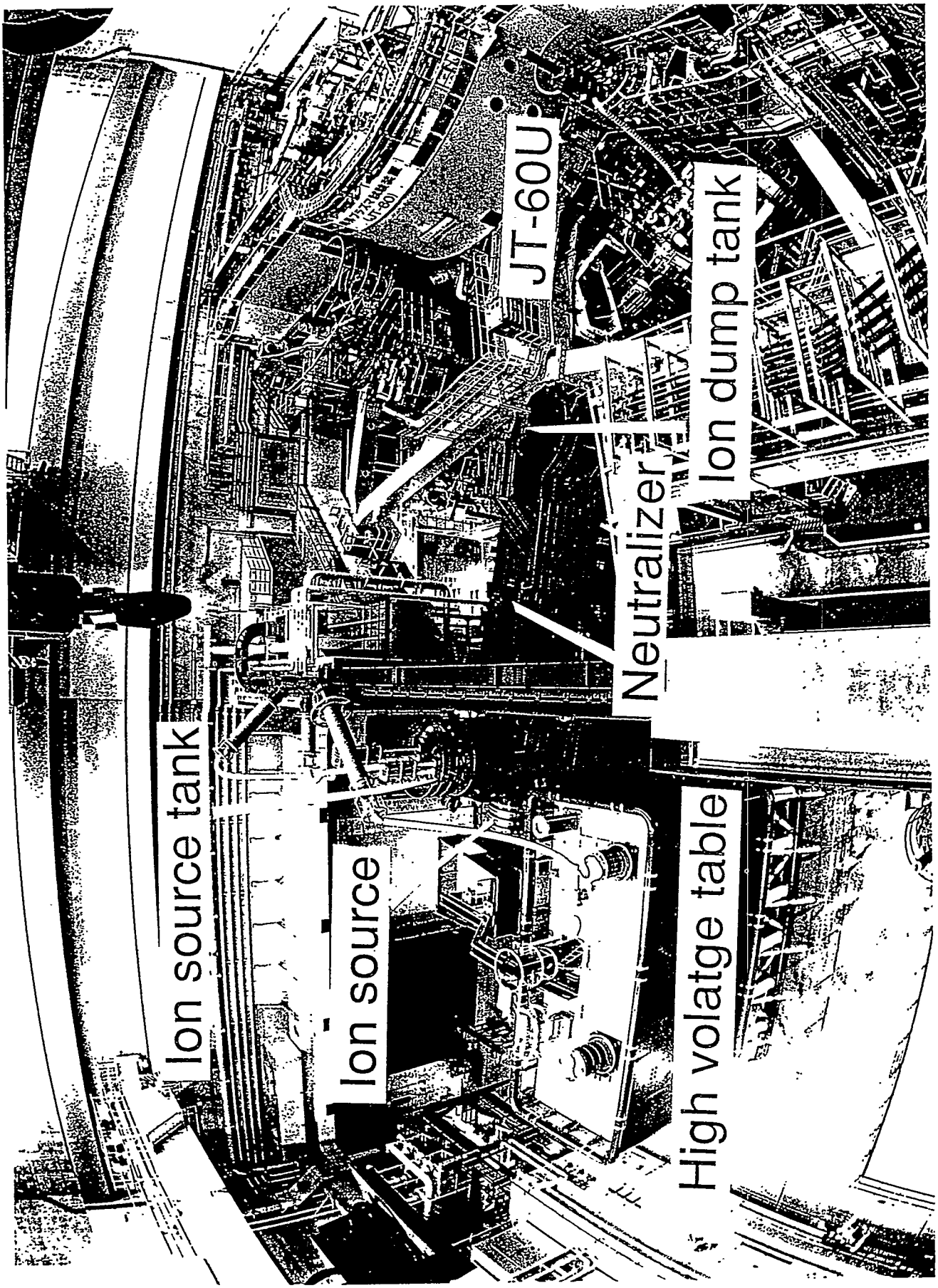
Ion source tank
Ion source
JT-60U
Neutralizer
Ion dump tank
High volatge table

Experience with the Tore Supra Phase III
Outboard Pump Limiter

by

Richard E. Nygren
Sandia National Laboratories

Tore Supra High Heat Flux Components

US Japan Workshop --- Colorado Springs CO, January 9-11, 1996

US-CEA Collaboration: Pumping and Particle Control

Sandia: Richard Nygren, Tom Lutz, Joel Miller, Ben Tafoya, Bob McGrath, Joe Koski, Jon Watkins

CE : Thierry Loarer, Jean Jacques Cordier, Dominique Guilhem, Philippe Chappuis, Jean-Yves Journeaux, Jacques Schlosser, Stephan Vartanian, Philippe Valenza, many others

ORNL: Peter Mioduszewski, John Hogan, Tanner Uckan, Chris Klepper, Steve Tobin (MFE Fellow, U. Mich.)

Sandia National Laboratories

1454.140/REN/052395

Brief Review of Some Tore Supra PFC Activities

- Future development of PFCs at Tore Supra
- Hot spot on Phase III Vertical Pump Limiter
- Phase III Outboard Pump Limiter Experience

  Design/Fabrication issues

  Operation/Monitoring/Safety issues

  Reference List
  - *publications*
  - *some being completed (3-5 papers)*
  - *special issue of Fusion Tech. with Tore Supra PFCs*

Sandia National Laboratories

1454.140/REN/052395

Locations of some PFCs on Tore Supra

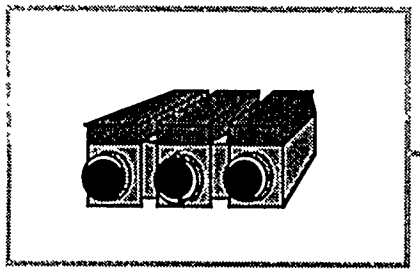

inner wall segment

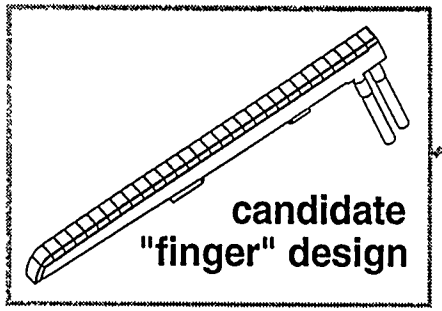

Phase IV bottom toroidal limiter (future option)

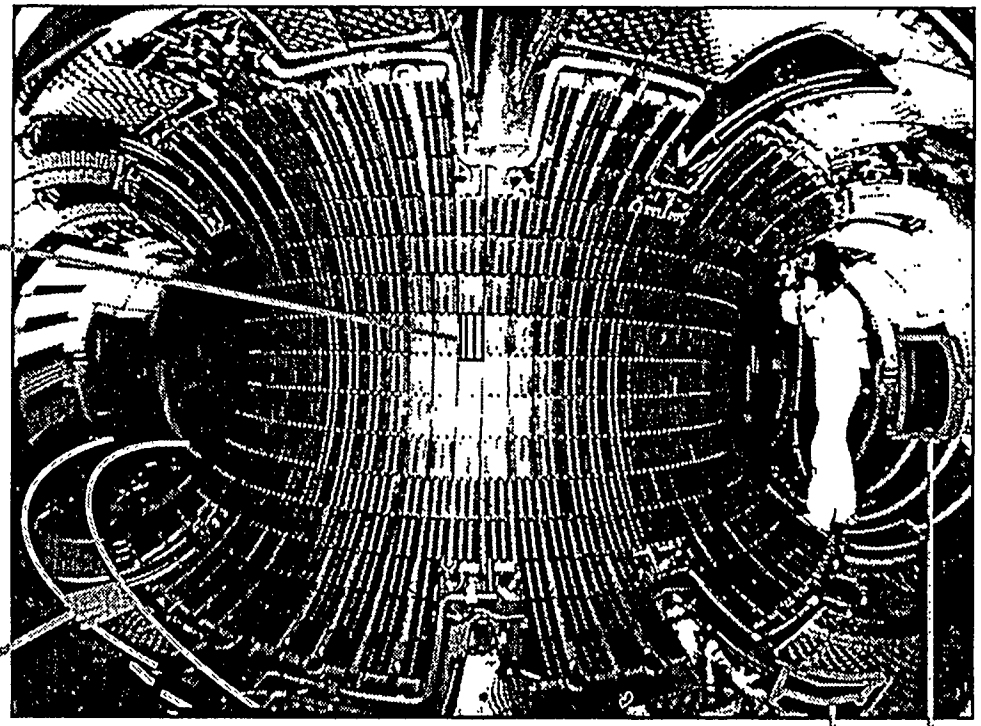

Midplane location, as for Outboard Pump Limiter, and bottom location for one Vertical Limiter are shown.

Sandia National Laboratories

1454.140/REN/091294

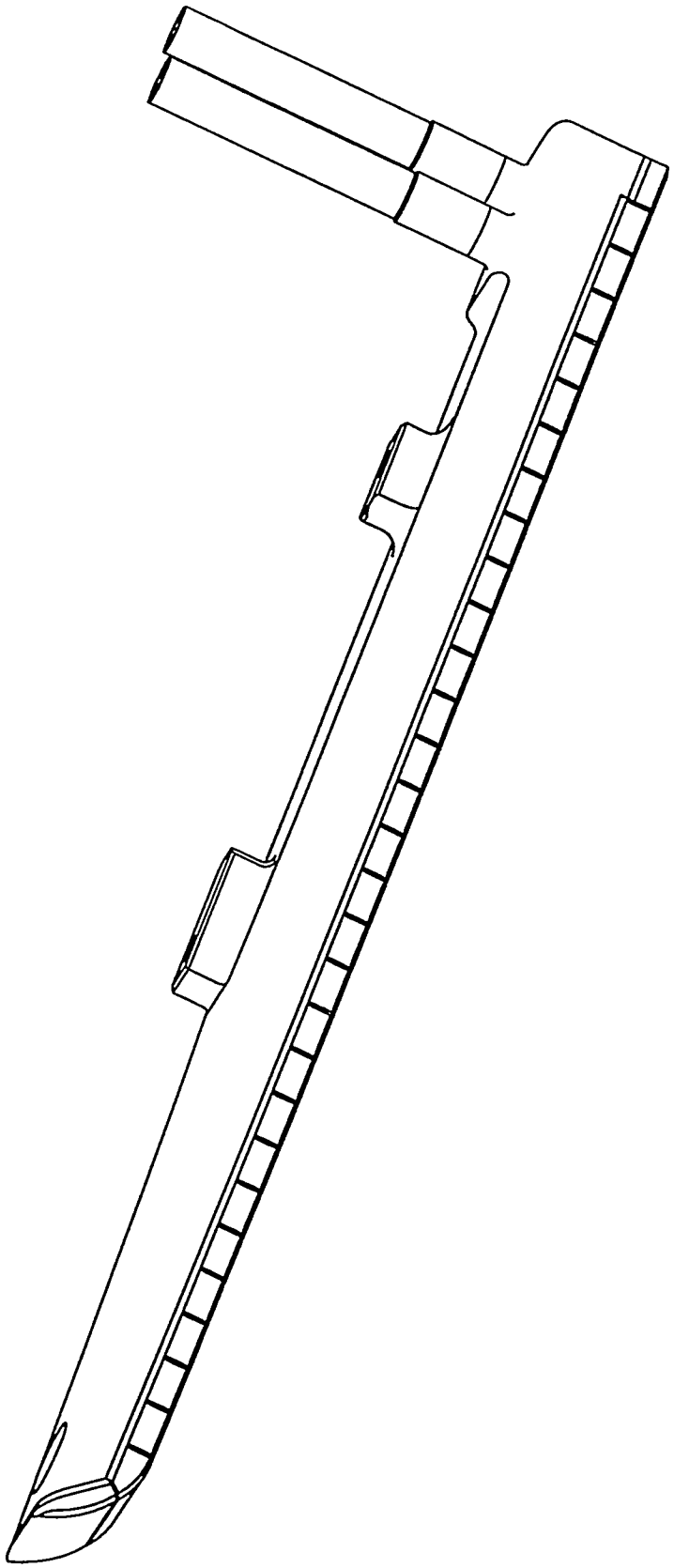

REN Observations: Future Tore Supra PFCs

- Physics mission requires increased power handling, but PFCs (inner wall, limiters, ergodic divertor) limit this.

- Interest in radiative layers and ergodic divertor --

  unproven physics solutions, experimental confirmation needed

- Interest in water-cooled PFCs, e.g. belt limiter --

  "proven" technology solution, technology development needed

Dilemma mirrors that of fusion community and ITER.

Tore Supra will continue to provide relevant experience in both physics and technology.

Sandia National Laboratories

1454.140/REN/052395

Tore Supra Phase III Vertical Limiter

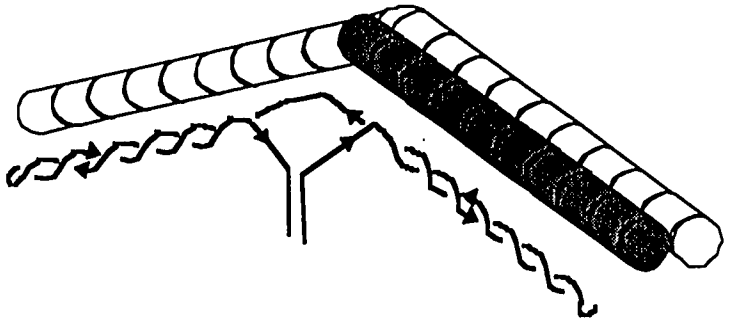

six locations bottom ports

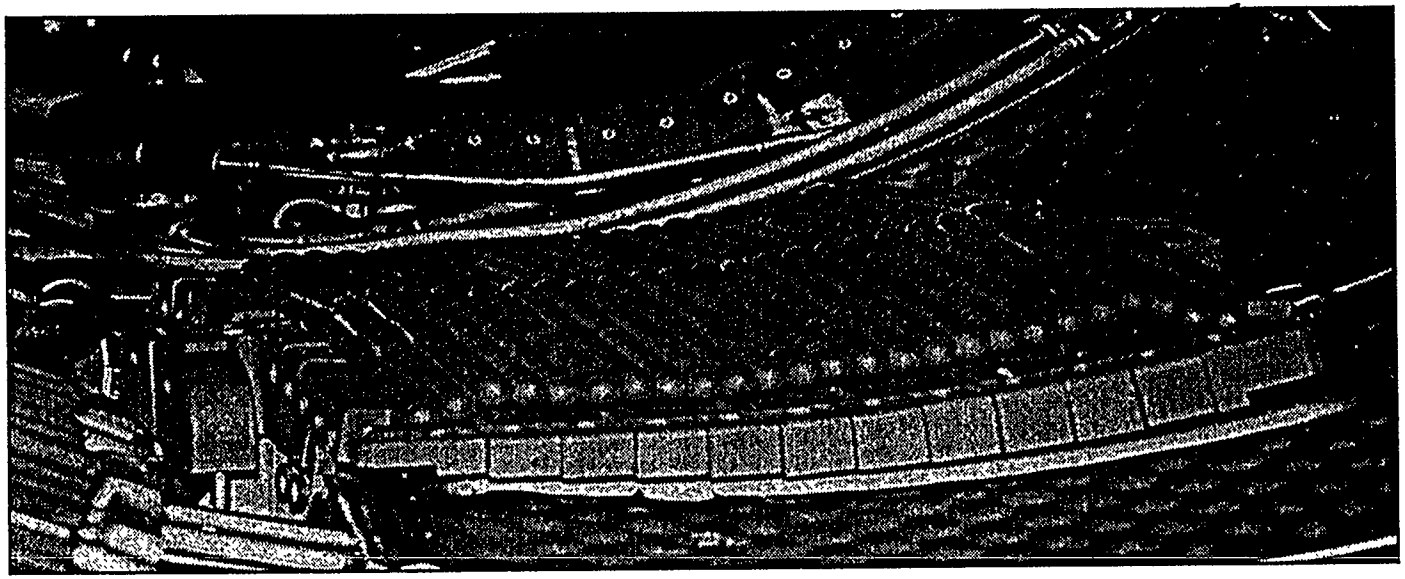

Sandia National Laboratories

1454.140/REN/091294

shot 5746: Hot Spot on Phase III Vertical Limiter

IR image at 6.4 s (right)

T history of 3 points (below)

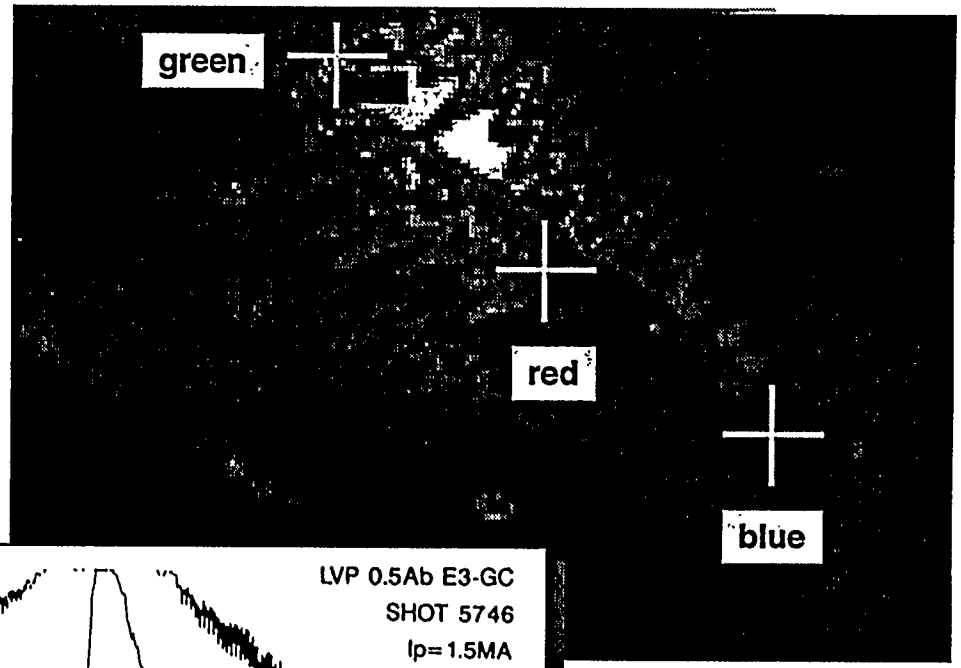

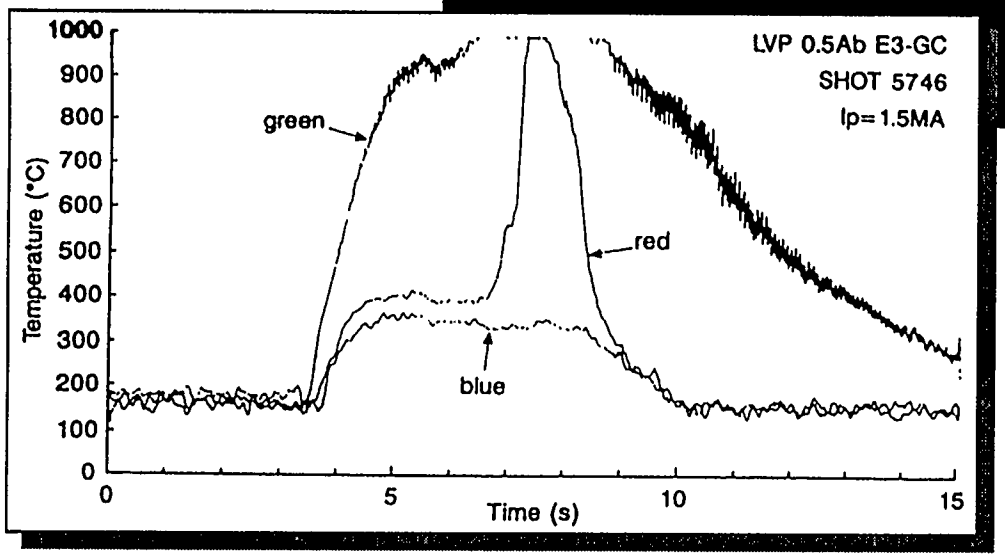

D. Guilhem et al., JNM 196-198 ('92) p759-765 (Monterey PSI)

Sandia National Laboratories

1454.140/REN/052395

"Super Brilliance" on Phase III Vertical Limiter

- Phenomenon poses a significant threat to actively cooled PFCs.
  Must we add another safety factor of 2-3 for future PFCs?
  Can we mitigate this effect?

- Event: hot spot associated with a sheath instability*at plasma edge;
  started on poorly bonded tile at crown of vertical limiter;
  expanded slowly to include neighboring, well bonded tile;
  seemed to stabilize, (escalations in T and C-II emission).
- Trigger: $T_{armor} > T_{threshold}$;
  flux of incoming carbon may be important;
  secondary electron emission may be important.

refs: Guilhem et al., "Actively cooled pump limiters and power scrape-off length measurements in Tore Supra," JNM 196-98 (1992) p759

Sandia National Laboratories

1454.140/REN/052395

"Super Brilliance" continued

Using conditions for runaway erosion (ala Brooks) and modifying variables, such as C sputtering and e^- emission, Hogan (ORNL) showed a restricted window of stable behavior (plot of surface temperature versus accelerating voltage). Instability results in a "runaway" in the yields of carbon, at least initially.

[ref: Hogan et al., EPS-95, Bournemouth]

Food for thought:

The initial "trigger" for super brilliance and carbon blooms may be similar. Temperature increases on non-actively-cooled PFCs led to runaway instabilities (C-blooms). In Tore Supra, excess heating due to the sheath instability was stabilized on a water-cooled PFC.

Cold electrons from secondary emission and stripping of sputtered C seem to be an important factor. These evidently depress the sheath potential and enhance the power conducted locally via electrons.

There is no reason in theory why this event cannot happen with metal armor under appropriate conditions.

Tore Supra Vented Limiter

concept: Franck-Condon dissociation near surface produces some neutrals which scatter back into vents.

Vented Limiter is used in port for Vertical Limiter.

Experiments performed on pumping and gas injection in the 1995 campaign.

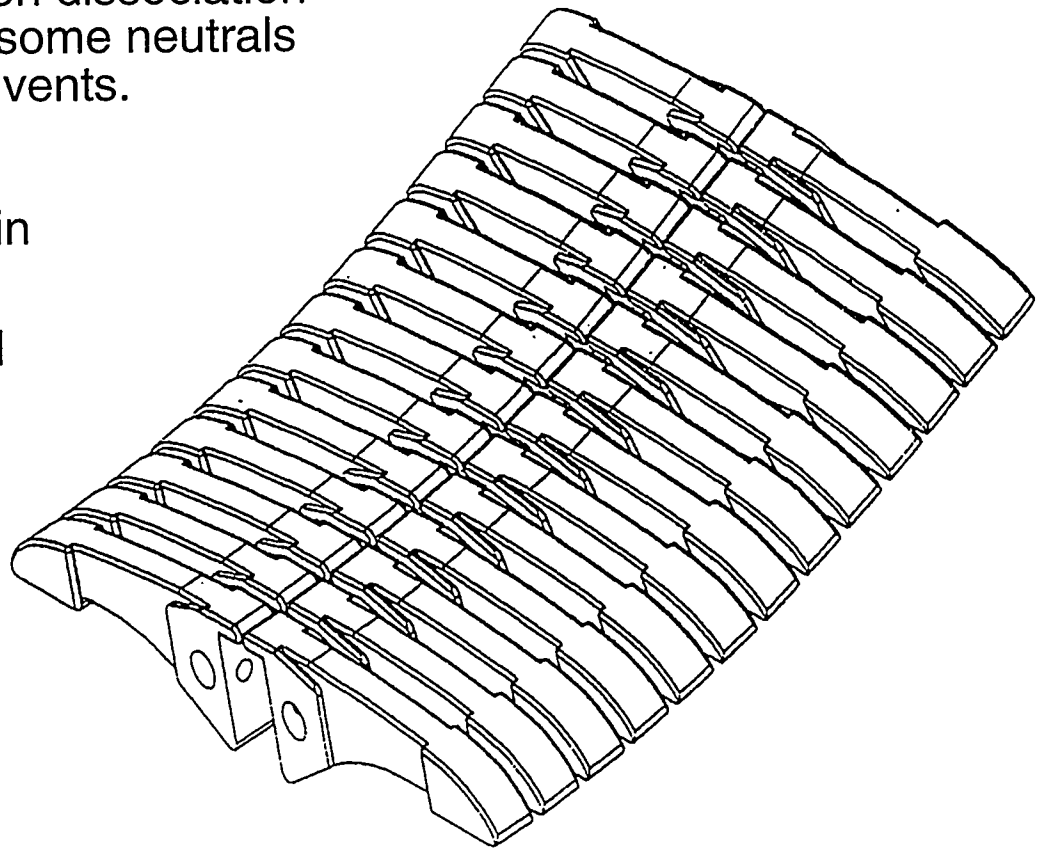

Sandia National Laboratories

1454.140/REN/052395

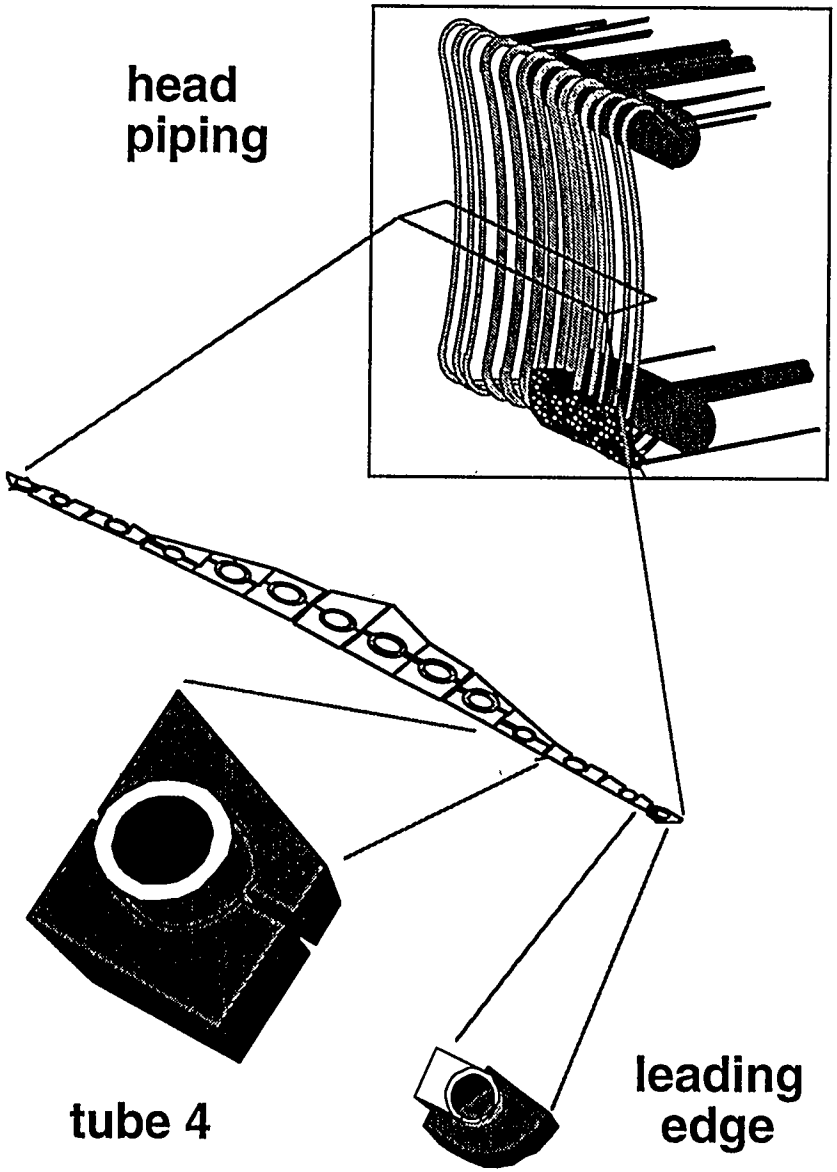

Tore Supra Phase III Outboard Pump Limiter

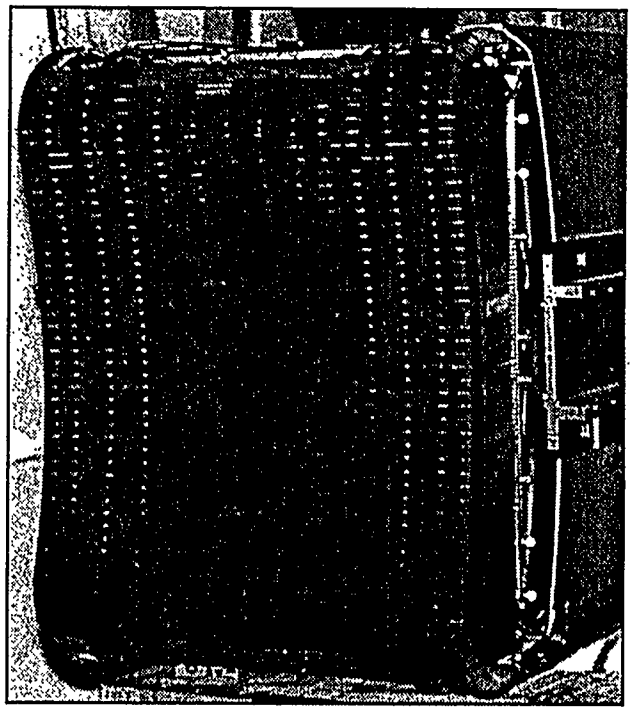

Sandia National Laboratories

1454.140/REN/091294

Results with Phase III OPL

Pumping Data

- 4 densities, ohmic shots, R & a constant
- 3 OPL positions (R_1,R_2,R_3), ohmic shots, a & n_e constant

Power Deposition

- up to ~0.8 MW
- detailed IR views of OPL (basis for "flaw map")
- dilemma of cracked leading edge tile
- runaway electron event - breach of electron side leading edge

Operational Systems

- redesigned and tested safety interlock system
- IR trigger system
- excellent calorimetry (user format developed)

Sandia National Laboratories

1454.140/REN/091294

Summary of Damage to Phase III OPL

1993: "Burnout" of leading edge tube resulted from coolant water to OPL shut off just before shot. *water leak*

1994: Hot spot was observed; experiment was restarted after review of thermal analysis of hot spot.

1994: Runaway electrons from disruption pierced leading edge tube; Phase III head was retired. *water leak*

Rebuilt Phase II head will be used in 1995.

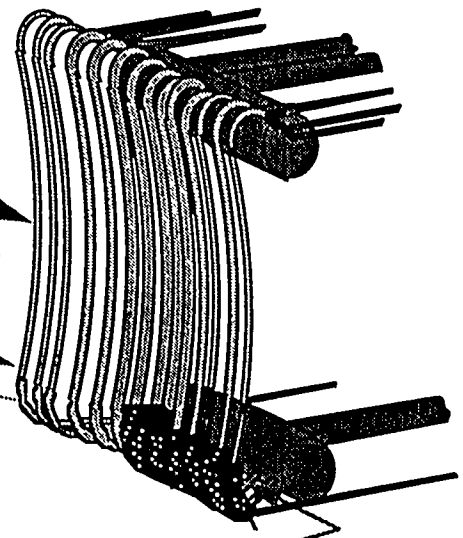

Sandia National Laboratories

1454.140/REN/091294

Cracked Tile Dilemma

July 12 last shot: "hot spot" temperature excursion seen with IR

July 13 first shot: obvious tile problem

Does observed hot spot imply greater chance of burnout?

Should OPL experiments proceed?

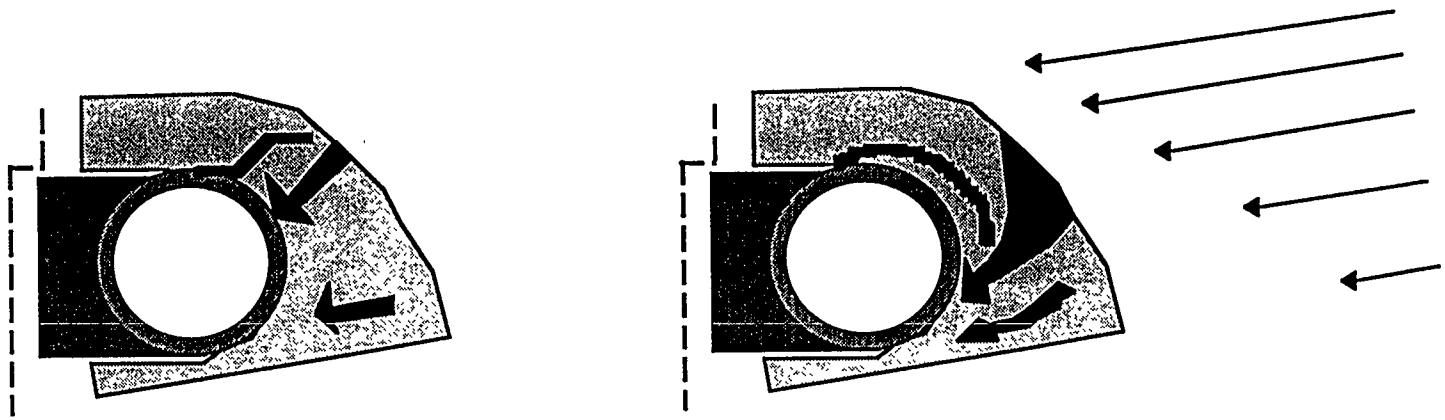

Sandia National Laboratories

1454.140/REN/091294

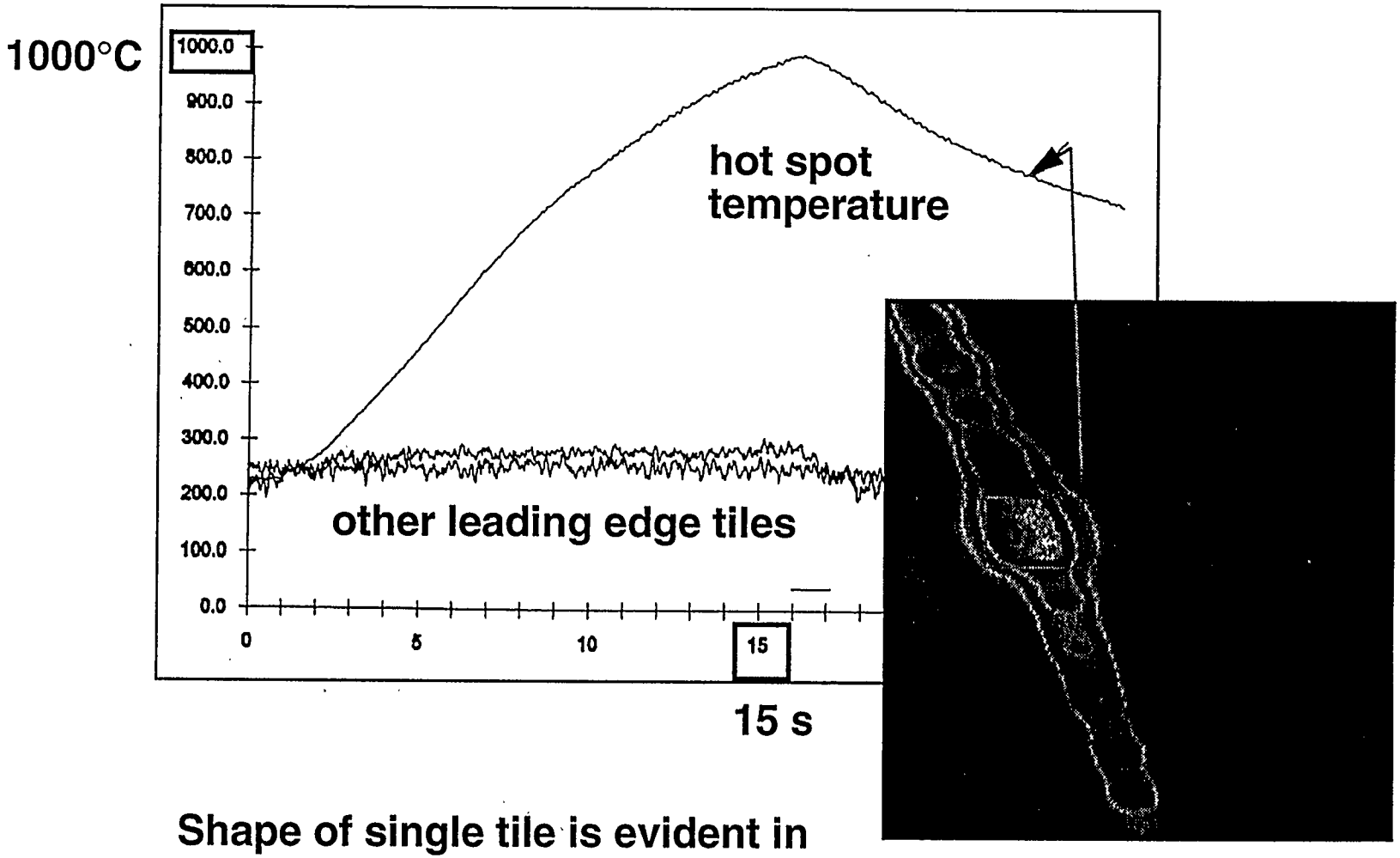

Shape of single tile is evident in IR view of hot spot, shot 14772 July 13.

Sandia National Laboratories

1454.140/REN/091294

Cracked Tile Dilemma

7/13: request for help
Sandia 2-D analysis

7/18: weekly Tore Supra meeting
- **analysis* presented**
- **decision to proceed**

7/19: continued operation

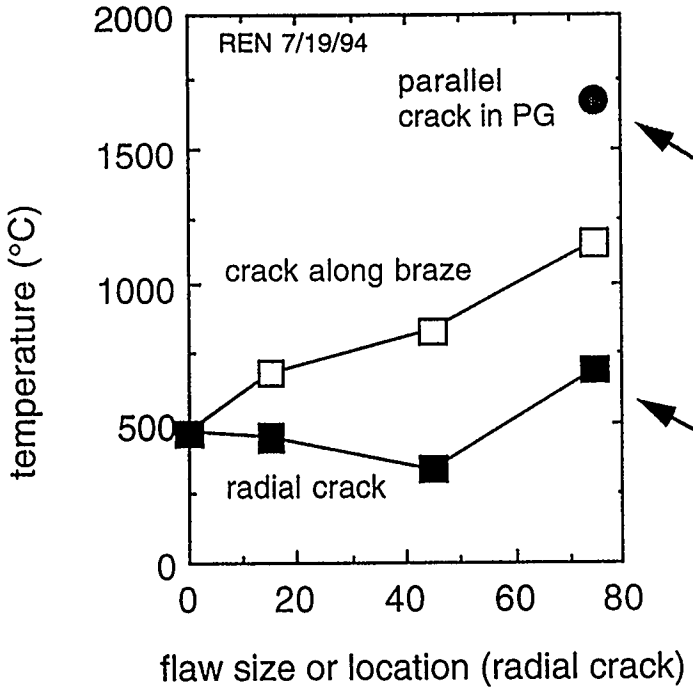

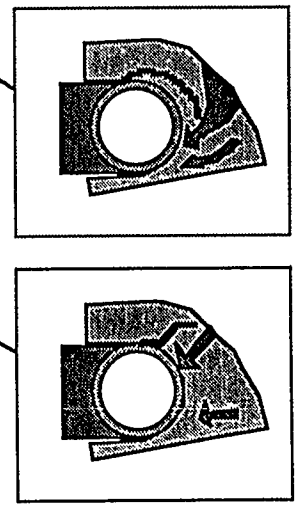

***A subsequent more detailed crack analysis by Mitteau (CE) was consistent with Sandia's preliminary evaluation.**

Sandia National Laboratories

1454.140/REN/091294

Runaway Electron Event

shot 18483: 1.5 MA I_p + 1.5 MW LH planned

- initial ramp up
- premature start-up of LH
- disruption resulted

- production of runaway electron "tail" observed in I_p
- neutron production observed at disruption time
- IR evidence of strikes on OPL face and leading edge

Sandia National Laboratories

1454.140/REN/091294

Shot 14843: Shot data and IR views

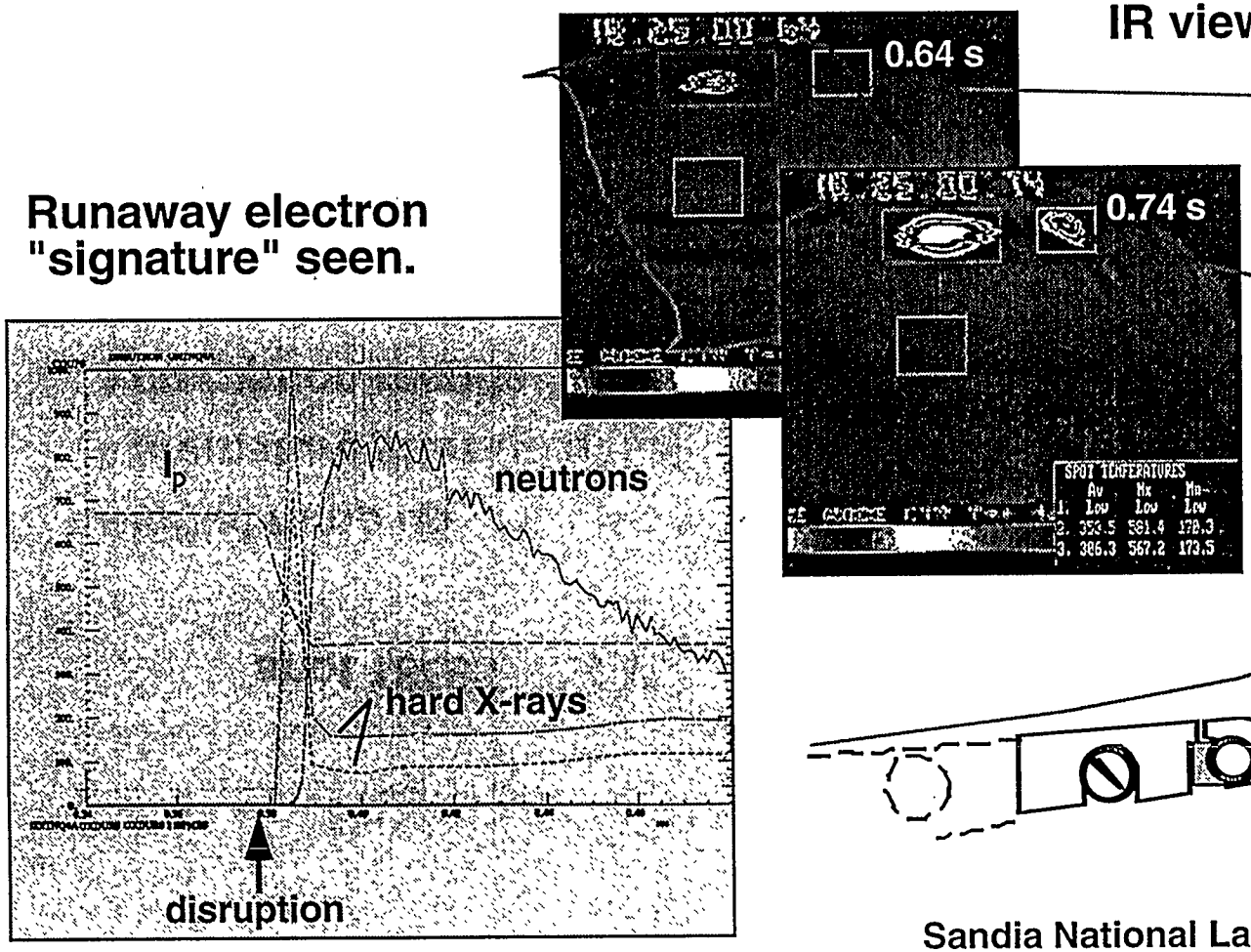

IR views (180° rot.)

Hot spot
bottom center

Second hot spot
e-side leading edge bottom

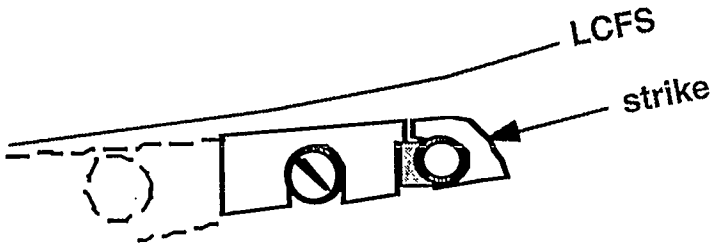

Sandia National Laboratories

1454.140/REN/091294

Runaway Event: Explanation by G. Martin, CE

A lateral X-point can be formed in Tore Supra with a relatively low current (~250 kA) of high energy (~100 keV) electrons.
[At outside midplane v_{Drift} ($\alpha\ \gamma_{rel.\ mass}$) cancels v_θ ($\alpha\ I_p$) e.]

Outside X-point, in each toroidal pass the rotational transform produces large outward step.

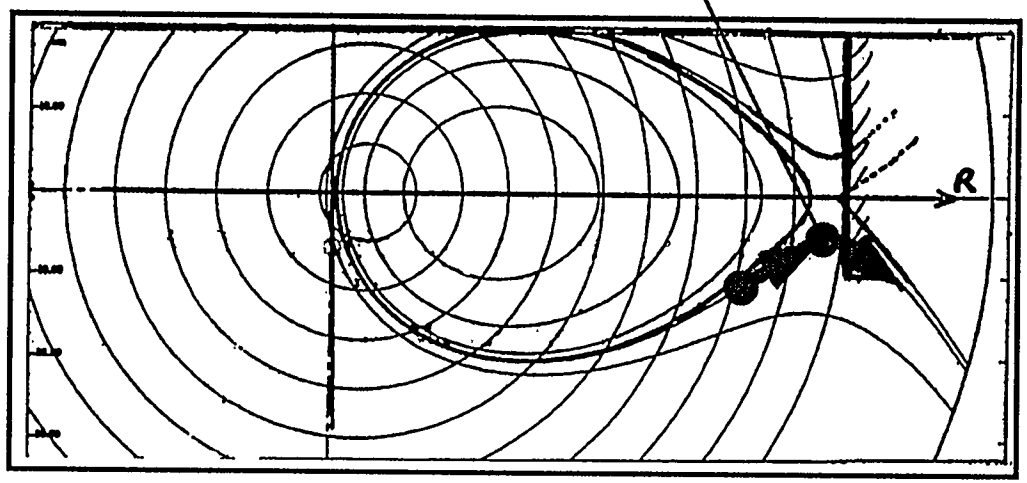

trajectory plot: flux surfaces for 240 kA runaway current
(G. Martin, CE, 1994 Tore Supra Executive Committee Meeting)

Sandia National Laboratories

1454.140/REN/091294

Lessons for the Future

ISFNT paper (Los Angeles 1994)

In-service monitoring of PFCs

Phase III OPL (~.3 m^2) had

- 34 thermocouples
- 10 flow meters
- infrared camera views.

If we do detect changes in real time (e.g., overheating), can we react?

How will PFCs in ITER and LHD be monitored?

Do we need new technology?

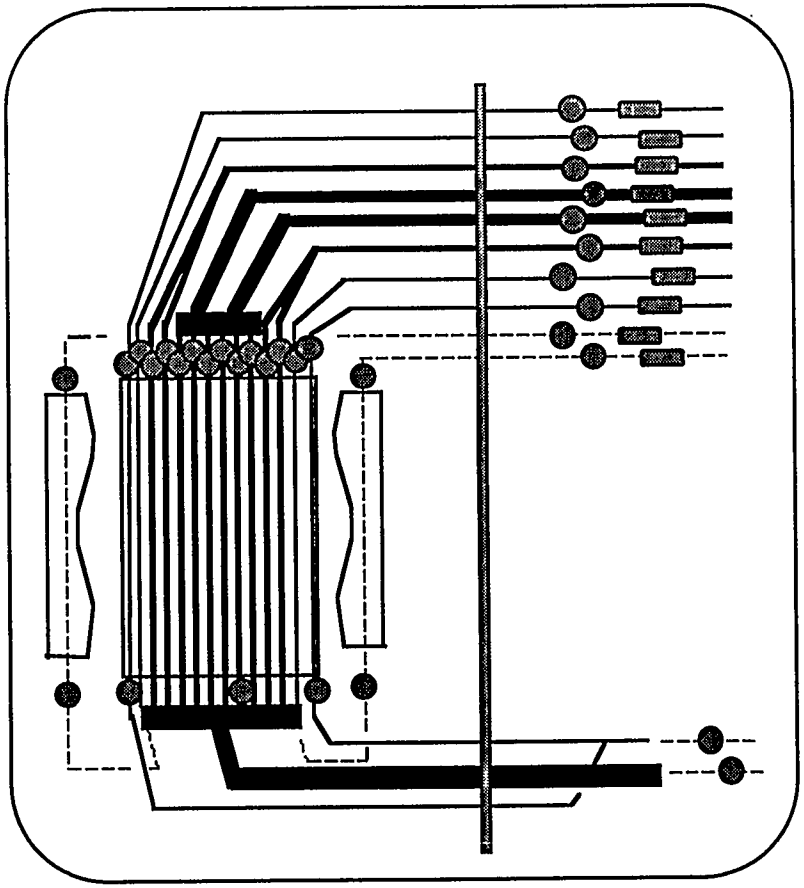

Phase III OPL piping layout

Sandia National Laboratories

1454.140/REN/091294

Lessons for the Future

ISFNT paper (Los Angeles 1994)

Quality Assurance

Design and R&D should confirm techniques and criteria for QA.

Thermal-hydraulics

Allowance for and analyses of joining flaws seems prudent.

Critical Heat Flux

Data is sparse one-side heating.

There is no universal model.

Correlations must be verified with tests.

How do we manage risks and safety margins for ITER and LHD?

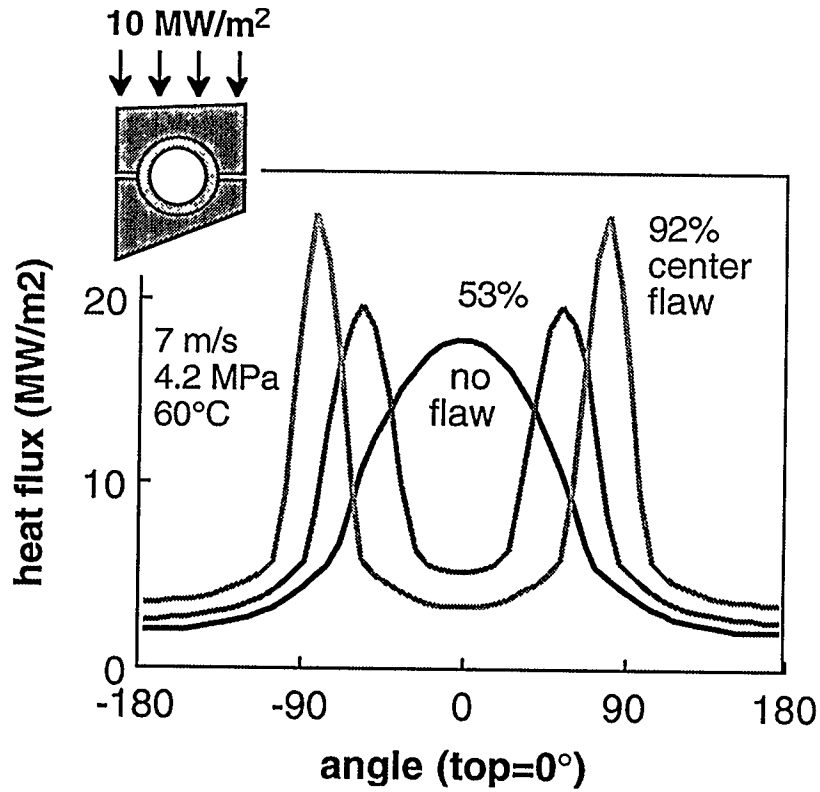

effect of flaw size on peak heat flux

Selected References on Tore Supra Actively Cooled Limiters

R. Nygren, T. Lutz, D. Walsh, G. Martin, T. Loarer and D. Guilhem, ""Runaway Electron Damage to the Tore Supra Phase III Outboard Pump Limiter" (96PSI abstract)

R. Nygren, T. Lutz), D. Guilhem and T. Loarer, "Operational Experience with the Tore Supra Phase III Outboard Pump Limiter" (96PSI abstract)

T. Lutz, R. Nygren, D. Guilhem and F. Moreau, "Results from Calorimetry on the Actively Cooled Outboard Pump Limiter in Tore Supra" (96PSI abstract)

Equipe Tore Supra, "Towards Long Pulse High Performance Discharges in Tore Supra: Experimental Knowledge and Technological Developments for Heat Exhaust," to be published in Fusion Technology

R. E. Nygren and J. D. Miller, "How Braze Flaws Affect the Thermal-hydraulic Performance of The Tore Supra Phase III Limiter" to be published in Fusion Technology

T. Uckan, ... R. Nygren, "Particle Exhaust of Helium Plasmas with Actively Cooled Outboard Pump Limiter on Tore Supra," 22nd EPS Conf. 1995, Bournemouth

D. Guilhem and Tore Supra Equipe, "Steady State Plasma Control for Long Pulse Operation with Actively Cooled Plasma Facing Components," 15th IAEA Int. Conf. on Plasma Physics and Controlled Nuclear Fusion Research, Madrid 1994

R. Nygren, T. Lutz, J. Miller, G. Dale and R. McGrath, "Assessing Braze Quality in the Actively Cooled Tore Supra Phase III Outboard Pump Limiter," Fusion Eng. and Design 29 Part C, p421, 1995 (ISFNT94)

R. Nygren, "High Quality Actively Cooled Plasma Facing Components for Fusion," Fusion Eng. and Design 29 Part B, p3, 1995 (ISFNT94)

R. Nygren, J. Koski, T. Lutz, R. McGrath, J. Miller, J. Watkins, D. Guilhem, P. Chappuis, J. Cordier and T. Loarer, "Steady-State Heat and Particle Removal with the Actively Cooled Phase III Outboard Pump Limiter in Tore Supra," JNM 220-222, p526-530, 1995 (1994PSI)

R. Nygren, C. Walker, T. Lutz and R. McGrath, "Brazing of the Tore Supra Outboard Pump Limiter," JNM 212-215, p1621-26, 1994 (ICRFM93)

R. Nygren, J. Miller and T. Lutz, "Initial Report on Calorimetry for the Tore Supra Outboard Pump Limiter, Sandia National Laboratories, SAND93-1922

D. Guilhem et al., "Actively Cooled Pump Limiters and Power Scrape-off Length Measurments in Tore Supra," J. Nucl. Mat., p196-98, 1992 (1992PSI)

J. Koski, "Thermal-hydraulic Considerations in the Surface Contouring of a Limiter Head for Tore Supra", 7th Proc. of Nuclear Thermo-hydraulics, ANS 1992 Winter Mtg. 1991 San Francisco ISBN 0-89448-170-3 p7

Session III

Developments of High Heat Flux Components

Chaired by: *K. Sato and R. Watson*

III.1	**Sato**/Akiba	PFC Developments at JAERI
III.2	**Watson**	Overview of US T-221 Activities
III.3	**Dombrowski**	Recent Results - Bonding S-65C Grade Be
III.4	**Dombrowski**	Fundamental Aspects of Be Oxidation
III.5	**Cadden**/Bonivert Odegard/Watson	Copper-Beryllium Joining Technology
III.6	**Ting**	Materials & Joining Development for PFCs
III.7	**Castro**/Stanek Elliott/Bartlett/Walsh Youchison/Watson	Structure, Properties and Performance of Plasma Sprayed Beryllium
III.8	**Davis**/Slattery Ulrickson	Development of Tungsten Structures for PFCs
III.9	**Youchison**	T-222 R&D Activities
III.10	**Driemeyer**	Divertor Mockup Design and Fabrication
III.11	**Yamazaki**	Manufacturing of ITER PFCs
III.12	**Sato**	The CHF Experiment in Screw Tube
III.13	**Zhan**	Thermal Hydraulic Analyses of ITER
III.14	**Marshall**	Post-CHF and LOFA Experiments at Sandia

JAERI

PFC Developments at JAERI

presented by K. Sato (JAERI)

M. Akiba, M. Araki, K. Nakamura, S. Suzuki
K. Sato, M. Dairaku, K. Yokoyama

- Overview of 1995
- Recent Topics

ITER Design Requirements

- Armour materials: Be, W, CFCs
  - Be 5 -10 mm thick, silver-free braze
  - W 5 - 20 mm thick, silver-free braze
  - CFC 30 - 40 mm thick, silver-free braze
- Steady surface heat load:
  5 MW/m², ~1000 s, 10,000 cycles
- Transient surface heat load: 15 MW/m², <10 s
- Incident critical heat flux of the cooling tube: 20 MW/m²
- Cooling conditions;
  - Inlet pressure: 4 MPa
  - Inlet temperature: 150 °C

R&D Target by the middle of 1996

- Select reference grade of Be, W, CFCs (+neutron irradiation)
- Select reference bonding technology (+neutron irradiation)
  - silver-free braze, thermal bond
  - thick armour tiles
- Define manufacturing method for the large scale components
- Develop CHF data at the ITER relevant flow conditions
- Define detailed design of the divertor components

R&D's above have started already, and results will come out in 1996.

R&D Progress in 1995

- Manufacturing and testing on the middle-scale mock-ups have successfully been performed.
  - Wing Edge Mock-up (JAERI design)
  - Vertical Target Mock-up (JAERI design)
- Silver-free joining technologies have developed extensively.
  - CVD-W coating on Cu alloy
  - CFC to Cu Functionally Graded Material
  - Thermal bond layer
- CHF data on new cooling tubes have intensively accumulated.
  - Screw Tube
- Neutron irradiation on duplex structures will start soon in JMTR. Operation of the Ooarai Hot-cell Electron Beam Irradiation System, OHBIS, has started.

Recent Topics

- Heating Tests on Edge part of Wing mock-up
- Heating Tests on Vertical target mock-up
- Heating Tests on CVD-W/Cu alloys mock-up

Heat Flux Profile on the Wing

- JAERI proposes the monobloc type Wing to reduce electro magnetic force during disruptic
- Peak heat flux will locate on th edge of the Wing

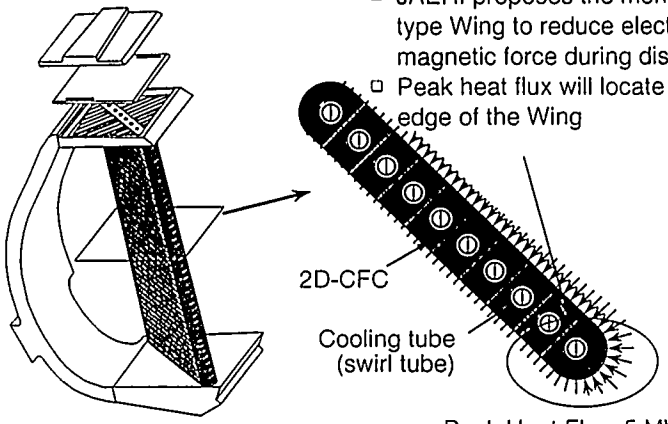

Peak Heat Flux, 5 MW/m²

Divertor Cassette

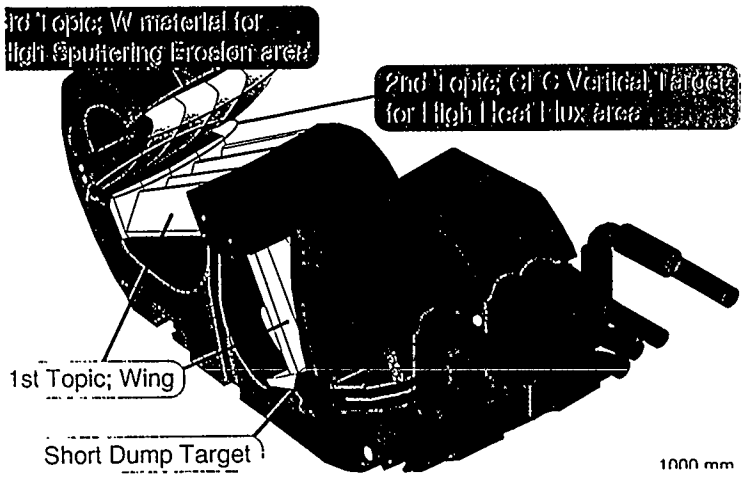

Wing Edge Mock-up

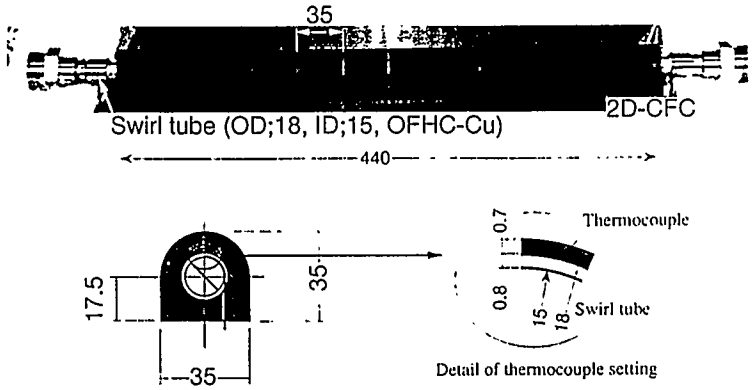

ased on numerical analyses, the heating condition of
5 MW/m², 1 s was selected to simulate the interface
·mperature at a steady heat flux of 10 MW/m²

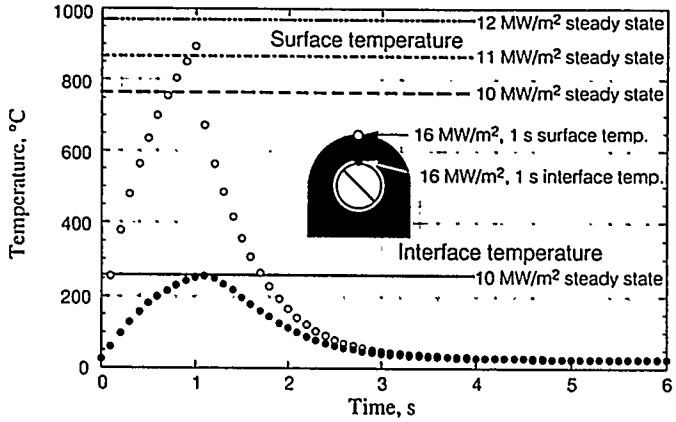

No degradation of thermal performance was observed

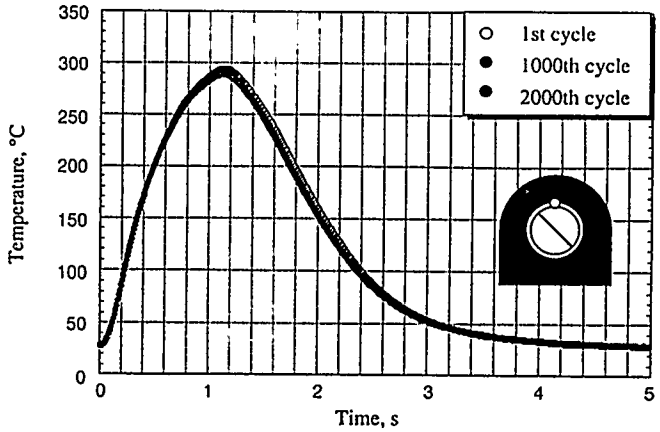

Vertical Target Mock-up (JAERI design)

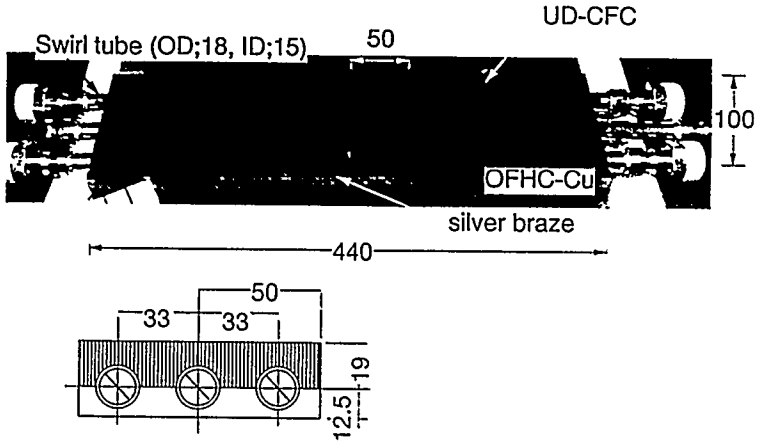

Testing Conditions of Vertical Target Mock-up

- Heating conditions;
  - Steady heat load
    - 5 MW/m², 1,000 - 10,000 s
    - 5 MW/m², 15 s
  - Transient heat load
    - 15 MW/m², 15 s
- Cooling conditions;
  - Axial flow velocity 4 m/s
  - Local pressure ~ 2.0 MPa
  - Inlet temperature ~ 30 °C

Surface temperature was almost constant during 10000 s

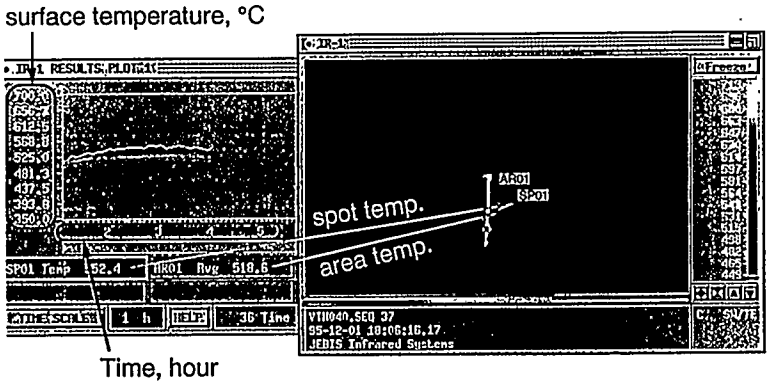

Tungsten material will be used in upper half of the Vertical Target where is high sputtering erosion area.

- The disruption erosion of CVD-W was two times less than that of powder sintered W.
- As one of the silver free bonding techniques, JAERI propoese CVD-W coated on Cu alloy divertor for high sputtering erosion area.

Heating Tests of Vertical Target Mock-up

- Results
  - The mock-up successfully endured a heat flux of 5 MW/m^2, 15 s for more than 10,000 thermal cycles.
  - No degradation of thermal performance was observed at 15 MW/m^2 for 15 s which is ITER slow transient condition
  - Surface temperature was almost constant during 10,000 s which is 10 times longer than ITER requirement.
- Future Plan
  - Large scale mock-up will be fabricated for VT application.

CVD-W/Cu alloy Mock-ups

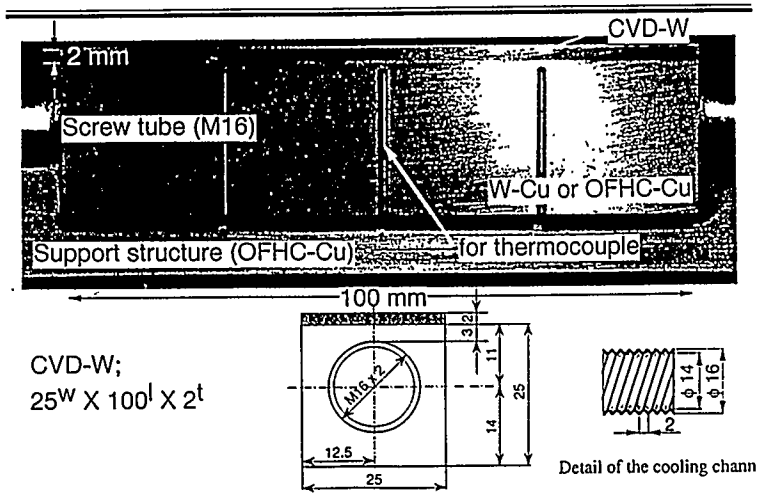

Testing condition on CVD-W/Cu alloy mock-up

- Thermal Cycling Test
  - Heating conditions; 15 MW/m^2, 0.3 s (= 5 MW/m^2, steady state)
    1,000 cycles
  - Cooling conditions;
    - Axial flow velocity 4 m/s
    - Pressure 1.0 MPa

- Result

  No degradation of thermal performance was found after 1,000 cycles.

Summary

	ITER requirement	JAERI achieved	
Normal Operation			
Surface heat flux	5 MW/m^2,	5 MW/m^2	5 MW/m^2
Duration	1,000 s	10,000 s	15 s
Cycles	10,000	1	10,000
Off-normal events			
Surface heat flux, duration	15 MW/m^2, <10 s	15 MW/m^2, 15 s	
Cooling condition			
Velocity	≤ (10 m/s)	4 m/s	
Pressure	4 MPa	~ 2.0 MPa	
Inlet temperature	150 °C	RT	

US-Japan Workshop, Q219, on High Heat Flux Components for Plasma Surface Interactions for Next Fusion Devices
Jan. 9-11, 1996, Colorado Springs, CO.

Overview of US T-221 Activities

Robert D. Watson
Task Leader

Sandia National Laboratories

The US Home Team is working on 4 of the 6 Sub-Tasks.

221.1	Be Properties	2100 IUA
221.2	W Properties	500 IUA
221.3	CFC Properties	0 IUA
221.4	Be/Cu Joining	1100 IUA
221.5	W/Cu Joining	500 IUA
221.6	CFC/Cu Joining	0 IUA

Total 4200 IUA

Sandia National Laboratories

T-221 Schedule

- Select reference grade of Be, W — June '96
- Select reference joining methods — June '96
- Mechanical tests, unirradiated Be,W — Sept. '96
- Complete neutron irradiations Be — Dec. '96
- Post-irradiation tests, e-beam tests — Dec. '97

Sandia National Laboratories

Many US institutions contribute to T-221 activities.

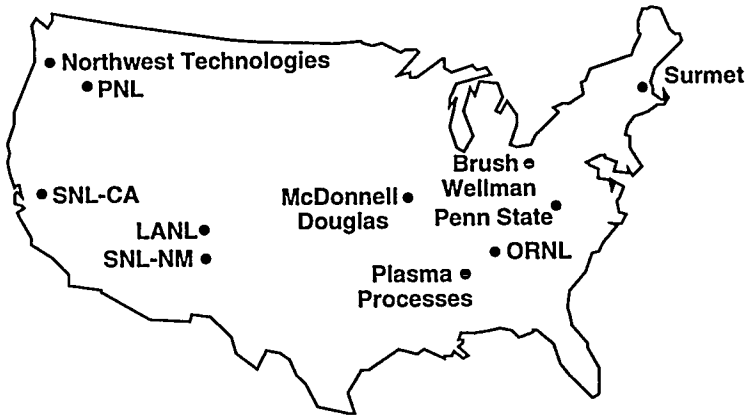

Sandia National Laboratories

T-221 has 7 major deliverables.

1. Select best grade of Be and W.
2. Measure thermal and mechanical properties of Be and W.
3. Develop silverless Be/Cu and W/Cu joints.
4. Quantify thermal fatigue reliability of Be/Cu and W/Cu joints up to 10,000 HHF cycles *(small-scale e-beam mockups).*
5. Determine effects of neutron irradiation and hydrogen on both bulk and joint properties.
6. Evaluate concept of the beryllium, tungsten "brush".
7. Evaluate composites of tungsten + Mg or Li .

Mechanical testing of unirradiated beryllium will start soon (Ben Odegard, SNL-CA).

- S-65C beryllium *(ITER reference grade)*
- Tensile stress/strain tests
- Compressive stress/strain tests *(@ Rocky Flats)*
- Isothermal fatigue tests
- RT, 100, 200, 300, 400, and 500 C

Properties of vacuum plasma sprayed beryllium have improved dramatically (Rich Castro, LANL).

- 98% dense as-sprayed coating
- Recrystallized, elongated grain structure
- Thermal conductivity = 95% of theoretical
- Improved adhesion from transferred arc cleaning
- *Key question is what copper substrate temperature to use during spraying.*

E-beam thermal fatigue tests of unirradiated Be are encouraging (Dennis Youchison, SNL).

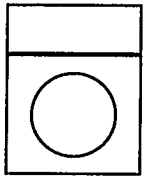

- 5 mm thick Russian TGP-56 beryllium, diffusion bonded to water-cooled copper heat sink.
- No evidence of bulk or surface fatigue cracking after 9200 steady-state thermal cycles at 5 MW/m2 (Be/Cu joint failed at 9200 cycles).

Initial Results of Laser Consolidated Vacuum Plasma Sprayed Be - CO_2 Laser

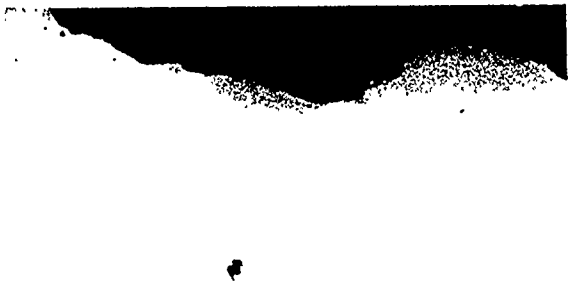

- Photomicrograph showing high density achieved after laser treating, 100x.

- Photomicrograph showing the same region as above, but polarized light was used to reveal the microstructure of the consolidated region, 100x.

Initial Results of Laser Consolidated Vacuum Plasma Sprayed Be - YAG Laser

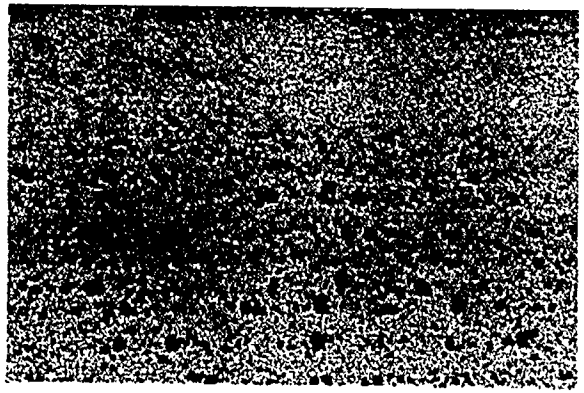

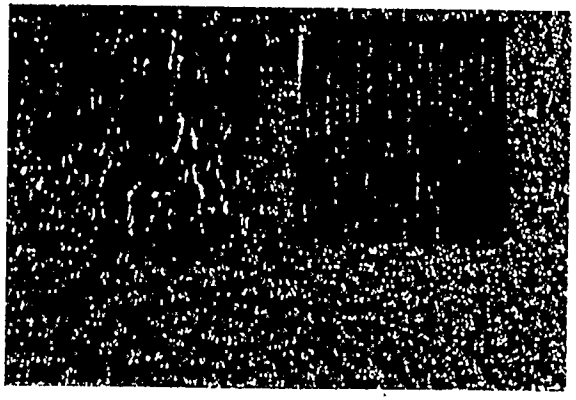

- Improvement in density from 94% as-sprayed (bottom) to 98% after YAG laser consolidation (top), 20x.
- Photograph contrasting the difference between the as-sprayed surface and two YAG laser consolidated patches.

"Laser Processing of Thermal Sprayed Be PFCs"

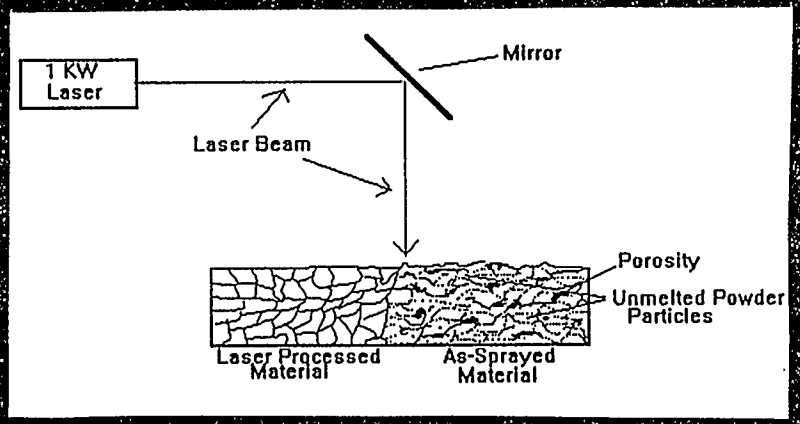

New DOE/PPI/LLNL/LANL/ORNL/SNL STTR Phase I

Objective: demo improved Be by laser processing

IPS Be @ ORNL & VPS Be @ LANL

Laser consolidate @ LLNL (Dr. Hanafee)

Neutron irradiation of beryllium is progressing well. (Lance Snead, ORNL).

- ORNL has irradiated 4 grades of Be in HFIR to 1 dpa at 150 and 300 °C.
  - Brush Wellman S-65-C
  - LANL plasma sprayed *(non-optimized)*
  - Max Planck zone-refined
  - KBI "P-0" high purity
- Post-Irradiation Examination (PIE) will include:
  - thermal conductivity *(no change)*
  - swelling *(none)*
  - hardness
  - elastic modulus
  - tritium rentention (@ TPE)

RDW-9 Watson US-Japan Colorado Springs-96

Sandia National Laboratories

Future plans for neutron irradiation of beryllium (ORNL):

- ORNL will irradiate 2 grades in HFIR at 250 °C and 500 °C to 0.1, 0.5, and 1 dpa:
  - Brush Wellman S-65C
  - KBI "P-0" high purity
- Post-Irradiation Examination (PIE) will include:
  - Strength
  - Elongation
  - TEM (also Max Planck zone refined Be)

RDW-10 Watson US-Japan Colorado Springs-96

Sandia National Laboratories

The US has recently supplied 2 types of Be/Cu joints to Russia for neutron irradiation (Dan Edwards, PNL).

- Explosion bonded
- Electroplated

- They will be irradiated in RBT-10 in Dimitrovgrad at 120 and 300 °C to a level of 0.2 dpa.
- Objective is to study growth of Be/Cu intermetallic phases during n-irradiation (if any).

RDW-11 Watson US-Japan Colorado Springs-96

Sandia National Laboratories

Joining Strategy

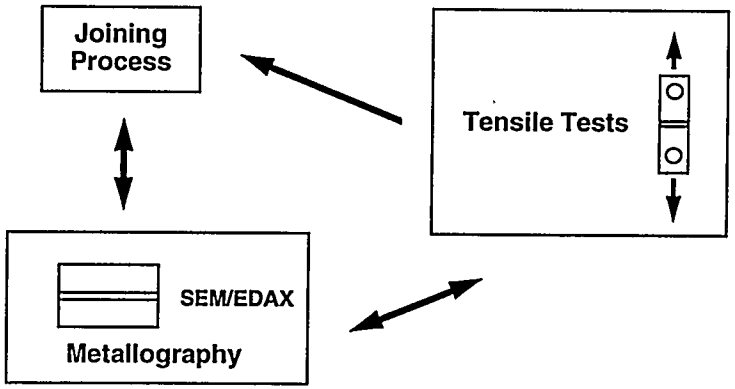

RDW-12 Watson US-Japan Colorado Springs-96

Sandia National Laboratories

Joining Strategy, cont'd

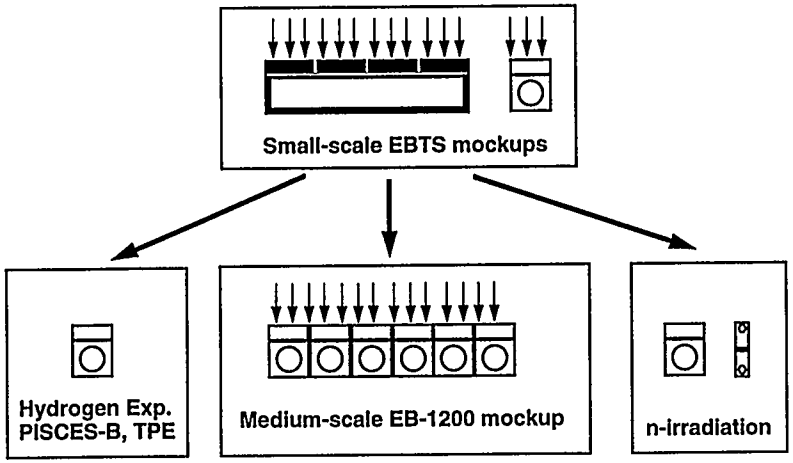

RDW-13 Watson US-Japan Colorado Springs-96

Sandia National Laboratories

Joining Strategy, cont'd

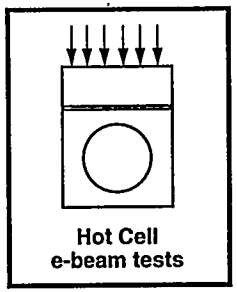

(JUDITH, OHBIS)

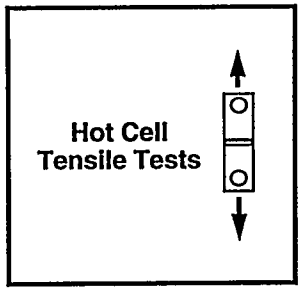

RDW-14 Watson US-Japan Colorado Springs-96

Sandia National Laboratories

Joining beryllium to copper alloys is a challenging task.

- Beryllium reacts with copper at elevated temperatures to form brittle intermetallic compounds (BeCu, Be2Cu).
- Al, Ge, Si, Ag, Zn are the only elements which do not form intermetallic phases with beryllium.
- Zinc has too high a vapor pressure.
- Silver transmutates to cadmium, and is high activation.
- Al, Ge, and Si are acceptable elements.
- BeO is very stable, and difficult to wet with brazes.

RDW-15 Watson US-Japan Colorado Springs-96

Sandia National Laboratories

Our goal is to meet or exceed the Be/Cu joining process developed by JET for their actively-cooled divertor without using silver or gold.

<u>JET "Silver Standard"</u>

- Induction brazed with InCuSil-ABA.

  59% Ag, 27% Cu, 13% In, 1.25% Ti
  solidus = 605 C, liquidus = 715 C

- Shear strengths = 220-250 MPa.
- Be tiles brazed to CuCrZr hypervapotrons fail "explosively" at heat fluxes 18-20 MW/m2 in the brazed joint.

RDW-16 Watson US-Japan Colorado Springs-96

Sandia National Laboratories

We tried brazing with aluminum-12% silicon eutectic. (Chuck Cadden, SNL-CA).

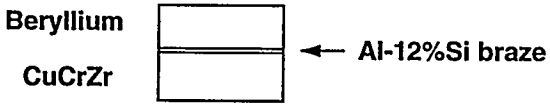

Intermetallic phases resulted in low fracture strength.

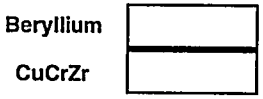

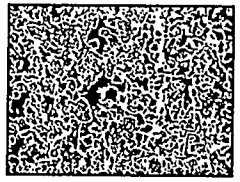

Fracture Stress = 42 MPa

- Braze condition was 675°C for 5 minutes *in vacuo.*
- A continuous film of intermetallic phase is seen on the fracture surface. Fracture was in the Be_2Cu phase.

Explosion bonding Be to Cu was tried (Don Butler, NTI).

- Appears to be an excellent mechanical joint.
- No intermetallics can be seen.
- Some vertical cracks in the beryllium.

Electroplated copper on beryllium gives a strong joint. (Bill Bonivert, SNL-CA)

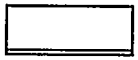

- Copper cyanide solution.
- High strength, > 300 MPa (ring shear test).
- 100 % joint efficiency (failure not at the bondline).
- No intermetallics (room temperature process).
- Will confirm strength with tensile test coupons.
- *Formation of BeCu intermetallics during operation?*

We used HIP to diffusion bond electroplated copper to CuNiBe (Hycon) copper alloy. (SNL-CA & Kevin Slattery, MDA).

CuNiBe
Electoplated Copper
CuNiBe

Hot Isostatic Pressing

- 450 °C
- 180 minutes
- 105 MPa pressure
- 320 grit roughening

Tensile strength = 340 MPa

We will combine electroplating and HIPing. (SNL, MDA, BWI)

Beryllium
EP Copper
CuNiBe

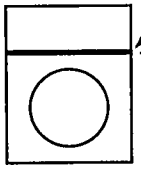

Electroplate copper on Be (step #1)

HIP bond Cu to Cu 450 C (step #2)

- Low-temperature process should prevent intermetallics.
- HIPing will improve properties of electroplated layer.

We will combine electroplating and HIPing with a diffusion barrier coating. (SNL, MDA, BWI, Suri Sastri, Surmet)

Beryllium
DBC
EP Copper
CuNiBe

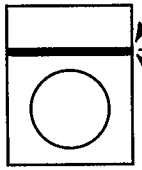

PVD diffusion barrier coating (Step #1)

Electroplate copper on Be (step #2)

HIP bond Cu to Cu 450 C (step #3)

- Low-temperature process should prevent intermetallics.
- HIPing will improve properties of electroplated layer.

We will combine explosion bonding with brazing. (SNL, NTI, MDA, Surmet or LANL)

Beryllium
Aluminum
Al-12Si
Aluminum
Titanium
CuCrZr

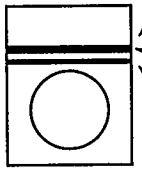

PVD aluminum coating on Be (Step #2)

Braze Al to Al with Al-12%Si (step #3)

Explosion bond 1100 Al with titanium diffusion barrier to CuCrZr (step #1)

- Multi-step process eliminates intermetallics.
- Aluminum will be acid etched or coated with silicon to promote good wetting by Al-12Si braze alloy.

We will combine explosion bonding with HIPing. (SNL, NTI, MDA, BWI)

Beryllium
AlBeMet-150
Titanium
CuNiBe

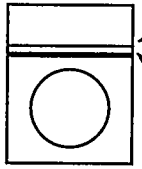

HIP Be to AlBeMet at 600 °C (step #2)

Explosion bond AlBeMet-150 with Ti diffusion barrier to CuNiBe (step #1)

- Multi-step process eliminates intermetallics.
- AlBeMet will be acid etched to preferentially remove aluminum and leave beryllium "islands" before HIPing.

We will try plasma sprayed beryllium on copper (LANL)

VPS Beryllium
DBC
GlidCop Al-25

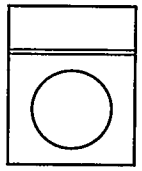

Plasma spray beryllium (Step #3)

Plasma spray W, V, Ti, or Ni diffusion barrier coating (Step #2)

Transfer arc clean copper. (Step #1)

- Excellent option for coating curved surfaces.
- Can be HIP'ed after spraying to reach 100% density. (no HIP can required)

We will try plasma sprayed Be+Al functionally graded joint. (LANL, Tim McKechnie at Plasma Processes, Inc.)

Beryllium
Be + Al FGM
GlidCop Al-25

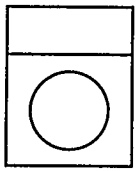

Plasma sprayed functionally graded Be-Al layer.

- Functionally graded Be/Al interlayer should reduce CTE-mismatch stresses.
- May require a diffusion barrier coating (e.g. Ti).

A simple EBTS mockup design will be used for Be/Cu and W/Cu thermal fatigue tests.

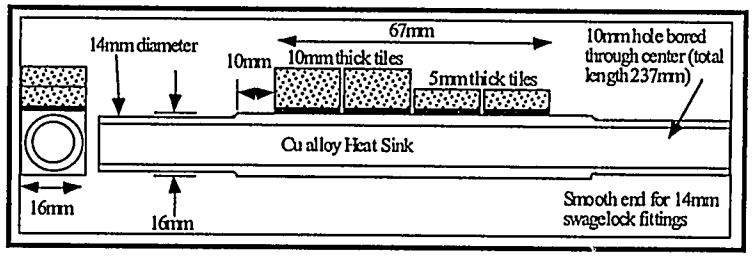

- Basic copper monoblock configuration
- Single circular cooling channel
- Ends turned down to standard tube diameter
- Compression fittings (no welds or brazes)
- Flat surface for joining armor tiles
- Standard set of thermocouple holes

Each divertor mockup will have 16 thermocouples.

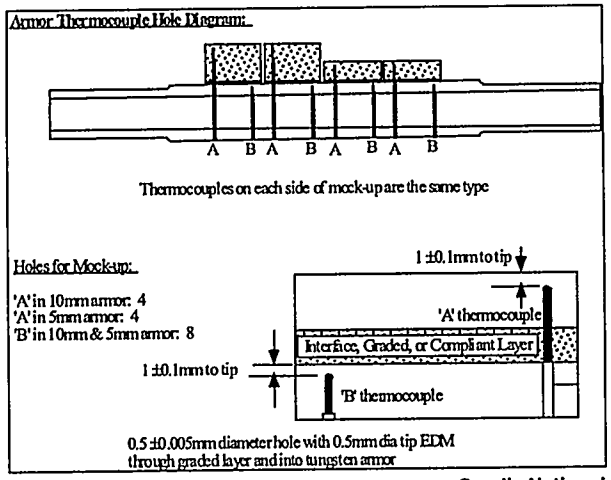

RDW-29 Watson US-Japan Colorado Springs-96

Sandia National Laboratories

ITER funded small-scale EBTS divertor mockups.

NAME	ARMOR	HEAT SINK	OTHER LAYERS	ATTACHMENT METHOD	DATE AVAIL
PB-1	S-65C	Hycon	0.5mm E-plate Cu	450°C HIP DB	TBD
PB-2	S-65C	Hycon	PVD diffusion barrier, 0.5mm E-plate C	450°C HIP DB	TBD
PB-3	S-65C	Elbrodur-G	Al coating on Be, Exp Bond Ti & Al	Al-Si braze	TBD
PB-4	S-65C	Hycon	Exp Bond Ti & AlBeMet 150	600°C HIP DB (Gil London)	TBD
PB-5	S-65C	Hycon	?	B-W Proprietary	TBD
LB-1	PS Be	GlidCop Al-25	none	Plasma Spray	TBD
LB-2	PS Be	GlidCop Al-25	TBD barrier coating	Plasma Spray	TBD
LB-3	PS Be	Elbrodur-G	Exp bond Ti & Al	Plasma Spray	TBD
PW-1	W bar	Hycon	1mm cast Cu	450°C HIP DB	29-Mar-96
PW-2	W bar	GlidCop Al-25	Cu/W graded layer, Cu deposit on W	450°C - 1000°C HIP DB	29-Mar-96
PW-5	PS W	TBD	PS Cu/W graded layer	Plasma spray & HIP	30-Aug-96

RDW-30 Watson US-Japan Colorado Springs-96

Sandia National Laboratories

SBIR funded small-scale EBTS divertor mockups.

NAME	ARMOR	HEAT SINK	OTHER LAYERS	ATTACHMENT METHOD	DATE AVAIL
SB-1	S-65C	GlidCop Al-25	Diffusion Barrier Coating	Alloy or ternary eutectic braz	TBD
MB-1	PS Be	GlidCop Al-25	Cu/Al/Be FGM	Plasma Spray	1-May-96
MB-2	PS Be	GlidCop Al-25	Cu/Al/Be FGM	Plasma Spray	1-May-96

RDW-31 Watson US-Japan Colorado Springs-96

Sandia National Laboratories

Conclusions

- Silverless joining of beryllium and tungsten is a challenging task.
- We have made very good progress and will soon be fabricating small-scale divertor mockups for e-beam testing.
- We are on schedule to meet ITER milestones.

RDW-32 Watson US-Japan Colorado Springs-96

Sandia National Laboratories

RECENT RESULTS FOR BONDING S-65C GRADE Be TO COPPER ALLOYS

David E. Dombrowski

Brush Wellman Inc.

Presented at US-Japan Workshop Q219 on High Heat Flux Components and Plasma Surface Interactions for Next Fusion Devices

9-11 January 1996
Colorado Springs, Colorado

Brush Wellman

Outline

- Background on Bond Strengths in Be Bonding Processes
- Bond Strengths Achieved in Present Work
- Significance of Bond Strength Results
- Failure Modes
- Effect of Test Specimen Geometry
- Conclusions
- Future Work

Brush Wellman

Background

Bond Strengths (MPa) Achieved in Other Candidate Processes

	Process	Room Temperature	200 °C	400 °C
JET (1993) Be to Cu Alloy	Ag Based Induction Brazing	220 MPa	≈ 215 at 250°C	≈ 157
MSC (1993) Be to Cu Alloy	Ag Sputtered on Be and Cu followed by HIP	32.5	NA	NA
O'Brien, Rice, and Olson (1976) Be to Be	Ag sputtered on Be followed by Diffusion Bonding	434	NA	NA
Be to Be	Al Based Brazing	102	64	NA
Be to Be	Zn Based Brazing	88	52	20

Brush Wellman

Bond Strength Determination

S-65C grade Be Bonded to Cu (C10100)

Rectangular Tensile Samples

	Tensile Strength of Bond (MPa)		
Process	Room Temp.	200°C	400°C
A	73.8	NA	49.6
B	49.6	NA	35.2

Reduced Section Tensile Samples

	Tensile Strength of Bond (MPa)		
Process	Room Temp.	200°C	400°C
A	142	141	96.5 95.8
B	88.2	112	90.3 94.5

Brush Wellman

Significance of Results

- No Ag Used
- All Materials Used Have Lower Radiation Hazard Than Ag
- Room Temperature Bond Strength Exceeds MSC HIP Bond Process
- Elevated Temperature Strength Exceeds Al Based and Zn Based Be to Be Brazing
- Some Elevated Temperature Failures Were In the Copper Reduced Section
    - Good sign when Bond is Stronger Than Base Metal
- Bonds Are Robust Enough That Conventional Machining Methods Can Be Used to Make Reduced Section Specimens

Brush Wellman

Comparison of Macroscopic Appearance of Room Temperature and 400°C Straight Sided Rectangular Tensile Specimens

BWI Process A

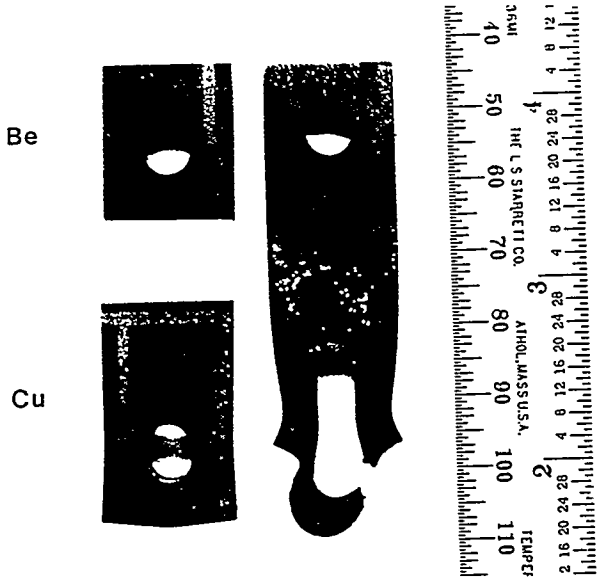

Comparison of Macroscopic Appearance of Room Temperature and 400°C Straight Sided Rectangular Tensile Specimens

BWI Process B

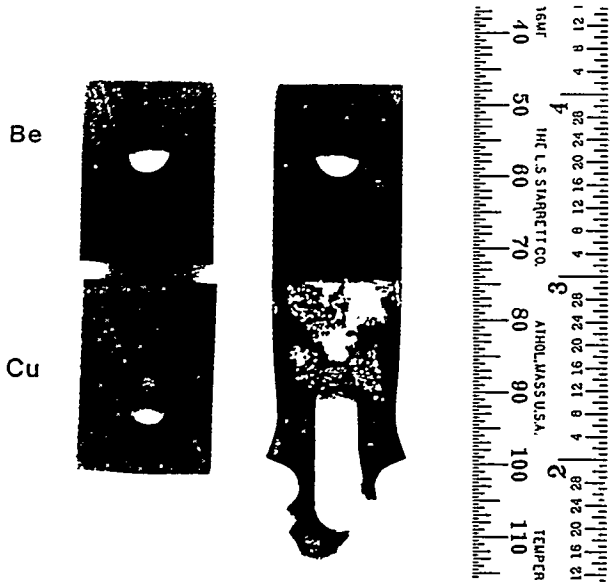

Brush

Comparison of Macroscopic Appearance of Room Temperature, 200°C, and 400°C Reduced Section Tensile Specimens

BWI Process A

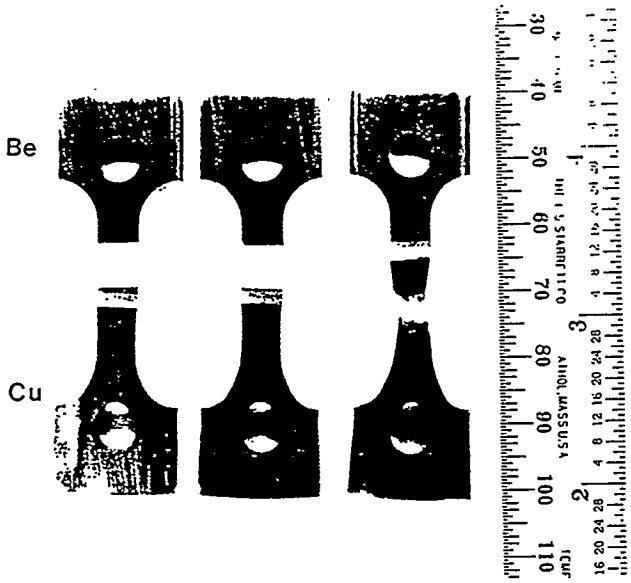

Brush Wellman

Comparison of Macroscopic Appearance of Room Temperature, 200°C, and 400°C Reduced Section Tensile Specimens

BWI Process B

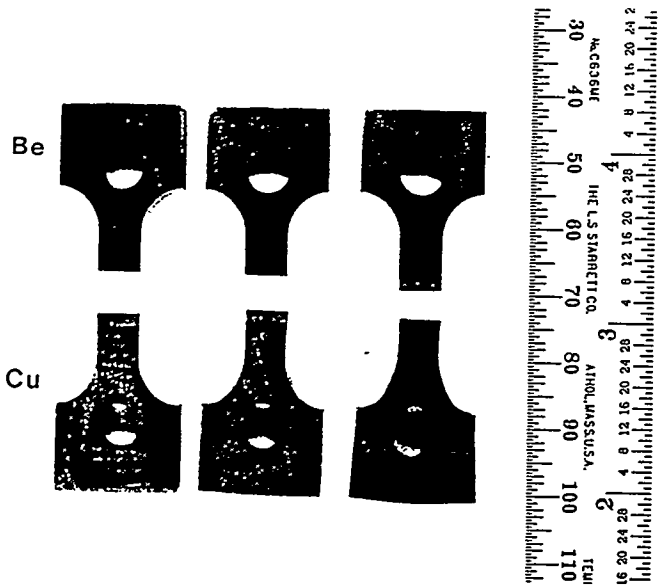

Brush Wellman

Comparison of Macroscopic Appearance of 400°C Rectangular and Reduced Section Tensile Specimens Specimens

BWI Process A

Be

Cu

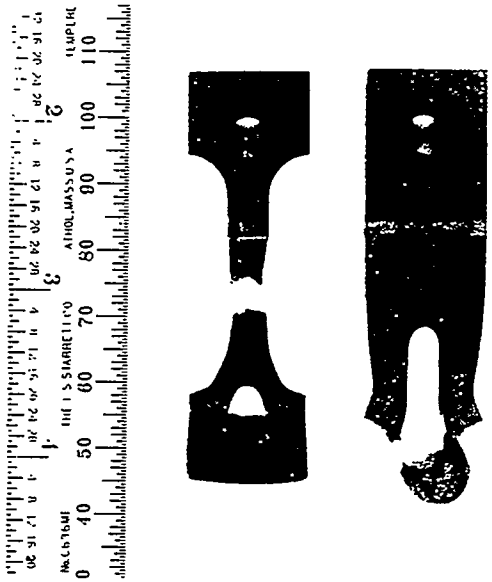

Comparison of Macroscopic Appearance of 400°C Rectangular and Reduced Section Tensile Specimens Specimens

BWI Process B

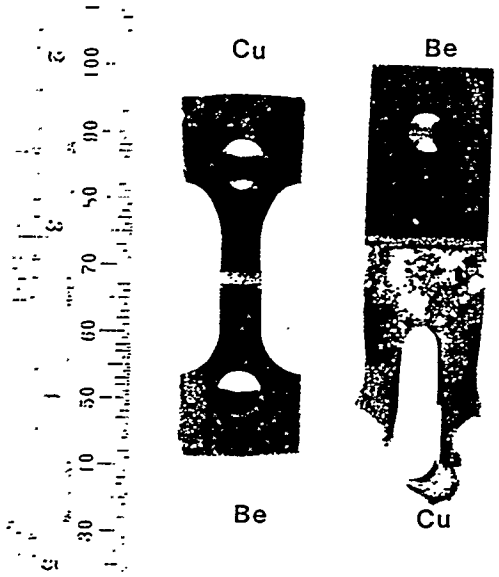

Brush Wellman

Summary of Tensile Sample Failure Location

	Process A		Process B	
	Rect.	Reduced Section	Rect.	Reduced Section
Room Temp.	Flat Fracture at Be/Bond Interface	Flat Fracture in Bond	Flat Fracture at Be/Bond Interface	Flat Fracture at Be/Bond Interface
200 °C	NA	Uneven Fracture in Bond	NA	Flat Fracture at Be/Bond Interface
400 °C	Failed In Cu Pin Hole	Failed in Main Body of Cu	Failed In Cu Pin Hole	Uneven Fracture in Bond and at Be/Bond Interface

NA = Not Available

Brush Wellman

Discussion of Effect of Test Specimen Geometry on Measured Bond Strength

- Straight Sided Rectangular Tensile Specimens with Pin Hole Grips
  - Provide Easy to Machine Geometry for Low Strength Bonds
  - Measured Bond Strengths Are Lower Than Those Derived With Reduced Section Specimens
  - Indicated Magnitude of Difference Between BWI Process A and B at Room Temperature
  - Elevated Temperature Testing Fails in Pin Hole Grips
- **Reduced Section** Tensile Specimens With Pin Hole Grips
  - Constrains location of highest strain
  - Can be made when moderate bond strength achieved
  - Bond Strengths are higher than those measured with simple rectangular geometry
  - Avoid Failure in Pin Hole Grips at Elevated temperature

Brush Wellman

CONCLUSIONS

- Novel Brush Wellman Processes Show Promising Bond Strengths Without Use of Ag
  - Reduced Section Tensile Strengths of >140 MPa at Room Temperature and 200°C were achieved
  - The strengths at elevated temperatures exceed those for beryllium to beryllium bonding using aluminum based and zinc based brazing processes.
  - Bond resistance to degradation during handling and machining is good.
- There is a significant difference in bond strengths measured by straight sided rectangular and reduced section tensile specimens.
  - Bond strengths measured with reduced section specimens are twice as high as when measured with straight sided, rectangular specimens.
  - Straight sided, rectangular specimens should only be used to indicate room temperature trends.

Brush Wellman

Recommendations

- Future work should include optimization of the process parameters.
- Now that the robust nature of the bond is known, testing should be conducted with thinner but better designed sample geometries.
- Accurate characterization of elevated temperature bond strength can only be done with copper alloys which have higher elevated temperature strength, are thermally stable during the bonding process and are age hardenable.
- High heat flux testing of the bonds should be delayed until the bond characteristics are optimized for use with a higher strength copper alloy.

Brush Wellman

Fundamental Aspects of Be Oxidation and Implications for Fusion Experiments

by

David E. Dombrowski

Brush Wellman, Inc.
Cleveland, OH
USA

Presented at US-Japan Workshop Q219 on High Heat Flux Components and Plasma Surface Interactions for Next Fusion Devices

9-11 January 1996
Colorado Springs, Colorado

BRUSH WELLMAN INC.

Outline

- Reasons to Examine Fundamentals of Be oxidation
- Two Fundamental limits: Thermodynamics and Kinetics
  - Thermodynamics of Oxidation
  - General Kinetics of Metal Oxidation
  - Kinetics of Be Oxidation
  - Kinetics of Oxidation in Vacuum
- Colors on Be Surface: Interference Films
- Implications for Fusion Research

BRUSH WELLMAN INC.

Reasons to Examine Fundamentals of Be Oxidation

- Phenomological Questions from High Heat Flux Testing and Low Cycle Thermal Fatigue Testing
  - Significance of 700°C
  - Significance of color change
  - Significance of emissivity change
- Questions Related to Development of Be to Cu Alloy Bonding
  - Can surface condition be improved by heating in vacuum?
  - What is baseline surface condition?
  - Can there be Be metal on top of Be oxide?
- Questions Related to Be Characterization Studies in Moderate to High Vacuum
  - What is baseline surface condition?

BRUSH WELLMAN INC.

Two Fundamental Limits:

Thermodynamics and Kinetics

- Thermodynamics:
  - Is there sufficient chemical driving force for a reaction to occur?

- Kinetics:

If there is sufficient chemical driving force, how quickly will the reaction occur?

Thermodynamics of Oxidation

Simple Case: Oxygen Gas

$$Be + 1/2\ O_2 \rightarrow BeO$$

ΔG_R = Chemical Driving Force for Reaction at Temperature T

$\Delta G_R < 0$: Enough Chemical Driving Force for reaction to Proceed

$\Delta G_R = 0$: Dividing Point Between Sufficient and Insufficient Chemical Driving Force

$\Delta G_R > 0$: <u>Not</u> enough Chemical Driving Force for reaction to Proceed

$$\Delta G_R = \Delta G^\circ_f(BeO) - \Delta G^\circ_f(Be) - \Delta G^\circ_f(O_2)$$

$$+ \ RT \ln (a_{BeO}/(a_{Be} \times p_{O2}^{1/2})$$

$$p_{O2} = e^{(\Delta G^\circ f(BeO)/0.5RT)}$$

BRUSH WELLMAN INC.

Thermodynamics of Oxidation, cont.

Simple Case: Oxygen Gas

- As shown on the Ellingham Diagram, BeO formation from Be and O_2 is very energetically favorable

- Can only decrease energy available if p_{O2} is decreased.

  - How low would p_{O2} need to be decreased to stop reaction?

    - At Room Temperature, p_{O2} would need to be lower than 1.6E-197 torr

    - At 700°C, p_{O2} would need to be lower than 3.7E-50 torr

BRUSH WELLMAN INC.

Critical H_2O to H_2 Partial Pressure Ratio for Be Oxidation

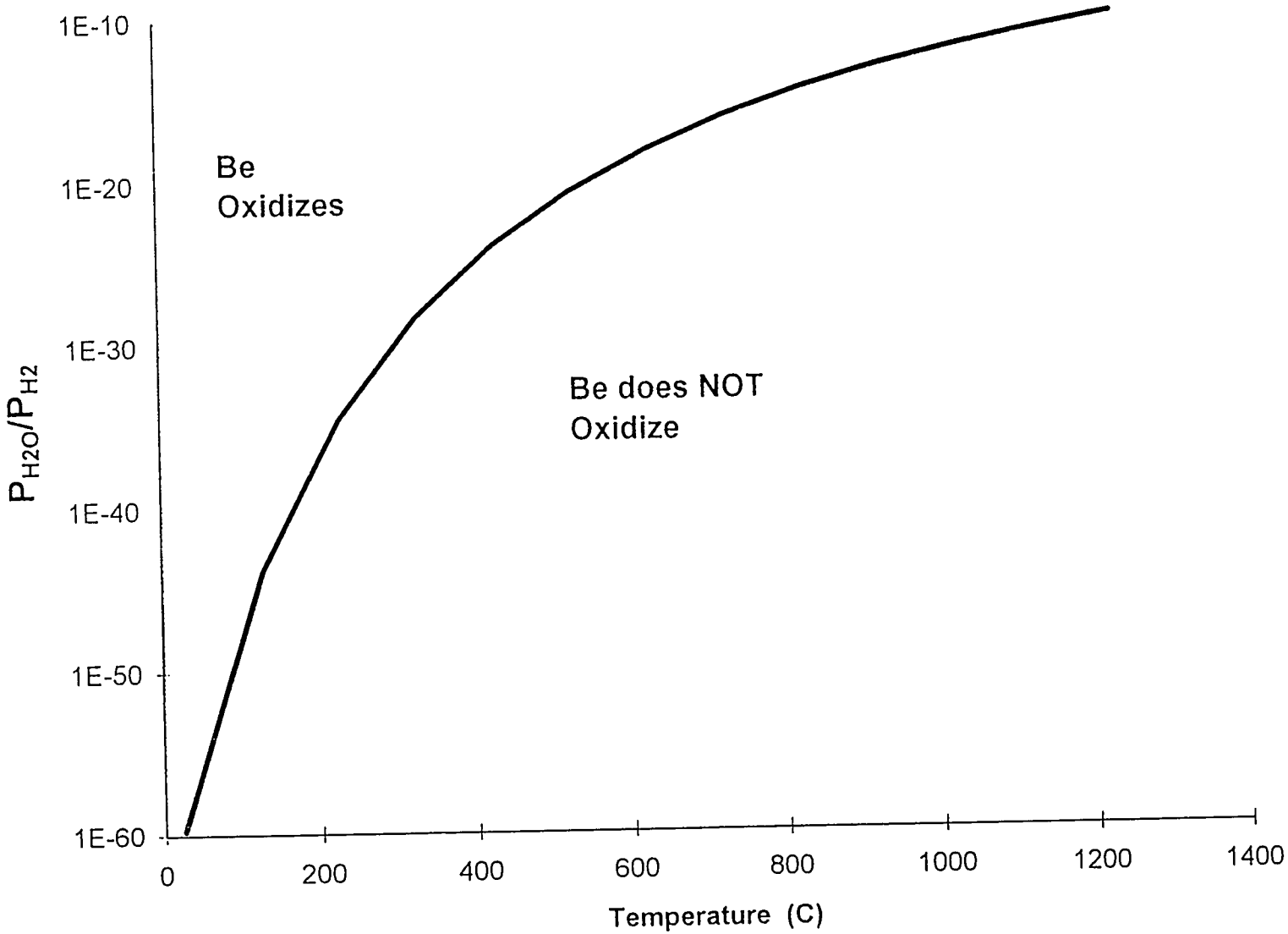

Thermodynamics of Oxidation

- Other Oxidizing Species
  - N_2
  - CO_2/CO
  - H_2O/H_2
- Analysis is similar to that for oxygen gas.

BRUSH WELLMAN INC.

Critical H_2O to H_2 Partial Pressure Ratio for Be Oxidation

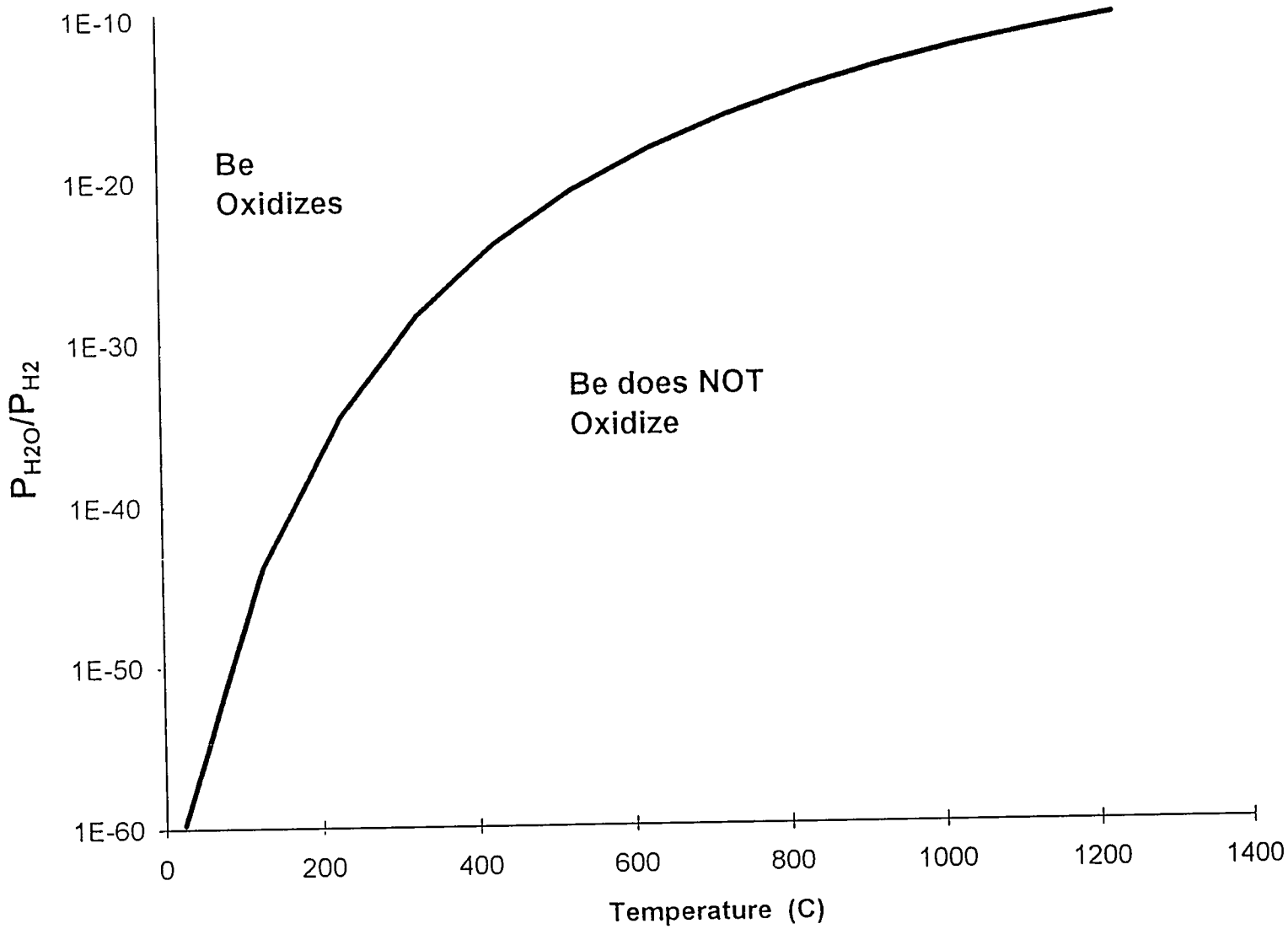

Thermodynamics of Oxidation:

Implications for Fusion Issues

- Phenomological Observations at 700°C
  - *NOT due to BeO decomposition*
- BeO will form and continue to grow in most low and high vacuum regimes
- Cannot decompose BeO to Be metal by heat treatment at elevated temperatures
  - Even in vacuum
- Unlikely that Be metal will diffuse through BeO and form metallic layer on top of BeO
  - Thermodynamic calculations do not support this
  - All fundamental theories of oxidation are based on diffusion of cations and anions through the oxide lattice

BRUSH WELLMAN INC.

General Kinetics of Metal Oxidation

- Kinetics are usually limited by one of two processes
  - diffusion of metal cation (ex.: Be^{2+})
  - diffusion of oxygen anion (O^{2-})
- Structure of Oxide Layer Can Affect These Kinetics
  - Tight Coherent Oxide Layers vs. Porous Oxide Layers
- Experimental Techniques
  - Weight Gain vs. Exposure Time
  - Tracer Diffusion Measurements vs. Time
- General Forms of Equations for Weight Gain vs. Time
  - logarithmic
  - parabolic

BRUSH WELLMAN INC.

Kinetics of Be Oxidation

- Parabolic Oxidation Kinetics at $T < 700°C$
  - $w^2 = k_p t + C$
  - Ervin and Mackay have shown that k_p varies with oxygen pressure according to p^n where $n = 1/4.6$
  - k_p = parabolic rate constant
    - For old production grade of Be
      - $k_p = 1.8 \times 10^{-12} \exp(-8{,}500/RT)\ g^2/cm^4$ from 350 - 700°C
  - Effect of Impurity Content and Fabrication Method
    - Impurities (Be_2C, Fe, etc.) Enhance Corrosion Rate
    - Value of k_p and C vary with Impurity Content and Fabrication Method
    - Temperature range of Parabolic Oxidation Behavior varies

BRUSH WELLMAN INC.

Kinetics of Be Oxidation

- Linear or Accelerating Kinetics at T > 700°C
  - "Breakaway" Oxidation

$$w = Kt$$

    - For 1960's production grades of Be at 930°C
      - $K = 0.055\ mg/cm^2\text{-}min$

    (approx. 0.2 μm thick BeO layer in 1 min.)

  - Lattice Mismatch Stresses in Thicker Oxide Layers
  - Cation Vacancy Accumulation
  - Intergranular Attack
    - Below ≈1050°C
  - Projecting Needles and Flakes Can Form

BRUSH WELLMAN INC.

Kinetics of Oxidation in Vacuum

- Kinetics of Monolayer Formation as a function of chamber pressure
  - it takes about one second for a monolayer to form in a vacuum chamber at 10^{-6} torr and
  - 5 seconds for a monolayer to form at 10^{-7} torr.
- Once a Monolayer is formed, oxidation should be rapid
- p^n relationship used to extrapolate oxidation rates to lower pressures
  - indicates that at 10^{-6} torr oxidation rate is 2% of 1 atm rate
    - Still rapid
- Oxidation of Be at 0.1 atm O_2 (Gulbransen and Andrew)
  - 1 $\mu g/cm^2$-hr at 350°C
  - 88 $\mu g/cm^2$-hr at 950°C (4.7 nm BeO/min)

BRUSH WELLMAN INC.

Russian research clearly shows that beryllium emissivity varies dramatically depending on film thickness and morphology

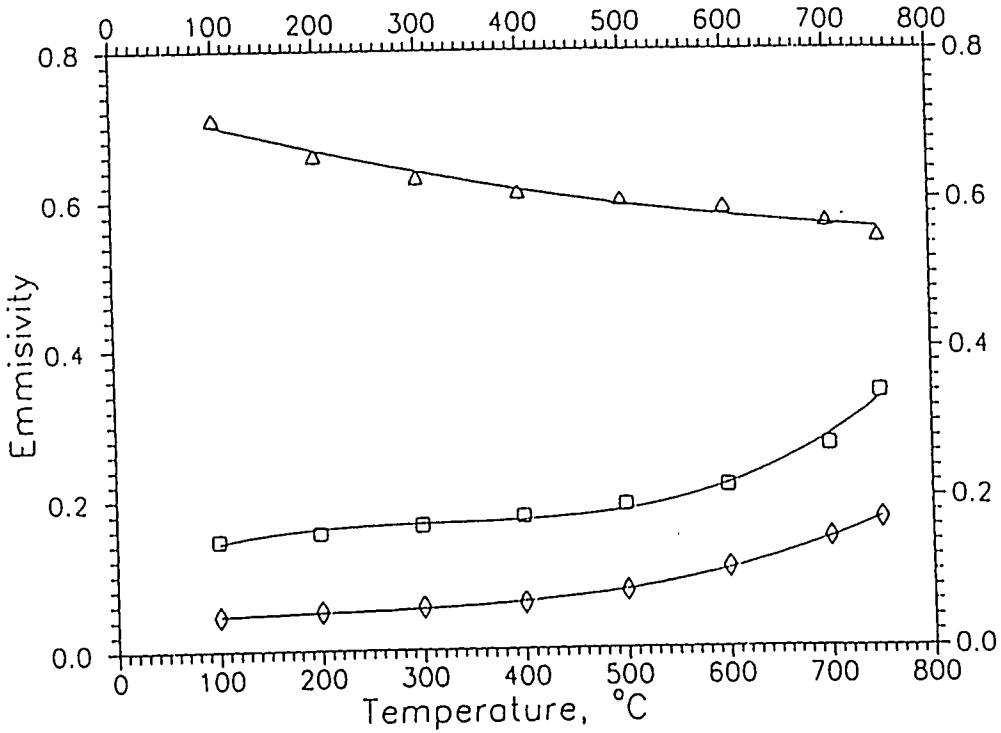

□□□□□ – TGP-56 (1)
◊◊◊◊◊ – TGP-56, etched (2)
△△△△△ – TGP-56, anoded (3)

Filling function:
1 – $Y = A + Bx + Cx^2 + Dx^3$
$A = 0.097$, $B = 0.00061$,
$C = -1.81 \cdot 10^{-6}$, $D = 1.89 \cdot 10^{-9}$,
2,3 – $Y = A + Bx + Cx^2$
2 – $A = 0.038$, $B = 0.00010$,
$C = -3.50 \cdot 10^{-7}$;
3 – $A = 0.79$, $B = -0.00097$,
$C = 1.81 \cdot 10^{-6}$.

D.V.Efremov Research Institute of Electrophysical apparatus	File: EMMISBE2	Date: April 21, 1994

BRUSH WELLMAN INC.

Colors on Be Surface: Interference Films

- Interference of White Light Beams reflected from front and back surfaces of a thin parallel films yield Newton's Colors
  - A uniform series of colors dependent on film thickness starting at thicknesses as low as 18 nm
- Uniform thickness and a smooth, surface morphology results in an uniform series of colors which is a function of thickness.
  - As soon as you mix thicknesses and increase roughness you deviate from that series.
- Scott looked at the growth of BeO on Be single crystals.
  - 600°C: projecting needles of BeO up to 5 μm in length and thin distorted BeO flakes form.\
  - 800°C: pronounced (001) habit of randomly developed BeO crystals was developed.
  - Conclusion: *Above 600°C the <u>surface roughness</u> increases due to a number of mechanisms.*

Implications for Fusion Research

- Phenomological Questions from High Heat Flux Testing and Low Cycle Thermal Fatigue Testing
  - Significance of 700°C: *Increased Oxidation Rate with subsequent Change in Oxide Structure*
  - Significance of color change: *Interference Film Effects*
  - Significance of emissivity change: *Surface Roughness and Morphology*
- Questions Related to Development of Be to Cu Alloy Bonding
  - Can surface condition be improved by heating in vacuum?
    - *NO*
  - What is baseline surface condition?
    - *BeO whose thickness and morphology depend on impurities and processing*
  - Can there be Be metal on top of Be oxide?: *NO*
- Questions Related to Be Characterization Studies in Moderate to High Vacuum
  - What is baseline surface condition? *(See Above)*

BRUSH WELLMAN INC.

Current Be-Cu Joining Technology at Sandia National Laboratory-CA

C. H. Cadden — Sandia National Laboratories (CA), USA

B. C. Odegard — Sandia National Laboratories (CA), USA

W. D. Bonivert — Sandia National Laboratories (CA), USA

S. J. Goods — Sandia National Laboratories (CA), USA

R. D. Watson — Sandia National Laboratories (NM), USA

Japan-US Workshop, January 9-11, 1996
Colorado Springs, Colorado

Sandia National Laboratories
California, USA

Be/Cu Joining Approaches - Sandia

- Brazing
  - Isolate Be and Cu
- Diffusion Bonding
  - HIP Process
- Electroplate Cu on Be
  - Subsequent Cu/Cu Joint

Diffusion Barriers

Diffusion Barriers are used to eliminate the formation of intermetallics:

- Between the filler metals and substrates in a braze;
- Between the substrate materials in a solid state bond

Diffusion Barrier:
Ti, Ta, Ni, Cr

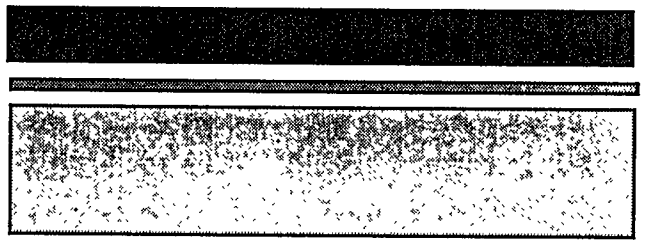

Compliant Layer

- An aluminum or Al-Be compliant layer will reduce thermal stresses generated at the interface.

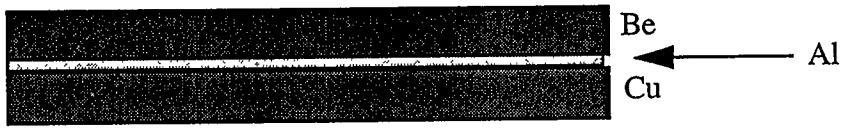

Explosively Bonded Assembly

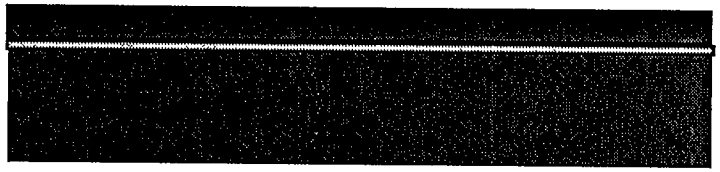

Al (Alloy 1100)

Ti, Ta Diffusion Barrier

Cu (Alloy 110)

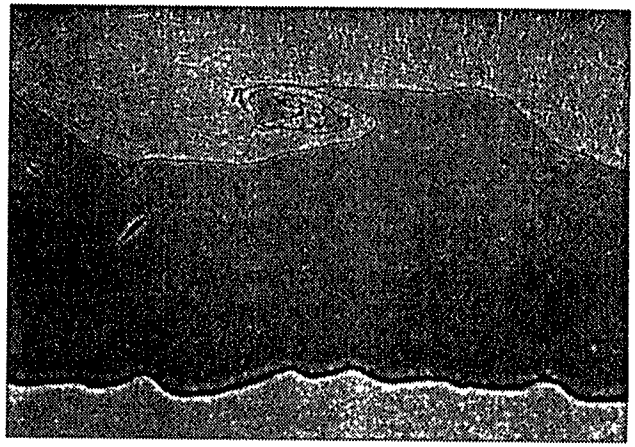

1 mm

Braze Tile using an Explosive Bonded Assembly

- A titanium diffusion barrier to eliminate intermetallics between the Al - Cu explosive bond.
- An Al/AlBeMet 150 compliant layer to reduce thermal stresses at the bond interface.
- Aluminum substrate to bond to the beryllium

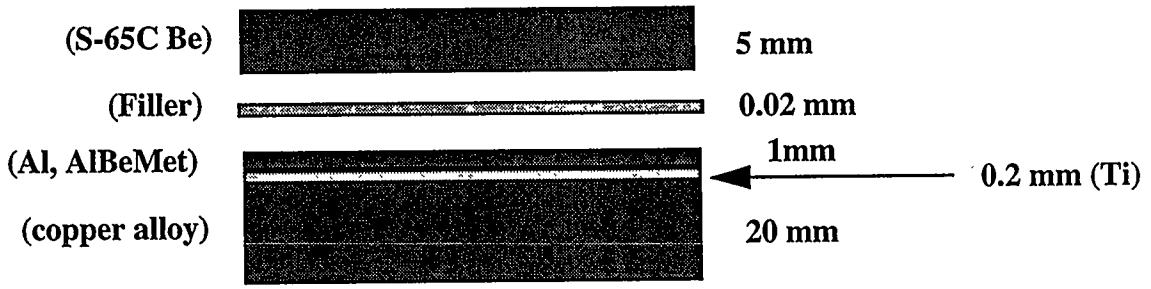

Diffusion Bond using an Explosive Bonded Assembly

- A titanium diffusion barrier to eliminate intermetallics between Al and Cu explosive bond;
- An AlBeMet 150 compliant layer to reduce thermal stresses at the bond interface;
- AlBeMet 150 substrate to diffusion bond to the beryllium instead of a copper substrate copper;
- Etch AlBeMet to produce a rough Be surface.

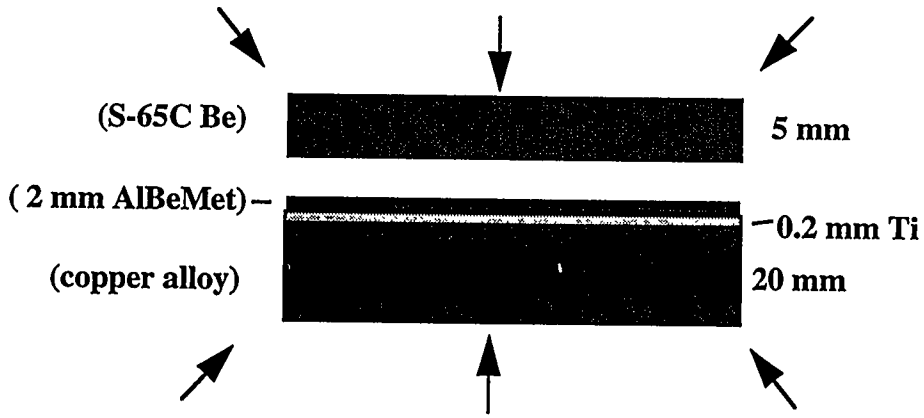

High Magnification of AlBeMet 150 surface

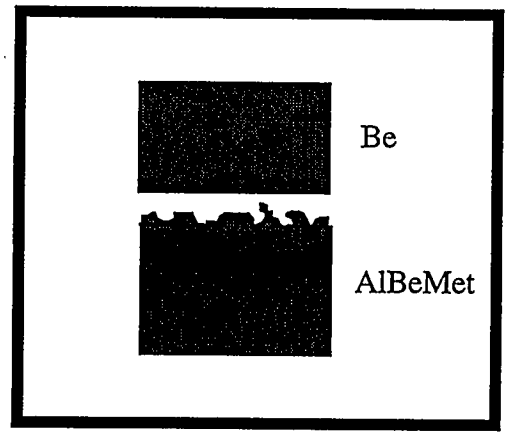

Vacuum Furnace Braze

- < 1 micron Zn Coated Be
- < 1 micron Cu Coated Al
- Al-28%Ge Filler Metal
- 660°C, 1 minutes, in vacuum

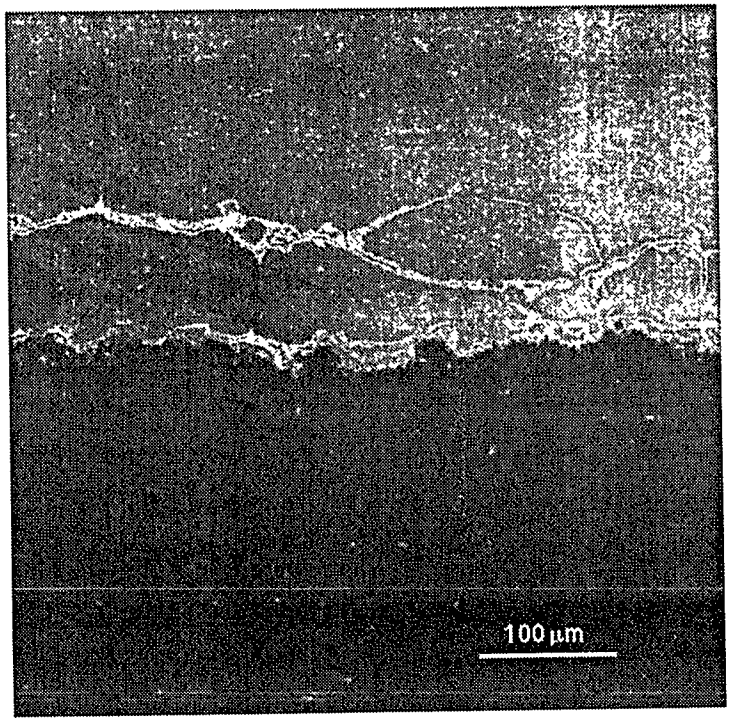

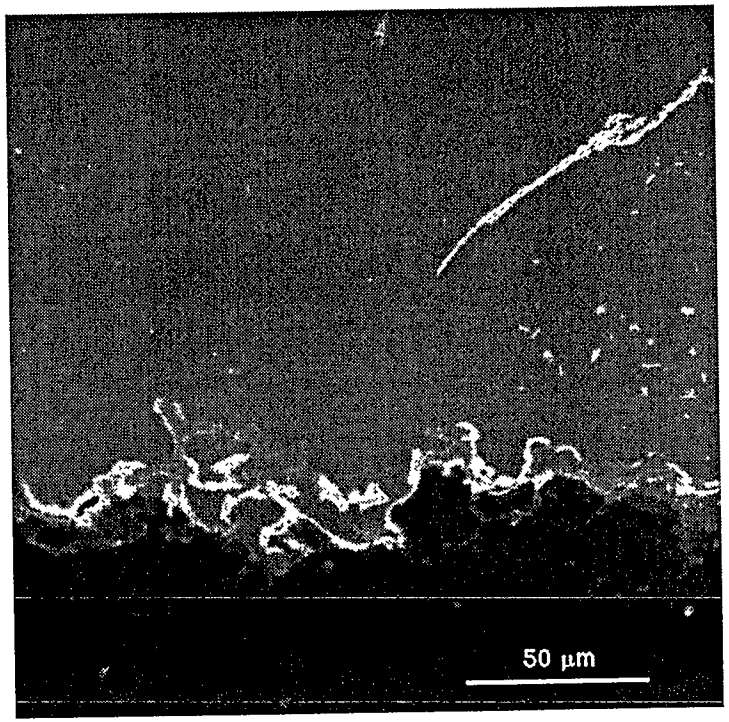

Vacuum Furnace Braze

- etched Al - etched Al
- Al-12%Si Filler Metal
- 660°C, 5 minutes, in vacuum

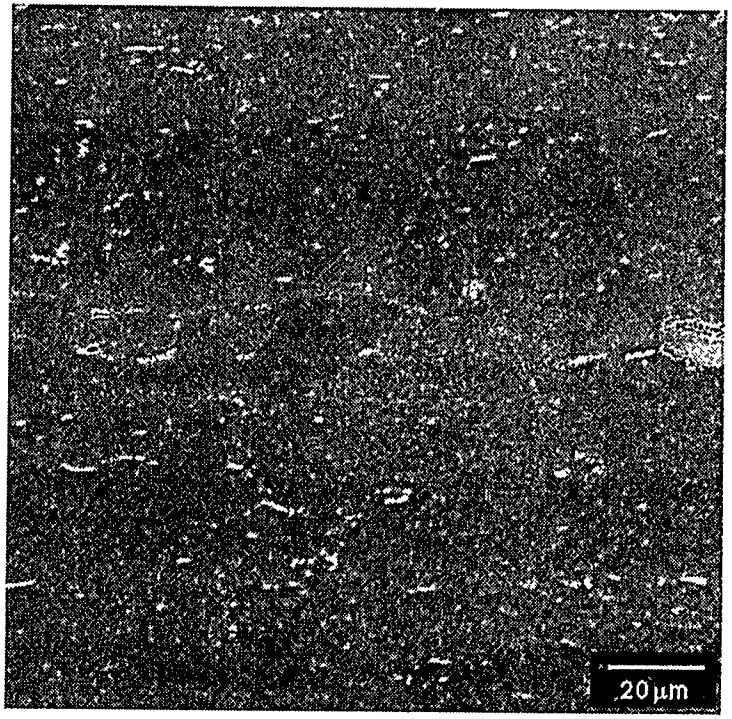

Vacuum Furnace Braze

- 25 micron Al Coated Be
- etched Al

- Al-12%Si Filler Metal
- 660°C, 5 minutes, in vacuum

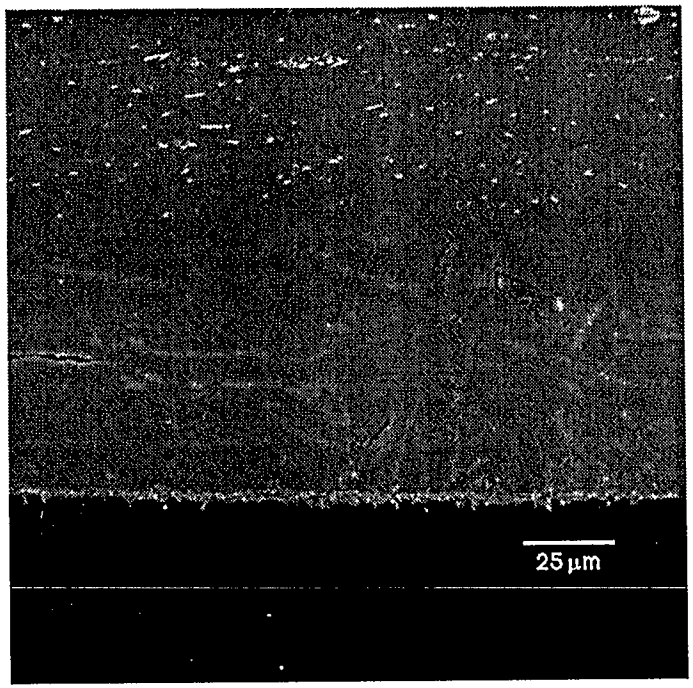

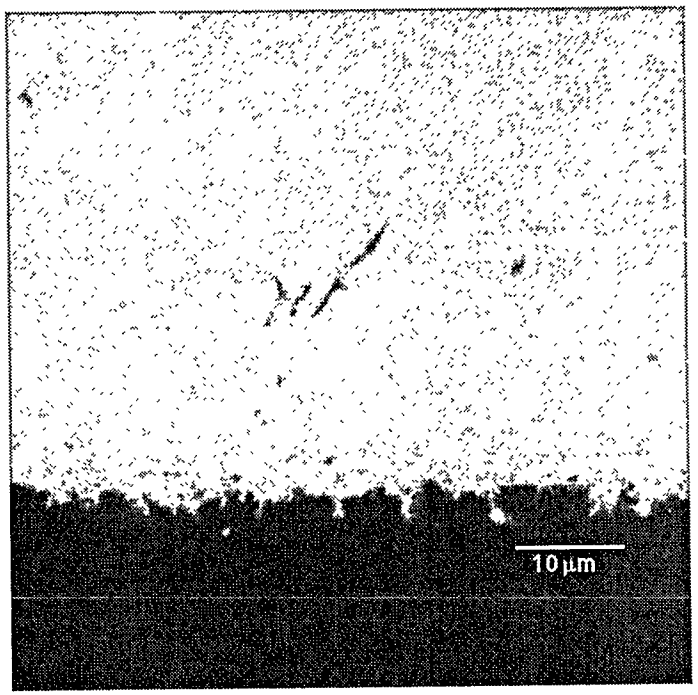

Hycon 3-Hycon 3 Diffusion Bond - MDA

- 105 MPa HIP Pressure
- Fracture Stress
  1. Ni assist - 123 MPa
     450°C, 3 hours
  2. Sn assist - 77 MPa
     350°C, 4 hours
  3. ED Cu - 350 MPa
     450°C, 3 hours

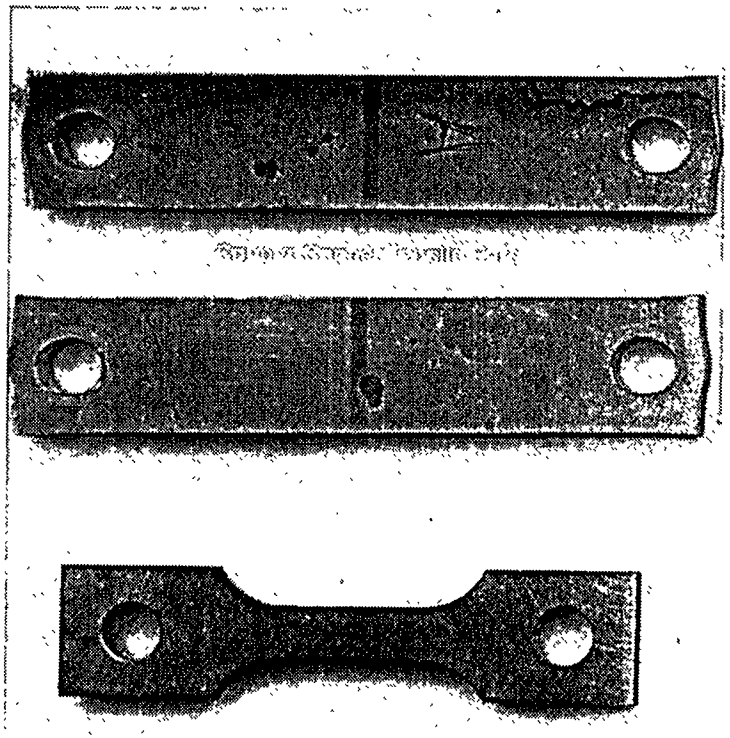

Ongoing Work

- Diffusion Bonding
- Vacuum Plasma Spray Al on Be
  look at thicker (>200μm) Al layers
- Explosive Bonded AlBeMet to Cu for
  Brazing and Diffusion Bonding trials
- Electroplated Cu on Be incorporating
  Diffusion Barriers

Materials and Joining Developments for Plasma Facing Components

Jyh-Ming Ting
Applied Sciences, Inc.
Cedarville, OH 45314

US-Japan Workshop Q219 on
High Heat Flux Components and Plasma Surface Interactions for Next Fusion Devices

Colorado Springs, CO
January 9-11, 1996

Outline

- Background
- Development of High κ Carbon Fiber for Heat Removal
- Composites Materials for PFM
- Joining Strategy for PFC
- Summary

BACKGROUND

- Carbon Composites based on Vapor Grown Carbon Fiber (Pyrograf-I™) as PFM
  - Fiber development
  - Densification techniques
- C-fiber Reinforced Beryllium Composite
  - Fiber surface modification
- Joining Carbon Composites or Beryllium to Glidcop
  - Interface engineering

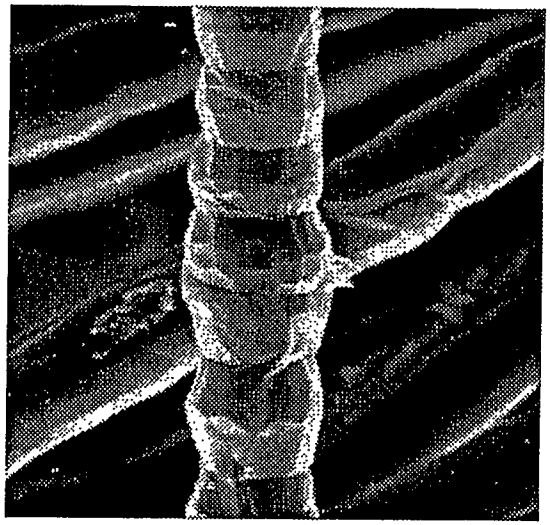

Vapor Grown Carbon Fiber

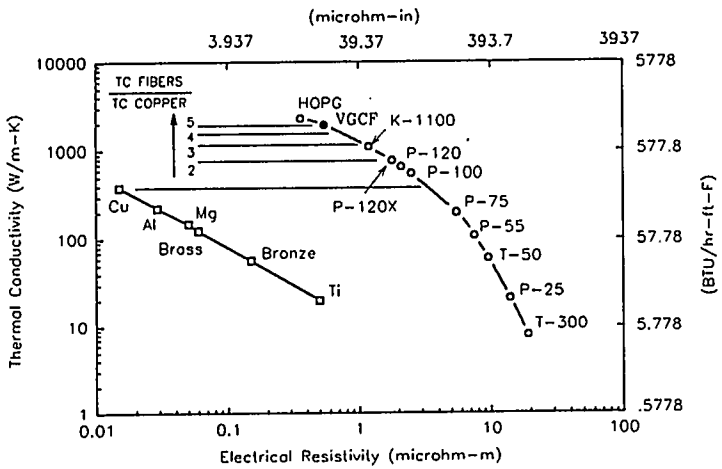

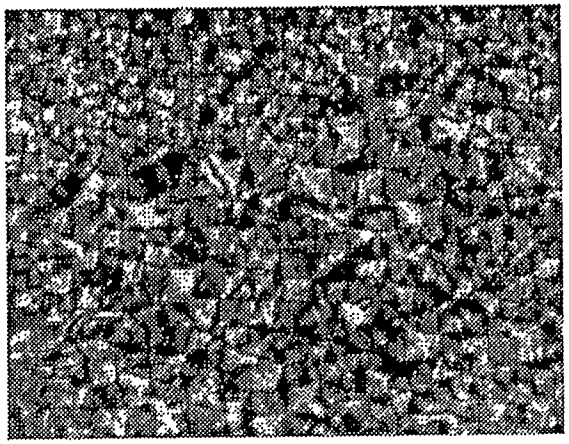

VGCF/C Composite

Thermal conductivity of 1D VGCF/C composite specimens prepared by different densification methods at different processing conditions.

Densification Condition	None	Chemical Vapor Infiltration				Pitch Infiltration		
		A	B	C	D	a	b	c
Conductivity (W/m-K)	481	559	460	590	568	463	647	736
Density (g/cc)	1.13	1.55	1.55	1.62	1.60	1.56	1.70	1.79
Cond/D (W/m-K)/(g/cc)	428	361	297	364	355	297	381	411

Thermal conductivity of VGCF/C composites with different fiber volume fraction (V_f) and densities.

ID	V_f (%)	Density (g/cc)	Thermal Conductivity (W/m-K)
L1	25%	1.26	326 (X), 36 (Y), 12 (Z)
L2	25%	1.32	344 (X), - -
L3	25%	1.51	372 (X), 38 (Y), 16 (Z)
M1	29%	1.15	362 (X), 49 (Y), 12 (Z)
M2	29%	1.35	374 (X), 52 (Y), 14 (Z)
M3	29%	1.49	431 (X), - -
H1	36%	1.32	502 (X), - -
H2	36%	1.48	528 (X), 72 (Y), 18 (Z)
H3	36%	1.59	564 (X), 75 (Y), 19 (Z)

Thermal conductivity of VGCF/C composites with high fiber loading.

ID	FV(%) X/Y	ρ(G/cc)	Conductivity X/Y/X
14	55/0	1.70	824/89/24
01	65/0	1.88	910/84/33
03	45/15	1.80	635/373/21

VGCF/Be Composites

To manifest the Advantages of VGCF and BE and Enhance the Performance of Be Tiles.

- Increasing thermal conductivity
- Enhancing thermal shock resistance
- Stabilizing melt run-off
- ***Reaction between VGCF and BE***

Pressure Infiltration of VGCF/Be Composites

- **Preforms: 20 v/o and 40 v/o VGCF Preforms.**
- **Conditions:**
  - **–1,100 psi in N_2.**
  - **–20 min. to above 1350 C.**
  - **–VGCF in contact w/ molten Be for approximately 5 min.**
  - **–Cool down to RT in 3 hrs.**
- **Results:**
  - **–First cast failed due to broken alumina tube.**
  - **–Second cast resulted infiltration of only one preform (40 v/o.)**

Be Composites by HIP Process

- Be: SP-200SF powders. 14.3g
- VGCF: Pyrograf I and Pyrograf III. 0.3g
- Pressure: 103.4 Mpa.

Can#	Fiber	Temp. (°C)
1368	AG-Pyrograf I	600
1369	HT-Pyrograf I	750
1370	HT-Pyrograf I	600
1371	AG-Pyrograf III	750
1372	HT-Pyrograf III	600

- **Analysis: OM and X-ray Diffraction.**

d-spacing (A)	No. 1370 Relative Intensity (%)		No. 1372 Relative Intensity (%)	Phase
3.36	5	3		*graphite*
2.51	2	3		Be_2C
1.99	33	33		Be
1.80	27	28		Be
1.74	100		100	Be
1.53	1	2		Be_2C
1.33	13	13		Be
1.15	14	15		Be

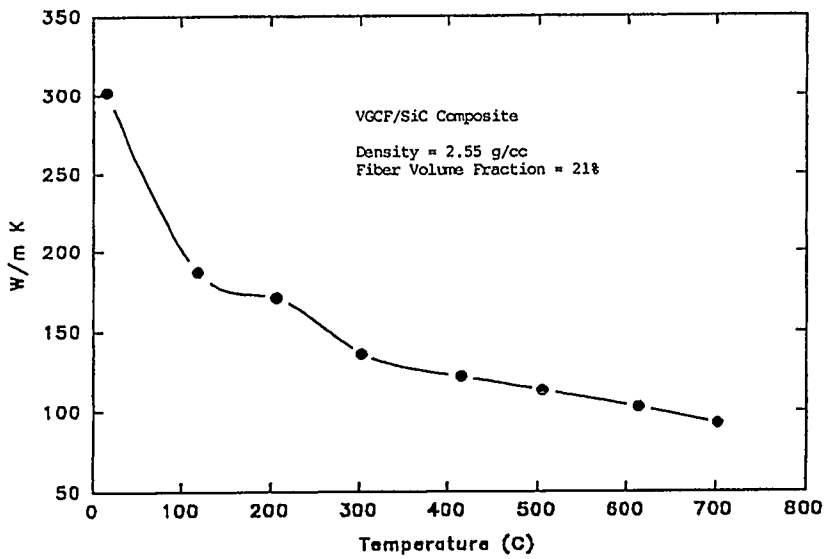

Brazing Residual Stresses in Glidcop-$Al_{12}Si$-Be*

- Determined by finite element method.
- Temperature-dependent elastic properties and coefficient of thermal expansions have been used.
- **Plastic deformation of $Al_{12}Si$ has been considered based on experimental stress-strain relationship at different temperatures.**
- Effect of brazing layer thickness was examined.

* P. Dadras, J.-M. Ting, and M.L. Lake, "Brazing Residual Stresses in Glidcop-$Al_{12}Si$-Be," J. Nuclear Mat. (1996).

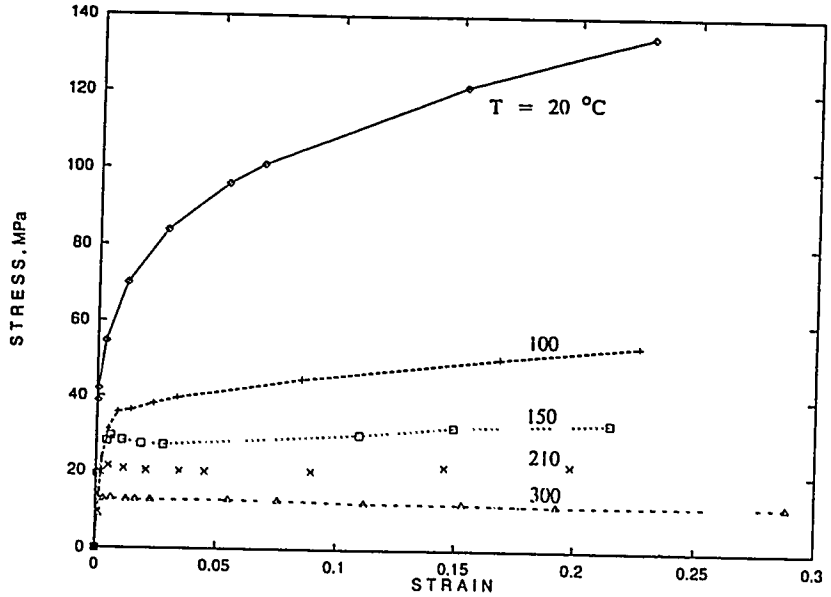
STRESS, MPa
STRAIN
T = 20 °C
100
150
210
300

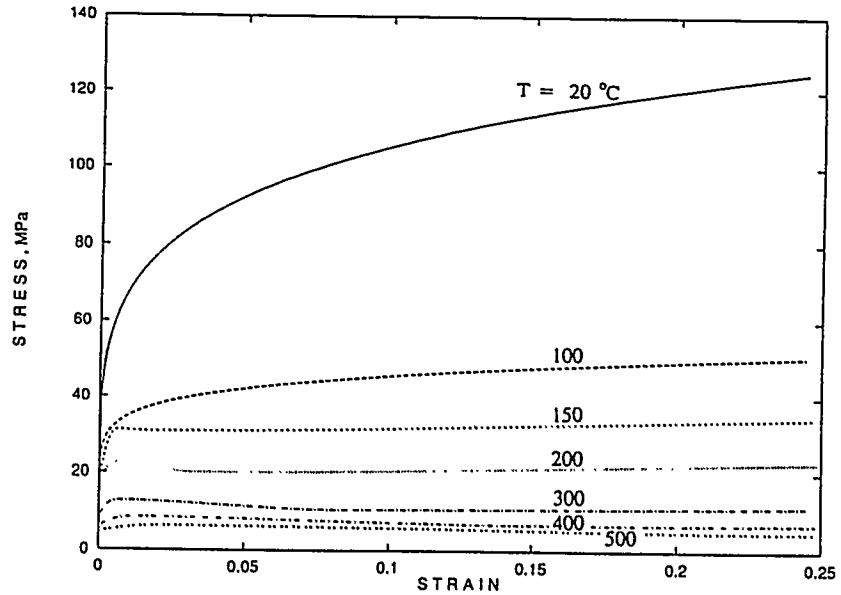
STRESS, MPa
STRAIN
T = 20 °C
100
150
200
300
400
500

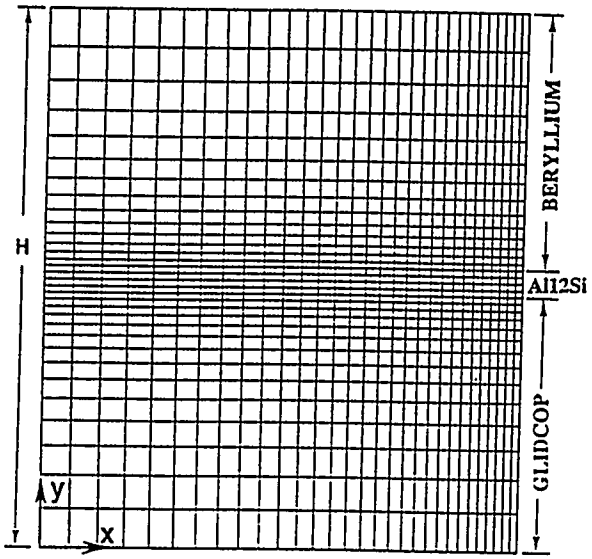
H
y
x
BERYLLIUM
Al12Si
GLIDCOP

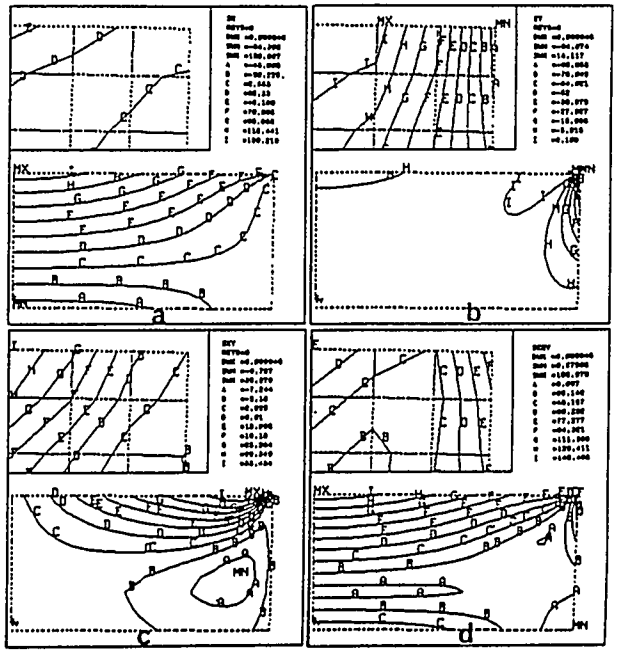
a
b
c
d

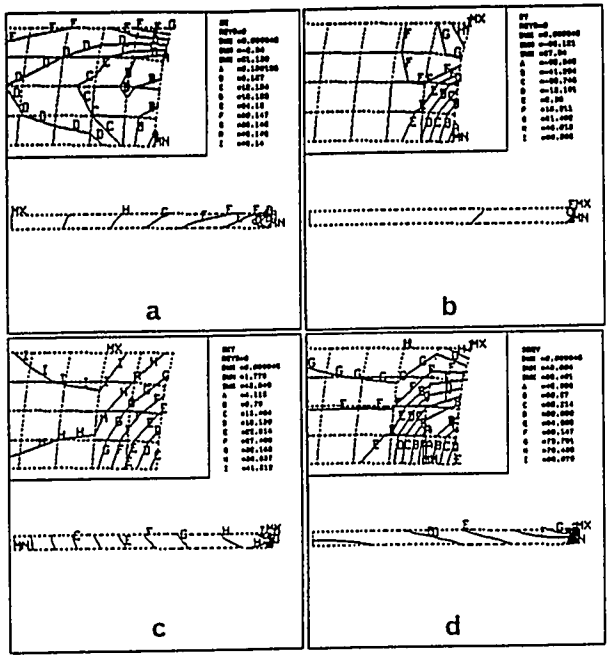

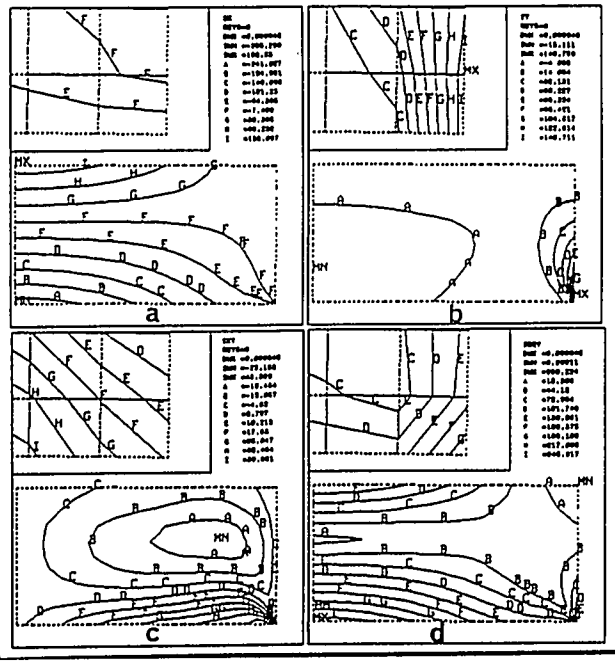

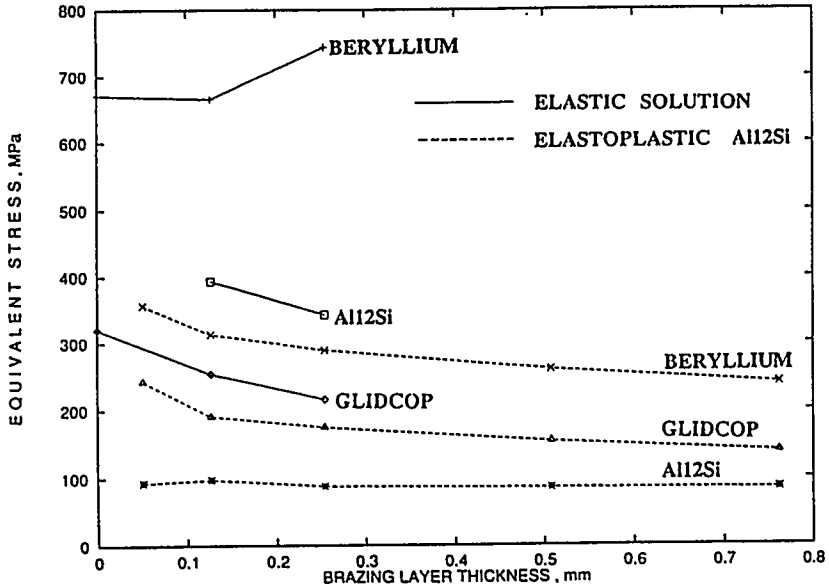

SUMMARY

- Composites, based on Vapor Grown Carbon Fiber (VGCF), for high heat flux were investigated.
  - VGCF/C, VGCF/Be, and VGCF/Si
  - 910 W/m-K
- Joining - experimental and theoretical.
  - C/C to Cu
  - Be to Cu.
- Issue of interface engineering.

The Structure, Properties and Performance of Plasma-Sprayed Beryllium for Fusion Applications

R.G. Castro, P.W. Stanek and K.E. Elliott
Los Alamos National Laboratory

D.L. Youchinson, R.D. Watson and D.S. Walsh
Sandia National Laboratory

US-Japan Workshop Q219 on High Heat Flux Components and Plasma Surface Interactions for Next Fusion Devices

January 9-11, 1996
Colorado Springs, Colorado

Outline

- ITER Requirements
- Critical R&D Issues
- Results:
  - Plasma-spraying with H_2 (κ, α)
  - (-) transferred-arc cleaning
  - Coating of ISX-B beryllium limiter tiles
- Conclusion/Future R&D Activities

Beryllium Atomization and Thermal Spray Facility (BATSF)

- Centrifugal gas atomizer - powder production
- Remote manipulations and CNC control of plasma torch (35 cm x 40 cm)
- 40 and 120 kW plasma torches
- 2000 amp power supply for scale-up operations
- Transferred-arc spraying/cleaning for surface preparation
- (2) vacuum tight beryllium powder feeders
- Hydrogen secondary gas approval to 4%
- BATSF a U.S. user facility

General Performance Requirements Maintenance and Testing:

S 10 GDRD 1 95-02-10 W 1.2

Section 2.3.3.5

To further minimize intervention time, reduce generation of waste and lower the risk of spread of contamination and exposure to personnel, maintenance strategies shall be based on a "multi-level" approach whereby first *in-situ* repair is considered before contemplating the exchange of components. When a system or component cannot be maintained by *in-situ* repair, maintenance shall be accomplished by (in order of priority) removal of a subcomponent, and then by removal of the complete component, if required.

Section 5.4.4.2

The divertor shall be designed for relatively frequent fully remote assembly and disassembly.

Section 5.5.1.3.1

The primary wall, limiters and baffles shall be designed for full remote repair and replacement. The first wall may be installed and replaced together with and as part of blanket/shield modules.

Divertor Design

The Reference Design is based on beryllium bonded to a water-cooled heat sink.

- Divertor is assembled in a cassette structure
- *In situ* or off-site repair using plasma-spraying technology
- 3 to 10 mm of beryllium coatings

First Wall/Blanket Shield Design

The reference Design for the Basic Performance Phase is a water-cooled stainless steel shield. The first wall is a stainless steel/copper alloy laminate with a beryllium armor surface.

- 1 to 5 mm of beryllium over approximately 1000 m^2
- Beryllium plasma-spraying as either initial fabrication and/or *in situ* repair

1 mm Be coating:

1 m^3 = 1850 kg of Be = 1.85 metric tons (100% D.E.)
2.5 metric tons (70% D.E.)

Critical R&D Issues for Beryllium Plasma-Spraying for ITER

Objectives:

- Optimizes thermal conductivity for maximum heat transfer
- Optimize bonding of coating to Be, Cu
- Mechanical properties and performance (irradiated and non-irradiated)
- Remote maintenance and *in situ* repair
- Inspection and process control
- Reclamation/recycling of beryllium powder
- Scale-up and technology transfer

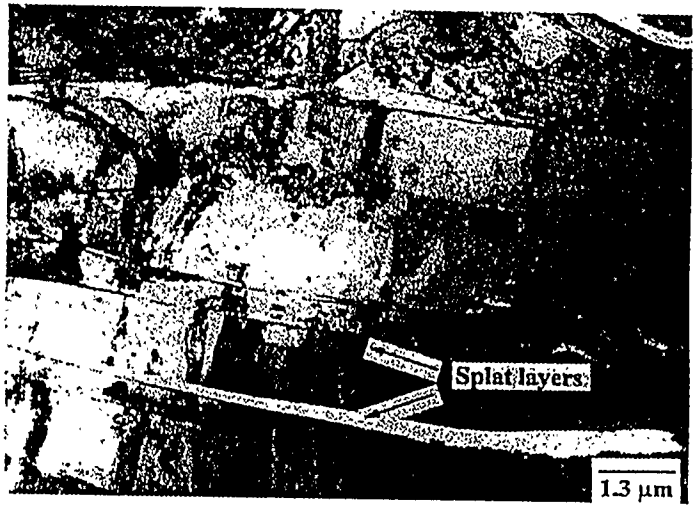

TEM microstructure of plasma-sprayed beryllium

The Effect of Hydrogen Gas Additions on Plasma-Sprayed Beryllium

- Brush Wellman Powder (-38 μm +10 μm)
- 350 Torr Chamber Pressure

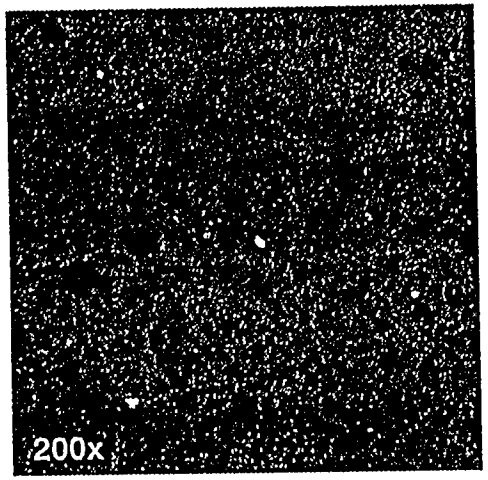

10-slm He
s.s. temp ~ 700°C
ρ = 94% of T.D.
κ = 115 W/m•K

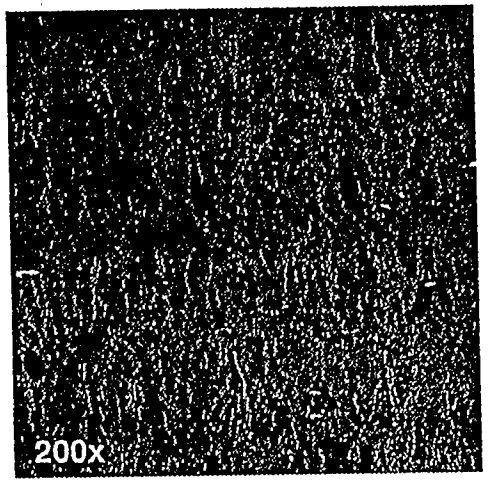

1-slm H_2
s.s. temp ~ 500°C
ρ = 96% of T.D.
κ = 150 $\rightarrow$165 W/m•K

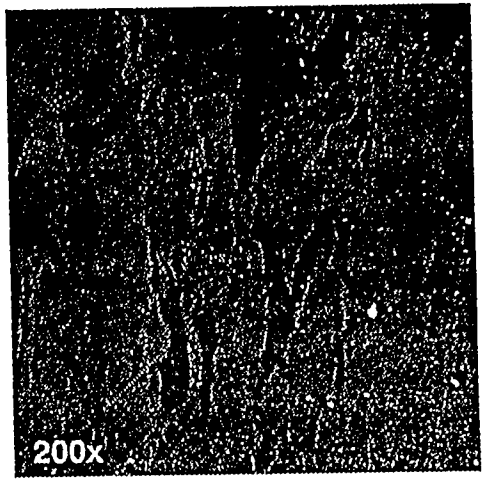

4-slm H_2
s.s. temp ~ 650°C
ρ = 98% of T.D.
κ = ?

Improved Thermal Conductivity of Plasma-Sprayed Beryllium

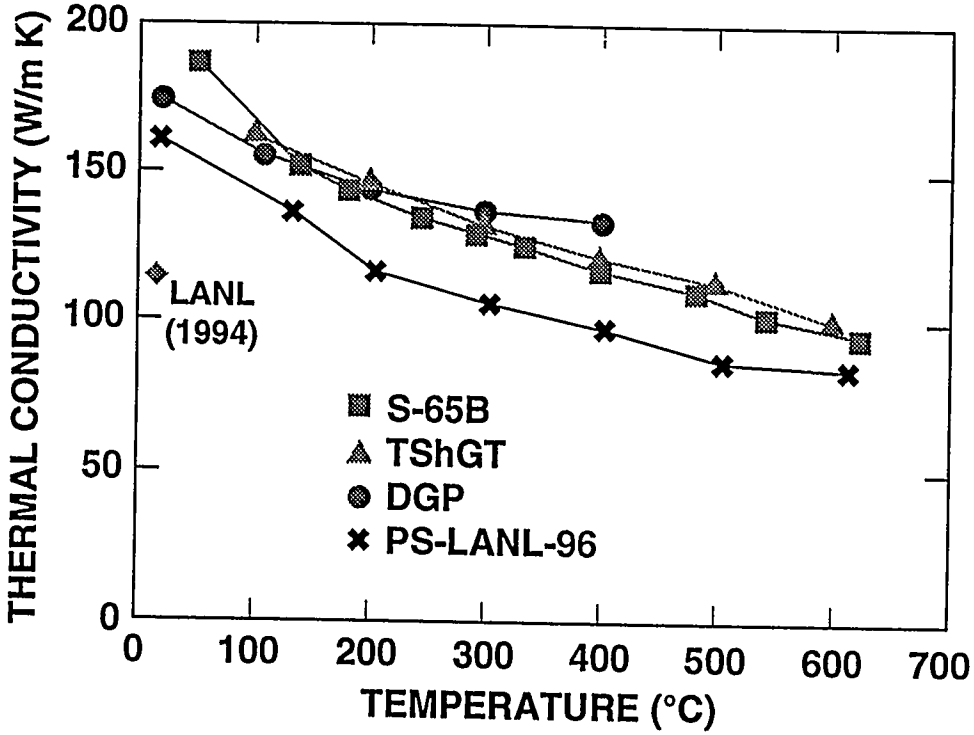

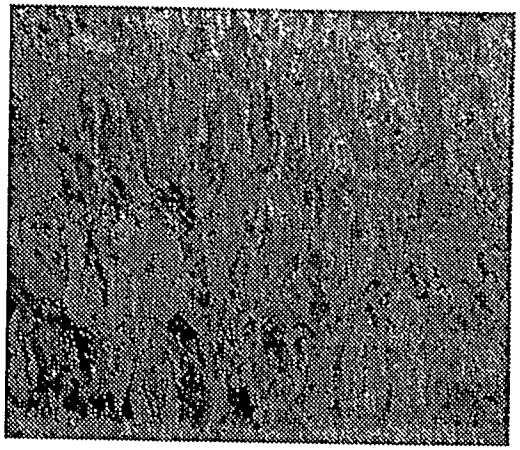

As-Deposited Beryllium
Elongated Grain Structure
(25-30 μm)

S-65B – Vacuum Hot Pressed
TShGT – Technical Purity, punched from hot pressed product
DGP – Distillation Purity, sintered hot pressed
PS-LANL-96 – VPS Beryllium - 96% T.D.

Reference: V. Barabash, "Recommended Data on Be Thermochemical Properties for Plasma Facing Components"

Improved Thermal Conductivity of Plasma-Sprayed Beryllium

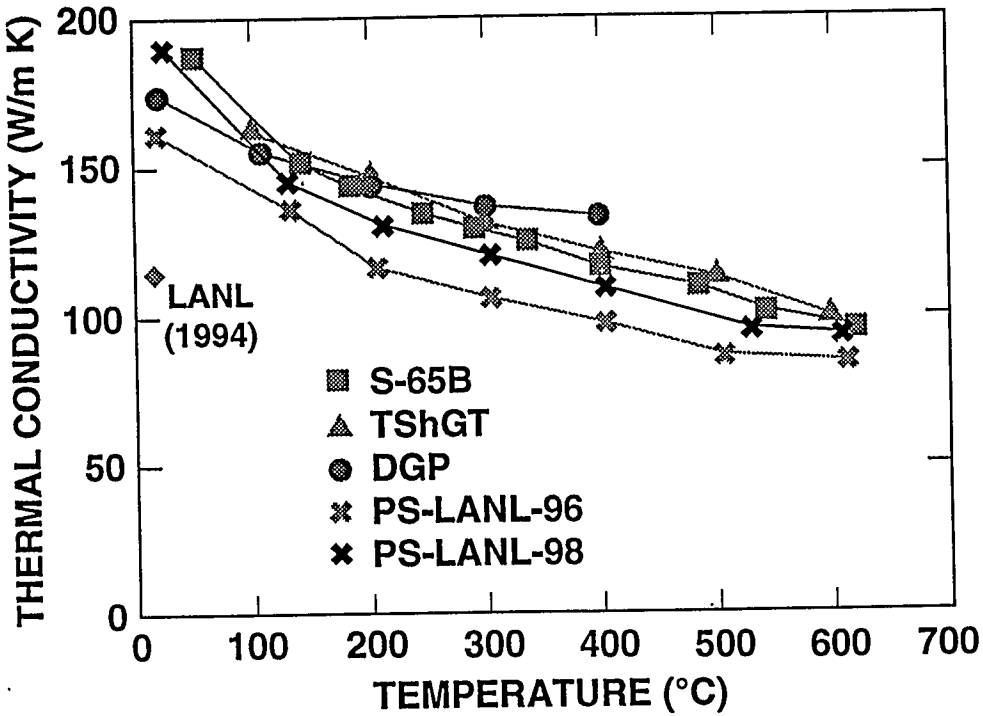

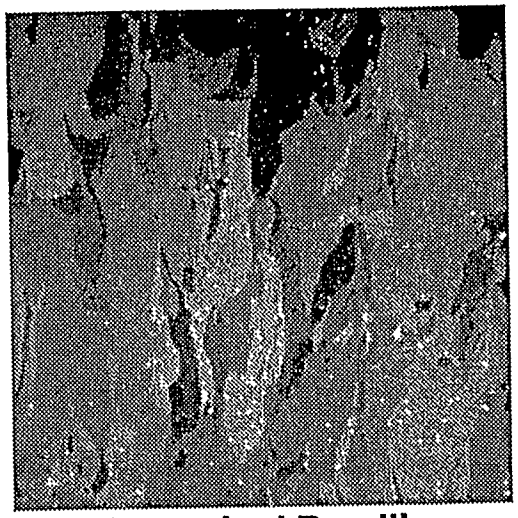

As-Deposited Beryllium
Elongated Grain Structure
(100-150 μm)

S-65B – Vacuum Hot Pressed
TShGT – Technical Purity, punched from hot pressed product
DGP – Distillation Purity, sintered hot pressed
PS-LANL-96 – VPS Beryllium - 96% T.D.
PS-LANL-98 – VPS Beryllium - 98% T.D.

Reference: V. Barabash, "Recommended Data on Be Thermochemical Properties for Plasma Facing Components"

Thermal Diffusivity: Coating - Interface - Substrate

Substrate Temperature: Started - 500°C
During - 650°C

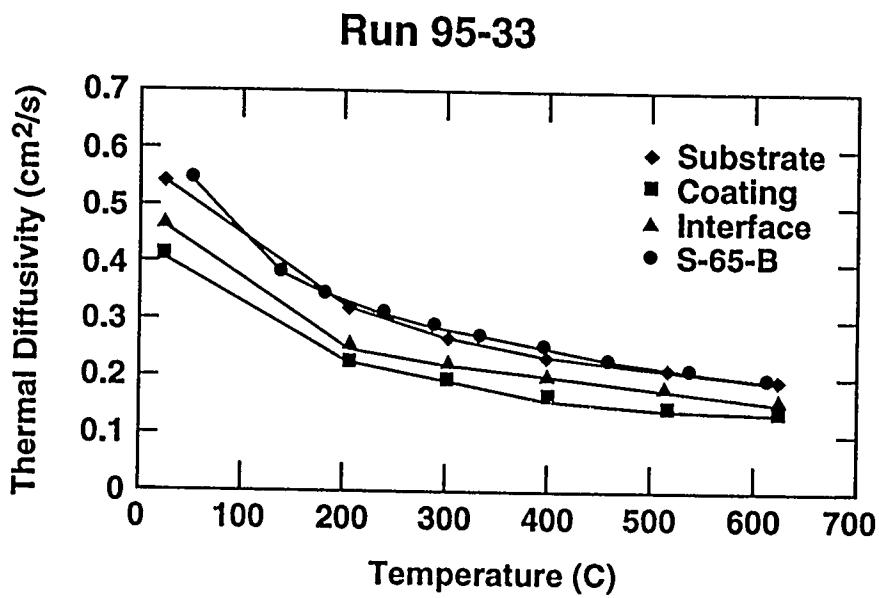

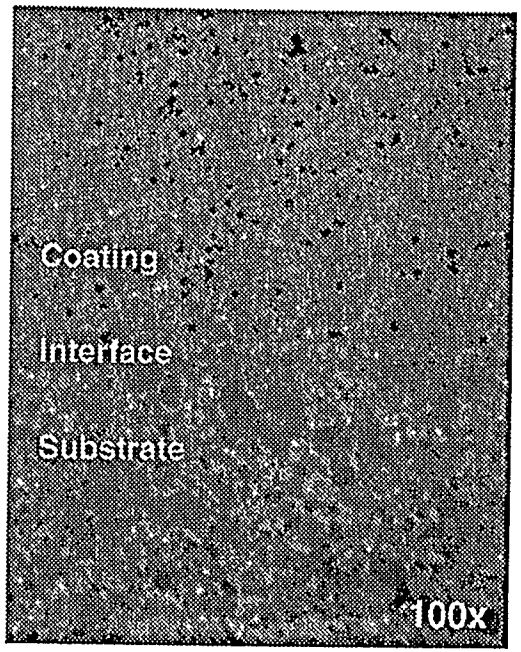

Thermal Diffusivity: Coating - Interface - Substrate

Substrate Temperature: Started - 600°C
During - 700°C

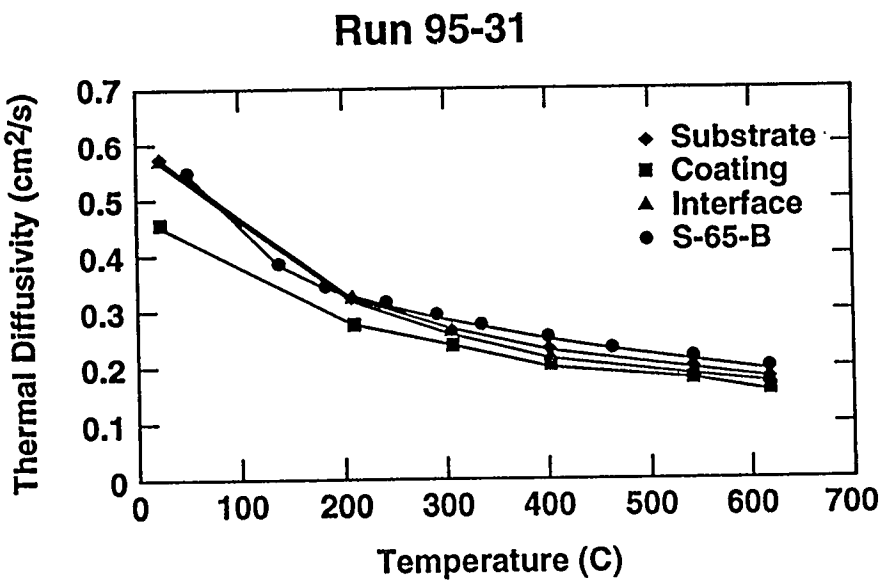

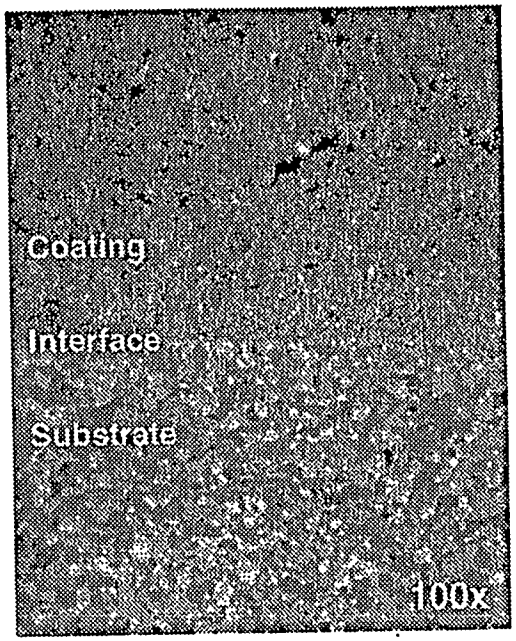

Thermal Diffusivity: Coating - Interface - Substrate

Substrate Temperature: Started - 700°C
During - 900°C

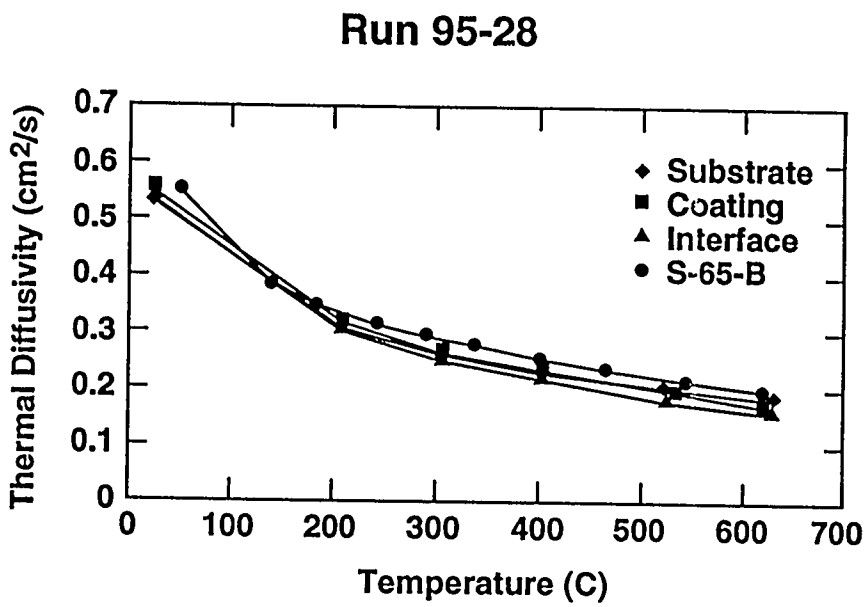

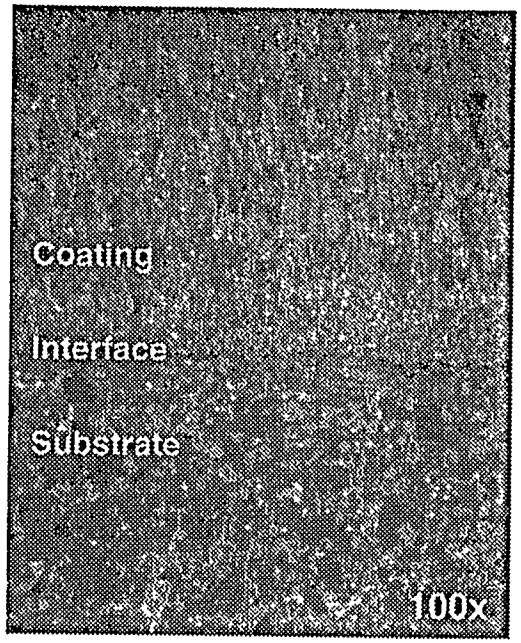

Thermal Diffusivity: Coating - Interface - Substrate

Substrate Temperature: Started - 800°C
During - 1000°C

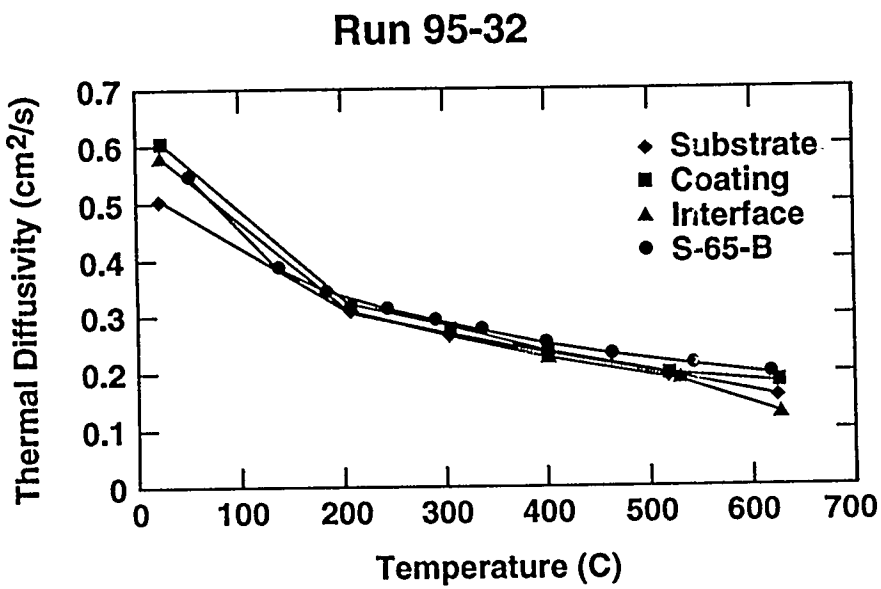

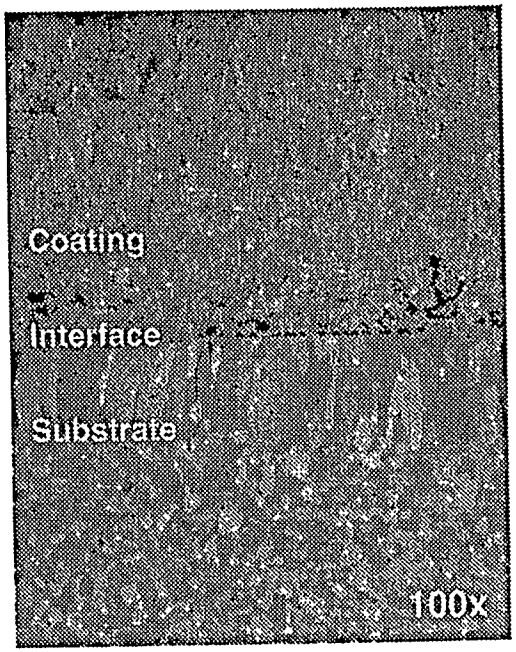

Four-Point Bend Testing of Plasma -Sprayed Be on Be

Room temperature testing
Strain rate = 5×10^{-4}

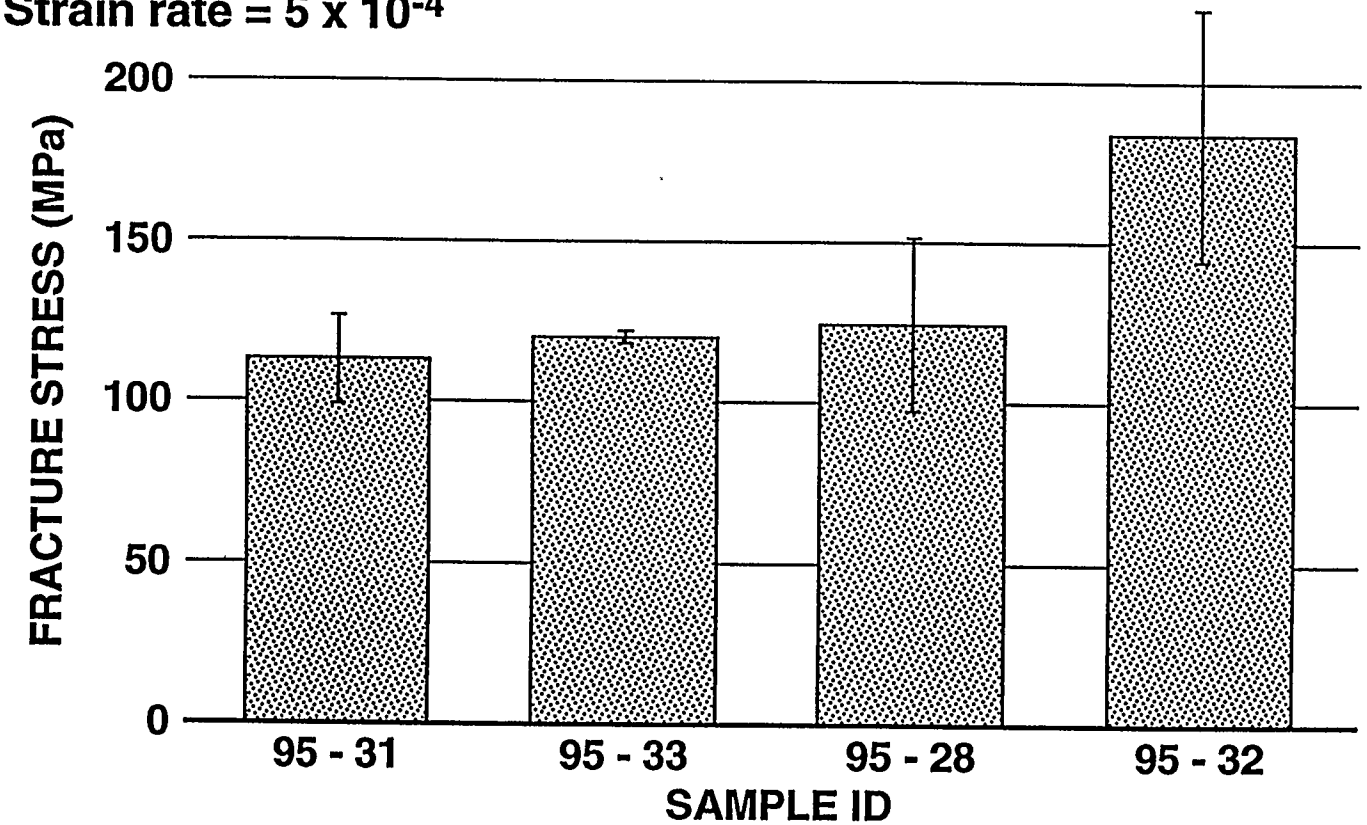

Negative Transferred-Arc Cleaning of Beryllium

- A cathodic condition is established at the substrate by applying a voltage between the plasma torch and the substrate
- Microscopic cathode arc spots form on the thin dielectric oxide layers on the surface of the material to be coated
- Electrons are emitted from the oxide films as a result of the very high electric fields at the cathode arc spots
- Melting of surface oxides results from high electric currents (10^8 A/cm^2) at arc spot

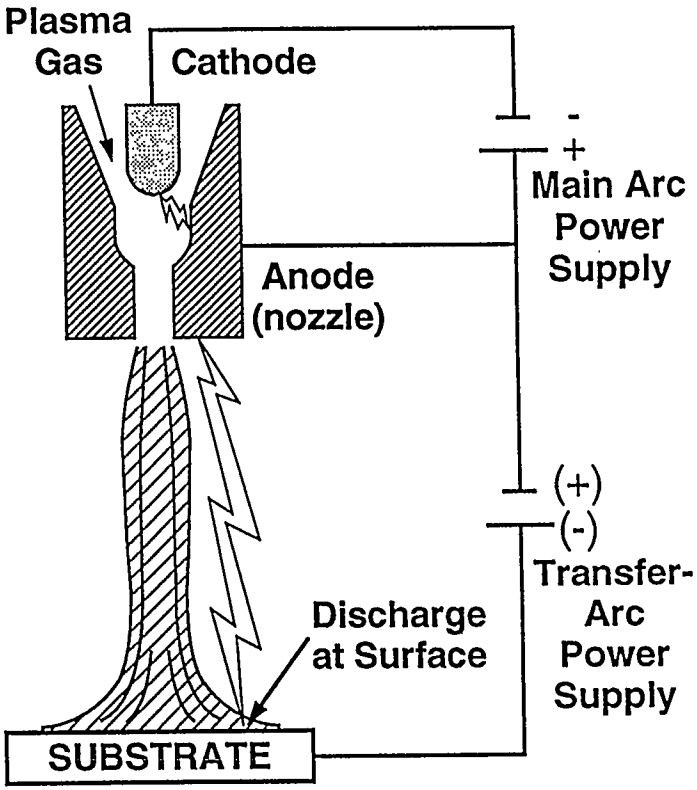

Deliverables/Major Milestones: Negative Transferred-Arc Cleaning of Beryllium

- Removed sputtered deposited carbon films from beryllium surfaces ($<10^{13}$ atoms/cm^2)
- Sputtered deposited tungsten films were reduced by an order of magnitude
- A thinner BeO layer on the surface of Be was identified (50 - 100 angstroms)
- Results were confirmed by both RBS and XPS analysis

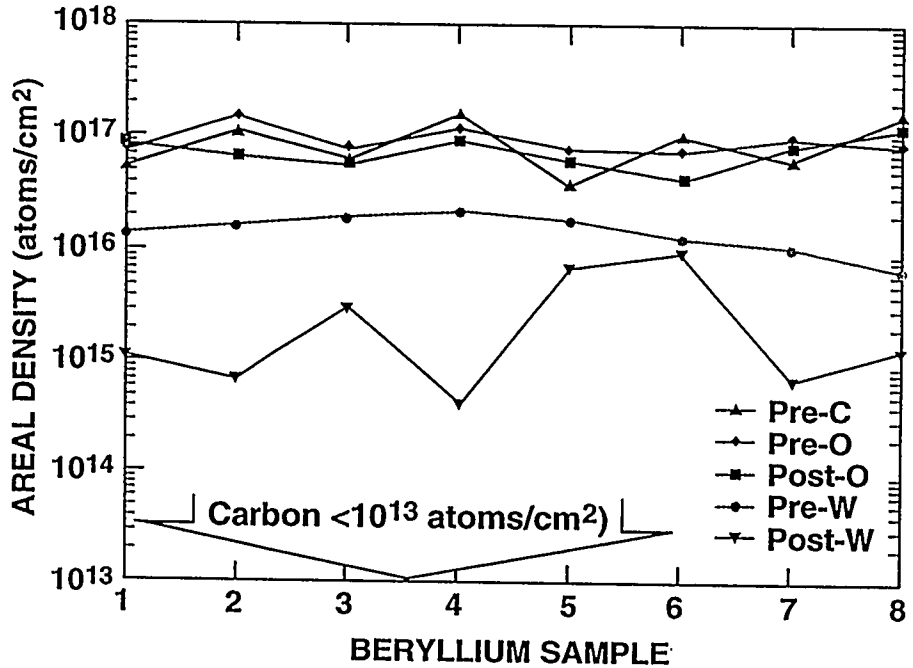

RBS Measurements of Pre and Post Cleaned Beryllium Surfaces

Transferred-Arc Cleaning of Diffusion Barrier Coatings on Copper

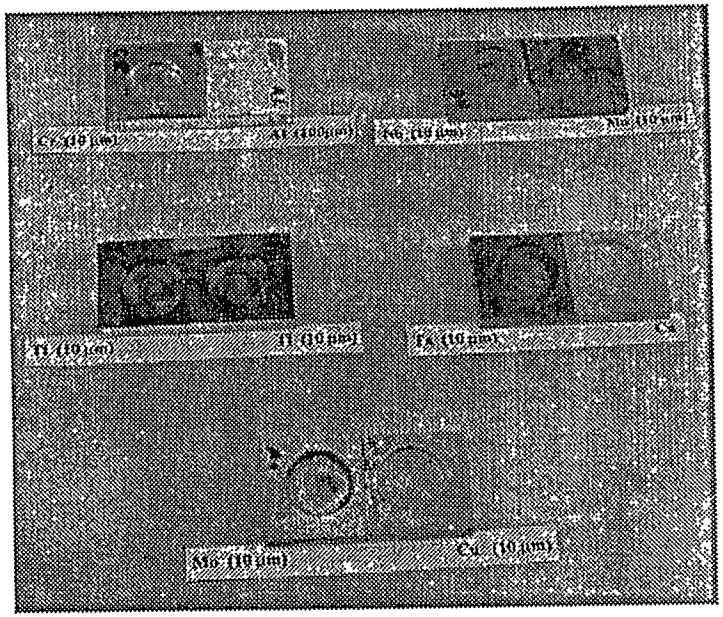

Before

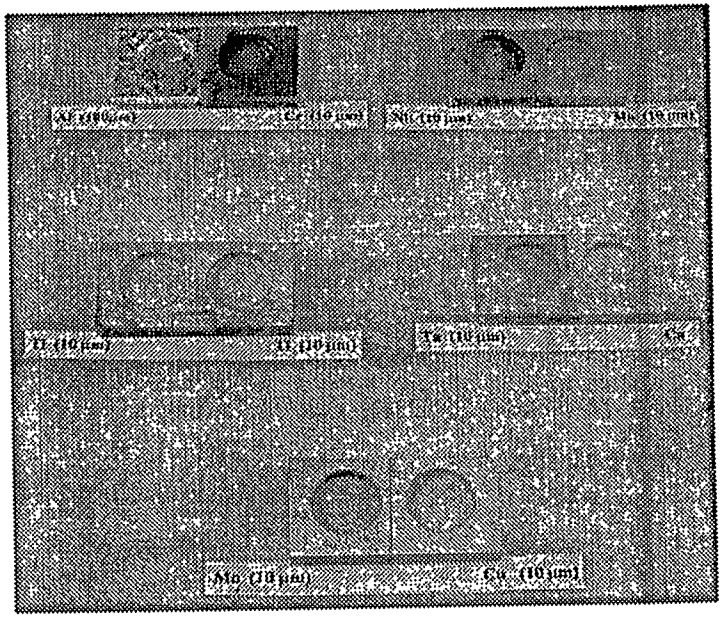

After

Repair of ISX-B Beryllium Limiter Tiles

Objective: Demonstrate the feasibility of coating and repairing beryllium plasma-facing components using plasma-spraying technology.

- Undamaged tile surfaces
- Melted and cracked tile surfaces
- Surface Contamination

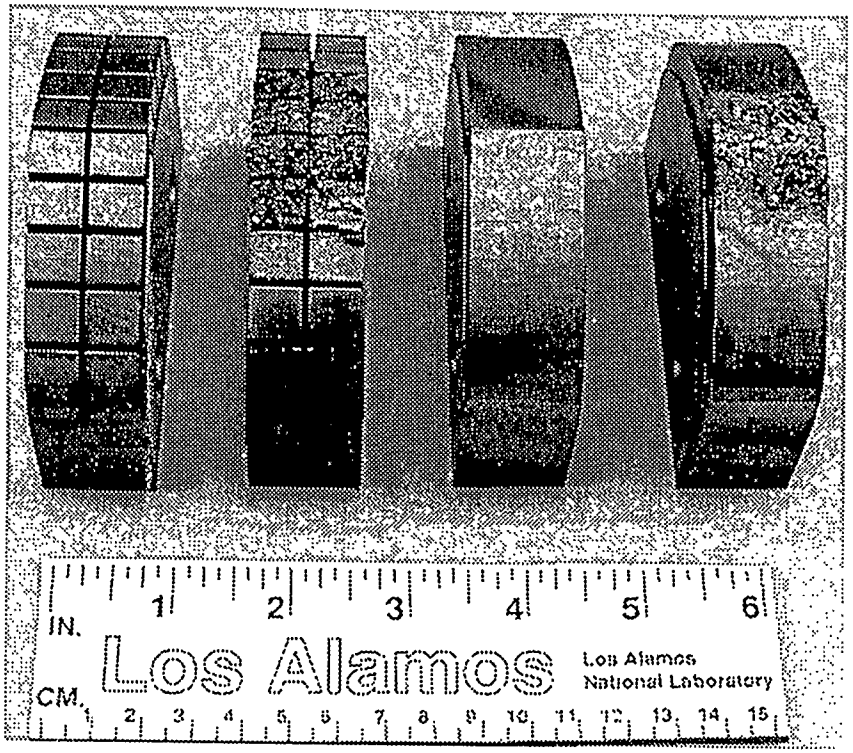

Beryllium Coating on Damaged ISX-B Beryllium Limiter Tile

- Thermal fatigue cracks propagated through the coating thickness and extended along the columnar grain boundaries in the remelted region of the damaged tile
- Coating thickness - 1.0 mm thick with approximately 10% to 12% porosity
- Coating microstructure - fine grain microstructure
- Survived 680 thermal cycles using 10 s cycle times with 60 s cool-downs at an ITER relevant heat flux slightly in excess of 5 MW/m^2

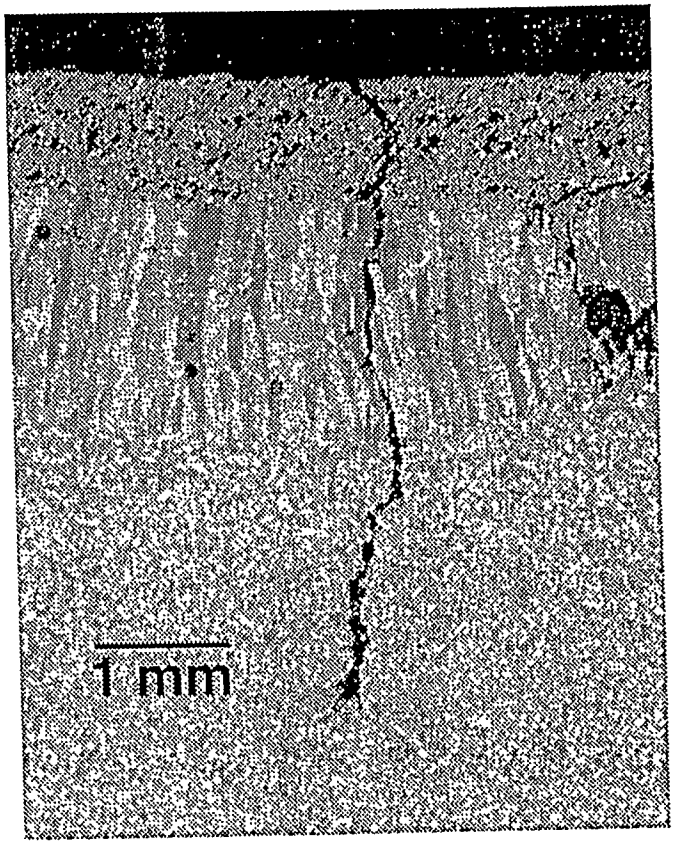

Beryllium Coating on Undamaged ISX-B Beryllium Limiter Tile

- Thermal fatigue cracks propagated through the coating thickness and extended along the coating/tile interface
- Coating thickness - 1.5 mm thick with approximately 7% porosity
- Coating microstructure - intermixed regions of columnar grains surrounded by a fine grain beryllium matrix
- Survived 80 thermal cycles using 10 s cycle times with 60 s cool-downs at an ITER relevant heat flux slightly in excess of 5 MW/m^2

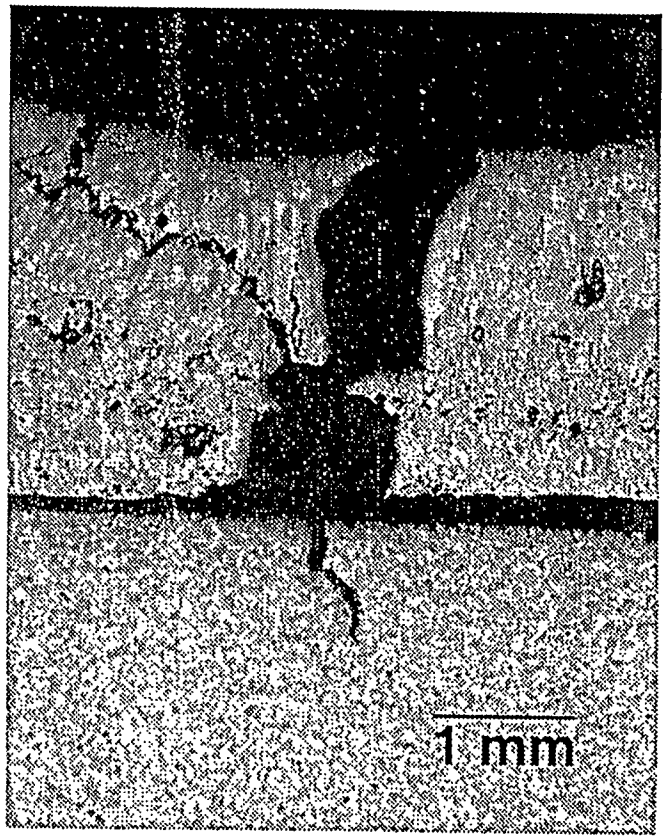

Future Activities Task 223A: Coating Technology

- Fabricate beryllium/copper armor structure by plasma spraying
  - Beryllium on copper
  - Beryllium on explosive bonded Al/Ti/Cu
  - Beryllium on diffusion barrier coatings (W, Ni, Ti, Va) produced by plasma spraying and Surmet process
  - Coat aluminum on beryllium followed by bonding experiments
  - Investigate FGM's of BeAl and Be
- Evaluate bond strength of beryllium on copper
- Coat actively cooled diverter mockup for high heat flux testing
- Provide plasma sprayed beryllium samples for thermal shock tests
- Produce samples for mechanical and thermal property measurements
- Support plasma spraying of copper on tungsten
- Continue collaboration with KFA-Judith Facility (J. Linke et al.)

U.S. Industrial Team

Tungsten Armor Materials and Tungsten - Copper Joining for ITER

U.S. - Japan Workshop on Fusion
9 January 1996

J.W. Davis
K.T. Slattery

ITER Plasma Facing Components

U.S. Industrial Team

TUNGSTEN ARMOR AND TUNGSTEN-COPPER JOINING DEVELOPMENT

INITIAL LIST	STATUS	NEXT STEP
MATERIALS		
Armor		
Wrought (sheet, bar, upset forged)	Pure & LaO_2 doped being evaluated	Thermal fatigue testing
Wrought & Recrystallized	Dropped - no ductility	
Pressed & Sintered	Dropped - poor availability & no ductility	
Infiltrated	Mg & Li infiltrants with Cu baseline	Thermal shock testing
Plasma Sprayed	Demonstration of existing technology	Fabrication of EBTS mock-up
Functionally Graded Materials		
HIP Powder	Layers HIPped between W and Cu	Diffusion bond & mechanical test
Liquid Phase Sintered	Fabrication of individual layers demonstrated	Diffusion bond & mechanical test
Plasma Sprayed	Application of related technologies to ITER	Fabrication of EBTS mock-up
JOINING		
Roll Bonding	Dropped - intitial studies unsuccessful	
Brazing	Research being performed by RF, JA	
Diffusion Bonding	Variety of options being pursued	Fabrication of mechanical test joints
Explosion Bonding	Suspended due to budget cuts	
Plasma Spraying	Demonstration of existing technology	Fabrication of EBTS mock-up

ITER Plasma Facing Components

U.S. Industrial Team

CONTRIBUTORS

- SANDIA NATIONAL LABS - NEW MEXICO
  - M. Ulrickson, R. Watson
- SANDIA NATIONAL LABS - CALIFORNIA
  - W. Bonivert, C. Cadden, B. Odegard
- LOS ALAMOS NATIONAL LABS
  - R. Castro
- ARGONNE NATIONAL LABORATORY
  - D. Smith
- MCDONNELL DOUGLAS AEROSPACE
  - J. Davis, D. Deuser, D. Driemeyer, D. Lederich, K. Slattery, J. Wille
- UNIVERSITY OF ILLINOIS
  - J. Shang
- SURMET CORPORATION
  - S. Sastri

ITER Plasma Facing Components

U.S. Industrial Team

CRITICAL ISSUES

- COEFFICIENT OF THERMAL EXPANSION (CTE) MISMATCH BETWEEN COPPER AND TUNGSTEN
- THERMAL STRAINS DUE TO DISRUPTIONS
- DUCTILE-BRITTLE TRANSITION TEMPERATURE (DBTT) - STRAIN RATE SENSITIVITY

ITER Plasma Facing Components

POTENTIAL SOLUTIONS

U.S. Industrial Team

- COEFFICIENT OF THERMAL EXPANSION MISMATCH
  - FUNCTIONALLY GRADED TRANSITION*
  - LOW TEMPERATURE BONDING*
- THERMAL STRESS
  - FUNCTIONALLY GRADED TRANSITION*
  - TRANSPIRATION COOLING*
  - THIN SECTIONS OF PURE TUNGSTEN
  - REDUCED TEMPERATURE JOINING TO Cu
- DUCTILE-BRITTLE TRANSITION TEMPERATURE
  - COLD WORKING (WROUGHT TUNGSTEN)*
  - DOPED TUNGSTEN (TiO_2, La_2O_3)

* Being Worked on by U.S

ITER Plasma Facing Components

TUNGSTEN ARMOR FORM ISSUES

U.S. Industrial Team

- SHEET
  - NONPOROUS/FULLY DENSE
  - SOME DUCTILITY AT LOW TEMPERATURES
  - ELONGATED MICROSTRUCTURE
  - CONTROLLED THICKNESS WITHOUT MACHINING OR GRINDING
  - NO FURTHER PROCESSING OF ARMOR REQUIRED
  - LOWER DBTT THAN PRESSED AND SINTERED MATERIAL
- BAR - SAME AS SHEET EXCEPT:
  - SAME PROPERTIES OF SHEET WITH GRAIN DIRECTION PARALLEL TO HEAT FLUX
  - CUT TO THICKNESS
- UPSET FORGED - SAME AS BAR WITH EQUIAXED MICROSTRUCTURE

ITER Plasma Facing Components

DBTT OF TUNGSTEN CAN BE AFFECTED BY SEVERAL VARIABLES

U.S. Industrial Team

- GRAIN SIZE
- COLD WORK
- PURITY
- RADIATION

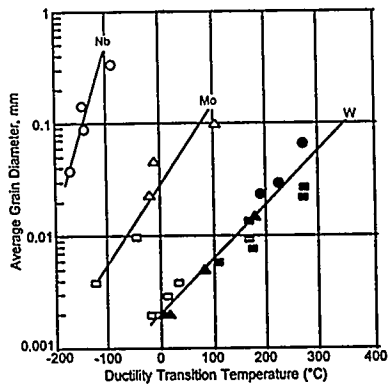

ITER Plasma Facing Components

ARMOR FORMS (CONTINUED)

U.S. Industrial Team

- SINTERED POWDER
  - LOW COST RAW MATERIAL
  - HIGHER DUCTILE-BRITTLE TRANSITION TEMPERATURE
  - EQUIAXED MICROSTRUCTURE
  - TYPICAL DENSITY 92% - 94% OF THEORETICAL
- PLASMA SPRAYED
  - EXISTING TECHNOLOGY
  - LOW COST RAW MATERIAL
  - SLOWEST PROCESSING
  - POROSITY CONTENT AND CONTROL AN ISSUE
  - OXIDE CONTENT AND CONTROL AND ISSUE
  - HIGH PRE-HEATING OF SUBSTRATE REQUIRED
  - POTENTIAL FOR ONE-STEP PROCESSING, REPAIR METHOD
  - GRAIN SIZE AND DBTT DIFFICULT TO CONTROL IN THICK SECTIONS

ITER Plasma Facing Components

ARMOR FORMS (CONCLUDED)

U.S. Industrial Team

- INFILTRATED
  - TRANSPIRATION COOLING
  - 'OFF THE SHELF' TECHNOLOGY (copper and silver infiltration)
  - POTENTIAL FOR GRADED LAYER INCORPORATION
  - COPPER INFILTRATED HAS HIGHEST THERMAL CONDUCTIVITY
  - LOOKING AT OTHER INFILTRANTS (Li, Mg, Li-Mg alloy)

ITER Plasma Facing Components

INFILTRANTS ARE UNIFORMLY DISTRIBUTED THROUGH MICROSTRUCTURE

U.S. Industrial Team

- POROSITY IS INTERCONNECTED
- SYSTEM WILL PUMP INFILTRANT
- LIFETIME CONTROLLED BY RESERVOIR OF INFILTRANT

W-Ag

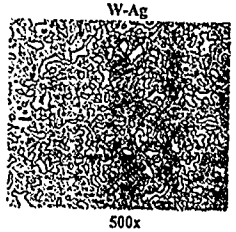

500x
Dark Area - Tungsten
White Area - Silver

W-Cu

500x
Continuous Area - Tungsten
Dispersed Area - Copper

LITHIUM OR MAGNESIUM ARE POTENTIAL LOW Z INFILTRANTS

ITER Plasma Facing Components

EVAPORATION HEAT LOSS

U.S. Industrial Team

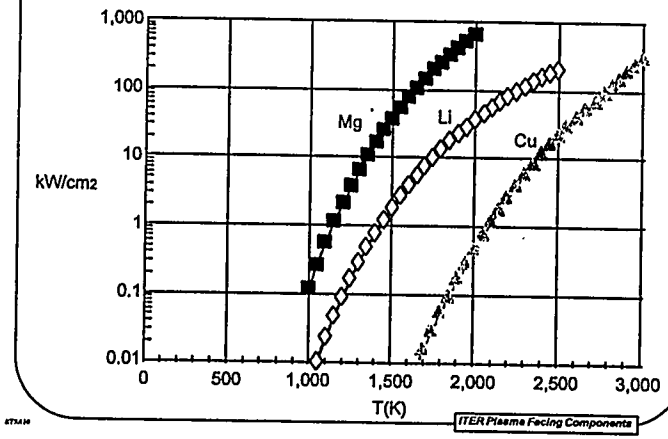

ITER Plasma Facing Components

BONDING METHOD

U.S. Industrial Team

- ROLL BONDING
  - DIRECT W-Cu BONDS
  - HIGH OUTPUT POTENTIAL
- BRAZING
  - PRODUCE W-Cu JOINT USING OTHER METHODS AND UTILIZE METHODS DEVELOPED UNDER Cu-Cu BRAZING STUDIES
- LIQUID PHASE SINTERING
  - METHOD OF FABRICATING GRADED LAYER
  - BRAZE OR DIFFUSION BOND TO Cu SUBSTRATE
- DIFFUSION BONDING (HOT PRESSING, HIP)
  - JOIN W (SINTERED, SHEET, OR INFILTRATED) TO GRADED POWDER LAYERS AND Cu WHILE COMPACTING LAYER
  - POTENTIAL FOR 1-STEP FABRICATION
- EXPLOSION BONDING
  - LOW COST JOINING METHOD
  - SOME EXISTING TECHNOLOGY AVAILABLE

ITER Plasma Facing Components

DEVELOPMENT COMBINATIONS

U.S. Industrial Team

- LIQUID PHASE SINTERING
  - DIFFUSION BOND WROUGHT W TO SERIES OF PRE-SINTERED FULL-DENSITY GRADED LAYERS
- PLASMA SPRAYED
  - SPRAY GRADED LAYER AND ARMOR
  - SPRAY GRADED LAYER TO WROUGHT W ARMOR
    - HIP TO FULL DENSIFICATION
    - LOW TEMPERATURE DIFFUSION BOND TO HEAT SINK
- POWDER HIPPING
  - W AND SERIES OF Cu/W GRADED LAYERS
    - HIGH TEMPERATURE HIP TO FULL DENSITY
    - LOW TEMPERATURE DIFFUSION BOND TO HEAT SINK
  - W TO SERIES OF TAPE CAST OR PRESSED POWDER GRADED LAYERS AND HEAT SINK - SINGLE HIP OPERATION

ITER Plasma Facing Components

TUNGSTEN - COPPER JOINING

U.S. Industrial Team

- ROLL BONDING
- DIFFUSION BONDING
- GRADED LAYERS
  - SOLID HOT ISOSTATICALLY PRESSED (HIP)
  - LIQUID PHASE SINTERES
  - PLASMA-SPRAYED FUNCTIONALLY GRADED MATERIAL
- EXPLOSION BONDING
- EBTS MOCK-UP PLANS

ITER Plasma Facing Components

THERMAL FATIGUE AND THERMAL SHOCK EVALUATION

U.S. Industrial Team

GRADE	PRODUCT FORM	DIMENSIONS (mm)			THERMAL FATIGUE		THERMAL SHOCK	SPARE
		Length	Width	Thickness	Flat	Edge		
Pure	CR Bar	25 25	25 25	5 10	2 2	2 2		1 1
Pure	Upset Forged	25 25	25 25	5 10	2 2	2 2		1 1
Pure	CR Sheet	25 25	25 25	5 10	2 2	2 2		1 1
Lanthanated	CR Bar	25 25	25 25	5 10	2 2	2 2		1 1
Lanthanated	Upset Forged	25 25	25 25	5 10	2 2	2 2		1 1
Cu	Infil	25 25	25 25	5 10	1 1	1 1	1 1	1 1
Li	Infil	19 dia	19 dia	10			1	
Mg	Infil	19 dia 19 dia	19 dia 19 dia	5 10	1 1	1 1	1 1	1 1

Product Forms:
CR Sheet - Cold-Rolled and Stress-Relieved Sheet - Grain orientation perpendicular to thickness
CR Sheet - Cold-Rolled and Stress-Relieved Sheet - Grain orientation parallel to thickness
Upset Forged - Upset forged material - Grain orientation roughly equiaxed.
Infil - Cu, Mg, or Li infiltrated 74% dense W

ITER Plasma Facing Components

ROLL BONDING

U.S. Industrial Team

Trial #	ACTIVATION LAYER				DIFFUSION BONDING						ROLL BONDING				RESULT
	Alloy	Application	Time		Pre/Post Roll	Temp	Press	Envir	Time		Temp	Red/Pass	# Pass	Tot Red	
IB-1	Ti	PVD	2000A		Bending Only	450°C	150MPa	LaVac	1 hr						debonded
IB-2	Ti	PVD	2000A		Bending Only	450°C	75MPa	LaVac	1 hr						20MPa
IB-3	Ti	PVD	2000A		Bending Only	450°C	80MPa	LaVac	1 hr						14MPa
HR-1	Ti	PVD	2000A								550C	2.5%	10	25.0%	debond
HR-2	Ti	PVD	2000A								550C	2.9%	7	20.0%	debond
HR-3	Ti	PVD	2000A								550C	20.0%	1	20.0%	debond
HR-4	Ti	PVD	2000A								550C	2.9%	7	20.0%	OK
CR-1	Ti	PVD	2000A								RT	2.5%	1	2.5%	debond
CR-2	Co	PVD	2000A								RT	2.5%	1	2.5%	debond
CR-3	Ni	PVD	2000A								RT	2.5%	1	2.5%	debond
CR-4	none	N.A.	N.A.								RT	2.5%	1	2.5%	debond
SC-1	Ti	PVD	2000A		Pre-rolling	450°C	75MPa	LaVac	1 hr		550°C	2.5%	8	20.0%	OK
SC-2	Co	PVD	2000A		Pre-rolling	450°C	75MPa	LaVac	1 hr		550°C	2.5%	1	2.5%	partial
SC-3	Ni	PVD	2000A		Pre-rolling	450°C	75MPa	LaVac	1 hr		550°C	2.5%	1	2.5%	partial
SC-4	none	N.A.	N.A.		Pre-rolling	450°C	75MPa	LaVac	1 hr		550°C	2.5%	1	2.5%	no bonding
HTR-1	Ti	PVD	2000A		Pre-rolling	450°C	75MPa	LaVac	1 hr		550C	2.5%	8	20.0%	33MPa
HTR-2	Ti	PVD	2000A		Pre-rolling	450°C	75MPa	LaVac	1 hr		650C	2.5%	4	10.0%	debond
HTR-3	Ti	PVD	2000A		Pre-rolling	450°C	75MPa	LaVac	1 hr		750C	2.5%	1	2.5%	debond
Best	Ti	PVD	2000A		Pre-Rolling	450C	75MPa	LaVac	1 hrs		550C	20.0%	1	20.0%	33MPa

Copper Alloy: UNS 11100, 1.5mm to 4.5mm thick, polished
Tungsten Alloy: Commercially pure sheet, 0.5mm thick, polished and etched in HF

Study Abbreviations:
IB - Initial Bonding
HR - Hot Rolling
CR - Cold Rolling
SC - Surface Coating
HTR - High Temperature Rolling

- CONCLUSIONS:
  - ROLL BONDING GAVE LITTLE IMPROVEMENT IN PROPERTIES
  - PURSUE DIFFUSION BONDING AT HIGHER TEMPERATURES

ITER Plasma Facing Components

DIFFUSION BONDING

U.S. Industrial Team

- TENSILE TESTS AT 350°C

MATERIAL		INTERLAYER	TEST			Strength (MPa)	
Cu	W		Type	Temp (°C)	Spec I.D.	Indiv.	Avg
Hycon	1.5mm 89% P&S	Ni	tensile	350	101A-1 101A-2 101A-3	19** [redacted]	20
Hycon	1.5mm 89% P&S	Ti	tensile	350	102A-1 102A-2 102A-3		
Hycon	0.5mm CR & SR	Ni	tensile	350	101B-1 101B-2 101B-3	[redacted]	2.7
Hycon	0.5mm CR & SR	Ti	tensile	350	102B-1 102B-2 102B-3	1.6** [redacted]	1.2

** Failure initiated at interface and grew in tungsten (evidence of pre-cracking)

[redacted] Failure initiated and grew in tungsten

[redacted] Tensile specimens not available for test (broke during machining)

* Specimen broke during installation into test fixture

Metallographic specimens also taken from each section

ITER Plasma Facing Components

W - Cu GRADED LAYERS

U.S. Industrial Team

- BASELINE DESIGN:
  - 2mm THICK
  - 4 LAYERS WITH 20% TRANSITION
- PROCESSING METHODS:
  - SOLID HIP
  - LIQUID-PHASE SINTERED
  - PLASMA SPRAYED
- FLEXIBLE DESIGN/PROCESSING
- EVALUATION:
  - 4-POINT BENDING AND TORSIONAL SHEAR
  - HIGH HEAT FLUX

GRADED LAYER

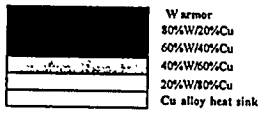

Graded composition of Cu and W (high W near W armor & high Cu alloy near Cu heat sink)

ITER Plasma Facing Components

DIFFUSION BONDING

U.S. Industrial Team

- CONCLUSIONS
  - DUE TO FAILURE IN W, RESULTS INCONCLUSIVE
  - OTHER TUNGSTEN PRODUCT FORM DESIREABLE FOR TENSILE SPECIMENT - WILL USE ROLLED BAR WITH GRAIN ORIENTATION IN TENSILE DIRECTION
  - NEED FOR REPEAT TESTS
- LOOK AT DIRECT APPLICATION OF Cu TO W
  - PLASMA VAPOR DEPOSITION
  - ELECTROPLATING
  - CASTING OF THIN

ITER Plasma Facing Components

HOT ISOSTATIC PRESSING DEVELOPMENT

U.S. Industrial Team

- UTILIZE HOT ISOSTATIC PRESSING (HIP) TO DENSIFY MIXTURE
- DETERMINE HIP PARAMETERS
- MIXTURE OF W POWDER SIZES FOR HIGH W CONTENT LAYERS
- HOMOGENEOUS AND GRADED CHARGES
- DETERMINE DENSITY
- METALLOGRAPHY
- COLD-PRESS GRADED PREFORMS

ITER Plasma Facing Components

INITIAL HIP MATRIX

U.S. Industrial Team

%Cu	%W	W Particle Size (microns)			
				88% large	70% large
100	0	N.A.			
80	20	70			
60	40	70			
40	60	70	10		
30	70	70	10	70 & 10	
20	80	70		70 & 10	70 & 10

Used to make four layer graded specimen

Total number of specimens per HIP run: 12

Temperatures Evaluated (°C)	600	800	1000
T/Tm for Cu:	0.64	0.79	0.94
T/Tm for W:	0.24	0.29	0.35

- Pressure Evaluated: 105MPa (15ksi)
- Time and Temperature: 15min, 60min, 240min, 960min
- Heat-up Rate: 20°C/min with 15min hold
- Total Number of HIP Runs: 12
- Total Number of Specimens: 144

ITER Plasma Facing Components

RESULTS

U.S. Industrial Team

- 80% W - BINARY AND TERNARY W MIXTURES

SPEC #	PRESSURE (MPa)		Tmax (°C)	TIME (min)	VOLUME %				THEO DENSITY (g/cc)	DENSITY (g/cc)	% THEO
	Cold	Hot			Cu	70μ W	10μ W	1μ W			
8113	75.7	105	1000	240	19.9%	52.6%	17.1%	10.5%	17.24	15.89	92.1%
8213	75.7	105	1000	240	20.1%	58.7%	21.3%	0.0%	17.23	15.71	91.2%
8313	75.7	105	1000	240	20.1%	58.8%	0.0%	21.1%	17.22	15.74	91.4%
8413	75.7	105	1000	240	19.9%	56.1%	0.0%	24.0%	17.24	15.87	92.1%
8114	75.7	105	1000	960	19.8%	52.5%	17.2%	10.5%	17.25	16.22	94.0%
8214	75.7	105	1000	960	20.1%	58.7%	0.0%	21.2%	17.22	16.14	93.7%
8314	75.7	105	1000	960	19.9%	58.8%	0.0%	21.3%	17.24	16.24	94.2%
8414	75.7	105	1000	960	20.0%	55.9%	0.0%	24.1%	17.23	16.29	94.5%

ITER Plasma Facing Components

RESULTS

U.S. Industrial Team

- MINIMUM PARAMETERS TABLE - UNITARY AND BINARY W MIXTURES

SPEC #	PRESSURE (MPa)		Tmax (°C)	TIME (min)	VOLUME %			THEO DENSITY (g/cc)	DENSITY (g/cc)	% THEO
	Cold	Hot			Cu	70μ W	10μ W			
008	75.7	105	800	15	100.0%	0.0%	0.0%	8.96	9.21	102.8%
207	75.7	105	800	60	80.0%	20.0%	0.0%	11.03	11.33	102.7%
210	75.7	105	800	240	80.0%	20.0%	0.0%	11.03	11.31	102.5%
411	75.7	105	800	15	60.1%	39.9%	0.0%	13.09	13.23	101.1%
805	75.7	105	800	960	39.9%	60.1%	0.0%	15.17	15.41	101.6%
835	75.7	105	800	240	40.1%	0.0%	59.9%	15.16	15.14	99.9%
705	75.7	105	800	960	30.0%	70.0%	0.0%	16.20	16.34	100.9%
733	75.7	105	1000	60	30.0%	0.0%	70.0%	16.20	16.18	99.9%
735	75.7	105	800	960	29.9%	0.0%	70.1%	16.21	16.46	101.6%
761	75.7	105	1000	240	29.9%	61.6%	8.5%	16.21	15.88	98.0%
765	75.7	105	800	960	30.1%	61.6%	8.3%	16.18	15.88	98.2%
805	75.7	105	800	960	20.0%	80.0%	0.0%	17.23	15.55	90.3%
885	75.7	105	800	960	19.8%	56.2%	24.0%	17.25	16.12	93.4%

ITER Plasma Facing Components

GRADED LAYER DEMONSTRATION

U.S. Industrial Team

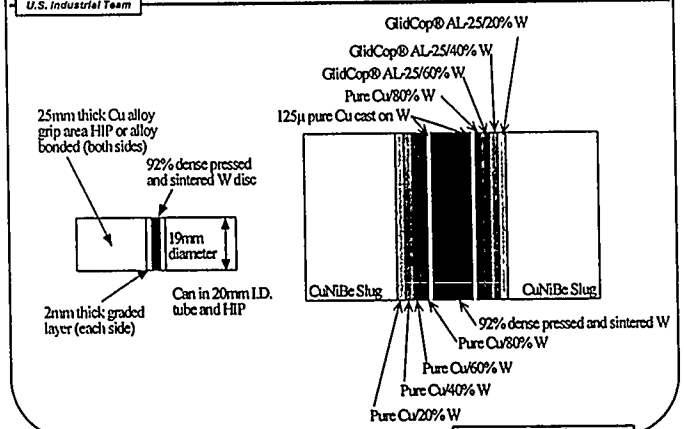

ITER Plasma Facing Components

COPPER - TUNGSTEN HIPPED GRADED LAYER

U.S. Industrial Team

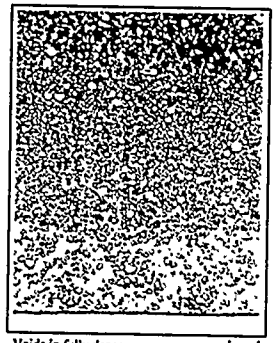

80% W (porous)

60% W (fully dense)

40% W (fully dense)

20% W (fully dense)

Unbond due to improper cleaning

CuNiBe Slug

Voids in fully dense regions due to pull-out

200μ

PROCESSING
1000°C
105MPa
960min

Cu POWDER: SCM HGS (40μ)
W POWDER: Kulite KSP (70μ)
Kulite KMP-110 (10μ)

ITER Plasma Facing Components

COPPER - TUNGSTEN HIPPED GRADED LAYER
INTERFACE WITH COPPER COATED TUNGSTEN

U.S. Industrial Team

PROCESSING
1000°C
105MPa
960min

Cu POWDER: SCM HGS (40μ)
W POWDER: Kulite KSP (70μ)
Kulite KMP-110 (10μ)

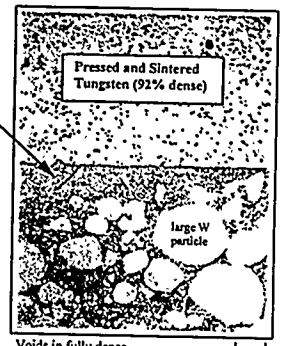

80% W (fully dense in region next to Cu coating due to infiltration by Cu from coating)

Voids in fully dense regions due to pull-out

25μ

ITER Plasma Facing Components

COPPER - TUNGSTEN HIPPED GRADED LAYER
WITH GLIDCOP ® AL-25 COPPER POWDER

U.S. Industrial Team

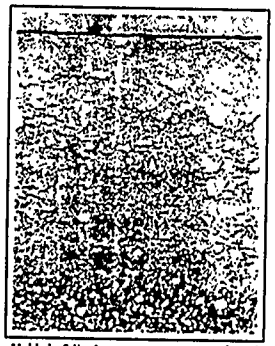

CuNiBe Slug

Unbond due to improper cleaning

20% W (fully dense)

40% W (fully dense)

60% W (fully dense)

80% W (porous)

Voids in fully dense regions due to pull-out

200μ

PROCESSING
1000°C
105MPa
960min

20% - 60% W:
Cu POWDER: SCM GlidCop® AL-25 (170μ)
W POWDER: Kulite KMP-101 (1.3μ)

80% W:
Cu POWDER: SCM HGS (40μ)
W POWDER: Kulite KSP (70μ)
Kulite KMP-110 (10μ)

ITER Plasma Facing Components

LIQUID PHASE SINTERING

U.S. Industrial Team

- SMALLER POWDERS USED TO IMPROVE DENSIFICATION
  - TUNGSTEN: 0.3μ AND 1.0μ
  - COPPER: 30μ
- 50mm x 50mm PIECES FABRICATED
- 20, 40 AND 60 VOLUME % W FULLY DENSIFIED
- MAXIMUM TUNGSTEN CONTENT TO FULLY DENSIFY
  - 72 VOLUME %
  - ACHIEVED USING 0.35% Co
- WILL BE JOINED TO W AND Cu USING DIFFUSION BONDING

ITER Plasma Facing Components

EBTS MOCK-UPS

U.S. Industrial Team

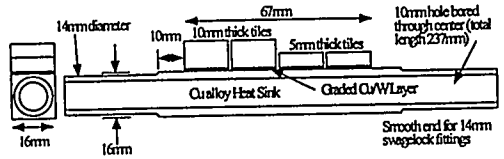

NAME	ARMOR	HEAT SINK	OTHER LAYERS	ATTACHMENT METHOD	DATE AVAIL
PW-1	W bar	Hycon	1mm cast Cu	450°C HIP DB	29-Mar-96
PW-2	W bar	GlidCop Al-25	Cu/W graded layer, Cu deposit on W	450°C - 1000°C HIP DB	29-Mar-96
PW-5	PS W	TBD	PS Cu/W graded layer	Plasma spray & HIP	30-Aug-96

ITER Plasma Facing Components

MECHANICAL TESTING OF GRADED LAYERS

U.S. Industrial Team

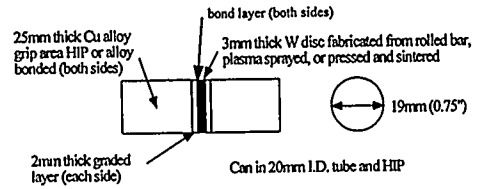

4 Point Bend or Torsional Shear: EDM out four (4) 6 ± 0.1 mm x 6 ± 0.1mm specimens and test.

Offal piece for metallography

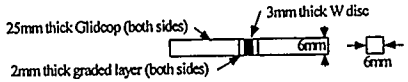

ITER Plasma Facing Components

MECHANICAL TESTING OF GRADED LAYERS

U.S. Industrial Team

- FABRICATE INITIAL MECHANICAL TEST SPECIMENS
  - VARIETY OF JOINTS AND LAYERS
  - 1 HIPPED JOINT, 4 SPECIMENS, 3 TESTS
  - 350°C TEST TEMPERATURE
  - COMPLETE BY 12-FEB-96
- EVALUATE FABRICATION AND PROPERTIES FOR BEST APPROACH
- FOLLOW-UP TESTING:
  - FURTHER 4-POINT BENDING TESTING
    - STATISTICAL SIGNIFICANCE
    - PROCESSING VARIABILITY EFFECTS
    - OTHER TEMPERATURES (150°C, 600°C)
  - TORSIONAL SHEAR
  - EBTS MOCK-UPS
  - IRRADIATION TESTING
  - VERIFY FOR HEAT SINK (Cu) AND ARMOR (W) MATERIALS

ITER Plasma Facing Components

TEST MATRIX

U.S. Industrial Team

GRADING	MATERIAL				TEST		
	Cu Grip	Cu Powder	W	Bond	Type	Temp (°C)	# of Tests
LPS	AL-25	pure	CR & SR bar	PVD Cu	4-point	350	3
LPS	AL-25	pure	CR & SR bar	Cu-ABA	4-point	350	3
LPS	AL-25	pure	CR & SR bar	Ni	4-point	350	3
HIP powder	AL-25	pure	CR & SR bar	PVD Cu	4-point	350	3
HIP powder	AL-25	pure	CR & SR bar	Cu-ABA	4-point	350	3
HIP powder	AL-25	pure	CR & SR bar	Elec Cu	4-point	350	3
HIP powder	AL-25	pure	CR & SR bar	Cu-Mn	4-point	350	3
HIP powder	AL-25	pure	CR & SR bar	Cu-Ti	4-point	350	3
HIP Powder	AL-25	pure	CR & SR bar	PS Cu	4-point	350	3
HIP powder	AL-25	AL-25	CR & SR bar	PS Cu	4-point	350	3
						Total	30

ITER Plasma Facing Components

PLASMA SPRAYING

U.S. Industrial Team

- ITER POTENTIAL:
  - REPAIR OF DAMAGED COMPONENTS
  - ONE STEP APPLICATION OF GRADED LAYER TO W TILE
- TECHNIQUES
  - PRODUCTION - SPRAY AND HIP TO FULL DENSITY
  - REPAIR - SPRAY ONLY
- EBTS MOCK-UPS AND MATERIAL EVALUATION COUPONS
- STATUS: ABILITY TO SPRAY GRADED LAYER DEMONSTRATED

ITER Plasma Facing Components

CONCLUSIONS/STATUS

U.S. Industrial Team

- TUNGSTEN PRODUCT FORMS
  - LARGE VARIETY PROVIDES FLEXIBILITY OF PROPERTIES
  - THERMAL FATIGUE TESTING WILL SELECT FORM
- TUNGSTEN-COPPER JOINING
  - VIABILITY OF DIFFUSION BONDING TO BE DEMONSTRATED SHORTLY
  - CLEANING OF SURFACES IMPORTANT
  - USE OF GRADED (W/Cu) LAYER vs COMPLIANT (pure Cu) LAYER WILL BE DETERMINED BY THERMAL FATIGUE (EBTS) TESTING
  - GRADED LAYER FORM WILL BE DETERMINED BY COST CONSIDERATIONS
  - PLASMA SPRAY BEST OPTION FOR REPAIR, SERVICE LIFE NEEDS TO BE DETERMINED

ITER Plasma Facing Components

US-Japan Workshop Q219 - HHFC and PSI for Next Fusion Devices

ITER

Task T-222: Manufacturing and Testing of Permanent Components

T-222 R&D Activities

Dennis L. Youchison

January 09, 1996
Colorado Springs, CO

Sandia National Laboratories

Task T-222: Manufacturing and Testing of Permanent Components

OUTLINE

I. The 1996 US Program for T-222

II. 1996 T-222 Objectives

III. Status of T-222.4 and T-222.5

IV. HHF Testing of Medium-scale Mock-ups

V. Synopsis

Sandia National Laboratories

Overview: How does T-222 fit into ITER?

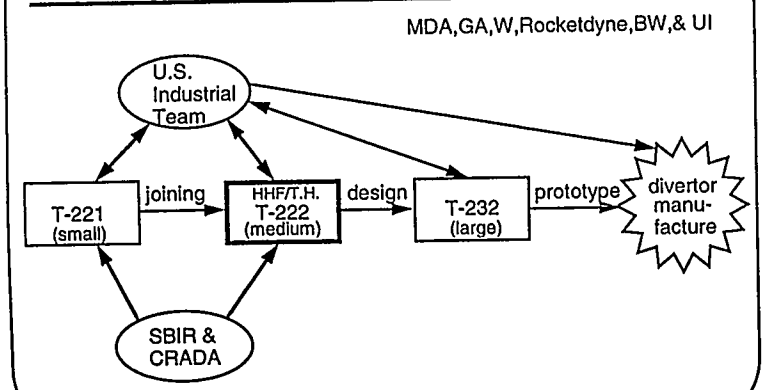

Sandia National Laboratories

T-222 Sub-Tasks

T-222.1	Be/Cu Medium-scale Mock-ups
T-222.2	W/Cu Medium-scale Mock-ups
(T-222.3)	(CFC/Cu Medium-scale HHF Tests)
T-222.4	Critical Heat Flux Tests
T-222.5	NDE Techniques

Sandia National Laboratories

U.S. has many T-222 objectives in 1996.

Complete HHF tests of MDA ribbed channel medium mock-ups	May
Complete HHF tests of GA hypervapotron medium mock-up	June
Complete HHF tests of GA helical-finned medium mock-up	July
Complete design/manufacture of Be/Cu medium mock-up	October
Complete HHF tests of RF porous-coated mock-ups	December
Complete design/manufacture of W/Cu medium mock-up	December
Down-select NDE technique for Be and W joining	December

Sandia National Laboratories

The eight T-222.4 bare copper medium-scale mock-ups include 6 designs and 3 copper alloys.

RF

(3 circular channel plates, 16 mm cell size, 10 mm channel, one smooth, two with porous surface treatment)

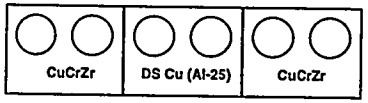

MDA/RF

(Three separate plates with ribbed cooling channels, one to receive RF porous surface treatment)

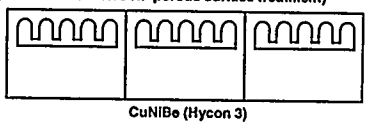

CuNiBe (Hycon 3)

GA

(Circular channel plate with annular swirl finned rod inserts, TBD mm cell size, TBD cells wide,)

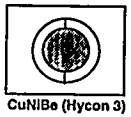

CuNiBe (Hycon 3)

GA

(Hypervapotron plate design optimized for ITER coolant conditions: 4 MPa, 150°C)

CuNiBe (Hycon 3)

Sandia National Laboratories

T-222.4 mock-ups will fulfill many objectives.

- Develop the design process and manufacturing procedures needed for the construction of robust high heat flux (HHF) components
- Verify their thermal hydraulic performance under ITER relevant conditions (4-5 MPa, 150 °C, 5 - 25 MW/m²)
- Assess / compare Critical Heat Flux capability of proposed and alternative diverter target design concepts
- Verify their mechanical performance (distortions etc.) during / following HHF loading
- Begin developing NDE processes / database for ITER-relevant hardware
- Post-test analyses of HHF experiments to establish design correlations, guidelines and margins for selected concepts
- Initial assessment of divertor component lifetime and failure criteria

Sandia National Laboratories

The EB-1200 has a versatile mock-up mount.

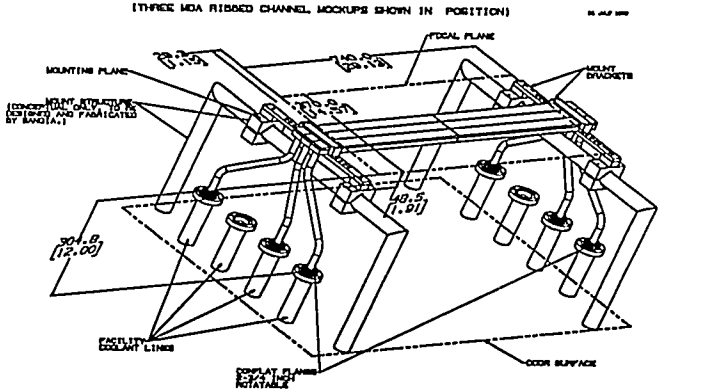

Sandia National Laboratories

All U.S. medium-scale mock-ups use the EB-1200 mount.

- Inlet / Outlet coolant line hardware does not interfere with mounting hardware
- Unique coolant line adapters for each mock-up location
- Mock-up alignment / mechanical support provided by separate mounting structure to ease coolant line manufacturing tolerances
- Force common mock-up thickness and connections so center mock-up is interchangable
- High-pressure coolant lines float inside low-pressure vacuum bellows
- Outer mock-ups absorb high power edge beam spill-over during CHF testing of center mock-up.
- Separate coolant supply / instrumentation to each mock-up for independent testing

Sandia National Laboratories

T-222 HHF tests will use Sandia's new EB-1200 facility.

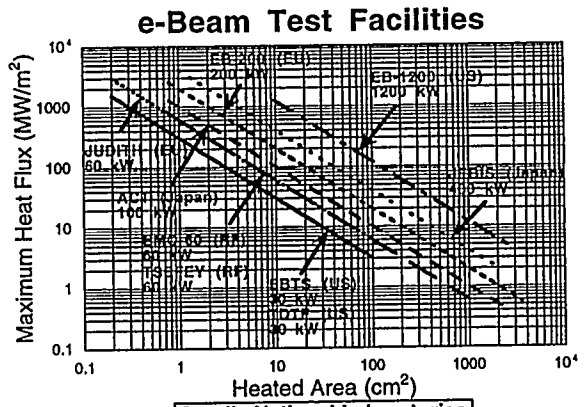

Sandia National Laboratories

Sandia's EB-1200 is a flexible HHF facility.

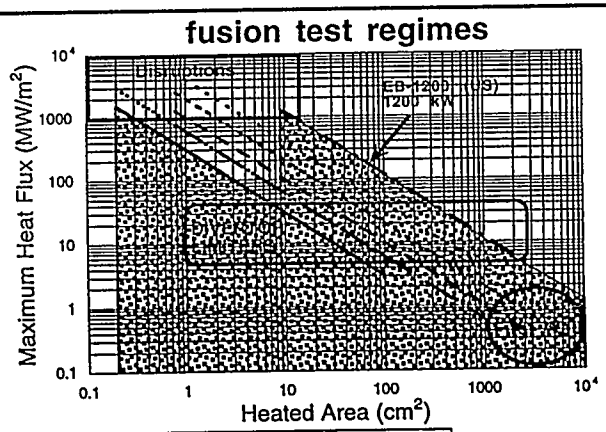

Sandia National Laboratories

The EB-1200 System offers enormous flexibility.

Beam Power (2 guns)	0 to 1200 kW (cw)
Accelerating Voltage	0 to 40 kV
Beam Current	15 amperes each gun
Angle of Beam Incidence	0° to 90 °
Cathode Lifetime	≥ 200 hours
Magnetic Lenses	2
Magnetic Deflection	X-Y direction
Max. Angle of Beam Deflection	±30° at < 200 Hz ±7° at 10 kHz
Maximum Raster Frequency	10 kHz
Spot Diameter at 600 kW and a Distance of 1.5 m	4 cm
Maximum Heat Flux (unrastered)	>1000 MW/m^2
Maximum Heated Area @ 1.5 m, 10 kHz	37 cm X 3½ cm
Heat Flux @ Maximum Area	8.7 MW/m
Maximum Pressure in Chamber	≤3 Pa_3
Cooling Water Consumption	2.2 m /hr

Sandia National Laboratories

EB-1200 has a variety of diagnostics.

Diagnostic	Purpose
Pyrometers (4)	Surface temperatures
Infrared Camera & video digitizer (2)	Surface temperature profiles
Thermocouples (48)	Bulk temperatures
Pressure Gauges (9)	Absolute pressure
Differential Pressure (2)	Delta-P across targets
Strain gauges, LVDT's	Bulk response
Residual Gas Analyzer	Partial pressures
Water calorimetry (3)	Heat removal capability
Bore scopes (3)	*In situ* surface observations
TV monitoring system	Visual records

Sandia National Laboratories

EB-1200 and EBTS both received upgrades.

- digital beam rastering system with reliable deflection amplifiers
- state-of-the-art infrared colorizing/digitizing system
- computer-controlled 100 amu RGA system
- low temperature pyrometers (150 °C to 550 °C), (80 °C to 200 °C)
- low noise isolation amplifier modules for TC's and other transducers
- *in-vacuo* ΔT blocks for calorimetry
- ΔP differential pressure transducers
- LVDT deflection measurement system
- laser interferometry system for target deflection measurements

Sandia National Laboratories

T-222.4 mock-ups are well instrumented.

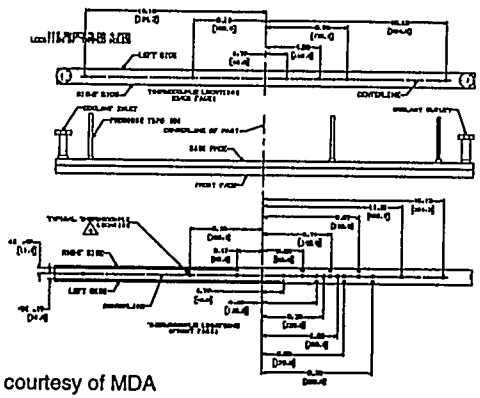

drawing courtesy of MDA

Sandia National Laboratories

Modifications to permit beryllium testing in the EB-1200 and EBTS with T_{In}=150 °C are under way.

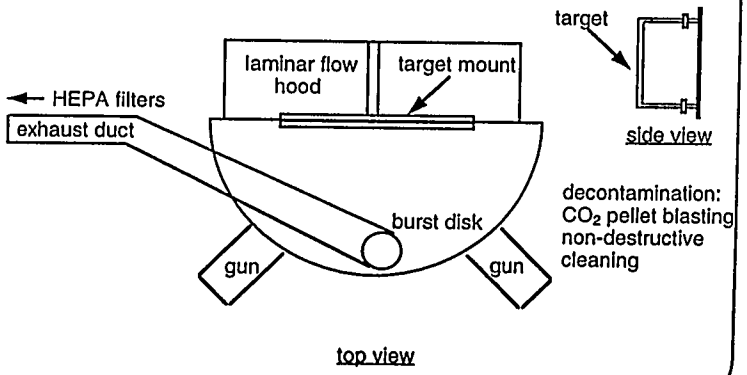

Sandia National Laboratories

T-222.5: Many institutions are involved in NDE research.

- McDonnell Douglas
- Karta Technologies ($600k SBIR phase-II)
- Sandia Laboratories
- Lawrence Livermore Laboratory
- University of Illinois
- Mississippi State University

Sandia National Laboratories

Many different NDE techniques are under evaluation.

- DEMONSTRATED/IN-PRODUCTION
  - PIEZO-ELECTRIC TIME-DOMAIN ULTRASONICS
  - FILM & COMPUTED RADIOGRAPHY
  - COMPUTED TOMOGRAPHY
  - PULSED INFRARED THERMOGRAPHY
- POTENTIAL
  - PIEZO-ELECTRIC FREQUENCY DOMAIN ULTRASONICS
  - LASER OR EMAT/LASER ULTRASONICS
  - TIME-RESOLVED INFRARED THERMOGRAPHY
  - HIGH HEAT FLUX INFRARED THERMOGRAPHY

Sandia National Laboratories

NDE trials performed on Cu/Be AND Cu/Cu joints.

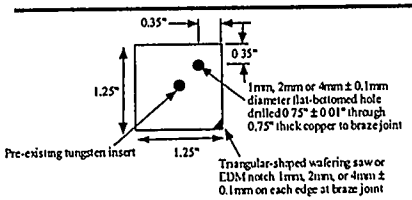

Braze Coupon Specimens - Plan View

SAMPLE #	JOINT	HOLE DIAMETER (mm)	NOTCH DIMENSIONS (mm)
37	Cu/Cu	1	1 x 1
38	Cu/Cu	2	2 x 2
39	Cu/Cu	4	4 x 4
40	Be/Cu	1	1 x 1
41	Be/Cu	2	2 x 2
42	Be/Cu	4	4 x 4

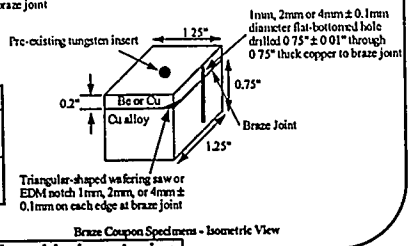

Braze Coupon Specimens - Isometric View

Sandia National Laboratories

Test plan approved by JCT.

- Performance validation for ITER Off-nominal heat flux profile
  - Validate 1.3x margin at 15 MW/m² for reference coolant conditions
  - Proposed Test Conditions: 4, 5 MPa — 100, 150°C; 5, 10, 15 m/s — 15, 20, 25 MW/m²
- Critical Heat Flux performance characterization with flat profiles
  - Evaluate ICHF / CHF for different heated lengths, same total power
  - Proposed Test Conditions: 4, 5 MPa — 100, 150°C; 5, 10, 15 m/s — 10, 15, 20 MW/m²
- Critical Heat Flux performance characterization with peaked ITER profile
  - Evaluate CHF for ITER Off-nominal profile

Sandia National Laboratories

ITER off-nominal divertor profiles simulated in EB-1200.

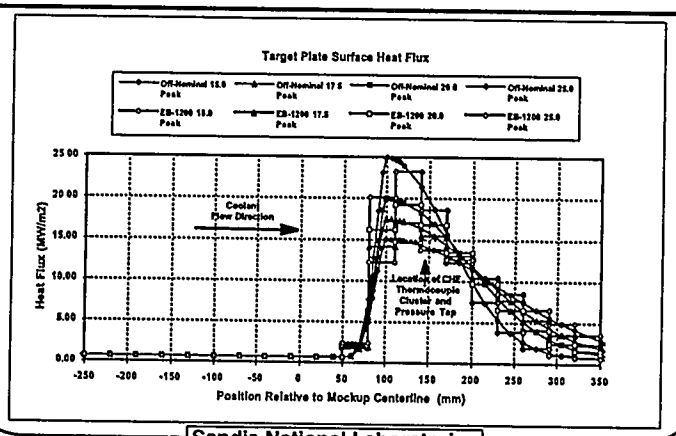

Sandia National Laboratories

Uniform CHF Test Profiles will also be used.

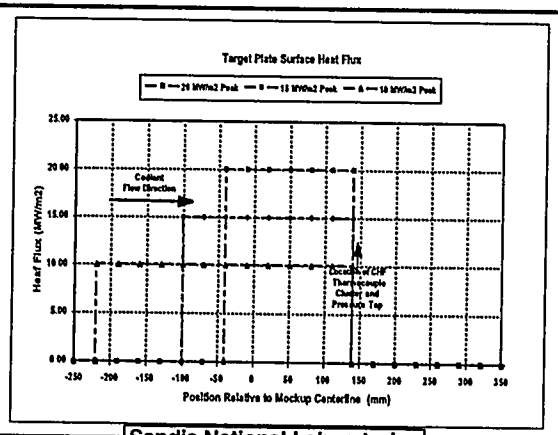

Sandia National Laboratories

Synopsis

All T-222 tasks will be well under way in 1996.

- Testing of 8 medium-scale mock-ups will begin in 3/96 for T-222.4.
- MDA and Karta Tech Inc. are developing NDE techniques for T-222.5.
- Begin fabrication of Be/Cu medium-scale mock-ups pending T-221 results.
- Begin fabrication of W/Cu medium-scale mock-ups pending T-221 results.

Sandia National Laboratories

Divertor Mockup Design and Fabrication

Permanent Component Development and Testing
ITER Task T222

US-Japan Workshop Q219
on HHF Components and PSI for Next Fusion Devices

Colorado Springs, Colorado
9-11 January, 1996

Presented by
Dan Driemeyer
McDonnell Douglas Aerospace

Task T222 Contributors

U.S. Home Team

Sandia National Laboratories (HHF Testing)
- D. Youchison, R. Watson, R. Nygren, M. Ulrickson

McDonnell Douglas (RC, HV Mockup Design/Mfg, Mfg Development)
- D. Driemeyer, T. Ganley, T. Hellwig, D. Kubik, H. Mantz, M. McSmith, K. Slattery, G. Wille

General Atomics (SRI, HV Mockup Design/Mfg, Mfg Development)
- C. Baxi, L. Sevier, P. Trester, B. Laycock

Rockwell Rocketdyne (Mockup Mfg Development)
- J. Yuen, R. Walters, D. Tentsch

University of Illinois (HV Flow Testing)
- B. Jones, J. Butler

Westinghouse STC (Corrosion Testing, CHF Test Planning)
- L. Green, R. Jacko

Efremov Institute, RF (PC Mockup Design/Mfg, Mfg Development)
- I. Mazul, R. Guiniantouline

Talk Outline

U.S. Home Team

- Mockup Design and Analysis
- Manufacturing Development
- Thermal-structural Analysis Summary
- HHF Testing Plans

Medium-Scale Mockup Objectives

U.S. Home Team

- Develop the design process and manufacturing procedures needed for the construction of robust high heat flux (HHF) components
- Verify their thermal hydraulic performance under ITER relevant conditions (4 MPa, 150°C, 5 - 20 MW/m^2)
- Assess / compare Critical Heat Flux capability of proposed and alternative diverter target design concepts
- Verify their mechanical performance (distortions etc.) during / following HHF loading
- Begin developing NDE processes / database for ITER-relevant hardware
- Post-test analyses of HHF experiments to establish design correlations, guidelines and margins for selected concepts
- Initial assessment of divertor component lifetime and failure criteria

Proposed Mockup Configurations

U.S. Home Team

RF

(3 circular channel plates, 16 mm cell size, 10 mm channel, one smooth, two with porous surface treatment)

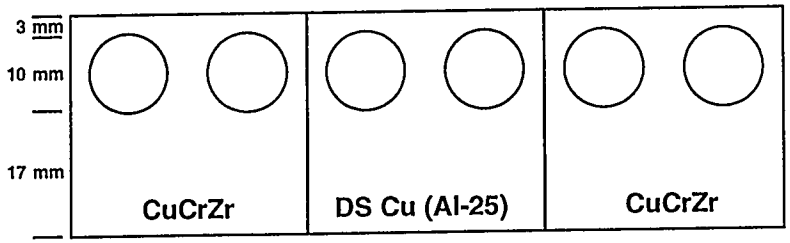

MDA/RF

(Two separate plates with ribbed cooling channels, third to receive RF porous surface treatment)

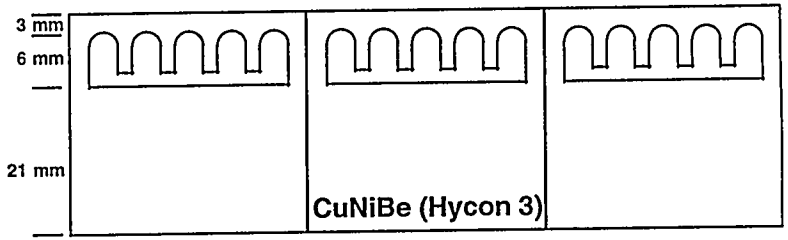

GA

(Circular channel plate with annular swirl finned rod inserts, 33 mm width, single cell wide)

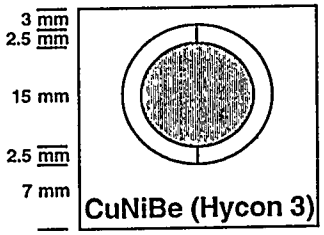

GA/MDA

(Hypervapotron plate design optimized for ITER coolant conditions: 4 MPa, 150ºC)

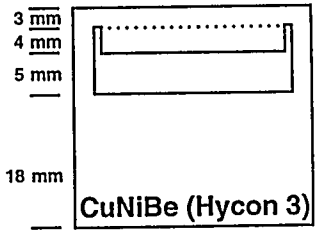

DED-5

ITER Plasma Facing Components

1/8/96

Ribbed Channel Design Overview

U.S. Home Team

Mockup Cross Section

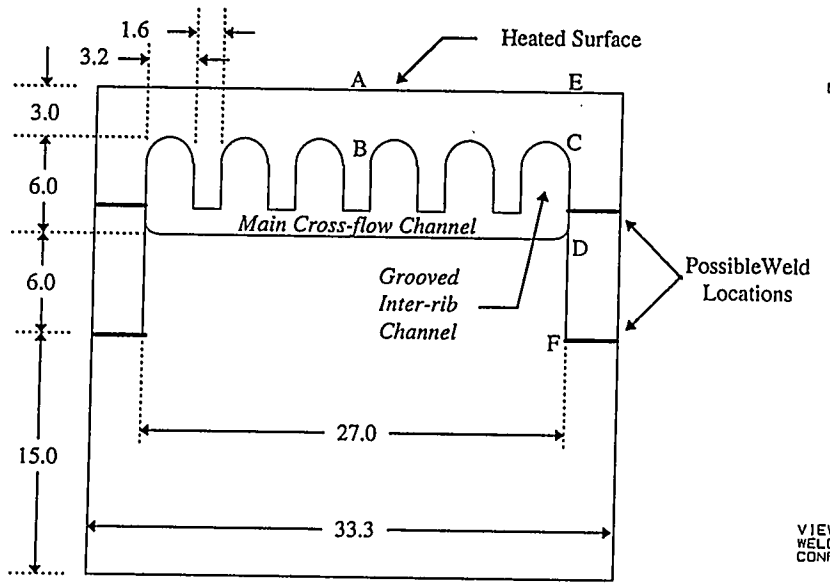

3-D Internal View

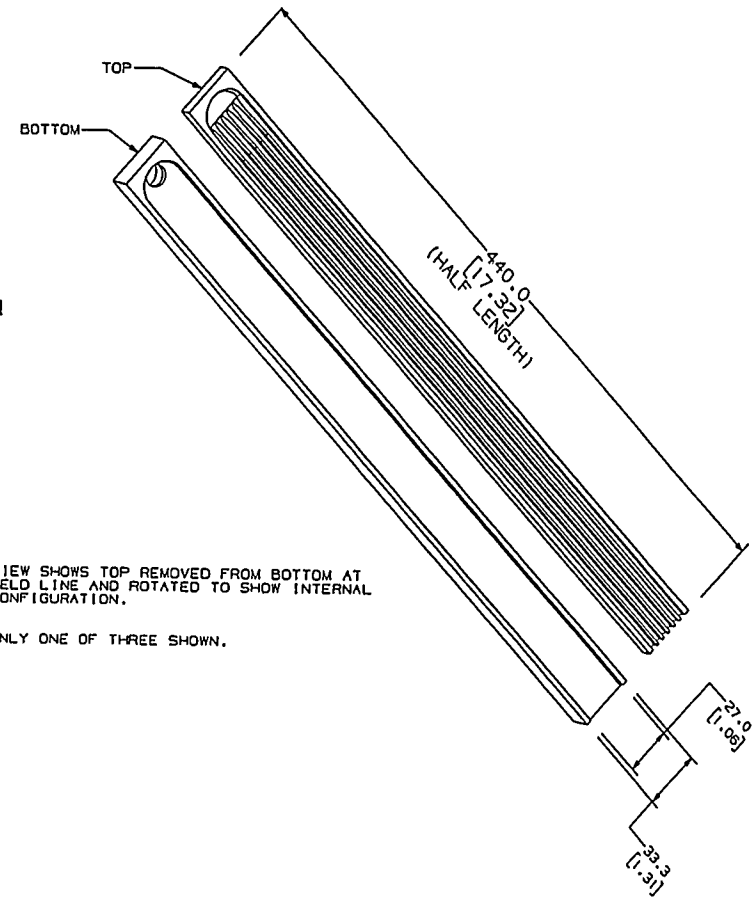

VIEW SHOWS TOP REMOVED FROM BOTTOM AT WELD LINE AND ROTATED TO SHOW INTERNAL CONFIGURATION.

ONLY ONE OF THREE SHOWN.

Basis for Ribbed Channel Configuration

U.S. Home Team

- Modification of LBL beam dump plate design tested at 20 MW/m^2
  - Thermal-hydraulic design updated for ITER conditions (150°C, 4 MPa, 10 m/s)
  - Main channel / groove dimensions selected based on ΔP and fin heat transfer models
  - Reference design provides 1.3x CHF margin for 15 MW/m^2 profile
  - Alternate design enhances mixing in grooves, should improve CHF
  - Need to establish CHF design correlations for these concepts
- Thermal-Structural analysis indicates design is viable
  - Meets ITER criteria at 15 MW/m^2 for reference Hycon properties
  - Will yield in locally at higher heat fluxes, cycles to failure being evaluated
  - Testing underway to verify material properties at elevated temperature
- Manufacturing development studies underway to determine baseline fabrication approach
  - Welding (TIG and E-beam, Cu-Cu and Cu-SS) and brazing
  - High speed machining

Comparison with Beam Dump Panel Design

U.S. Home Team

Parameter	LBL Panel	MDA Mockup
Flow area (mm^2)	9.2	122.5
Hydraulic diameter, D_h (mm)	1.35	4.88
Channel width (mm)	5.7	27.0
Number fins	3	5
Ratio heated length to D_h	159	152
Ratio fin height to width / Optimum ratio	2.5 / 2.1	1.7 / 1.5
Ratio cross flow to total area	0.31	0.37
Inlet temperature (°C)	55	150
Inlet pressure (MPa)	1.4	4.0
Outlet pressure (MPa)	0.83	3.8
T_{sat} at exit (°C)	172	251
T_{bulk} at exit (°C)	101	170
T_{sub} at exit (°C)	71	81
Inlet velocity (m/s)	12.7	10
Peak heat flux (MW/m^2)	>20	20
Length with heat flux > 11 MW/m^2 (mm)	220	200
Pressure drop (MPa)	0.29	0.2
Total flow length (mm)	220	860

GA Swirl Rod Insert Mockup

U.S. Home Team

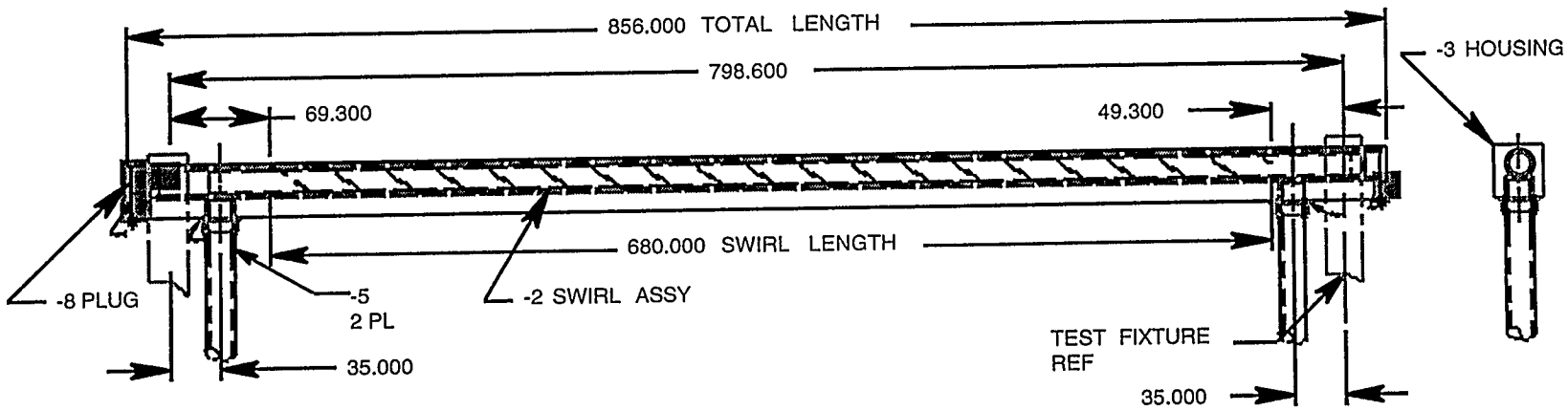

ALL DIMENSIONS ARE FOR REFERENCE ONLY.

- Single 20 mm ID gun-drilled cooling channel
- 15 mm OD swirl rod insert
- Rod supported at ends by e-beam welded plug inserts
- Explosion-bonded SS316 back plate to increase stiffness
- Coolant line and plug welds identical to MDA mockups

Efremov Institute Mockups

U.S. Home Team

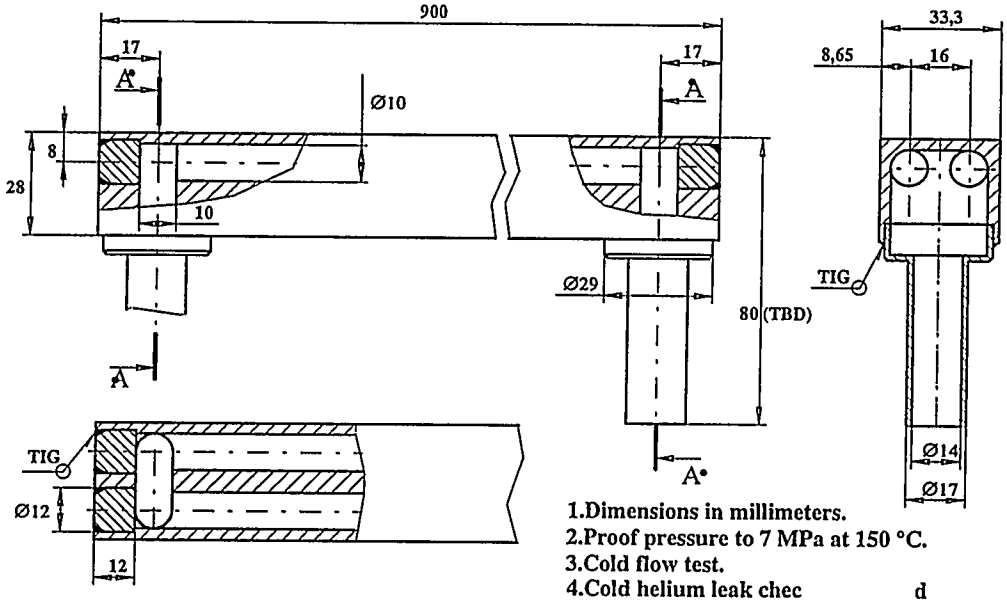

1.Dimensions in millimeters.
2.Proof pressure to 7 MPa at 150 °C.
3.Cold flow test.
4.Cold helium leak chec d

- Three mockups with dual, 10 mm circular channels
- Width consistent with other US mockups (33.3 mm)
- Side-by-side comparison of porous coating with other heat transfer enhancement techniques
- Two mockups fabricated from CuCrZr and one from Glidcop CuAl-25
  - Porous coating applied to one CuCrZr and the CuAl-25 mockup
- Subcontract in-place and preliminary design studies underway
  - Glidcop bar purchased from SCM and in-shipment to Efremov
- Samples of the Hycon-3 alloy provided to Efremov for process development studies

First set of Mockups to be Evaluated

U.S. Home Team

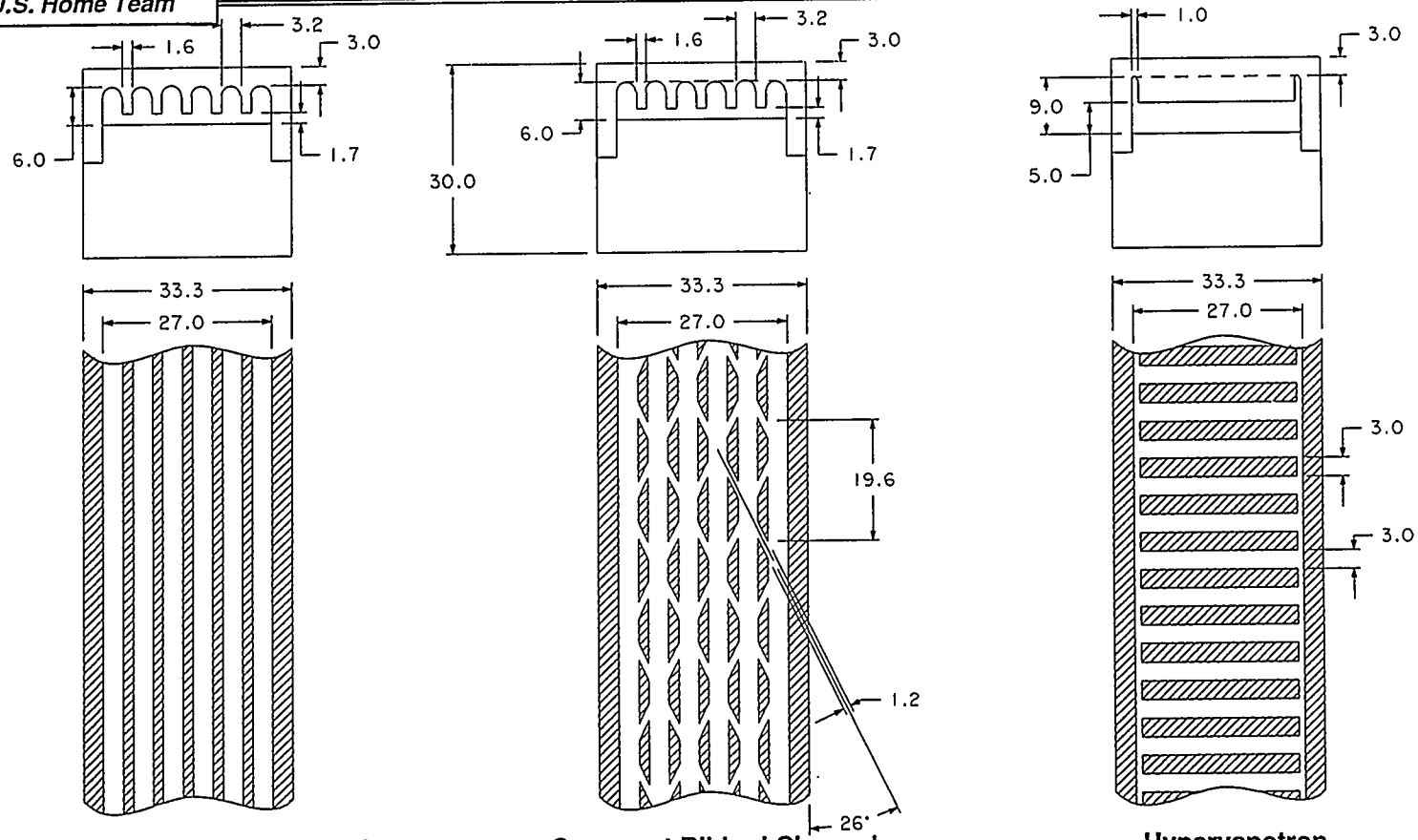

Baseline Ribbed Channel

Five 1.6 x 4.3 mm ribs

Also combined with porous coating

Cross-cut Ribbed Channel

Same geometry as baseline

Restarts boundary layer

Enhances mixing in long grooves

Hypervapotron

Replicates EU HV-1 design

3 x 4 mm teeth on 6 mm pitch

5 x 27 mm channel

HIGH-SPEED MACHINING DEVELOPMENT AND DEMONSTRATION

U.S. Home Team

- PERFORMED UNDER MDA INTERNAL RESEARCH
- INITIAL DEMONSTRATIONS ON CuCrZr ALLOY (ELBRODUR-G)
  - PART 1:
    - 9.5mm DIAMETER, 0mm RADIUS CUTTER
    - 330cm/min @ 20000rpm
    - 11mm DEEP CUT IN 11mm PASS - CHATTER & CUTTER BROKE
    - 11mm DEEP CUT IN 2.54mm PASSES - SMOOTH SURFACE
  - PART 2:
    - 3.2mm DIAMETER, 0.25mm RADIUS CUTTER
    - 250cm/min @ 18000rpm
    - 1mm DEEP CUT IN 1mm PASS
    - DEEPER CUTS CAN BE MADE, BUT PASS SHOULD BE KEPT TO 1mm TO AVOID CHATTER
- WILL USE FOR CuNiBe (HYCON-3) ARTICLES FOR T222
- ALSO LOOKING AT MACHINING 316LN STAINLESS

Divertor Mid Scale Module Analysis Update

U.S. Industrial Team

UPDATED GEOMETRY
- Increased Backplate Thickness 9mm, From 12 to 21mm
- Moved Weld Location From Mid-channel to 15mm From Heated Surface

UPDATED BOILING SUBROUTINE
- Film Temperature Computed Locally at Each Element
- Water Properties Based on Local Film Temperature
- h_c Calculated Internal to Program Based on Local Conditions
- Iteration Performed to Calculate Boiling Onset Temperature
- Wall cooling Based on Local Wall & Saturation Temperature & Pressure

COMPARED 2D STRUCTURAL MODELING METHODOLOGIES
- Plane Stress
- Plane Strain
- Generalized Plane Strain

Mid Scale Mockup Peak Temperature Summary

U.S. Industrial Team

HEAT FLUX MW/m^2	PRESSURE MPa	TEMPERATURE °C PEAK @ CORNER E	HEATED SURFACE A	WELD F	OUTER CHANNEL C
25	4	666	591	209	325
	5	687	612	213	345
20	4	577	520	205	314
	5	596	540	208	334
15	4	490	450	200	300
	5	506	467	203	320

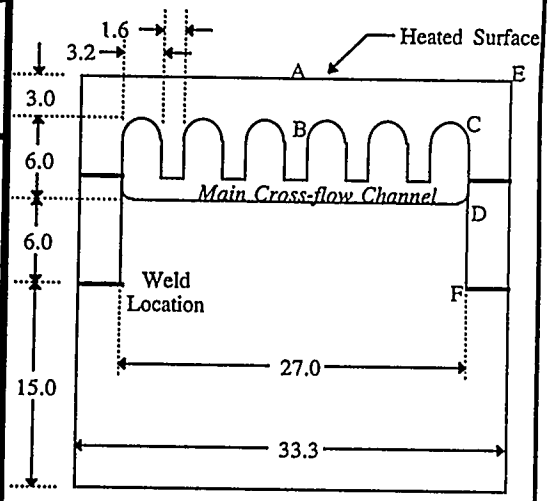

PFC 1

ITER Plasma Facing Components

10/27/9 5

DIVERTOR MOCK-UP
TEMPERATURE DISTRIBUTION

HEAT FLUX = 23.3 MW/m^2
BOILING HEAT TRANSFER INCLUDED
COOLANT TEMPERATURE = 161 C
COOLANT PRESSURE = 5 MPa

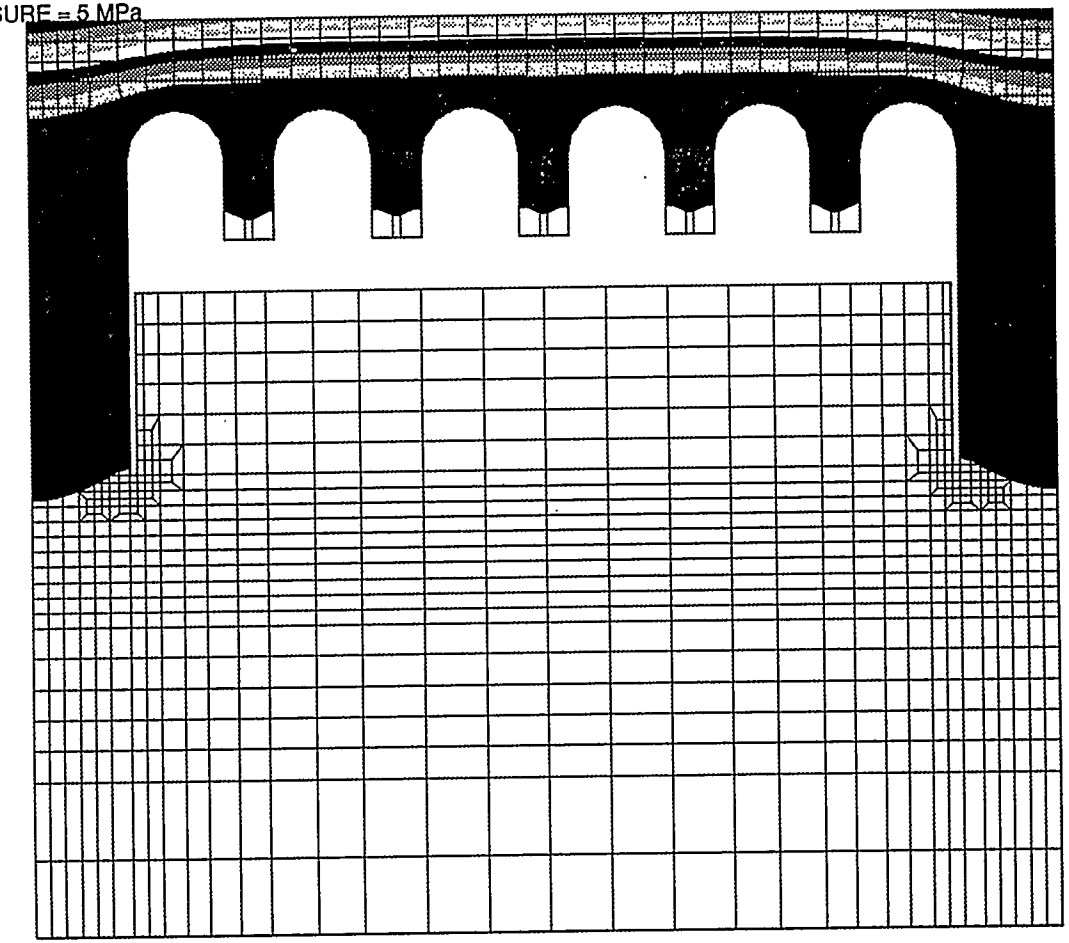

TEMPERATURE- C

653.3
620.8
588.4
555.9
523.5
491.0
458.6
426.1
393.7
361.2
328.8
296.3
263.9
231.4
199.0
166.5

RIB CHANNEL MOCKUP

YIELDED ELEMENTS

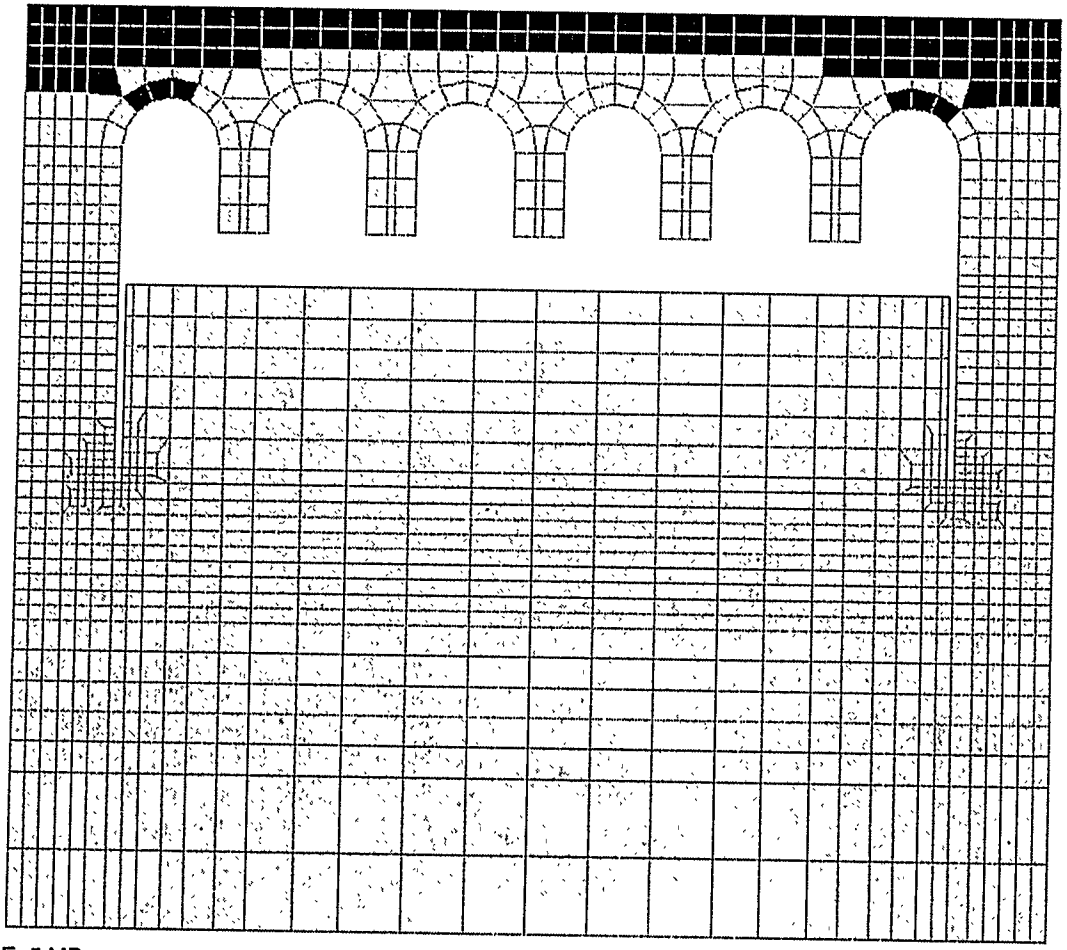

INTERNAL PRESSURE=5 MPa
SURFACE HEAT FLUX=25 MW/m^2

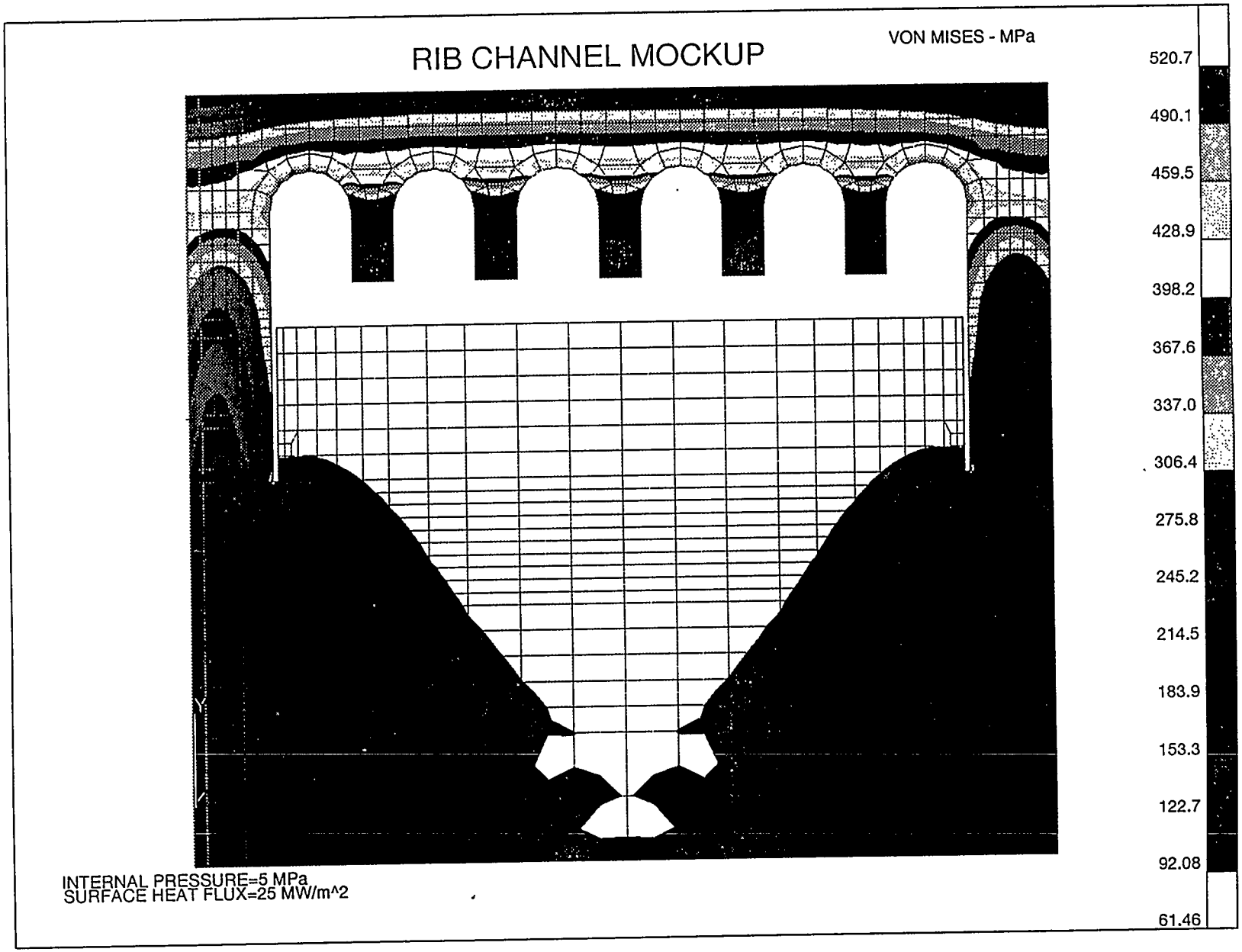
RIB CHANNEL MOCKUP
VON MISES - MPa
520.7
490.1
459.5
428.9
398.2
367.6
337.0
306.4
275.8
245.2
214.5
183.9
153.3
122.7
92.08
61.46
Y
INTERNAL PRESSURE=5 MPa
SURFACE HEAT FLUX=25 MW/m^2

RIB CHANNEL MOCKUP

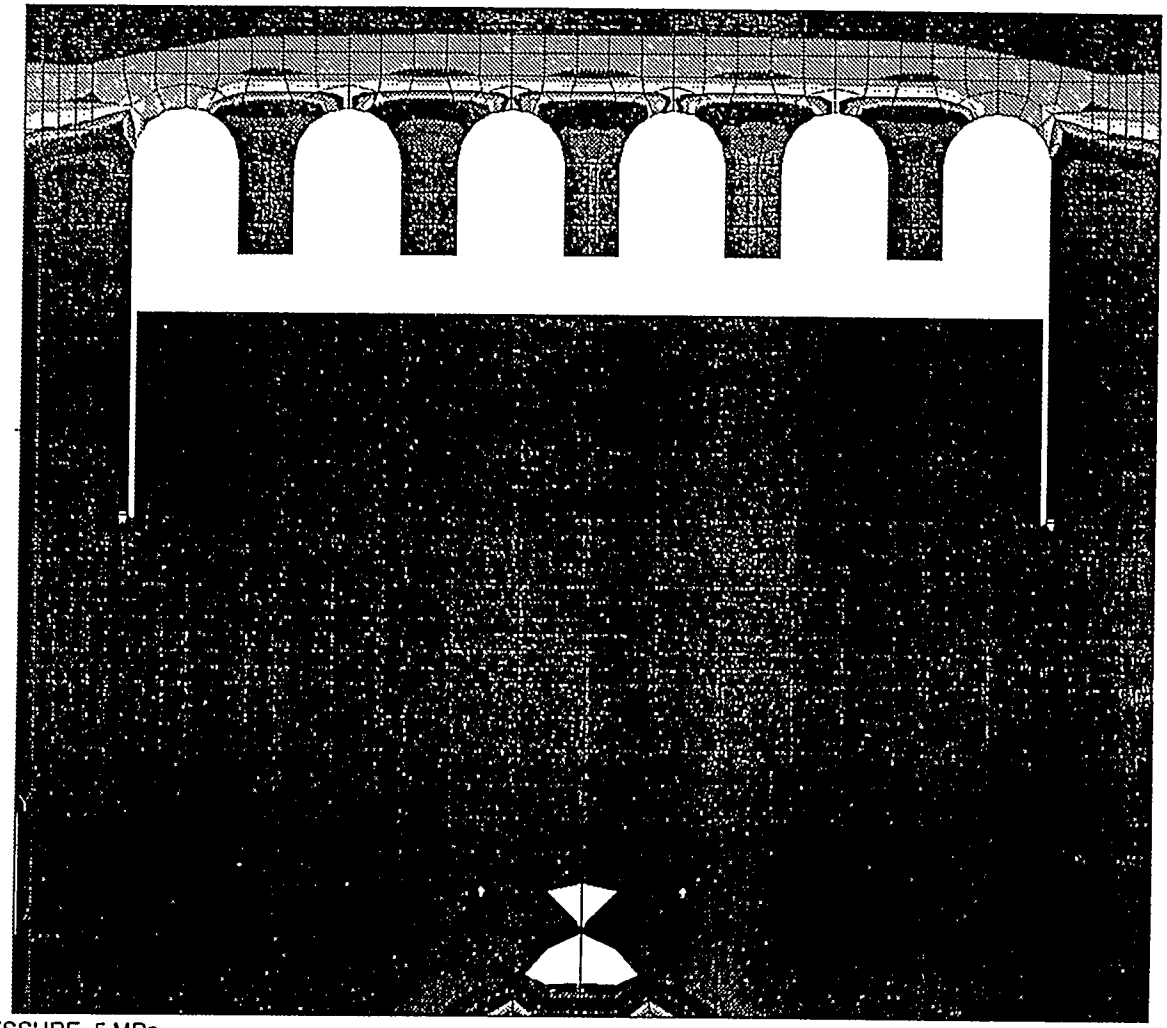

VON MISES - MPa

584.2
564.2
544.2
524.2
504.1
484.1
464.1
444.0
424.0
404.0
384.0
363.9
343.9
323.9
303.9
283.8

INTERNAL PRESSURE=5 MPa
SURFACE HEAT FLUX=25 MW/m^2

Mockup HHF Test Plan Overview

U.S. Home Team

- Performance validation for ITER Off-nominal heat flux profile
  - Validate 1.3x margin at 15 MW/m^2 for reference coolant conditions
  - Proposed Test Conditions:

3, 4, 5 MPa	100, 125, 150°C
5, 7.5, 10, 12.5, 15 m/s	10, 15, 17.5, 20, 22.5, 25 MW/m^2

- Critical Heat Flux performance characterization with flat profiles
  - Evaluate ICHF / CHF for different flow velocities and inlet conditions
  - Proposed Test Conditions:

3, 4, 5 MPa	100 - 150°C
5, 10, 15 m/s	10, 15, 20, 25 MW/m^2

- Critical Heat Flux performance characterization with peaked ITER profile
  - Evaluate CHF for ITER Off-nominal profile based on results of uniform profile testing

ITER-Off Nominal Test Profiles

U.S. Home Team

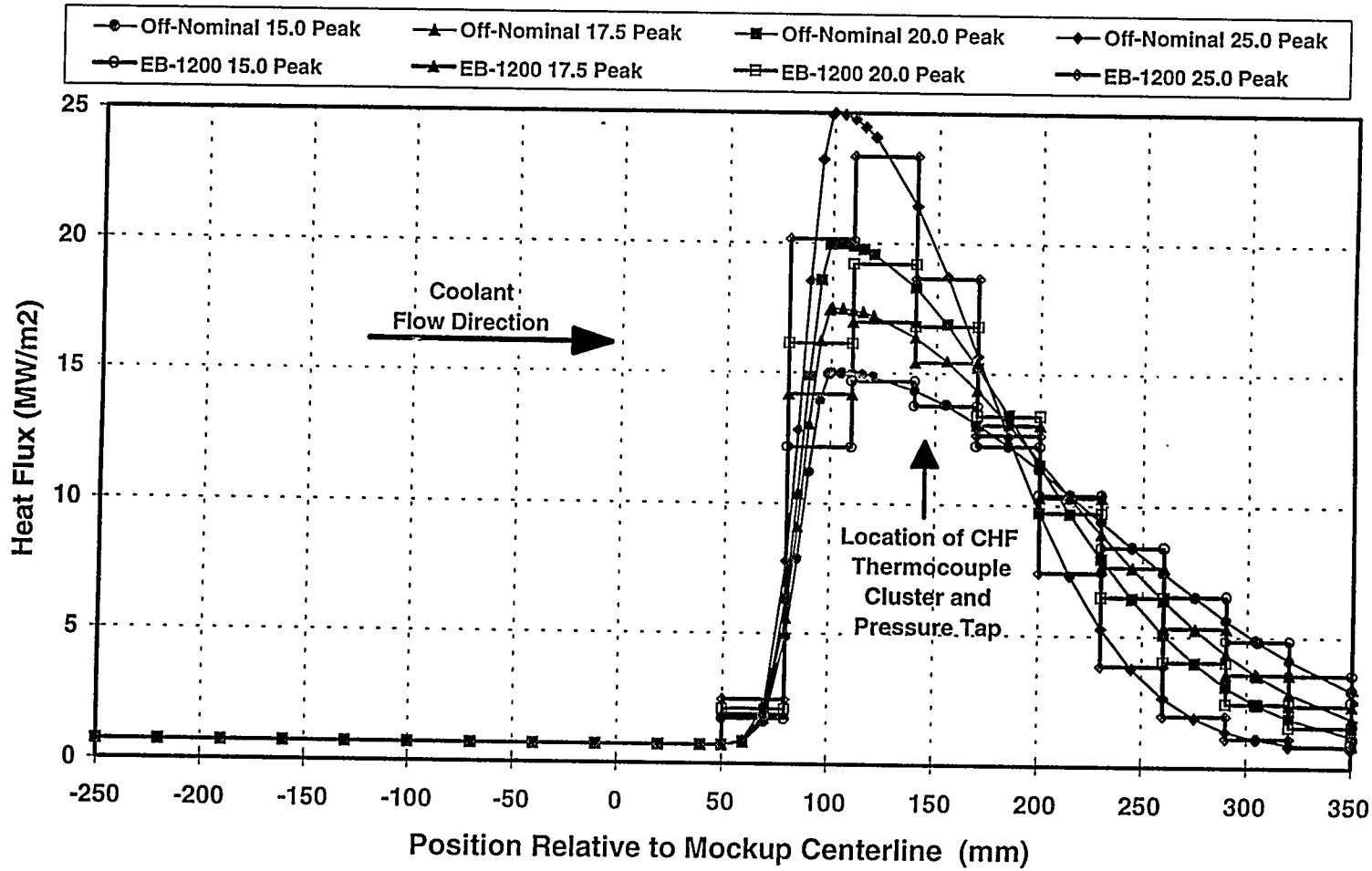

DED-11

ITER Plasma Facing Components

1/8/96

Critical Heat Flux Test Profiles

U.S. Home Team

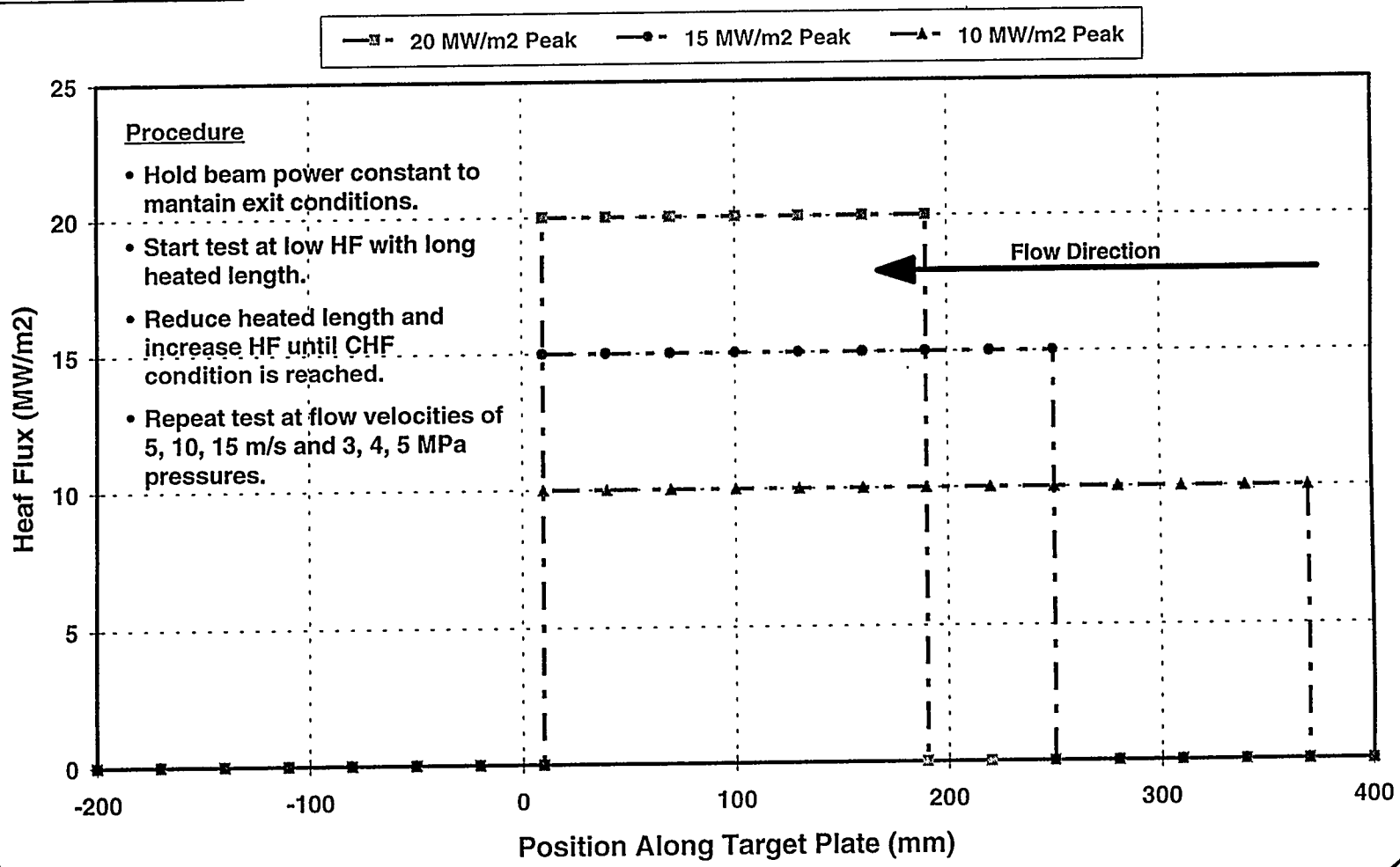

DED-12

ITER Plasma Facing Components

1/8/96

Typical Mockup Instrumentation

U.S. Home Team

Proposed Thermocouple Locations

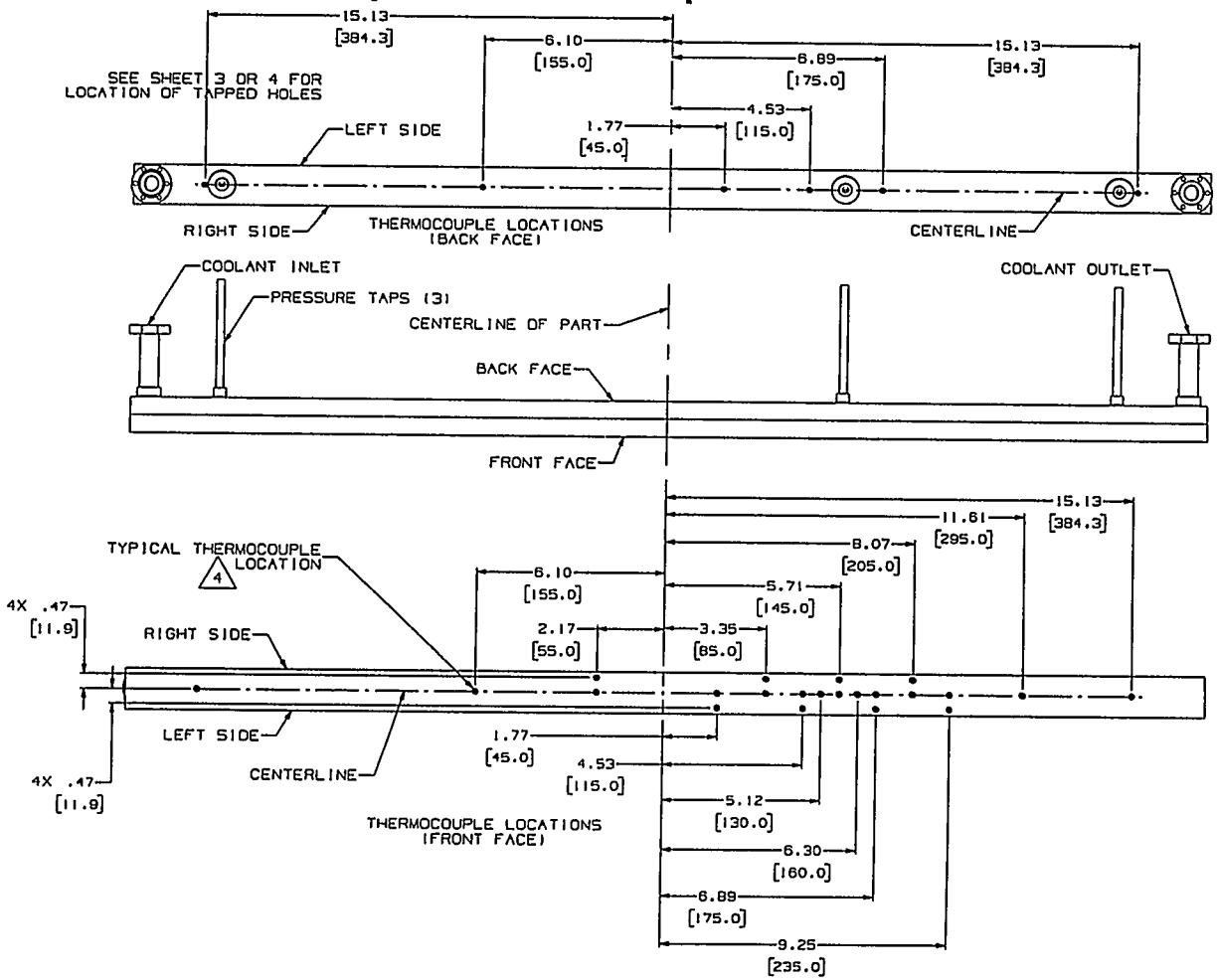

DED-13

ITER Plasma Facing Components

1/8/96

Mockup Development Summary

U.S. Home Team

- Compare several alternative cooling channel configurations in side-by-side testing
- Include baseline hypervapotron and annular swirl tape concepts proposed by JCT for dome and vertical target
- Adopt standardized mockup envelope, mounting arrangement and coolant line interfaces for interchangeability
- Manufacturing development testing underway
- Detailed designs complete by mid-~~October~~ December 95
- Staged mockup deliveries for ITER profile and CHF testing in EB-1200 facility beginning in ~~December~~ March 96
- Complete initial testing campaign in ~~March~~ June 96
- Select two best concepts based on testing / manufacturing results for medium-scale fabrication / testing with armor in FY'97

MANUFACTURING OF ITER PLASMA FACING COMPONENTS

PRESENTED AT
US-JAPAN WORKSHOP Q219
ON HIGH HEAT FLUX COMPONENTS AND PLASMA SURFACE INTERACTIONS FOR NEXT DEVICES

JANUARY 9-11, 1996, Sheraton Colorado Springs Hotel

Seiichiro YAMAZAKI — Kawasaki Heavy Industries, LTD.
Masato AKIBA — Japan Atomic Energy Research Institute
Hideyuki TAKATSU — Japan Atomic Energy Research Institute

MANUFACTURING OF DIVERTOR WING

MANUFACTURING OF DIVERTOR WING

IMPROVEMENT OF BRAZING TECHNIQUES FOR CARBON-COPPER JOINT

LOWER TEMPERATURE BRAZING
NON-SILVER BRAZING

Carbon Material : uni-directional CFC (MFC-1)
Copper Materials : OFCu, Ag-OFCu, Cu-Zr Alloy, DSCu

Brazing material survey,
Brazing tests and bending tests of carbon-Cu joints

MANUFACTURE OF MOCKUPS

Heat load and thermal-cycle test in JAERI

IMPROVEMENT OF BRAZING TECHNIQUE
LOWER TEMPERATURE BRAZING

ESTABLISHED BRAZING TECHNIQUE

- Ti is most effective additive to activate carbon surface.
- Braze at optimized temperature i.e. ab. 850°C using Ti-Cu-Ag.

Provide reliable carbon-copper joint.

WHY LOWER TEMPERATURE BRAZING?

- To keep integrity of copper alloys at brazing temperature.
  Suppress growth of crystal and decrease of strength.
- To provide reliable in-situ maintenance of armor tiles.

HOW LOWER TEMPERATURE BRAZING?

- To apply Ti contained brazing material with lower brazing temperatures.
  Brazing was successfully performed at ab. 750°C using Ti-In-Cu-Ag.
- To apply two step brazing.
  Before brazing, metalize the rear surface of carbon armor with Ti contained metal.
  Braze with non-Ti brazing material at lower temperature.

IMPROVEMENT OF BRAZING TECHNIQUE
NON-SILVER BRAZING

ESTABLISHED BRAZING TECHNIQUE

- A lot of experiences using silver based alloys as the brazing material.
- Braze using Ti-Cu-Ag as the brazing material.

Provide reliable carbon-copper joint.

WHY NON-SILVER BRAZING?

- To avoid the effect of Cd, that has high vapor pressure transmuted from Ag on plasma characteristics, though it is not obvious.

HOW NON-SILVER BRAZING?

- From the results of experimental study, Ti-Cu will be available for carbon-copper joint. Au-V may be also feasible.

CANDIDATE BRAZING MATERIALS

CHEMICAL COMPOSITION	SOLIDUS(℃)	LIQUIDUS(℃)	REMARKS
72Ag-28Cu	780	780	JIS BAg-8
63Ag-35Cu-2Ti	780	815	ref. 850 ℃
59Ag-27Cu-13In-1Ti	605	715	low T alt. 750 ℃
60Ag-30Cu-10Sn	602	718	low T
62Ag-28Cu-10In	690	720	low T
93Cu-3Si-2Al-2Ti	958	1024	non Ag
82Au-15.5Ni-1.75V-0.75Mo	940	960	non Ag
70Ti-15Cu-15Ni	910	960	non Ag
88Al-12Si	577	580	two step
96Pb-4Ag	305	330	two step

Kawasaki Heavy Industries, LTD. *Japan Atomic Energy Research Institute*

MOCK-UP OF DIVERTOR MODULE WITH RAIL SLIDING SUPPORT STRUCTURES

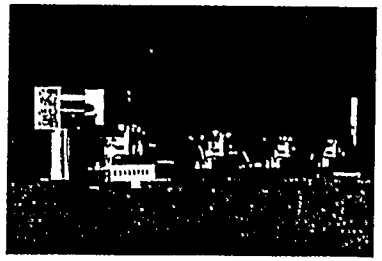

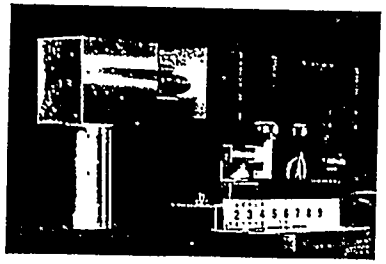

Total length of the mockup is about 1 meter. Sliding rail supports made of stainless steel with a pitch of 250 mm was applied. CFC(CX-2002U) and copper swirl tube were used as the armor tile and the coolant tube.

Kawasaki Heavy Industries, LTD. *Japan Atomic Energy Research Institute*

MICROSTRUCTURES OF BRAZED REGION

IFC-1/Ti-Cu-Ag/OFCu(850 ℃)

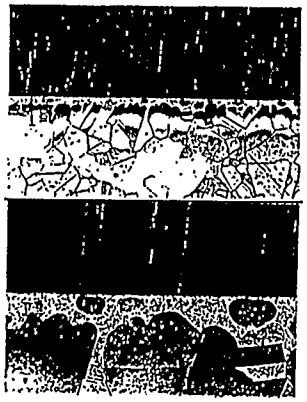

MFC-1/Ti-In-Cu-Ag/OFCu(750 ℃)

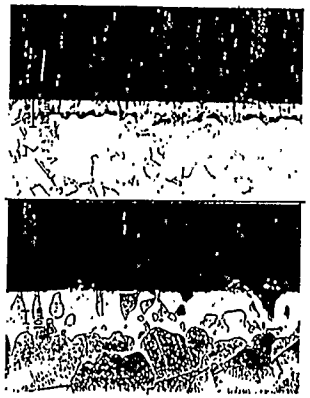

Kawasaki Heavy Industries, LTD. *Japan Atomic Energy Research Institute*

APPEARANCE OF SMALL-SIZE MOCKUP OF THE ITER DIVERTOR WING

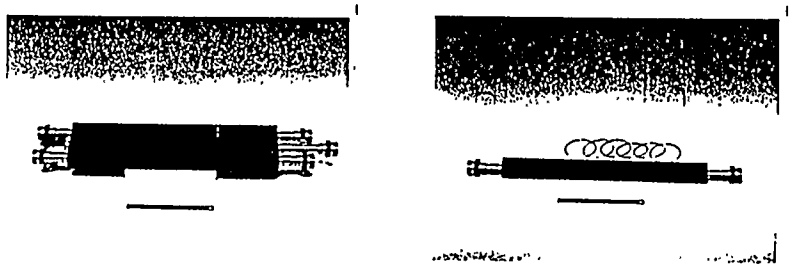

Kawasaki Heavy Industries, LTD. *Japan Atomic Energy Research Institute*

MANUFACTURING OF FIRST WALL

Kawasaki Heavy Industries, LTD. *Japan Atomic Energy Research Institute*

MANUFACTURING OF FIRST WALL

MANUFACTURING PROCEDURE WITH HIPing OF DSCu AND 316 STAINLESS STEEL

Optimization of HIP conditions,
Tensile, fatigue, creep and impact tests of HIPed joint
Microscopic observation

MANUFACTURE OF MOCKUPS

Heat load and thermal-cycle test in JAERI

[1] Sato S. et al., Fabrication of HIPed First Wall Panel for Fusion Experimental Reactor and Preliminary Analyses for Its Thermo-Mechanical Test, Proc. 16th SOFE , Champaign (1995,10)
[2] Furuya K. et al., Design Development of Shielding Blanket for Fusion Experimental Reactors, ibid.

Kawasaki Heavy Industries, LTD. *Japan Atomic Energy Research Institute*

CUT-AWAY VIEW OF THE ITER SHIELDING BLANKET AND FIRST WALL

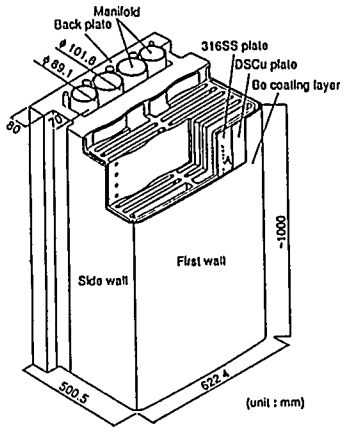

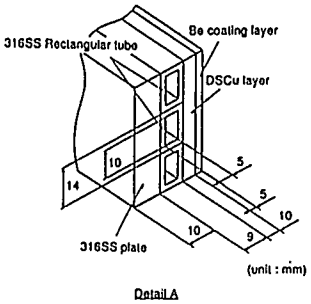

Kawasaki Heavy Industries, LTD. *Japan Atomic Energy Research Institute*

MANUFACTURING PROCEDURE OF THE ITER FIRST WALL MOCKUP

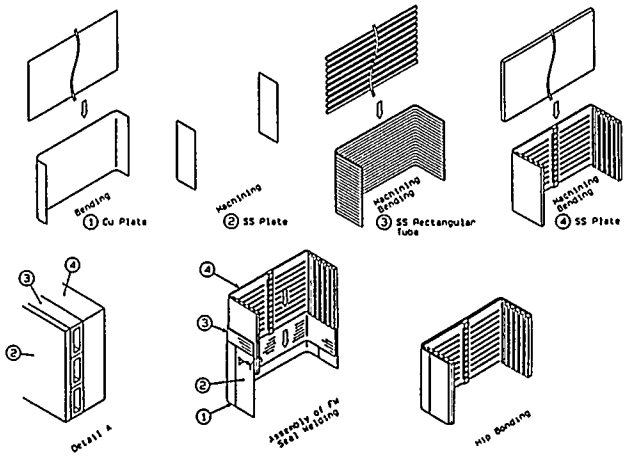

Kawasaki Heavy Industries, LTD. *Japan Atomic Energy Research Institute*

CROSS SECTION AT HIPed REGION OF THE ITER FIRST WALL MOCKUP

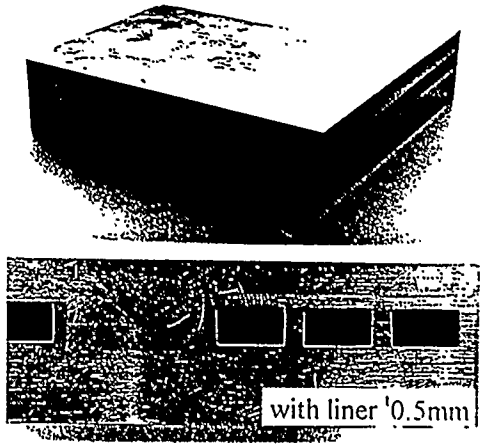

SUMMARY *Divertor Wing*

Improvement study of brazing technique for carbon coppe joint were performed.

Brazing at lower temperature is available using In-Ti-Cu-Ag a the brazing material.

Ti-Cu will be applicable as a non-Ag brazing material to avoi high vapor pressure Cd generation due to transmutation of Ag

A small mockup of divertor wing with three parallel coolan paths and mono block type CFC armor was successfull manufactured.

A real size mockup of divertor wing was designed, and will b manufactured by the end of March, 1996.

APPEARANCE OF THE ITER FIRST WALL MOCKUP (HIPed)

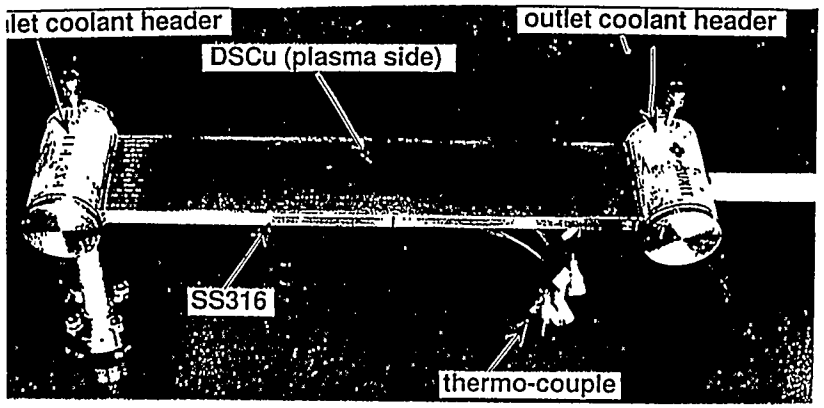

Temperature 1050℃, Pressure 150MPa, Holding Time 2hr

SUMMARY *First Wall*

Manufacturing procedure of the ITER first wall and shielding blanket structure was studied. The HIP joining method is applied for DSCu and stainless steel joint.

HIPing conditions were optimized, and mechanical tests were performed for the joints. It was proved that the joints has enough mechanical properties.

A mockup of the ITER Cu-SS first wall was successfully manufactured with HIP technique. Heating and thermal cycle tests for the mockup were performed in JAERI.

Critical heat flux experiment on the screw tube under one-sided heating conditions

M. Araki, K. Sato, S. Suzuki and M. Akiba

Naka-Fusion Research Establishment,
Japan Atomic Energy Research Institute

This result has been submitted for publication to Fusion Technology.

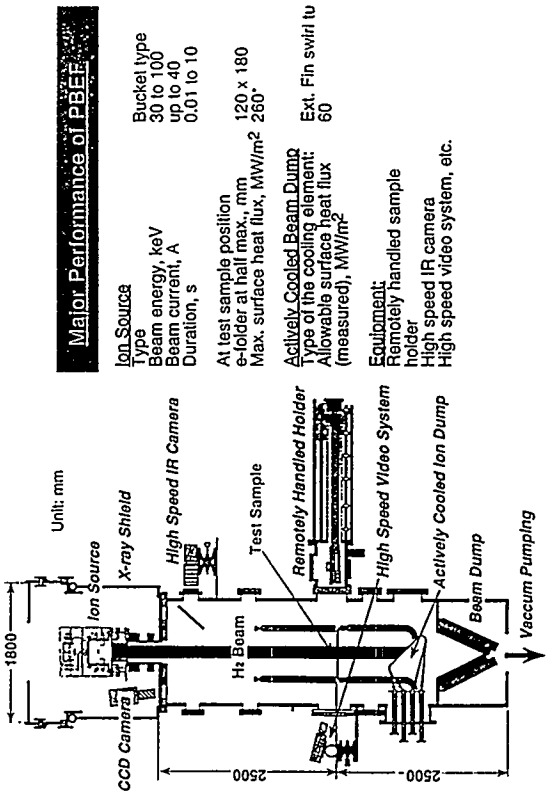

Major Performance of PBEF

Ion Source	
Type	Bucket type
Beam energy, keV	30 to 100
Beam current, A	up to 40
Duration, s	0.01 to 10
At test sample position	
e-folder at half max., mm	120 x 180
Max. surface heat flux, MW/m^2	260*
Actively Cooled Beam Dump	
Type of the cooling element:	Ext. Fin swirl tu
Allowable surface heat flux (measured), MW/m^2	60
Equipment:	
Remotely handled sample holder	
High speed IR camera	
High speed video system, etc.	

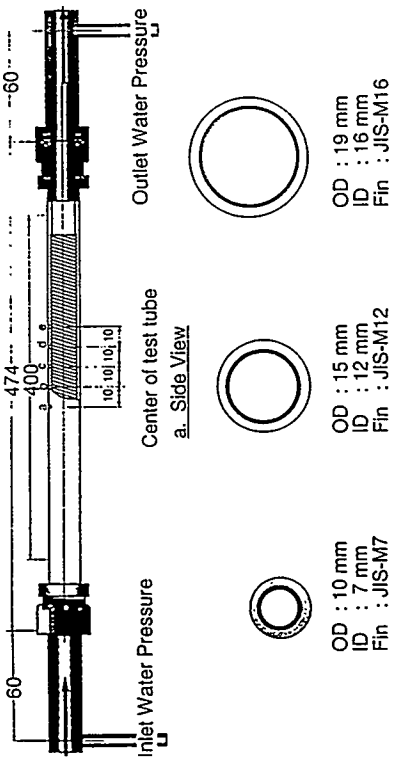

Schematic of Screw Tube Test Samples.

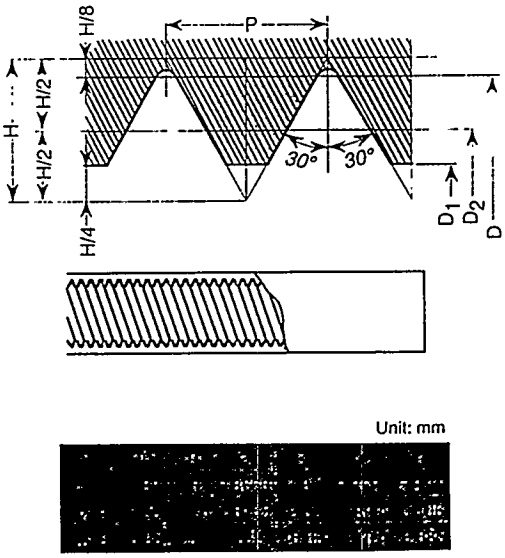

All sample tubes were machined based on ISO 261 (ISO general purpose screw thread-General plan) standard.

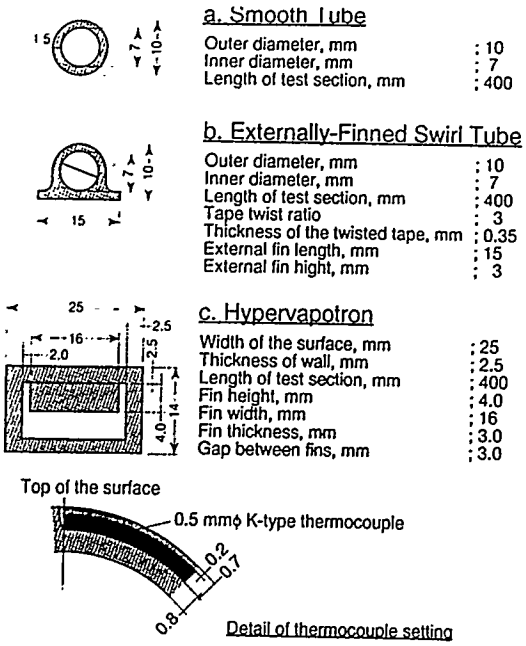

Cross sectional views of the other test samples.

All test samples were made of oxygen free high conductivity copper. Thermocouples were bonded into a grooves of the test sample to measure temperature response and catch the critical heat flux during heating.

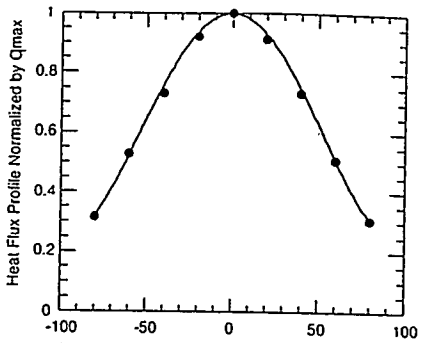

(a) Surface heat flux distribution normalized by the peak flux

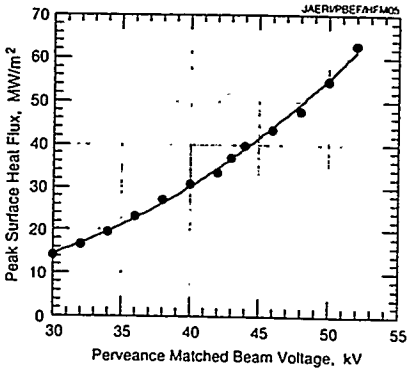

(b) Peak surface heat flux.

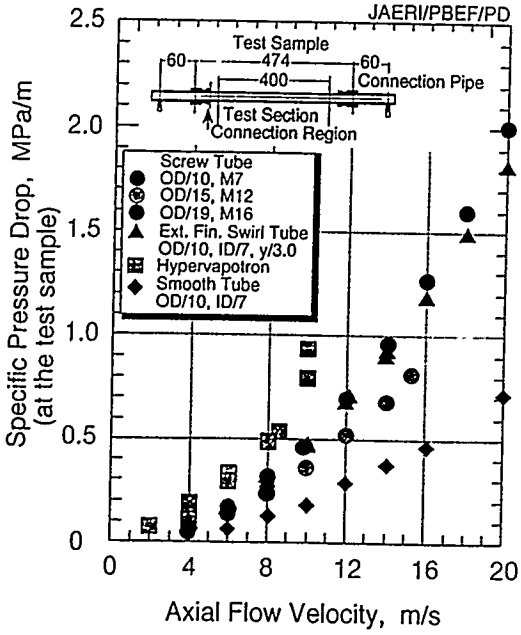

Pressure drop of the test samples as room temperautre.

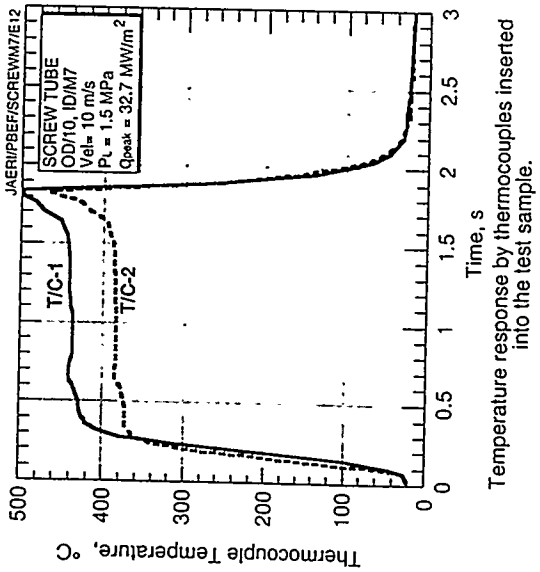

Temperature response by thermocouples inserted into the test sample.

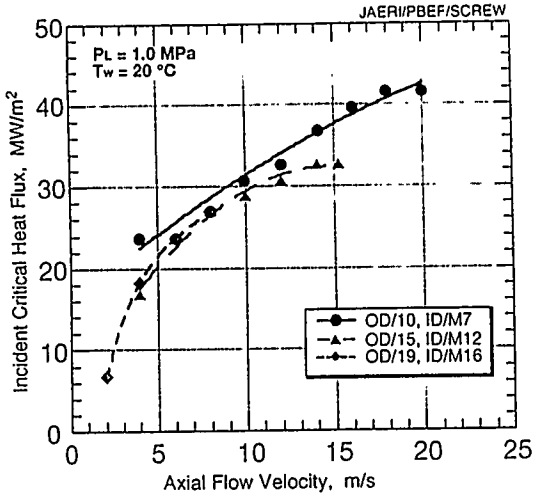

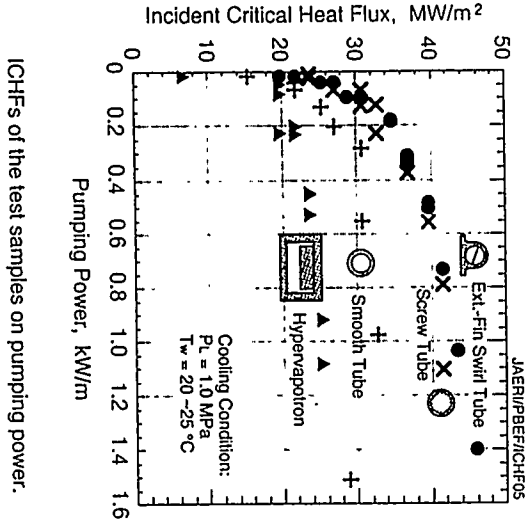

ICHFs of the test samples on pumping power.

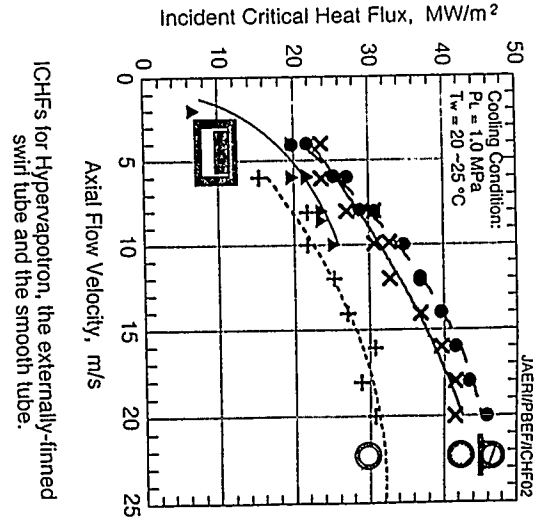

ICHFs for Hypervapotron, the externally-finned swirl tube and the smooth tube.

Concluding Remarks

ICHF experiments on various cooling structures have been performed at the axial flow velocity ranged from 4 to 20 m/s with the local pressure of 1.0 and 1.5 MPa for the inlet water temperature of 20 to 25 °C.

The screw tube of M7 has a factor by 1.5 times higher ICHFs compared to the smooth tube at a constant axial flow velocity and similar performance to the externally-finned swirl tube.

Thermal Hydraulic Analyses for the ITER Divertor High Heat Flux Components

N. J. Zhan

Westinghouse STC

1/9/96

Viewgraph 1
NJZ
1/8/96

Westinghouse
Science & Technology Center

PRESENTATION OUTLINE

- Divertor cassette geometry
- Power distribution among the PFC's
- Requirements for an acceptable cooling system
- JCT reference cooling channel designs
- Various cooling arrangements
- Conclusions and recommendations

Viewgraph 2
NJZ
1/8/96

Westinghouse
Science & Technology Center

DIVERTOR CASSETTE GEOMETRY

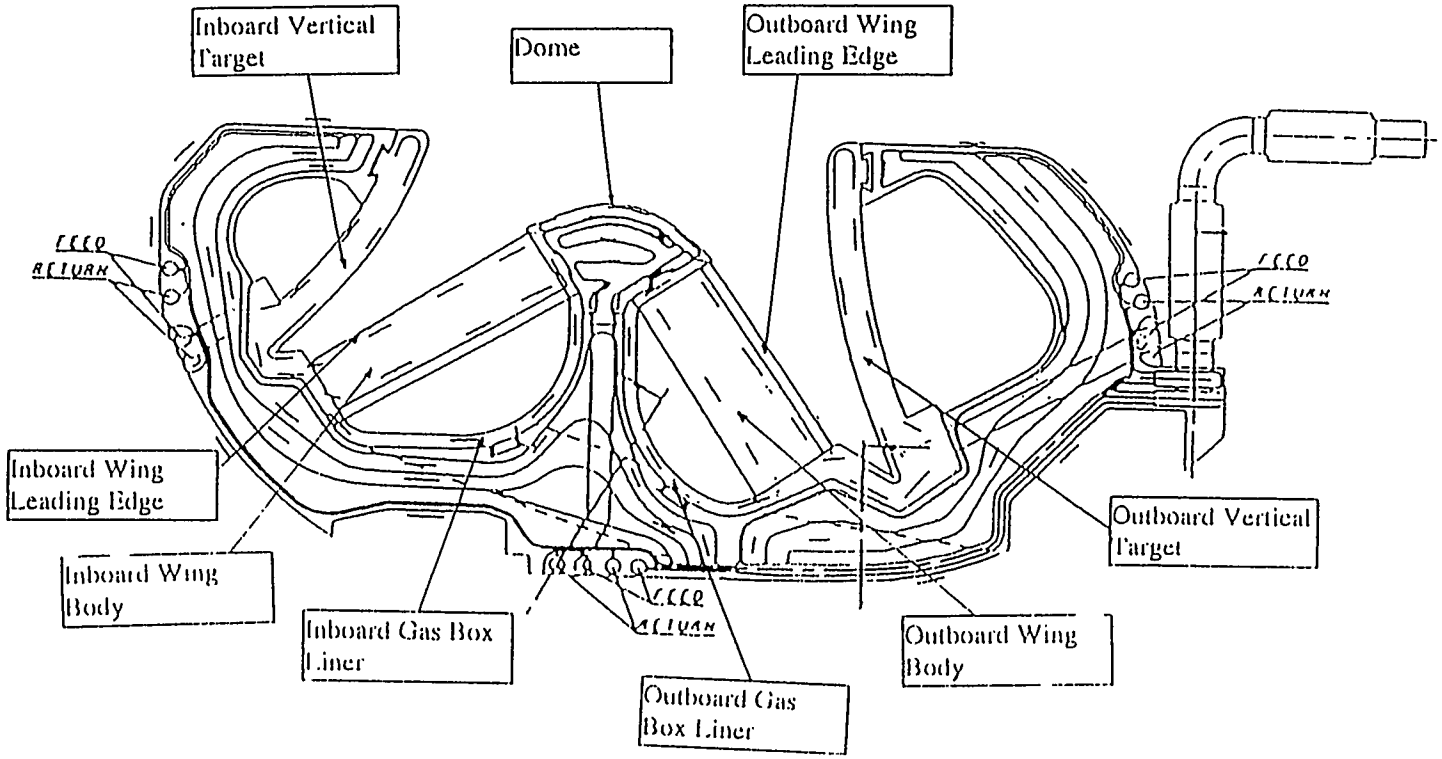

Viewgraph 3
NJZ
1/8/96

Westinghouse
Science & Technology Center

POWER DISTRIBUTION AMONG THE HHFC's

	Max. Incidental Heat Flux (MW/m2)	Max. Integrated Power (MW)
Outboard Vertical Target	15	200
Outboard Wing	5	100
Dome	5	100
Inboard Vertical Target	15	150
Inboard Wing	5	75

Viewgraph 4
NJZ
1/8/96

Westinghouse
Science & Technology Center

REQUIREMENTS AND INLET CONDITIONS

Requirements for an acceptable divertor hydraulic design:

- Coolant temperature rise of 20°C - 50°C
- Minimum critical heat flux (CHF) margin of 1.3
- Pressure drop less than 1.0 MPa

Inlet Coolant Conditions:

T = 150°C

P = 4.0 MPa

Viewgraph 5
NJZ
1/8/96

Westinghouse
Science & Technology Center

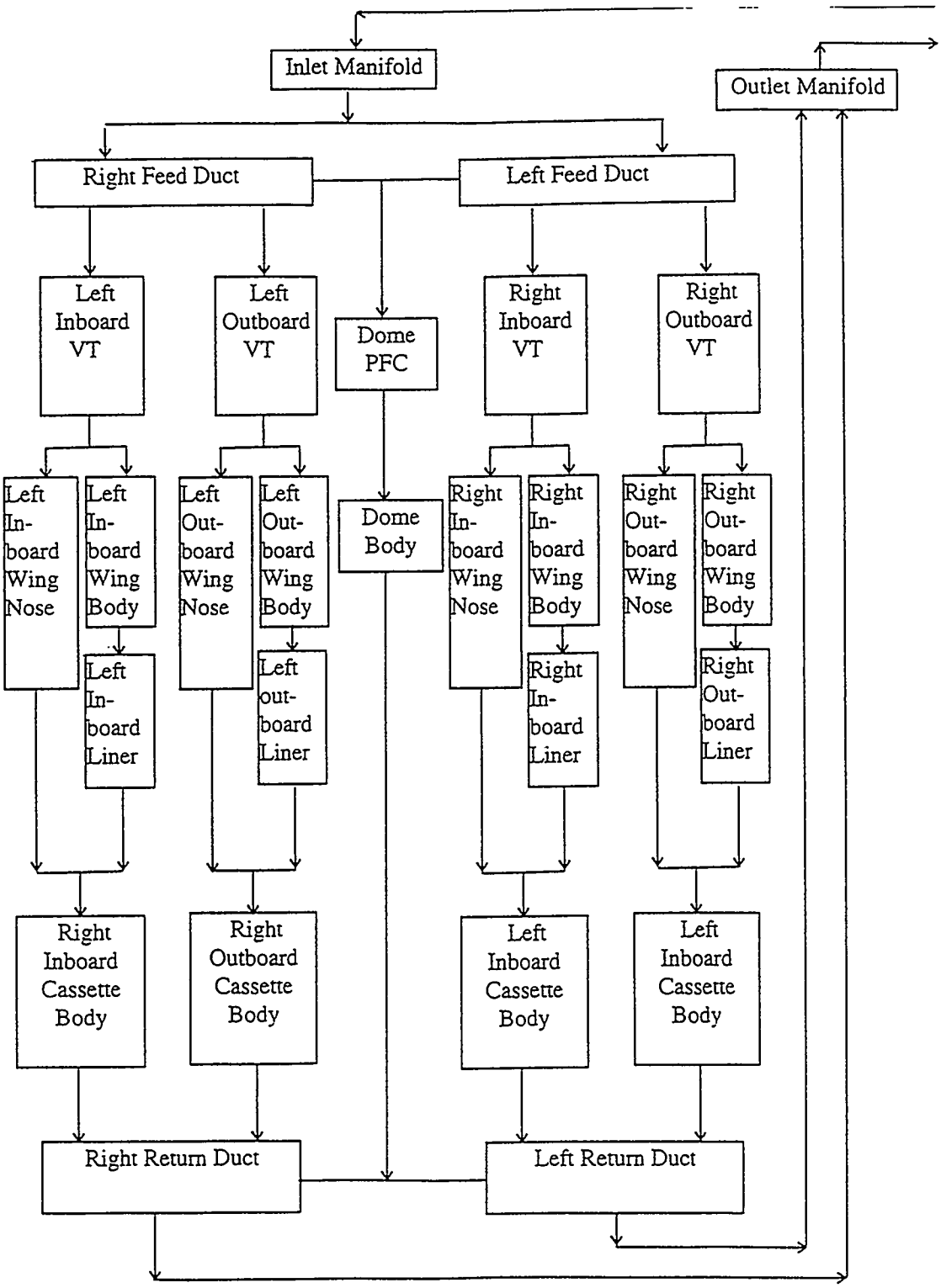

The JCT Concept

Viewgraph 6
NJZ
1/8/96

Westinghouse
Science & Technology Center

THE REFERENCE DESIGN CONCEPT

	V (m/s)	Flow Rate (liters/s)	ΔT (°C)	ΔP (MPa)	CHF Margin
Out Target	10.1	16.7	25.1	0.500	1.50
Out Wing Nose	7.00	2.45	12.9	0.226	1.67
Out Wing Body	7.07	14.2	12.8	0.131	6.72
Out Liner	7.11	14.2	N/A	0.094	N/A
In Target	10.1	12.1	25.8	0.450	1.50
In Wing Nose	4.80	1.78	13.2	0.138	1.83
In Wing Body	5.14	10.3	12.9	0.076	5.69
In Liner	5.17	10.3	N/A	0.062	N/A
Dome	5.90	10.5	41.4	0.159	1.69
Total	N/A	4.09E+03	25.2	0.726	N/A

Pumping Power = 3.0 MW

Viewgraph 7
NJZ
1/8/96

Westinghouse
Science & Technology Center

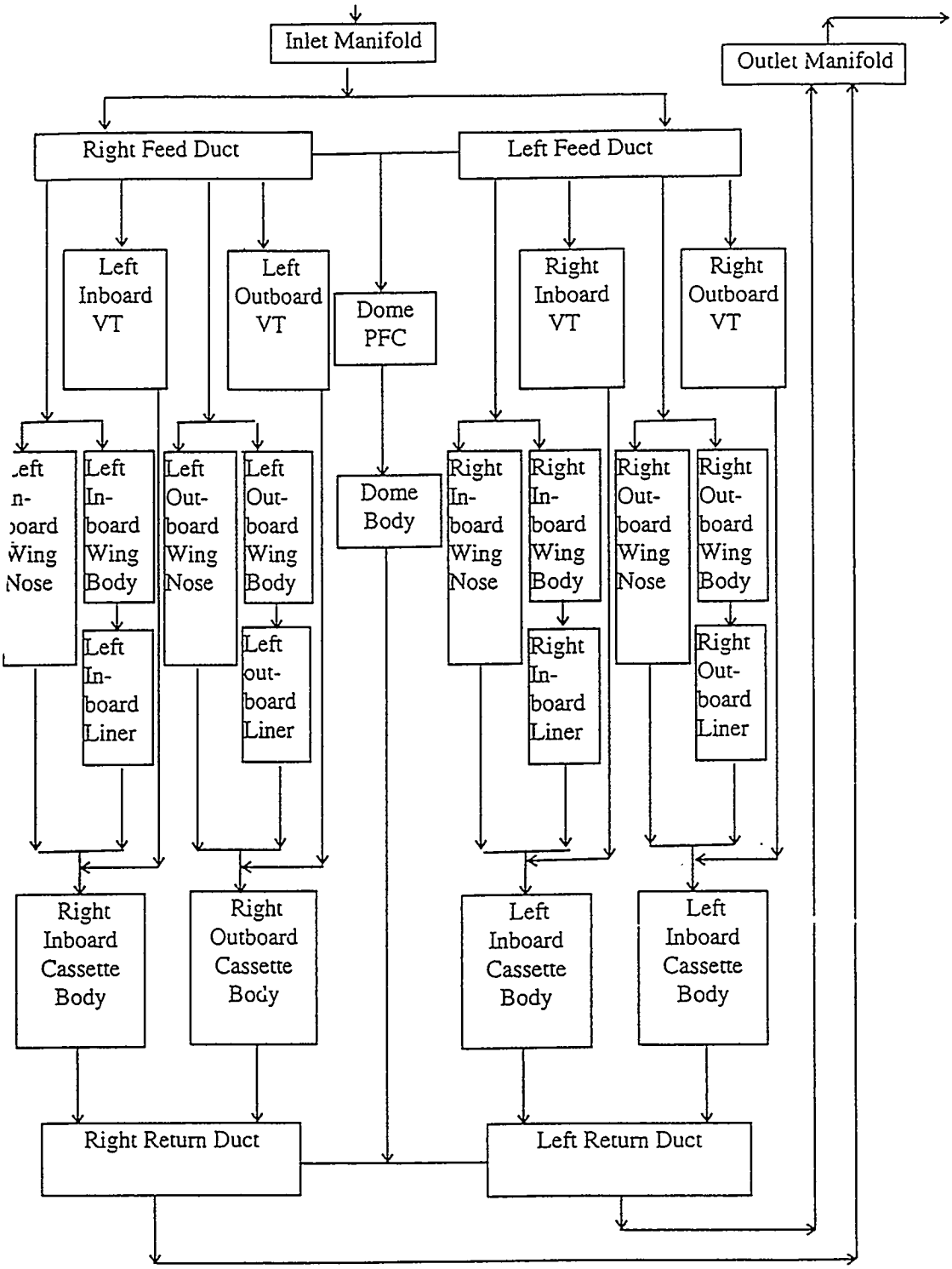

Concept A

Viewgraph 8
NJZ
1/8/96

Westinghouse
Science & Technology Center

CONCEPT A-1

(Verical Target Separately Cooled; Dump Target in Series with Vertical Target)

	V (m/s)	Flow Rate (liters/s)	ΔT (°C)	ΔP (MPa)	CHF Margin
Out Target	10.1	16.7	25.1	0.500	1.50
Out Wing Nose	3.8	1.33	24.2	0.046	1.68
Out Wing Body	3.0	6.03	30.2	0.026	4.4
Out Liner	3.02	6.03	N/A	0.019	N/A
In Target	10.1	12.1	25.9	0.450	1.50
In Wing Nose	3.50	1.22	19.7	0.044	1.67
In Wing Body	2.80	5.63	24.2	0.024	4.33
In Liner	2.81	5.63	N/A	0.020	N/A
Dome	5.9	10.5	41.4	0.159	1.65
Total	N/A	5.16E+03	20.0	0.50	N/A

Pumping Power = 2.6 MW

Viewgraph 9
NJZ
1/8/96

Westinghouse
Science & Technology Center

CONCEPT A-2

(Verical Target Separately Cooled; Dump Target in Series with Wing)

	V (m/s)	Flow Rate (liters/s)	ΔT (°C)	ΔP (MPa)	CHF Margin
Out target	10	16.5	26.0	0.365	1.50
Out Dump Target	7.7	12.7	N/A	0.121	1.50
Out wing nose	5.1	17.8	18.0	0.145	2.06
Out wing body	5.44	10.9	16.6	0.081	6.37
Out liner	5.46	10.9	N/A	0.060	N/A
In Target	10	12.0	26.9	0.316	1.50
In Dump Target	7.7	9.24	N/A	0.121	1.50
In wing nose	3.70	1.29	18.6	0.086	1.71
In wing body	3.91	7.86	17.3	0.046	5.18
In liner	3.93	7.86	N/A	0.038	N/A
Dome	5.9	1.05	41.4	0.159	1.65
Total	N/A	6.69E+03	15.4	0.365	N/A

PUMPING POWER = 2.5 MW

Viewgraph 10
NJZ
1/8/96

Westinghouse
Science & Technology Center

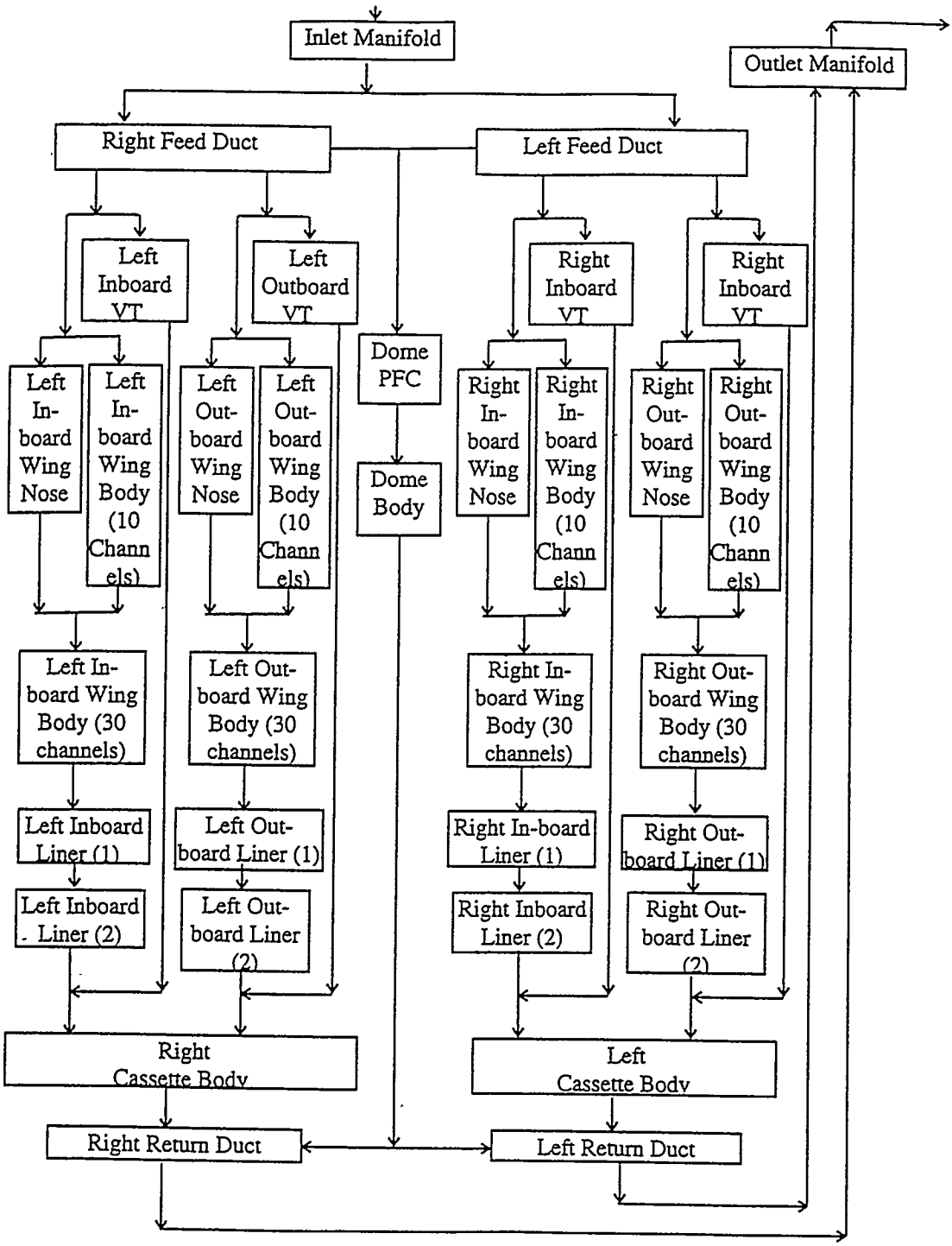

Concept B

Viewgraph 11
NJZ
1/8/96

Westinghouse
Science & Technology Cente

CONCEPT B

(Separate Vertical Target and Split Wing Routing)

	V (m/s)	Flow Rate (liters/s)	ΔT (°C)	ΔP (MPa)	CHF Margin
Out Target	10.1	16.7	25.1	0.500	1.50
Out Wing Nose	3.10	1.08	29.7	0.032	1.50
Out Wing Body In	3.70	1.86	N/A	0.026	N/A
Out Wing Body Out	1.95	2.94	24.9	0.012	3.38
Out Liner	2.94	2.94	N/A	0.040	N/A
In Target	10.1	12.1	25.9	0.450	1.50
In Wing Nose	3.10	1.08	22.2	0.035	1.53
In Wing Body In	3.40	1.71	N/A	0.029	N/A
In Wing Body Out	1.85	2.79	20.0	0.011	3.39
In Liner	2.8	2.79	N/A	0.044	N/A
Dome	5.9	10.5	41.4	0.159	1.69
Total	N/A	4.77E+03	21.6	0.50	N/A

Pumping Power = 2.4 MW

Viewgraph 12
NJZ
1/8/96

Westinghouse
Science & Technology Center

CONCEPT C-1-1

(Separate Vertical Target and Wing/Dome Routing; Dump Target in Series with Wing)

	V (m/s)	Flow Rate (liters/s)	ΔT (°C)	ΔP (MPa)	CHF Margin
Out Target	10	16.5	26.0	0.365	1.50
Out Dump Target	7.7	12.7	N/A	0.121	1.50
Out Wing Nose	5.20	1.82	18.0	0.080	2.07
Out Wing Body	5.42	10.9	16.7	0.080	6.37
Out Liner	4.84	9.68	N/A	0.045	N/A
In Target	10	12.0	26.9	0.316	1.50
In Dump Target	7.7	9.24	N/A	0.117	1.50
In Wing Nose	3.62	1.27	19.0	0.047	1.71
In Wing Body	3.97	7.98	17.1	0.047	5.28
In Liner	3.11	6.21	N/A	0.022	N/A
Dome	6.8	12.1	36.8	0.197	1.50
Total	N/A	6.05E+03	17.0	0.398	N/A

Pumping Power = 2.4 MW

Viewgraph 14
NJZ
1/8/96

Westinghouse
Science & Technology Center

CONCEPT C-1-2

(Separate Vertical Target and Wing/Dome Routing; Dump Target in Series with Vertical Target)

	V (m/s)	Flow Rate (liters/s)	ΔT (°C)	ΔP (Pa)	CHF Margin
Out Target	10.1	16.7	25.1	0.500	1.50
Out Wing Nose	3.7	1.29	24.9	0.044	1.64
Out Wing Body	3.90	7.84	23.3	0.043	5.09
Out Liner	2.87	5.75	N/A	0.017	N/A
In Target	10.1	12.1	25.9	0.450	1.50
In Wing Nose	3.50	1.22	19.7	0.044	1.67
In Wing Body	3.80	7.64	17.8	0.043	5.16
In Liner	2.74	5.48	N/A	0.018	N/A
Dome	7.6	13.5	33.0	0.240	1.50
Total	N/A	5.61E+03	18.3	0.50	N/A

Pumping Power = 2.8 MW

Viewgraph 15
NJZ
1/8/96

Westinghouse
Science & Technology Center

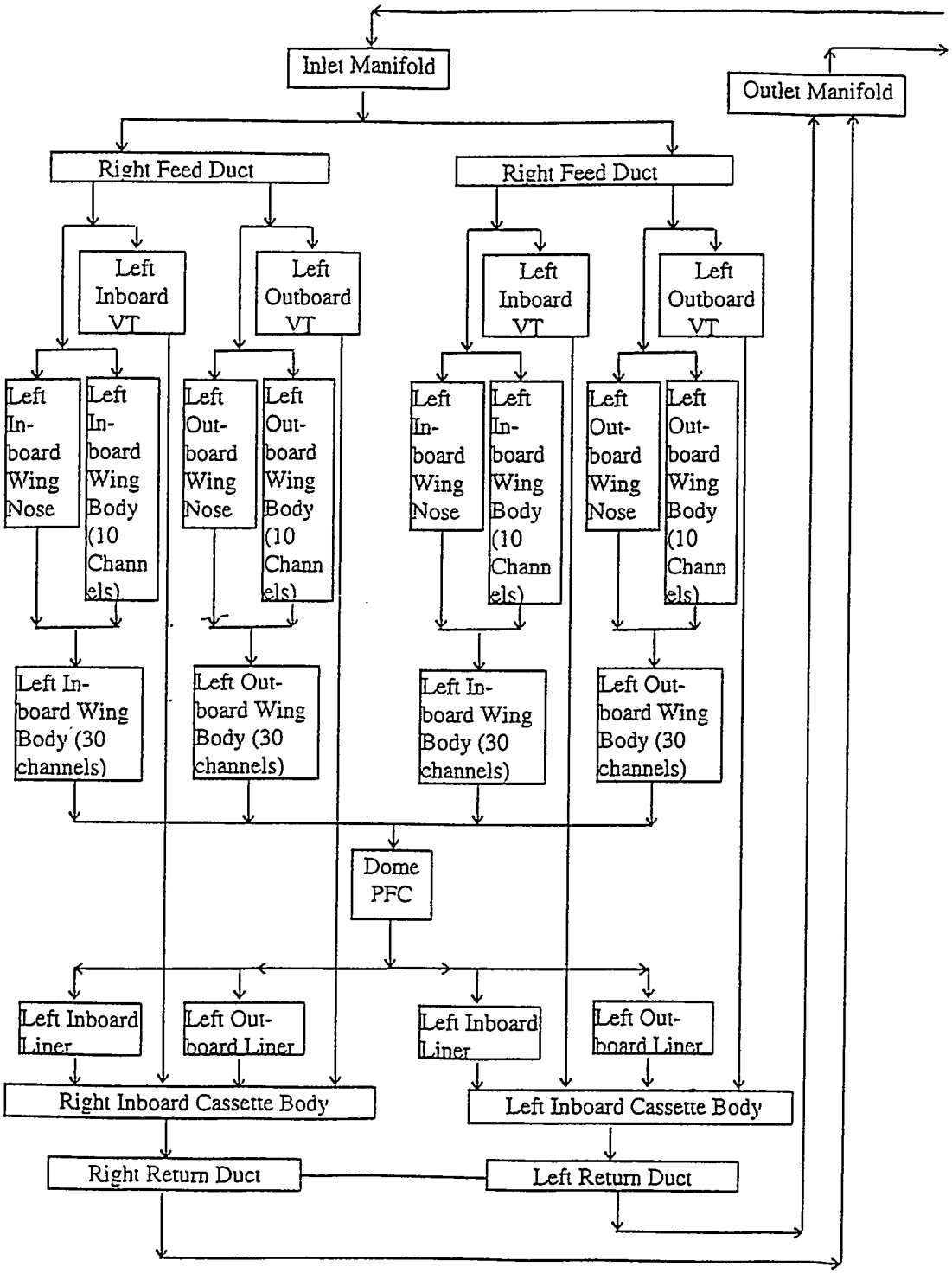

Concept C-2

Viewgraph 16
NJZ
1/8/96

Westinghouse
Science & Technology Center

CONCEPT C-2

(Separate Vertical Target, Split Wings Plus Dome)

	V (m/s)	Flow Rate (liters/s)	ΔT (°C)	ΔP (MPa)	CHF Margin
Out Target	10.1	16.7	25.1	0.500	1.50
Out Wing Nose	4.80	1.68	19.1	0.057	1.50
Out Wing Body In	4.40	2.21	N/A	0.036	N/A
Out Wing Body Out	2.58	3.89	20.5	0.020	4.08
Out Liner	1.94	3.89	N/A	0.008	N/A
In Target	10.1	12.1	25.9	0.450	1.50
In Wing Nose	5.40	1.89	12.7	0.077	1.62
In Wing Body In	4.20	2.11	N/A	0.040	N/A
In Wing Body Out	2.65	4.00	16.1	0.022	4.28
In Liner	2.00	4.00	N/A	0.011	N/A
Dome	8.85	15.8	27.2	0.315	1.52
Total	N/A	4.40E+03	23.4	0.50	N/A

Pumping Power = 2.2 MW

Viewgraph 17
NJZ
1/8/96

Westinghouse
Science & Technology Center

SUMMARY

Concept	Flow Rate (liters/s)	ΔT (°C)	ΔP (MPa)	Pumping Power (MW)
JCT	4.09 E+03	25.2	0.73	3.0
A-1	5.16 E+03	20.0	0.50	2.6
A-2	6.69 E+03	15.4	0.37	2.5
B	4.77 E+03	21.6	0.50	2.4
C-1-1	6.05 E+03	17.0	0.39	2.4
C-1-2	5.61 E+03	18.3	0.50	2.8
C-2	4.40E+03	23.4	0.50	2.2

Viewgraph 18
NJZ
1/8/96

Westinghouse
Science & Technology Center

CONCLUSIONS

- Pressure drop in the vertical target dominates the overall system pressure drop
- Separating the vertical target from low heat flux components will increase the flow rate, but reduce the system pressure drop
- Combining the dump target in series with the wing cooling channels will further reduce the pressure drop, but result in an excessive use of coolant
- Coolant flow rate can be reduced if the coolant use is optimized in the wing (Concepts B and C-2)
- Combining the dome with the wings and optimizing the coolant use at the wings (Concept C-2) reduce the power consumption by 26% from the JCT concept, and require a slight increase in flow rate

Viewgraph 19
NJZ
1/8/96

Westinghouse
Science & Technology Center

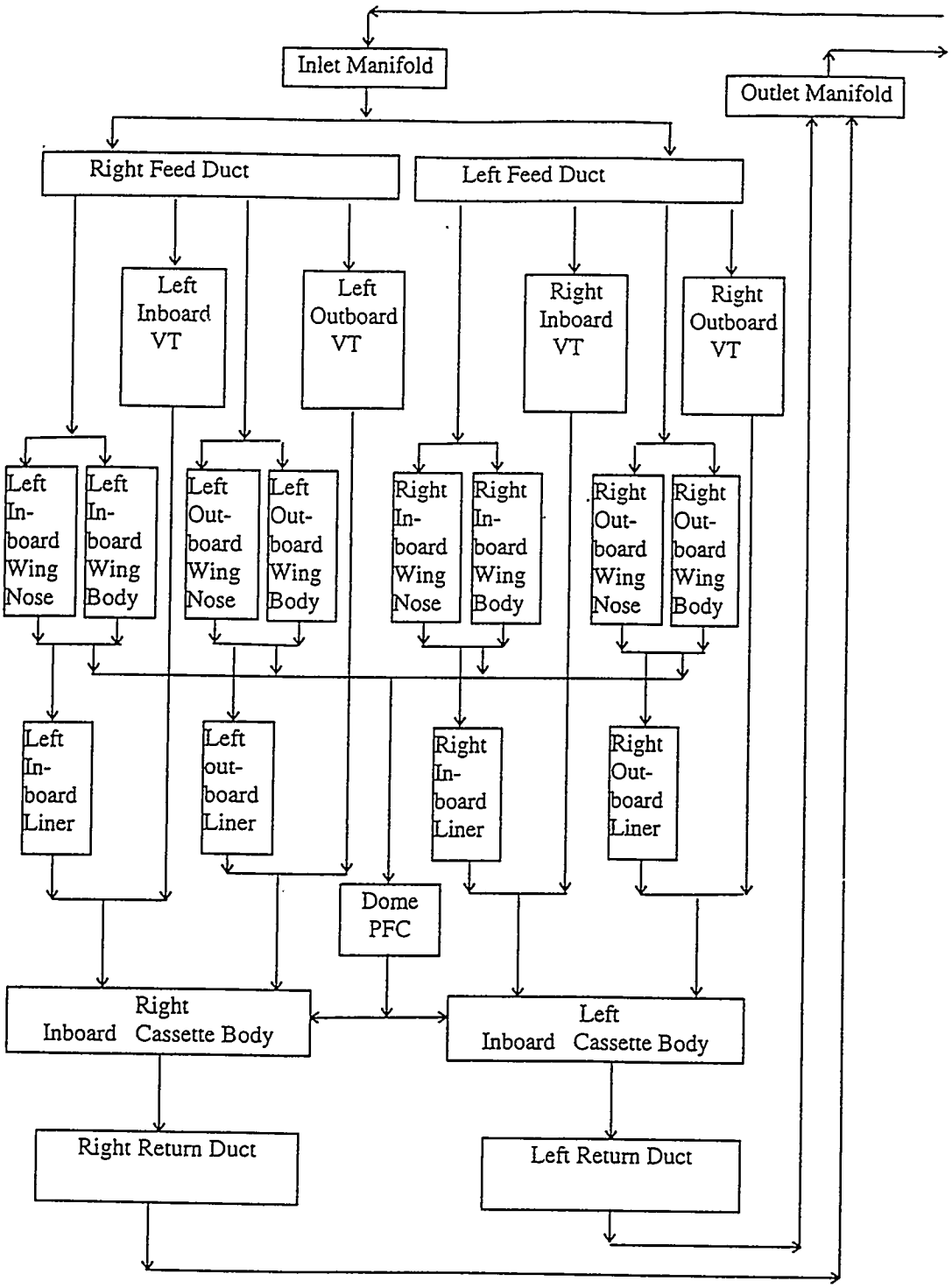

Concept C-1

Viewgraph 13
NJZ
1/8/96

Westinghouse
Science & Technology Center

1996 U.S./Japan Workshop Q219

Post-Critical Heat Flux and Loss of Flow Accident Experiments at Sandia

Theron Marshall

Rensselaer Polytechnic Institute

(505) 845-3136; TDMARSH@sandia.gov

Robert Watson Jimmie McDonald Dennis Youchison

La Wanda Wold Lee Cadwallader (INEL)

TDM 010596

Sandia National Laboratories

Introduction to Post-CHF research.

- Goals
  - Exceed the local CHF point using EBTS,
  - Demonstrate existence of stable Post-CHF mockup temperatures.
- Results
  - Stable surface temperatures beyond the local CHF point,
  - Local CHF point exceeded by 80%.

TDM 010596

Sandia National Laboratories

With one-sided heating, simultaneous coexistence of all heat transfer regimes is possible. (Boyd/Tanchuk)

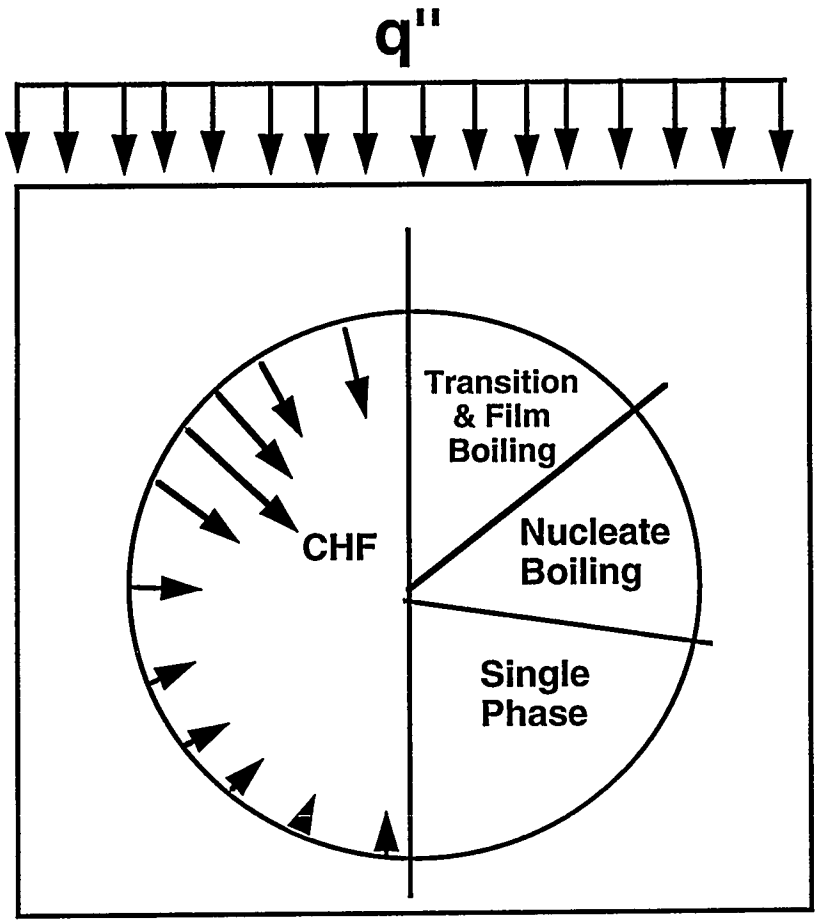

TDM 010596

Sandia National Laboratories

Incident heating was provided by Sandia's 30 kW electron beam test system (EBTS)

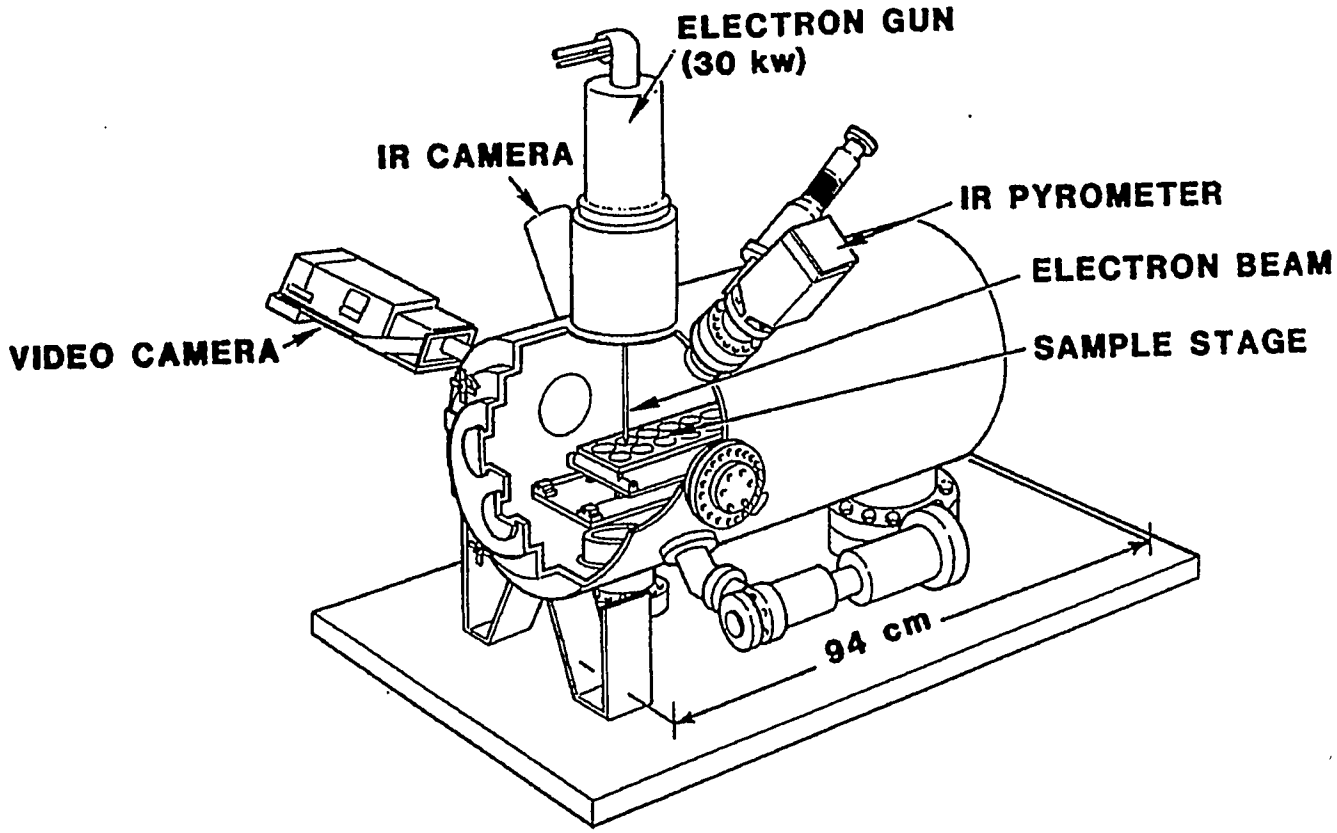

TDM 010596

Sandia National Laboratories

Mockup had H_L= 40 mm, H_w= 16 mm, ID= 7.7 mm, and Type-K thermocouples 0.5 mm from heated surface.

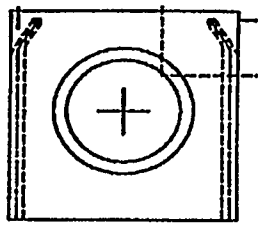

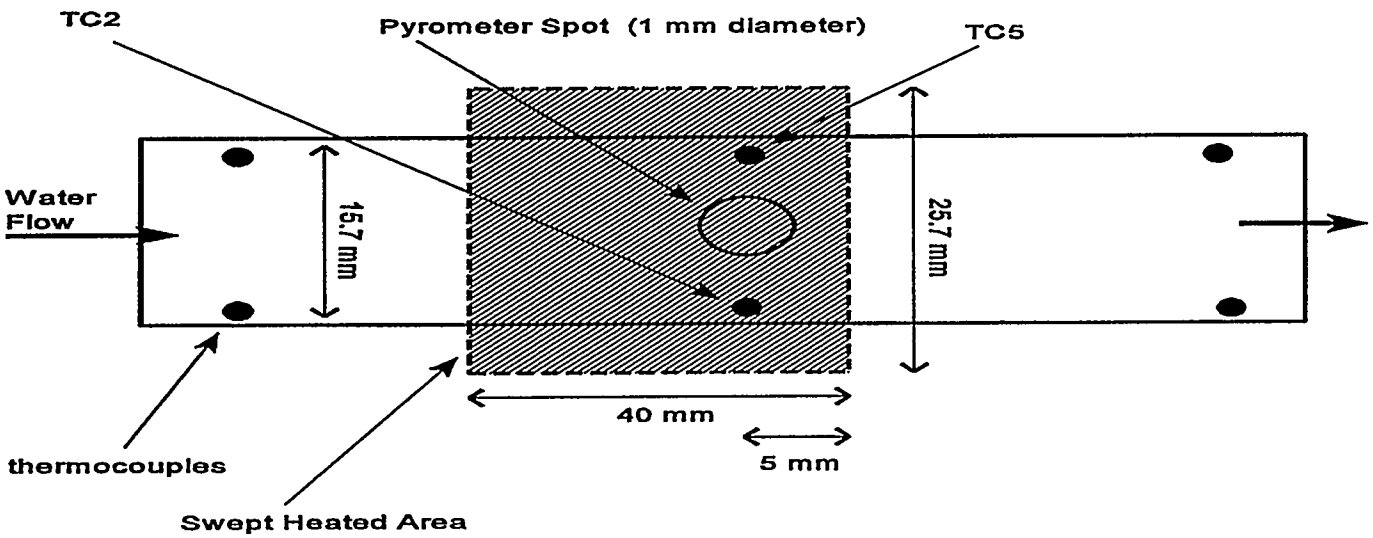

TDM 010596

Sandia National Laboratories

Temperatures in the single phase, nucleate boiling and Post-CHF regimes were experimentally measured

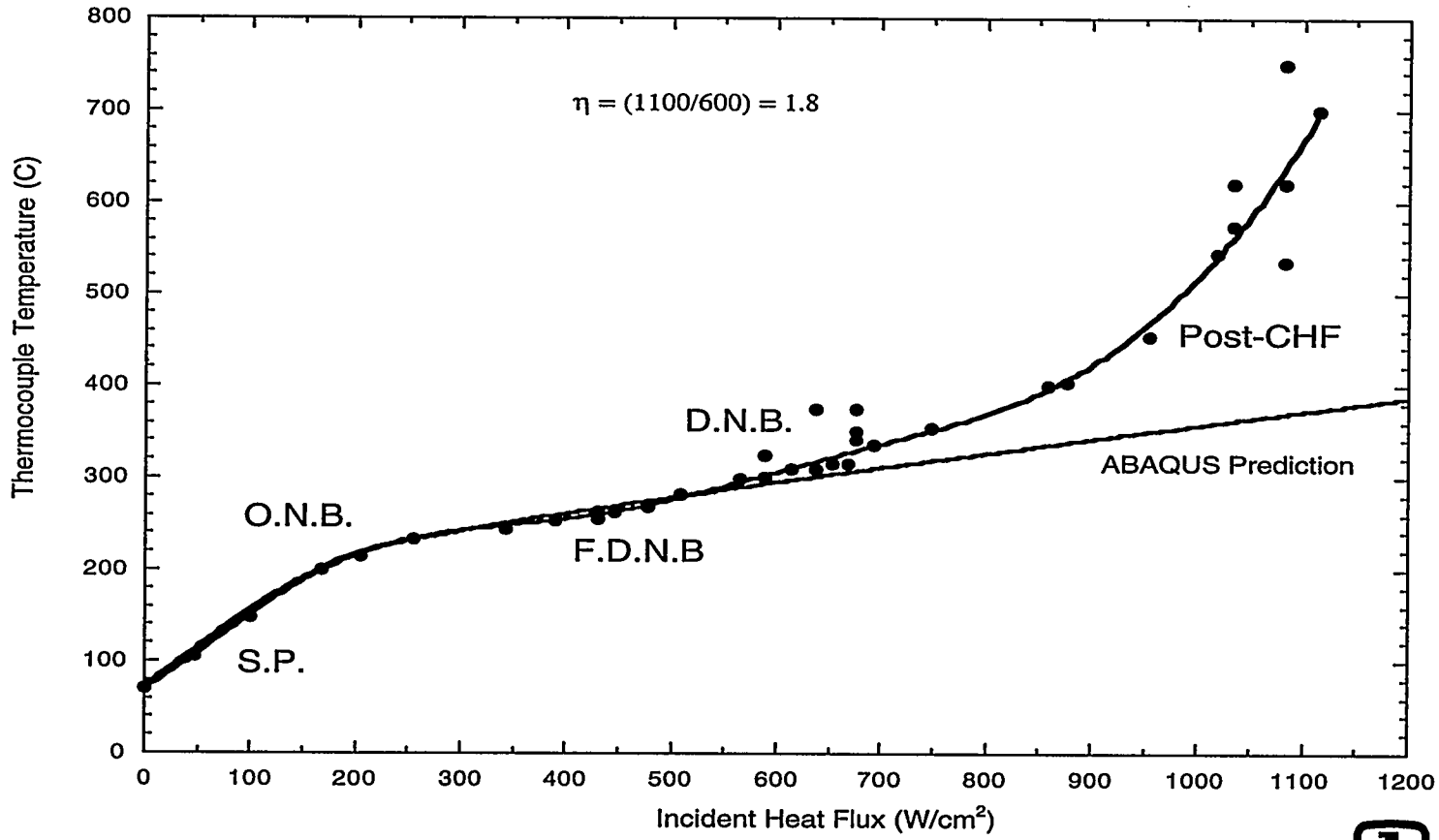

TDM 010596

Sandia National Laboratories

Introduction to LOFA research

- Goal
  - generate experimental time-to-burnout data for prototypical divertor plate during a simulated Loss of Flow Accident (LOFA).
- Results
  - eight experimental time-to-burnout data points,
  - preliminary experimental indication on the influence of steady-state inlet velocity,
  - preliminary experimental indication on the influence of steady state incident heating.

The LOFA is an unexamined ITER concern.

- Tore Supra experienced the equivalent of a LOFA in 1991.
- LOFA are anticipated for ITER
  - divertor tube blockage, frequency: 8E-2/yr
  - pump seizure, frequency: 2E-02/yr
  - all pumps coast down, frequency: 0.26/yr
- No experimental LOFA data published.

Time-to-burnout is the time to reach high temperature trip after pump has been tripped off.

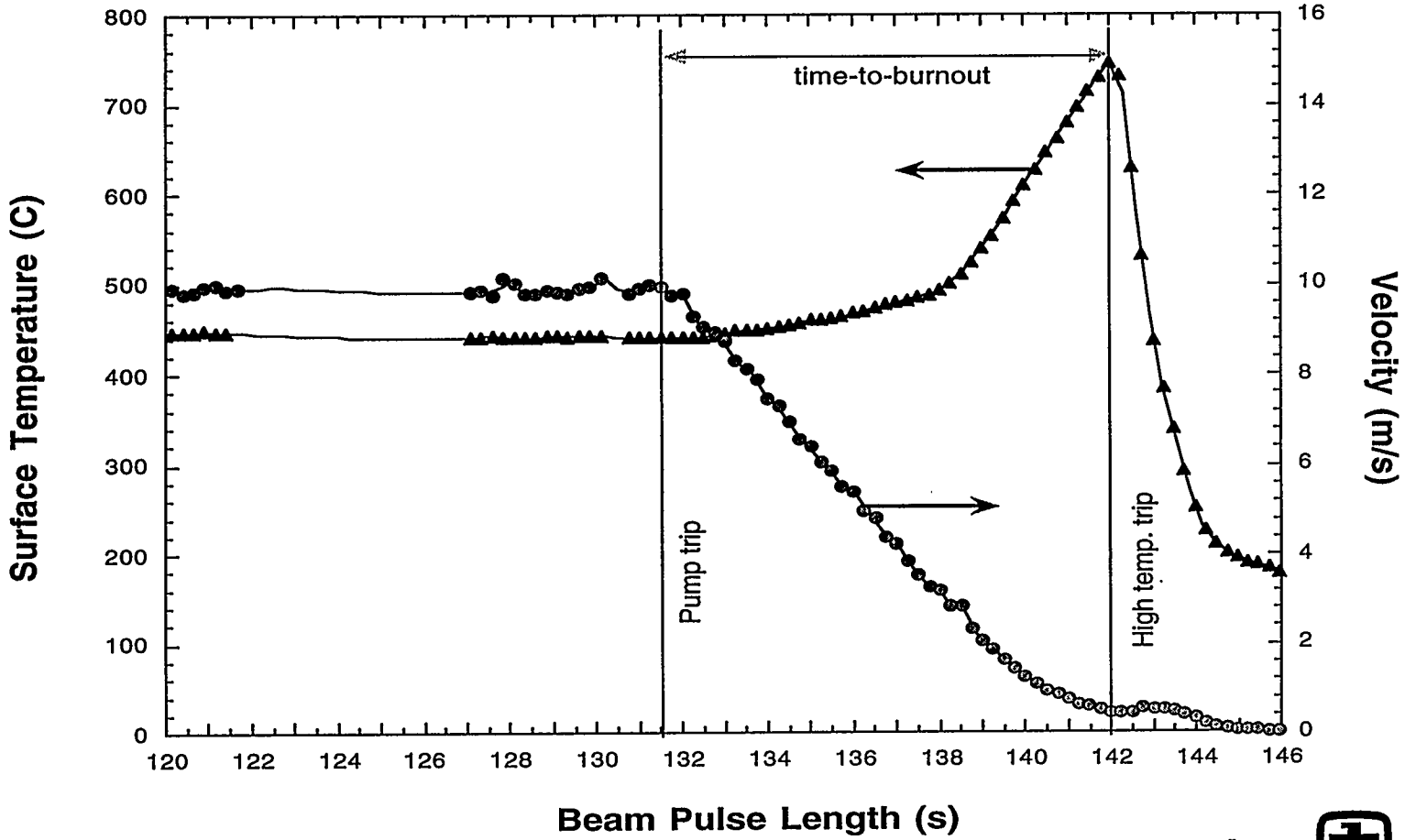

TDM 010596

Sandia National Laboratories

Time-to-burnout vs. velocity response for inlet conditions of 1 MPa, 70 C, 5 MW/m²

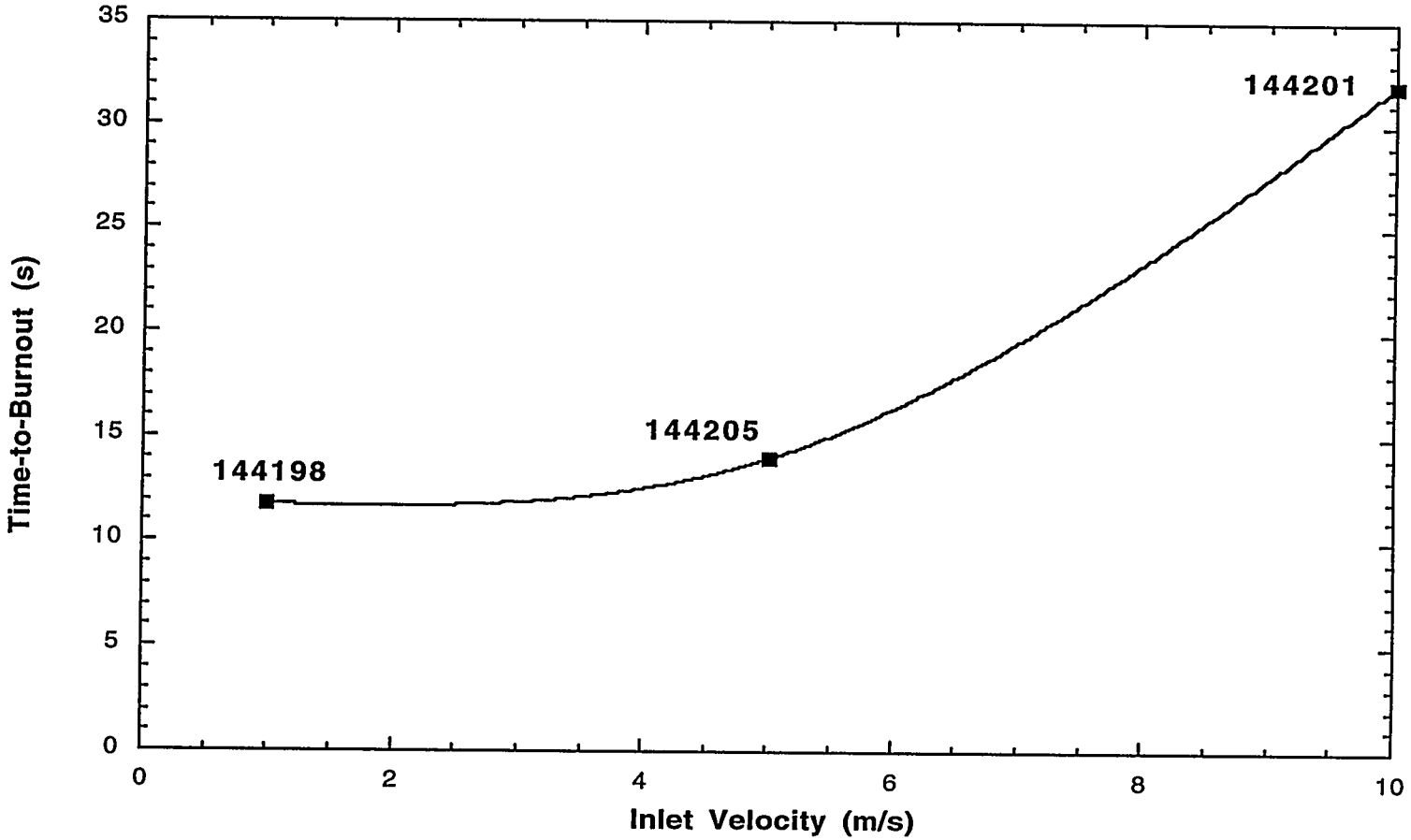

TDM 010596

Sandia National Laboratories

Time-to-burnout vs. incident heat flux for inlet conditions of: 1 MPa, 11 C, 10 m/s

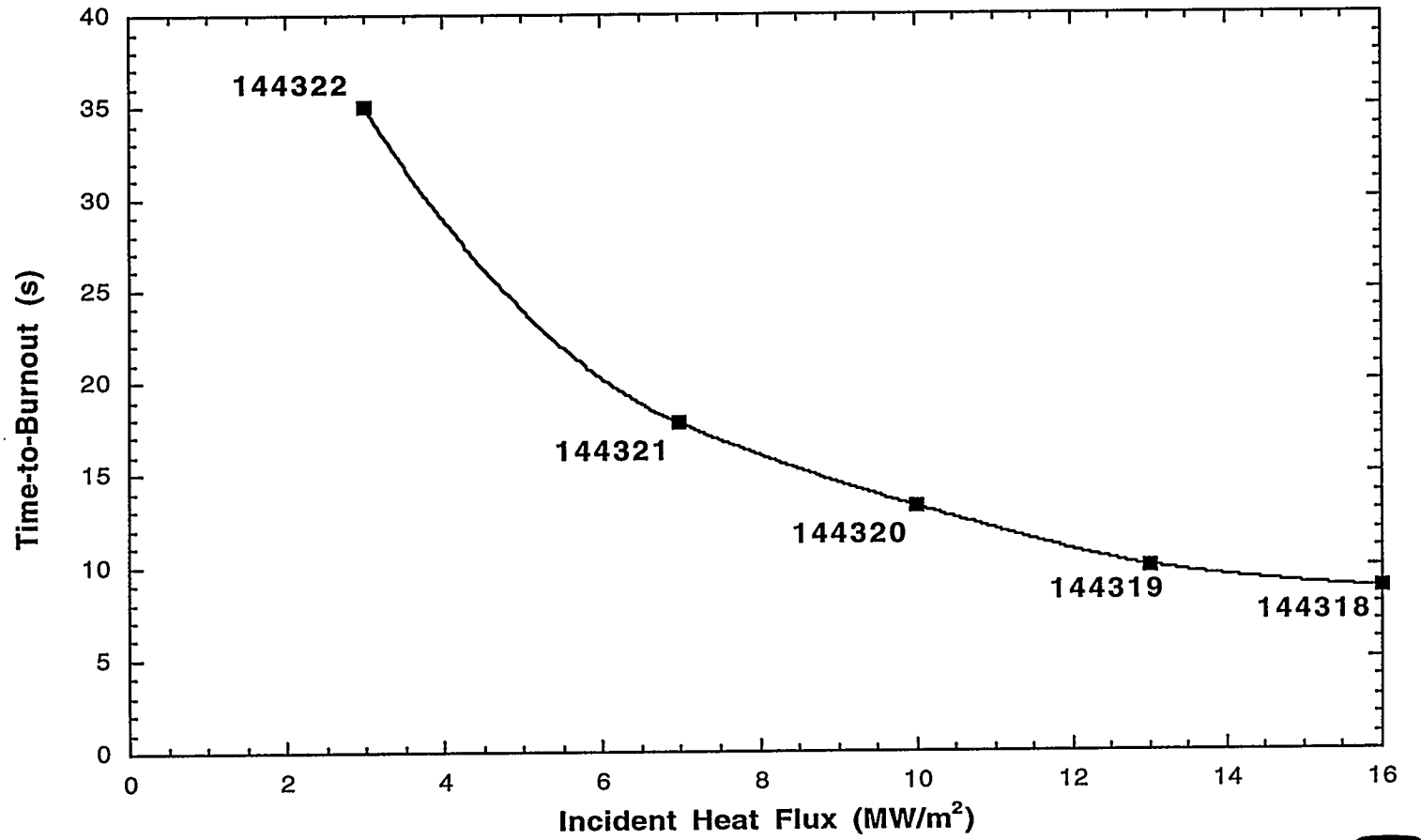

TDM 010596

Sandia National Laboratories

Finite element modeling of LOFA does not agree well with experimental results.

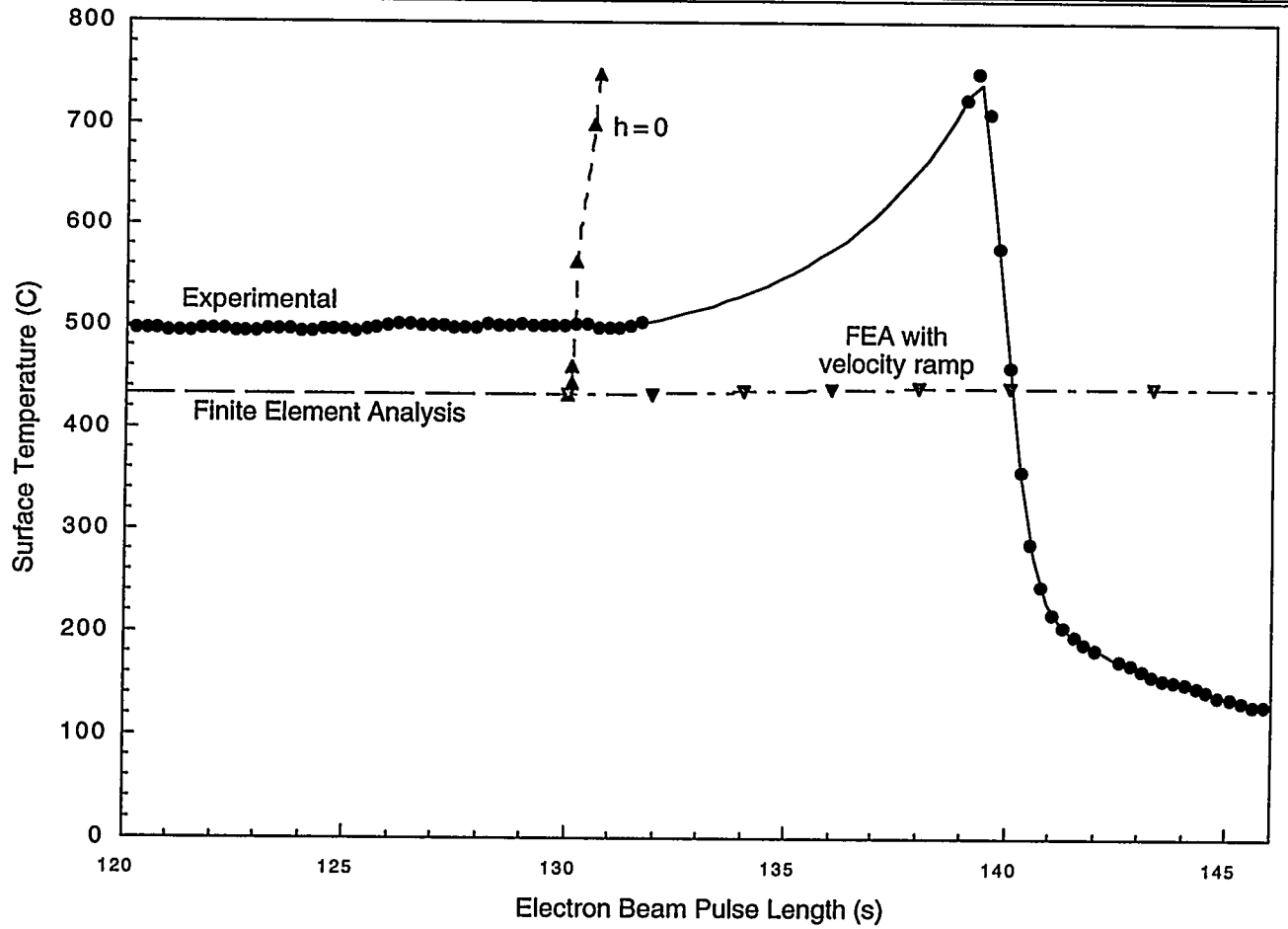

TDM 010596

Sandia National Laboratories

Phase II mockups are being fabricated

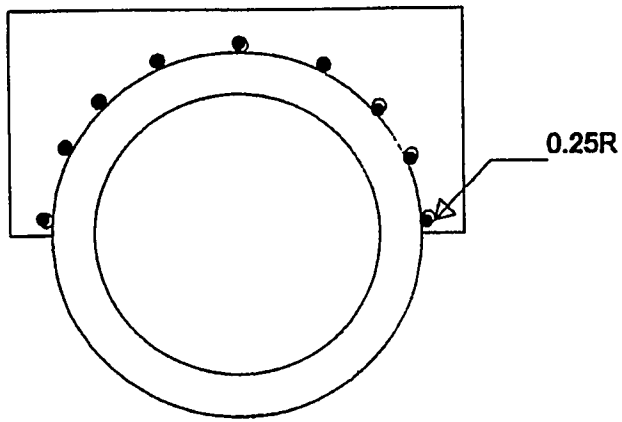

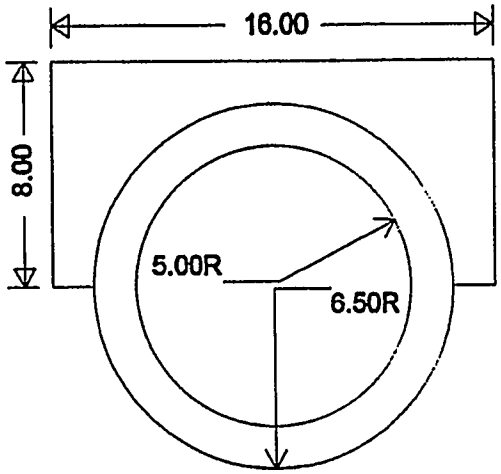

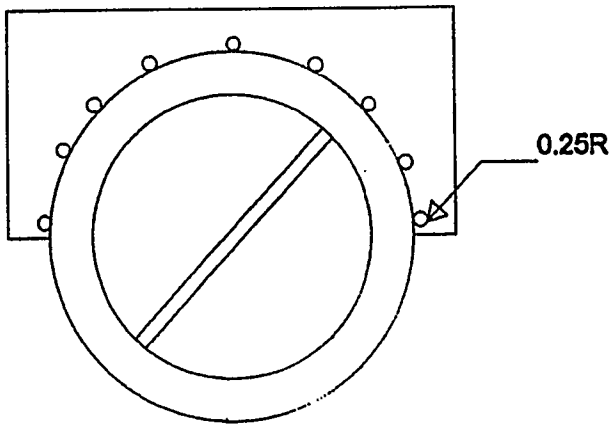

Will use inverse heat conduction analysis to calculate h_{film}, q_{wall}, and T_{wall} from TC data.

All units are in millimeters (mm)

TDM 010596

Sandia National Laboratories

Test matrix for Phase II swirl tube mockup

Research Area	E-beam shots	Heated Length (cm)	Pressure (MPa)	Velocity (m/s)	Temperature (C)
Heat Transfer	120	80	1, 4	1, 7 ,15	70, 150
LOFA	24	10, 80	1, 4	1, 7 ,15	70, 150
CHF	156	10, 50, 80	1, 4	1, 3, 7 ,15	70, 150

TDM 010596

Sandia National Laboratories

Test matrix for Phase III ribbed channel mockup

Research Area	E-beam shots	Heated Length (cm)	Pressure (MPa)	Velocity (m/s)	Temperature (C)
Heat Transfer	76	80	1, 4	1, 7 ,15	70, 150
LOFA	24	50, 80	1, 4	1, 7 ,15	70, 150
CHF	200	80	1, 4	1, 3, 7 ,15, 20	20, 70, 150

TDM 010596

Sandia National Laboratories

Concluding Remarks

- Post-CHF Experiment:
  - Experimental maximum achievable heat flux exceeded local critical heat flux by 80%, due to Post-CHF enhancement.
- LOFA Experiment:
  - time-to-burnout increases parabolically with increasing initial inlet velocity.
  - time-to-burnout decreases parabolically with increasing incident heat flux.
- Future experiments with more ITER relevant mockups will further examine the above observations.

Session IV

Plasma Surface Interactions and Plasma Facing Materials

Chaired by: *A. Hassanein and Y. Hirohata*

IV.1	**Hirohata**/Hino	PSI Studies at Hokkaido University
IV.2	**Tokunaga**/ Yoshida	Erosion and Gas Impurity Emission of B_4C Converted CFC
IV.3	**Doerner**	Reduced Be Erosion in PISCES-B
IV.4	**Hirooka**	Be Erosion and Compatibility with C and W as Other PFM
IV.5	Brooks/ **Hassanein**	Erosion and Redeposition Analysis for ITER and DIII-D
IV.6	Cohen/**Skinner**	Arc Jets for PFC - High Heat Flux Testing
IV.7	Cohen/**Skinner**	Studies of Thermally Collapsed Plasmas

PSI Studies at Hokkaido University

Presented by Y. Hirohata and T. Hino

Major Studies at Hokkaido Univ.

(i) Reduction of heat flux (Concept)
(Divertor configuration
Vapor shielding)

(ii) Disruption Erosion (Modeling)
(Particle emission)

(iii) Reduction of He ash concentration (Concept)
(Use of selective pumping metal
Divertor configuration

(iv) Hydrogen adsorption of Ti-alloy (Data)
with Toshiba
(Ti-V-Al alloy)

(v) Gas desorption of CFC/Cu brazed material (Data)
with JAERI

(vi) Hydrogen retention and oxygen gettering of boron film (Data) with NIFS

(vii) Oxygen gettering of lithium (Data)

(viii) Thermal response of boronized or siliconized CFC/Cu brazed material (Data) with NIFS

(ix) Hydrogen retention properties of several plasma facing materials (Data)
(C, B_4C, SiC, W)

(x) Helium selective pumping properties of nickel and tungsten (Data)

(xi) Analysis for loss of coolant accident, LOCA (Concept)

We here introduce the subjects of (ix) and (x).

Hydrogen Retention Properties of SiC Converted Graphite

Yuji YAMAUCHI, Tomoaki HINO, Yuko HIROHATA and Toshiro YAMASHINA

Department of Nuclear Engineering, Hokkaido University

Present study

SiC converted graphite

○**Evaluation Hydrogen Retention Properties**

Total amount of retained hydrogen

Temperature dependence of hydrogen retention

○**Reduction of retained hydrogen by helium ion impact desorption**

⇩

Comparison for results of isotropic graphite and B_4C converted graphite

Experiment

Sample

SiC converted graphite
(Toyo Tanso Co.Ltd.)

$SiO+2C \rightarrow SiC+CO$

Si concentration : 40 at.%

Isotropic graphite (Hitachi Chemical)

B_4C converted graphite
(Hitachi Chemical)

Ion Irradiation (H_3^+ or He^+)

ECR Ion Irradiation Apparatus

Evaluation Method

Thermal Desorption Spectroscopy (TDS)

ECR Ion Source

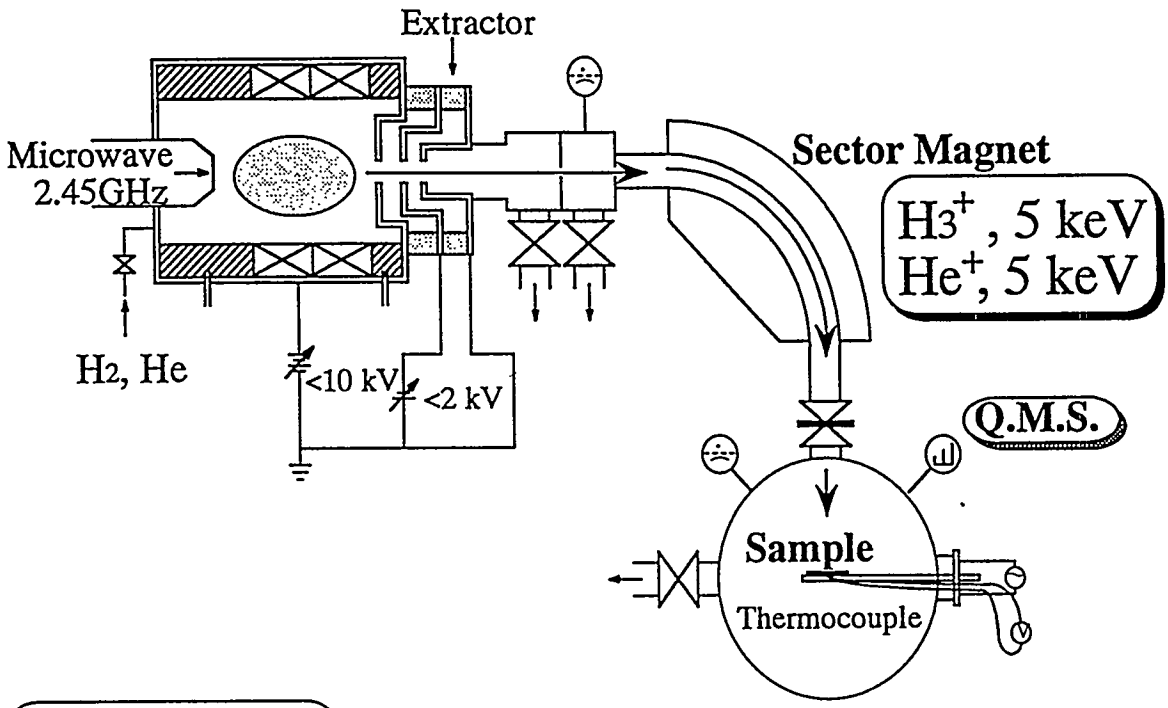

Procedure

(1) Evaluation of hydrogen retention properties

H_3^+ irradiation → TDS
(5×10^{18} H/cm^2)

(2) Reduction of hydrogen by He^+ bombardment

H_3^+ irradiation → He^+ irradiation
(up to 3×10^{18} He/cm^2)
→ TDS

TDS Condition

RT−1000 °C

Resistive heating (50 °C/min)

Results 1

Hydrogen Retention Properties of SiC Converted Graphite

(1)Thermal Desorption Spectra of H_2

H^+ Fluence=$5x10^{18}$ H/cm^2 Irrad.Temp.=RT

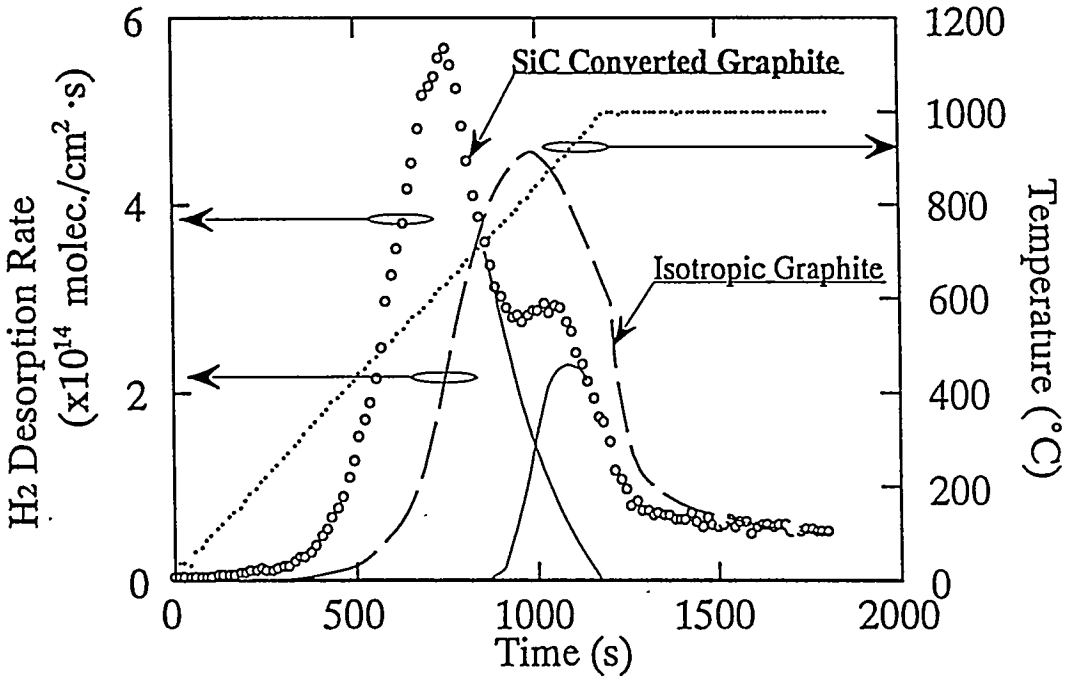

○H_2 desorption for Si-H bonding・・・600℃

◎**Si-H >C-H**

2 : 1

(2)Thermal Desorption Spectra of CH_4

H^+ Fluence=$5x10^{18}$ H/cm^2 Irrad.Temp.=RT

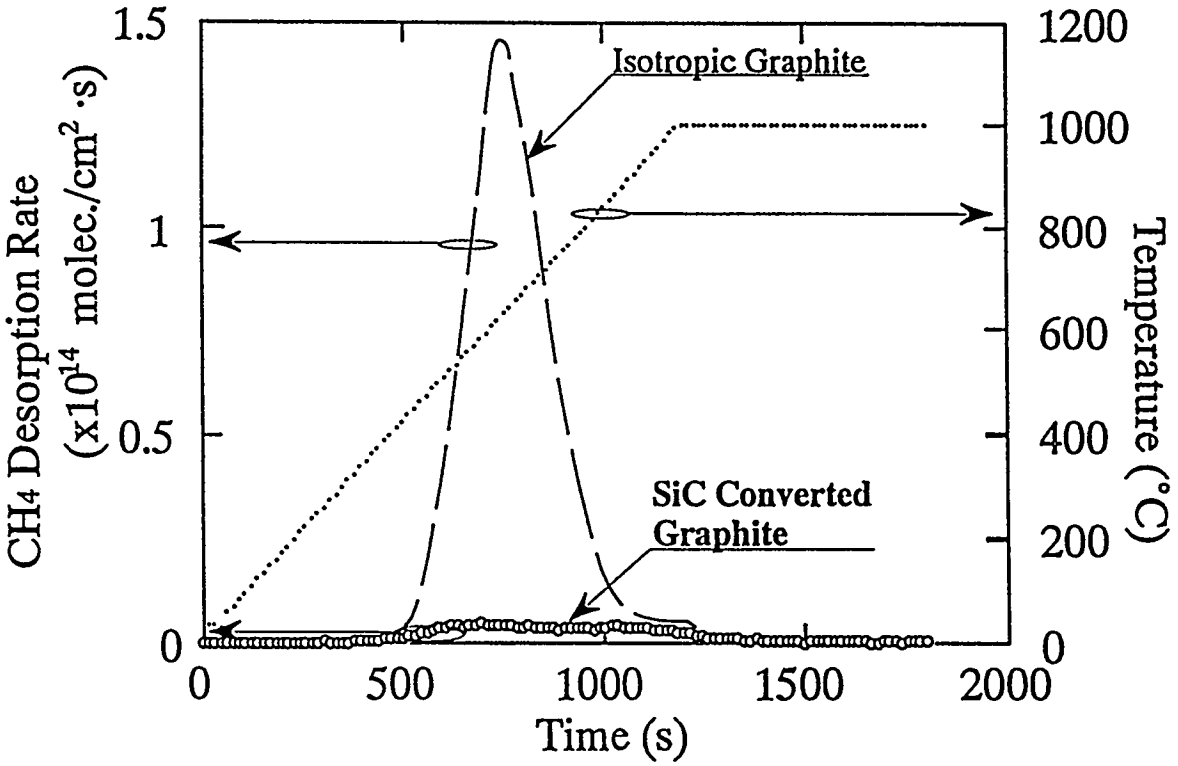

◎Chemical sputtering yield
10 times smaller than that of isotropic graphite

Hydrogen Retention Properties of B_4C Converted Graphite

(3)Thermal Desorption Spectra of H_2

H^+ Fluence=$5x10^{18}$ H/cm^2 Irrad.Temp.=RT

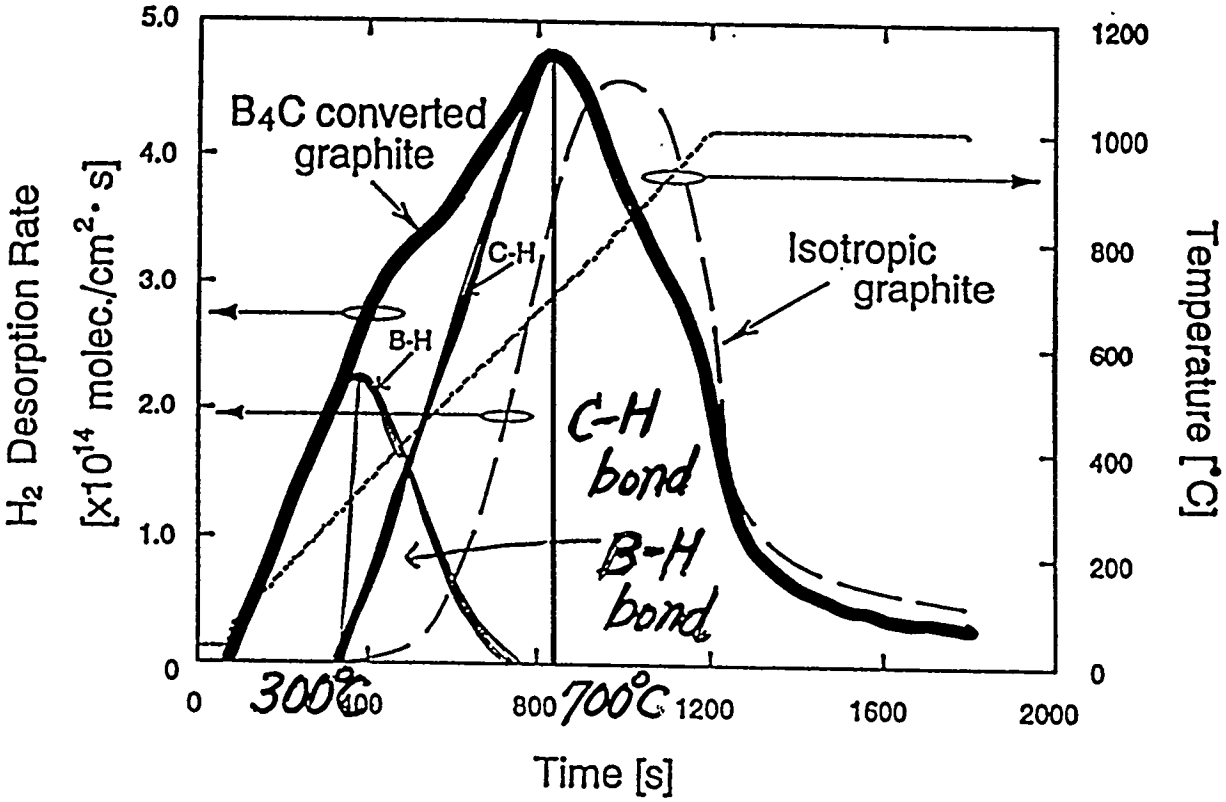

○H_2 desorption for B-H bonding・・・300℃

◎**B-H < C-H**

1 : 3

(4) Comparison:Hydrogen Desorption Amounts

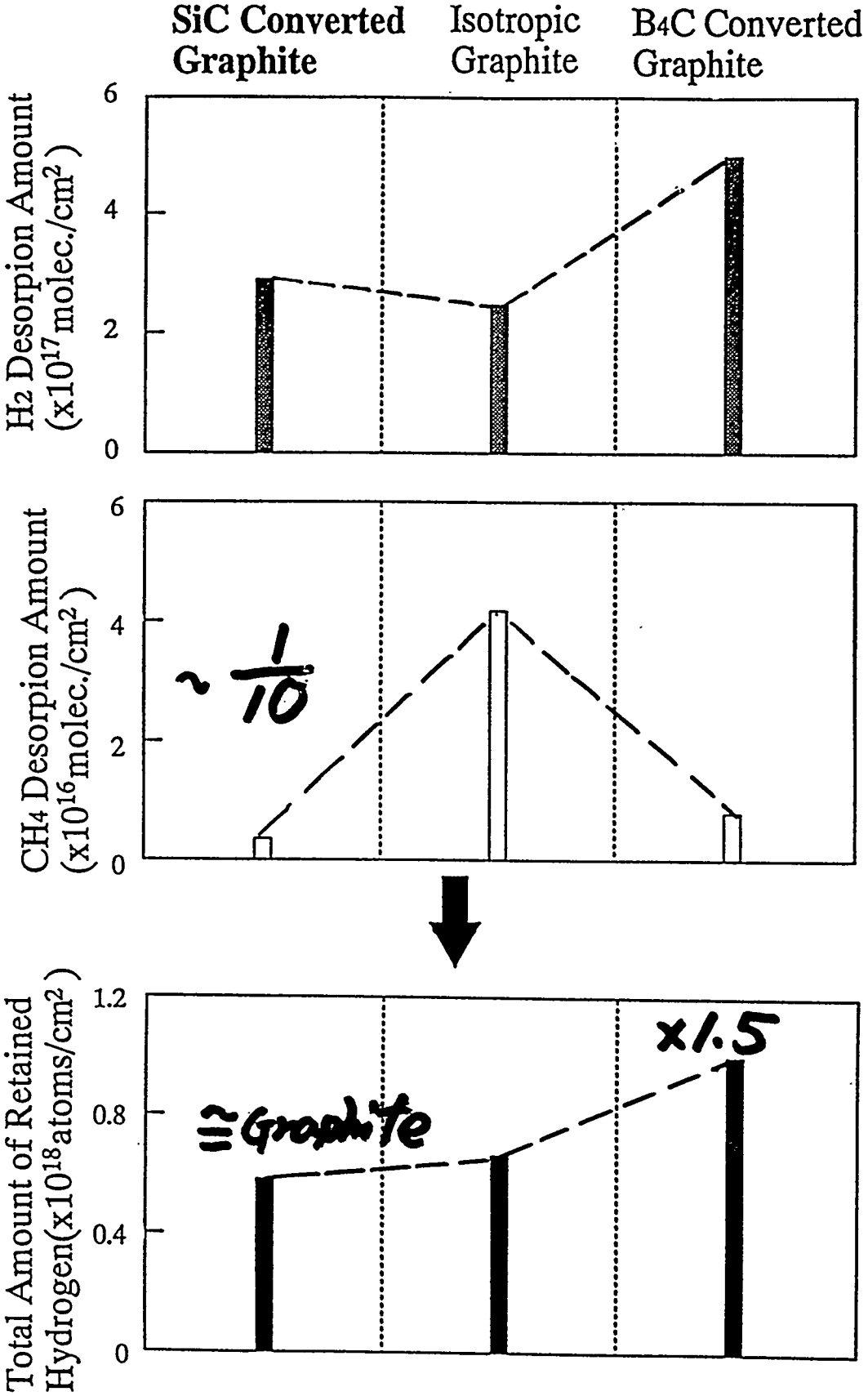

(5)Annealing Temperature Dependence of Hydrogen Retention

H^+ Fluence=$5x10^{18}$ H/cm^2 Irrad.Temp.=RT

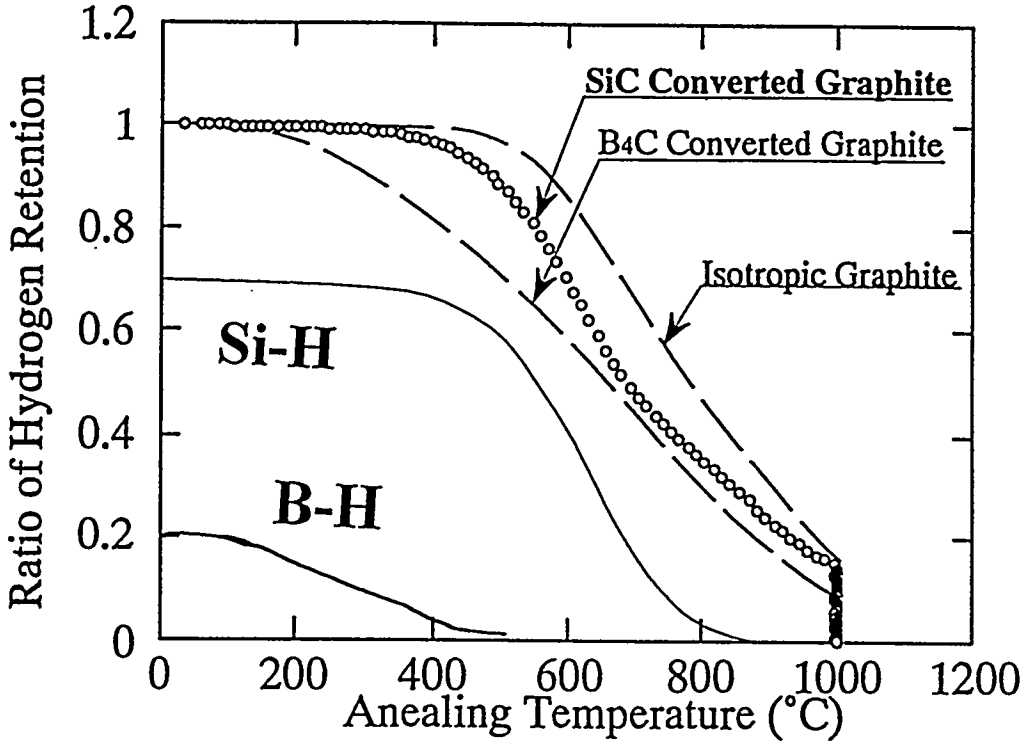

○SiC Converted graphite

Temperature to become a half :
-100℃ lower than that of isotropic graphite

⇩

due to desorption of Si-H bondings

○B_4C Converted graphite : rapid decrease

⇩

due to desorption of B-H bondings
-10% removed by baking (300℃)

Results 2

Helium Ion Impact Desorption for SiC Converted Graphite

(1) H_2 Desorption Spectrum after He Ion Bombardment

H^+ Fluence=$5x10^{18}$ H/cm^2 Irrad.Temp.=RT

He^+ Bombardment=$2.9x10^{18}$ He/cm^2

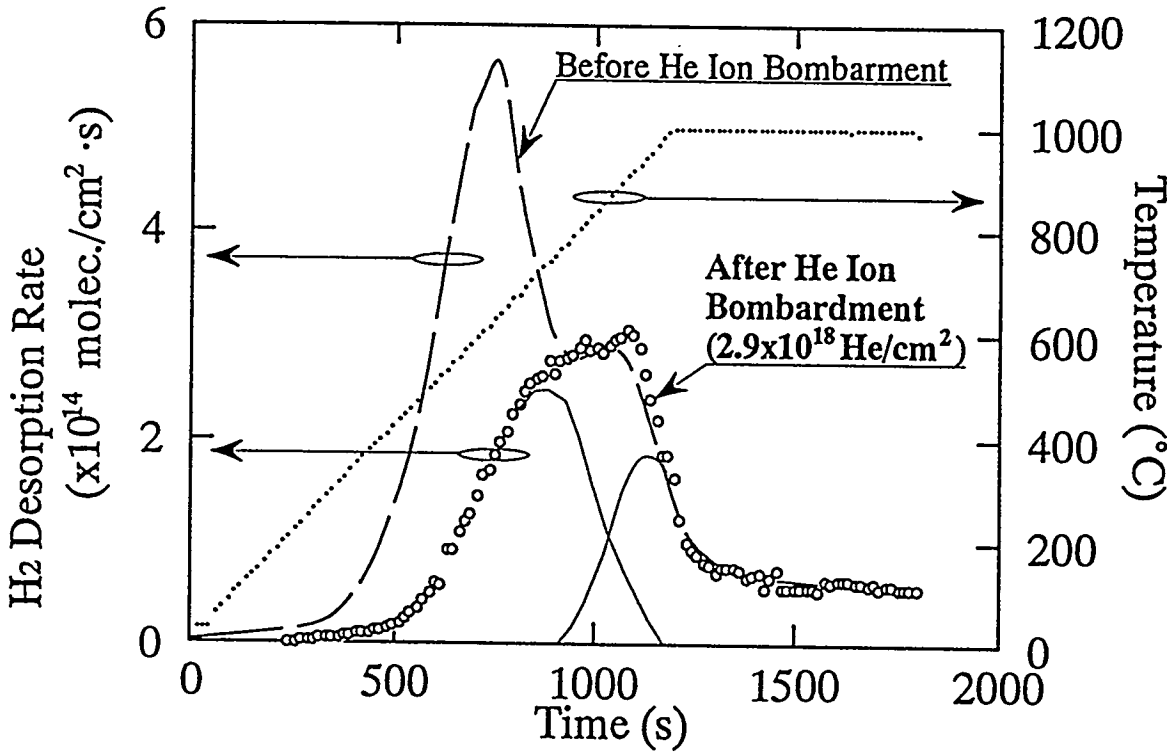

◎Total amount of retained hydrogen・・・
40 % reduced

◎Hydrogen amount in form of S-H bonding
・・・largely reduced (50%)

(2) He Ion Fluence Dependence of Hydrogen Retention

H^+ Fluence=$5x10^{18}$ H/cm^2 Irrad.Temp.=RT
He^+ Bombardment: (0.75-2.9)$x10^{18}$ He/cm^2

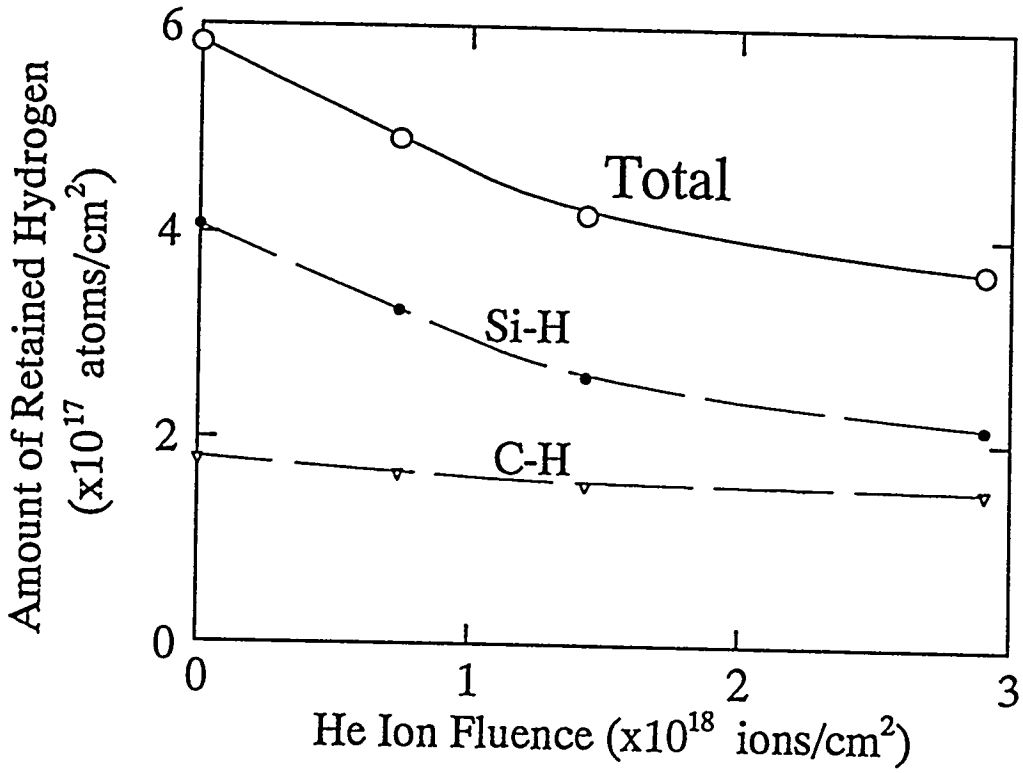

◎Total amount of Si-H bonding
rapid decrease within fluence up to $1x10^{18}$ He/cm^2
◎C-H bonding・・・**little decreased by He ion impact**

(3) Comparison : Effects of He Ion Impact Desorption

H^+ Fluence=$5x10^{18}$ H/cm^2 Irrad.Temp.=RT
He^+ Bombardment: (0.75-2.9)$x10^{18}$ He/cm^2

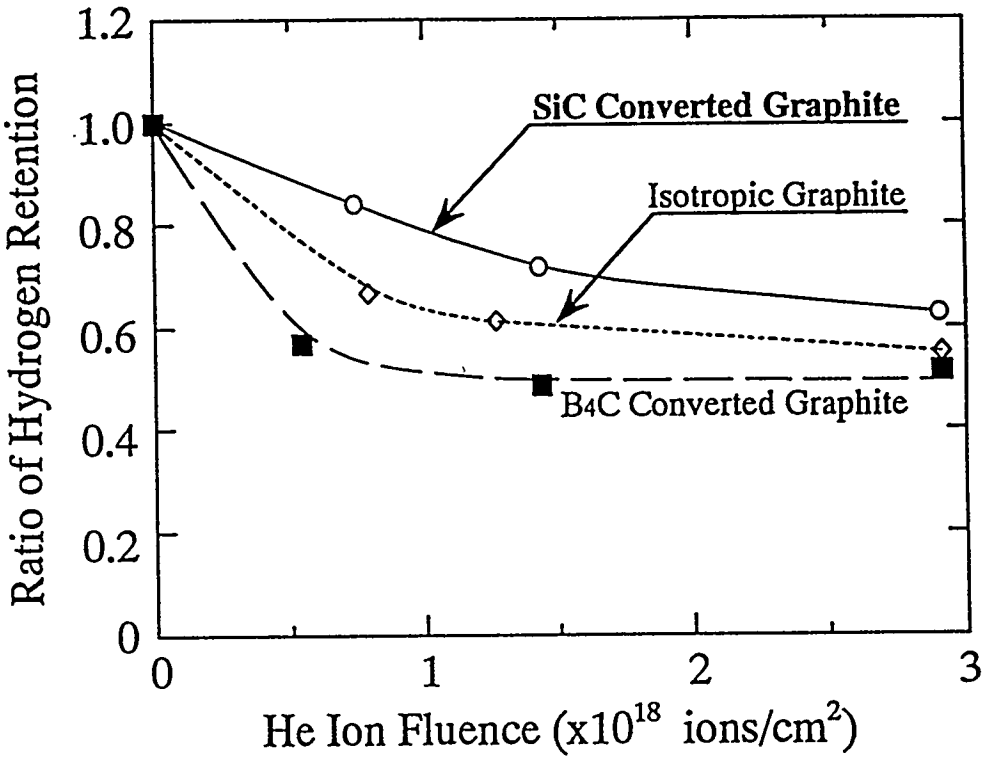

○**SiC Converted graphite**
Ratio of decrease : not large

○B_4C Converted graphite
very rapidly decreased
largely reduced also by He ion impact

Summary

Hydrogen Retention Properties of SiC Converted Graphite

○ Two peaks appeared in H_2 desorption spectrum, corresponding to detrappings of Si-H and C-H bonds.

○ Amount of retained hydrogen was comparable with that of isotropic graphite.

◎ Hydrogen retention of SiC converted graphite becomes a half at ~600 °C, which is approximately 100 °C lower than that of isotropic graphite.

Helium Ion Impact Desorption for SiC Converted Graphite

○ By He ion impact, amount of retained hydrogen was as high as 40 % reduced.

◎ In particular, hydrogen amount in form of Si-H bond was largely reduced.

Helium pumping properties of nickel and tungsten

H. Yanagihara, T. Hino, Y. Hirohata, T. Yamashina

Department of Nuclear Engineering, Hokkaido University

Present study

Ni and W metals

○ **Evaluation Helium Selective Pumping Properties**

⇧

Relative ratio of trapped amounts between helium and hydrogen

○ **Total amount of trapped He**

Temperature dependence (Ni&W)

Fluence dependence (Ni)

Energy dependence(Ni)

⇩

○ **Suitable use of Nikel as a Pumping Material**

Experiment

1.Sample: Nickel (99.9%)
Tungsten (99.95%)

2. Plasma irradiation

ECR plasma irradiation apparatus

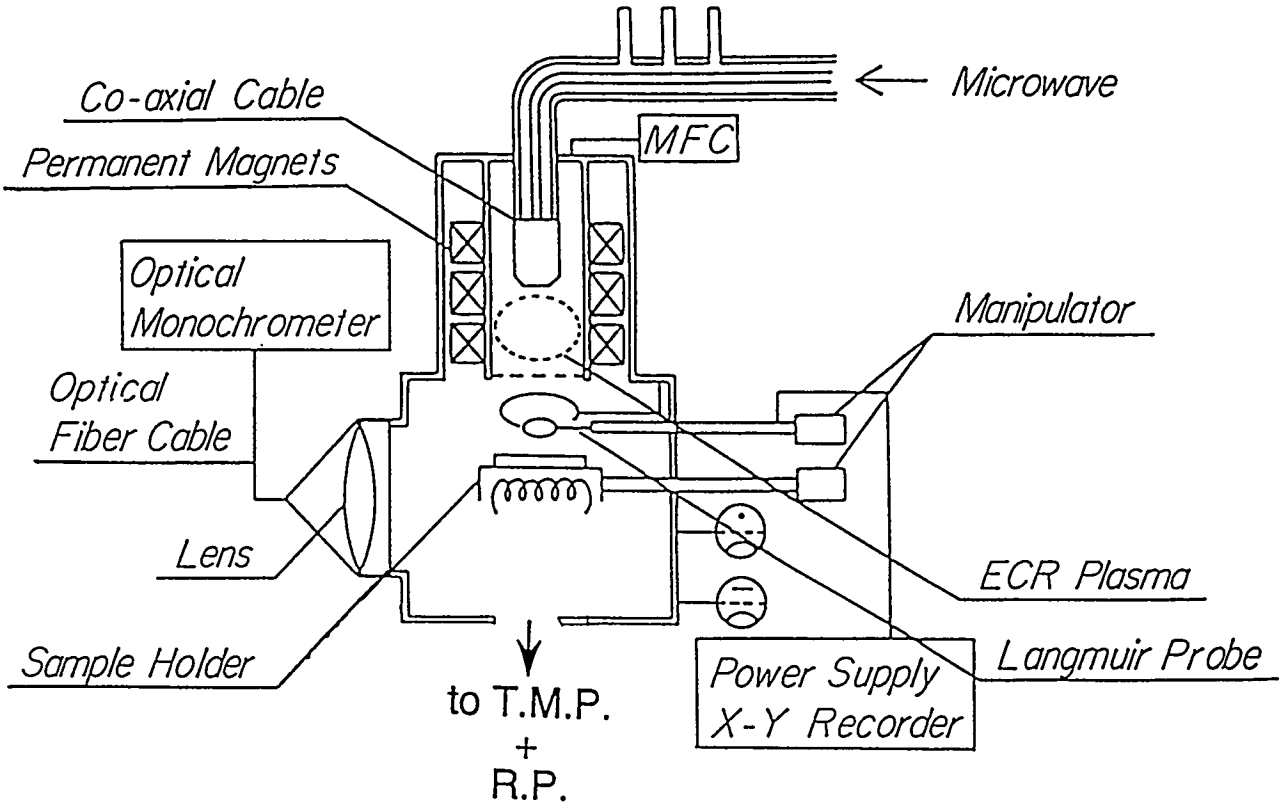

Pre-treatment
Degassing : 800°C, 2hrs
↓
Irradiation

2. Condition of plasma irradiation

Irradiation temperature dependence
(Ni and W)

He or H plasma irradiation
- ·He or H fluence : ~5×10^{18} #/cm^2
- ·Bias voltage : -1 kV
- ·Irradiation temperature : RT~700°C

He fluence dependence of Ni (He plasma)

- ·(0~7)$\times10^{18}$ He/cm^2
- ·-1 kV
- ·200°C, 600°C

He energy dependence of Ni (He plasma)

- ·~2×10^{18} He/cm^2
- ·0~-1 kV
- ·200°C, 600°C

3.Evaluation method of trapped He

Thermal desorption spectroscopy(TDS)

Heating rate : 10°C/min
Range : RT~1000°C
(Holding at 1000°C for 30 min)

Results 1

He selective pumping (Ni and W)

1. Irradiation Temperature Dependence for Trapped He-Thermal Desorption Spectra

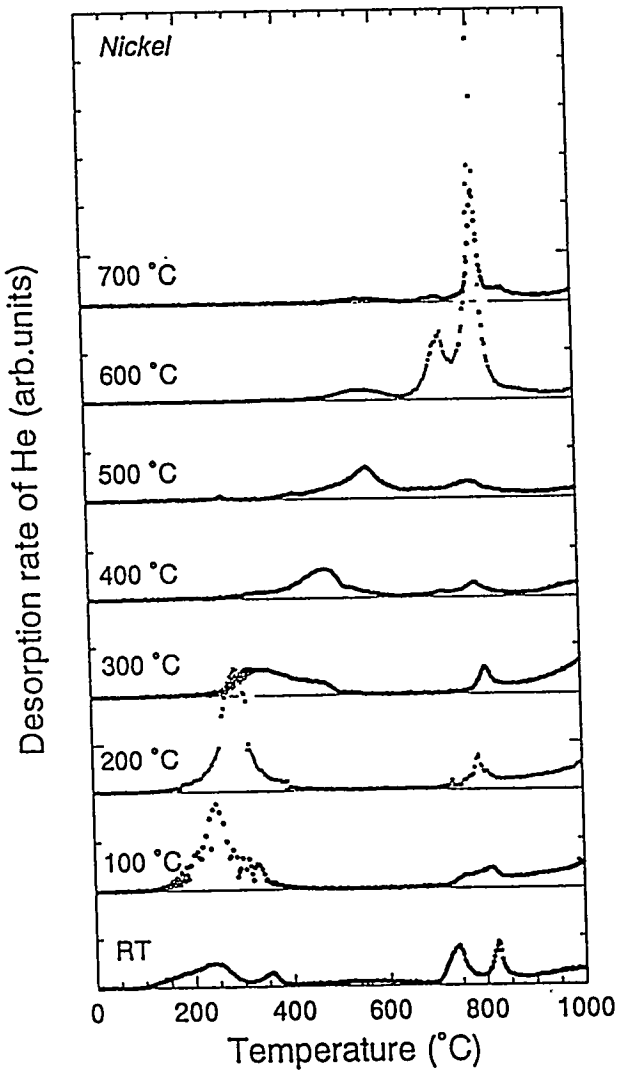

Two desorption peaks :Peak-L, Peak-H
L-Peak temperature shift to higher Temp. with increase of irrad .Temp.

2. Irradiation Temperature Dependence for Amount of Trapped He or H in Ni

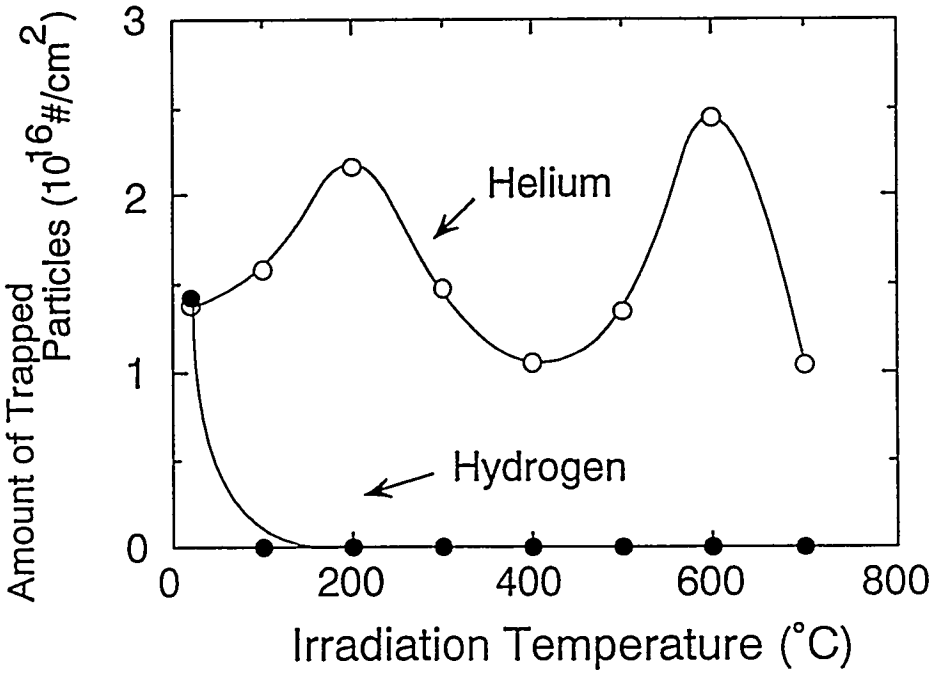

- ≤100°C ⟶ No H trapping
- Total amount of trapped He
  Maximum at ~200°C, ~600°C

↓

Nickel can selectively trap He

3. Irradiation Temperature Dependence for Amount of Trapped He or H in W

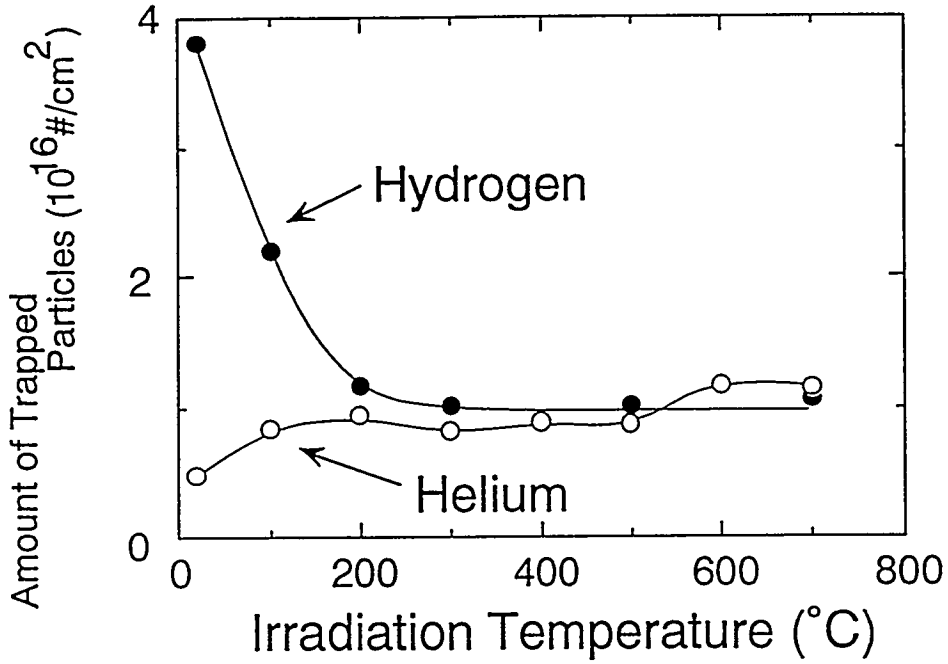

Amount of trapped He did not exceed that of trapped H in entire temperature range.

↓

No He selective pumping

Results 2

He fluence and energy dependences of trapped He in nickel

1. He fluence dependence of trapped He in **nickel**

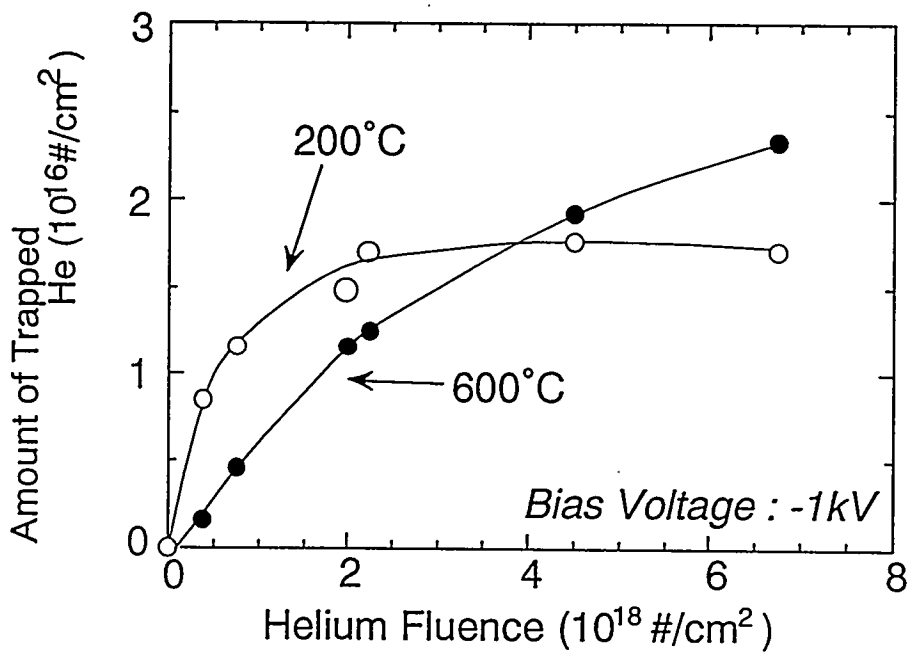

- 200°C

  Saturation of trapped He ··· ~2×10^{16}He/cm^2

- 600°C

  Increase of trapped amount

  ↘

  Diffusion of He into bulk

2. He energy dependence of trapped He in **nickel**

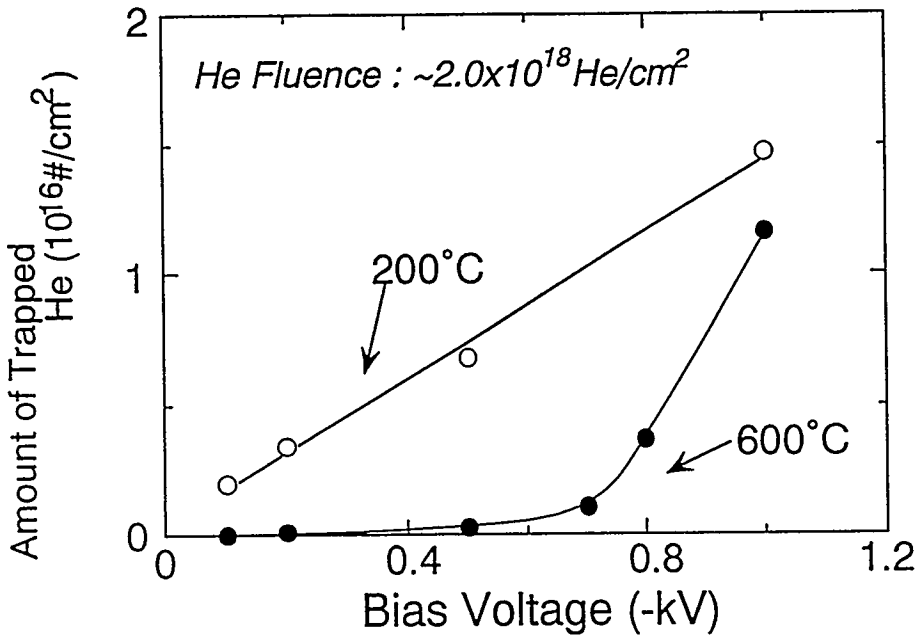

- 200°C
  Amount of trapped He linearly increased.
- 600°C
  No He trapping below |-0.7 kV|

Application of nickel to fusion reactor

Temperature in vicinity of divertor : ~ 300°C

·Trapping amount : 1.5×10^{16} He/cm^2

↓

Suitable temperature : 200°C or 600°C

·Trapping amount : $(2 \sim 3) \times 10^{16}$ He/cm^2

Summary

1. Helium selective pumping (nickel and tungsten)

- Nickel has He selective pumping capability.
- For Nickel, two peaks of trapped He appeared at 200°C and 600°C.

2. He fluence and energy dependences for amount of trapped He in nickel

- At low irradiation temperature, trapped He amount saturated at low fluence. Saturation level was small.
- At high irradiation temperature, energy of He ion has to be higher than some critical level.

US-Japan Workshop Q219 on High Heat Flux Components and
Plasma Surface Interactions for Next Fusion Devices,
January 9-11, 1996, Colorado Springs, Colorado

Erosion and Gas Impurity Emission of B_4C Converted CFC by High Heat Load

K. Tokunaga, N. Yoshida, M. Kugimiya

Research Institute for Applied Mechanics,
Kyushu University

T. Ando

ITER EDA, Garching Co-center

K. Masaki and M. Saidoh

JAERI

Purpose of present study

B_4C converted CFC tiles have been installed in JT-60U as divertor armor.

↓

Good PMI performance (30 MW NBI, 2 sec)

- Reduction of carbon and oxygen impurity (100 μ m B_4C, B/C=2.7)
- Drastic reduction of of oxygen impurity, melting and evaporation of B_4C layer (300 μ m B_4C, B/C=3.8)

Remarkable melting and erosion have occurred.

Purpose of present study :

- To evaluate the high heat resistance of B_4C converted CFC.
- To investigate emission of gases and particle and damage of materials.

High heat load experiments using electron beam were carried out.

SEM observation of B_4C converted CFC and bare CFC

(1)B_4C converted CFC(PCC-2S) made by a chemical vapor reaction (Hitach Chemical Co. Ltd.)

$$2B_2O_3 + 7C \quad B_4C + 6CO \uparrow$$

(2)Size : 20 mm x 20 mm x 10mm, Outgas : 1000 ℃, 30 min(vacuum)

CFC (PCC-2S)

B_4C (80 μm, B/C =2.7)

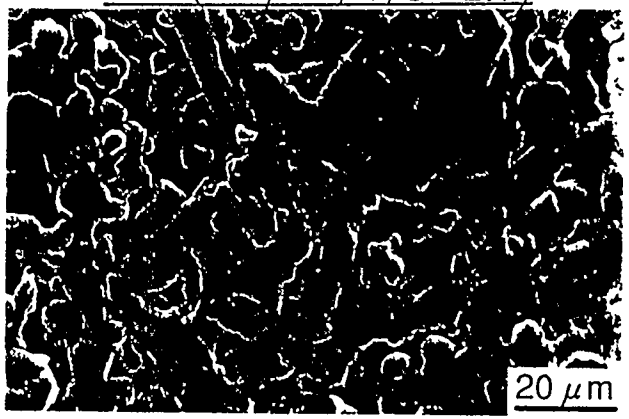

B_4C (140 μm, B/C = 3.9)

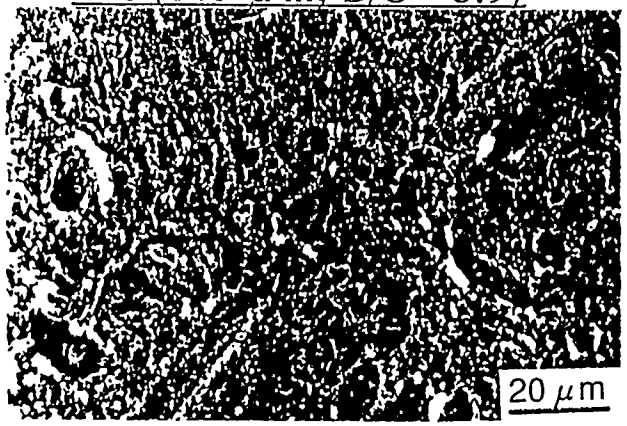

Cross section of B_4C(140 μm, B/C = 3.9)

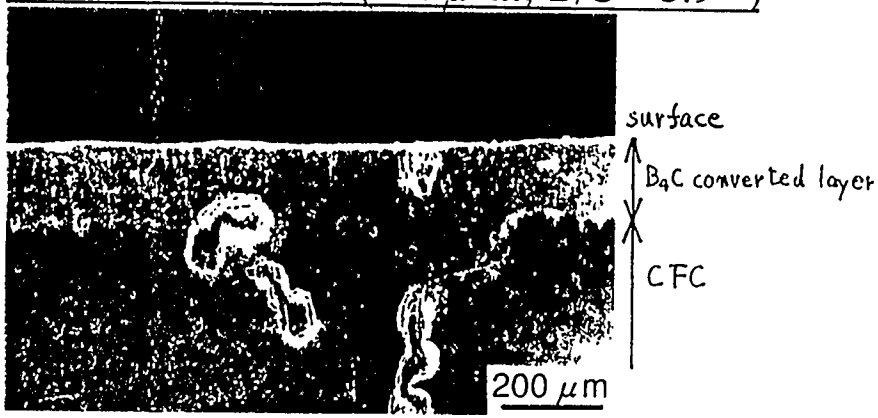

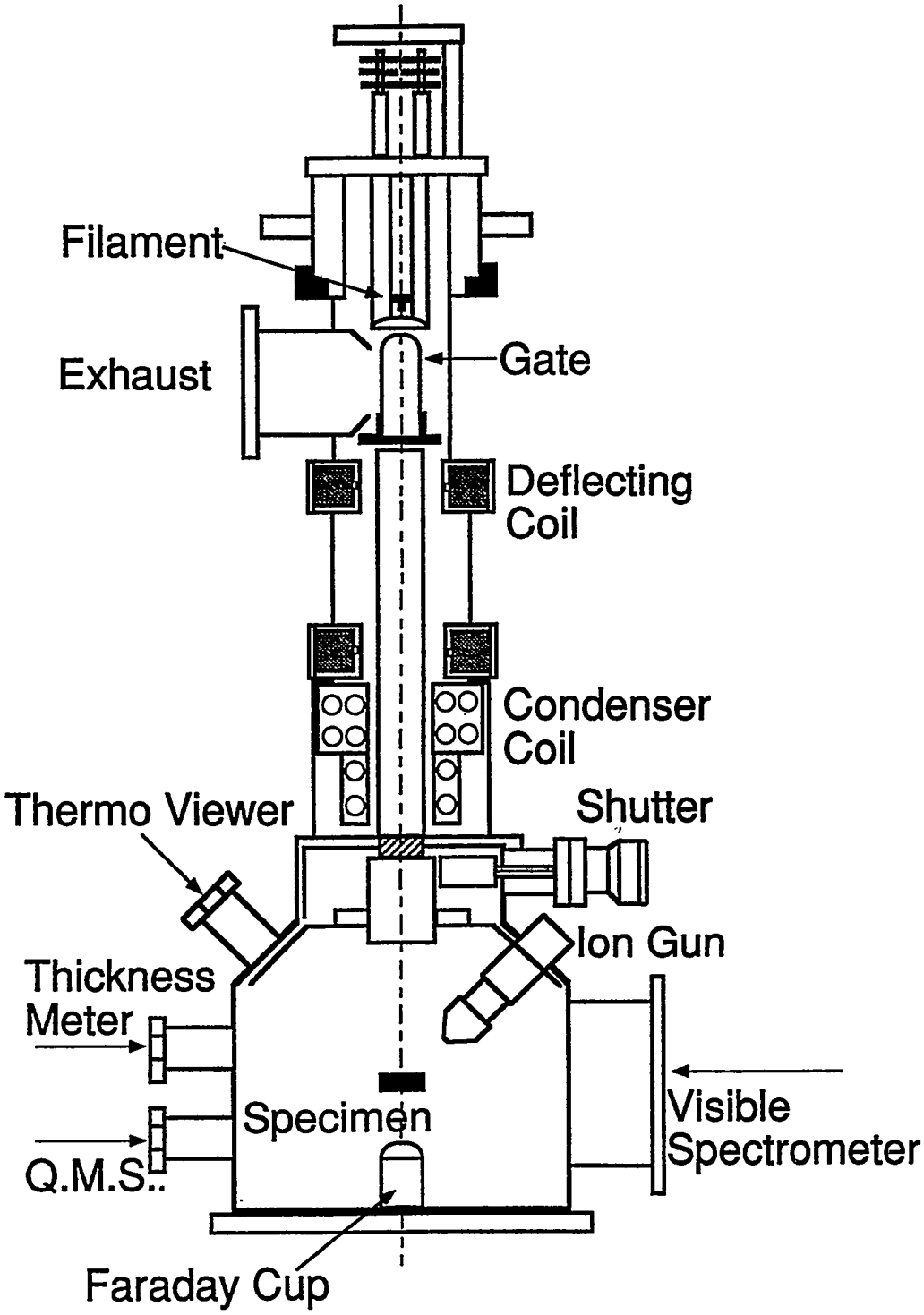

Electron beam irradiation heat flux test simulator

High vacuum electron beam irradiation test simulator

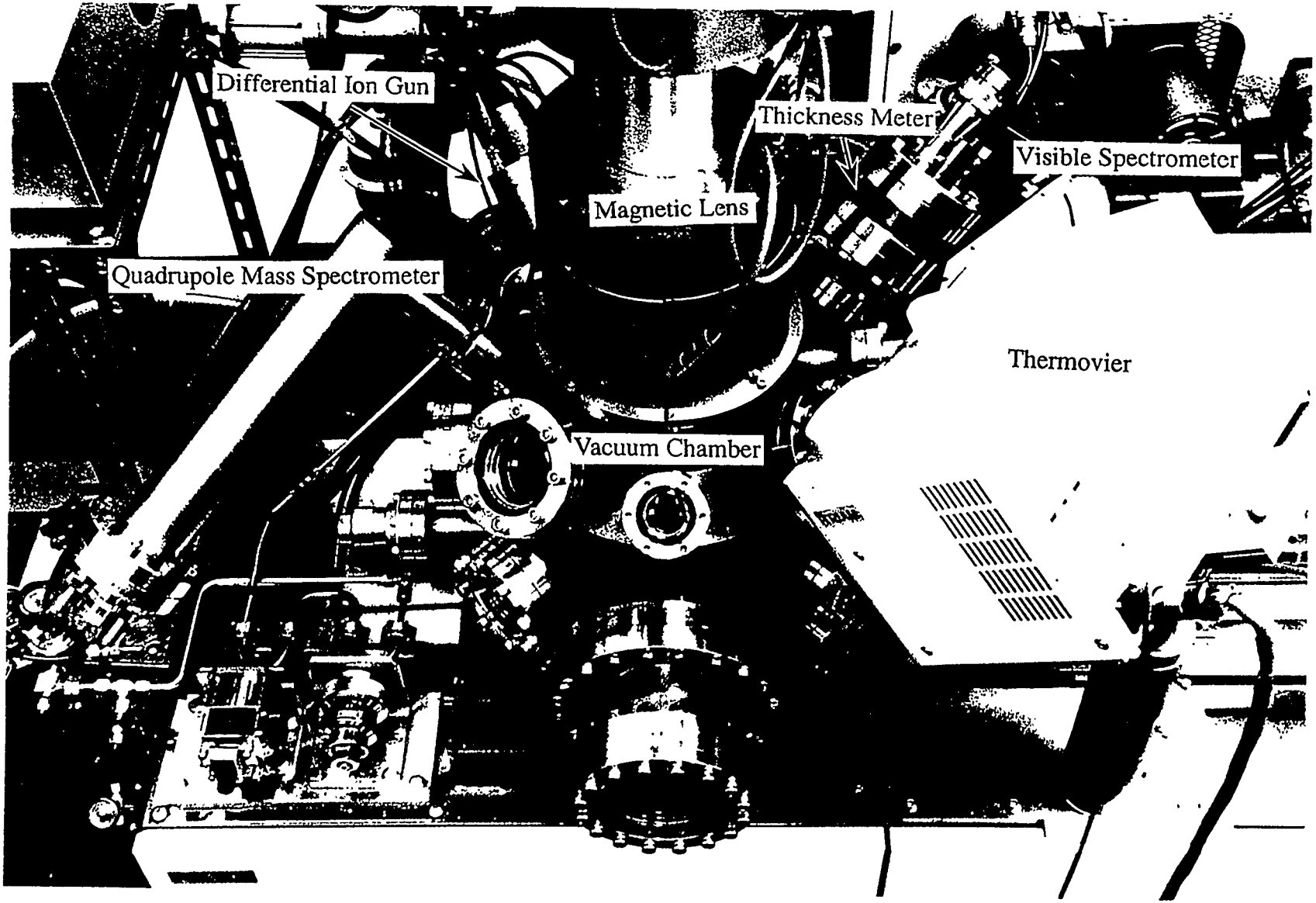

Experimental

(1) Experimental device : Electron beam irradiation test simulator of Kyushu University

(2) Experimental condition:

Electron energy : 20 keV
Heat flux : 20 MW/m^2
Irradiation time : 60 sec
Beam diameter : 8 mm ϕ
Pressure in a vacuum chamber(before irradiation) : 1×10^{-5} Pa

(3)Measurement : Surface temperature : Two-color optical pyrometer
Surface temperature distribution : Thermoviewer
Emitted Gases : Quadrupole mass spectrometer(QMS)
Deposited thickness : Quartz crystal thickness meter(QCTM)
Emitted macroscopic particle : CCD camera
Amount of erosion : Weight loss
Sample electric current : Heat flux

Surface modification : Scanning electron microscope(SEM)

Increase of surface temperature during e-beam irradiation

Heat flux : 20 MW/m^2, 60 sec, 8 mm ϕ

CFC(PCC-2S)
Sublimation point : 3367 ℃
Thermal conductivity : 280 W/mK(parallel)
150 W/mk(normal)

B_4C converted layer
Melting point : 2450 ℃
Thermal conductivity : (29 W/mK)

CFC (PCC-2S)

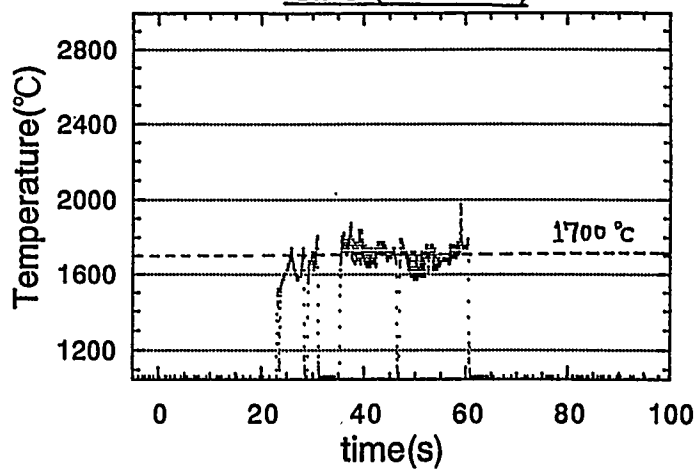

B_4C (80 μm, B/C =2.7)

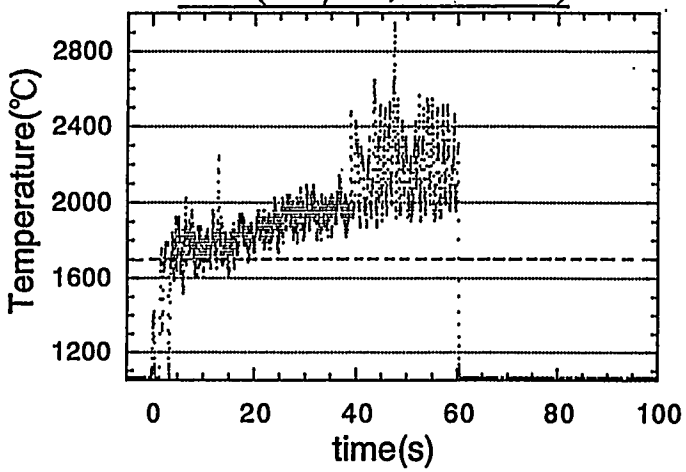

B_4C (140 μm, B/C = 3.9)

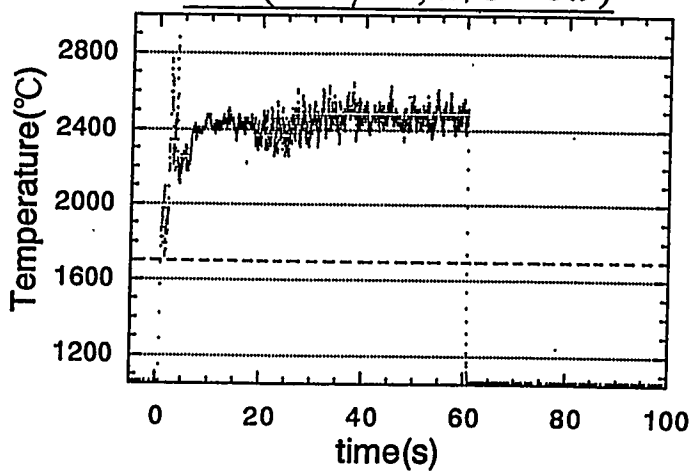

Increase of vacuum pressure during e-beam irradiation

Heat flux : 20 MW/m^2, 60 sec, 8 mm ϕ

Surface temperature :

CFC : 1600℃～1800 ℃
B_4C(80 μm)/CFC : 1900℃ ～2300 ℃
B_4C(140 μm)/CFC : 2300℃ ～2500 ℃

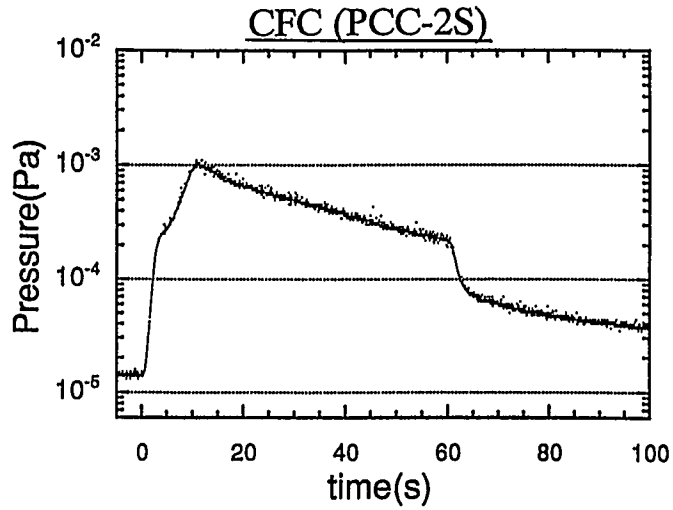

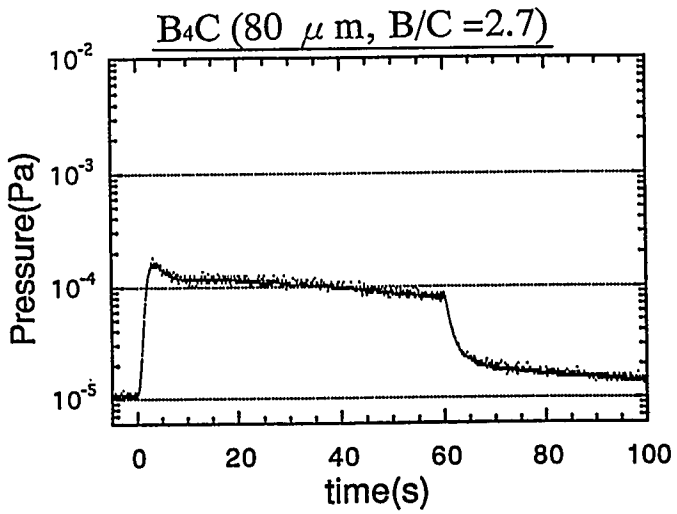

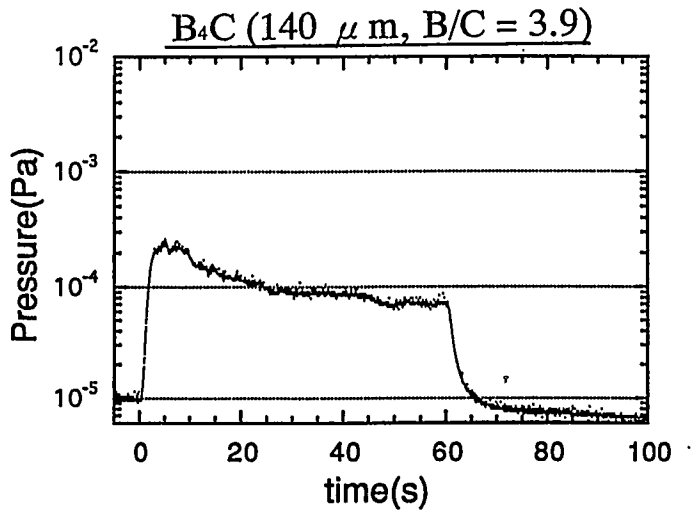

Gas emission during electron beam irradiation

At 6sec after irradiation started

Heat flux : 20 MW/m^2, 60 sec, 8 mm ϕ

Surface temperature :

CFC : 1600℃～1800 ℃

B_4C(80 μm)/CFC : 1900℃ ～2300 ℃

B_4C(140 μm)/CFC : 2300℃ ～2500 ℃

CFC (PCC-2S)

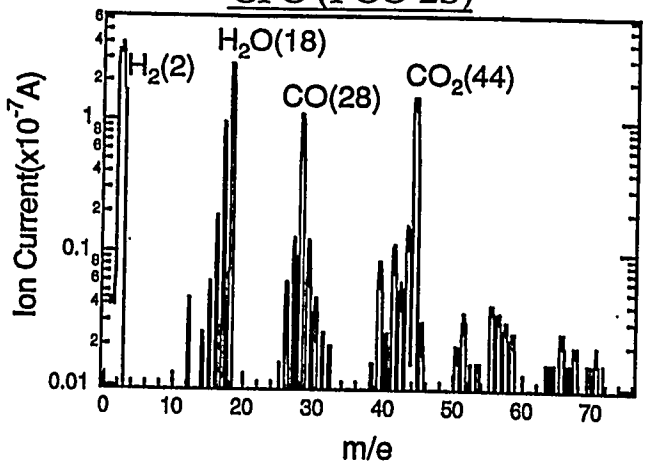

B_4C (80 μm, B/C =2.7)

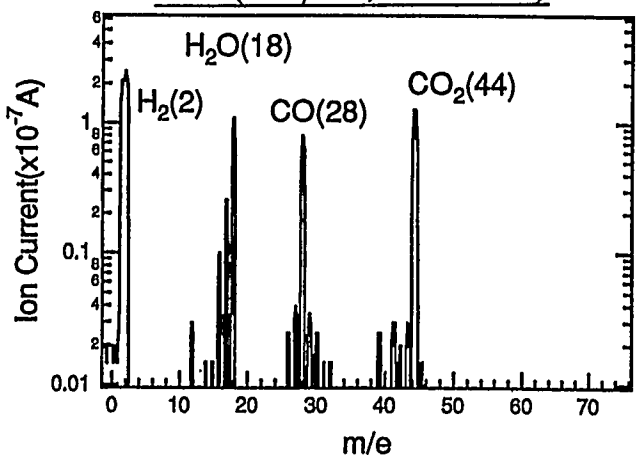

B_4C (140 μm, B/C = 3.9)

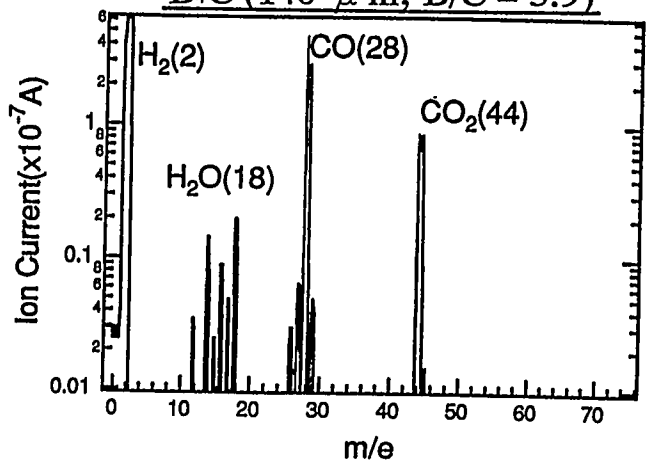

Time evolution of gases during e-beam irradiation

Heat flux : 20 MW/m^2, 60 sec, 8 mm ϕ

Surface temperature :

CFC : 1600℃～1800 ℃
B_4C(80 μm)/CFC : 1900℃ ～2300 ℃
B_4C(140 μm)/CFC : 2300℃ ～2500 ℃

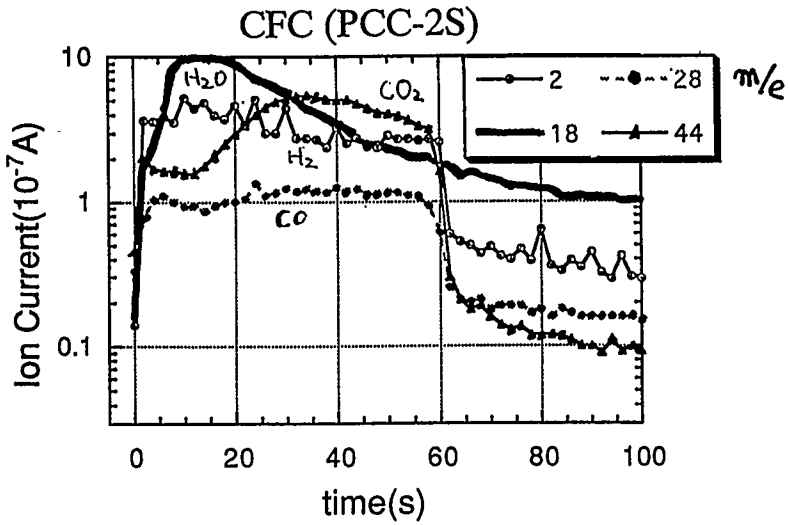

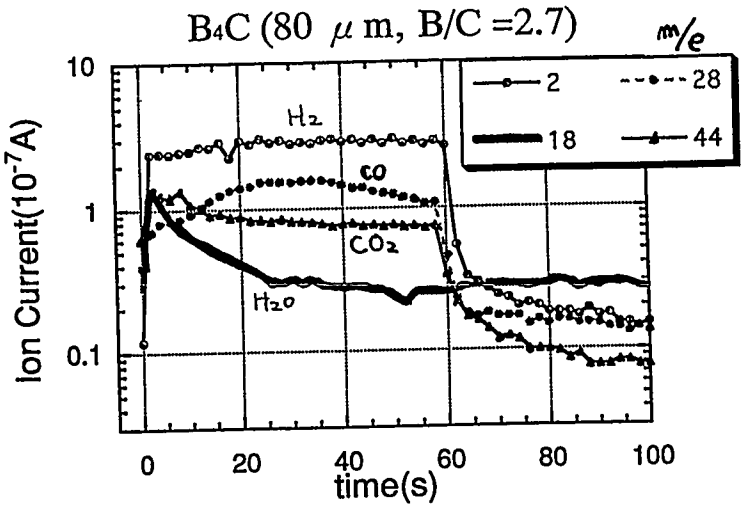

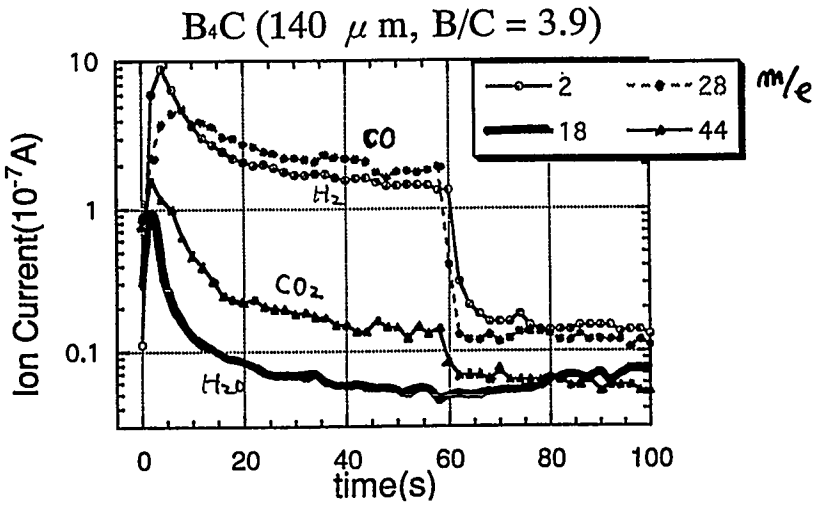

Time evolution of gases during e-beam irradiation

Heat flux : 20 MW/m², 60 sec, 8 mm ϕ

Surface temperature :

CFC : 1600℃～1800 ℃
B_4C(80 μ m)/CFC : 1900℃ ～2300 ℃
B_4C(140 μ m)/CFC : 2300℃ ～2500 ℃

CFC (PCC-2S)

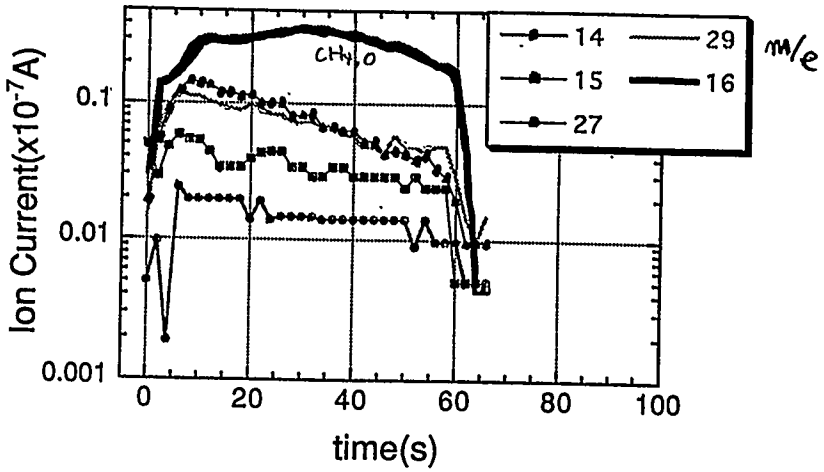

B_4C (80 μ m, B/C =2.7)

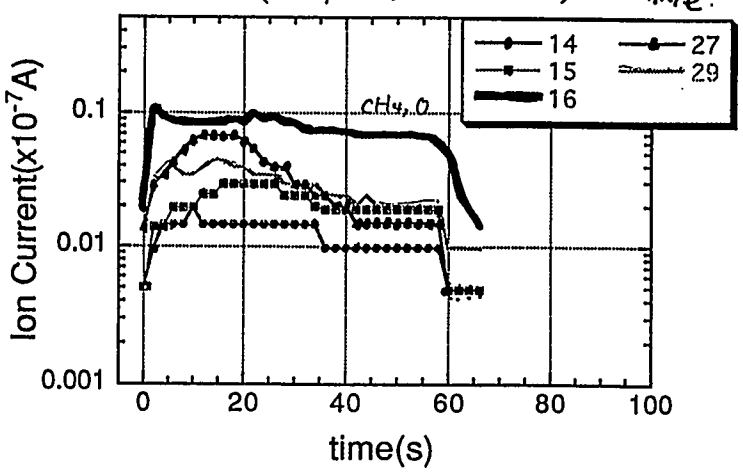

B_4C (140 μ m, B/C = 3.9)

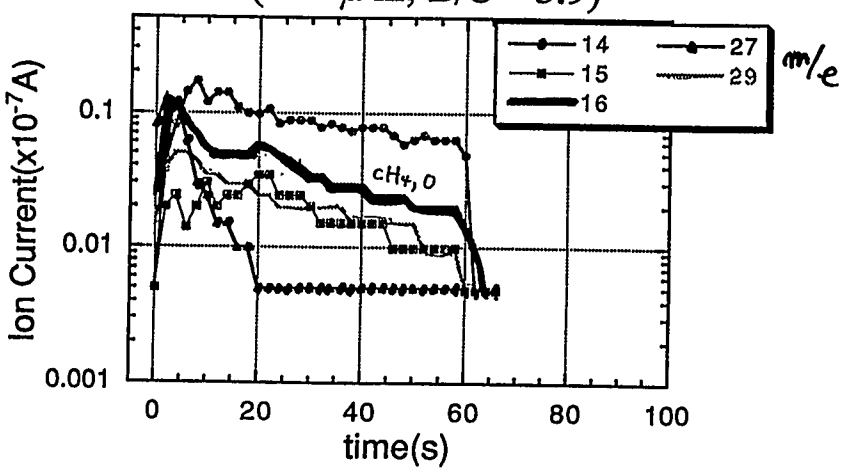

Time evolution of gases during e-beam irradiation

Heat flux : 20 MW/m^2, 60 sec, 8 mm ϕ

Surface temperature :

CFC : 1600℃～1800 ℃
B_4C(80 μm)/CFC : 1900℃ ～2300 ℃
B_4C(140 μm)/CFC : 2300℃ ～2500 ℃

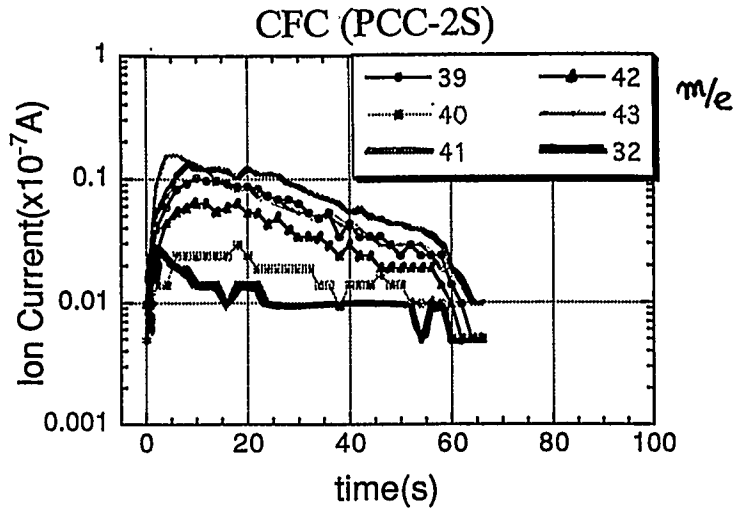

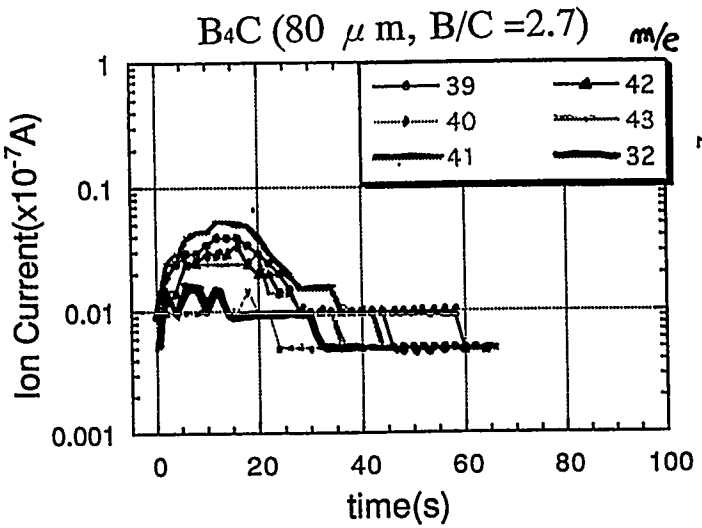

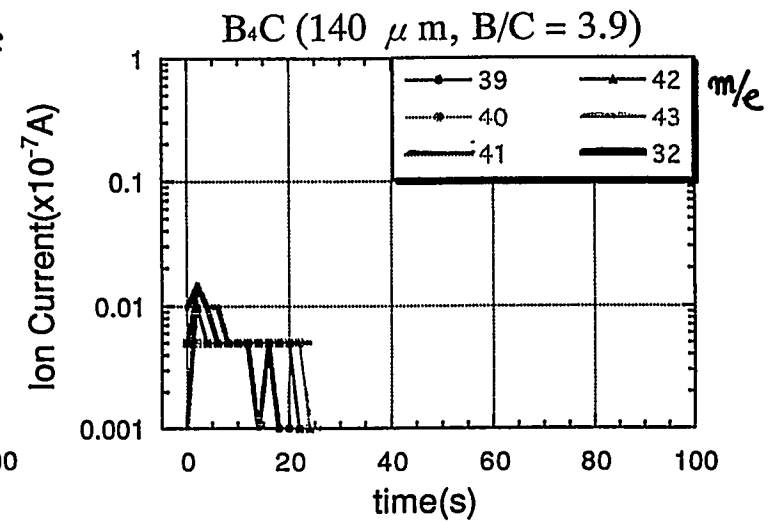

Erosion of B_4C-conv. CFC by electron beam irradiation

B_4C(80 μm, B/C = 2.7)

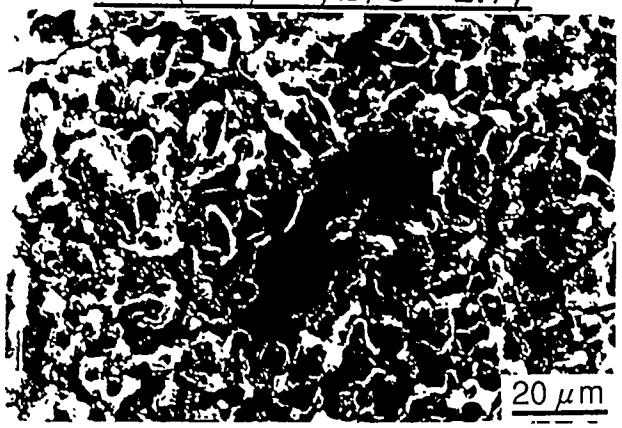

B_4C (140 μm, B/C = 3.9)

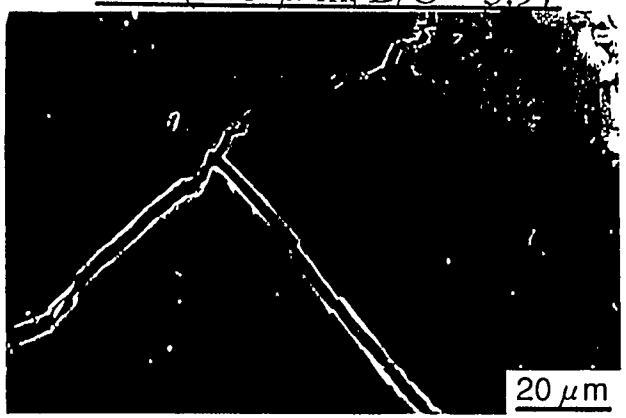

Cross sectional view during irradiation
B_4C (140 μm, B/C = 3.9)

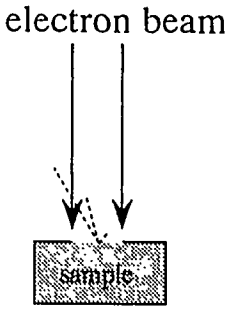

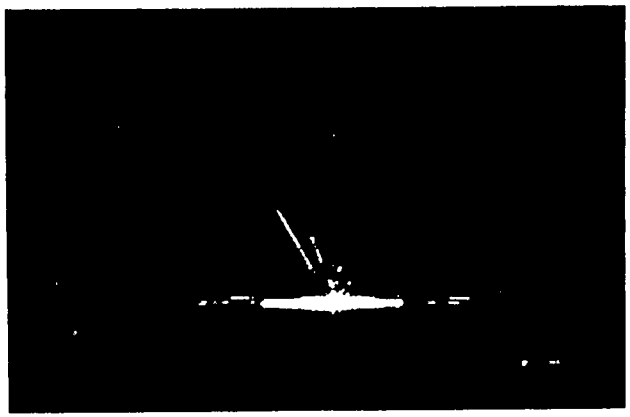

Erosion of B_4C converted CFC by electron beam irradiation

• Heat flux : 20 MW/m^2, 60 sec, 8 mm ϕ

sample (Temperature)	weight loss (expriment)	weight loss (calculation)	deposited thickness(wall) (thicknes meter)
80 μm (B/C=2.7) (1800℃～2200℃)	3.0×10^{-5} g	0.08×10^{-3} g	< 0.16 nm
140 μm (B/C=3.9) (2500℃, meltng)	1.2×10^{-3} g	0.42×10^{-3} g	4.0 nm

Langmuir's equation : $J = P(T)(2\pi mkT)^{-1/2}$

P(T) : equilibrium vapor presssure, k : Boltzmann constant, T : surface temperature

Summary

High heat loading experiments using an electron beam were carried out to evaluate the high heat load resistance of the B_4C converted CFC in the view point of materials damage and gases and particle emission.

(1) The surface temperature of the B_4C converted CFC during the electron beam irradiation was higher than that of the CFC. This is expected to be due to lower thermal conductivity of the B_4C converted layer.

(2)On the other hand, increase of the vacuum pressure for the B_4C converted CFC was about 1/5 of that of the CFC. Peak of partial pressure of H_2O and CO_2 for the B_4C converted CFC was 1/5 and 1/10 of that of the CFC, respectively.

(3)When the surface layer of the B_4C was melt, the vacuum pressure decreased comparing with that of before the irradiation. It is confirmed that getter effect due to evaporated B occurred.

(4)The present results suggest that a B/C ratio and thickness of B_4C layer should be optimized to control the surface temperature increase by heat load.

Observation of Reduced Beryllium Erosion in PISCES-B PSI Experiments

presented by
Russ Doerner

Work performed by the PISCES-B Materials Team
R. Boivin, R. Doerner, Y. Hirooka, S. Luckhardt, D. Sze and J. Won

US-Japan Workshop on High Heat Flux Component and
Plasma Surface Interactions for Next Fusion Devices
January 9-11, 1996
Colorado Springs, Colorado

Outline of Talk

- Motivation of Experiments
- PISCES-B Facility and Parameters

* Beryllium Sputtering Yield Results

* Description of 'Protective' Surface Impurity Layer

* Implications for Divertor Designs

References
- Y. Hirooka, J. Won, R. Boivin et al., accepted for publication in the J. Nuc. Mat.
- J. Won, Y. Hirooka, R. Boivin et al., presented at 42nd AVS (to be published in J. of Vac. Sci. & Tech.)
- Y. Hirooka, J. Won, S. Keller et al., Fusion Technology 26 (1994) 540.

The Goals of the PISCES-B Experimental Program Focus on ITER

- Provide a Safe Environment to Examine Plasma-Surface Interactions using Toxic Material Samples

- Measure PFC Relevant Properties of Beryllium
  - Sputtering Yield
  - Deuterium Retention
  - Surface Modifications

- Investigate Mixed Material Scenarios
  - Be, C, W

UC SAN DIEGO PISCES EXPERIMENTAL PROGRAM

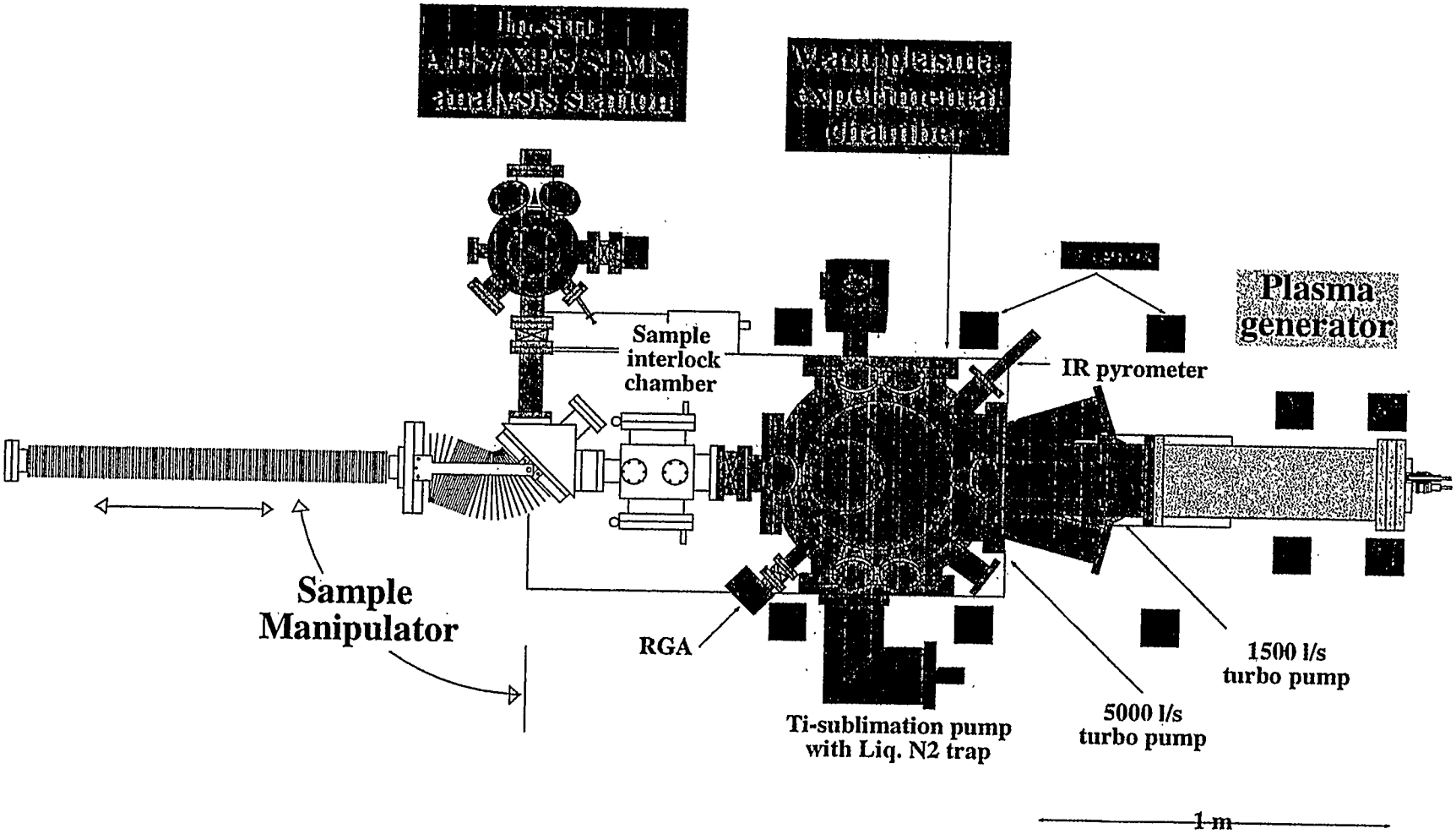

THE PISCES-B FACILITY

UC, San Diego PISCES-B
PLASMA-BERYLLIUM TEST FACILITY

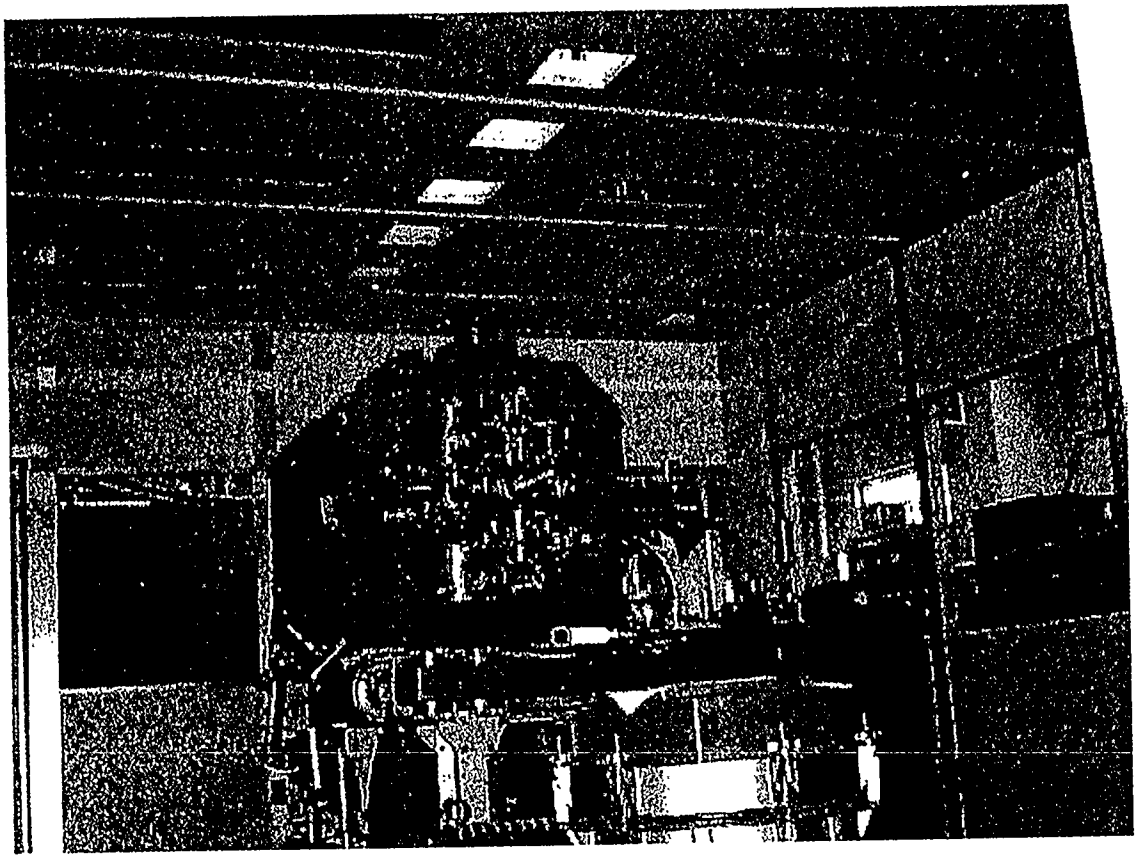

12-95

UCSD FUSION ENERGY RESEARCH PROGRAM

BERYLLIUM HANDLING FACILITY

1. Airborne Beryllium limit (< 0.1 $\mu g/m^3$)
   - 2 $\mu g/m^3$ (OSHA Industrial Limit)

2. Clean room with high ventilation and HEPA-filtered exhaust

3. Negative internal pressure

4. Double door entry with computer-controlled interlock safety system

5. Operation in full-face, air-supplied respirator

6. Surface- and air-sampling for beryllium contamination

COMPARISON BETWEEN PISCES-B AND ITER DIVERTOR PLASMA CONDITIONS

Plasma conditions	PISCES-B Mod	ITER DIVERTOR
Plasma density (m^{-3})	3×10^{19}	1×10^{20}
Electron temperature (eV)	5 - 30	1 - 150
Ion bombarding flux (m^{-2} sec^{-1})	2×10^{23}	10^{23} - 10^{24}
Ion bombarding energy (eV)	20 - 300	10 - 100
Power load (MW/m^2)	1 - 10	1 - 5

PISCES-B Is Supplying Valuable Experimental Data on the Behavior of Beryllium/Plasma Interactions

- **Erosion/Redeposition Measurements**
  - Sputtering Yield vs. Incident Ion Energy
  - Sputtering Yield vs. Plasma Impurity Concentration
  - Sputtering Yield vs. Surface Temperature

- **Formation of 'Protective' Surface Impurity Layers**
  - Conditions for Impurity Layer Formation
  - Physical Structure of Protective Layers
  - Chemical Structure of Protective Layers

- **Deuterium Retention**
  - In Bulk Beryllium
  - In 'Protective' Impurity Layers

Impurity Layers Form on Beryllium Samples which are Exposed to Plasma at High Temperature

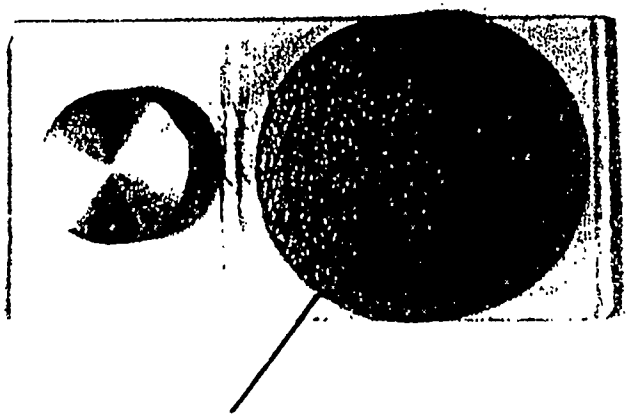

Room Temperature Exposure
Clean Surface After Bombardment
(high erosion rate)

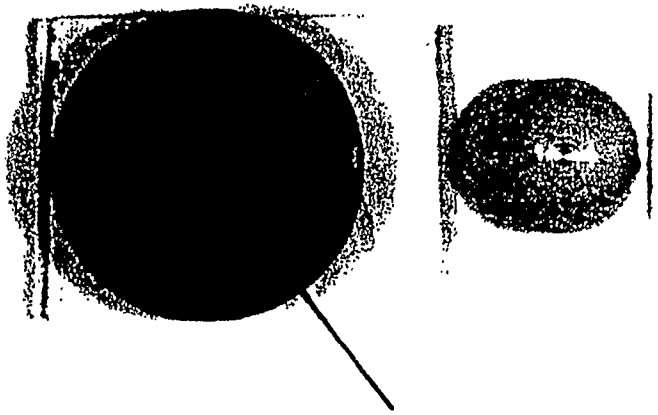

High Temperature Exposure
Coated Surface After Bombardment
(low erosion rate)

AT HIGH TARGET TEMPERATURE (≥ 250 degree C), BERYLLIUM EROSION IS *REDUCED UP TO TWO ORDERS OF MAGNITUDE* BY PLASMA IMPURITY EFFECTS IN PISCES-B.

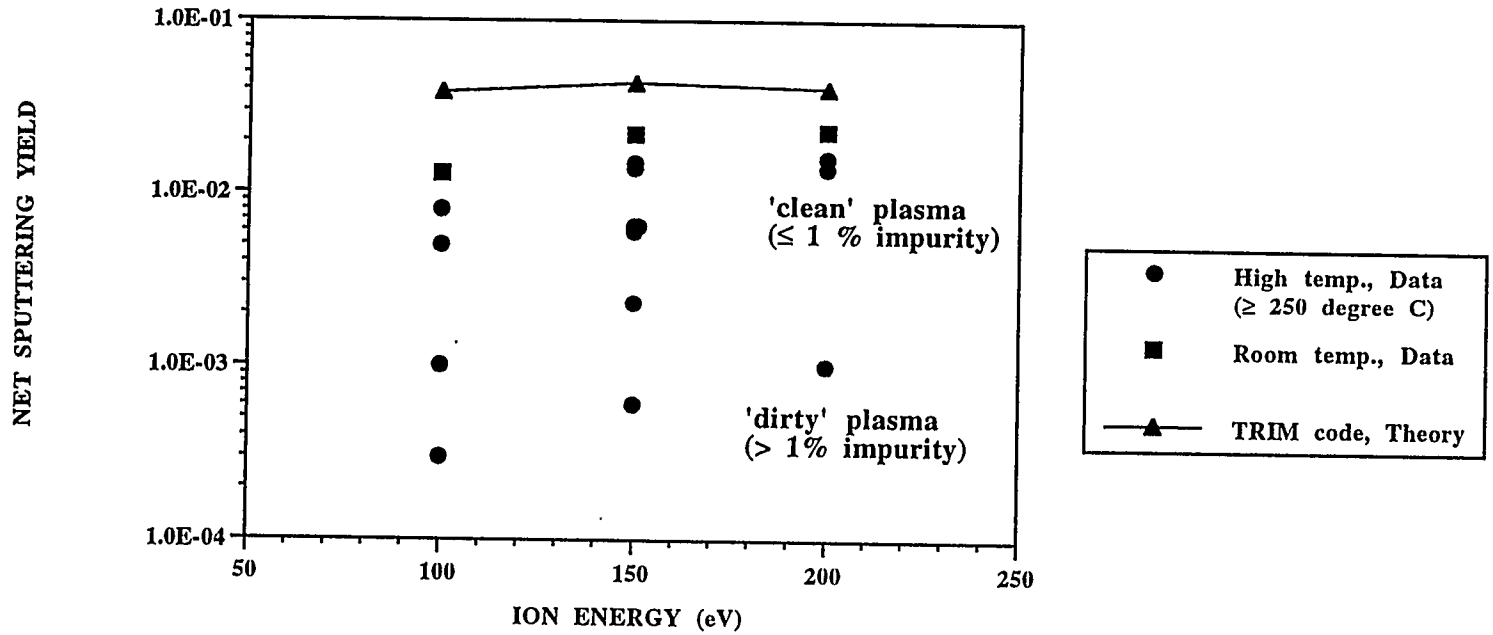

1. Sputtering yields decrease with increasing plasma impurity content causing a range of yield values.

2. This effect does not occur at lower temperatures (~30 degree C).

AT ELEVATED TARGET TEMPERATURE, Be II LINE INTENSITY IS REDUCED TO LESS THAN 10 % OF THE INITIAL MAXIMUM DUE TO IMPURITY DEPOSITION.

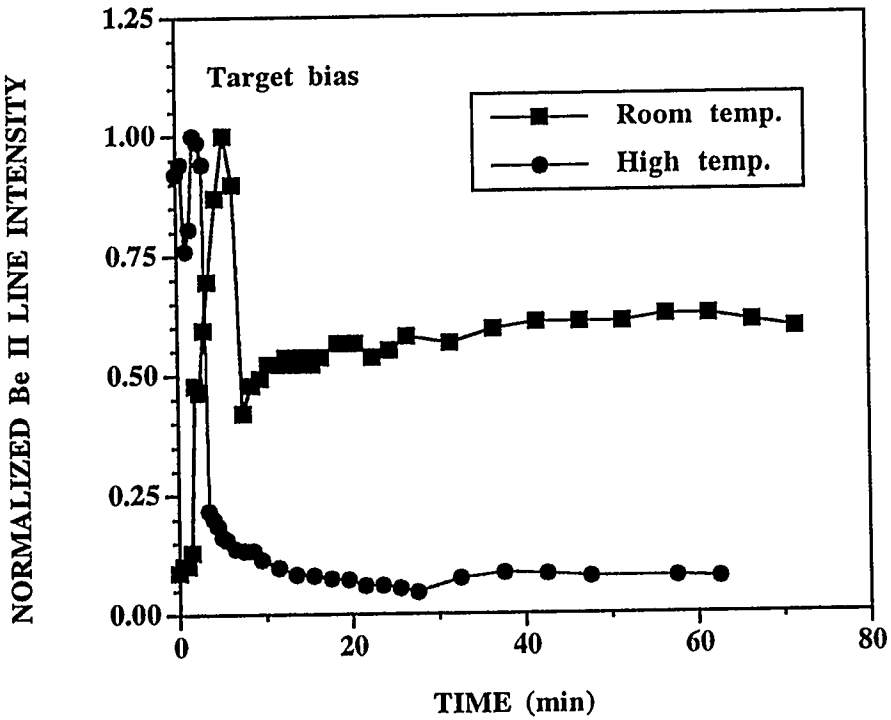

Comparison of the Be II line (313 nm) intensity during plasma bombardment under different surface temperature conditions.

Protective Surface Layers have been Subjected to Extensive Materials Analysis Techniques

* SEM pictures before and after plasma exposure to determine surface morphology change

* Depth profile AES to identify elemental composition of the impurity layer

* XPS for analysis of chemical structure within the surface layer

- Be samples were sliced to measure film thickness and porosity
  (≈100nm thick)

- Grazing incidence XRD to identify any crystalline formation in the surface layer
  (crystaline BeO detected, no crystaline formation of Be2C, Be3N2)

- Electrical conductivity of coating checked
  (conductive)

Impurity Surface Layers Form on Beryllium Samples at High Temperature

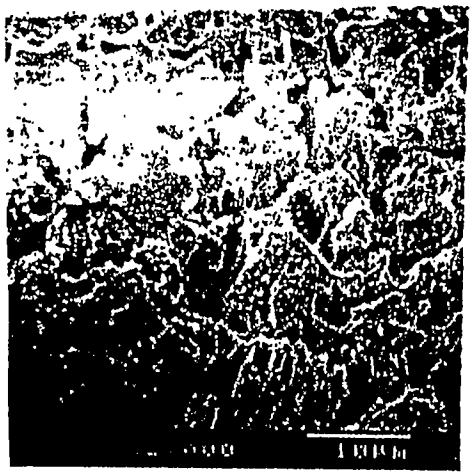

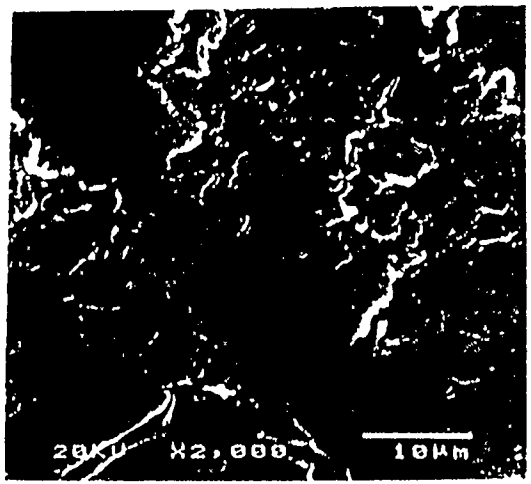

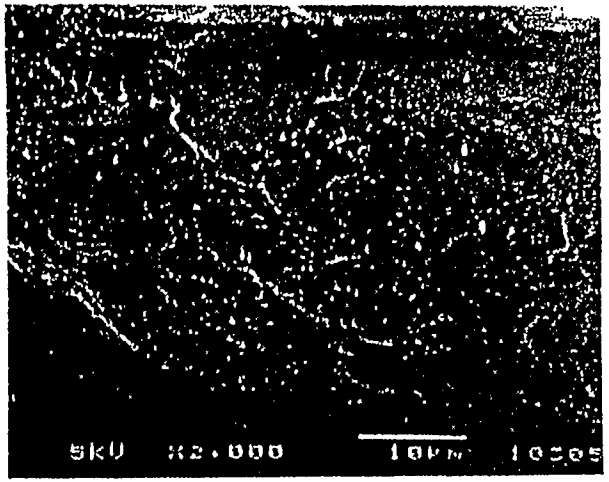

Impurity Layer Formed During High Temperature Exposure Exhibits a Rough Surface

As received Brush-Wellman Sample

Low Temperature Exposure Results in a Smooth Surface

PLASMA-EXPOSED BERYLLIUM SAMPLES EXHIBIT A MIXED SURFACE IMPURITY LAYER AS DETECTED BY DEPTH-PROFILE AES ANALYSIS.

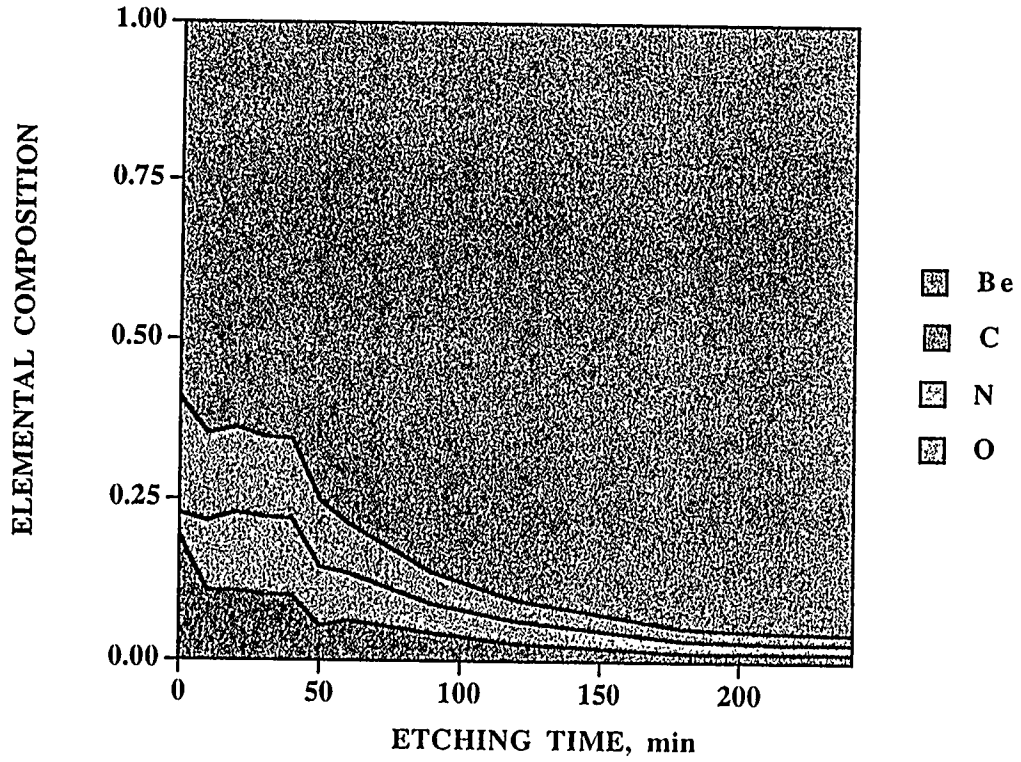

XPS Analysis Detects Little Carbide Formation within the Impurity Surface Layer

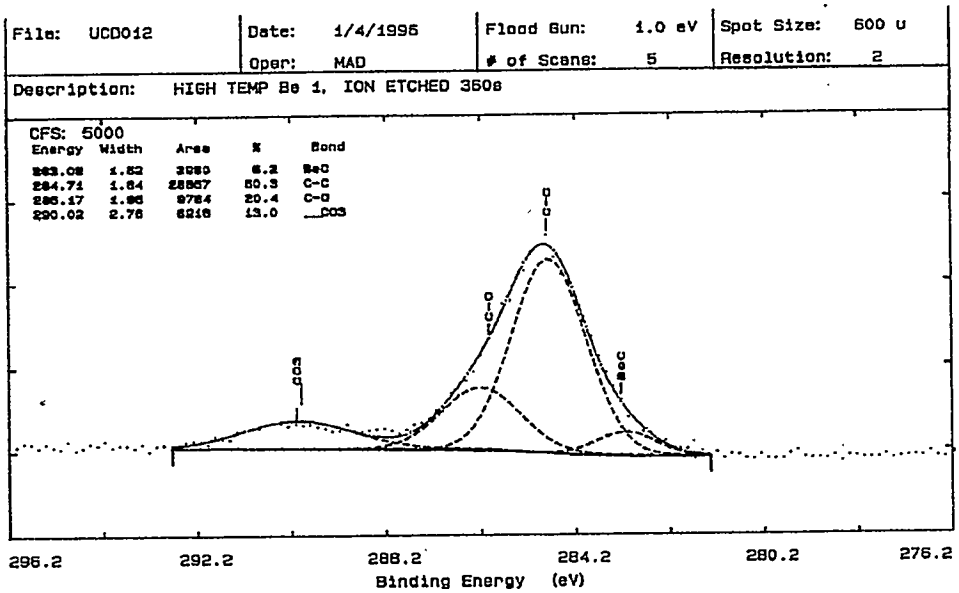

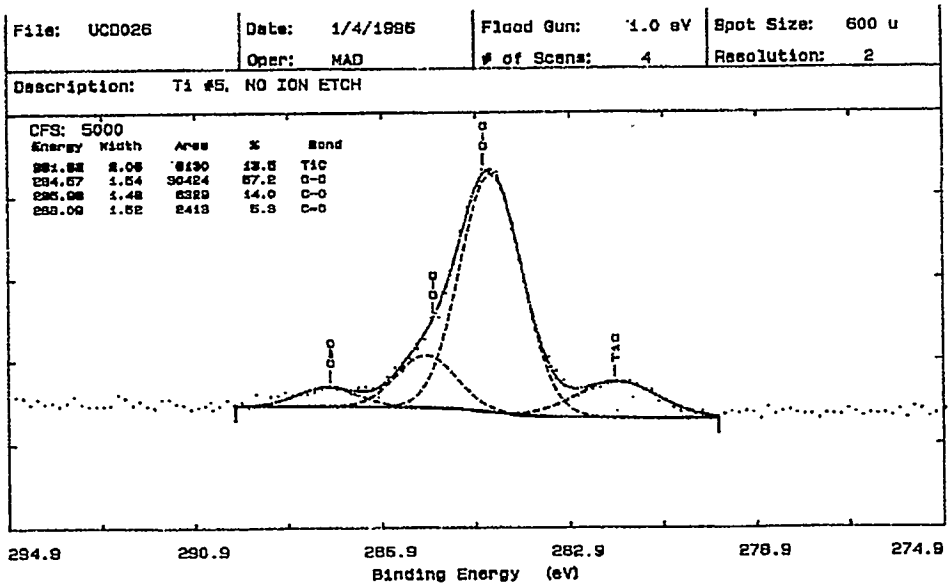

What Is Known About These Protective Impurity Layers

- Coating forms at high sample temperature (≈250°C)
- Elemental composition of 60% Be, 15% each C, N, O throughout the coating
- Carbon is predominantly present as amorphous C
- Coatings are ≈100nm thick (30 min. exposure), very porous and electrically conductive
- Coatings may lower the deuterium desorption temperature
- Potential formation process identified (see Y. Hirooka talk)

What Is Unknown About Coatings

- Growth rate/saturation thickness of coating
- Mechanical properties
- Will coating occur on surfaces shielded from direct plasma bombardment
- Additional theoretical calculations & model validation needed to address these issues

Implications for ITER and Next Fusion Devices

- Designs of PFCs must address the issue of 'mixed material' (Be, C, W) coatings.
- Clearly these mixed material coatings will have characteristics different from the pure substrates (erosion rates, thermal conductivity, tritium retention, mechanical properties).
- In the case of Beryllium, PISCES-B found the coatings formed at high temperature protect the Beryllium substrate and reduce the net erosion from the plasma flux exposed surface.
- Are there benefits to the overall divertor design arising from mixed material coatings?
  - example, Tritium retention in films can be addressed by controlling surface growth rate and devising between shot burn-off techniques

Beryllium erosion and compatibility with carbon and tungsten under DT-plasma bombardment

US-Japan Workshop on PMI/HHF
Colorado Springs
Jan. 9-11th, 1996

Yoshi Hirooka

Fusion Energy Research Program
University of California, San Diego

FERP-UCSD

Table of Contents

1. Highlight data from recent Be experiments

   Carbon impurity effect ("C-poisoning" over Be)

2. Dynamic compatibility analysis for Be, C, W under DT-plasma bombardment

   Be-poisoning over C and W
   W-poisoning over Be and C

3. Conclusion

FERP-UCSD

Erosion of Be, C, W by D-plasma bombardment

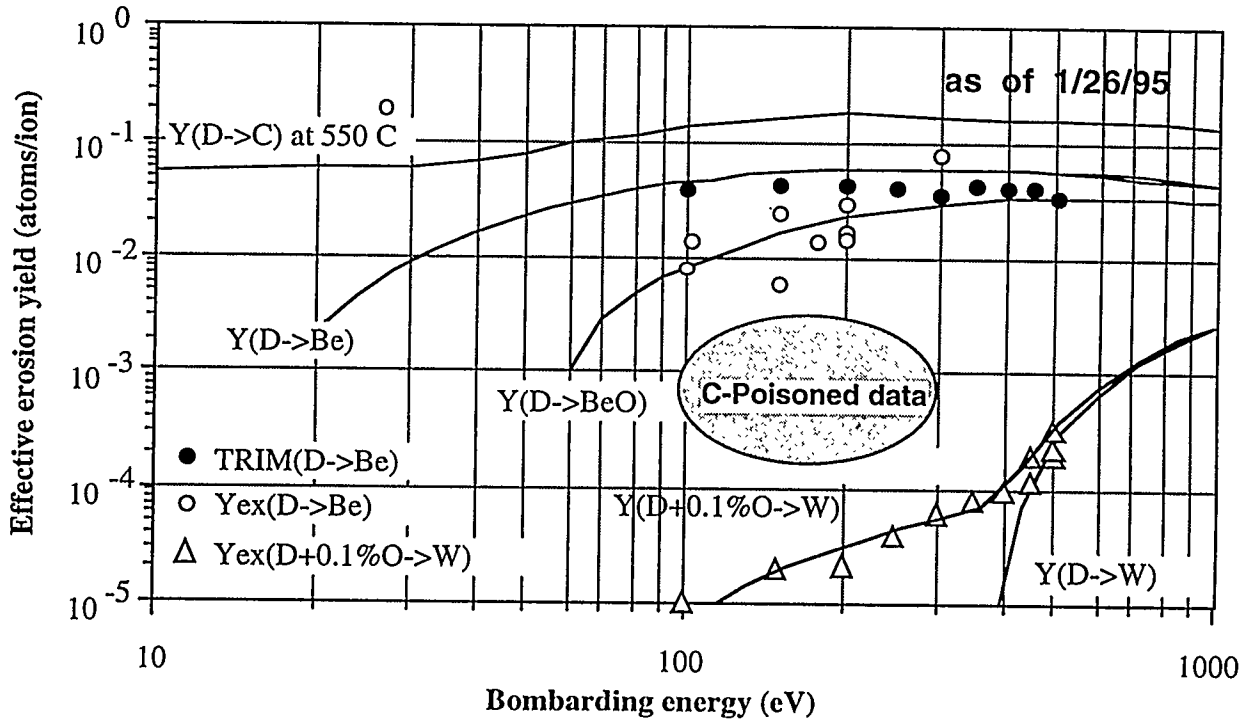

Remarks: Y(D->C at 550C) after Roth (IPP, Garching)
Y(D->BeO) after Eckstein (IPP, Garching)

after Y.Hirooka et al. Fusion Tech. 26(1994)540. (Proc. ANS Topical Meeting on the Technology of Fusion Energy, Jun 19-23, 1994, New Oriens)

FERP-UCSD

"After-the-fact" evidence of carbon posioining effect

1. C-poisoned surface layer is incorporated with othere impurities such as O, N (reactive surface).
2. Thickness depends on the exposure time.
3. Potential danger of increased T-inventory due to co-deposition.

AES-analysis data

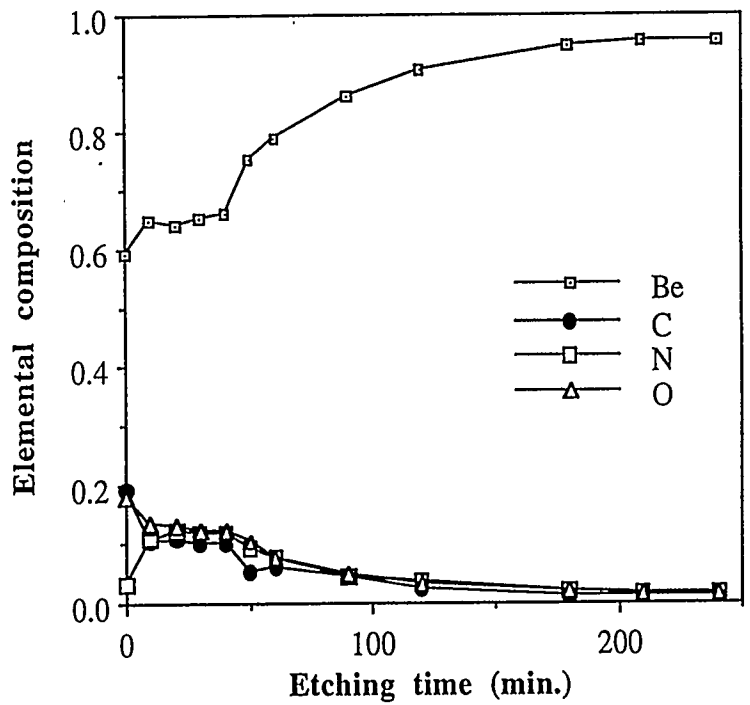

After J.Won et al. presented at 94 Fall APS

FERP-UCSD

"Real-time" evidence of carbon poisoining effect

(1) As soon as C-poisoning starts, Be-II rapidly decreases to BG-level. A sign of reduced erosion of Be.

(2) Possible carbon sources are: C_xH_y fragmented ions from pump oil or CO from the hot cathode(L_6B).

Be-II spectroscopy data

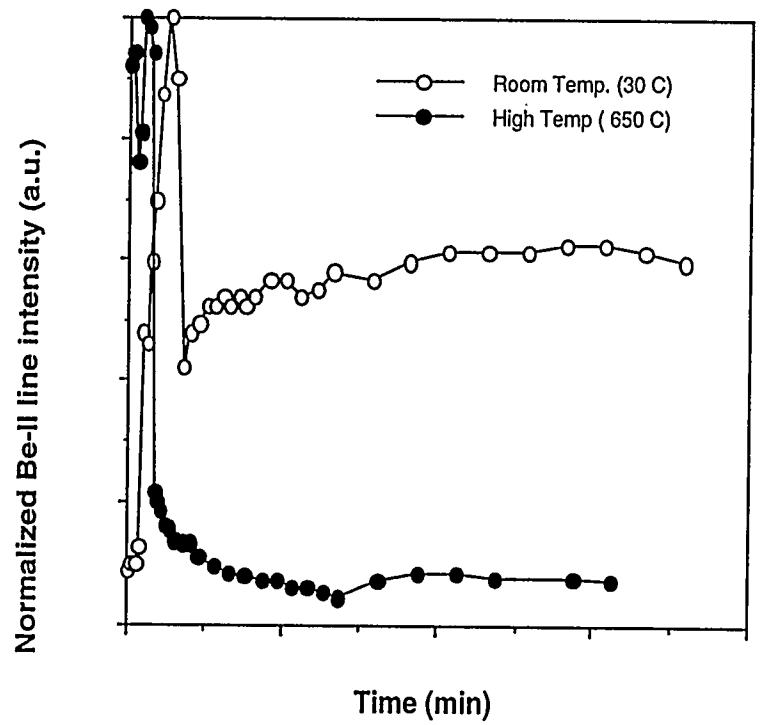

FERP-UCSD

Key process to the carbon poisoning effect-II
- Beryllium carbide formation -

XPS data indicate that at elevated temperatures (above 300 C), beryllium reacts with carbon to form some carbide (After Ashida et al. in NIFS-report ISSN: 0915-6348).

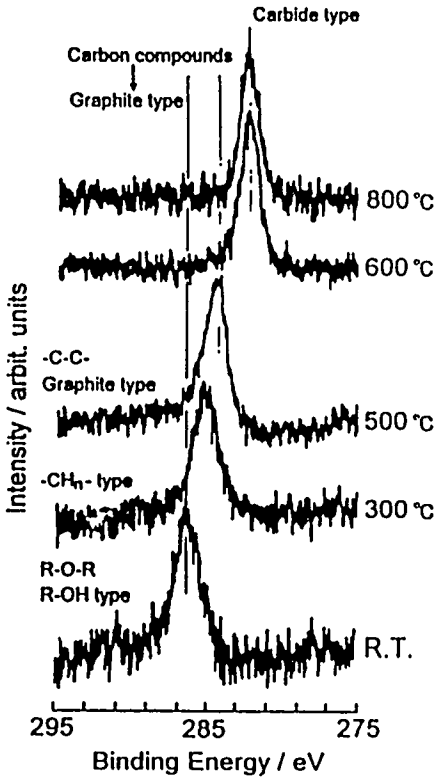

Fig.4. Temperature dependence of the narrow range C1s spectra for Be sample covered with evaporated carbon film.

FERP-UCSD

Critical impurity-to-DT flux ratio for poisoning

(1) Dynamic surface concentration of impurity-X under competitive erosion and deposition (trapping) conditions:

$$dC_x/dt = \Gamma_{in} - \Gamma_{out} \text{ , where}$$

$$= \nu_{trap}\Gamma_x - (Y_{ss}\Gamma_x + Y_s\Gamma_{DT})$$

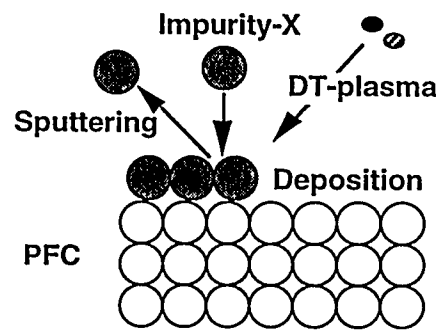

(2) Critical flux ratio above which "poisoning with impurity -X" occurs:

For a steady state, dCi/dt = 0

$$\Gamma_x / \Gamma_{DT} = \frac{Y_s(E, \Theta, T_s)}{(\nu_{trap}(E, \Theta) - Y_{ss}(E, \Theta))}$$

where the denominator must be positive.

FERP-UCSD

Surface temperature effect on C-poisoning over Be

1. Due to chemical sputtering and RES, the critical flux ratio goes up and down as temp. changes.

2. (Be+C) mixed layer seem to have reduced erosion* even at elevated temps. This leads to a lower critical flux for C-poisoning over Be.

* Catalytic effect to enhance molecular recombination.

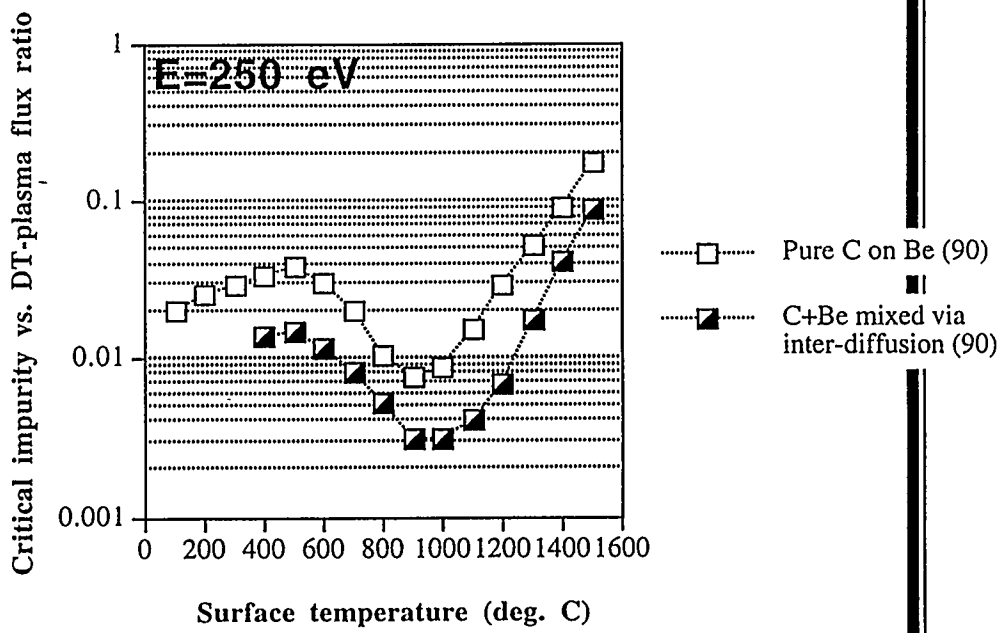

Above data assume the same erosion rates for (B + C) and (Be +C) mixed materials. Data for (B+C) are after Hirooka et al. J.Nucl.Mater. [1990).

FERP-UCSD

C-poisoning over W is less likely than Be

1. Due to high reflection, C-poisoning over W requires higher impurity levels than over Be.

2. Due to an increase in sputtering yield, non-normal incidece makes the critical flux ratio higher, meaning that C-poisoning is less likely.

** Axis converted to the edge plasma temp., assuming $T_i = T_e$ and $E_i = 6kT_e$.

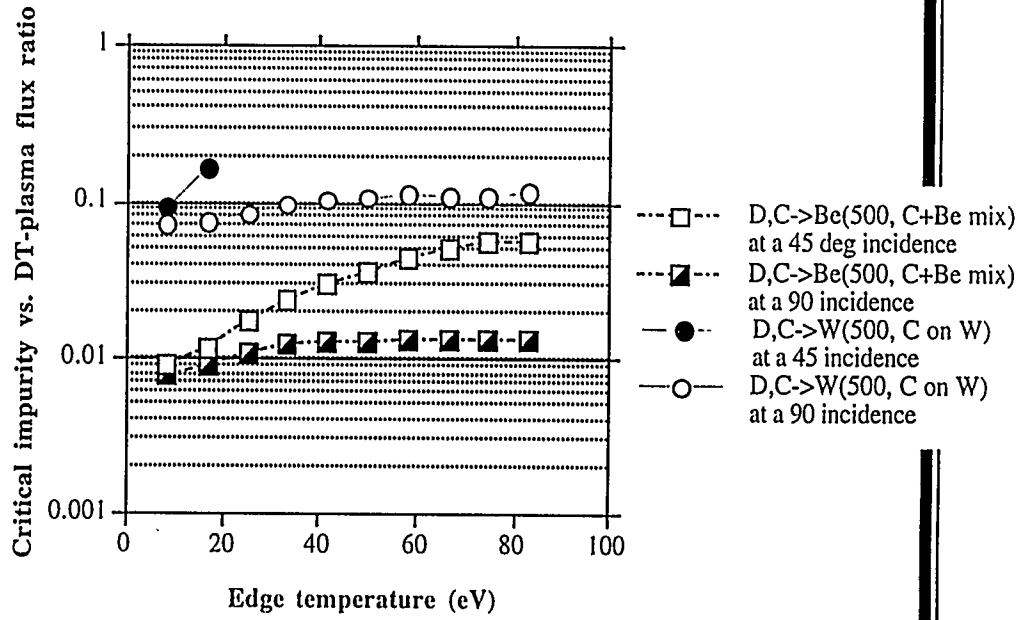

FERP-UCSD

Substrate mass effect on C-poisoning

1. Due to high reflection, heavier elements are less suceptible to C-poisoning at RT.

2. At elevated temps., low diffusivity into carbon deposits makes heavy elements further less succeptible to C-poisoning (no metal catalysis).

** Axis converted to the edge plasma temp., assuming $T_i = T_e$ and $E_i = 6kT_e$.

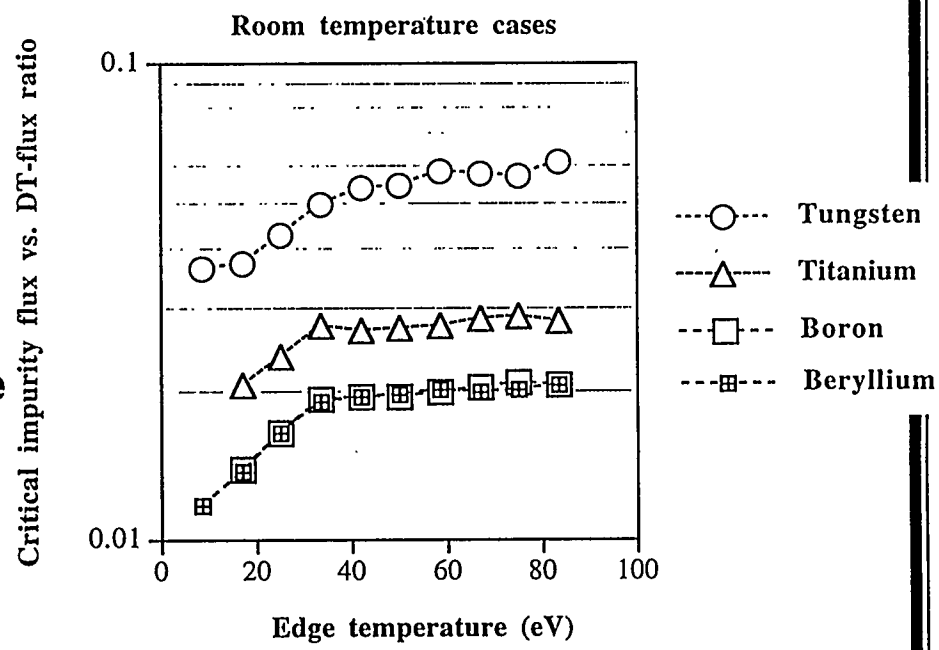

FERP-UCSD

Be-poisoning NOT likely over W-surfaces !

1. Be-poisoning occurs both on W and C at a 90 deg. incident angle. But, C is much more suseptible to Be-poisoning than W.

2. At a 45 deg. incident angle, Be-poisoning is found less likely (Not possible for W).

3. D or T isotope effect is not so significant.

4. Multiple-charged (2+) case occurs at 90 deg but not likely at 45 deg.

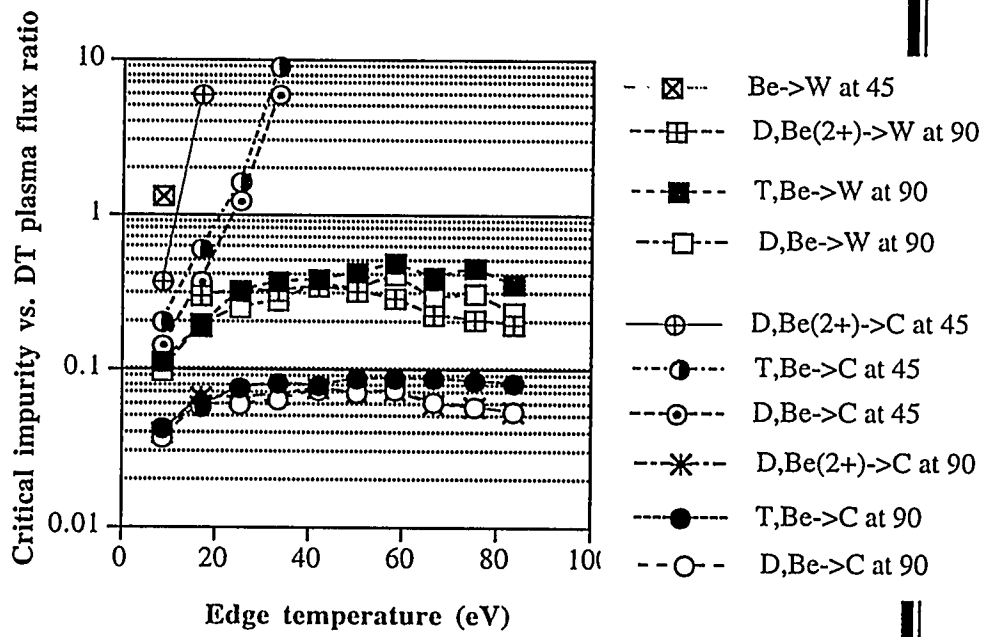

FERP-UCSD

W-poisoning over Be, C is highly possible at low Te

1. Both Be and C are extremely suseptible to W-poisoning at low Te (< 50 eV).

2. Be and C behave similarly in terms of W-poisoning.

3. At higher Te (> 50 eV), W-poisoning is very unlikely due to high self-sputtering yield ($Y_{ss} > 1$ at $E_i > 450$ eV at 45 deg incidence).

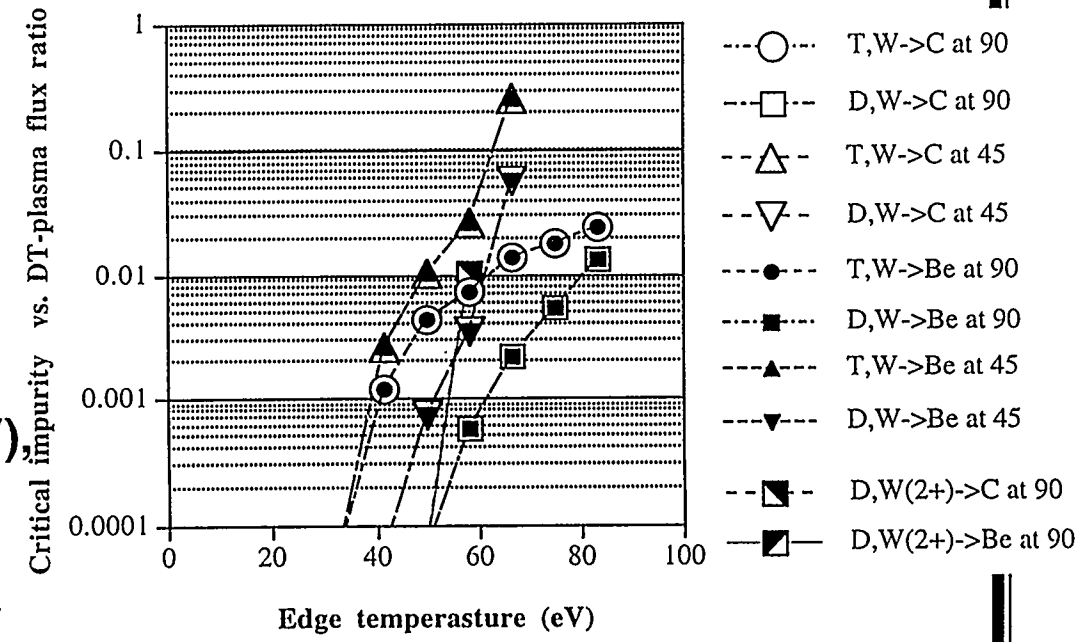

FERP-UCSD

Conclusion

1. Materials "communication" is NOT always two-way street.

2. W is likely to stay "clean" while it poisons Be and C.

3. Be and C can poison each other, forming (Be+C) surface layers, which have reduced erosion relative to pure Be and C. However, C-poisoning over Be can lead to an increase in T-inventory.

4. Non-normal incidence makes poisoning less likely. Also, multiple-charged impurities are not likely to poison other surfaces due to their high self-sputtering yields.

Materials exchange diagram

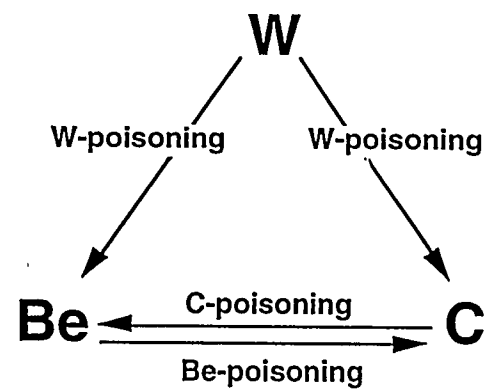

FERP-UCSD

Erosion/Redeposition Modeling for ITER and DIII-D

Jeffrey N. Brooks
(Ahmed Hassanein)
Argonne National Laboratory
9700 South Cass Avenue
Argonne, Illinois 60439 USA

U.S - JAPAN WORKSHOP

JANUARY 1996

COLORADO SPRINGS

Erosion/Redeposition Modeling for ITER and DIII-D

Objectives: Analyze erosion lifetime, plasma contamination, and tritium co-deposition for ITER PFC's; benchmark erosion codes.

Current Activities:

- ITER Vertical Divertor Erosion Analysis [with JCT,SNL,U of ILL.]
  - Be, C, W erosion, T co-dep. WBC and REDEP code analysis for several plasma solutions including radiative plasma solution (Coster et al. ~1% neon), and detached plasma solution (Kukushkin et al.) .
- ITER Sheath Analysis
  - BPHI sheath code analysis of oblique - incidence sheath conditions with in-sheath ionization of surface emitted particles.
- DIII-D DiMES Probe Erosion Analysis [with GA, SNL]
  - Be, C, V, Mo, W sputtered particle transport along divertor analyzed and compared to data.

ITER Vertical Divertor Erosion/Redeposition Analysis

- Radiative plasma solution of Coster et al., used in REDEP/WBC

  (~1% neon SOL seeding, $T_e \leq 10$ eV, $N_e \approx 10^{21}$ m^{-3} at strike point)

– Results (without neon near-surface recycle considered)

  – Peak gross erosion rate (Be) ≈ 600 cm/burn·yr

  – Peak net erosion rate (Be) ≈ 30 cm/burn·yr

  – Net erosion rate (W) ≈ 0

- Results for Be are up to an order of magnitude better than gas-bag geometry (depending on assumed plasma solution for the latter).

- Higher redeposition rate is due to: a) non-tangential field-line geometry, b) high plasma density.

- Little contamination of core plasma by divertor sputtering predicted.

– Results with neon near-surface recycling examined in detail (J.. N. Brooks "Analysis of Noble Gas Recycling at a Fusion Plasma Divertor", Physics of Plasmas, to be published):

- Inhibited backflow to SOL, high sputtering and other effects predicted for neon/Be case. Factor of ~100 surface neon flux amplification appears possible.

- Neon/W case does not result in apparent problems due to high neon <u>reflection</u> at surface.

- Results are speculative- data, additional analysis required.

ITER vertical divertor/REDEP analysis,
radiative plasma conditions

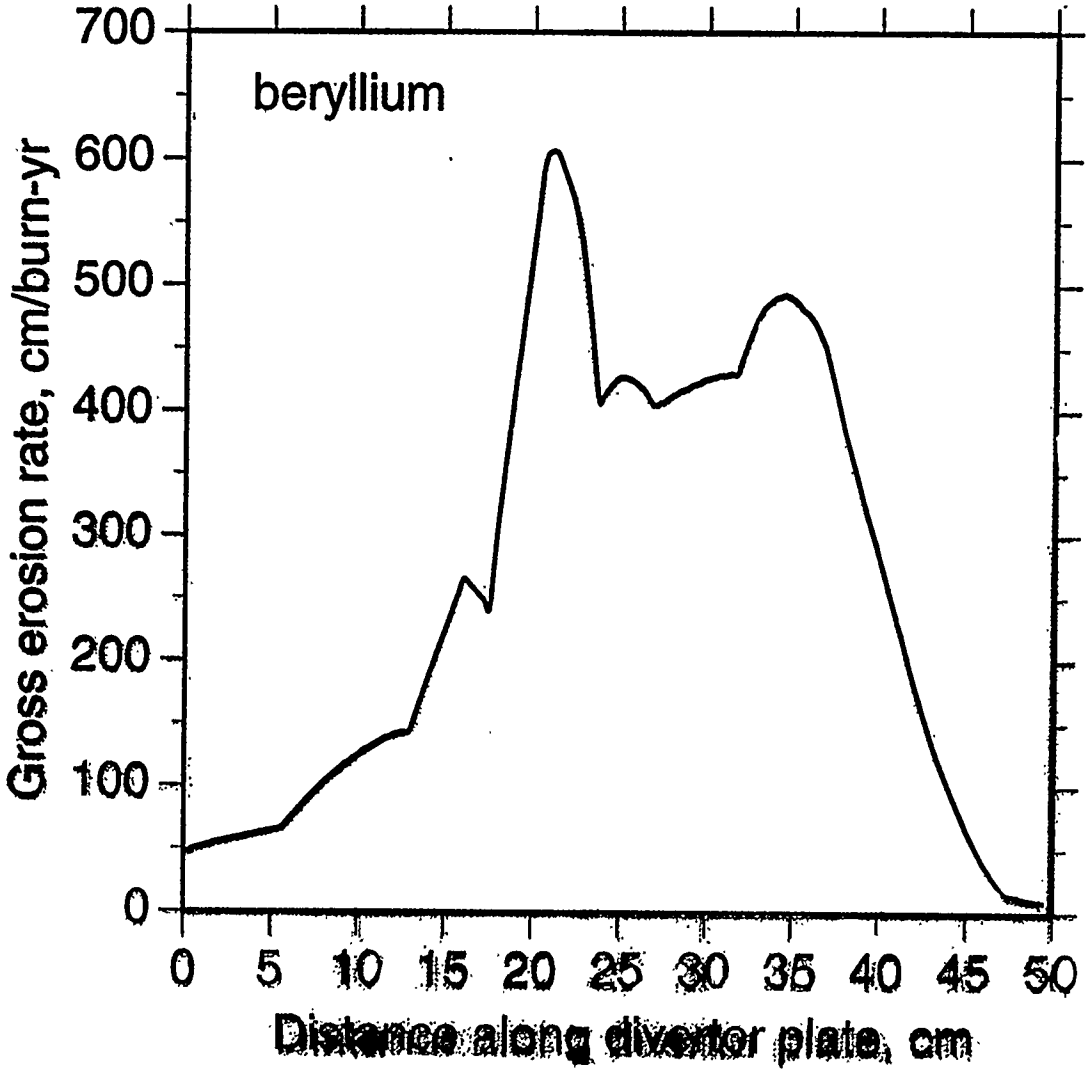

ITER vertical divertor/REDEP analysis,
radiative plasma conditions

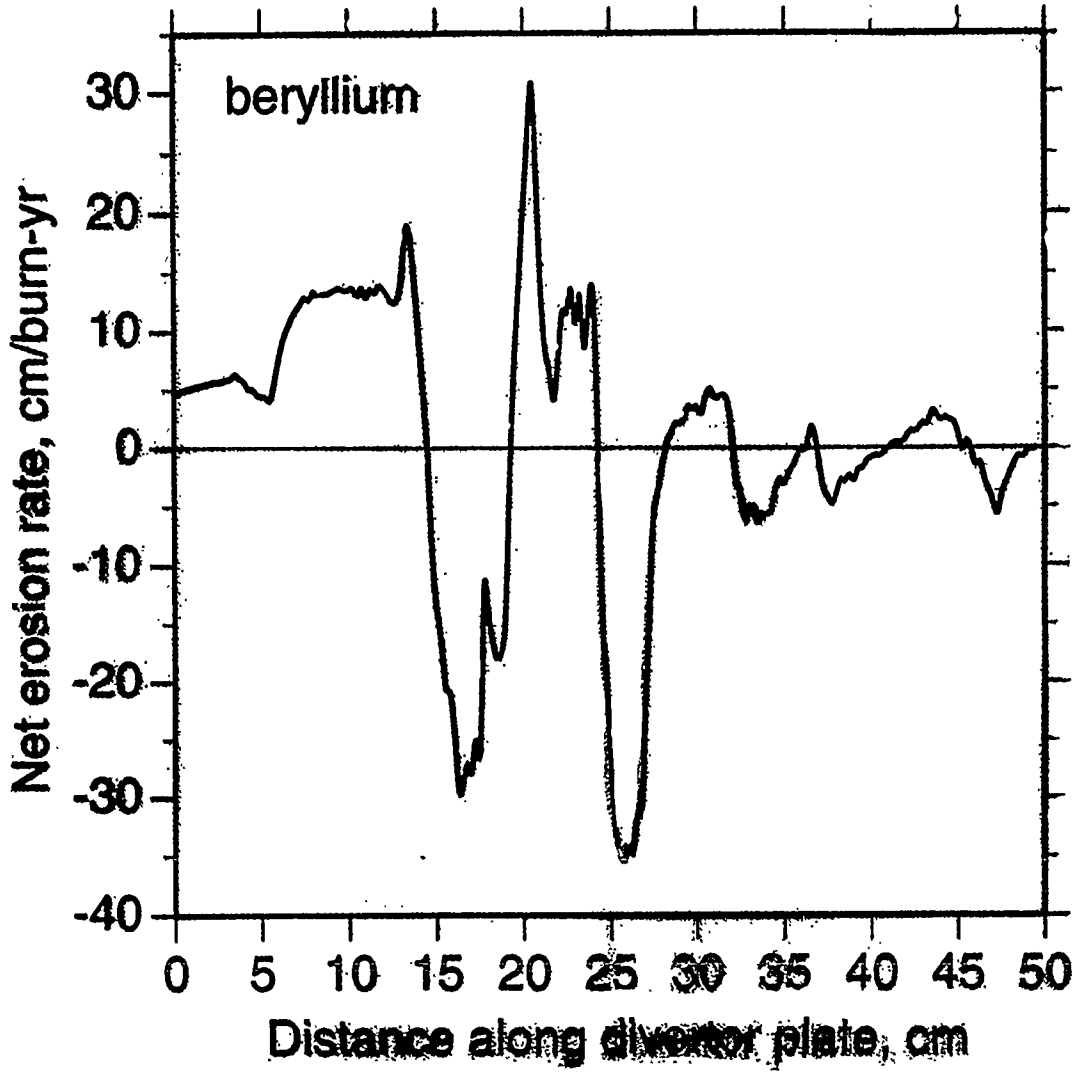

ITER vertical divertor/REDEP analysis

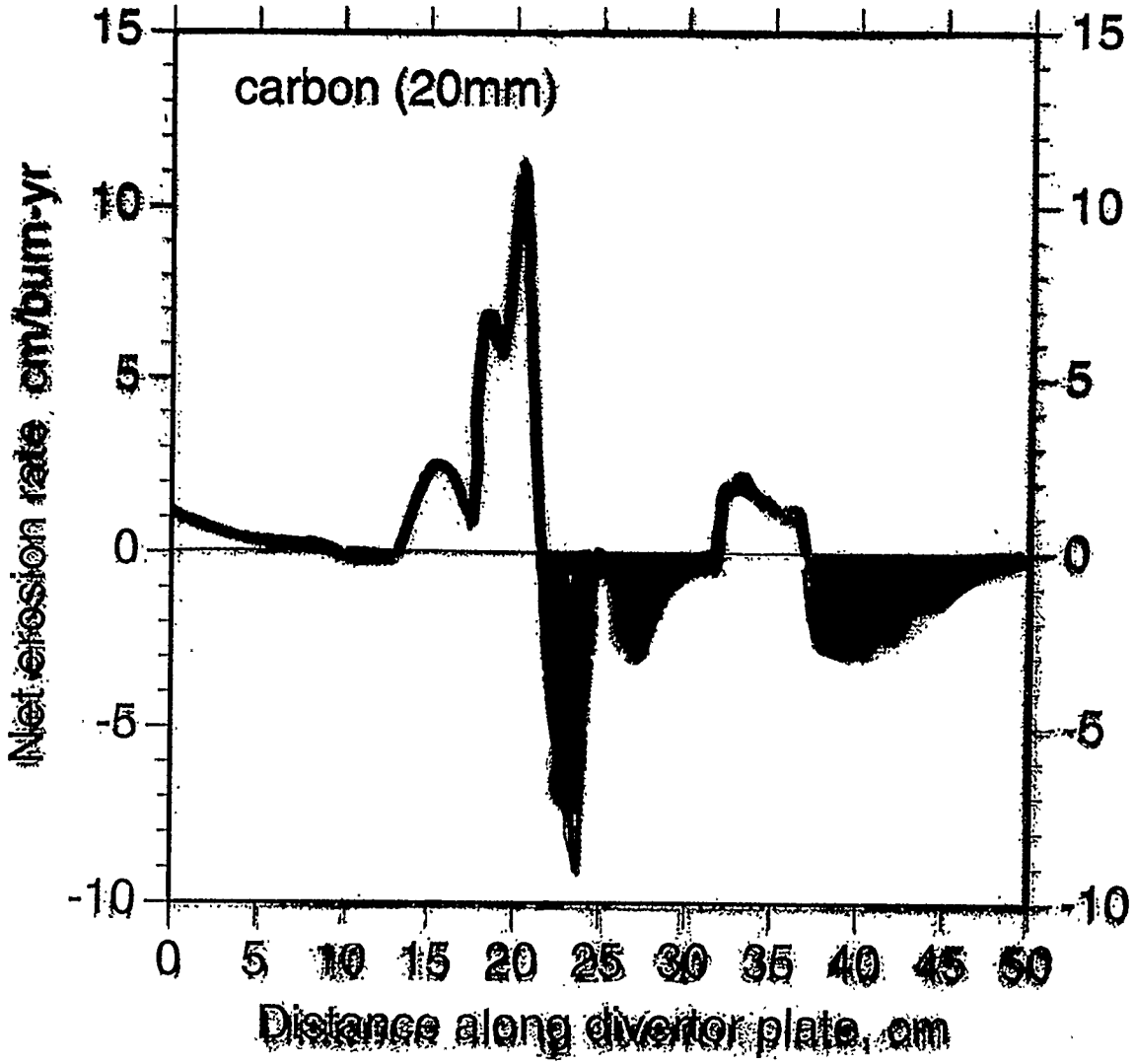

— GROWTH REGIO
TRITIUM
CO-DEPOSITI

Lifetime Estimation - "Vertical Divertor" (for 5 mm coating thickness)*

Material	Peak Net Erosion rate, cm/burn·yr	Duty cycle	Lifetime**
Beryllium	~30	100% 2%	6 days 0.8 yrs
Carbon	~12	100% 2%	15 days 2 yrs
Tungsten	~0	100%	~unlimited

* REDEP/ITER analysis (7/95), radiative plasma solution (Coster et al.) w/o neon surface effect

** due to sputtering erosion

WBC Analysis - DIMES71

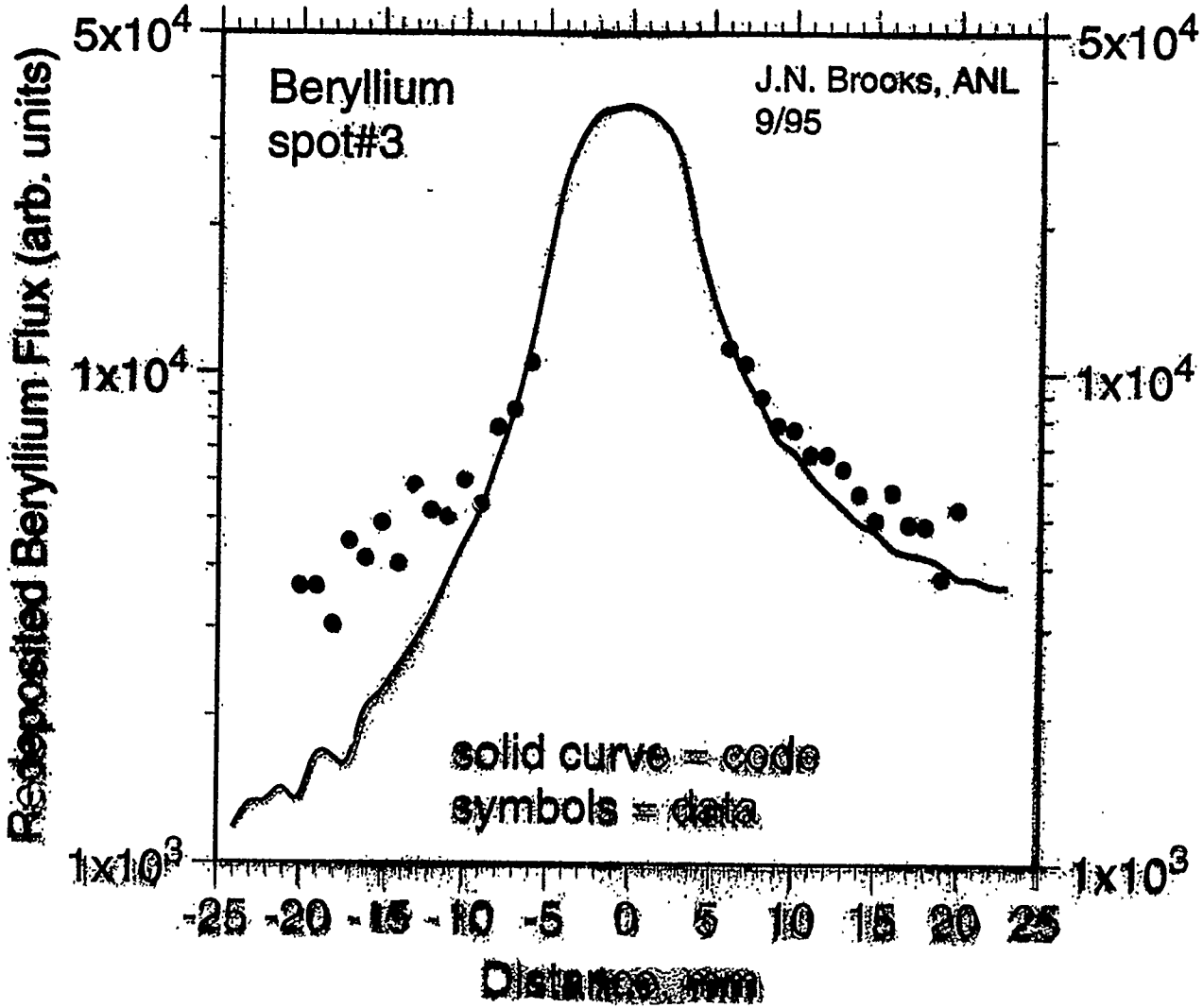

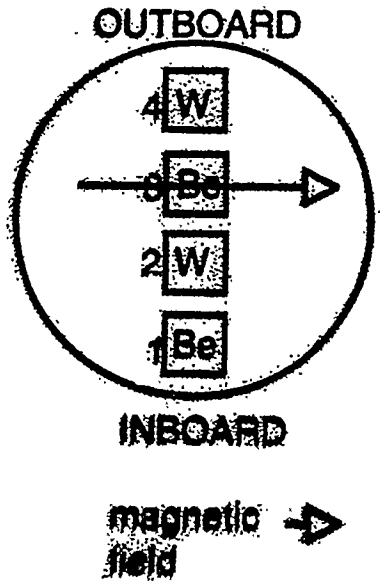

WBC Analysis - DiMES71

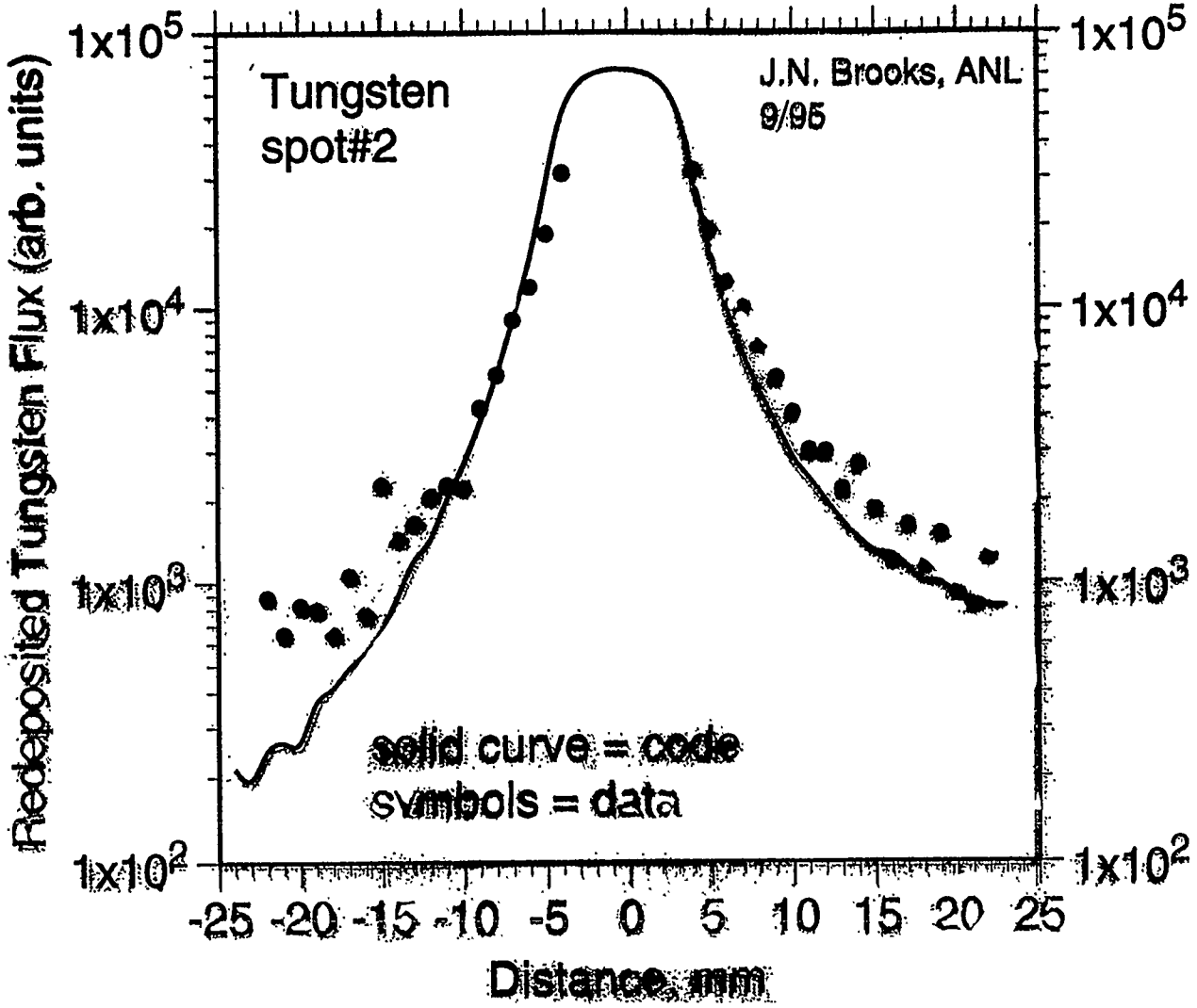

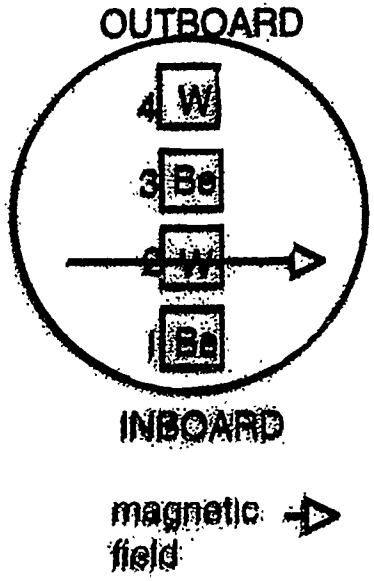

Required Future Work

- ITER Divertor - Plasma Surface Interactions
  - Neon/beryllium compatibility
  - Carbon erosion/co-deposition with rigorous chemical sputtering analysis and surrounding divertor region transport, and with additional plasma solutions.
  - Tungsten - impurity effects, plasma temperature limits
  - Sheath issues/performance e.g. overheating effects, geometry effects
  - Tri-material (C, Be, W) effects
  - 1st wall erosion
  - ICRF faraday screen and related RF component erosion, particularly due to RF induced sputtering

Conclusions

- The erosion/redeposition process is critical to ITER divertor performance, e.g., net Be erosion is ~1/10 gross erosion. Erosion/ redeposition data generation and code validation is a critical need for ITER.

- Net erosion rates for the vertical divertor are an order of magnitude lower then the gas-bag design. Predicted core contamination by sputtering is low. Tritium co-deposition in carbon is high. (All results are uncertain.)

- Plasma Radiation Seeding may not work with low-Z materials. We are formulating plans for experimental tests of this issue in, e.g., PISCES.

- Erosion code benchmarking with DiMES is encouraging - good agreement with Be, W, Mo, C redeposition data. Modeling results explain the substantial difference in sputtered transport distances between Be and W.

- Work is ongoing to examine some of the critical plasma surface interaction issues, e.g., sensitivity to plasma solutions, tri-material (C, Be, W) effects and sheath issues.

Lifetesting of Divertor and Plasma-facing Components

Samuel A. Cohen
Plasma Physics Laboratory
Princeton University
8 January 1996

Full-scale prototype models of divertor and plasma-facing components, such as

- divertor tiles,
- wall tiles,
- tile support,
- tile attachment, e.g., braze joints,
- cooling structures,
- ducts to pumps, and
- pumps

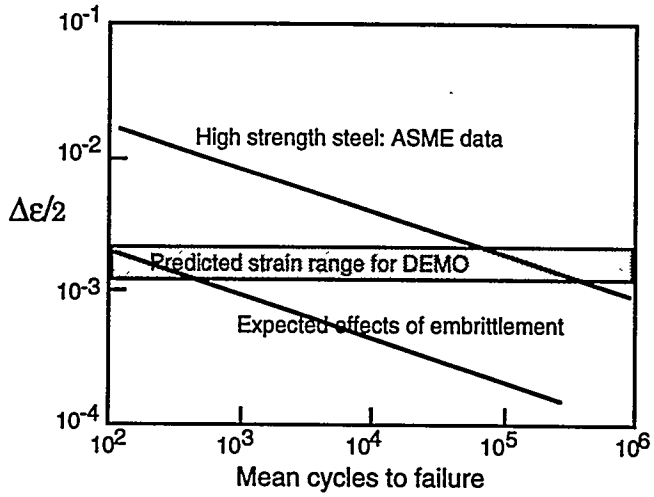

must be qualified, *via* full lifecycle testing, in a high heat flux environment, complete with exposure to reactive, hyperthermal ionic, atomic, and molecular hydrogen. These tests will include heat flux limits, thermal fatigue, pumping speed, and radiating layers.

Heat flux facilities that can produce the necessary environment have been used for decades in the aerospace industry. These devices, arcjets, produce steady streams of high enthalpy plasma.

Experimental facilities presently used in the fusion program to develop the divertor operational scenarios

Devices	Number (Total/US)	Power (MW)	Pulse length /duty factor
Tokamaks	12/5	50	$10/10^{-4}$
Linear plasma	10/5	1	$1/10^{-1}$
E-beams	4	1	CW
Neutral beams	5	10	$10/10^{-1}$

Gaps in the present program

low duty factor
low hydrogen fluence
poor accessibility
understanding of
  radiation and energy transport
  ablation
full life testing of large scale prototypes

Important fusion-related experiments could be carried out in Arcjet facilities

- Materials and component qualification
- Fatigue lifetime
- Erosion lifetime

- Hydrogen inventory in materials

- Pump qualification

- Radiation transport

- Melt layer ablation

The use of arcjets for fusion would be a cooperative effort between US goverment agencies.

Typical arcjet geometries

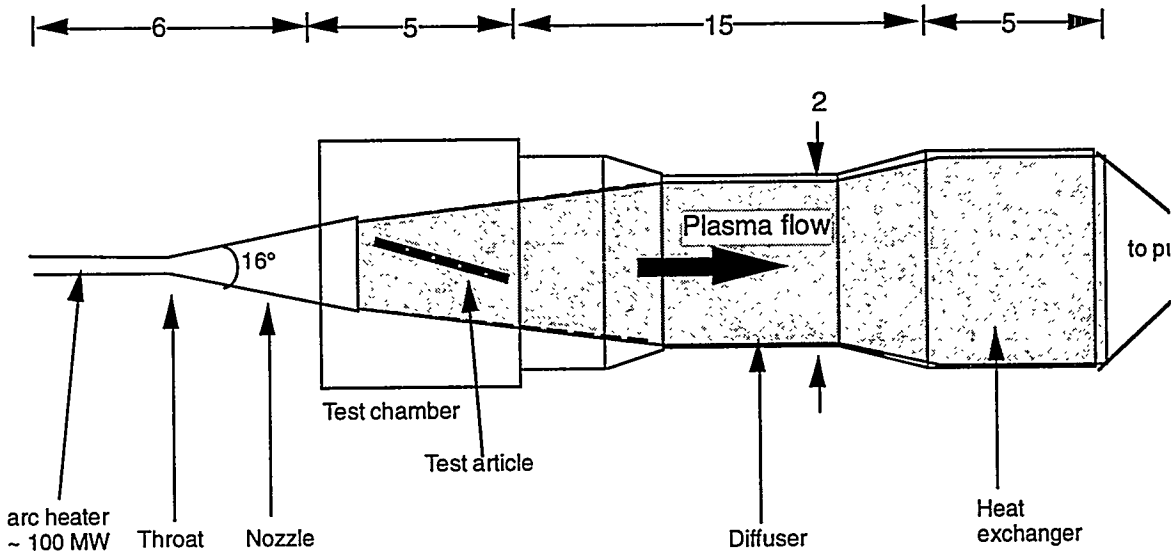

Typical arcjet geometries
(all dimensions in meters)

In the US, at least two <u>hydrogen</u> arcjets have been operated.

- Scramjet Combustor Facility
- Giant Planet Facility (GPF) qualified tile materials for spacecraft entry into the Jovian atmosphere (Galileo exp.)

Scramjet: Rarely used, but still assembled
100 MW,
10 kV, 10 kA, ~1m x 1m x 1 m test chamber

GPF: Now "on the shelf", ~3m x 2m x 2 m test chamber
85H-15He mixture, 110 MW heating power ->400 MJ/kg
Measured heat flows (blunt surfaces) > 250 MW/m^2
80 MW/m^2 radiation (note relation to ITER)

LOCAL CONDITIONS FOR PEAK HEATING
h_t = 10 - 29 MJ/kg (4300 - 12,500 Btu/lb_m)
M = 5 - 8 (LOCAL VALVES, WINDWARD SIDE)
TIME = 1000 sec

REGION I. BOUNDARY-LAYER FLOW
TRANSITIONAL/TURBULENT FLOW
$\dot{q}$: 20 W/cm²
p: 0.006 - 0.028 atm
SIZE: CHARACTERISTIC SIZE: 61 cm (2 ft)

REGION II. STAGNATION FLOW
LAMINAR BOUNDARY LAYER
$\dot{q}$: 105 W/cm²
p: 0.033 - 0.105 atm
SIZE: CHARACTERISTIC SIZE: 61-cm (2 ft) diam

Figure 4. Heating simulation requirements for the shuttle orbiter.

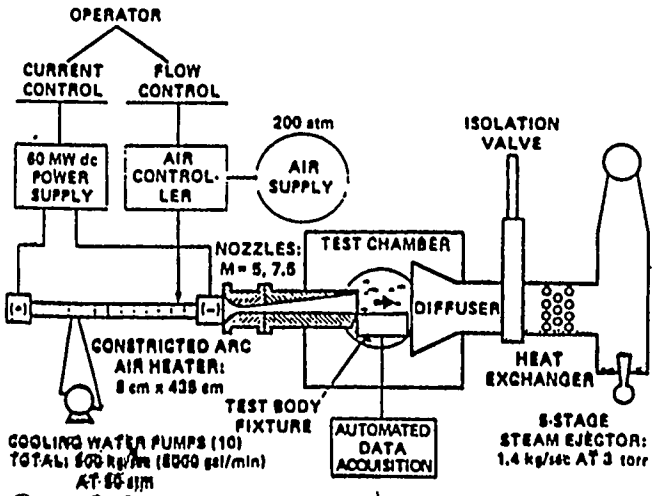

Figure 5. Schematic diagram of the 60-MW shuttle interaction heating facility.

Now qualified to 100 MW

FACILITY DESCRIPTION

The ~~60~~-MW Shuttle Interaction Heating Facility is a continuous flow, electric-arc-heated, hypersonic wind-tunnel system. A schematic representation of the facility is shown in Figure 5. The major components of the facility include a constricted-arc air heater, a 60-MW power supply, two interchangeable hypersonic Mach number nozzles, a walk-in test chamber, and ancillary sub-

60-MW RATING
PRESSURE 12 atm
CURRENT 5400 A
VOLTAGE 11000 V
FLOW RATE 1.4 kg/sec

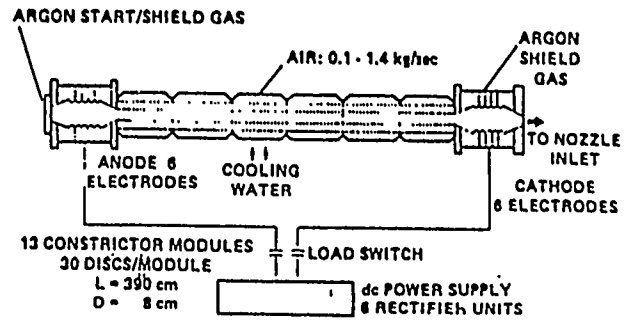

PHYSICAL SPECIFICATIONS

WORKING FLUID	AIR, 1.3% Ar
ARC BORE	8 cm
SINGLE CONSTRICTOR THICKNESS	1 cm
CONSTRICTOR LENGTH	390 cm
ELECTRODE ASSEMBLY LENGTH	32 cm
OVERALL ARC LENGTH	412 cm
ELECTRODES (TWO)	SIX, MAGNETICALLY SPUN, COPPER

Figure 6. The 8-cm-constricted-arc heater.

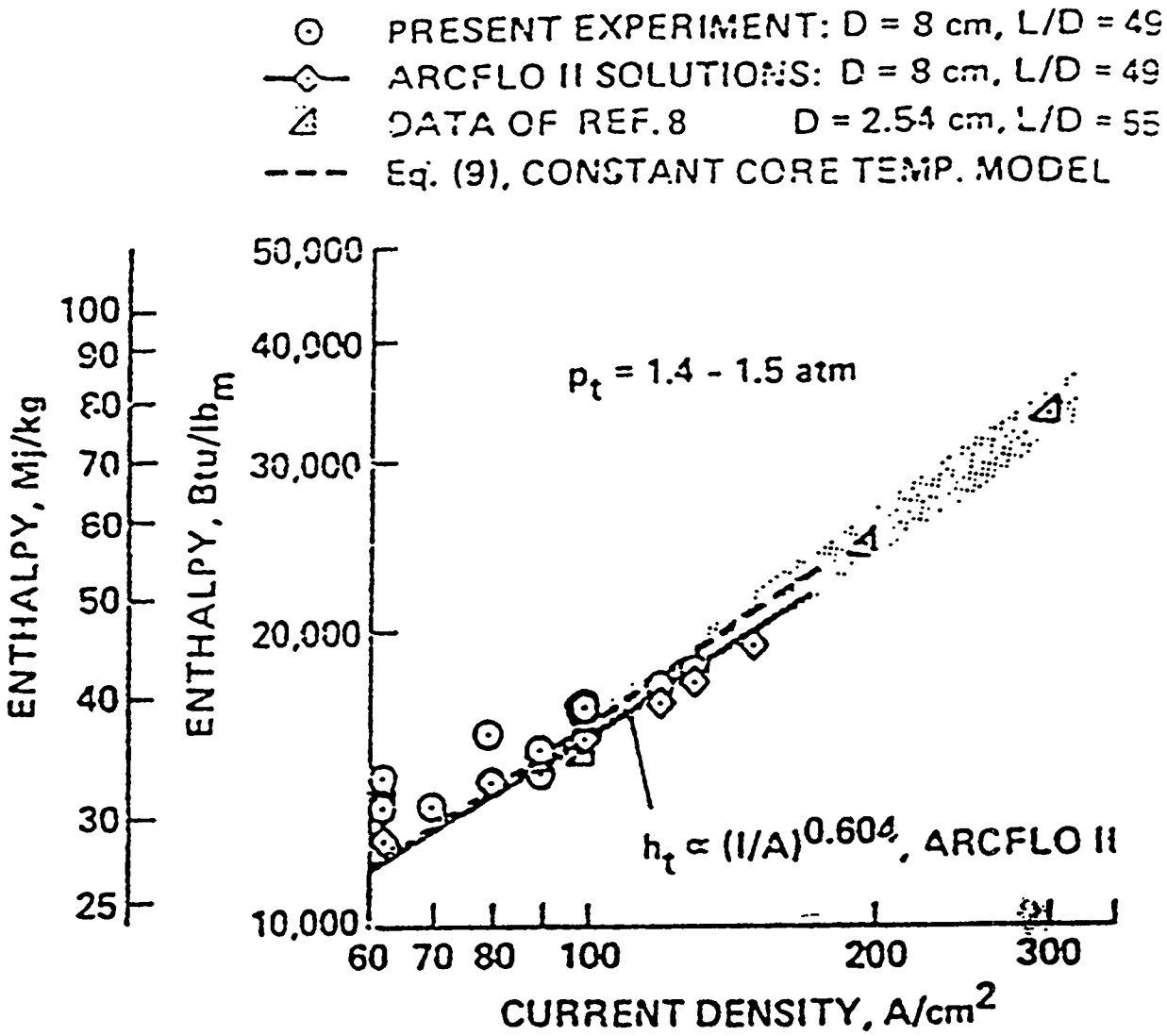

Fig. 7 General enthalpy scaling law for constricted-arc heaters at constant pressure and 49 < L/D < 55.

Radiative heat load

A radiant heat load on the test article and chamber will occur when a test article is in place. An incandescent gas layer is formed in the sharp longitudinal gradients surrounding its blunt surface. This gas cap region radiates a multiband spectrum nominally described as an optically thin black body, hence there is an approximate T^4 dependence on the gas temperature. The shock standoff distance, d_0, and the article radius, *a*, determine the radiating volume, in contrast to an optically thick black body whose power losses depends on surface area only.

Based on calculations and experiments performed for Earth, Tauber and Sutton, and Jupiter reentry, Winovich and Carlson for the 110 MW arcjet Giant Planet Facility (GPF), scaling relations have been determined as functions of Mach number and heat flow.

Figure 1 shows the radiative heat transfer coefficient, defined as $C_{Hr} \equiv q_r/(\rho U^2/2)$, where q_r is the radiant load onto the object. Essentially, C_{Hr} is the fraction of kinetic energy in the gas stream (initially flowing directly towards the test article) that is converted to radiation onto the target. Using the ρ_e and U_e values from a high enthalpy case we find the power flux density flowing towards the test article to be 43 MW/m^2. Higher values can be obtained at higher Mach numbers

Comparison of devices

	ITER requirement	Arc Jet capability
Characteristics		
Power input (MW)	~100 MW to SOL	to 110 MW
Enthalpy (MJ/kg)	3 (midplane)	1 to 400
Peak heat flow (GW/m^2)	2 ($B_{ll\text{-}SOL}$)	0.05 -> 20 (axial)
Plasma flow	?	to above Mach 10
T_e,T_i	1-2 eV desired	1-2 eV obtained
Power to side walls (MW/m^2)	turbulence desired	turbulence 0.1
Pulse length (minutes)	15	> 25
Pulses	10,000 in life	1000/year
Cyclic heat load (Hz)	0.1 (sweeping)	TBD
Hydrogen content	90H-10He	to 100%
Chemical erosion	expected	observed
Test area (m^2)	~60	3
Plasma width (m)	~ 0.1	0.05 -> 2 m
Conductance (m^3/s)	depends on gas	>1000 m^3/s
Pumping speed (m^3/s)	500	> 500
Pressure recovery	10 μ - 0.05 atm	yes, to 1 atm
Throughput (kg/s)	0.20	0.1-10.0
Throughput (atoms/sec)	5 x 10^{24}	->2 x 10^{26}

*Possible Elm and disruption testing via pulsed bias

Note: Arcjets have no magnetic field and hence are not suitable for testing the ITER divertor physics that occurs where the plasma is fully ionized. But one ITER plan is to promote plasma recombination away from the divertor plate. Then the physics of the hot, partially ionized plasma gas streams are similar. Navier-Stokes equations are being used to model both the ITER plasma gas and arcjet plasmas.

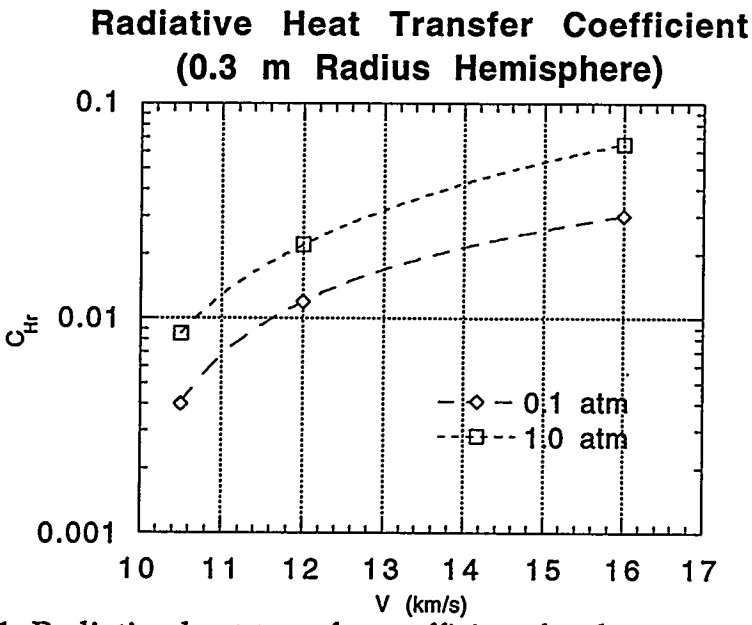

Figure 1. Radiative heat transfer coefficient for the motion of a 0.6 m diameter hemisphere through air.

The radiated power changes with stagnation pressure, Mach number, and operating gases.

Proposed workplan for ITER

Dates	Activity
1-4/96	1. Perform analytic derivations and numerical evaluations to find arc heater/diffuser regimes most representative to ITER divertor conditions: P, T, Ma, H^0/H_2 Balboni: NASA Ames Smits: Mechanical and Aerospace Engineering, Princeton Cohen: PPPL
4-8/96	2. Perform 1- and 2-d Navier Stokes calculations (with real gas chemistry) to determine gas flow properties and radiation levels relative to ITER divertor Balboni et al: NASA Ames Pigarov: Kurchatov, PPPL
8-12/96	3. Perform plasma calculations on heat flow to test samples, including effects of pulsed bias and radiative energy transfer Cohen, Vesey: PPPL Balboni: NASA Ames
1-6/97	4. Engineering analysis to determine facility lifetesting capability (incl. materials) and resiting PPPL engineering
6-12/97	5. Perform brief test runs in Interaction Heating Facility (IHF) with 95Ne-5H or 95He-5H to assess cyclic heat load capability, low pressure regimes, and radiation levels predicted in 1 and 2 Balboni, NASA Ames

1-6/98

6. Operation of scramjet facility in cyclic mode with 100%H or D
   a) no test article
   b) with test article (prototype divertor plate)

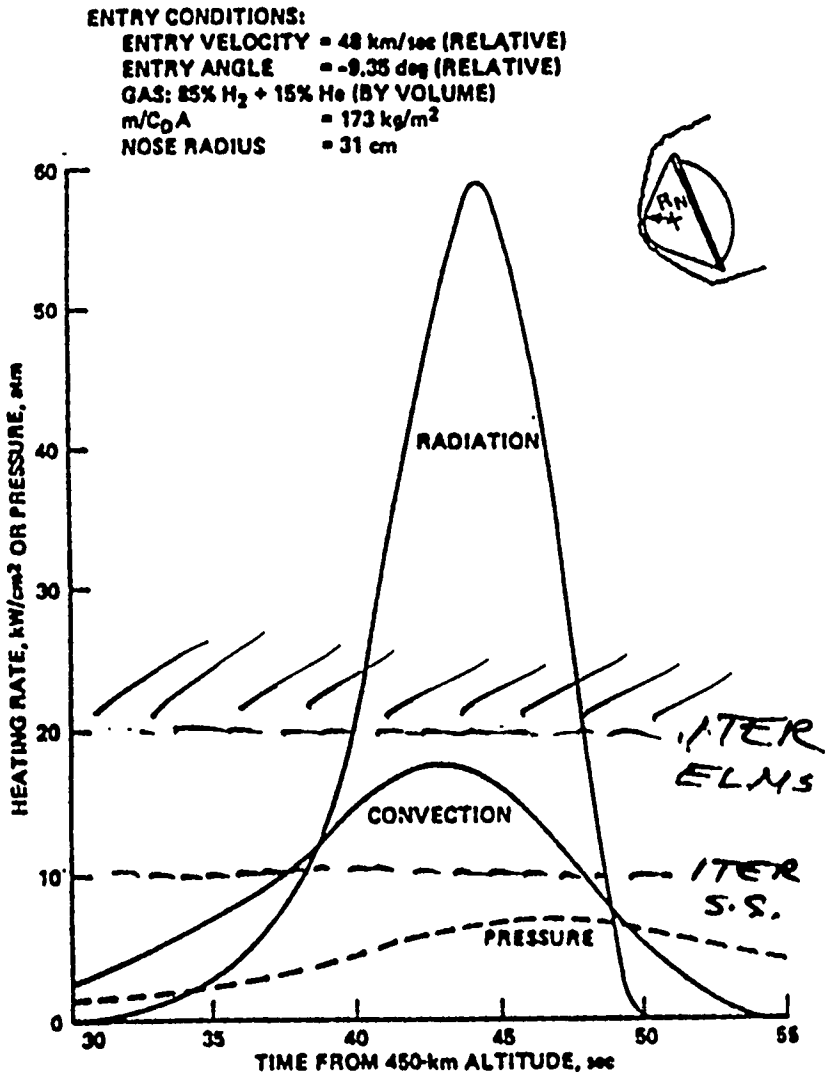

Figure 3 - Stagnation-Point Heat-Transfer Rates and Pressure for the Entry Probe.

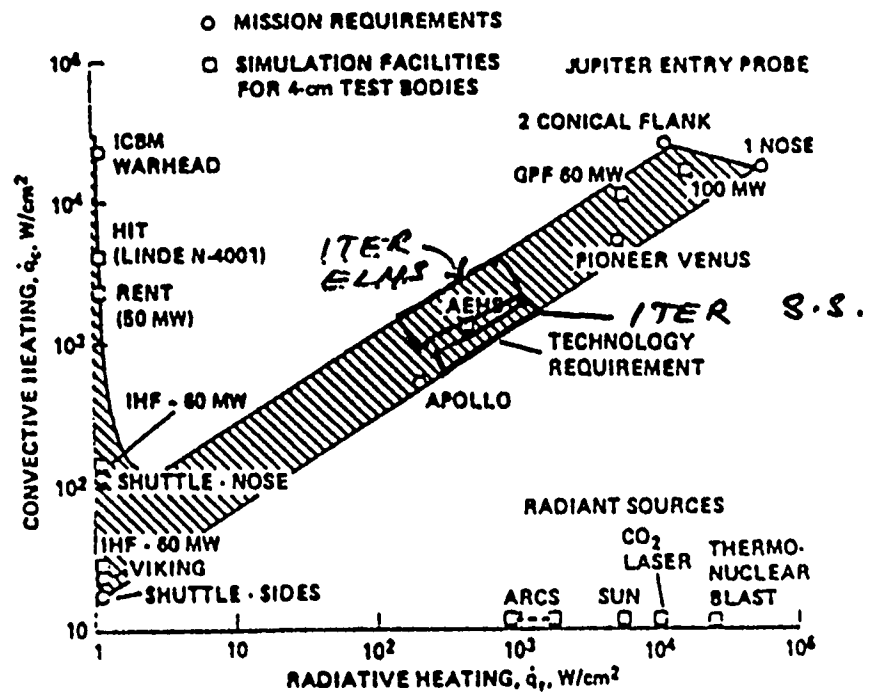

Figure 4 - Technology Requirements for Simulation of Entry Heating for Various Missions.

Further studies of thermally collapsed plasmas (STEPS)

J. Park, S. Cohen, G. Chiu
Princeton University
Plasma Physics Laboratory
Princeton, NJ

US/Japan Workshop on
Plasma Surface Interactions and
High Heat Flux Components in
Magnetic Confinement Fusion Reactors
Colorado Springs, Jan 1996

Motivation/history

Present tokamak experiments show high heat loads on plasma facing components during attached plasma operation.

Extrapolations to ITER indicate the heat loads and other related effects will be more severe, if standard (attached) tokamak operational modes occur.

We have continued studies of SOL plasma parameter regimes which have markedly reduced heat loads.

The mode we have studied, a thermally collapsed state nicknamed STEPS - Steep Temperature and Electric Potential Steps - is achieved by operating at increased neutral pressure, plasma density, and divertor depth. It may be related to detached divertor plasmas seen in tokamaks.

Our goals are:

- to understand the basic physics processes that cause the thermal collapse
- to assess which diagnostics are needed to compare detached modes in tokamaks and STEPS in linear machines, and
- to decide whether these modes can be useful to ITER

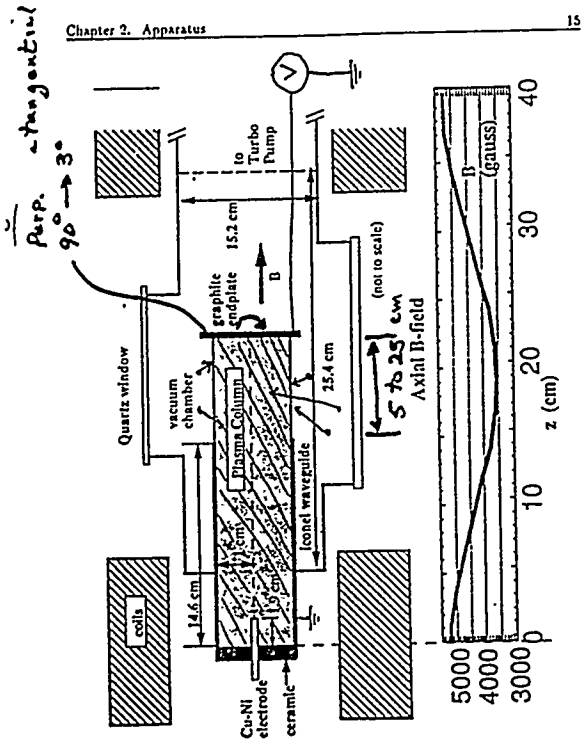

Figure 2.1. Schematic of PDS (Plasma Divertor Simulator): showing the plasma column, end target plate, vacuum chamber, and magnet coils. The nominal magnetic field intensity on axis is also plotted as a function of axial distance.

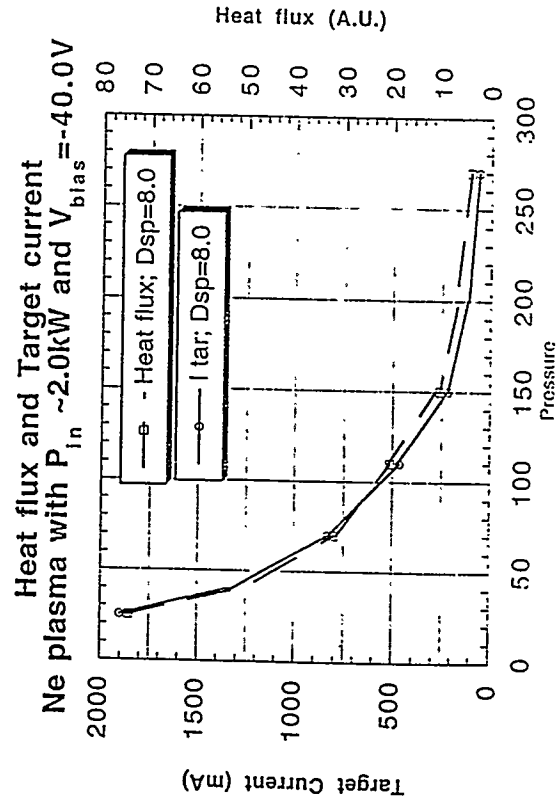

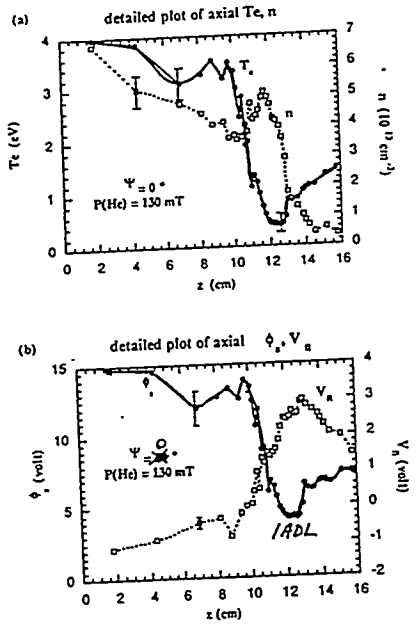

Figure 7.26. A detailed axial (a) density and T_e, and (b) floating and plasma potential profile of the thermally collapsed region at 130 mT

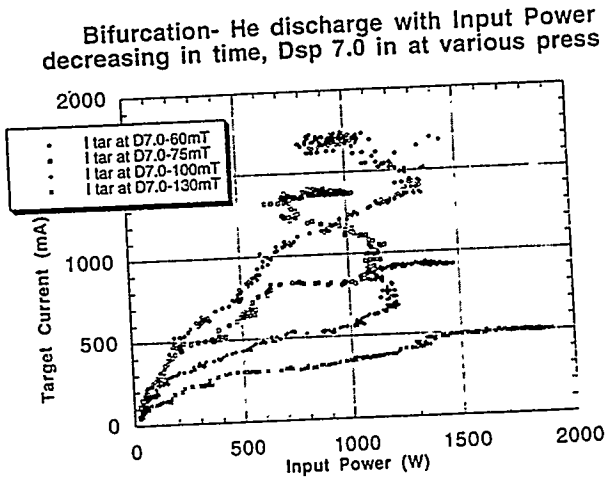

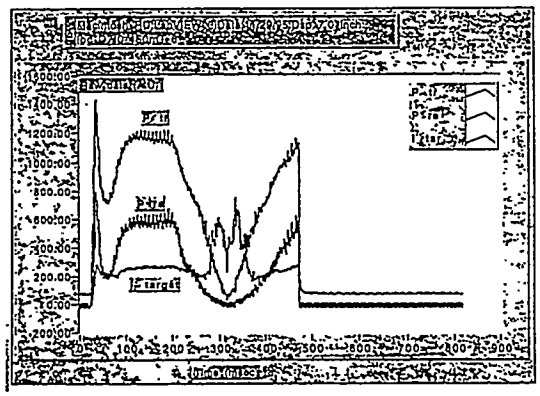

Summary

1. For $P_{\parallel}$ ~ 1 MW/m², high gas pressures and long channels, PL = 1 T·cm, cause He plasmas to undergo thermal collapse to T_e < 1 eV.
2. Neutral gas pressure exceeds plasma pressure
3. Recombination radiation (n = 9,3 -> 2) is observed. Resonance radiation is not.
4. For recombination rates to explain the density decrease, highly stagnated flow must occur. τ_p > 50 ms.
5. The cause of the thermal collapse is not simply radiative energy loss but the establishment of a strong $B_{\parallel}$ plasma potential gradient. The exact roles of electron/ion scattering by neutrals is not understood.
6. The measured space potential has a shape similar to that found in ion acoustic double layers.
7. Present tokamaks, e.g., C-mod, are operating in regimes where these conditions may be found.

Session V

Tritium

Chaired by: *B. Odegard and M. Saidoh*

V.1	O'hira/Okuno **Saidoh**	Study of Tritium Retention in Graphite by Simulating First Wall Circumstance
V.2	**Skinner**	Measurements of Tritium Recycling and Retention on TFTR
V.3	**Davis**	Graphites: Erosion and Retention
V.4	**Bastasz/Causey**	Results From Tritium Plasma Experiment

US-Japan Workshop Q219 on High Flux Components and Plasma Surface Interactions for Next Fusion Devices

Study of Tritium Retention in Graphite by Simulating First Wall Circumstances

JAERI

S. O'hira and K. Okuno

January 10, 1996

Tritium Retention Study at TPL

OBJECTIVES

Analysis of the chemical state of hydrogen isotopes and estimation of total tritium inventory in plasma-exposed PFMs

Apparatus:

- Apparatus for thermal desorption spectra measurement and chemical species analysis from plasma-exposed PFMs
- Tritium inventory measurement apparatus
- Plasma CVD, XPS, AUGER, SIMS (surface control & analysis)

Samples: graphite (isotropic, c/c composite etc.), Be and W

Parameters:

Sample temperature(r.t.-1473 K), flux(-10^{22}atoms/m^2s), fluence

Current Status:

Tritium experiments (D-T plasma exposure) are running.

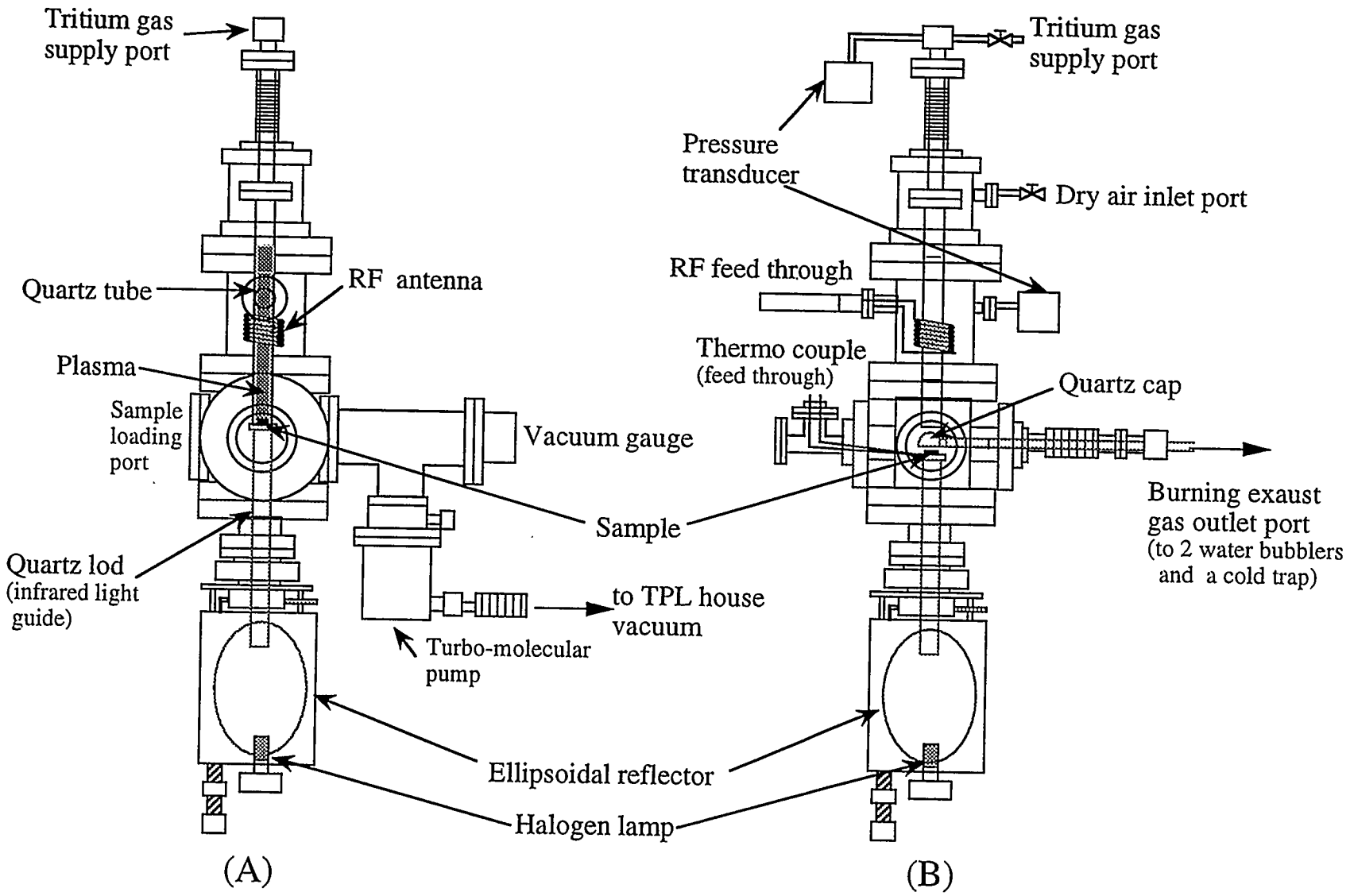

Experimental apparatus (A) Side view, (B) Front view

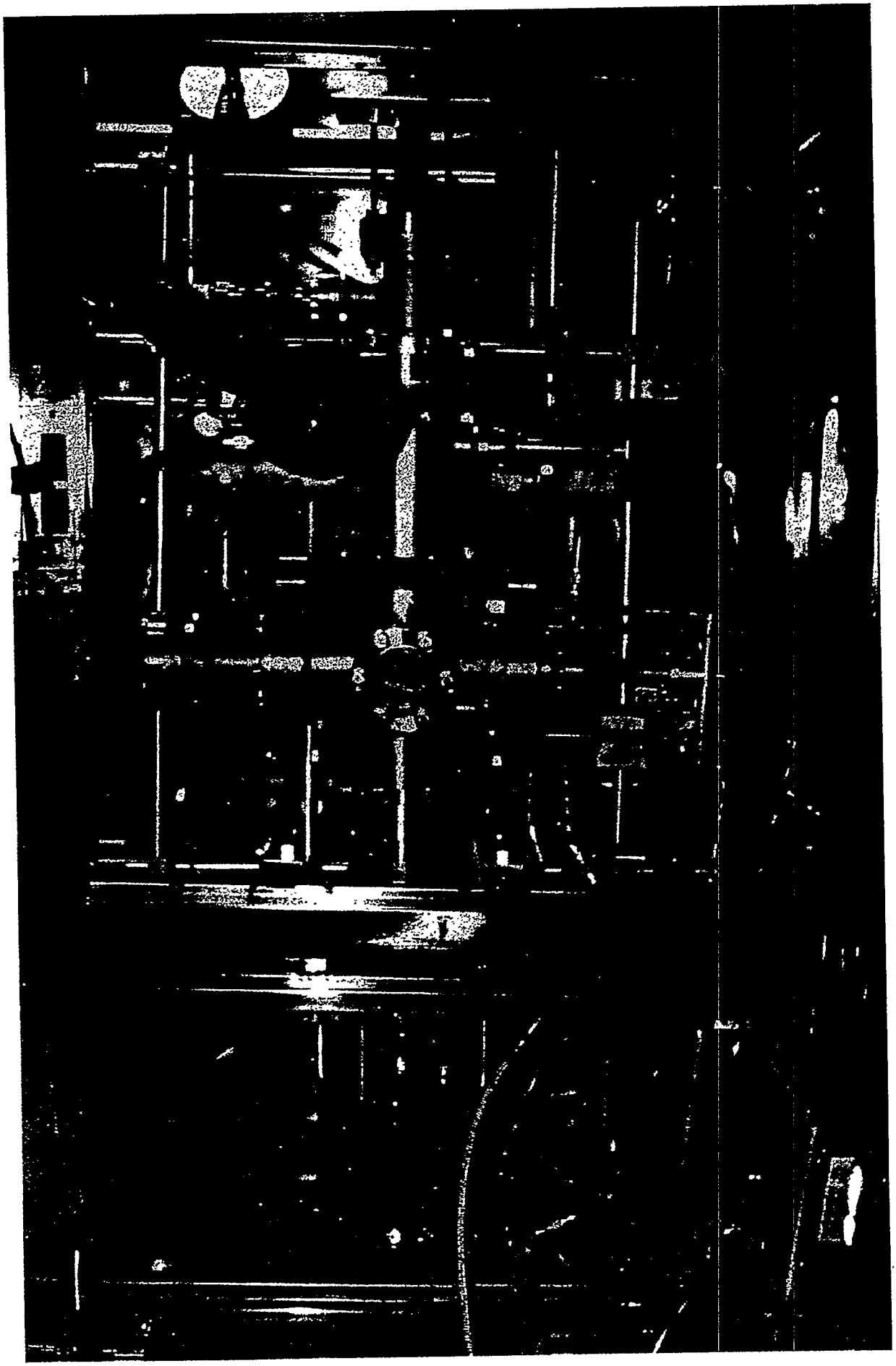

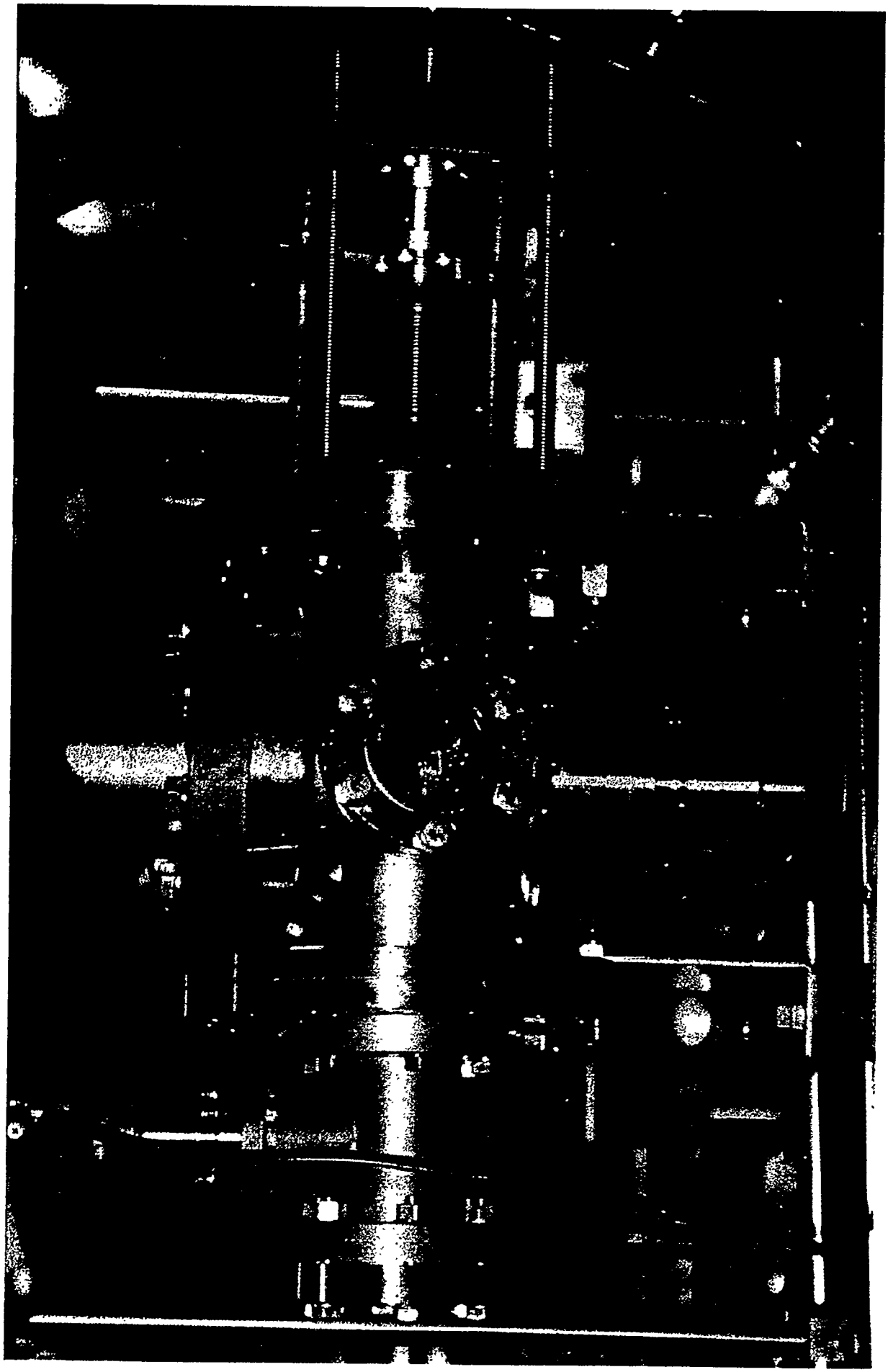

Experimental condition

-Sample-

Isotropic graphite ETP-10 10 mm ϕ 0.3 mm t

degassed at 1000 ℃ for 2 h ($\leqq 10^{-3}$ Pa)

-Plasma exposure-

Supplied gas	D_2-DT mixture D : T =1000 : 1
RF power	50 W
Gas flow rate	1 cc/min (flux 1×10^{22} atoms/m^2/s)
Pressure	6.7 Pa
Exposure time	20～480 min (fluence 1×10^{25}～3×10^{26} atoms/m^2)
Sample temperature	R. T. , 423 K , 500 K

-Combustion-

Temperature	700 ℃ (in dry air flow)
Trap	Two water bubblers + cold trap (−72 ℃)
Tritium measurement	Liquid scintillation counter

Experimental procedure

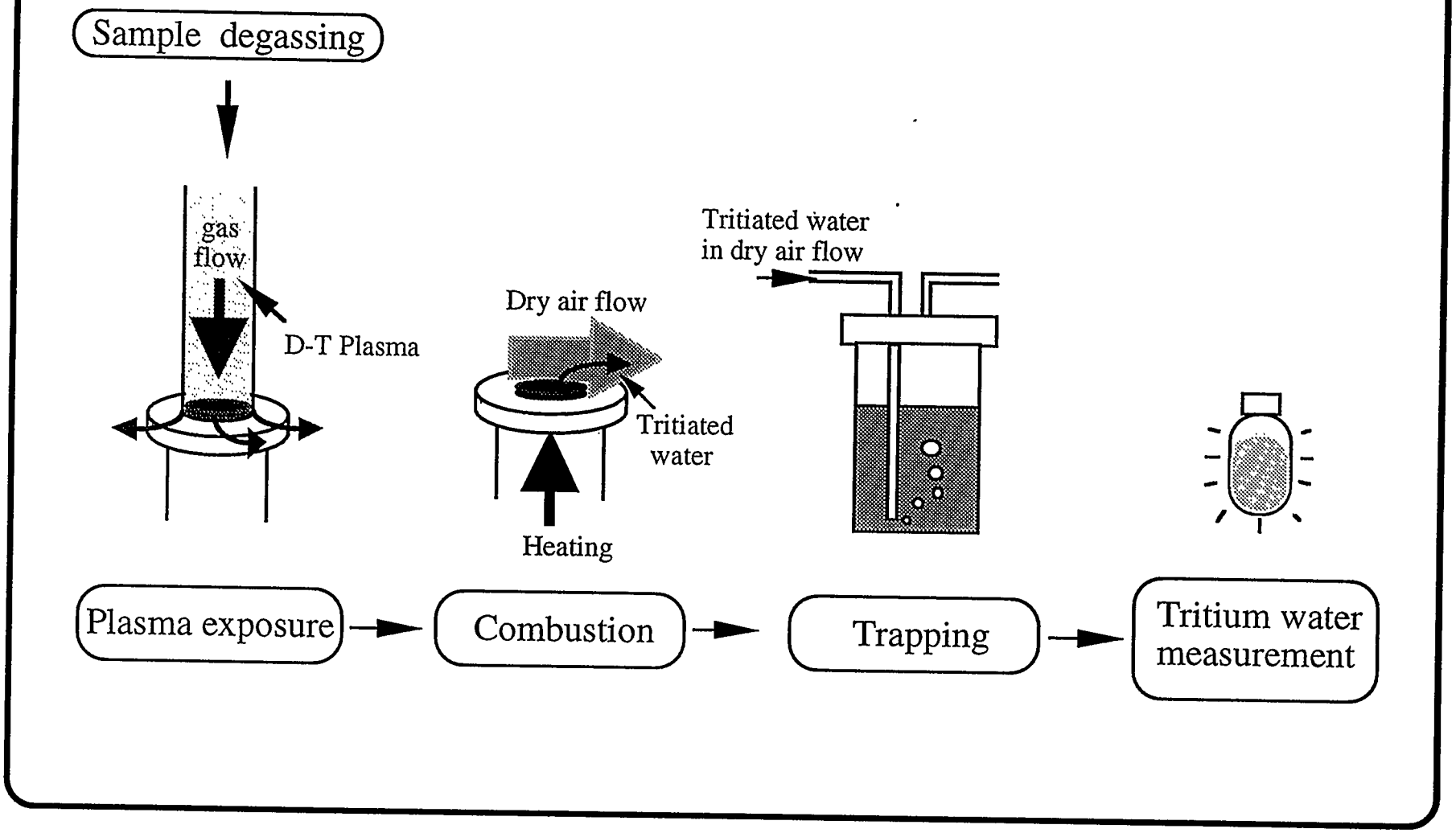

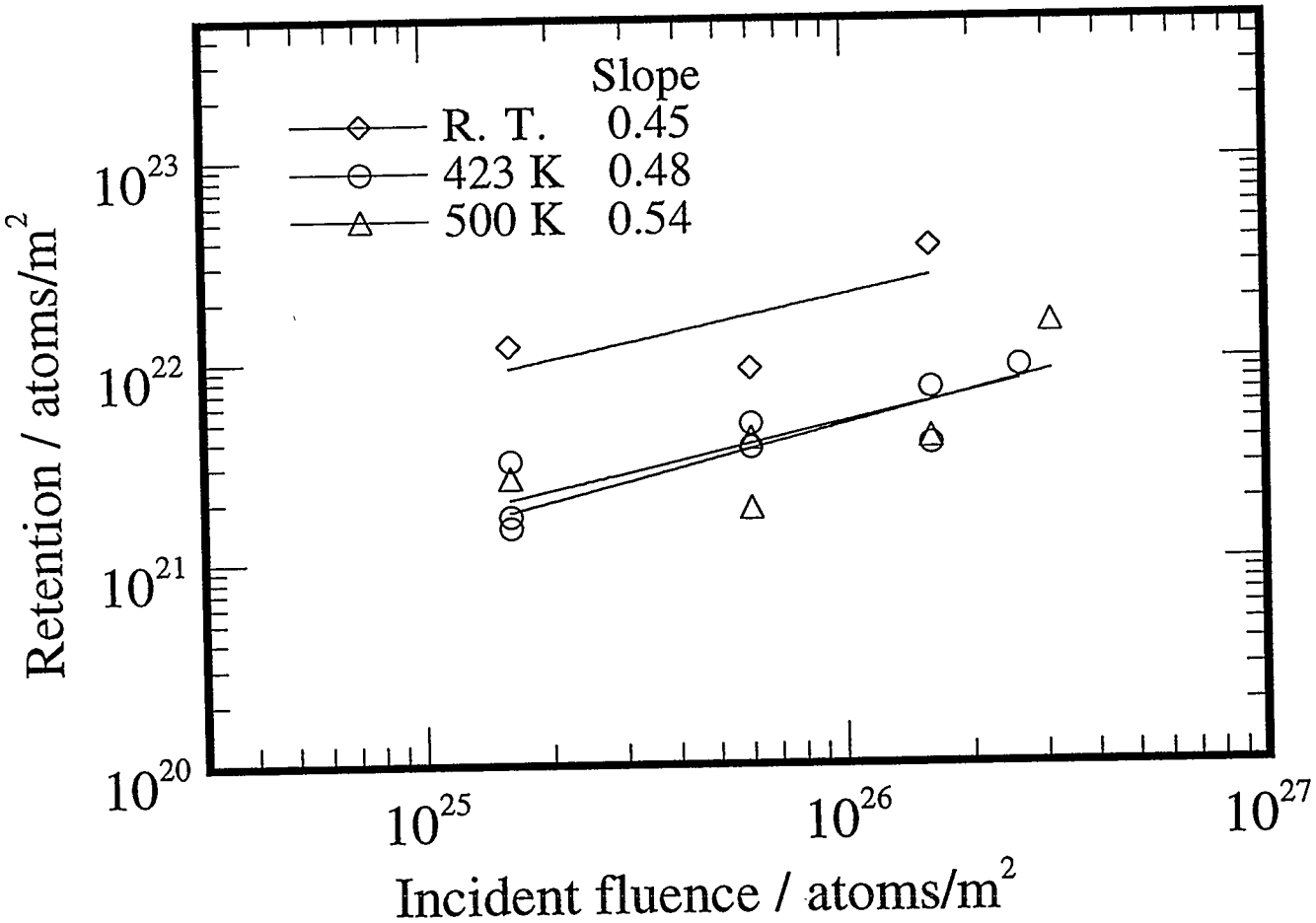

Fig. Hydrogen retention in ETP-10 exposed to D/T plasma

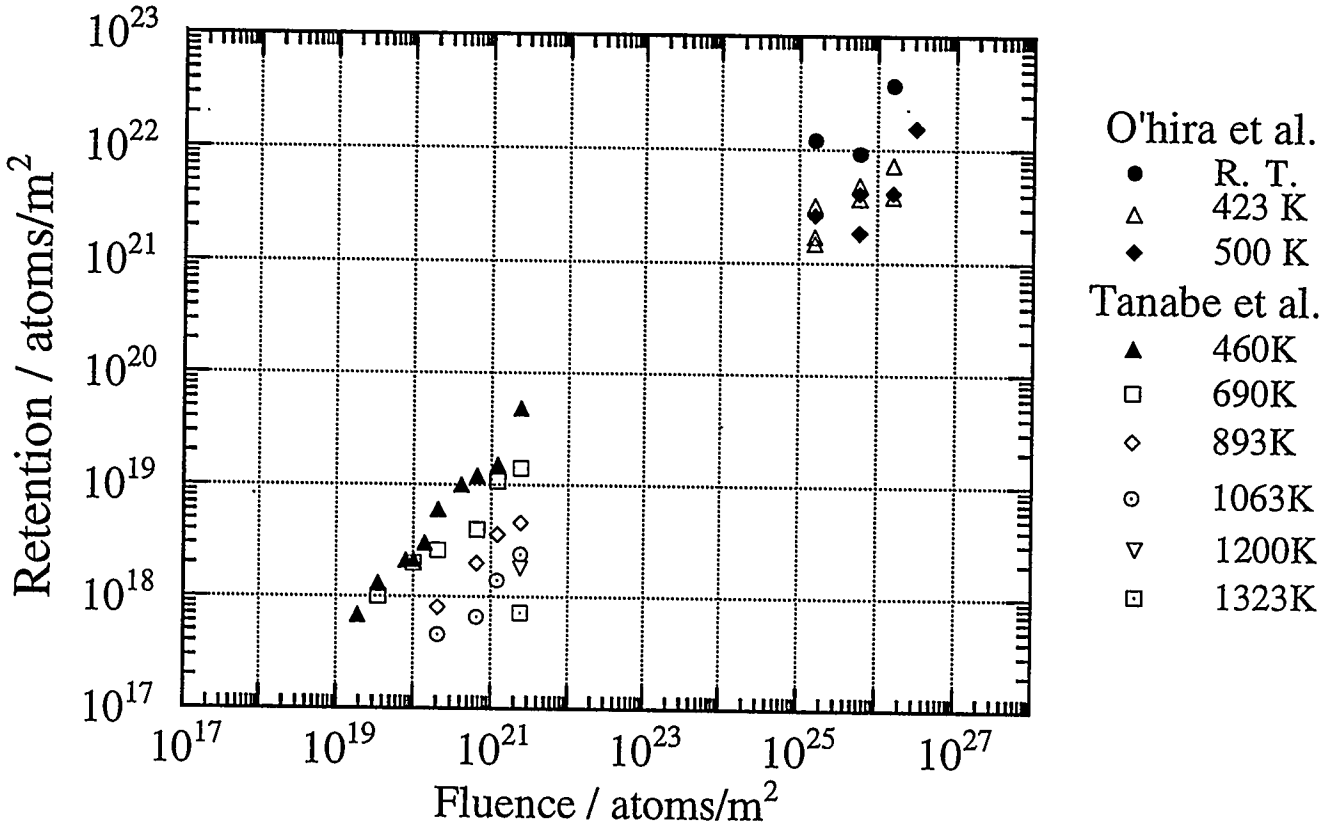

Fig. Hydrogen retention in ETP-10 exposed to atomized hydrogen isotopes

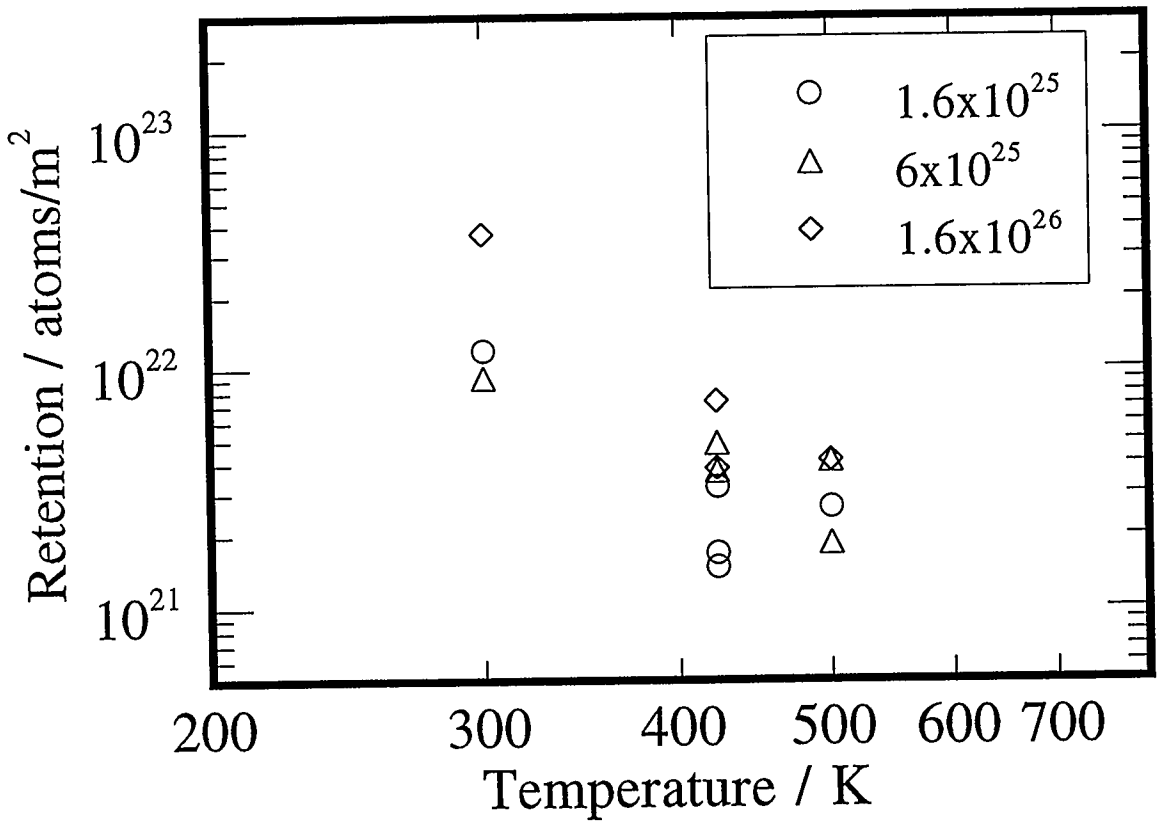

Fig. Temperature dependence of hydrogen retention

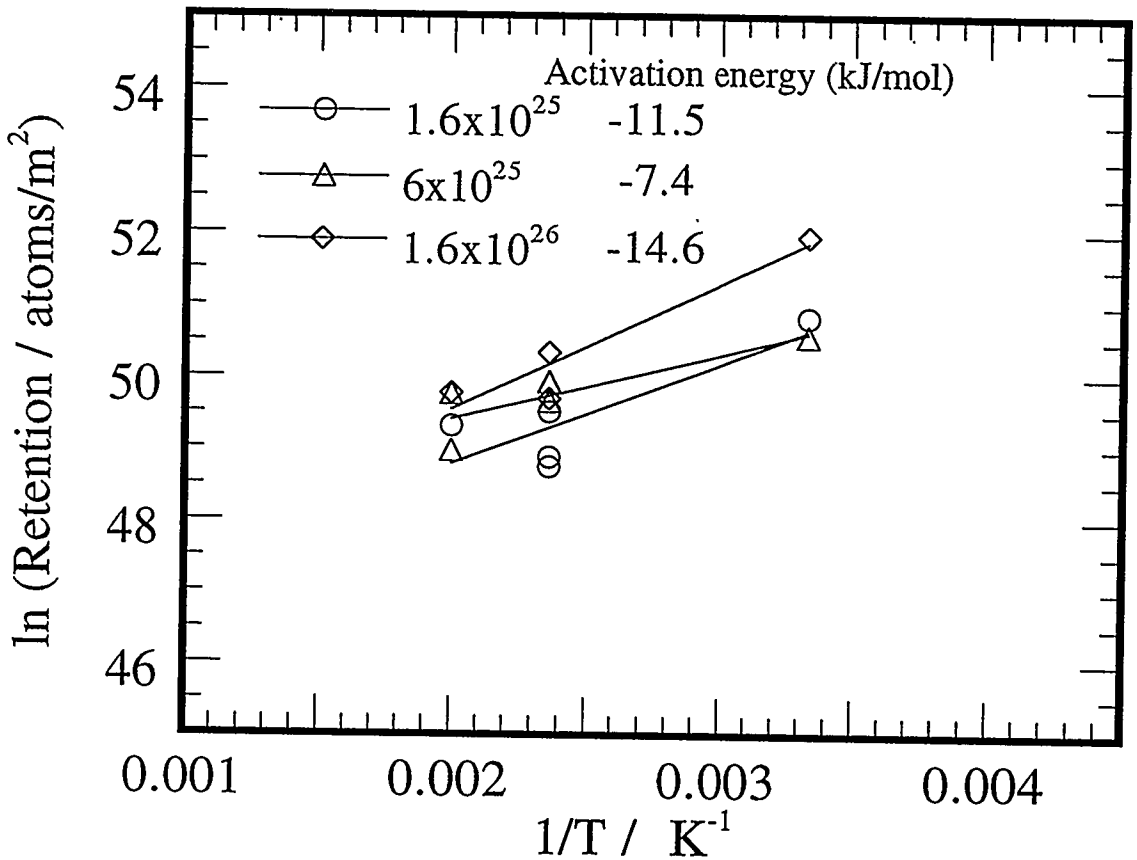

Fig. Arrhenius plot for hydrogen retention

CONCLUSIONS

Isotropic graphite (ETP-10) samples were exposed to the D-T atomized particles, and the total amounts of nydrogen isotopes retained in the samples were measured at a temeraure range of 300 - 500 K and a fluence range of 1.6×10^{25} - 1.6×10^{26} atoms·m^{-2}.

1) The amount of hydrogen isotopes retained in the isotropic graphite sample was in proportion to a half power of total incident fluence and no saturation has been observed up to 1.6×10^{26} atoms·m^{-2} at the temperature range.

2) The activation energies of retention of hydrogen isotopes in the isotropic graphite sample were around 11 kJ/mol (0.11 eV) at the fluence range.

Tritium inventory

First wall ~ 750 m^2

Divertor plates ~ 200 m^2

Total plasma facing surface ~ 1000 m^2

⇒ will be exposed to high fluence of D/T particles ($\geqq 10^{31}$ atoms/m^2) during ITER physical phase operation

Tritium inventory in plasma facing materials *

↓

6.6 kg

* calculated from retention data at 500 K
Duterium :Tritium(retained) = 1 : 1
Retention increase in proprtion to a half power of total fluence
(upto 10^{31} atoms/m^2)

Measurements of Tritium Recycling and Retention on TFTR

C H Skinner and the TFTR group

- Introduction to TFTR.
  Prior results.
- Spectroscopic measurements of hydrogen, deuterium, tritium influx. Isotope changeover during tritium injection.
- Tritium retention measurements.
  Efficacy of tritium removal techniques.
- Summary & conclusions.

Credits:

K.M McGuire, H. Adler, P. Alling, C Ancher, H. Anderson, J L. Anderson,[1] J W Anderson, V Arunasalam, G. Ascione, D. Ashcroft, Cris W Barnes,[1] G Barnes, S. Batha,[2] G Bateman, M. Beer, M G Bell, R. Bell, M. Bitter, W. Blanchard, N L. Bretz, C. Brunkhorst, R. Budny, C.E. Bush,[3] R Camp, M. Caorlin, H Carnevale, S Cauffman, Z Chang,[4] C. S Chang, C.Z. Cheng, J Chrzanowski, J Collins, G Coward M Cropper, D.S Darrow, R Daugert, J. DeLooper, W Dorland,[5] L. Dudek, H Duong,[6] R. Durst,[4] P.C. Efthimion, D Ernst,[7] H. Evenson,[4] N Fisch, R Fisher,[6] R.J Fonck,[4] E. Fredd, E Fredrickson, N Fromm, G.Y Fu, T. Fujita,[8] H P Furth, V Garzotto, C. Gentile, J. Gilbert, J. Gioia, N Gorelenkov,[9] B. Grek, L.R. Grisham, G. Hammett, G R. Hanson,[3] R.J. Hawryluk, W. Heidbrink,[10] H W. Herrmann, K.W. Hill, J. Hosea, H Hsuan, M Hughes,[11] R. Hulse, A. Janos, D.L. Jassby, F.C. Jobes, D.W Johnson, L.C. Johnson, M. Kalish, J Kamperschroer, J. Kesner,[7] H. Kugel, G Labik, N.T Lam,[4] P.H. LaMarche, E. Lawson, B. LeBlanc, J Levine, F.M. Levinton,[2] D. Loesser, D. Long, M.J. Loughlin,[12] J. Machuzak,[7] R. Majeski, D.K. Mansfield, E. S. Marmar,[7] R. Marsala, A. Martin, G. Martin, E. Mazzucato, M. Mauel,[13] M.P. McCarthy, J. McChesney,[6] B. McCormack, D.C. McCune, G. McKee,[4] D.M. Meade, S S. Medley, D.R. Mikkelsen, S.V. Mirnov,[9] D Mueller, M. Murakami,[3] J.A. Murphy, A. Nagy, G.A. Navratil,[13] R. Nazikian, R. Newman, M. Norris, T. O'Connor, M. Oldaker, J. Ongena,[14] M. Osakabe,[15] D.K. Owens, H. Park, W. Park, P. Parks,[6] S.F. Paul, G. Pearson, E. Perry, R. Persing, M. Petrov,[16] C.K. Phillips, M. Phillips,[11] S. Pitcher,[17] R. Pysher, A.L. Quaglis,[3] S. Raftopoulos, S. Ramakrishnan, A. Ramsey, D.A. Rasmussen,[3] M.H. Redi, G. Renda, G Rewoldt, D. Roberts,[4] J. Rogers, R. Rossmassler, A.L. Roquemore, E. Ruskov,[10] S.A. Sabbagh,[13] M. Sasao,[15] G. Schilling, J. Schivell, G.L. Schmidt, R. Scillia, S.D. Scott, I. Semenov,[9] T. Senko, S. Sesnic, R. Sissingh, C.H. Skinner, J. Snipes,[7] J. Stencel, J. Stevens, T. Stevenson, B.C. Stratton, J.D. Strachan, W. Stodiek, J. Swanson,[18] E. Synakowski, H. Takahashi, W. Tang, G. Taylor, J. Terry,[7] M.E. Thompson, W. Tigbe, J.R. Timberlake, K. Tobita,[8] H.H. Towner, M. Tuszewski,[1] A. von Halle, C. Vannoy, M. Viola, S. von Goeler, D. Voorhees, R.T. Walters, R. Wester, R. White, R. Wieland, J.B. Wilgen,[3] M. Williams, J.R. Wilson, J. Winston, K. Wright, K.L. Wong, P. Woskov[7] G.A. Wurden,[1] M. Yamada, S. Yoshikawa, K.M. Young, M.C. Zarnstorff, V. Zaveriev,[19] and S.J. Zweben
D P Stoder, E Amarasca, M Carey, M Gibson, M Kalish, J Langford, S Langish, R Mika, R Raucci, T Walters.

Plasma Physics Laboratory, Princeton University, Princeton, New Jersey 08543 USA
[1]Los Alamos National Laboratory, Los Alamos, New Mexico
[2]Fusion Physics and Technology, Torrance, California
[3]Oak Ridge National Laboratory, Oak Ridge, Tennessee
[4]University of Wisconsin, Madison, Wisconsin
[5]University of Texas, Institute for Fusion Studies, Texas
[6]General Atomics, San Diego, California
[7]Massachusetts Institute of Technology, Cambridge, Massachusetts
[8]JAERI Naka Fusion Research Establishment, Naka, Japan
[9]TRINITI, Moscow, Russia
[10]University of California, Irvine, California
[11]Grumman Corporation, Princeton, New Jersey
[12]JET Joint Undertaking, Abingdon, England
[13]Columbia University, New York, New York
[14]Ecole Royale Militaire, Brussels, Belgium
[15]National Institute of Fusion Studies, Nagoya, Japan
[16]Ioffe Physical-Technical Institute, Russia
[17]Canadian Fusion Fuels Technology Project, Toronto, Canada
[18]EBASCO, Division of Raytheon, New York, NY
[19]RRC Kurchatov Institute, Moscow, Russia

Interior of TFTR showing graphite limiter.

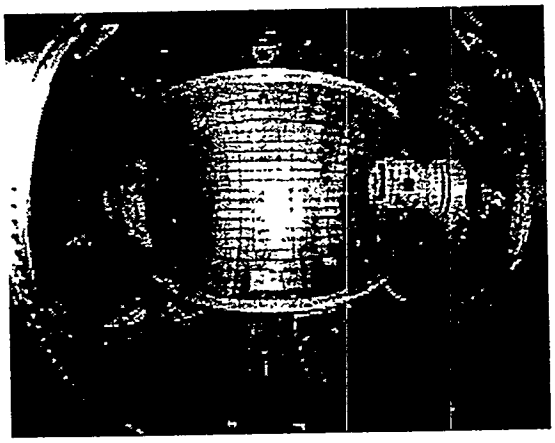

348 *B.E. Mills et al. / Characterization of*

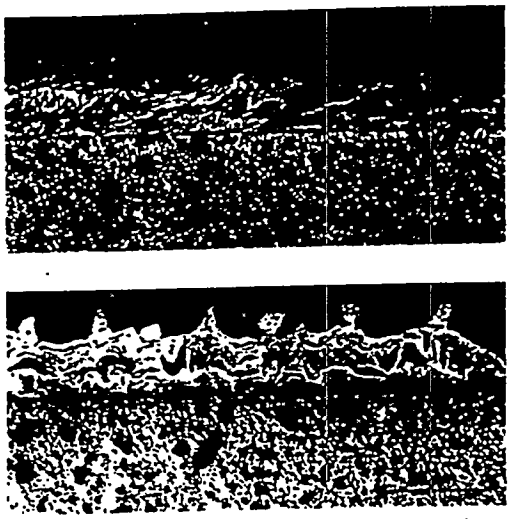

Fig. 5. Poloidal (top) and toroidal (bottom) cross-sections of the plasma-facing surface of a bumper limiter tile in the moderate deposition region, the surface of which is seen in figure 4C.

B E Mills et al. J Nucl. Mater. 343, 162 (1989)

Prior deuterium retention results:

- Nuclear reaction analysis of graphite tiles and wall coupons indicated the overall fractional retention of deuterium in TFTR was around 45%.

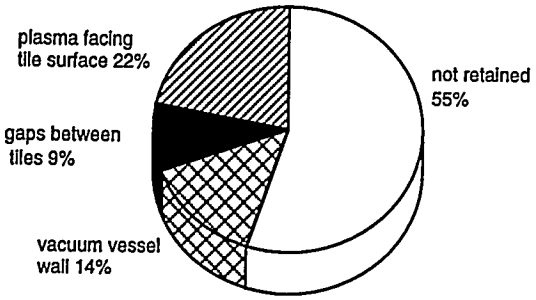

- Comparison of different run periods showed that the retention varied in the range 22% - 63%, correlated with the average neutral beam power. This pattern was attributed to increased edge and limiter temperatures leading to more co-deposition at high beam powers.

- ≈35% of the tritium produced in DD nuclear reactions was retained in the internal components of TFTR.

'Tritium Retention on TFTR',
H F Dylla and K L Wilson Ed.,
Princeton University, Plasma Physics Laboratory
Report PPPL-2523
(April 1988) 108 pp.

'Tritium Retention and Conditioning of Graphite Limiters in TFTR'
M Ulrickson et al. Nucl. Fus. Suppl. 3, 419 (1989)

TFTR has produced Reactor-Level Fusion Power Densities

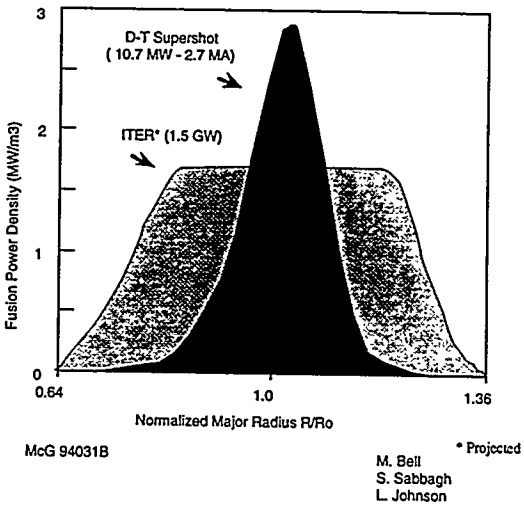

Significant fueling of plasma core by influx from limiter

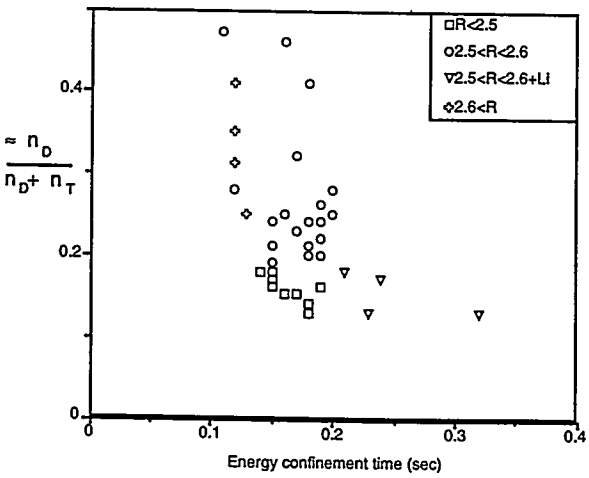

Select shots with tritium only beam fueling -
- DT neutron rate dependent on D influx from limiter.

Compare DT neutron rate with standard scaling for balanced D/T beam fueling.

Derive approximate $\frac{\approx n_D}{n_D + n_T}$

Emission from neutral hydrogen, deuterium observed by Fabry-Perot Interferometer

7.7 MW fusion power supershot

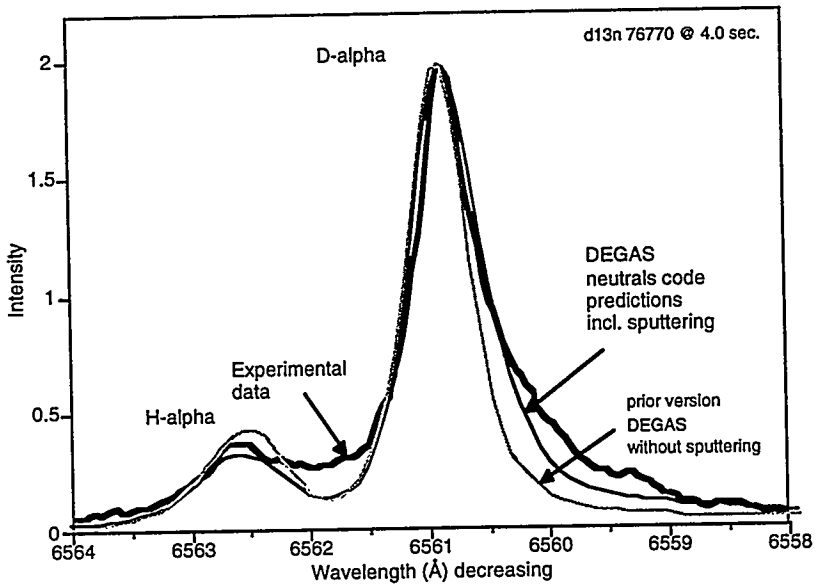

Predicted line profile convoluted with Fabry-Perot Instrument function.

Components of spectral profile predicted by DEGAS

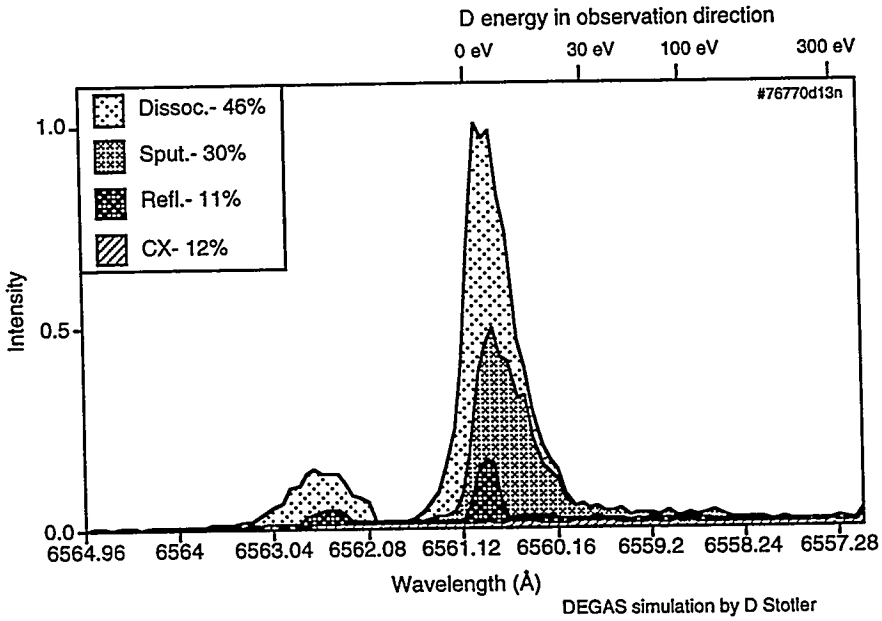

DEGAS simulation by D Stotler
Sputtering data from D Ruzic, B Turkot, U Illinois
H sputtering not included

Weak tritium-α emission on tritium neutral beam injection
7 T sources, no D sources

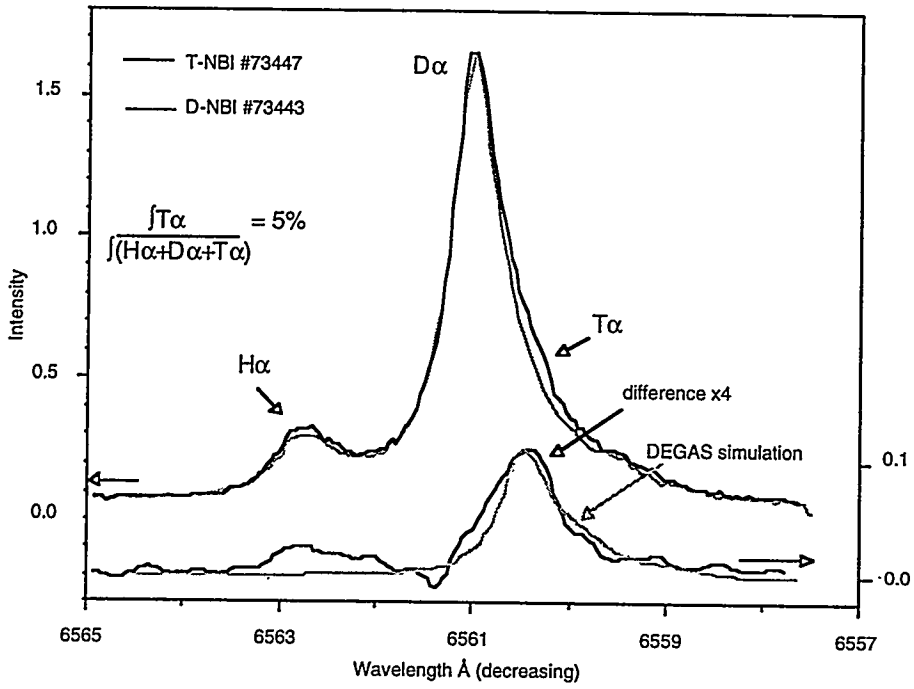

Tritium influx from limiter after tritium NBI

Ta and DT/DD neutron ratio in D-NBI discharges after T-NBI reflects depletion/burial of tritium in limiter.

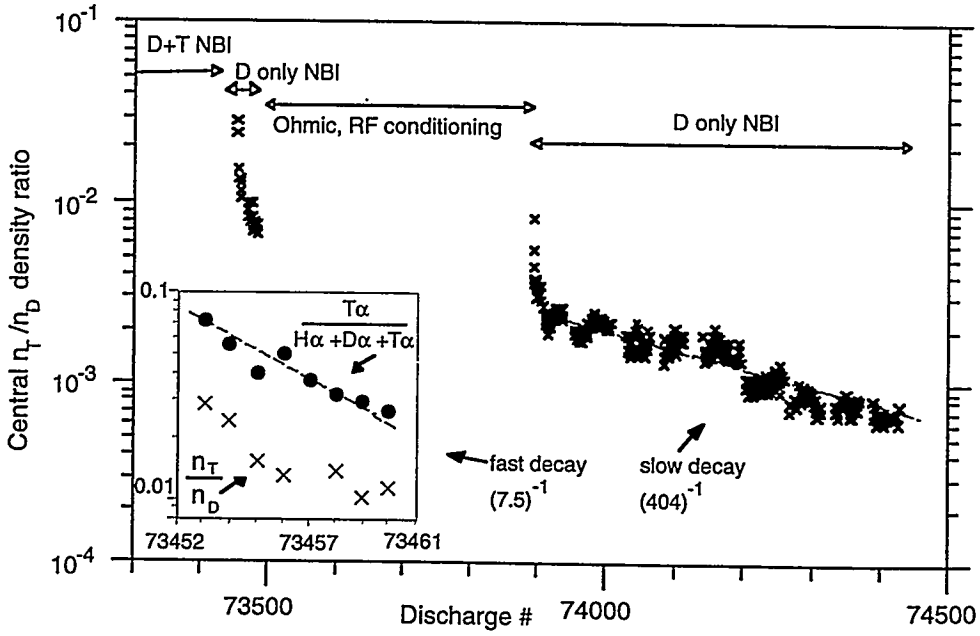

Emission from neutral hydrogen, deuterium, tritium
with tritium gas injection.

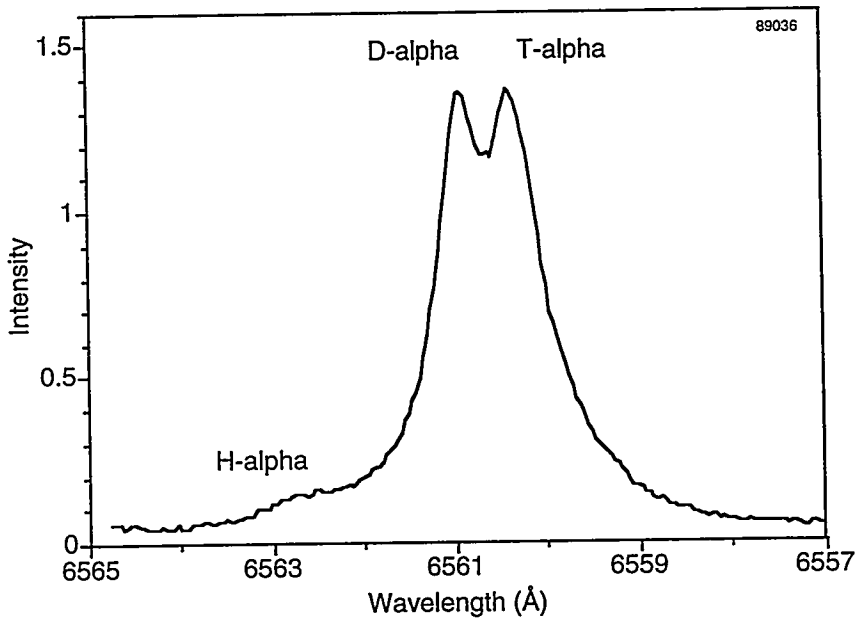

D,T velocities scale with √ mass

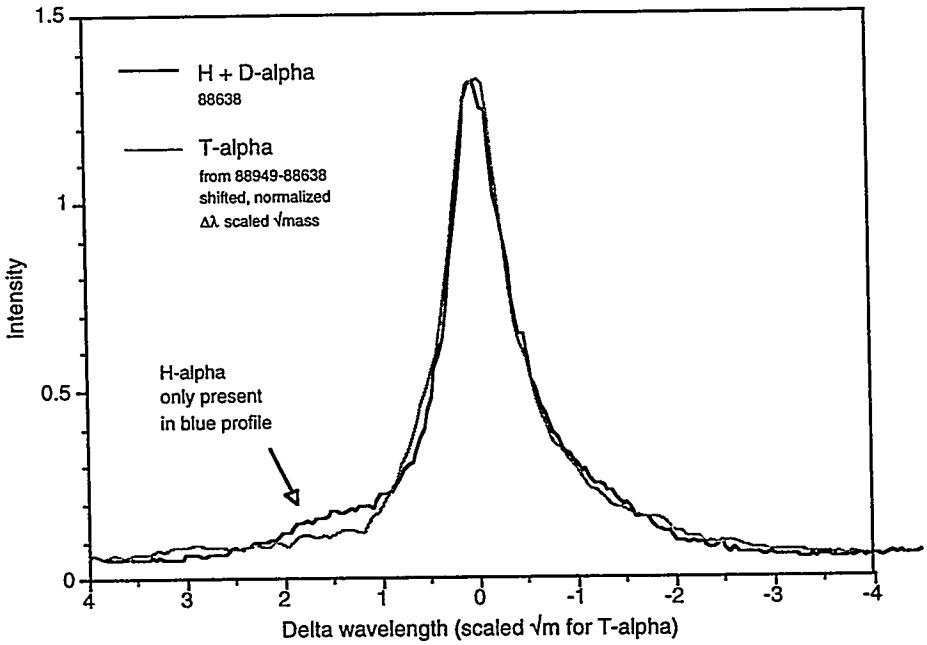

Spectral profile is Doppler broadened, velocities scale close to square root of mass.
Effect of differences in dissociation physics and spatial distributions small.

Tritium injection by gas puff and neutral beams (9/1/95)

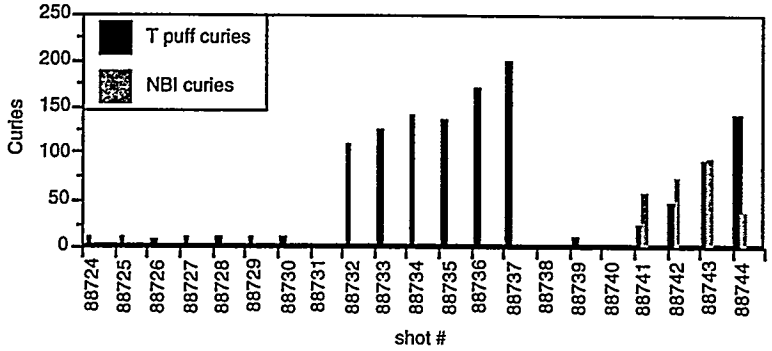

Tritium fraction in hydrogenic influx from limiter

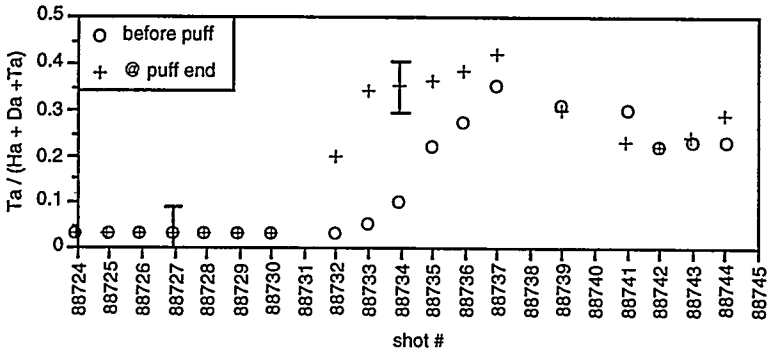

History of tritium injection, removal, Sep.-Nov. 1995

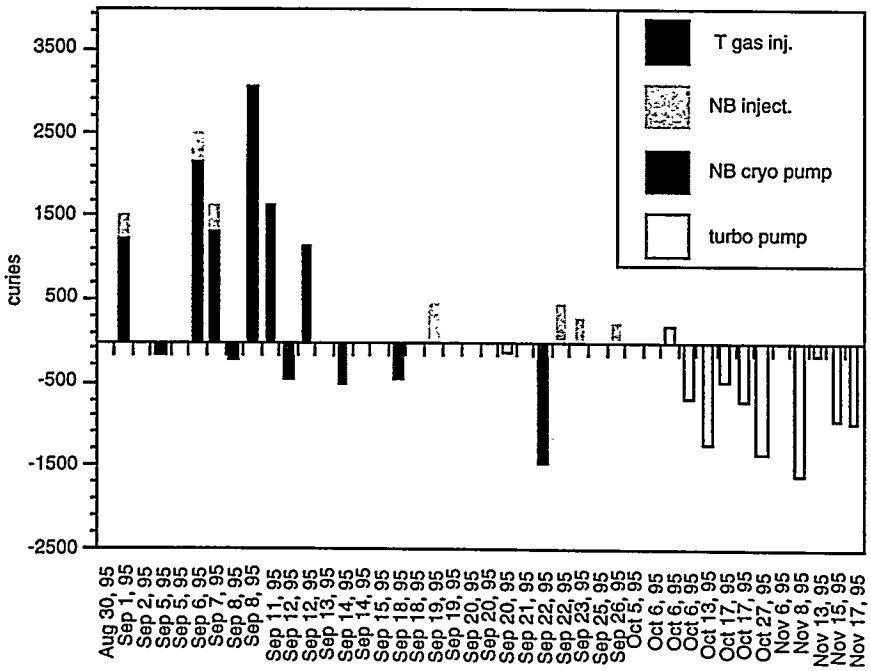

Tritium inventory, exhaust

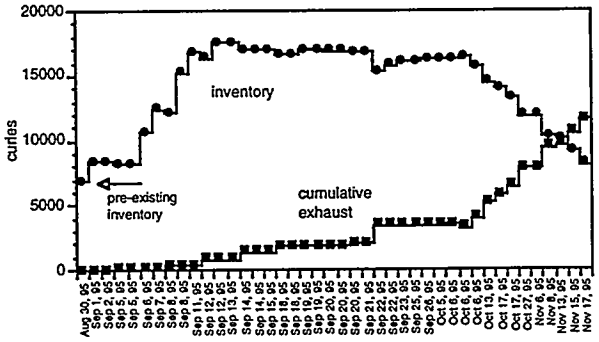

Retention of tritium input since 9/1/95

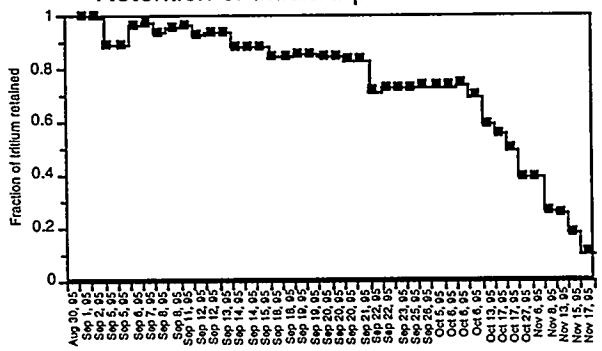

Tritium removal rate

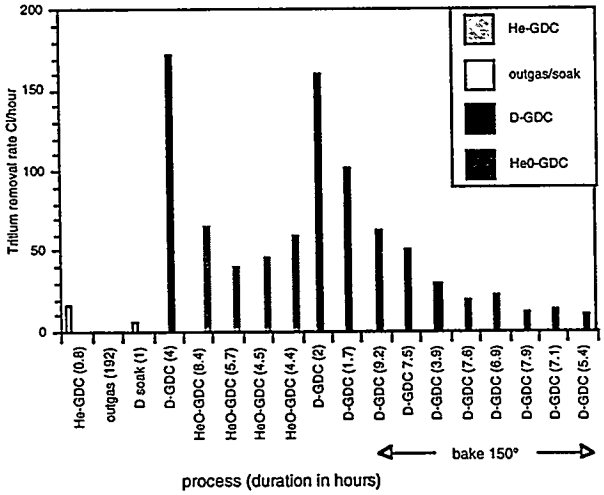

Summary

- TFTR has a special opportunity to study tritium recycling and retention since it has a graphite limiter which experiences erosion, codeposition and neutron flux from DT plasmas with core fusion power similar to that expected for ITER.
- Observations of hydrogen, deuterium, tritium - alpha spectral line shape benchmarks modelling code; .... monitors isotope changeover in limiter.
- *Active removal of tritium necessary to control inventory.* Short term tritium retention in TFTR high (>90%), tritium removal campaign sucessful. After 2 years of DT operation, present inventory less than 1/2 administrative limit.
- Analysis in progress: implications for current models of tritium retention in graphite.

References:

General:

- Review of deuterium-tritium results from the Tokomak Fusion Test Reactor,
  K M McGuire et al.
  Physics of Plasmas 2, 2176 (1995).

T recycling

- First Measurements of Tritium Recycling in TFTR
  C H Skinner, et al. .
  Nucl. Fus. 35, 143-151, (1995).
- Tritium Transport, Recycling, and Gas Fueling Experiments on TFTR
  P C Efthimion et al, .
  Proceedings of the 15th International Atomic Energy Agency Conference on Plasma Physics and Controlled Nuclear Fusion Research 1994 (September 1994, Seville Spain) to be published by IAEA Vienna, 1995.
- Spectroscopic Diagnostics of Tritium Recycling in TFTR
  C H Skinner, D P Stotler, R V Budny, H Adler, and A T Ramsey
  Review of Scientific Instruments, 66, 646-648, (1995).

US-Japan Workshop on High Heat Flux Components and Plasma Surface Interactions for Next Devices, January 9-11, 1996, Colorado Springs.

Graphites: Erosion and Hydrogen Retention

J. W. Davis, A. A. Haasz, B. V. Mech and A. Y. K. Chen

Fusion Research Group
University of Toronto Institute for Aerospace Studies
4925 Dufferin St., North York, Ontario, Canada, M3H 5T6

OUTLINE:

A. DEUTERIUM RETENTION IN DOPED GRAPHITES:

A.1 Introduction:

- Graphite has many properties which make it suitable for use as a plasma-facing material in fusion reactors.
- Its primary disadvantages are its susceptibility to erosion under H and O bombardment and high levels of hydrogen retention.
- It has long been recognized that some improvement of the erosion characteristics may be achieved through the addition of other elements to the graphite: doping.
- However, the doping may improve one characteristic property, while having a negative effect on others.
- We have tried to perform a comprehensive study of some doped graphites by looking at 4 properties of interest for fusion:
  - → Thermal conductivity
  - → Radiation-enhanced sublimation
  - → Chemical erosion
  - → Hydrogen retention and reemission

A. DEUTERIUM RETENTION IN DOPED GRAPHITES:

A.2 Doped Graphite Specimens:

- Doped graphites were produced by Ceramics Kingston Inc. (Ontario, Canada)
  - → high density (~ 2060 kg/m^3 for undoped specimens)
  - → dopants: B (2, 10 and 20 at%)
    - Si (3, 8 and 14 at%)
    - Ti (2, 8 and 16 at%)
    - Ni (10 at%)
    - W (10 at%)
    - Al (10 at%)
  - → Undoped reference specimens also prepared
- Mechanically, most of the specimens are brittle and difficult to work with.
- In the case of the Al-doped material, after several months of air exposure at room temperature, the specimen block completely disintegrated.
- Problems were also encountered with the Ni-doped specimen; Ni melting and evaporation.

A. DEUTERIUM RETENTION IN DOPED GRAPHITES:

A.3 Fluence Dependence of D Retention:

- Previously we have found that D retention in graphite at high fluences depends on the graphite structure.

  → Do dopants influence the transport and trapping of hydrogen beyond the implantation zone?

- 1 keV D^+ is loaded into the specimens through a 2 mm aperture in a mask.
- Specimens are heated on a separate heating stage.
- D retention is evaluated from D_2, HD and CD_4 observed in the residual gas.
- Retention at low fluences (< saturation of the implantation zone) is not greatly affected by the dopants.
- At high fluences, the doped specimens have a higher retention of hydrogen than the undoped specimens.

  → The effect of sample porosity may be significant.

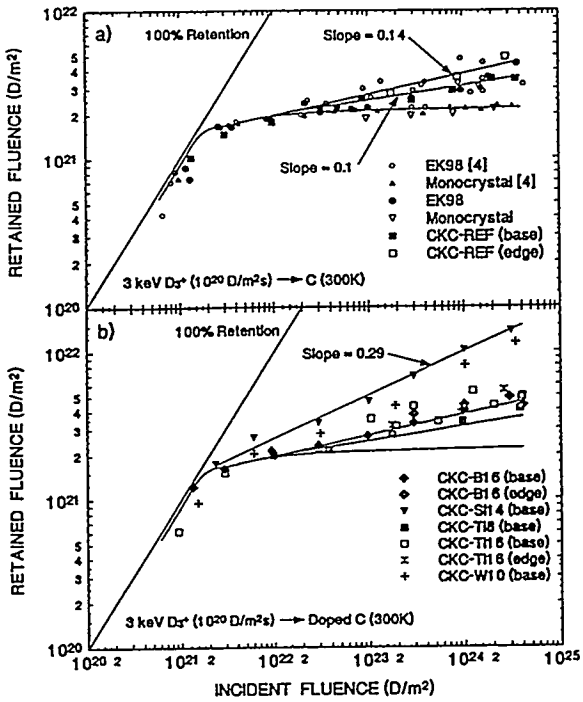

A. DEUTERIUM RETENTION IN DOPED GRAPHITES:

A.4 Thermal Desorption Spectra:

- This information is available as part of the previous study.
- Reference and EK98 are almost identical.
- Ti-doped specimen desorption spectrum has a clear 2-peak structure, ~ 20% of D released in low-temperature branch.
- Release from B- and Si-doped specimens also starts at lower temperature and has a high temperature shoulder.
- This is evidence of a change (reduction) in the D trapping energy in the doped specimens.
- At higher fluences, there is a blending together of the peaks.
- W-doped specimen behaves very similar to undoped graphites, except that the retention is larger.

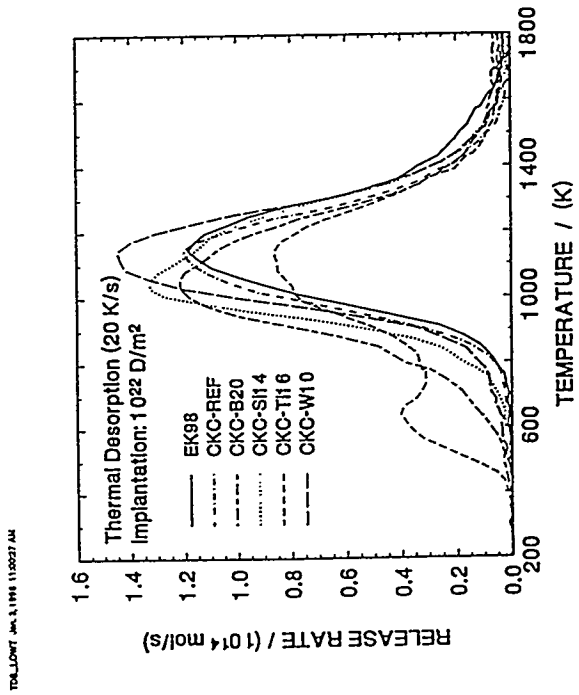

A. DEUTERIUM RETENTION IN DOPED GRAPHITES:

A.5 Temperature Dependence of D Retention:

- For these experiments, the samples could be heated in situ, however, the beam spot was not defined by a mask.
- Undoped graphites behave in a similar manner.
- Ti-doped specimen has a different behaviour, consistent with TDS spectra.
- B-doped specimen may have slightly different shape, but data is not good enough to draw conclusions.
- Direct comparison between samples is not possible as the beam spot is not well defined, and sample warping lead to different spot sizes.
- Other specimens could not be heated by direct current.

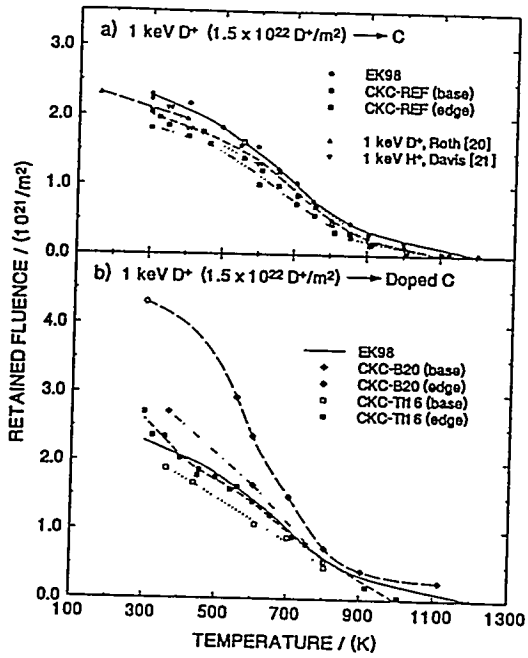

A. DEUTERIUM RETENTION IN DOPED GRAPHITES:

A.6 Atom Reemission for Temperatures > 1000K:

- Reemission experiments were performed using the line-of-sight detection system used for the RES experiments.
- As was found for graphite, the reemission of D atoms during D^+ bombardment was observed for temperatures > 1000 K.

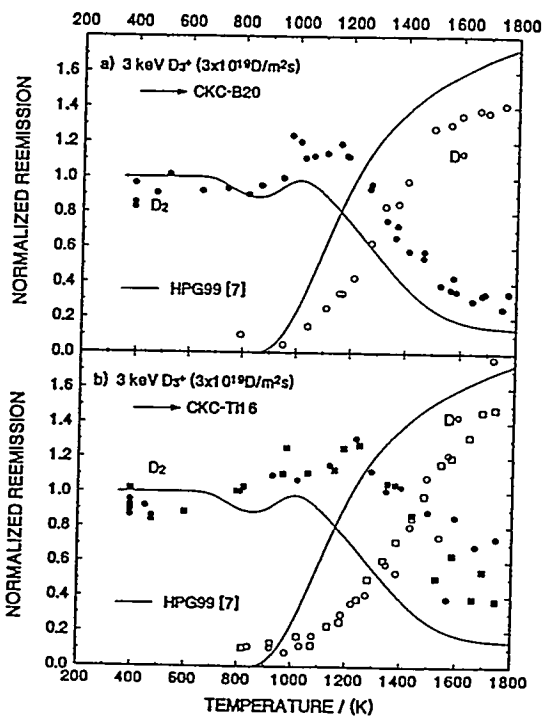

A. DEUTERIUM RETENTION IN DOPED GRAPHITES:

A.7 Summary:

- Generally higher levels of D are retained in the doped specimens, with the difference with undoped graphites increasing at high fluences. This may, however, be due to the specimen porosity/structure.
- For a Ti-doped specimen, different trapping energies have lead to as decrease in the amount of D retained in the 400 - 600K temperature range.
- As with graphite, D is found to recycle as atoms for temperatures > 1200K.

B. LOW ENERGY EROSION WITH H^+ AND D^+:

B.1 Objectives / Experiment:

- The prediction of lower and lower edge temperatures in ITER has stimulated the need for erosion results with lower and lower ion energies.
- Current experiments are under way using a mass selected ion gun modified by the addition of a deceleration stage.
  - → Measurements of beam profiles indicate that the deceleration stage is effectively slowing the beam without altering the beam spatial profile.
- Hydrocarbon products are measured in the residual gas with a QMS.
- Measurements have been carried out measuring CD_4 production for energies from 10 - 200 eV.
- Measurements with H^+ ions are under way in the same energy range; in these experiments we also hope to look for other hydrocarbons.

B. LOW ENERGY EROSION WITH H^+ AND D^+:

B.2 Results:

- In General our results have confirmed previous measurements which have shown a broadening of the temperature profiles at lower ion energies, leading to lower peak erosion yields, but higher yields at low temperatures.
- As the ion energy is decreased from 200 to 10 eV, the maximum erosion yield decreases from 6×10^{-2} to 9×10^{-3} and T_m decreases from ~725K to ~510K.
- The RT CD_4 yields are a factor of 2-3 lower than results by Roth and Bohdansky (1987) at 30, 50, 80, 100 eV.
- Temperature dependent results at 50 and 200 eV for CD_4 are in good agreement with Garcia-Rosales and Roth (1992), although our peak erosion yields are somewhat (30-40%) lower.
- For the lowest energies, we still see a temperature dependence, especially a decrease in yield above 500K.
- There is no evidence for an energy threshold for chemical erosion.
- At 500K, the yield is relatively insensitive to ion energy.
- At 800K, the yield decreases more than one order of magnitude
- At RT, the yield decreases for energies < 50 eV.

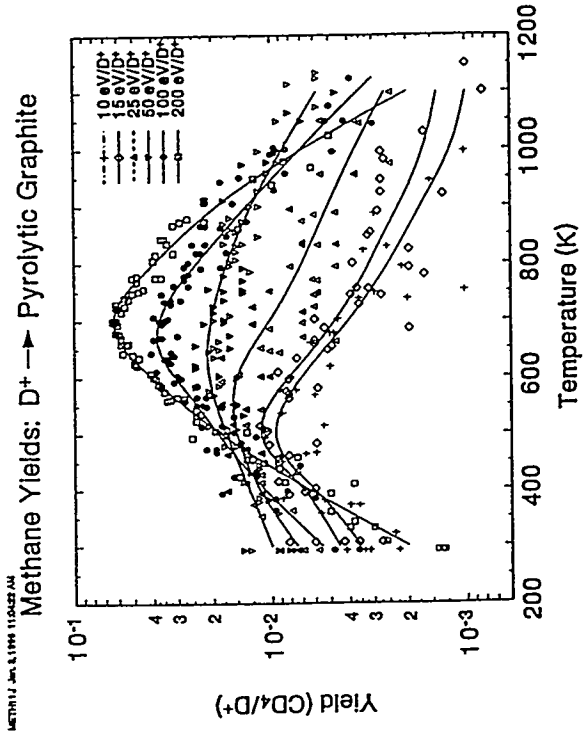

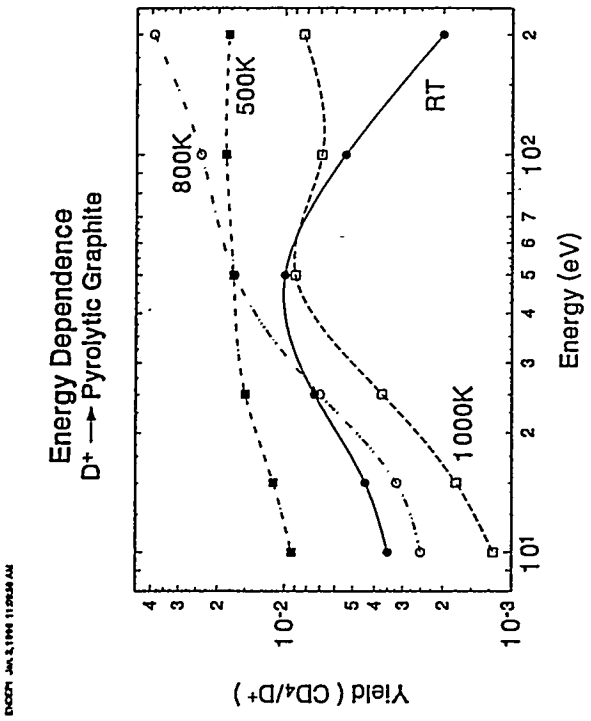

C. $O^+ + H^+$ CHEMICAL EROSION:

C.1 Objectives / Experiment:

- In a fusion reactor with carbon walls, oxygen is known to be one of the major plasma impurities.
- The production of CO by O^+ bombardment of carbon has been demonstrated previously.
  - → It is thought that O reaching the walls will recycle as CO with near 100% efficiency.
- In a reactor, there will also be a much larger flux of hydrogen; does this affect the CO production mechanism, ie., a negative synergistic effect?
- Experiment was performed with dual beam accelerator with beams of 1 keV H^+ and 6 keV O^+.
  - → Energies were chosen to provide the best overlap of implantation ranges, and the largest beam currents.
  - → ϕ_{H^+}/ϕ_{O^+} ~ 5 to 30
- Reaction products measured by line-of-sight quadrupole mass spectrometry and RGA.
- Observed H_2, CH_4, H_2O, CO and CO_2; specimen temperatures 300 to >1000 K.

C. $O^+ + H^+$ CHEMICAL EROSION:

C.2 Results:

- The production of H_2O is observed in the 600 to 1000K temperature range, containing as much as 20% of the incident oxygen.
- Corresponding reductions observed in CH_4 yield (due to the addition of O^+ to H^+) and in CO_2 yield (due to the addition of H^+ to O^+).
- Changes in the H_2 or CO signals difficult to determine.
- To first order, the H^+ and O^+ reaction mechanisms are independent, however, there is evidence of competing chemical reactions leading to the production of water instead of erosion products.

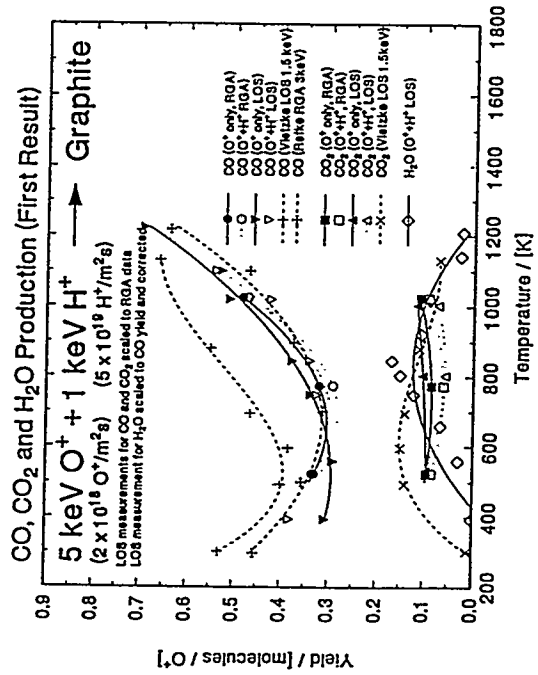

Session VI

Material Damage

Chaired by: *R. Bastasz and A. Sagara*

VI.1	**Yoshida**	Damage of Plasma Facing Materials Due to Low Energy Hydrogen or Helium Ion Irradiation
VI.2	**Watson**	Low Cycle Thermal Fatigue Damage of Beryllium
VI.3	**Bastasz**	Recent Results From the DiMES Experiment
VI.4	**Hassanein**	Recent Results of Comprehensive Plasma Disruption Modeling and Simulation
VI.5	**Rockett**	Utility of X-ray Imaging for Disruption Analysis

US-Japan Workshop Q-219(1996.1.9-11, Colorado Springs)

Damage of Plasma Facing Materials Due to Low Energy Hydrogen Ion Irradiation

N. Yoshida, S. Mizusawa, R. Sakamoto and H. Watanabe
Research Institute for Applied Mechanics, Kyushu University

Contents

Background & Objectives

FUSION REACTOR:

Low Energy but High Flux Hydrogen and Helium ⇒ PFM

⇓

Radiation Damage of Subsurface Region
(material degradation, hydrogen retention and recycling)

OBJECTIVES

- Radiation damage at atomic level by keV-energy hydrogen ions
- Its effects on hydrogen retention of PFM (Be, W, Mo, etc.)

⇓

Characteristics of H irradiation effects of each materials as PFM

Experimental Procedures

Materials

Be(Nippon Gaisi Co.) (wt%)

	Be	BeO	Fe	C	Al	Mg	Si
TEM, TDS	98.9	1.2	0.10	0.14	0.05	0.02	0.04
TDS	99.1	0.9	0.10	0.14	0.04	0.01	0.03

W(99.995%SC, 99.95%PC), Mo(99.995%SC, 99.95%PC)

Hydrogen Ion Irradiation

Ion energy: 0.5~8keV D_2^+ or H^+ (comparable to plasma energy)
Ion Dose: up to 5×10^{22}ions/m^2
Irrad. Temp.: 300~1073K

In situ TEM Observation under Irradiation

Hydrogen Ion Gun-TEM Interface

Thermal Desorption Experiments (D_2 Gas)

Microstructural Evolution under D Ion Irrad. in Be

300K, 8keV D_2^+, 5.0×10^{18}ions/m^{2}s

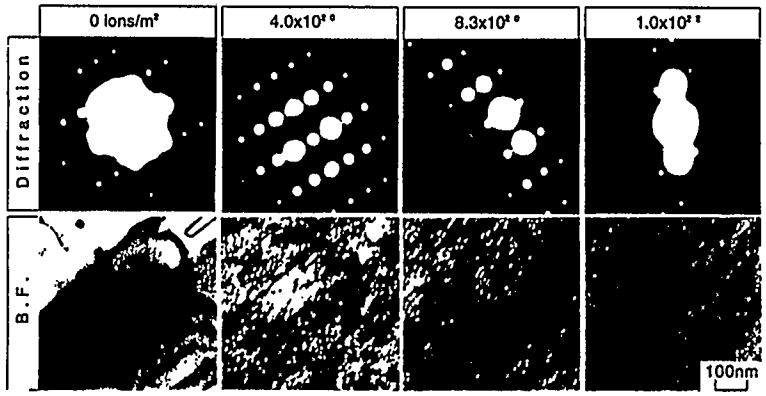

Evolution of Microstructure in Be under D Ion Irradiation

High Dose (≦30dpa)

Irradiation Conditions : 8keV-D_2^+, 5.2×10^{18} ions/m^2s, Room Temperature

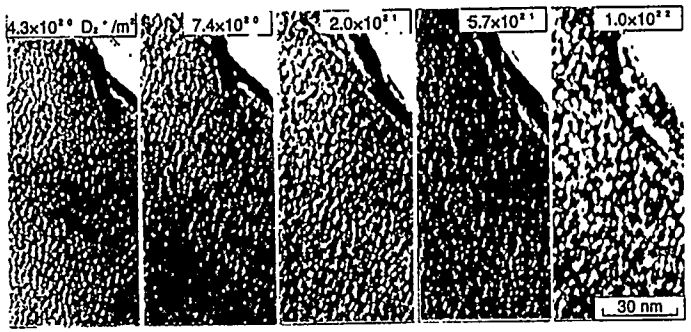

Isochronal Ann. of Be Irradiated by D_2^+

8keV-D_2^+, 1.4×10^{20}ions/m^2, R.Temp. 100K-Step, 30min

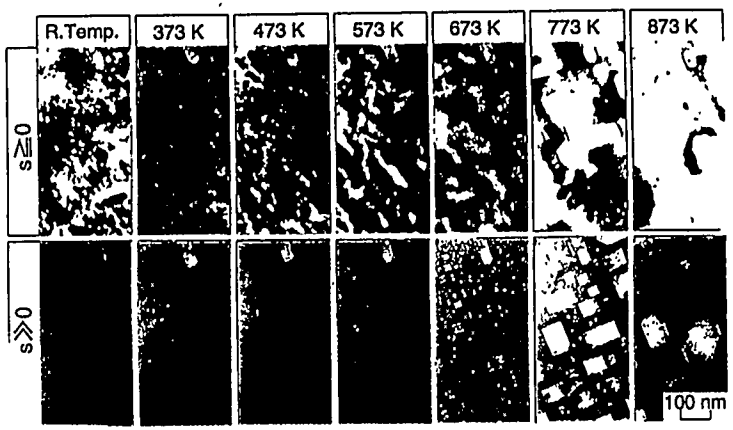

Isochronal Annealing of Cavities in Be Formed by D Ion Irr.

8keV-D_2^+, 1.0×10^{22} ions/m^2, Room Temperature, 100K-step, 300min.

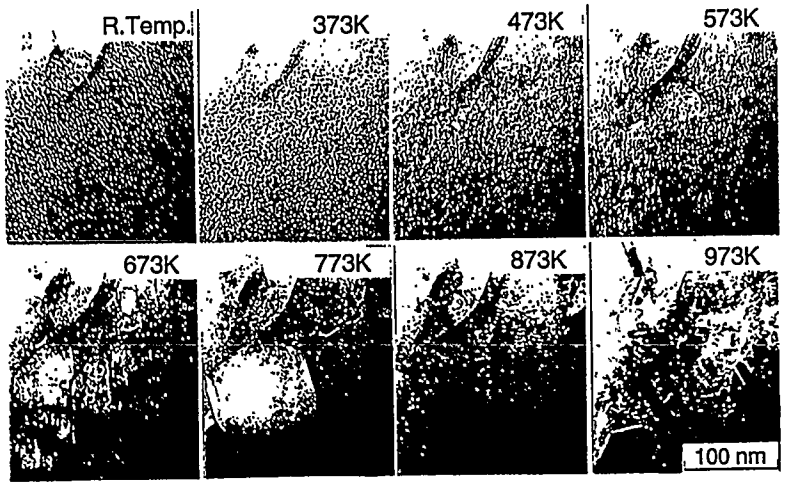

Desorption of D Gas from Be and W

8keV D_2^+, 1.0×10^{18} ions/m^2s, R.Temp., 1K/s

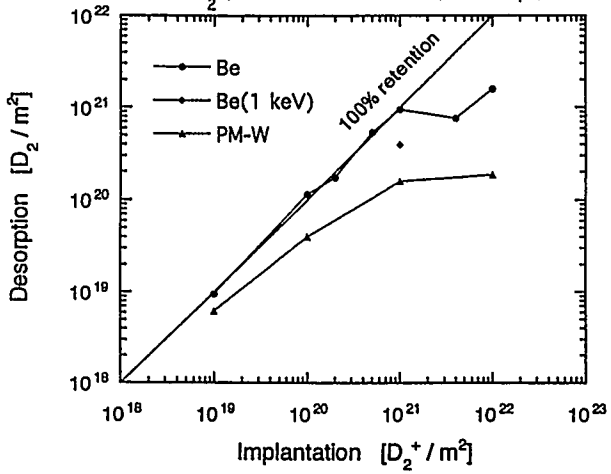

Dose Dependence of TDS of D Gas from Be

Irradiation Conditions : 8keV-D_2^+, 1.0×10^{18} Ions/m^2s, Room Temperature

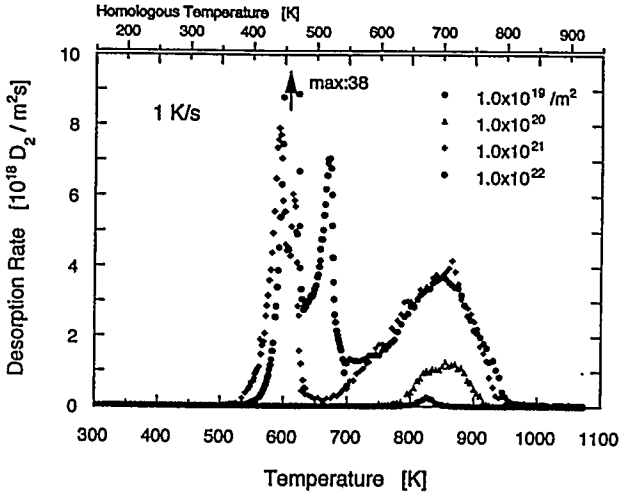

Ramping Rate Dependence of TDS of D Gas from Be

Irradiation Conditions : 8keV-D_2^+, 1.0×10^{21} Ions/m^2, Room Temperature

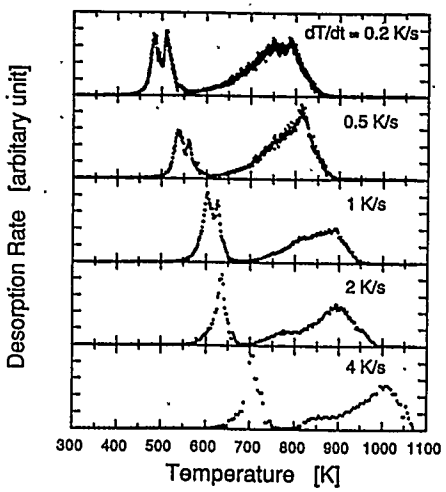

Detrapping Energy of Implanted Deuterium

Be, 8keV D_2^+, $1.0\times10^{21}D_2^+/m^2$, R. Temp

$$\ln\left(\frac{T_P^2}{a}\right) = \frac{E_D}{kT_P} + \ln\left(\frac{E_D}{\nu k}\right)$$

E_D : dissociation energy
T_P : peak temperature
a : ramping rate
ν : frequency factor
k : Boltzman factor

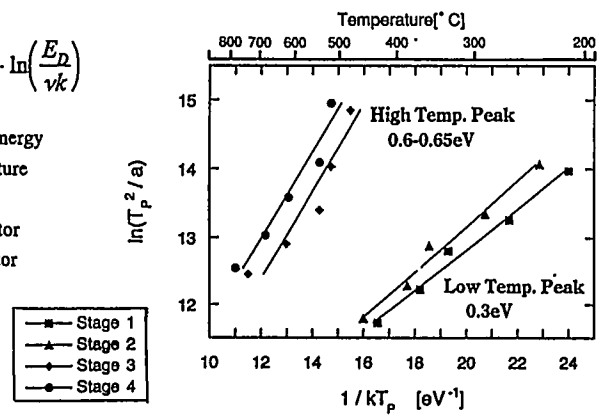

Microstructural Evolution under D Ion Irrad. in Be

573K, 8keV D_2^+, 5.0×10^{18}ions/m^2s

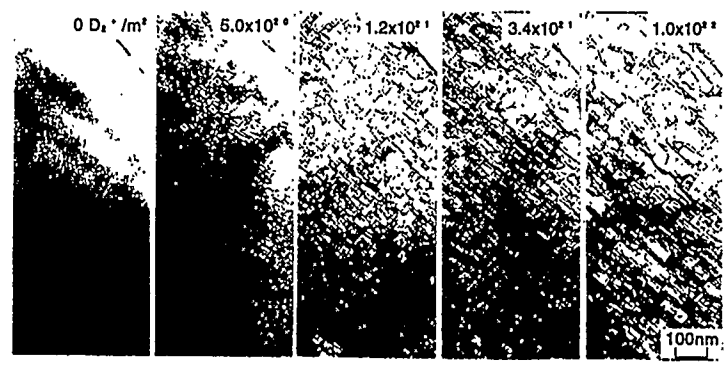

Microstructural Evolution under D Ion Irrad. in Be

773K, 8keV D_2^+, 5.0×10^{18} ions/m^{2}s

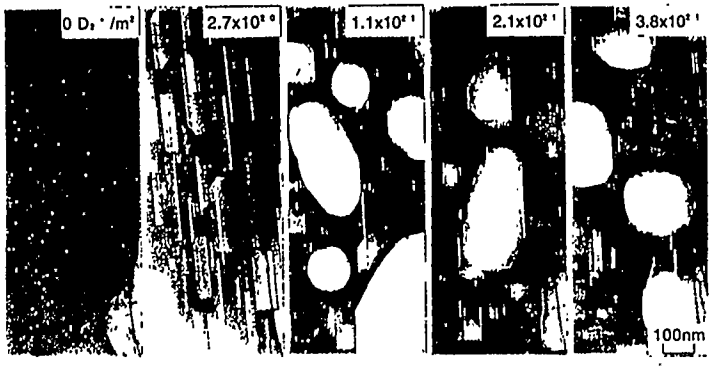

Irradiation Temp. Dependence of D Gas Desorption

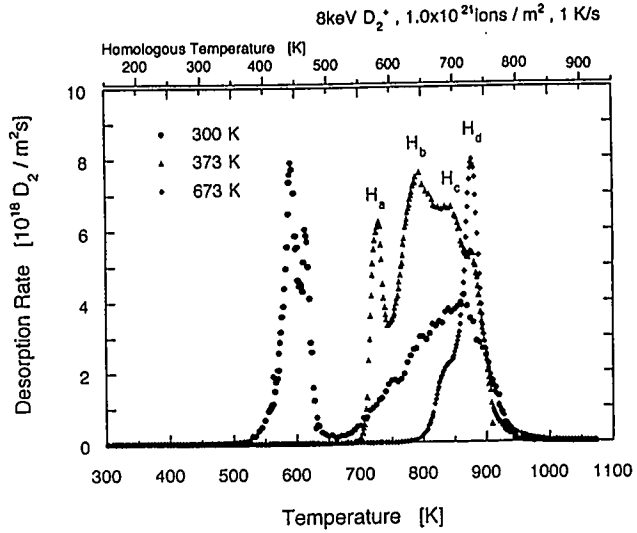

Damage Evolution in Mo at 773K under H^+ Irrad.

8keV H^+, 2.6×10^{18} H^+/m^{2}s

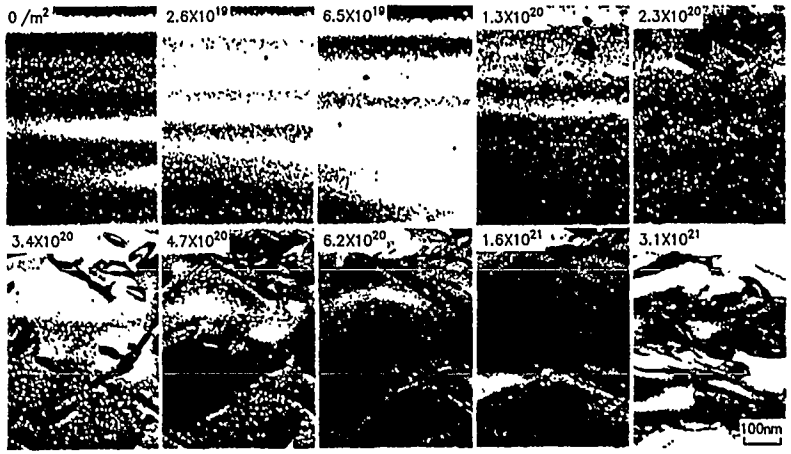

Damage Evolution in W at 573K under H^+ Irrad.

8keV H^+, 4.6×10^{18} H^+/m^{2}s

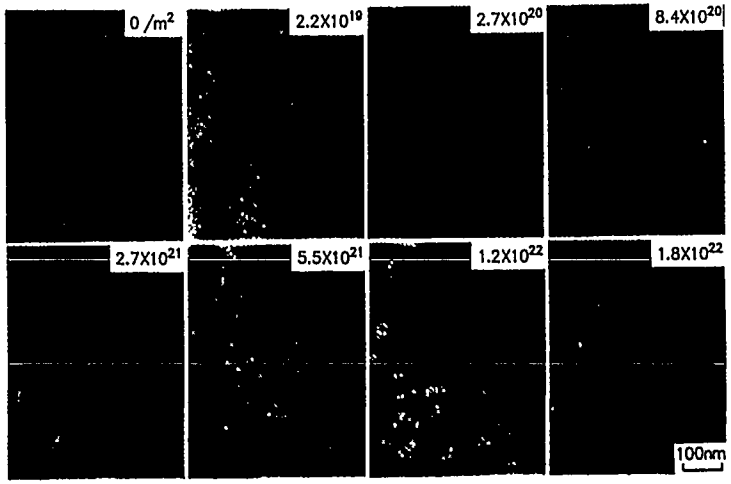

Desroption of D_2 from Various Materials Irr. by D Ions

Irr. Cond.; 300K, 8keV D_2^+, $1x10^{21}$ions/m^2, Ann. Cond. ; 1K/s

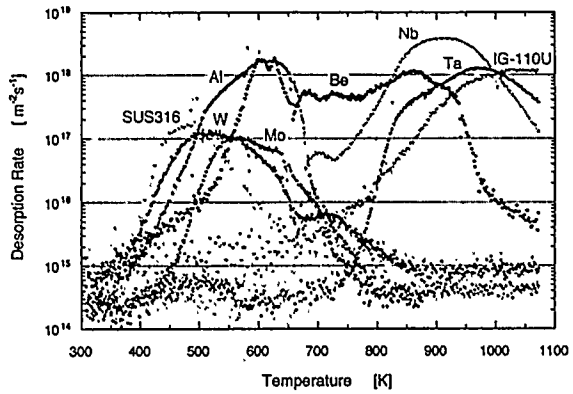

Irradiation Temperature Dependence of D_2 Desorption from D Ion Irradiated PM-Mo

Irr. Cond. ; 300K, 8keV D_2^+, $1x10^{21}$ions/m^2, Ann. Cond. ; 1K/s

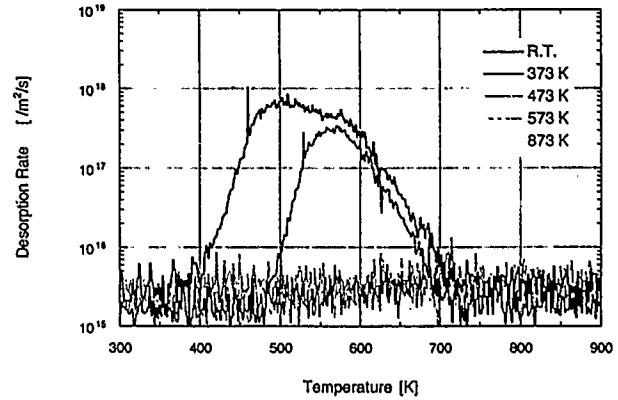

Identification of Desorption Stage (Mo & W)

Stage A & B
- --Low ion energy dependence
- --Purity dependence
  - ➡ *detrapping from impurity atoms*

Activation Energy of D_2 Detrapping(eV)

	stage A	stage B
Mo	0.39	0.43
W	0.48	0.61

Stage C
- --Enhanced by cold work
  - ➡ *detrapping from dislocations and dislocation loops*

(detrapping from vacancies occurs below stage A)

Characteristics of Radiation Damage by H Ions

Be

Microstructure: no dislocation loops, local distortion
bubbles, cavities ----large and high density

H trapping: vacancies, bubbles, ? ----very strong, above 900K

Mo

Microstructure: I-loops, tangled dislocations----high density
cavities----small and low density

H trapping: impurities (majority), dislocations
(no trapping above 473K)

W

Microstructure: I-loops----low density above 473K
cavities----small and very low density

H trapping: impurities (majority), dislocations
(no trapping above 473K)

From the stand point of hydrogen retention and radiation damage, W shows good performance, while Be has many problems.

16Th IEEE/NPSS Symposiom on Fusion Engineering
Champaign, Illinois Sept. 30-Oct. 5, 1995.

Thermal Fatigue Behavior of US and Russian Grades of Beryllium

R.D. Watson[a], D.L. Youchison[a], D.E. Dombrowski[b], R.N. Guiniatouline[c], I.B. Kupriynov[d]
[a]Sandia National Laboratories, MS-1129, P.O. Box 5800, Albuquerque, NM 87185
[b]Brush Wellman, Inc., 17876 St. Clair Ave, Cleveland, OH 44110
[c]Efremov Institute, P.O. Box 42, St. Petersburg, Russia 189631
[d]Russian Institute of Inorganic Materials, 5 Rogov St., Moscow, 123060, Russia, Box 369

ABSTRACT

A novel technique has been used to test the relative low cycle thermal fatigue resistance of different grades of US and Russian beryllium, which is proposed as plasma facing armor for fusion reactor first wall, limiter, and divertor components. The 30 kW electron beam test system at Sandia National Laboratories was used to sweep the beam spot along one direction at 1 Hz. This produces a localized temperature "spike" of 750 °C for each pass of the beam. Large thermal stresses in excess of the yield strength are generated due to very high spot heat flux, 250 MW/m^2. Cyclic plastic strains on the order of 0.6% produced visible cracking on the heated surface in less than 3000 cycles. An *in-vacuo* fiber optic borescope was used to visually inspect the beryllium surfaces for crack initiation. Grades of US beryllium tested included: S-65C, S-65H, S-200F, S-200F-H, SR-200, I-400, extruded high purity, HIP'd spherical powder, porous beryllium (94% and 98% dense), Be/30% BeO, Be/60% BeO, and $TiBe_{12}$. Russian grades included: TGP-56, TShGT, DShG-200, and TShG-56. Both the number of cycles to crack initiation, and the depth of crack propagation, were measured. The most fatigue resistant grades were S-65C, DShG-200, TShGT, and TShG-56. Rolled sheet Be (SR-200) showed excellent crack propagation resistance in the plane of rolling, despite early formation of delamination cracks. Only one sample showed no evidence of surface melting, Extruded (T). Metallographic and chemical analyses are provided. Good agreement was found between the measured depth of cracks and a 2-D elastic-plastic finite element stress analysis.

INTRODUCTION

Beryllium is proposed as a protective armor material on plasma facing components (PFC's) for the next generation of tokamak experiments, including the International Thermonuclear Experimental Reactor (ITER). Long-pulse operation will require active cooling to maintain steady-state surface temperatures of the 5-10 mm thick armor tiles in the range of 600-800 °C. Beryllium tiles are bonded to a water cooled copper alloy heat sink to provide active cooling. Cracking of the beryllium armor should be avoided if it leads to: (1) loss of material, (2) a reduction in thermal conductivity if cracks run across the direction of heat flow, or (3) a water leak if the cracks propagate through the tile and into the copper heat sink.

In this paper, we will describe how the e-beam test facility at Sandia National Laboratories (SNL) was used to screen the relative resistance to low cycle fatigue damage on 14 US and Russian grades of beryllium and 3 other beryllium materials. This work was performed in support of the ITER technology R&D task, T-221, "Beryllium and Other Armor Materials". This new screening technique reduces the high costs associated with traditional methods of fatigue testing of beryllium at elevated temperature, especially combined thermo-mechanical fatigue testing. A more detailed version of this paper was recently published [1].

FINITE ELEMENT ANALYSIS

The test geometry is shown in Fig. 1. Fourteen tiles were stacked side-by-side so that all samples were subjected to the same heat flux history.

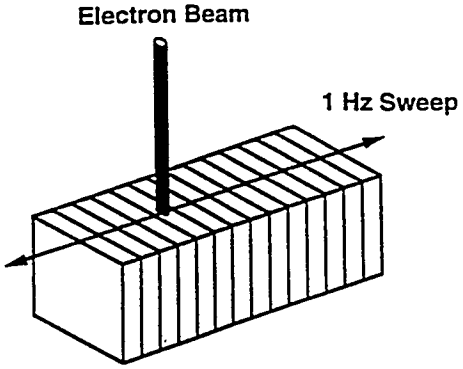

Fig. 1 Test setup showing 2 mm diameter electron beam spot swept at constant velocity across 14 tiles at 1 Hz.

A 2-D finite element mesh of the beryllium tile was generated with PATRAN, and analysed with a finite element code, ABAQUS 5.4, running on a HP 735/125 UNIX workstation. Because the tile is thin (5 mm) relative to its other dimensions (25.4 mm), a 2-D plane stress was used. First, a transient thermal analysis was performed, and then the resulting temperatures were then applied to an elastic-plastic stress analysis. The model consists of 3804 nodes and 1221 8-noded isoparametric quad elements (DC2D8 for thermal, and CPS8 for stress). A smaller mesh size was used in the region where the steepest gradients were expected, i.e. underneath the beam spot. The size of the smallest elements was 0.2 mm x 0.2

mm. Temperature-dependent thermal and mechanical properties of S-65C were used in the analysis [2].

A constant heat flux = 80 MW/m^2 was applied in ABAQUS over a 2 mm wide spot on top of the tile for a pulse length = 0.06 seconds, then turned off for 0.94 seconds. Fig. 2 shows the temperature response for a single on/off cycle at the hottest point on the surface of the beryllium tile directly underneath the beam spot. The peak temperature rises from 25 °C to 750 °C during the 0.06 heating pulse. This agrees well with experimental measurements. The hot spot has cooled back down to 35 °C at the end of the 1 s cycle, indicating that only a small amount of thermal ratcheting would occur with multiple cycles. The steep temperature profile is approximately 2 mm deep.

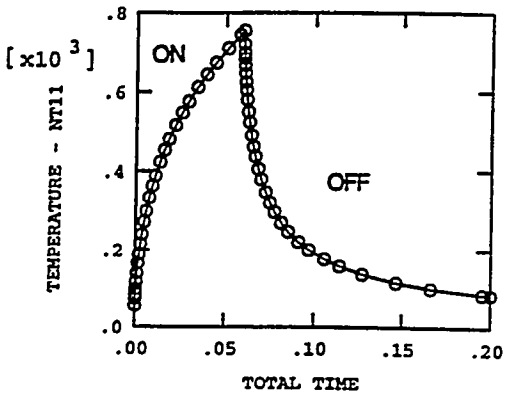

Fig. 2 Temperature (C) vs time (s) for the hottest element.

The same mesh used for the thermal analysis was subsequently used for an elastic-plastic stress analysis. A bi-linear stress/strain curve was used, with a kinematic hardening rule and temperature-dependent yield strength. Fig. 3 shows the deformed mesh plot (magnified by 200 times) at the end of the 0.06 s heating pulse.

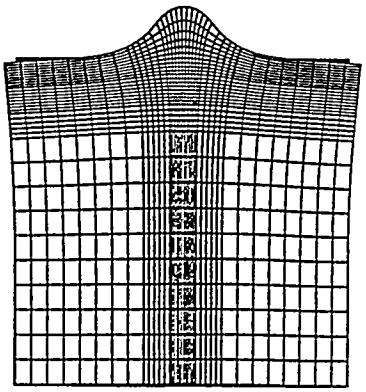

Fig. 3 Deformed ABAQUS mesh (magnified by 200 X) at the end of the heating pulse (t=0.06 s). Undeformed mesh is plotted underneath the deformed mesh.

Fig. 4 shows the X-direction stress vs plastic strain response of the hottest element underneath the beam spot for a total of 12 on/off cycles. The mechanical self-constraint of cold beryllium that surrounds the expanding hot spot creates a large compressive stress inside the hot spot during heating. The compressive stress increases rapidly up to a maximum value of -260 MPa (the yield strength) during the first 3 milliseconds when the temperature has risen about 100 °C. Then, with increasing temperature up to 750 °C, the yield strength decreases and the peak compressive stress likewise decreases to -130 MPa. Next, the heat flux is turned off, and the temperature gradient relaxes. The stress reverses sign and becomes tensile, first elastically, then plastically, as the yield strength is exceeded during cooldown. After 0.2 s, the temperature pulse has relaxed sufficiently that only small changes in the peak tensile stress (240 MPa) occur up to 1 s.

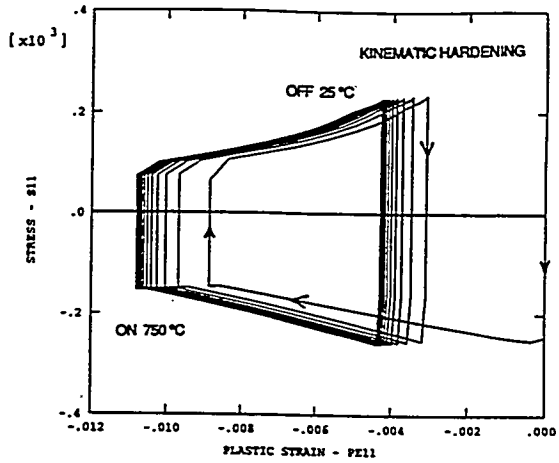

Fig. 4 Combined X-direction stress vs plastic strain for the element directly underneath the beam spot. Cyclic stress = 500 MPa and cyclic plastic strain = 0.65% after 12 cycles.

The plastic strain increases continuously up to a peak value of -0.9 % at the end of the first heating pulse. This value then decreases as the temperature pulse decays during the cooldown, leaving a permanent "residual" compressive plastic strain of -0.3% at the end of the first cycle. Shakedown to a stable response occurs during the first 6-8 cycles. The cyclic plastic strain for this element, i.e. the difference in plastic strain between the end of the heating pulse and the end of the cooling cycle, is 0.65%. Likewise, the cyclic stress is 500 MPa. The residual tensile stress at the heated surface is +240 MPa.

Fig. 5 plots the X-direction stress as a function of distance from the heated surface into the bulk at the end of the heating pulse, and at the end of the cooling cycle. The difference between these two curves is equal to the cyclic stress. The profile of cyclic stress remains rather constant for the first 1 mm, but then decays rapidly to zero at a depth of about 2 mm. This indicates that fatigue cracks, once initiated, should grow

rapidly through the first 1 mm, but then slow down at they approach a depth of 2 mm. The cyclic stress range is sufficiently high, 500 MPa, that rapid crack growth would be expected.

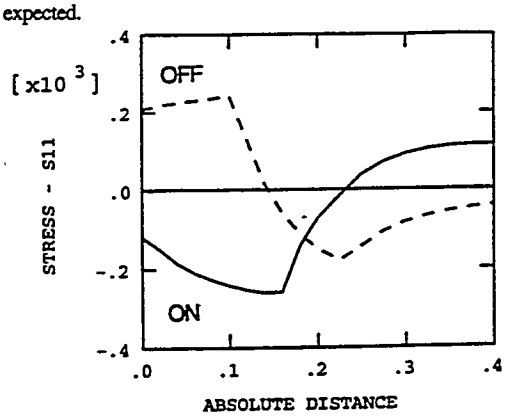

Fig. 5 Profile of X-direction stress through thickness (cm) at end of heating pulse (t=0.06 s) and end of cycle (t=1).

Fig. 6 plots the X-direction plastic strain as function of distance from the surface into the bulk at the end of the heating pulse, and at the end of the cooling cycle. The difference between these two curves is equal to the cyclic plastic strain. The profile of cyclic plastic strain decays rapidly to zero at a depth of 0.8 mm. This would indicate that fatigue crack initiation should be concentrated in a region than 0.8 mm deep. With the peak cyclic plastic strain values exceeding 0.6%, crack initiation would be expected to occur rather quickly.

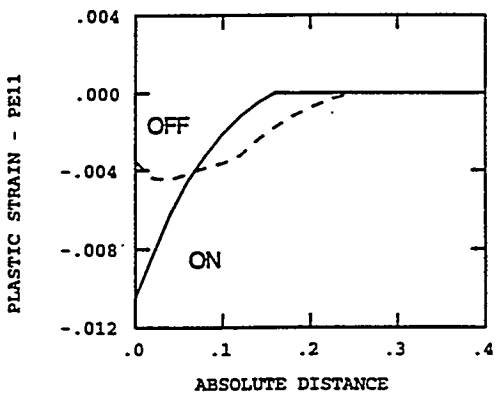

Fig. 6 Profile of X-direction plastic strain through thickness (cm) at end of heating pulse (t=0.06 s) and end of cycle (t=1).

EXPERIMENTAL PROCEDURE

Grades of US beryllium tested included: S-65C, S-65H, S-200F, S-200F-H, SR-200, I-400, extruded high purity, HIP'd spherical powder, porous beryllium (94% and 98% dense), Be/30% BeO, Be/60% BeO, and $TiBe_{12}$. Russian grades included: TGP-56, TShGT, DShG-200, and TShG-56. Each tile was 2.54 cm x 2.54 cm x 0.5 cm for the US grades, and 0.6 cm thick for the Russian grades. All of the US samples were chemically etched after machining, and degreased with an industrial grade, water based degreaser, then rinsed with acetone and methanol. Some of the Russian samples have a silvery, reflective finish which may be a the result of electropolishing. All grades typically have BeO contents on the order of 1 wt%, except I-400, which has 6 wt% BeO. The US grades showed a range of mean grain size from 5-12 microns. The mean grain size for DShG-200, 18.8 microns, is roughly twice as large as typical US grades. Also, the RF grade, TShG-56, showed an unusually large range of grain sizes, from 8 .to 105 microns, within one sample.

The 30 kW Electron Beam Test System (EBTS) was used to apply a highly concentrated heat pulse to the surface of each beryllium tile. This system, described in more detail in [3], consists of a 30 kV, 1 amp (max) electron beam that can be rastered in X- and Y-directions at frequencies up to 10 kHz. For this experiment we chose to raster the beam only in one direction at a frequency of 1 Hz with a constant velocity of 8.4 cm/s over a total length of 8.4 cm. A sawtooth raster pattern was used, with a 20X faster return at the end. The tiles were clamped on both sides by water-cooled copper blocks, including a Papyex graphite paper gasket, which removed the time-averaged power deposition and prevented thermal ratcheting.

Post-test examination of the heat affected zone indicated that the beam FWHM was approximately 2 mm wide. Rapid changes in the surface due to oxidation, microcracking, and melting prevented the use of optical pyrometry for accurate surface temperature measurements. However, visual observation of the color of the hot spot, after the beam had moved on to the next tile, indicated peak temperatures of at least 600 °C. Three cases (#3, 4, and 5) were run at 1300 W gun power. Each tile was inspected after every 100 cycles with an *in-vacuo* fiber optic borescope for any evidence of cracking or melting. Cycling was then continued on all 14 tiles until the last sample of the set had cracked (no more than 3000 cycles).

EXPERIMENTAL RESULTS

There are a number of common features among the samples. Looking down on the heated surface (top view) there is a clearly defined heat affected zone (HAZ) which is usually dark brown or black, with parallel bands of lighter color. It has the appearance of heavily oxidized metal. Many of the samples have a single major crack running down the middle of the HAZ parallel to the beam path, but rolled sheet and extruded samples have major cracks perpendicular to it.

The HAZ is typically 2 mm wide. In most samples, the HAZ is wider, and the damage was more severe, on the side where the beam exited the sample. Surface melting was also

observed, more so on the beam's exit side. On many samples, the tile's width is narrower in the HAZ, more on the beam exit side than on the entrance side, by as much as 0.4 mm. Some tiles that cracked perpendicular to the beam's path expanded in width, rather than contracting.

Looking perpendicular to the heated surface (side view), all samples show a elliptical-shaped discolored area underneath the beam spot, consisting of both darker and lighter bands. The sharp change in color from dark brown to a light gray may be caused by different thicknesses and morphology of the BeO layer. All samples have a raised hump 0.2-0.4 mm tall directly underneath the center of the beam path. This hump is also characterized by a network of many fine cracks.

Most samples showed evidence of surface melting. Some showed evidence of net erosion of material, especially the samples with high BeO content. Many samples show a single thin, straight crack descending from the highest point of the hump perpendicular to the heated surface. Crack depths range from 0.1 mm to 2.0 mm, with the average being about 1.0 mm. These cracks were usually deeper on the side of the tile where the beam exited the sample. A few samples showed lateral cracks running parallel to the heated surface at a depth of approximately 0.1 mm below the surface. Samples which showed no evidence of surface melting were SR-200, S-65 (T), and Extruded (T).

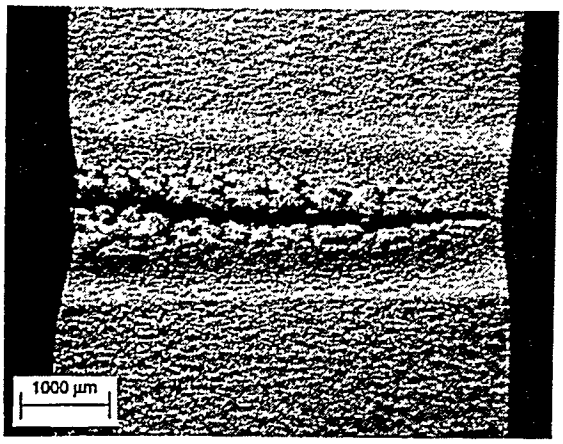

Fig. 7 Top view of S-200F after 2400 cycles. Longitudinal VHP billet orientation is parallel to heated surface. Mag 18X.

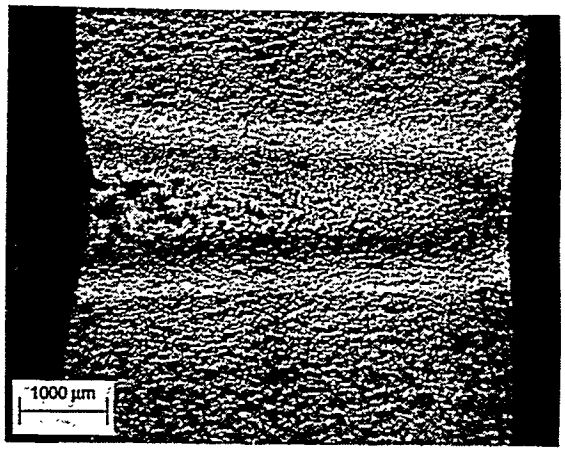

Fig. 9 Top view of S-65C after 2400 cycles. Longitudinal VHP billet orientation is parallel to heated surface. Mag 18X.

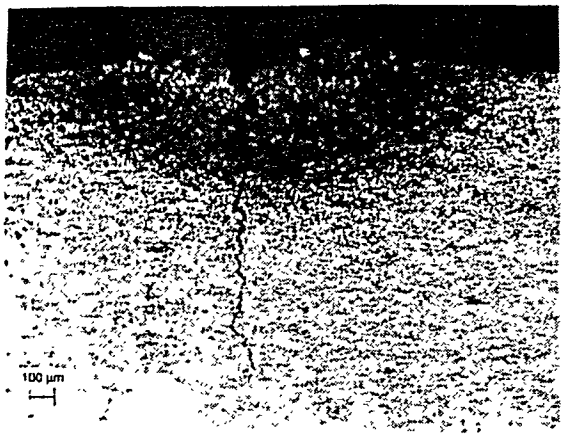

Fig. 8 Side view of S-200F after 2400 cycles. Longitudinal VHP billet orientation is parallel to heated surface. Mag 47X.

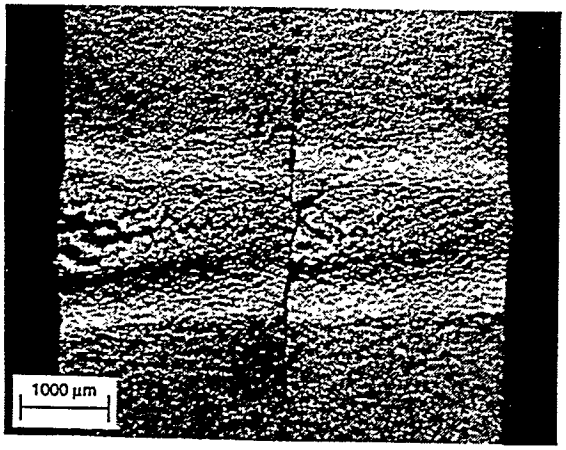

Fig. 10 Top view of SR-200 rolled sheet after 2400 cycles. Delamination crack is in the plane of rolling. Mag 18X.

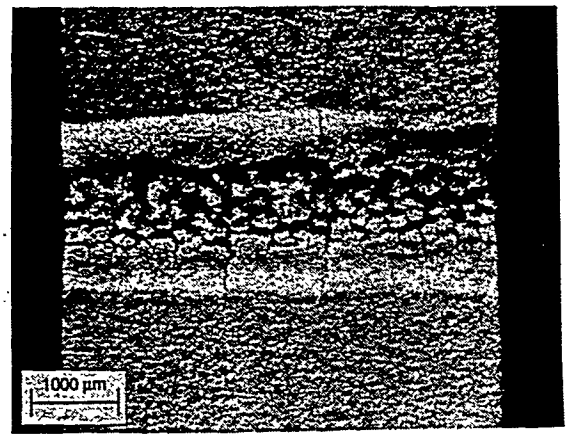

Fig. 11 Top view of I-400 after 2400 cycles. Longitudinal VHP billet orientation is parallel to heated surface. Mag 18X.

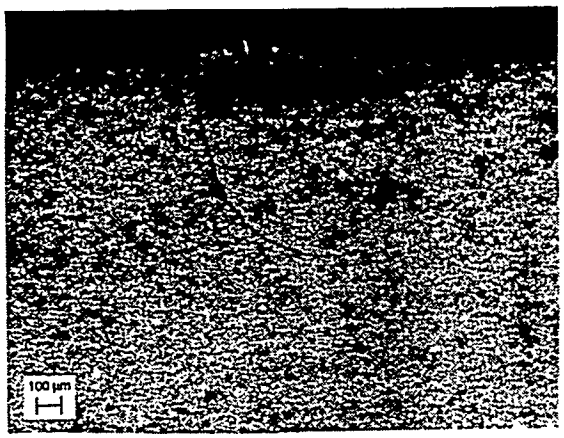

Fig. 12 Side view of I-400 after 2400 cycles. Longitudinal VHP billet orientation is parallel to heated surface. Lateral cracks can be seen running parallel to heated surface. Mag 47X.

The samples with the best resistance to crack initiation were: S-65C (L), DShG-200, S-65C (T), TShGT, S-65H, and TShG-56. The samples with the worst resistance to crack initiation were: TiBe12, Be/60wt% BeO, Be/30wt% BeO, I-400 (L), SR-200, 94% S-65. The samples with the shortest cracks were: SR-200, TShGT, S-65C (L), DShG-200, Be/60% BeO, and TShG-56. The samples with the longest cracks were: $TiBe_{12}$, Extruded (L), S-200F (L), I-400 (T) and TGP-56.

The cracks tended to fall into two categories: either straight, narrow and long or blunt, wide and short. The blunt, wide and short crack morphology was correlated with the best crack initiation resistance. Only one sample had both types of cracks: S-65C with the transverse direction parallel to the heated surface. This sample shows a long, straight, narrow crack propagation from one of the blunt cracks. There was no strong correlation with microstructural features such as grain size and inclusion concentration, but there was a complicated relationship with texture. The highly textured grades (sheet and extrusion) performed worse than partially textured grades such as VHP. HIP grades, which have minimal texture, performed worse than VHP grades. The average crack length of all the samples was 0.8 mm (excluding $TiBe_{12}$). Typically, the cracks on the beam's exit side were 20% longer than on the beam's entrance side.

DISCUSSION

Fig. 13 summarizes the experimental results; it shows both the crack initiation cycles and crack propagation depths. $TiBe_{12}$ is not shown, because the crack depths are off the scale (16 mm). If we look at just the grades of beryllium metal with isotropic and near-isotropic properties (S-65C, S-65H, S-200F, S-200F-H, 94% S-65, 98% S-65, I-400, TGP-56), we see a clear trend. Samples in this group with high number of cycles to crack initiation also have low crack propagation depths, and visa-versa. This could be because they are tougher, or simply because there haven't been many cycles after crack initiation to propagate cracks deeper. Likewise, samples which initiate cracks early on have more time (e.g. cycles) to grow the crack deeper.

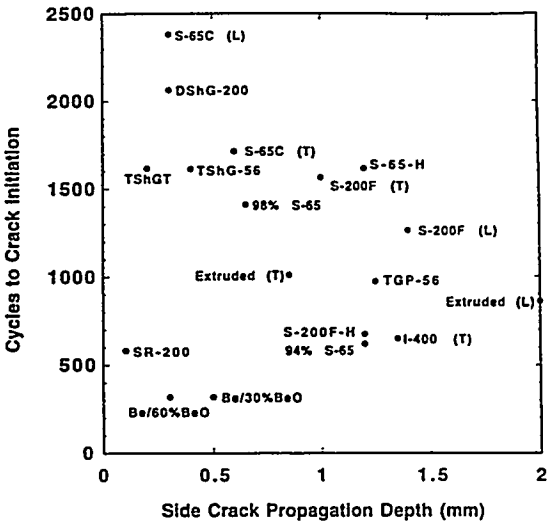

Fig. 13 Summary of experimental results. Samples with the best overall fatigue resistance are S-65C, DShG-200, TShGT, and TShG-56.

For the case of SR-200 (TShGT also), the low strength and ductility in the direction perpendicular to the plane of rolling explains why these samples formed a delamination crack relatively quickly. However, in-plane, vertical cracks (when

viewed from the side), show excellent resistance to growth. This is probably due to the outstanding mechanical properties in the plane of rolling (350 MPa Yield, 550 MPa Ultimate, and 25% elongation, at room temperature for SR-200, from Table 4). Use of beryllium in this form, as sheet "lamellae", bonded to a copper tube with the tube running perpendicular to the plane of the sheet, has been proposed for ITER high heat flux components by Merola et. al. [4].

The good resistance to melting of the SR-200 and S-65 samples correlate well to the short crack depths that was observed. In the case of extruded (T) sample, the lack of melting, despite a deeper crack (1 mm), indicates that the crack was vertical and did not hinder heat conduction.

The rankings shown here are only done to illustrate the differences in ranking which can result from the two different ranking measurements. The rankings are not statistically significant. Much more data is needed to make these rankings valid because fatigue measurements generally exhibit a large amount of scatter.

CONCLUSIONS

A novel technique has been developed to rapidly and efficiently determine the relative low cycle fatigue resistance of a number of different beryllium materials. Operating the electron beam at 1 Hz produces a localized temperature spike of sufficient intensity such that cyclic plastic strains on the order of 0.6% and cyclic stresses of 500 MPa are created, producing visible cracking in less than 3000 cycles.

A number of features were correctly predicted by a 2-D elastic-plastic finite element analysis, including: peak temperatures, width of the heat affected zone, orientation of the main crack, formation of a bump on the surface, depth of crack propagation, curvature of crack near a compressive zone, and residual tensile stresses causing crack opening upon cooldown. The 2-D, plane stress model did not account for two features: (1) out-of-plane stresses that caused delamination cracks in rolled sheet beryllium, and (2) narrowing of the tile due to plastic deformation. Future efforts in finite element modeling should include: (1) using a 3-D model, with a moving e-beam spot, (2) anisotropic material's properties, (3) improved description of the yield surfaces (e.g. kinematic vs isotropic hardening).

The most fatigue resistant grades were S-65C, DShG-200, TShGT, and TShG-56. Rolled sheet Be (SR-200) and TShGT showed excellent crack propagation resistance in the plane of rolling, despite early formation of delamination cracks. Only one sample showed no evidence of surface melting, extruded (T), despite cracking. The good thermal conduction is preserved because cracks only grow perpendicular to the heated surface because of the highly aligned grain structure in the extruded form.

The degree and morphology of cracking is strongly dependent on the metallographic texture. Vacuum hot pressed grades generally perform better than hot isostatic pressed grades. Likewise for the longitudinal direction oriented parallel to the heated surface. Lower metallic impurity contents correlates well with increased fatigue resistance, but BeO content does not correlate well. The use of highly textured beryllium, i.e. rolled sheet, in the form of thin "lamellae" proposed by Merola appears to be an attractive concept for improving fatigue lifetime of high heat flux components.

A second round of electron beam experiments is recommended in order to generate better statistics, and to improve our understanding of low cycle fatigue behavior. More tests using pre-cracked or notched samples could be performed to focus only on the crack propagation aspects. Also, samples which have previously been exposed to simulated plasma disruptions (plasma guns) could be tested. Neutron-irradiated samples could be tested in the JUDITH facility. Finally, samples of plasma sprayed beryllium should be tested.

ACKNOWLEDGMENTS

This work was performed at Sandia National Laboratories, supported by the US Department of Energy, Office of Fusion Energy, under contract DE-AC04-94AL85000. The authors wish to thank Brush Wellman, Inc. for their supply of the beryllium materials, and post-test examination, metallography, and chemical analyses. We wish to also thank Fred Bauer, Ken Trancosa, Jimmie McDonald, LaWonda Wold, and Wynona Sexson for their contributions contributions to operating the electron beam test system and computer network.

REFERENCES

[1] R.D. Watson, D.L Youchison, D.E. Dombrowski, R.N. Guiniatouline, I.B. Kupriynov, "Low Cycle Thermal Fatigue Testing of Beryllium Grades for ITER Plasma Facing Components", Proc. 2nd IEA International Workshop on Beryllium Technology for Fusion, Jackson, WY, Sept, 1995.

[2] R.D. Watson and J.B. Whitley, "Thermal Fatigue Tests of a Prototype Beryllium Limiter for JET", J. Nuclear Eng. and Design, Vol. 4, p. 49, (1986).

[3] D.L. Youchison, J.M. McDonald, L.S. Wold, "High Heat Flux Testing Capabilities at Sandia National Laboratories-New Mexico", ASME Heat Transfer in High Heat Flux Systems, HTD-Vol. 301, p. 31 (1994).

[4] M. Merola, R. Matera, G. Federici, S. Chiocchio, "Thermomechanical study of a new concept for a beryllium-protected high heat flux component", Fusion Eng. and Design, Vol. 28, p. 97 (1995).

DiMES Erosion Study: Test pairs provide direct comparisons of different divertor materials.

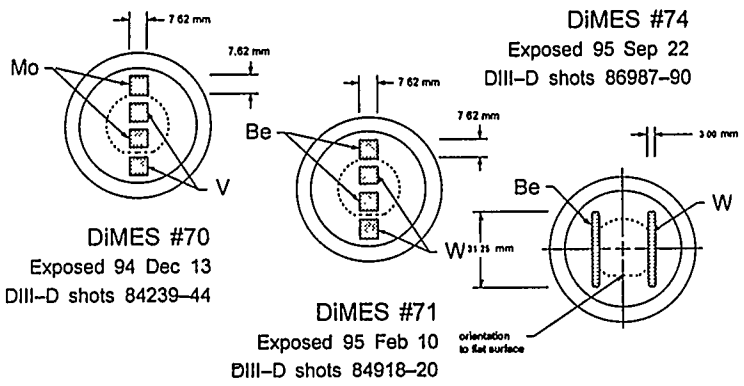

RB SNL 8716 96010509

DiMES Erosion Study: Exposure Conditions

- Samples exposed to normal H-mode deuterium plasmas (10^{22} D/m^2-s, ≈0.4 MW/m^2).
- Strike-point moved onto sample during steady-state portion of discharge (T_e: ≈ 30 eV, field angle: 1.2°).
- Plasma conditions kept constant throughout exposure.
- Length of exposure: 2–15 seconds, 1–6 plasmas.
- Samples retracted during wall conditioning.

RB SNL 8716 96010510

DiMES Erosion Study: Net Erosion Rates at the Strikepoint

- Carbon shows the highest erosion rate, tungsten the smallest. Their rates differ by nearly a factor of 50.

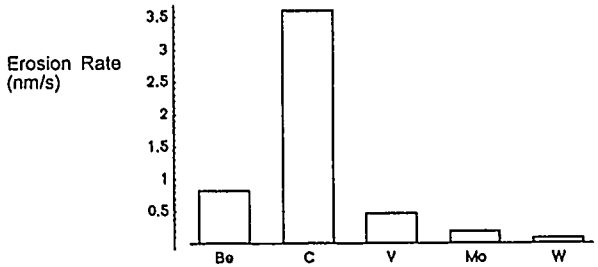

averaged data from DiMES #70 (C,V,Mo) and DiMES #71 (Be,C,W)

RB SNL 8716 96010511

DiMES Erosion Study: Deuterium Retention

- DiMES sample materials show differences in deuterium uptake following exposure in DIII–D.

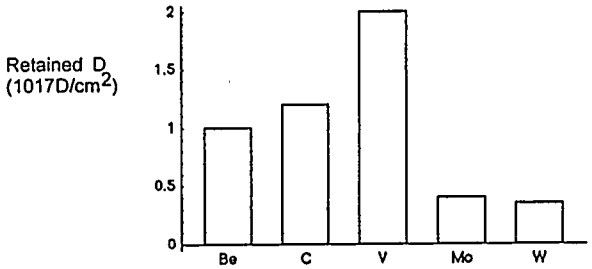

averaged data from DiMES #70 (C,V,Mo) and DiMES #71 (Be,C,W)

RB SNL 8716 96010512

DiMES Disruption Studies

- **Objective:**
  Characterize particles striking the divertor floor during a disruption.

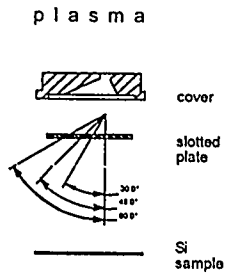

- **Experiment:**
  1. Place Si sample on DiMES behind a slotted aperture.
  2. Expose sample to a series of Ar induced disruptions.
  3. Measure amount of trapped D at each viewing angle.
  4. Measure D depth distribution at each viewing angle.
  5. Derive particle fluxes and energies.

RB SNL 8716 96010505

DiMES Disruption Study: Results

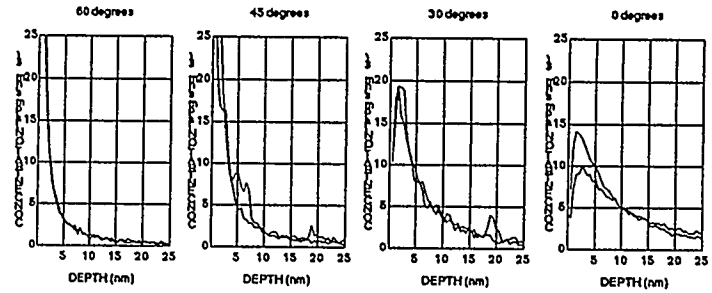

- Most of the trapped deuterium was found to reside within 10 nm of the surface.
- Deuterium was implanted deeper at the viewing angles closer to normal incidence.

RB SNL 8716 96010506

DiMES Disruption Study: Data Summary

Measured D in Si DiMES sample exposed to DIII–D shots 81166–8						
view angle a	[D] D/nm^2	[D]/cos(a) D/nm^2	peak depth nm	depth/cos(a) nm	energy eV	fluence D/nm^2
0°	160	160	2.1	2.1	100	252
30°	140	162	1.6	1.8	80	252
45°	130	184	<1	<2	<90	287
60°	90	180	<1	<2	<90	330

- The directional flux of deuterium appears to be nearly isotropic.
- Deuterium strikes the divertor floor at an average energy of up to 100 eV.
- A disruption model based on these results indicates that a cold neutral layer reduces the divertor heat load by about 30%.

RB SNL 8716 96010507

DiMES Erosion Studies

- DiMES has been used to make controlled-exposure measurements of divertor tile erosion.
- These measurements are used to:
  - Observe how various tokamak operating modes affect divertor erosion
  - Compare performance of different materials
  - Test models used to predict divertor lifetime.
- Materials examined to date:
  - carbon (ATJ graphite)
  - tungsten
  - molybdenum
  - vanadium
  - beryllium.

RB SNL 8716 96010508

Recent Results from the DiMES Experiment

Robert Bastasz for the DiMES Team

Sandia National Laboratories
Livermore, California

Presented at the US–Japan Workshop (Q219)
on High Heat Flux Components
and Plasma Surface Interactions for Next Devices
Colorado Springs, Colorado, January 9–11, 1996

RB SNL 8716 96010501

The DiMES Team:

General Atomics:

Neil Brooks, Terry Carlsness, Paul Parks, Phil West, Dennis Whyte, Clement Wong

Argonne National Laboratory:

Jeff Brooks, Dave Ehst, Ahmed Hassanein, Thanh Hua

Sandia National Laboratories:

Bob Bastasz, Dean Buchenauer, Dave Walsh, Bill Wampler, Josh Whaley

University of California, San Diego:

John Cuthbertson

RB SNL 8716 96010502

Recent DiMES Experiments

1. Disruption Studies:
   - Incident particle measurements during Ar induced disruptions.
2. Carbon Erosion Measurements:
   - Carbon erosion during H-mode operation.
3. Metals Erosion Measurements:
   - Be, V, Mo, W.
4. Materials Tests:
   - B4C versus graphite.
5. Conditioning Measurements:
   - Boronization effects on divertor surfaces.

RB SNL 8716 96010503

The Divertor Materials Exposure System transports samples to the DIII–D divertor floor

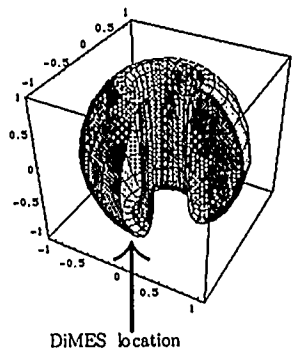

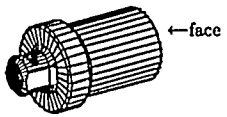

standard sample

- DiMES places samples near the center of the divertor floor (r=148.5 cm).
- Samples are typically made from graphite (type ATJ) and have a 4.8 cm diameter exposed face.

RB SNL 8716 96010504

DiMES Erosion Study: Summary of Results

- Net carbon erosion (4 nm/s) occurs in a narrow zone under the outer strikepoint in DIII-D .
- Tungsten erosion is very small (0.06 nm/s) and sputtered tungsten appears to be deposited locally.
- Be, V, and Mo erosion are all small (<1 nm/s).
- DiMES is providing benchmark data for the WBC/REDEP models used to predict erosion/deposition rates in ITER.

RD SNL 8716 96010513

Recent Results from the DiMES Experiment: Bibliography

1. "Measurements of carbon and tungsten erosion/deposition in the DIII–D divertor"
   R. Bastasz, W. R. Wampler, J. W. Cuthbertson, D. A. Buchenauer, N. Brooks, R. Junge, W. P. West, and C. P. C. Wong
   J. Nucl. Mater. 220–222 (1995) 310.
2. "Erosion and deposition of metals and carbon in the DIII–D divertor"
   W. R. Wampler, R. Bastasz, D. Buchenauer, D. Whyte, C. P. C. Wong, N. H. Brooks, and W. P. West
   J. Nucl. Mater. (1996) *in press.*
3. "First measurements of the ion energy distribution at the divertor strike-point during DIII–D disruptions"
   P. B. Parks, R. Bastasz, D. Whyte, N. H. Brooks, W. R. Wampler, W. P. West, and C. P. C. Wong
   Proc. of the 1995 SOFE Conference *in press.*

(as of 1995 December)

RD SNL 8716 96010514

Recent Results of Comprehensive Plasma Disruption Modeling and Simulations

Ahmed Hassanein

Argonne National Laboratory
Argonne, Illinois 60439 USA

US-Japan Workshop Q219

January 9-11, 1996

Colorado Springs, Colorado

Introduction

- Plasma disruptions are considered one of the most limiting factors for successful operation of magnetic fusion reactors.

- Comprehensive self-consistent model is developed and used to predict material erosion during plasma disruptions and simulation experiments.

- The model dynamically links target thermodynamics, vapor-cloud magneto-hydrodynamics, and photon transport for accurate evaluation of material erosion and lifetime.

- The model is extended to simulate various laboratory experiments on disruption. Results are in good agreement with recent data.

Major Disruption Effects

√ • Vaporization of plasma-facing components.

√ • Melting of metallic plasma-facing materials.

? • High temperatures and thermal stresses in structural materials.

? • Redeposition of eroded materials on various facing components.

Objectives

- Model and evaluate the erosion of plasma-facing components during reactor disruptions and ELMs.

- Model, analyze, and evaluate various disruption simulation experiments (e-beams, plasma-guns, etc...).

- Evaluate melt-layer behavior of metallic components under various forces during the disruption.

Stages of the Disruption Model

Three major modeling stages are required during the plasma/material interaction:

(1) Plasma - Material Interaction

(2) Plasma - Vapor Interaction

(3) Radiation Transport

A*Thermal-S Computer Code

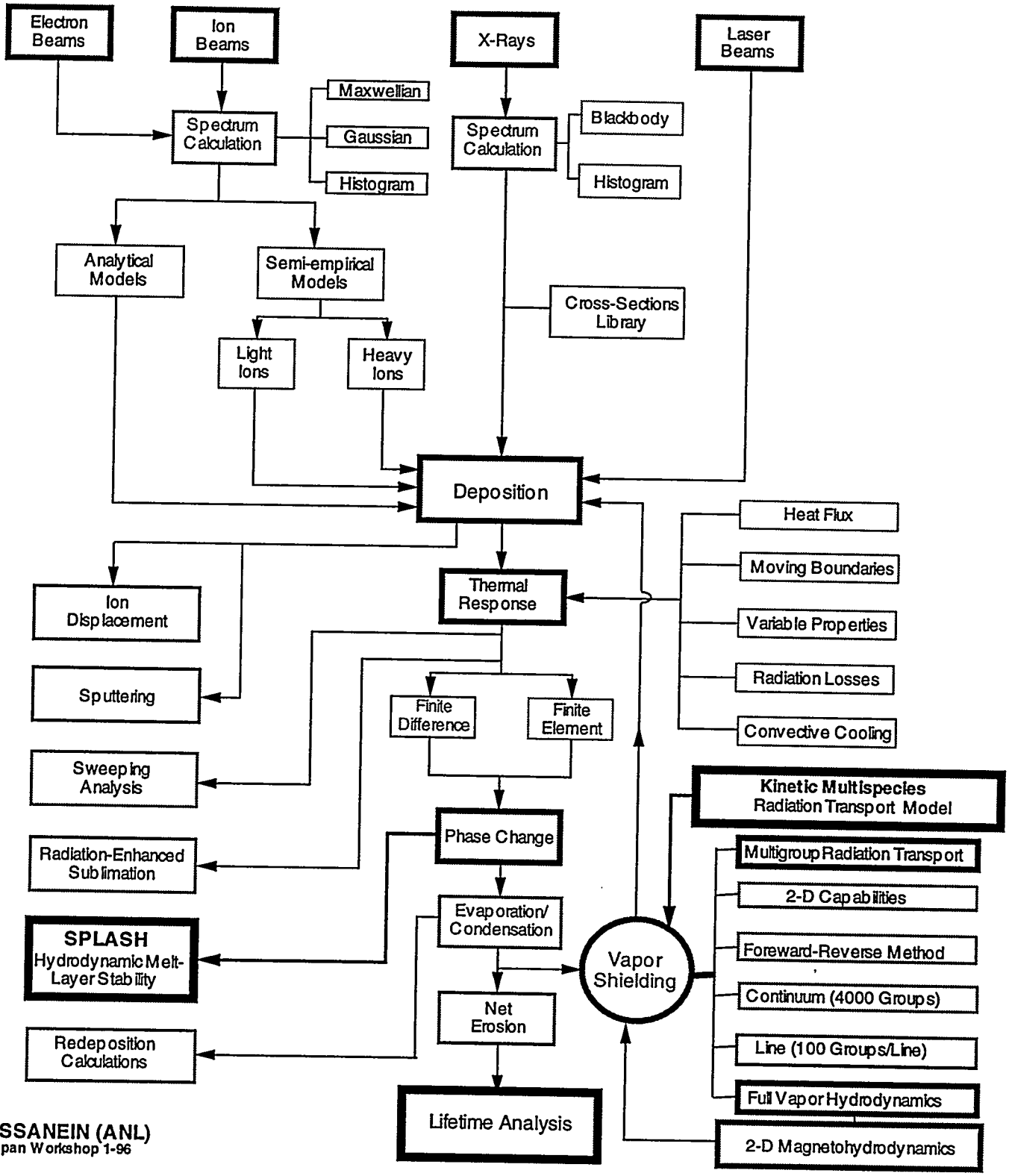

A. HASSANEIN (ANL)
US-Japan Workshop 1-96

Self-Consistent Kinetic Model

- Optical properties are calculated for a real plasma conditions.

- At each time step, quantities such as density, temperature, and spectral radiation flux are used to calculate absorption and emission coefficients.

- This is achieved by solving the kinetic equations for ion concentration and for level populations of each charge state.

- Calculation of emission and absorption coefficients includes the three kinds of radiation
  - bremsstrahlung radiation
  - recombination radiation
  - line radiation

(SUPERATOM Code)

- The atomic data base of the SUPERATOM code is used in these calculations.

- Some of the data includes:
  - Ionization potentials
  - Energy levels
  - Statistical weights
  - Quantum levels
  - Degeneracy levels
  - Oscillator force
  - Line transition probabilities
  - Ionization cross sections

Reactor-Disruption Parameters

- **Plasma-Particles:**

  Ions + Electrons
  Kinetic Energy (20 → 1 keV)

- **Energy Deposited:**

  Energy-Densities (10 → 200 MJ/m^2)

- **Deposition-Time:**

  Duration (0.1 → 10 ms)

- **Deposition-Area:**

  Size (tens of square-meters)

- **Plasma-Facing Materials:**

  Low-Z (Be and Carbon)
  High-Z (Tungsten)

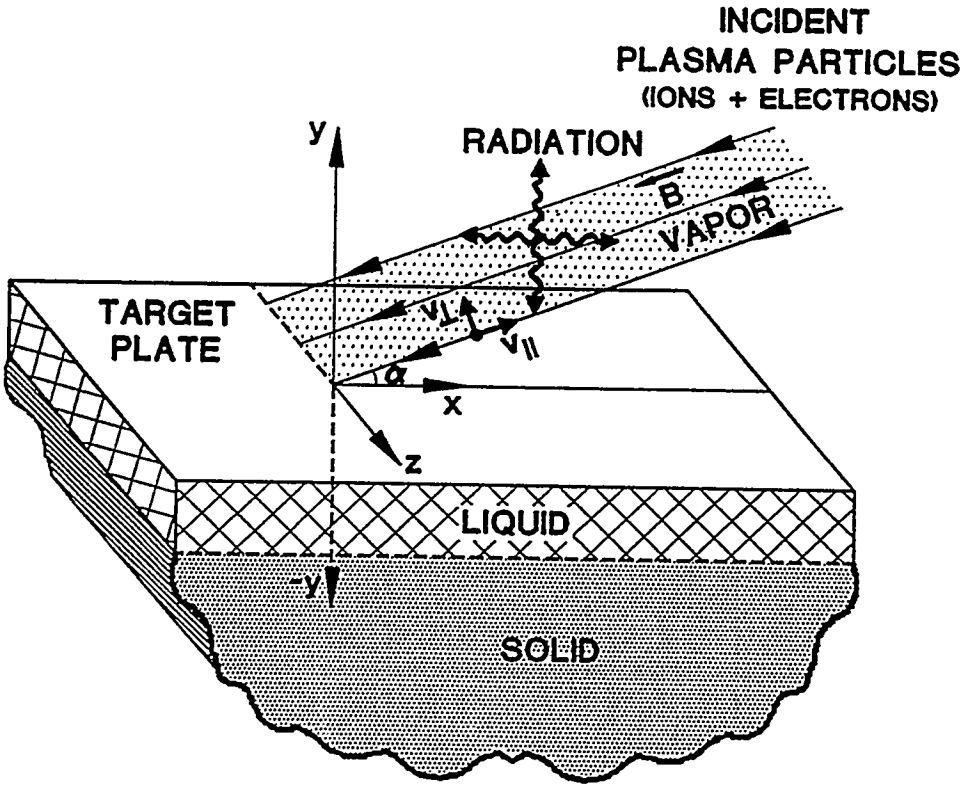

Hassanein, ANL

Fig 1

A*THERMAL-S Results

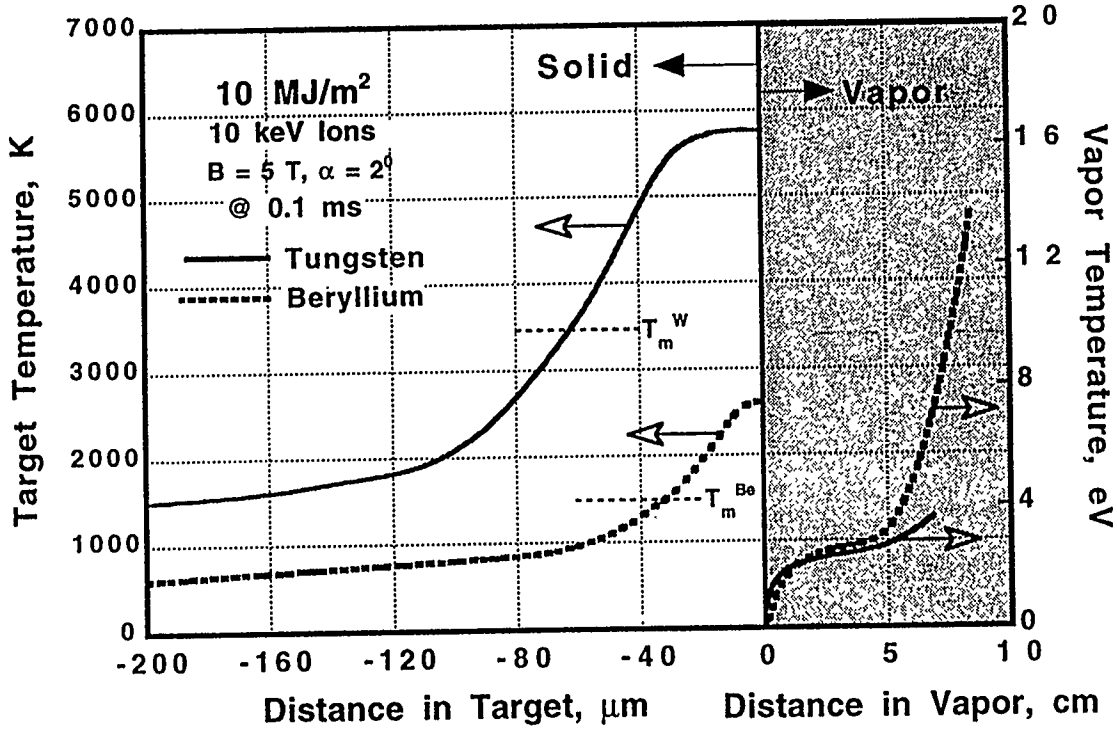

Hassanein, ANL

Fig. 2

A * THERMAL-S Results

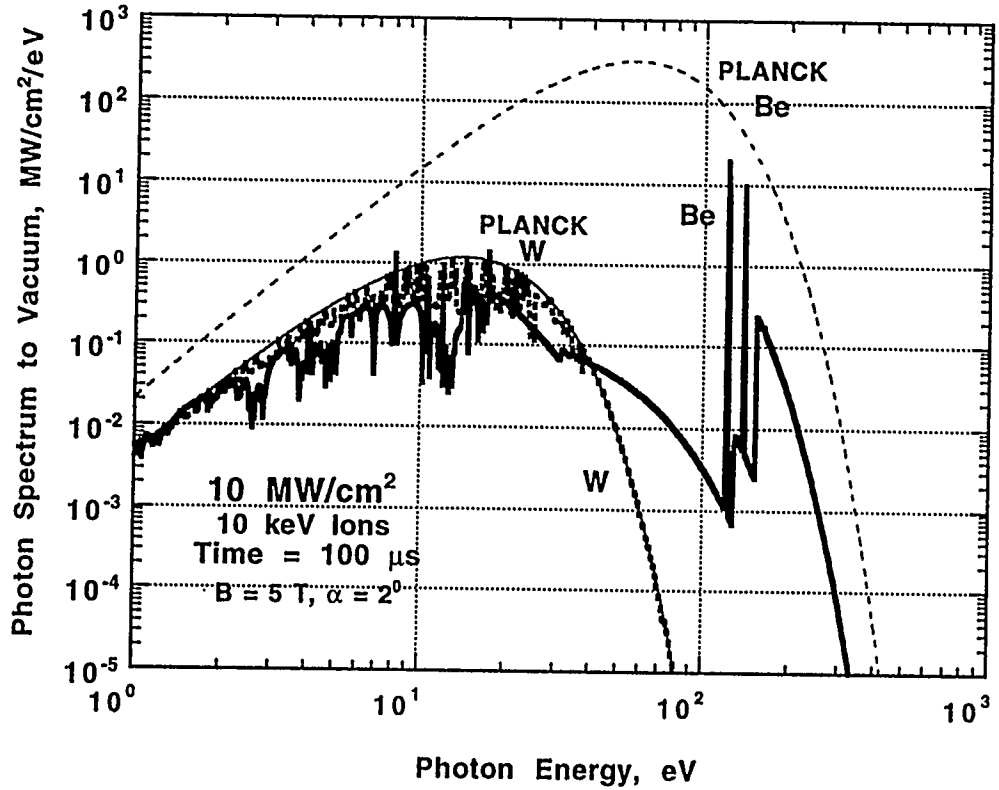

Hassanein, ANL

Fig 3

A*THERMAL-S Results

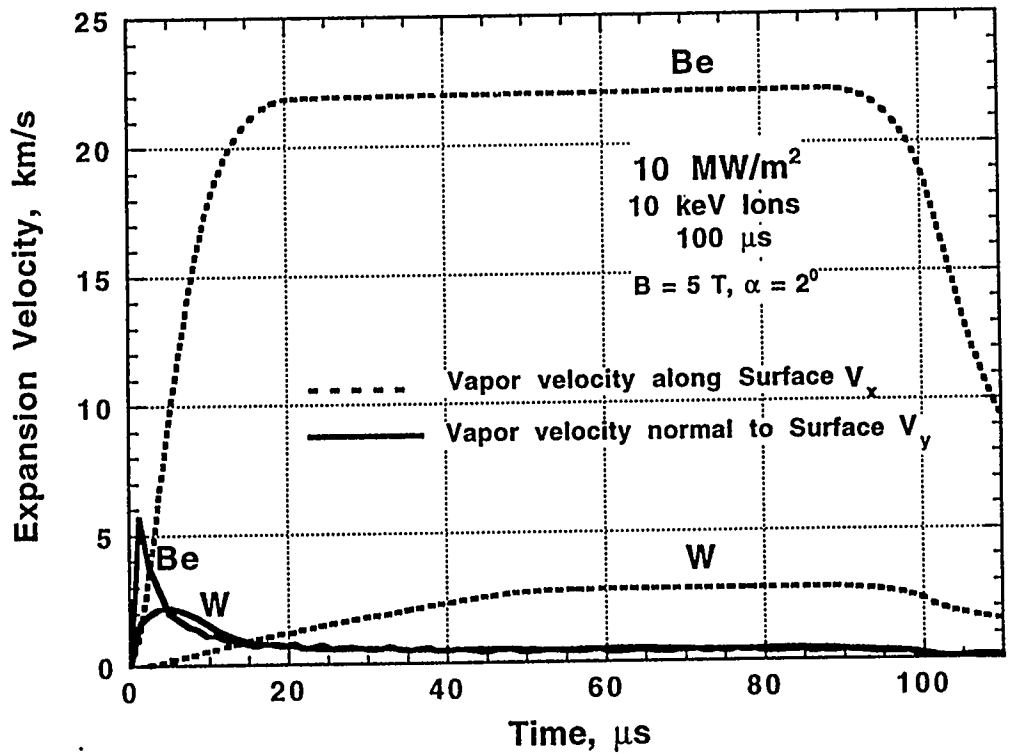

Hassanein, ANL

Fig (4)

A*THERMAL-5 Results

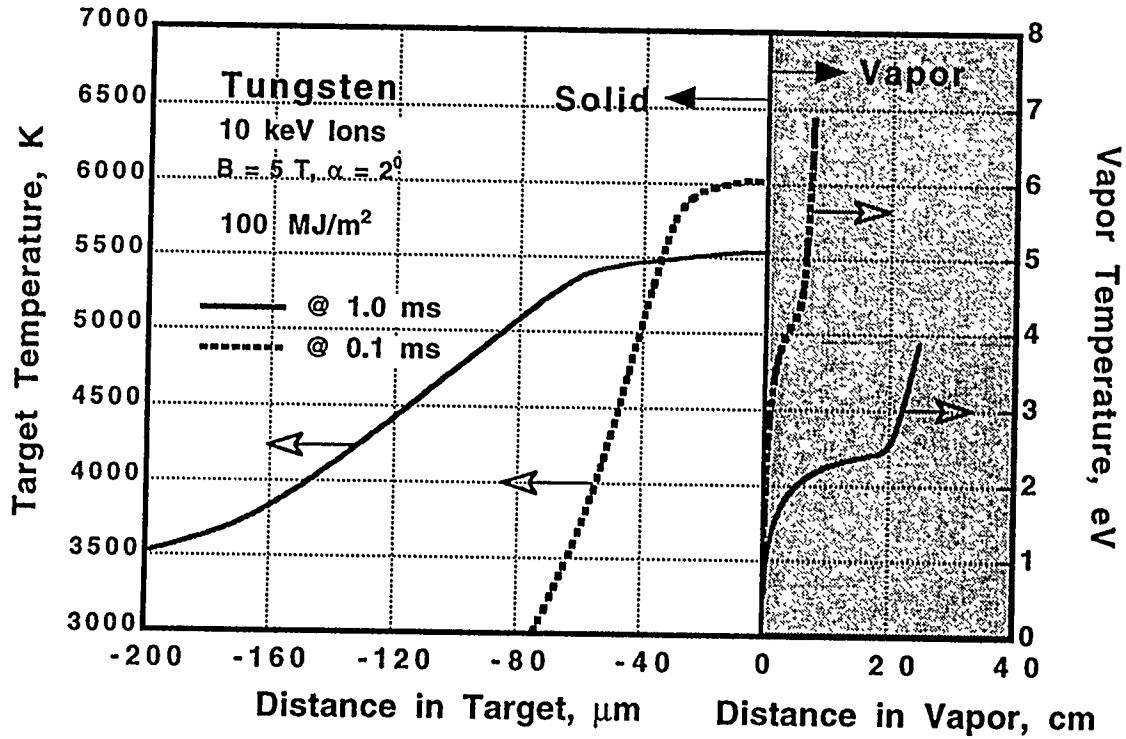

Hassanein, ANL

Fig 5

A*THERMAL-S Results

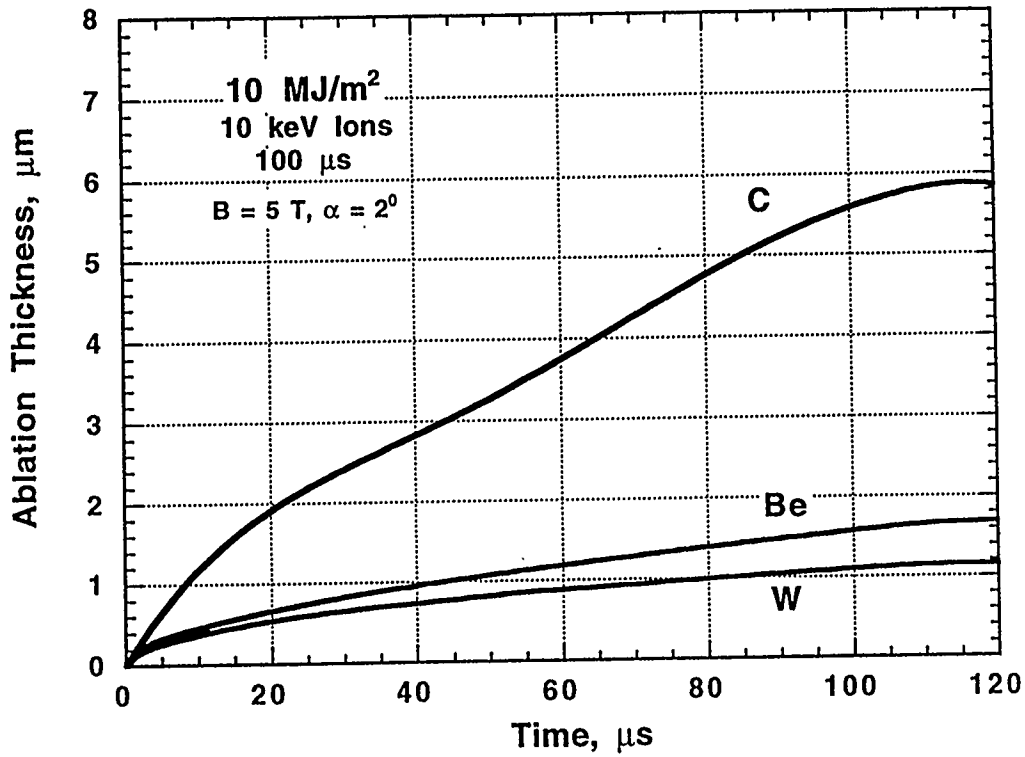

Hassanein, ANL

Fig 6

A*THERMAL-S Results

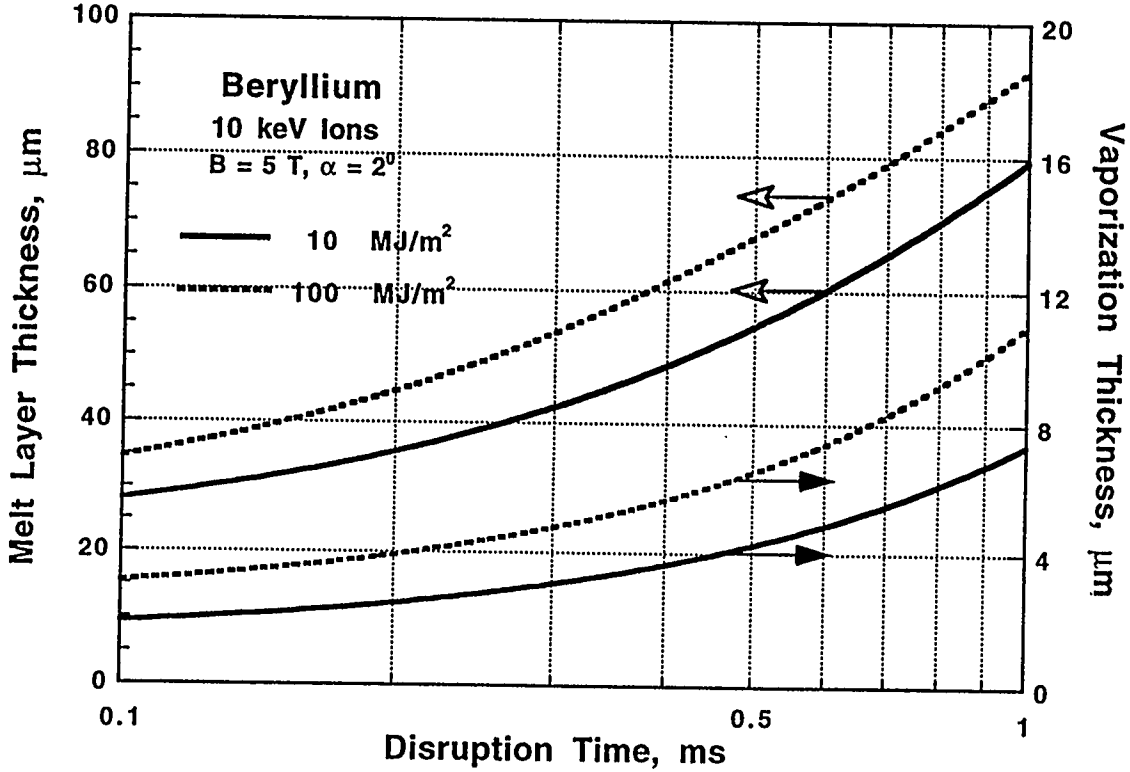

Hassanein, ANL

Fig 7

A*THERMAL-S Results

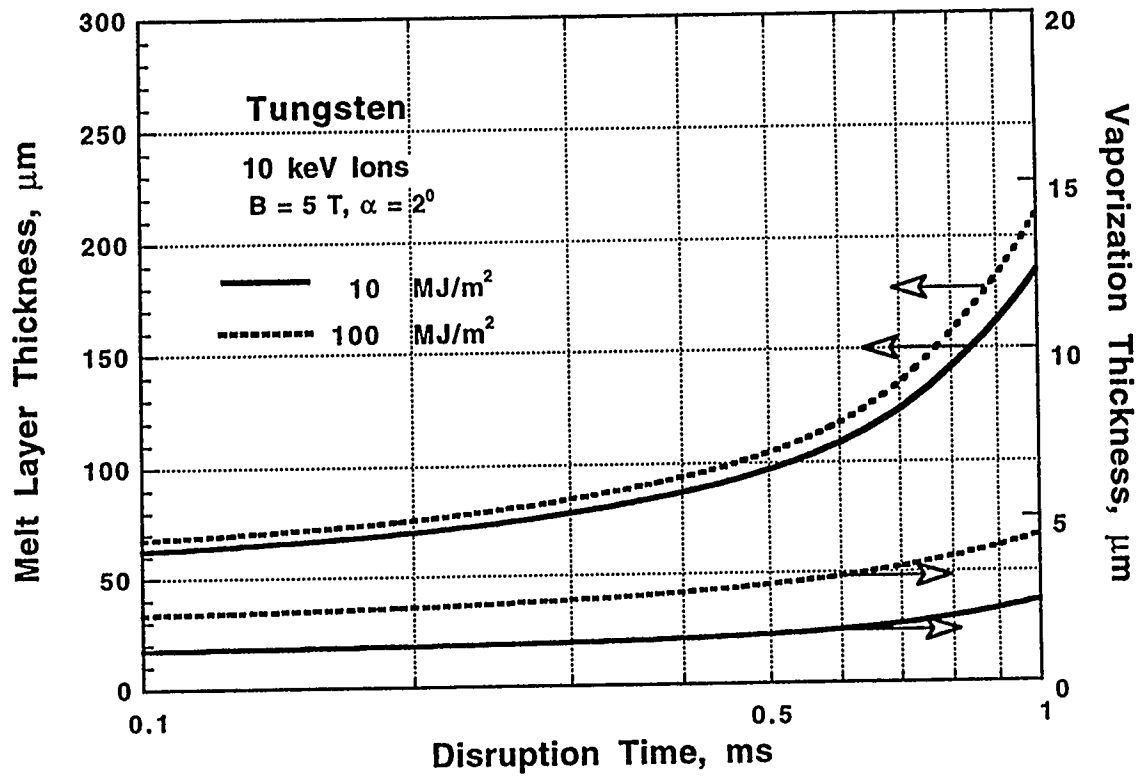

Hassanein, ANL

Fig 8

A*THERMAL-S Results

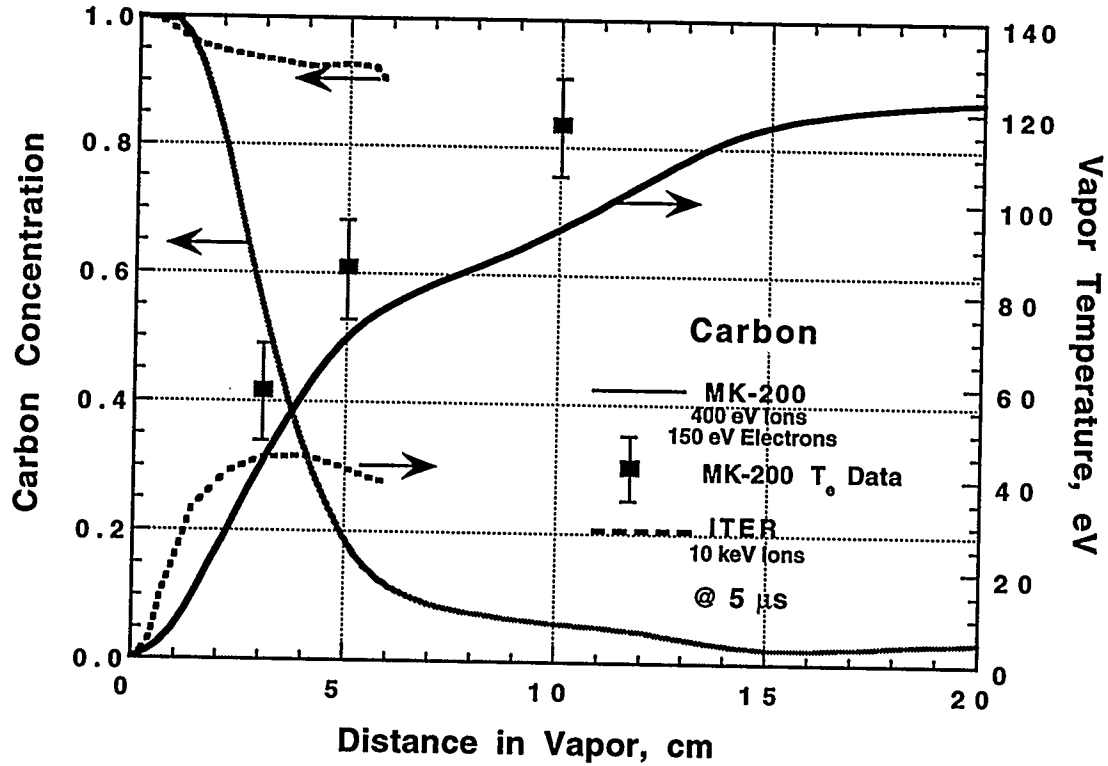

Hassanein, ANL

Fig 9

A * THERMAL-S Results

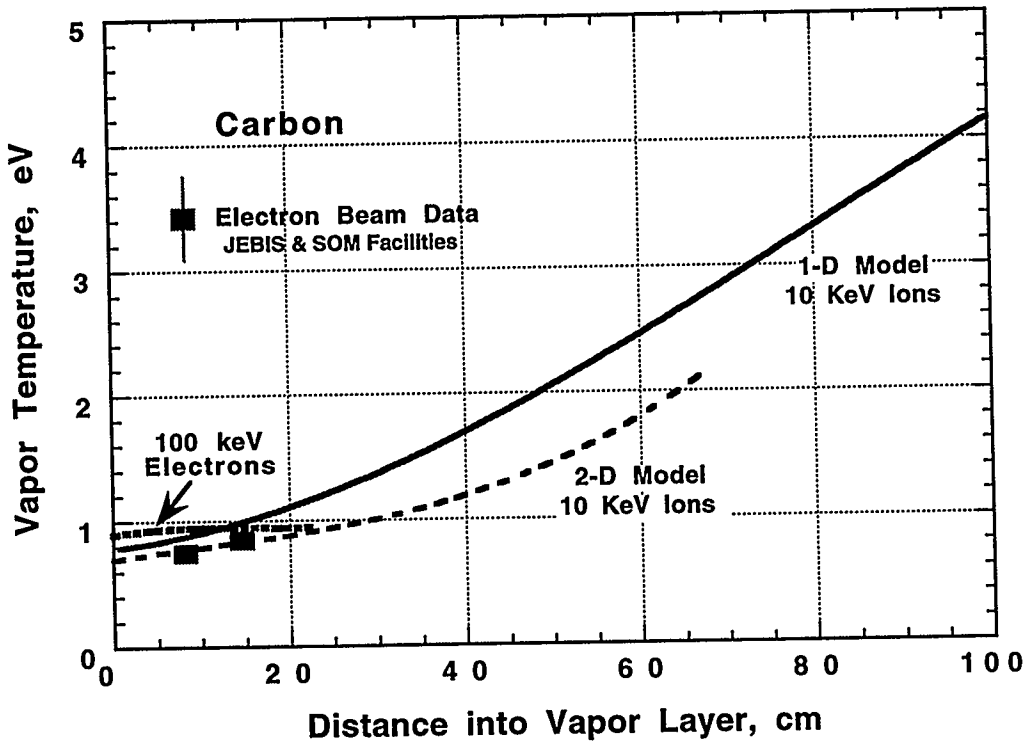

A. Hassanein, ANL

Fig (10)

Reactor Disruption vs. Experiments

- Higher plasma-particle kinetic and total energies will result in more erosion and less shielding effect.

- Vapor shielding may be less effective for electrons than for ions with the same particle energy.

- Longer disruption times ($\tau_d \approx 10$ ms) may result in less vapor shielding and more erosion.

- Magnetic field effects (oblique incidence).
  - Vapor diffusion
  - Edge effects

- Higher operating surface temperatures of plasma-facing components can result in more melting thickness for metallic materials.

Concerns and Future Studies

- **Vapor - Cloud Effects**
  - Turbulence
  - Instabilities
  - Expansion
- **Magnetic Field Effects**
  - Edge effects
  - Diffusion across magnetic field
- **Vapor - Plasma Mixing Effects**
  - Impurities effect
  - Disruption scenario
- **Melt-Layer Erosion**
  - Splashing
  - Hydrodynamic Instabilities
  - Flow and Dripping

Important Issues to Disruption Lifetime

- The developed vapor-cloud from initial vaporization is very important in protecting and further reducing erosion of the divertor plate.

- However, intense radiations from the expanding shielding layer can cause damage to other reactor components particularly in a closed-configuration design.

- More experimental data is required to evaluate disruption conditions relevant to ITER such as the influence of magnetic field, longer disruption time (τ_d ~ 1-5 ms), and high energy deposition (up to 100 MJ/m^2).

Melt-Layer Erosion

- The SPLASH code has been developed to study the erosion of melt layer during disruptions and ELMs.

- Hydrodynamic instabilities as well as melt-layer splashing from plasma-momentum and bubble vaporization can lead to melt-layer loss.

- Results are in good agreement with available experimental data.

- Melt-layer losses during disruptions and ELMs will significantly reduce the lifetime of metallic PFM.

- More-relevant simulation experiments are required to correctly evaluate melt-layer erosion in reactor environment.

Conclusions - I

- The self-consistent comprehensive numerical model (A*THERMAL-S Code) to evaluate PFC response to disruptions, ELMs, and high power excursions is enhanced to include a kinetic multispecies radiation transport model.

- The model integrate, with sufficient details, target thermodynamics with phase change, developed vapor-cloud magnetohydro-dynamics, and a time-dependent photon radiation transport field.

- Erosion from surface vaporization is determined by the complex interplay of material thermodynamics and properties, vapor magnetohydrodynamics, and detailed radiation properties linked in a self-consistent way to correctly evaluate divertor lifetime.

- Disruption simulation experiments using plasma guns and electron beams, with detail diagnostics, are in good agreement with the computer model.

Conclusions - II

- An order of magnitude increase in the disruption energy density ($10 \rightarrow 100$ MJ/m^2) only increases erosion rate by a factor of 2.

- Carbon ablation thickness is larger than that of beryllium for similar disruption conditions.

- Magnetic field appears to reduce erosion rate at lower energy densities by a factor of 30-50%.

- If the melt layer of metallic PFC is lost during the disruption (SPLASH code), the erosion lifetime will be drastically reduced.

P. D. Rockett and J. A. Hunter, Sandia National Labs, Albuquerque, NM, USA
S. Suzuki, K. Nakamura, and M. Akiba, JAERI, Naka, Japan

Utility of X-ray Imaging for Disruption Analysis

Paul D. Rockett

Org. 6428

Sandia National Laboratories

Presented to:

US/Japan Workshop
January 10, 1996

Colorado Springs, CO, USA

We used JEBIS to attempt to record the VUV spectra from POCO graphite targets irradiated by electrons with 70 kV, 2.8 A, and 1 msec.

The temperature at 2 x 10^9 W/m^2 was apparently too low. The VUV signal was unrecordable.

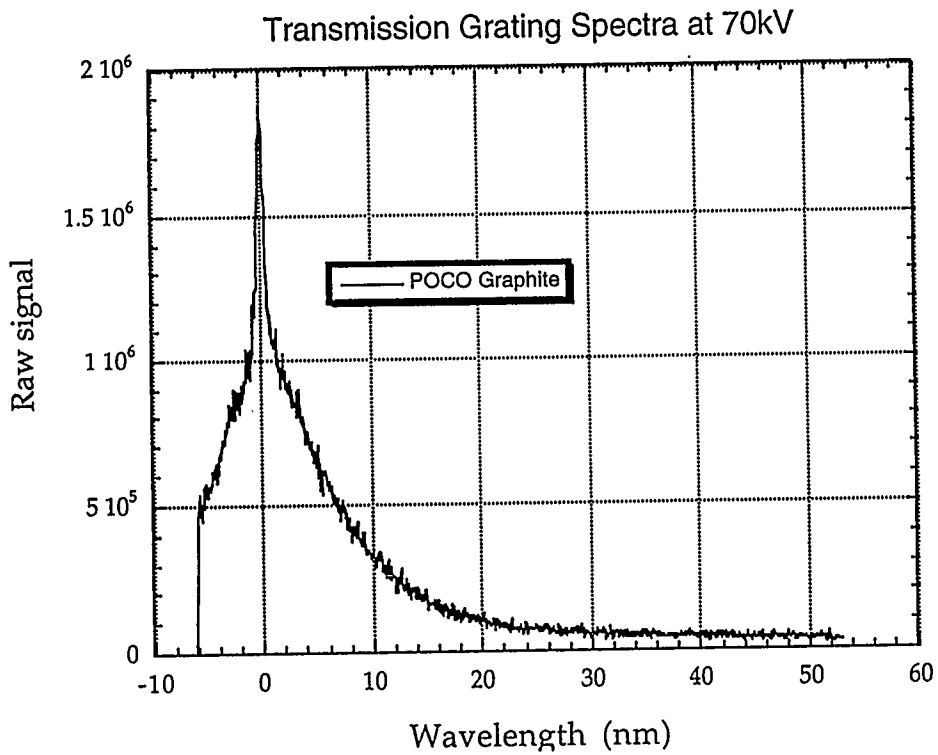

This raised the question: can one utilize the x-ray emissions from electron impacts on PFC's to infer the electron energy and the spatial energy distribution?

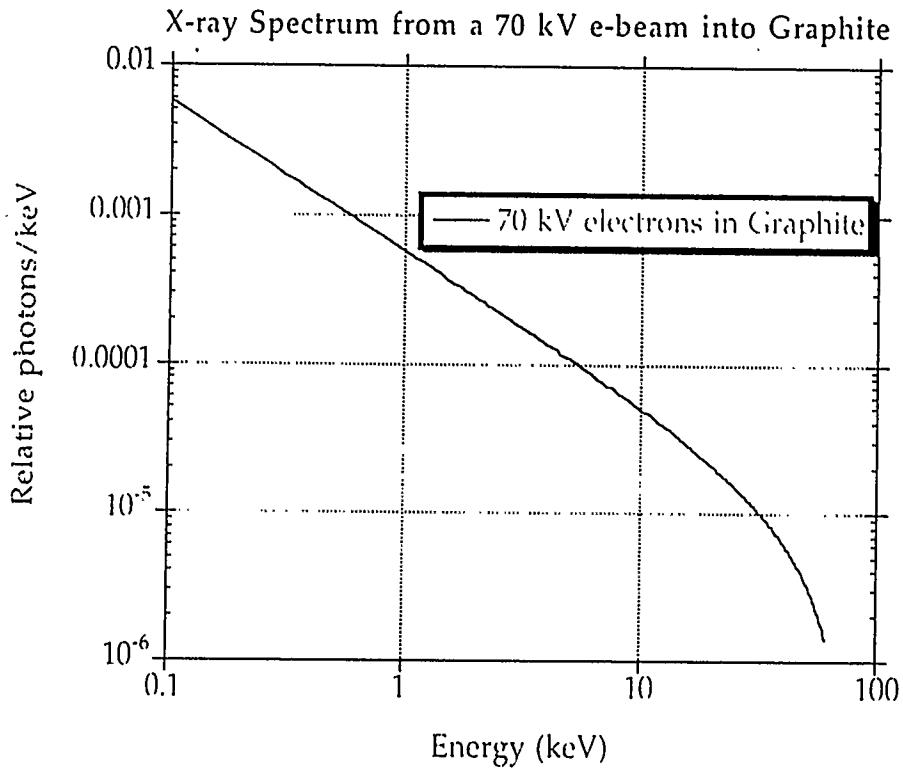

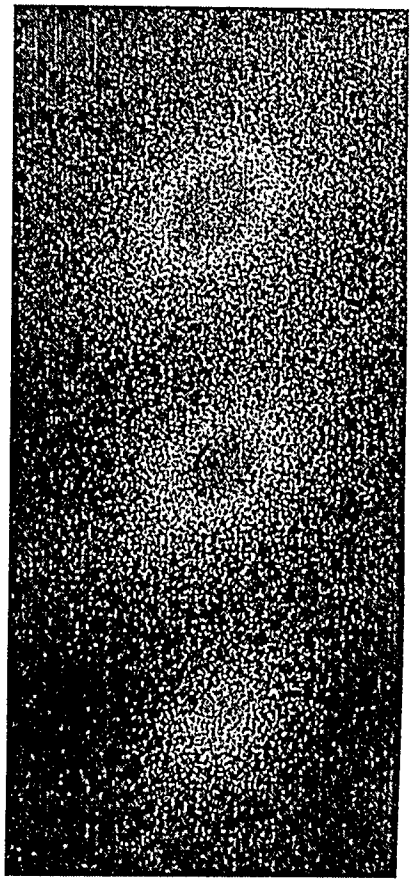

We designed an x-ray pinhole camera array to attempt to infer the incident *electron spectrum* and *spatial distribution* during a disruption.

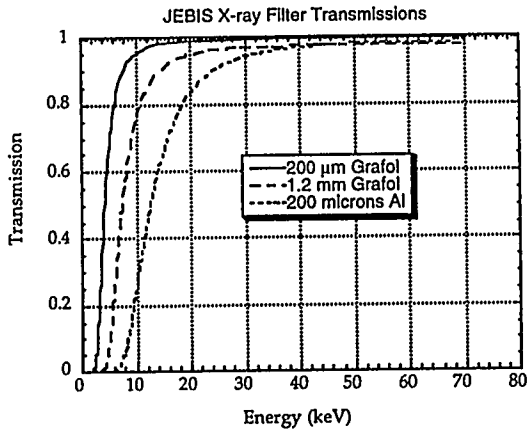

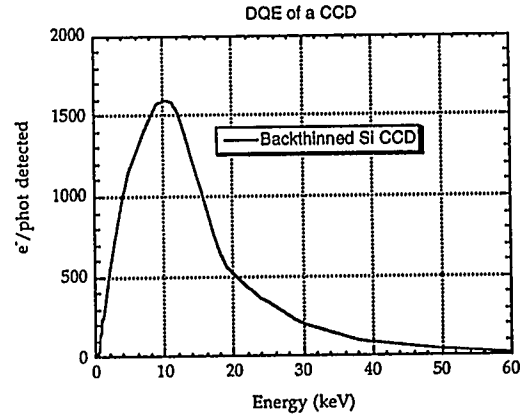

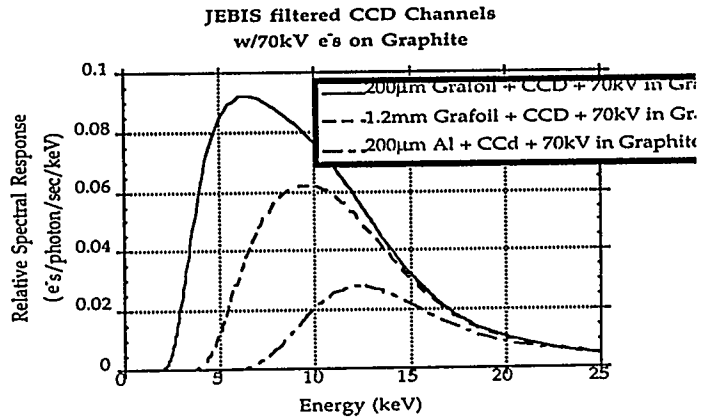

By measuring the ratios of the three signals with respect to one another we can:

1) approximatey reconstruct the incident electron energy spectrum, and

2) estimate the energy distribution in the impact area.

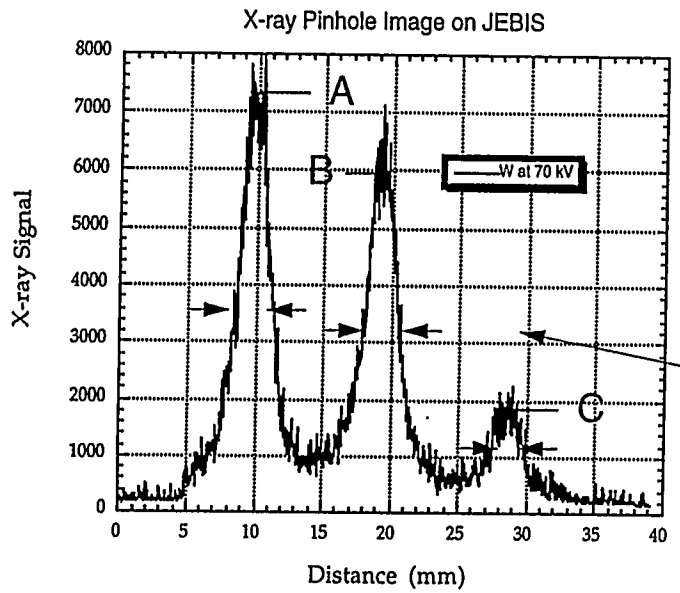

A/B
B/C
} yields inference of bremsstrahlung slope

FWHM for each filter yields estimate of electron energy distribution.

The pinhole geometry is a template for a more sophisticated in situ design within a Tokamak to infer disruption electron spectra.

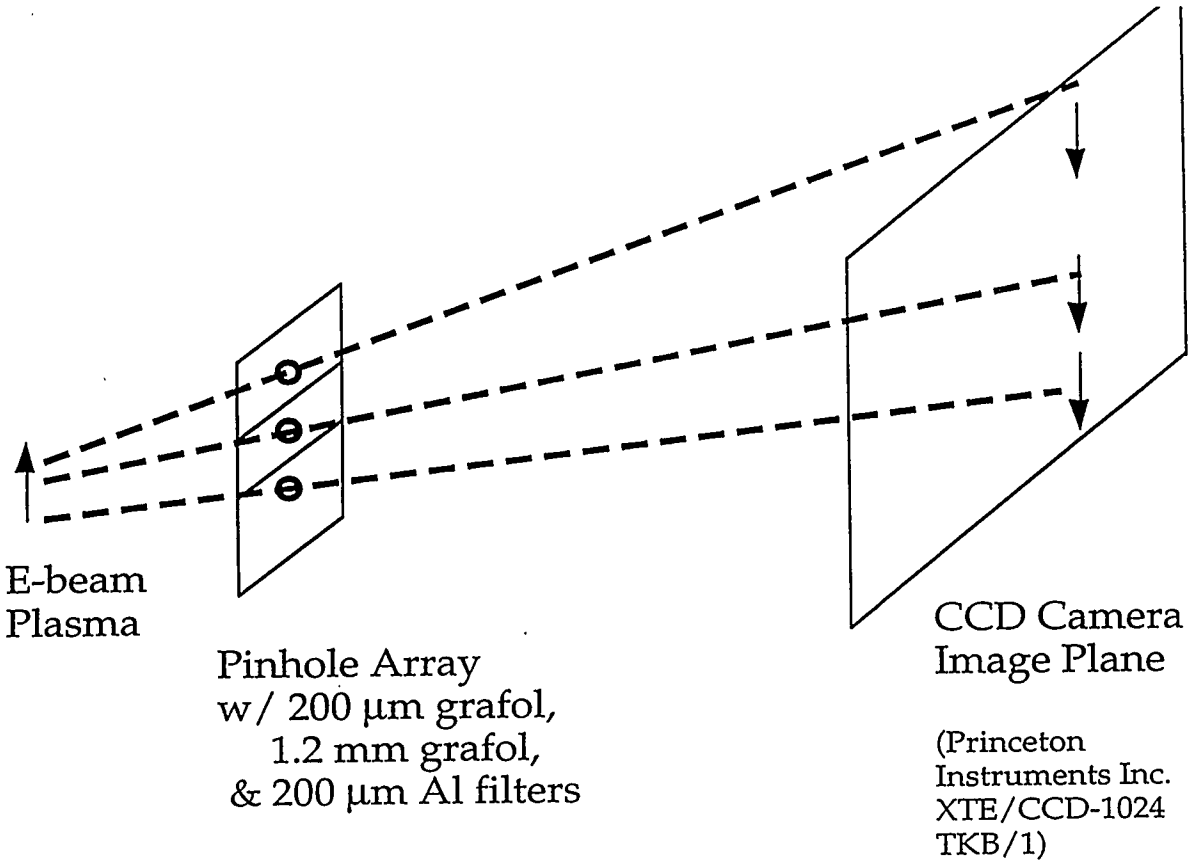

We chose to study a matrix of three materials and two different electron energies.

POCO Graphite	40 kV	70 kV
Molybdenum (sheet)	40 kV	70 kV
Tungsten (sintered and machined)	40 kV	70 kV

POCO Graphite with 70 kV electron irradiation:

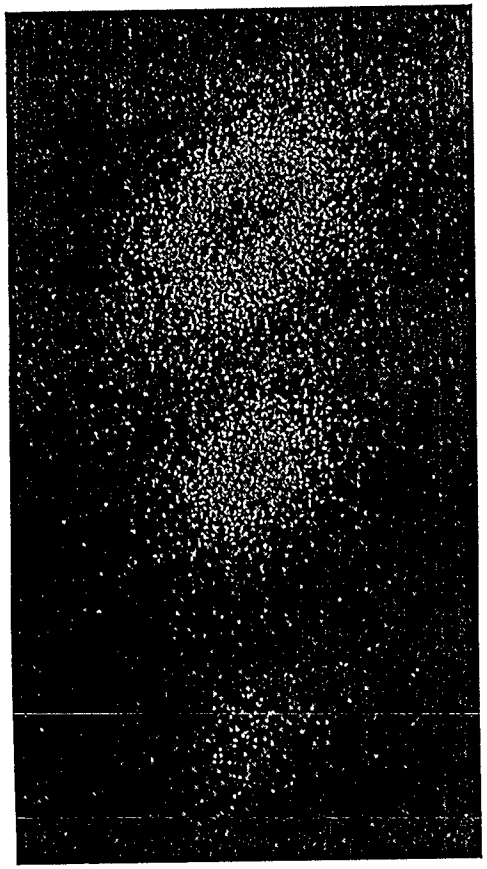

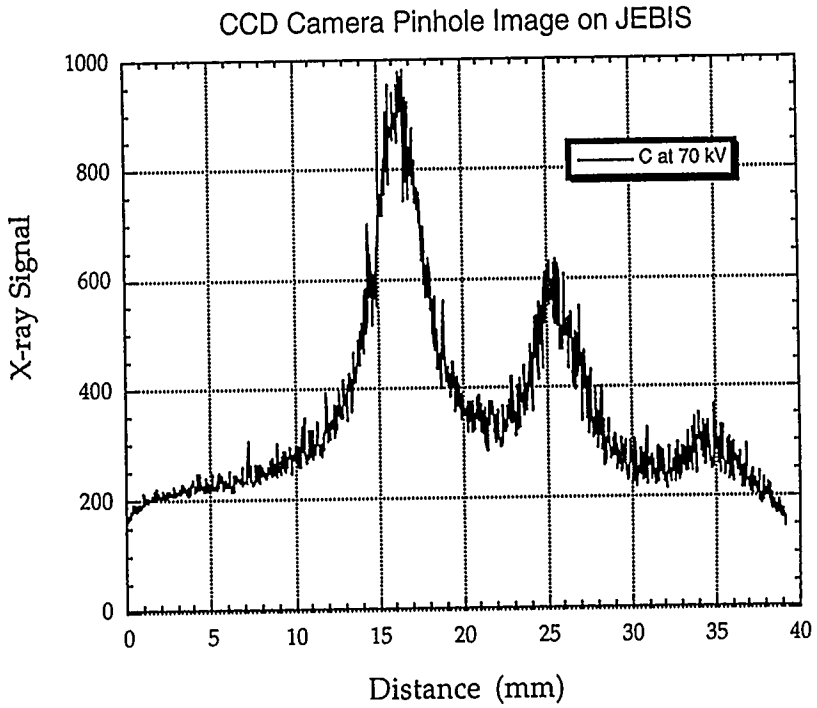

POCO Graphite with 40 kV electron irradiation:

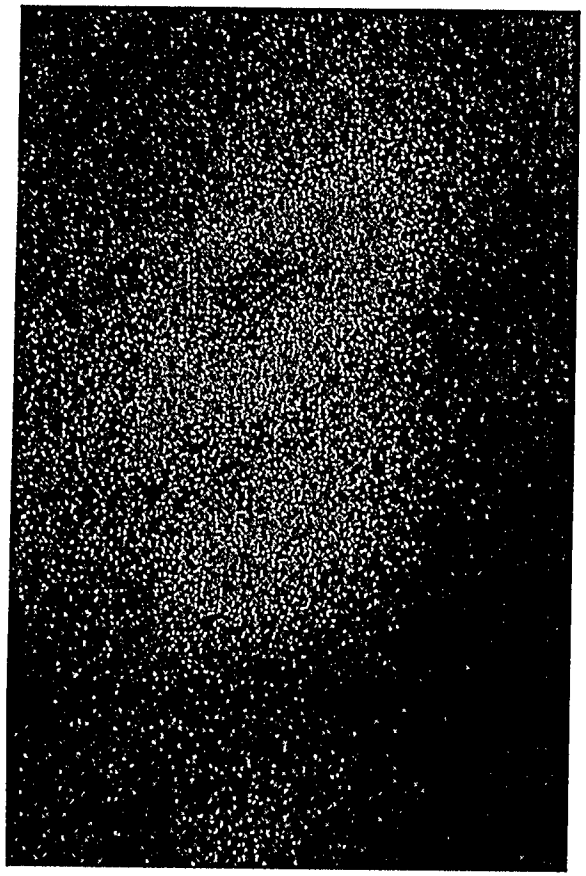

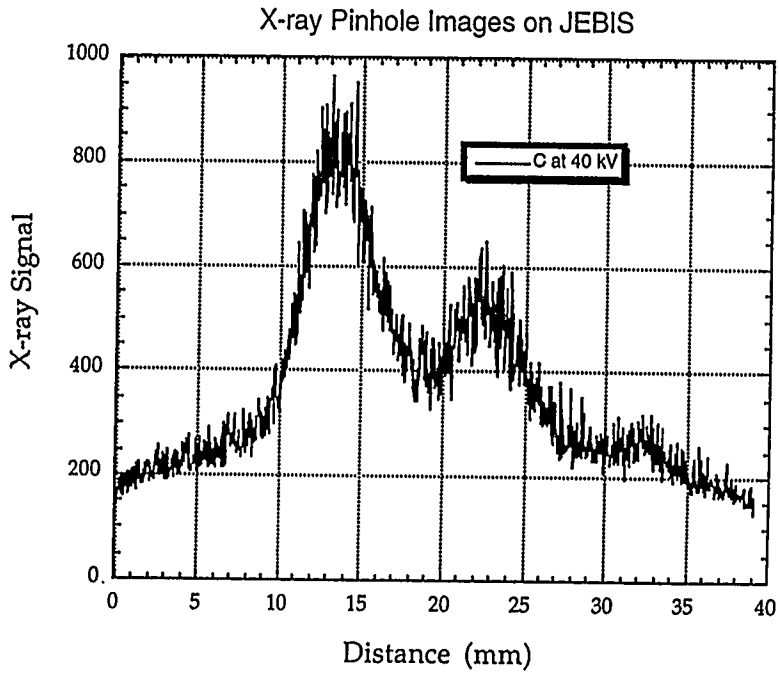

The circular electron beam was incident from above on the hypotenuse of a 45° wedge. When viewed from a side, the image appeared oval.

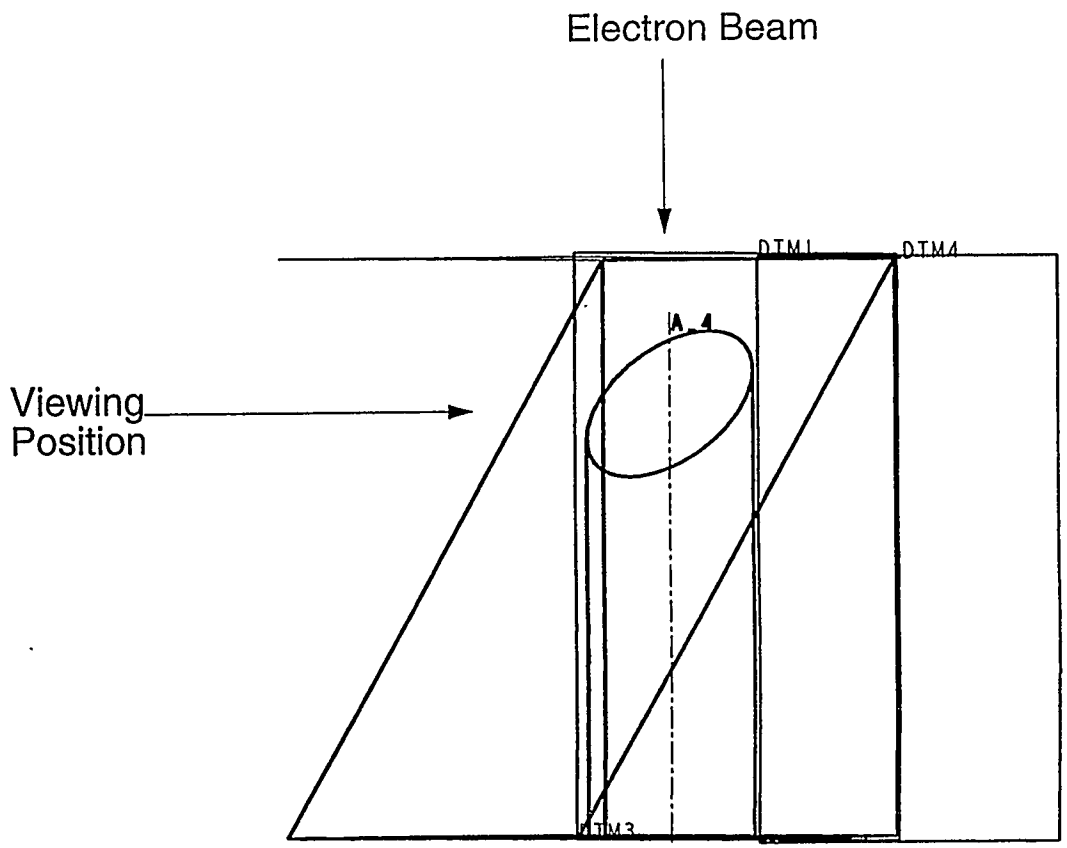

300 μm Mo sheet with70 kV electron irradiation:

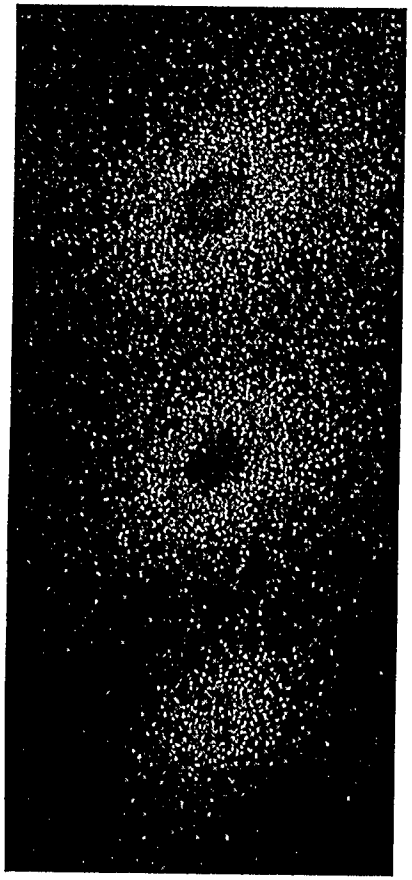

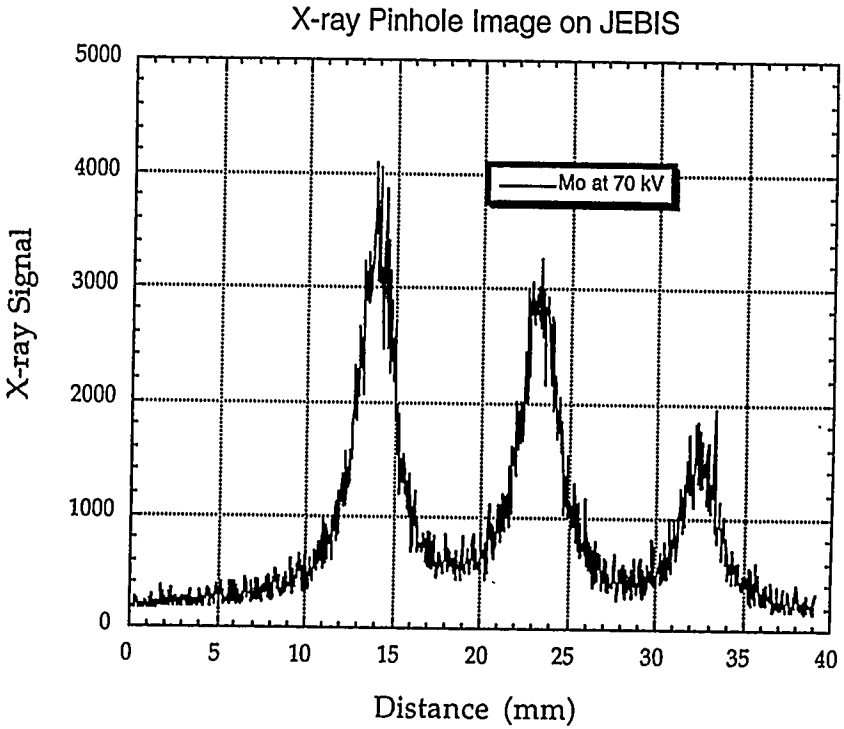

300 μm Mo sheet with 40 kV electron irradiation:

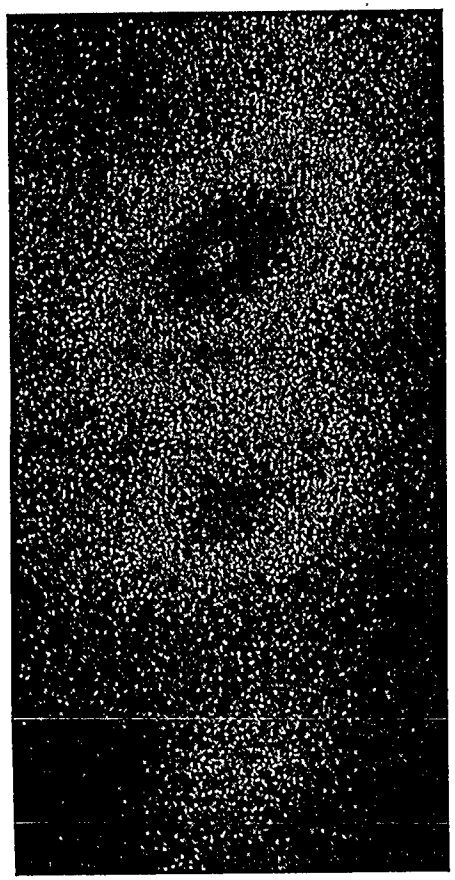

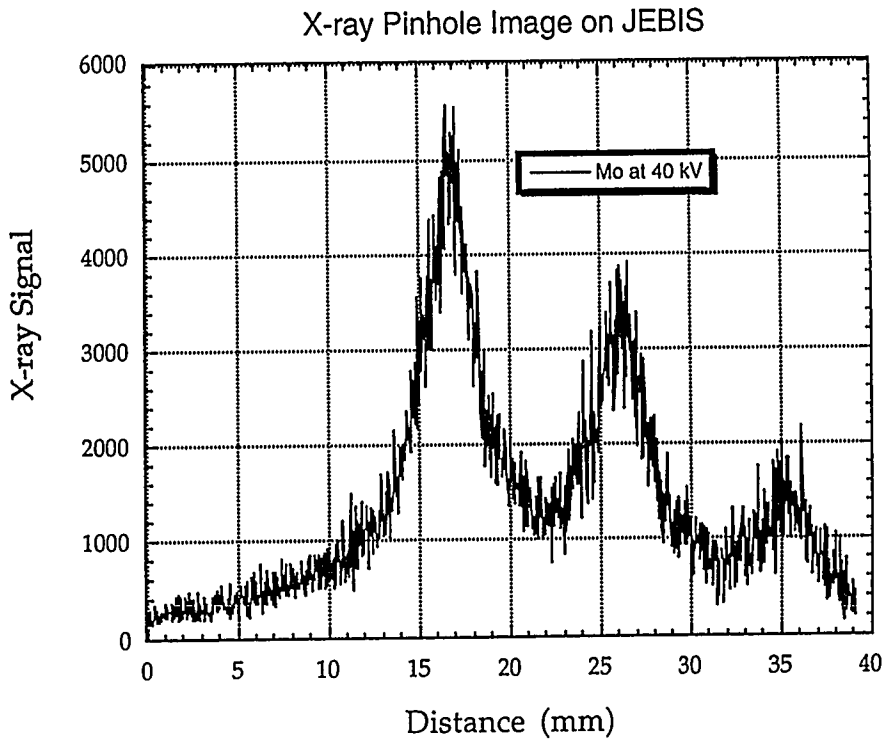

Tungsten with 70 kV electron irradiation:

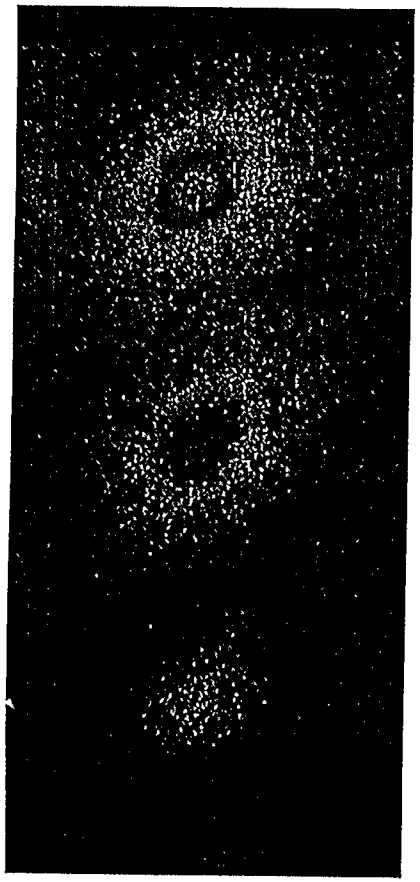

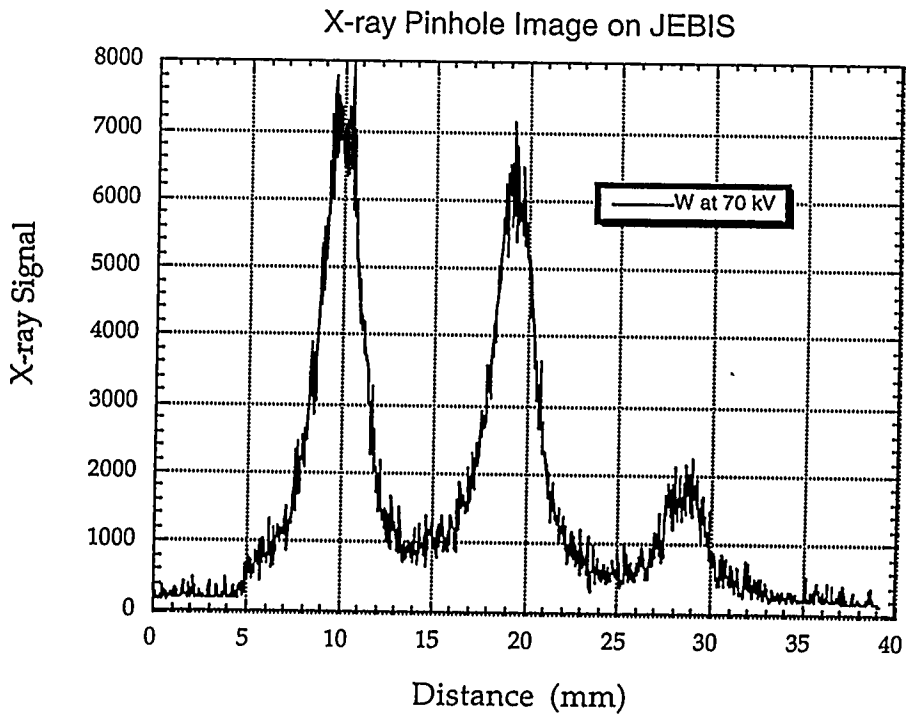

The closely spaced x-ray images can be unfolded using conventional spectroscopic techniques.

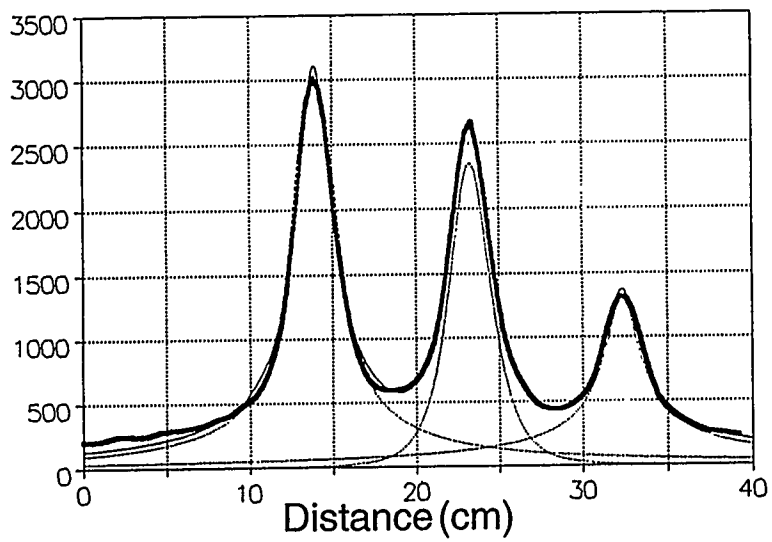

A peak-fitting routine has been used to calculate FWHM, as in this case with a Mo target at 70 kV.

Result is FWHM = 2.98 cm, 2.99 cm, and 3.19 cm respectively

An improved set of filters follows with their theoretical response to a 70 kV electron energy.

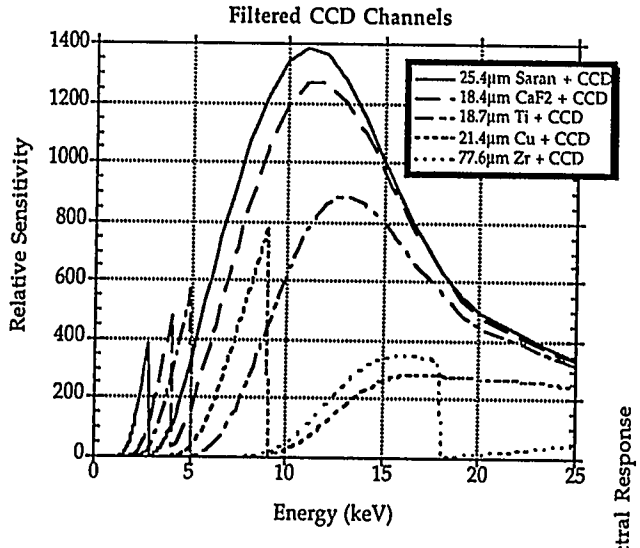

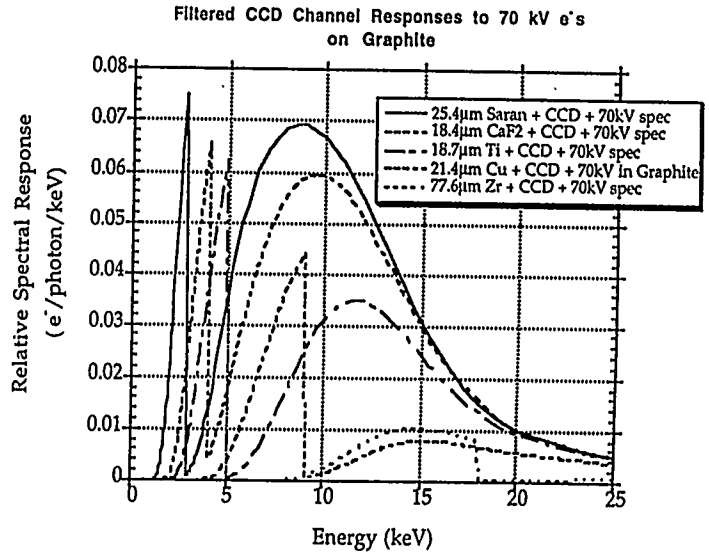

Filtered CCD Channel Responses to 40kV e⁻s on Graphite

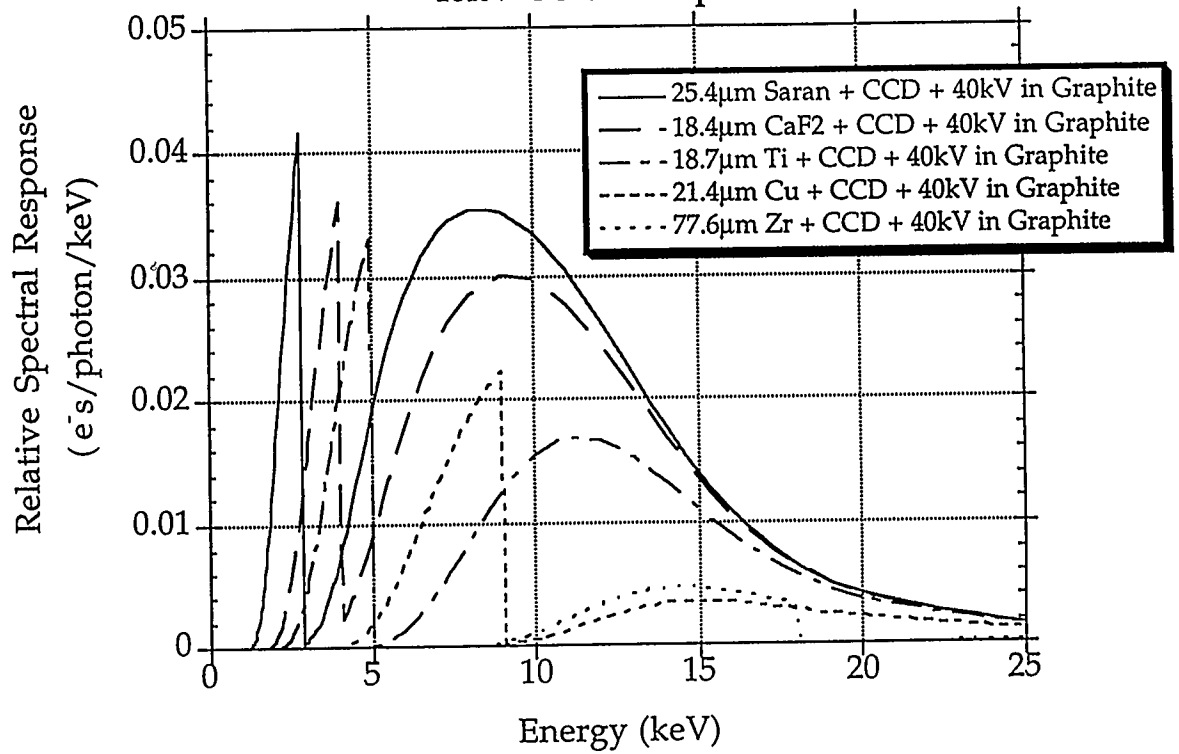

In response to the initial question of the utility of spectral x-ray imaging for disruption analysis, I answer as follows:

1. Given some a priori knowledge of the spectral shape one can infer electron spectra and energy distribution during a disruption.
2. The CCD response limits its usefulness to the measurement of relatively low electron energies (2-100 keV with a backthinned device).
3. At least four channels will be required for an estimate of temperature.

Session VII

Workshop Summary and Conclusion Viewgraphs

Compiled by

Robert Bastasz
Ahmed Hassanein
Tomoaki Hino
Richard Nygren
Michael Ulrickson
Robert Watson

Session II

PFC/PSI in Tokamak and Helical Devices

Summary Viewgraphs

Compiled by

R. Nygren

Summary of:

Session II

PFC/PSI in Tokamak and Helical Devices

Chaired by
R. Nygren and N. Yoshida

1.	PSI Under Long Pulse Operation in TRIAM-1M	Yoshida
2.	LID Experiments on CHS	Komori
3.	Study of Impurity Transport in LID Configuration in CHS	Masuzaki
4.	LID Design for LHD	Morisaki
5.	Wall Conditioning Scenario in LHD	Sagara
6.	PFC/PSI Studies in JT-60U	Saidoh
7.	Experience with the Tore Supra Phase III Outboard Pump Limiter	Nygren

Summary: PSI/PFC in Tokamak and Helical Devices

PSI Under Long Pulse Operation in TRIAM-IM (Yoshida, Kyasha)

- CX neutrals (0.5 - 3 KeV) produced significant sub-surface radiation damage to PFC armor materials inTRIAM-IM in ~ 10^{23} H/m^2.
- Codeposition and mixing of elements is likely to produce unexpected material forms on the surface of PFCs.

LHD Papers:

LID Design.for LHD	(Morisaki, NIFS)
CHS Experiments	(Komori, NIFS)
Wall Conditioning Scenario in LHD	(Sagara, NIFS)
Study of Impurity Transport in LID Configuration in CHS	(Masuzaki, NIFS)

- LHD design is specified and construction is proceeding. Operation in 1998 is planned. CHS experiments support LHD LID design.
- LID configuration produces changes in plasma parameters that increase the stored energy.
- Significantly increased pumping occurs with LID.
- IR data show power deposition away from leading edge of LID head.
- Several types of wall conditioning scenarios are being investigated, including development of alternative techniques, such as high power discharge cleaning between shots (with field on).

Summary: PSI/PFC in Tokamak and Helical Devices

PFC/PSI Studies in JT-60 (Saidoh ..., JAERI)

- Dueterated boronization ($He+D_2+H_{10}B_{14}$) produced (a) low Z_{eff}, (b) reduced oxygen levels in NB-heated plasmas for the first time, and (c) significant reduction in H/D in changeover experiments.
- Tritium (from D-D) is greater in divertor tiles than first wall and greater away from strike point than at strike point,
- Modified divertor with "W" configuration (central dome) and pumping behind baffle plates will be installed in early 1997.

Tore Supra High Het Flux Components (Nygren, Sandia)

- Tore Supra provides relevant experience with design, testing and operation of water-cooled PFCs.
- Observed hot spot due to sheath breakdown produced local increase of 2X in heat load; this may be important for design of future PFCs.
- A strategy is needed for monitoring PFCs for safe operation in ITER and LHD.
- Flaws in joining should be included in design and testing of PFCs; there should be a consistent treatment of joining flaws and QA procedures in design, testing, fabrication and qualification of PFCs.

Session III

Developments of High Heat Flux Components

Summary Viewgraphs

Compiled by

R. Watson

Summary of:

Session III

Developments of High Heat Flux Components

Chaired by K. Sato and R. Watson

1.	PFC Developments at JAERI	Sato
2.	Overview of US T-221 Activities	Watson
3.	Recent Results for Bonding S-65C Grade Be	Dombrowski
4.	Fundamental Aspects of Be Oxidation	Dombrowski
5.	Cu-Be Joining Tech	Cadden
6.	Materials & Joining Development for PFCs	Ting
7.	Structure, Properties & Performance of Plasma Sprayed Be	Castro
8.	Dev. of W Structures for PFCs	Davis
9.	T-222 R&D Activities	Youchison
10.	Divertor Mockup Design and Fabrication	Driemeyer
11.	Manufacturing of ITER PFCs	Yamazaki
12.	The CHF Experiment in Screw Tube	Sato
13.	Thermal Hydraulic Analysis of ITER	Zhan
14.	Post-CHF and LOFA Experiments at Sandia	Marshall

PFC Development

1. Armor Materials
2. Joining methods
3. HHF testing
4. CHF / thermal hydraulics
5. PFC monitoring

Armor Issues

- Does surface damage to PFCs from irradiation by CX neutrals pose a problem for LHD or ITER?
- What is the fatigue lifetime of Be and W coatings (pure and contaminated, W/Be, Be/W)?
- CX neutral irradiation may not cause additional problems in high erosion area, unless in low erosion area (e.g. blistering...)
- What is effect of resolidified metal layers (Be, W) on fatigue lifetime?
- What is optimum Be, W tile size (width)?

PFC / Cu Joining

- Simple strength tests (shear or tensile) are good for screening different joining methods. However, relationship between strength of joint and thermal fatigue lifetime is unclear.

- Measurements of joint ductility and toughness may provide a better understanding of fatigue lifetime because:

  - cyclic stresses are secondary,

  - flaws will be present at joint

Joining / Fabrication

1. What is the criteria for rating PFC bond quality?

   - strength?
   - ductility?
   - fatigue?
   - conductivity?
   - toughness?

2. What is correlation between mechanical tests and thermal fatigue results?

HHF Testing

Are small-scale e-beam mock-ups the primary screening method for determining preferred (joining) technique?

If yes, is there any important property for which this testing will not discriminate?

- Mechanical tests preferred for <u>initial</u> screening joining methods.
- Mechanical tests cannot replace HHF tests.
- However, HHF tests suffer from,
  - little creep damage
  - no neutrons
  - poor statistics
  - no EM forces
  - no combined disruptions + HHF
- Need improved NDE methods to eliminate HHF screening.
- Accelerated Creep with higher temps???

CHF / Thermal Hydraulics

- Experimental studies should be carried out so that complete heat transfer characteristics are known.

  - single phase flow
  - subcooling boiling
  - bulk boiling
  - CHF
  - corrosion test
  - parallel flow instabilities

- Need to downselect soon from:
  - twisted tape swirl flow
  - hypervapotron
  - porous coating
  - parallel fins
  - cross-cut fins
  - swirl rod insert

- Needs common basis for comparison:
  (figures of Merit)
  - $\frac{\text{CHF}}{\text{P.P.}}$
  - $\frac{\text{HT Coef.}}{\text{P.P.}}$
  - $\frac{\Delta P}{\text{P.P.}}$

→ Normal Flow

→ Accident (low) Flow

  - cost
  - stresses
  - corrosion

General

1) Develop strategies for monitoring of water cooled PFCs in LHD and ITER

2) Consider mixed material surfaces & impurities analyses of erosion and redeposition

Discussion of Strategy for Monitoring PFCs

Objective: strategy for design of PFCs diagnostics and philosophy of operation that provides safe operation.

Measurements: many techniques used but most imply large number of measurements.

Technique	Comment
1. IR monitoring	1a. Are all views available 1b. Cameras/ports overwhelming
2. TC's - calorimetry	2a. Many channels needed to locate hot spots
3. Strain gauges	3a. Operation in plasma may not work 3b. Too many s.q. required
4. Laser flash?	4 intermittent testing
5. Acoustic monitoring	5. Signal discrimination may not be well understood
6. Location tags of embedded elements	6. Volatization would show erosion or vaporization
7. In-situ inspection & metrology	7. High gamma-field effect on optics/electronics

Clear that some progress needs to be made toward this objective. Perhaps qualification testing of PFCs can produce some useful information for monitoring of PFCs during operation.

Group's General Comments

Focus on testing redeposited materials since this seems to be what will be in contact with plasma the majority of the time. Understand the structure and composition of the redeposited layer as well as its properties.

Is Cu - back plate safe from high energy charge exchange particles?

What are highest priority tasks for LANL Plasma Spraying Effort? Mockup fab? Mechanical and physical property Characteristics?

How select a W reference grade?

Selection of cooling option (heat transfer enhancement technique) for ITER divertor components completed in CY96.

Optimize wall conditioning for improved plasma performance in JT-60 (e.g. fast changeover D > H)

High heat flux fatigue lifetime of Be and W coatings.

Is transpiration cooling a viable approach to protect tungsten from melting during a disruption or ELM?

What tungsten microstructure is most resistant to thermal stresses or thermal shock?

What is the impact of porous coating process (1000° C) on properties of materials and thermal distortion of structure.

Does surface damage to PFCs from irradiation by CX neutrals pose problem for LHD or ITER?

Characterization of plasma-sprayed material (mechanical, thermal) irradiated, unirradiated

- Beryllium
- Tungsten
- Aluminum
- Graded Matls.

We assume plasma-sprayed material will behave like conventional process material.

What are the expected ITER operating conditions and operational requirements which must be met by the PFC's. Incorporate these requirements into a set of standards for prospective components. Also specify conditions not during plasma operation (bakeout, B fields present conditioning) so that no unexpected conditions are encountered during lifetime.

Consider mixed material surfaces and impurities in analyses of erosion and redeposition.

Impurity transport with LID configuration.

Development of new/alternative wall conditioning techniques for LHD (e.g. high power with field).

LID Experiments on CHS
The effect of the LID field itself is not clear.

Down selection of heat transfer enhancement schemes and development of <u>robust</u> CHF correlations.

Continuing cross checks or CHF correlations and results from various HHF facilities. Results need to be benchmarked in cross-testing so correlations can be standardized.

LID Design for LHD
The choice of materials for the divertor head, especially the plasma facing side (C/C or graphite).

Corrosion tests should be carried out for various channel geometries.

Develop strategies for monitoring of PFCs for safe operation in LHD and ITER.

Parallel channel flow instability for ITER vertical target and wing (if necessary) under abnormal operating conditions should be examined. Experimental studies which can help generate database for circular channel with twisted tape inserts and other channel geometries should be carried out so that complete heat transfer characteristics (single phase flow, subcool boiling, bulk boiling, and CHF) can be obtained.

The pumping speed at the position of the fast ion gauge is not clear.

Fabrication of real size (full size) mockup of the ITER divertor components, and shielding blanket module with the first wall.

What is the criteria for rating PFC bond quality? Strength? Ductility? Fatigue? Thermal conductivity?

Criteria for evaluating bond between beryllium to copper / beryllium to beryllium

- bond strength (4-pt bend, tensile, shear)
- interfacial energy
- fracture toughness
- others?

Standardized joining process evaluation / acceptance criteria. What is the correlation between mechanical testing and thermal fatigue results? Thermal fatigue is the ultimate objective.

What method should be used to rate PFC bonding performance?

Clearly define development path for silverless joining techniques for PFC armor to copper. What are downselect criteria?

Non-Ag brazing, if necessary, plasma facing material to copper heat sink, and D.A. of brazing parts.

Manufacturing aspects of ITER PFCs should be further addressed.

High heat flux fatigue lifetime and reliability of silverless Be/Cu joints.

Include joint flow analysis and QA in design and testing programs for PFCs.

Specifying manufacturing techniques for ITER divertor PFCs.

Thermal-hydraulic and thermo-mechanic tests for large size mockups with simulated boundary conditions.

LHD
Fabrication of the mechanical attached divertor module (introduced by Prof. Hino)

NDE criteria for bond joint interrogation
Maximum defect size criteria were presented based on thermal considerations. These are larger than those driven by fatigue and crack growth considerations. Work is needed to establish these more stringent defect conditions for the baseline ITER joining processes.

Are EBTS mock-ups the primary screening for determining preferred fabrication technique?
If yes - is there any important property for which this testing will not discriminate?

LHD
1. Develop new/alternative wall conditioning techniques for LHD (e.g. high power discharge cleaning)
2. Determine the effect of LID field on plasma performance and impurity transport.

Session IV

Plasma Surface Interactions and Plasma Facing Materials

Summary Viewgraphs

Compiled by

A. Hassanein

Summary of:

Session IV

Plasma Surface Interactions and Plasma Facing Materials

Chaired by A. Hassanein and Y. Hirohata

1.	PSI Studies at Hokkaido University	Hirohata
2.	Erosion and Gas Impurity Emission of B_4C Converted CFC	Tokunaga
3.	Reduced Be Erosion in PISCES-B	Doerner
4.	Be erosion and Compatibility with C and W as other PFM	Hirooka
5.	Erosion and Redeposition Analysis for ITER and DIII-D	Hassanein
6.	Arc Jets for PFC - HHFT	Skinner
7.	Further Studies of Thermally Collapsed Plasma	Skinner

PSI Studies at Hokkaido University

Major studies include:

1. Modeling of Disruption Erosion
2. Gas desorption / retention of various PFC
3. Effect of HE ion Impact Desorption
4. Lithium gettering properties
5. Analysis of Loss-of-coolant accidents.
6. Others

(3) Comparison : Effects of He Ion Impact Desorption

H^+ Fluence=5×10^{18} H/cm^2 Irrad.Temp.=RT
He^+ Bombardment: $(0.75\text{-}2.9) \times 10^{18}$ He/cm^2

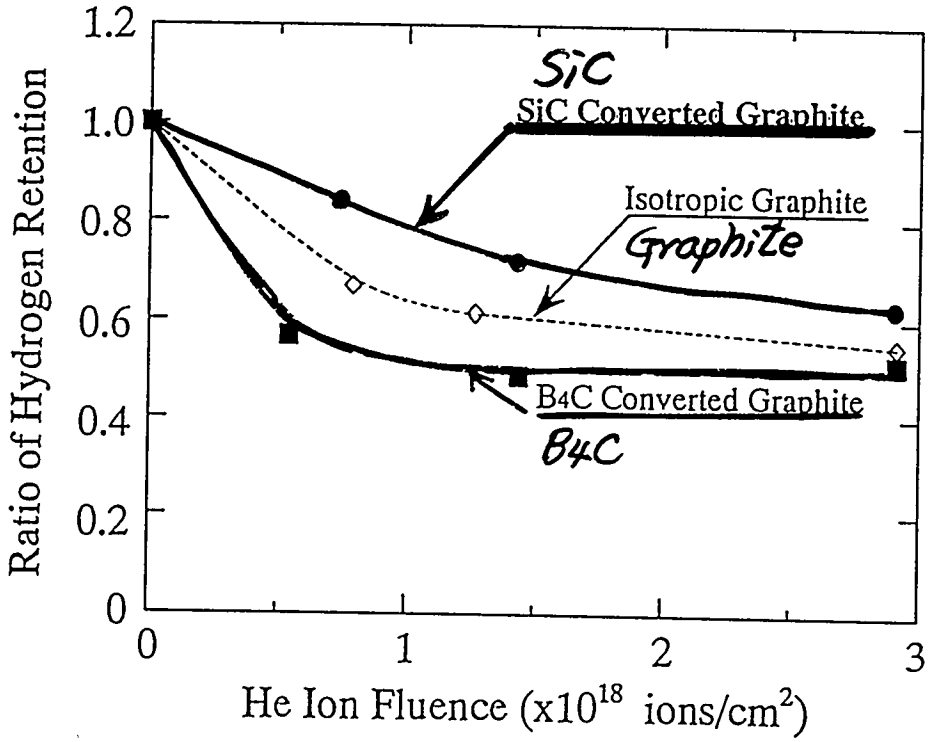

- **SiC Converted graphite**
  Ratio of decrease : not large
- B_4C Converted graphite
  very rapidly decresed
  largely reduced also by He ion impact

(5)Annealing Temperature Dependence of Hydrogen Retention

H^+ Fluence=5×10^{18} H/cm^2 Irrad.Temp.=RT

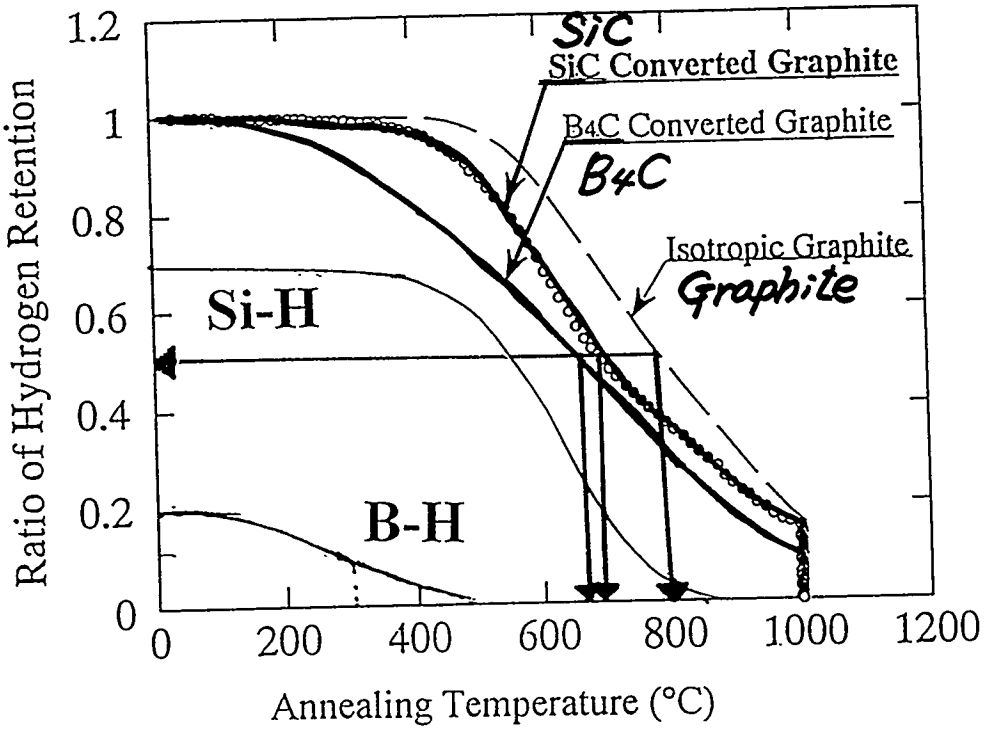

- **SiC Converted graphite**
  Temperature to become a half :
  ~100°C lower than that of isotropic graphite
  ⇩
  due to desorption of Si-H bondings

- B_4C Converted graphite : rapid decrese
  ⇩
  due to desorption of B-H bondings
  -10% removed by baking (300℃)

Erosion and Gas Impurity Emission of B_4C Converted CFC

- B_4C converted CFC tiles as divertor armor in JT-60 U showed good PMI performance
  - reduction of C and 0_2 impurities
- This reduction of impurities can be more enhanced by optimizing
  - B/C ratio
  - B_4C thickness
- This particular study evaluated HHFT of B_4C, emission of gases and particles, and resulting erosion damage.

Erosion of B_4C-conv. CFC by electron beam irradiation

B_4C(80 μm, B/C = 2.7)

B_4C (140 μm, B/C = 3.9)

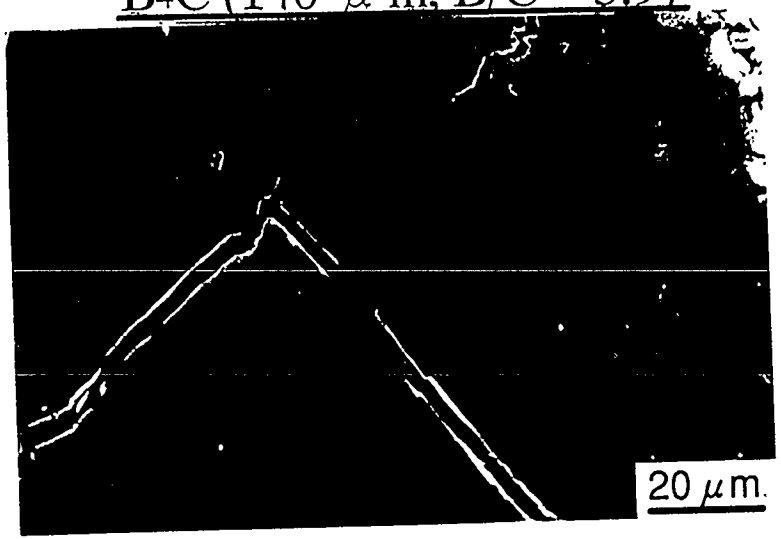

Cross sectional view during irradiation
B_4C (140 μm, B/C = 3.9)

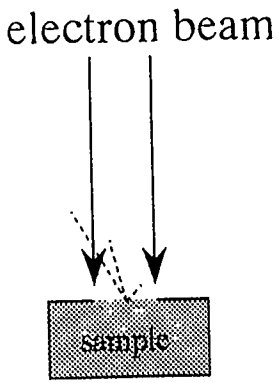

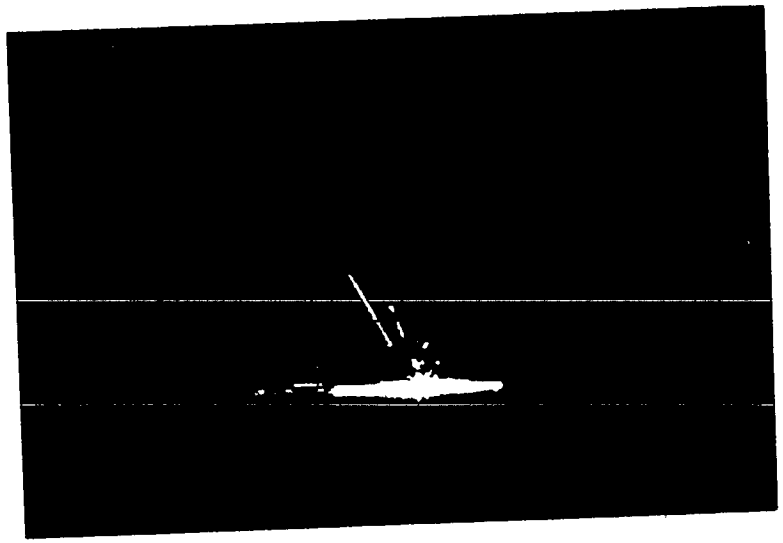

Summary

High heat loading experiments using an electron beam were carried out to evaluate the high heat load resistance of the B_4C converted CFC in the view point of materials damage and gases and particle emission.

(1) The surface temperature of the B_4C converted CFC during the electron beam irradiation was higher than that of the CFC. This is expected to be due to lower thermal conductivity of the B_4C converted layer.

(2)On the other hand, increase of the vacuum pressure for the B_4C converted CFC was about 1/5 of that of the CFC. Peak of partial pressure of H_2O and CO_2 for the B_4C converted CFC was 1/5 and 1/10 of that of the CFC, respectively.

(3)When the surface layer of the B_4C was melt, the vacuum pressure decreased comparing with that of before the irradiation. It is confirmed that getter effect due to evaporated B occurred.

(4)The present results suggest that a B/C ratio and thickness of B_4C layer should be optimized to control the surface temperature increase by heat load.

PISCES-B Be Erosion Experiments

1. "Protective" impurity coatings form on Be surfaces bombarded by plasma at elevated surface temperature (T_s > 250° C).

2. Net erosion of samples exposed at high temperature can be reduced by large factors (10 - 100) depending on the plasma impurity content.

3. Can these coating be controlled/manipulated to maximize their benefits in a tokamak environment?

Erosion of Be, C, W by D-plasma bombardment

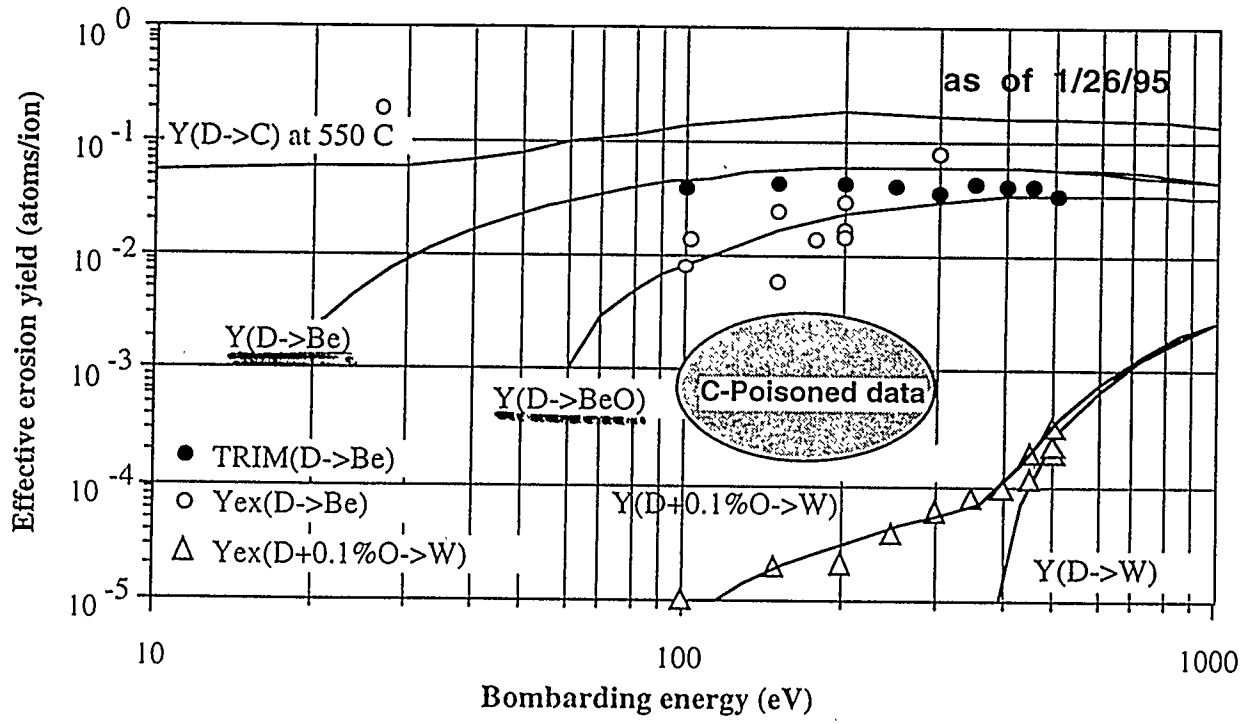

Remarks: Y(D->C at 550C) after Roth (IPP, Garching)
Y(D->BeO) after Eckstein (IPP, Garching)

after Y.Hirooka et al. Fusion Tech. 26(1994)540. (Proc. ANS Topical Meeting on the Technology of Fusion Energy, Jun 19-23, 1994, New Oriens)

FERP-UCSD

Yoshi

Conclusion

1. Materials "communication" is NOT always two-way street.

2. W is likely to stay "clean" while it poisons Be and C.

3. Be and C can poison each other, forming (Be+C) surface layers, which have reduced erosion relative to pure Be and C. However, C-poisoning over Be can lead to an increase in T-inventory.

4. Non-normal incidence makes poisoning less likely. Also, multiple-charged impurities are not likely to poison other surfaces due to their high self-sputtering yields.

Materials exchange diagram

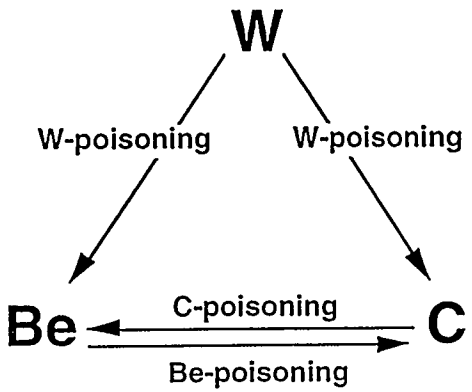

FERP-UCSD

Yoshi

Erosion and Redeposition Analysis for ITER and DIII-D

- Erosion/redeposition process is critical to ITER divertor performance. Data generation and modeling is a critical need for ITER.
- Low-Z materials (Be,C) have much higher erosion rates than the high-Z materials (W) for ITER plasma conditions.
- Net erosion rates for vertical divertor is much lower than gas-bag design. Tritium co-deposition in carbon is high (results are uncertain).
- Plasma radiation seeding may not work for low-Z materials.
- Good agreement of modeling work with DIMES experiments.

Proposal to Use Arc Jets for PFC High Heat Flux Testing

- Present E-beams, neutral beams, linear plasma, etc. Have low duty factor and low hydrogen fluence for full life testing of large scale prototypes.
- Hydrogen arc jets do exist in the US and can be used for various needed divertor testing.
- The use of arc jets for fusion would be a cooperative effort between US government agencies.

Comparison of devices

	ITER requirement	Arc Jet capability
Characteristics		
Power input (MW)	~100 MW to SOL	to 110 MW
Enthalpy (MJ/kg)	3 (midplane)	1 to 400
Peak heat flow (GW/m^2)	2 ($B_{\parallel\text{-SOL}}$)	0.05 -> 20 (axial)
Plasma flow	?	to above Mach 10
T_e, T_i	1-2 eV desired	1-2 eV obtained
Power to side walls (MW/m^2)	turbulence desired	turbulence 0.1
Pulse length (minutes)	15	> 25
Pulses	10,000 in life	1000/year
Cyclic heat load (Hz)	0.1 (sweeping)	TBD
Hydrogen content	90H-10He	to 100%
Chemical erosion	expected	observed
Test area (m^2)	~60	3
Plasma width (m)	~ 0.1	0.05 -> 2 m
Conductance (m^3/s)	depends on gas	>1000 m^3/s
Pumping speed (m^3/s)	500	> 500
Pressure recovery	10 μ - 0.05 atm	yes, to 1 atm
Throughput (kg/s)	0.20	0.1-10.0
Throughput (atoms/sec)	5×10^{24}	->2×10^{26}

*Possible Elm and disruption testing via pulsed bias

Note: Arcjets have no magnetic field and hence are not suitable for testing the ITER divertor physics that occurs where the plasma is fully ionized. But one ITER plan is to promote plasma recombination away from the divertor plate. Then the physics of the hot, partially ionized plasma gas streams are similar. Navier-Stokes equations are being used to model both the ITER plasma gas and arcjet plasmas.

Studies of Thermally Collapsed Plasmas

- Heat loads will be severe if standard (attached) tokamak operational modes occur.
- Steep temperature and electric potential steps (a detached plasma state) is achieved by operating at increased neutral pressure, plasma density, and divertor depth.
- Present tokamaks (e.g. C-mod), are operating in regimes where these conditions may be found.
- Basic physics processes that cause this thermal collapse are not well understood.
- Studies are underway to examine whether these modes can be useful to ITER.

Bifurcation- He discharge with Input Power decreasing in time, Dsp 7.0 in at various press

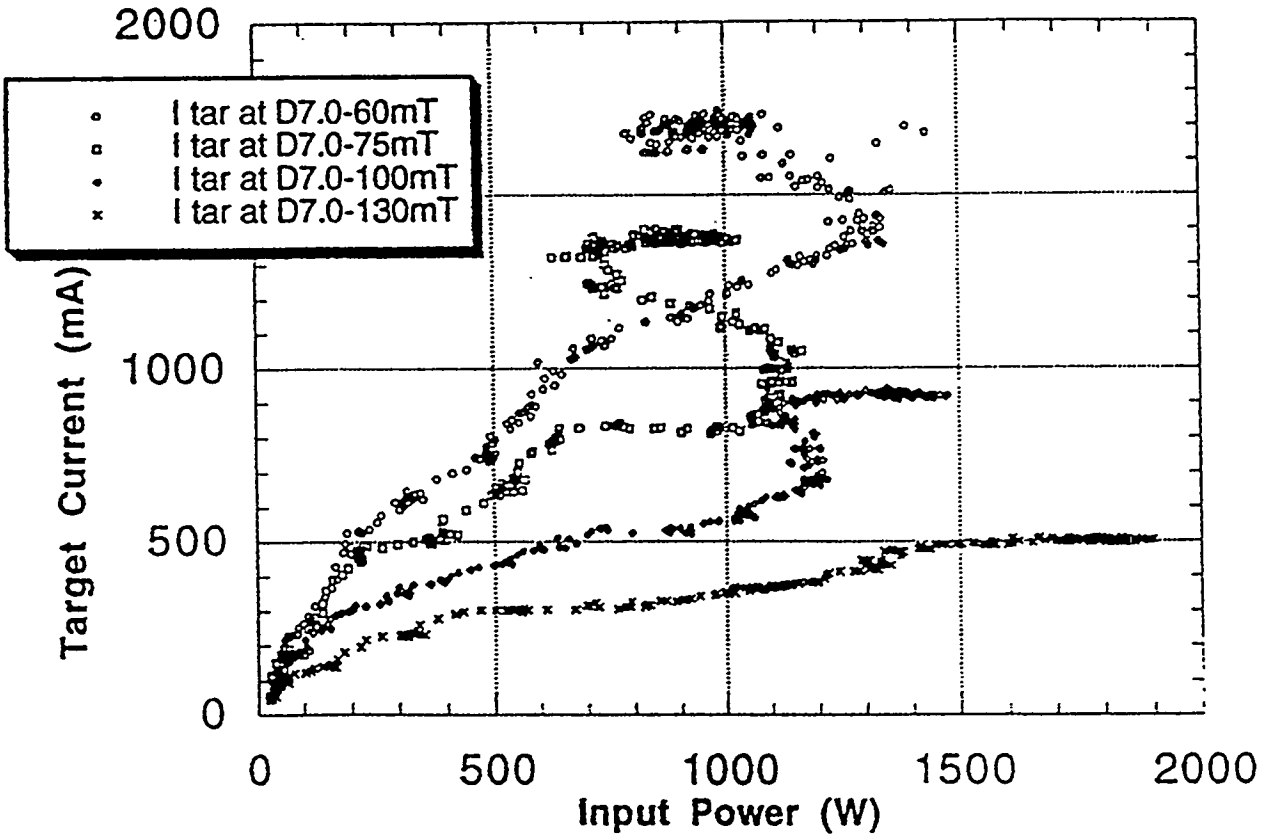

General Concerns/Comments

- Impurity Content and its effect on PFC
  - T - inventory
  - Disruption erosion
  - Sputtering erosion

- Melt-layer erosion during disruptions and other plasma instabilities.

- Further analysis of vapor shielding effect during thermal quench disruptions.

- DiMES experiments (erosion and disruption) are very important to continue.

- Coupling modeling codes (disruption and sputtering erosion to existing machines and facilities are important to ITER.

- Concerns about the use of mixed materials for ITER includes:
  - Actual erosion
  - Plasma contamination
  - Lack of existing data

Sessions IV, V, and VI

Plasma Surface Interactions and Plasma Facing Materials

Tritium

Material Damage

Summary Viewgraphs

Compiled by

R. Bastasz

Summary of:

Session V
Tritium

Chaired by
B. Odegard and M. Saidoh

1.	Study of Tritium Retention in Graphite by Simulating First Wall Circumstance	Saidoh
2.	Measurements of Tritium Recycling and Retention on TFTR	Skinner
3.	Graphites: Erosion and Retention	Davis
4.	Results from TPE	Bastasz

Session VI
Material Damage

Chaired by
R. Bastasz and A. Sagara

1.	Damage of PFMs Due to Low Energy Hydrogen	Yoshida
2.	Low Cycle Thermal Fatigue Damage of Be	Watson
3.	Recent Results from the DiMES Experiment	Bastasz
4.	Recent Results of Comprehensive Plasma Disruption Modeling and Simulation	Hassanein
5.	Utility of X-ray Imaging for Disruption Analysis	Rockett

Summary of Working Group Session On

- Plasma Surface Interactions & Plasma Facing Materials
- Tritium
- Material Damage

Participants:

N. Yoshida
C. Skinner
M. Saidoh
A. Sagara
P. Rockett
B. Odegard
Y. Hirooka
Y. Hirohata
A. Hassanein
J. Davis
R. Bastasz

Issues:

- Wall conditioning
- Erosion during normal operation
- Mixing of PFM / impurities
- Melt layer erosion during disruptions
- Thermal fatigue cracking
- Tritium inventory in co-deposited layers

Research Needs

PSI & PFM

1. Effects of O and CO impurities on tungsten
2. Mixed material properties (Be, C, W)
3. Steady state erosion / deposition measurements
4. Probe studies in machines (DIII-D, LHD)
5. Model benchmarking
6. Isotope effects in graphite co-deposition
7. Beryllium / carbon erosion rate measurements
8. Carbon erosion at very low particle energies
9. Characterization of disrupting plasmas near PFMs
10. Technique development as needed for above work

Tritium

1. Studies of tritium co-deposition
2. Mixed material effects on tritium inventory
3. Active control of tritium inventory

Material Damage

1. Modeling and measurement of melt layer erosion
2. Assessment of low-cycle thermal fatigue cracking (metals)
3. Effects of mixed materials on vapor layer properties
4. Characterization of melt layers at inclined angles

Summary of Material Damage Presentations

1. "Damage of PFM Due to Low-Energy H Ion Irradiation"
   N. Yoshida, et al.

   Damage Characteristics:

	Microstructure	H Trapping
Be:	Bubbles, cavities	very strong, above 900 K (no hydrid)
Mo:	I-loops, tangled dislocations	no trapping above 473 K
W:	Less damage, a few I-loops, cavities	no trapping above 473 K

   W shows good performance, Be has many problems

2. "Low-Cycle Thermal Fatigue Damage of Be"
   R. Watson, et al.

   - Novel technique using swept 30 Kw d-beam used to test 17 beryllium materials
   - S-65C (low oxygen) had best combined resistance to crack initiation and propagation.

3. "Recent Results From the DiMES Experiment"
   R. Bastasz, et al.

   Disruption Studies

   - Measurements of incident particles on the DIII-D divertor indicate an average energy of 100 V during AR-induced disruption
   - Disruption model suggests that cold neutral layer reduces divertor heat load by 30%

Erosion Measurements

- Net erosion beneath strikepoint during normal H-mode plasmas is:

C	≈	4 nm/s
Be, V, Mo	<	1 nm/s
W	<	0.1 nm/s

4. "Recent Results of Comprehensive Plasma Disruption Modeling and Simulation"
   A. Hassanein

   - Kinetic multispecies radiation transport model has been added to A* THERMAL-S code

   - Model includes: Target thermodynamics with phase change developed vapor-cloud magnetohydrodynamics time-dependent photon radiation transport field

   - Erosion from surface vaporization is determined in self-consistent way including all of the above physical processes

   - Disruption simulation experiments in good agreement with model

5. "Utility of X-Ray Imaging for Disruption Analysis"
   P. Rockett

   - Designed x-ray pin-hole camera array to measure incident e-spectrum and spatial distribution during a disruption

   - System tested in JEBIS using 3 materials (C, Mo, W) and 2 e-energies (40, 70 kV)

- Results encouraging and indicate technique is useful, especially with
  - a prior knowledge of spectral shape
  - low electron energies (2-100 KeV perhaps)
  - four channels to estimate temperature

Questions

1. Q: Can the TDS peaks be explained?
   A: Yes, peaks attributed to release from vacancy clusters, cavities, and other damage have been identified.

   Q: Any evidence for beryllium hydride formation?
   A: No.

2. Q: Tested plasma-sprayed beryllium?
   A: No, haven't received samples yet.

   Q: Did you try to measure crack growth rate?
   A: No.
   COMMENT: The B-W grades are actually rather anisotropic

3. Q: Have parametric studies been made to see if uncertainties in plasma parameters can account for discrepancy between data and model?
   A: Yes, it will account for some of the discrepancy.

   Q: Is carbon present on the metal surfaces after exposure?
   A: Yes, but some may also be due to environmental contamination.

   Q: Does surface roughness affect measurements?
   A: Possibly, but can use implant standards to check.

4. Q: Why is vapor cloud so energetic?
   A: Because shortly after disruption starts, vapor-cloud will completely stop plasma particles and absorb all of its energy. Vapor cloud can then damage other components, so vapor shield doesn't eliminate disruption damage.

5. Q: Does slow CCD response give temporal average?
   A: Yes, CCD averages both temporally and spatially

   Q: How does spot size of view compare with e-beam size?
   A: They are similar.

   Q: Could technique be used in 40 KV e-beam facility at SNL?
   A: Yes.

   Q: What are effects of surface contamination on measurements made on actual PFCs?
   A: Could be a problem.

Appendix A

Workshop Agenda

Agenda

US-Japan Workshop, Q219
High Heat Flux Components and Plasma Surface Interactions for Next Fusion Devices

January 9-11, 1996
Colorado Springs, Colorado

Tuesday
9-January-96

Session I	**Welcome, Organization and Overviews** ***Chaired by: T. Hino and M. Ulrickson***	
8:00	I-1. Opening	**T. Hino/M. Ulrickson**
8:10	I-2. Japanese Activities for PFC/PSI	**T. Hino**
8:20	I-3. US Activities for PFC/PSI	**M. Ulrickson**
Session II	**PFC/PSI in Tokamak and Helical Devices** ***Chaired by: R. Nygren and N. Yoshida***	
8:30	II-1. PSI Under Long Pulse Operation in TRIAM 1M	**N. Yoshida**
8:50	II-2. LID Experiments on CHS	**A. Komori**/O. Motojima
9:10	II-3. Study of Impurity Transport in LID Configuration in CHS	**S. Masuzaki**/O. Motojima
9:30	II-4. LID Design for LHD	**T. Morisaki**/O. Motojima
9:50	II-5. Wall Conditioning Scenario in LHD	**A. Sagara**/N. Noda/ N. Ohyabu/O. Motojima
10:10	**Break**	
10:30	II-6. PFC/PSI Studies in JT-60U	**M. Saidoh**
10:50	II-7. Experience with the Tore Supra Phase III Outboard Pump Limiter	**R. Nygren**

Tuesday
9-January-96

Session III	**Developments of High Heat Flux Components** ***Chaired by: K. Sato and R. Watson***	
11:10	III-1. PFC Developments at JAERI	**K. Sato/M. Akiba**
11:30	III-2. Overview of US T-221 Activities	**R. Watson**
11:50	**Lunch**	
1:00	III-3. Recent Results for Bonding S-65C Grade Be to Copper Alloys	**D. Dombrowski/D. Butler**
1:20	III-4. Fundamental Aspects of Be Oxidation and Implications for Fusion Experiments	**D. Dombrowski**
1:40	III-5. Copper-Beryllium Joining Technology	**C. Cadden/W. Bonivert/ B. Odegard/R. Watson**
2:00	III-6. Materials and Joining Development for Plasma Facing Components	**J. Ting**
2:20	III-7. Structure, Properties and Performance of Plasma Sprayed Beryllium	**R. Castro/P. Stanek/ K. Elliott/A. Bartlett/ D. Youchison/ R. Watson/D. Walsh**
2:40	III-8. Development of Tungsten Structures for PFCs	**J. Davis/K.Slattery/ M.Ulrickson**
3:00	**Break**	
3:20	III-9. T-222 R&D Activities	**D. Youchison**
3:40	III-10. Divertor Mockup Design and Fabrication	**D. Driemeyer**
4:00	III-11. Manufacturing of ITER Plasma Facing Components	**S. Yamazaki**
4:20	III-12. The CHF Experiment in Screw Tube	**M. Araki/K. Sato**
4:40	III-13. Thermal Hydraulic Analyses of the ITER Divertor High Heat Flux Components	**N. Zhan**
5:00	III-14. Post-CHF and LOFA Experiments at SNL	**T. Marshall**
6:30	**Reception - The Sheraton Garden Atrium**	

Session IV	**Plasma Surface Interactions and Plasma Facing Materials** ***Chaired by: A. Hassanein and Y. Hirohata***	
8:00	IV-1. PSI Studies at Hokkaido University	**Y. Hirohata**/T. Hino
8:20	IV-2. Erosion and Gas Impurity Emission of B_4C Converted CFC by High Heat Load	**K. Tokunaga**/Y. Yoshida
8:40	IV-3. Beryllium Erosion and Compatibility with Carbon and Tungsten under DT-Plasma Bombardment	**Y. Hirooka**
9:00	IV-4. Observation of Reduced Beryllium Erosion in PISCES-B PSI Experiments	**R. Doerner**
9:20	IV-5. Erosion and Redeposition Analysis for ITER and DIII-D	J. Brooks/**A. Hassanein**
9:40	IV-6. Arc Jets for PFC High Heat Flux Testing in a Reactive Hydrogen Environment	**S. Cohen**/T. Munsat/ J. Balboni
10:00	**Break**	
10:20	IV-7. Further Studies of Thermally Collapsed Plasmas	**S. Cohen**/J. Park
Session V	**Tritium** ***Chaired by: B. Odegard and M. Saidoh***	
10:40	V-1. Study of Tritium Retention in Graphite by Simulating First Wall Circumstance	S. O'hira/K. Okuno/ **M. Saidoh**
11:00	V-2. Measurements of Tritium Recycling and Retention on TFTR	**C. Skinner**
11:20	V-3. Graphites: Erosion and Retention	**J. W. Davis**
11:40	V-4. Results From Tritium Plasma Experiment	**R. Bastasz**/R. Causey
12:00	**Lunch**	

Wednesday
10-January-96

Session VI	**Material Damage** ***Chaired by: R. Bastasz and A. Sagara***	
1:20	VI-1. Damage of Plasma Facing Materials Due to Low Energy Hydrogen or Helium Ion Irradiation	**N. Yoshida**
1:40	VI-2. Low Cycle Thermal Fatigue Damage of Beryllium	**R. Watson**
2:00	VI-3. Recent Results From the DiMES Experiment	**R. Bastasz**
2:20	VI-4. Recent Results of Comprehensive Plasma Disruption Modeling and Simulation	**A. Hassanein**
2:40	VI-5. Utility of X-ray Imaging for Disruption Analysis	**P. Rockett**
3:00	**Break**	
3:20	**Working Group Sessions**	
7:00	**Group Dinner at Giuseppes Depot**	

Thursday
11-January-96

Session VII	**Working Group Session Summaries**	
8:00	PFC/PSI in Tokamak and Helical Devices	**N. Yoshida/R. Nygren**
8:20	Developments of High Heat Flux Components	**K. Sato/R. Watson**
8:40	Plasma Surface Interactions and Plasma Facing Materials	**Y. Hirohata/ A. Hassanein**
9:00	Tritium	**M. Saidoh/B. Odegard**
9:20	Material Damage	**A. Sagara/R. Bastasz**
9:40	Closing, Presentation of Next Meeting Site	**T. Hino/M. Ulrickson**

Appendix B

List of Participants and Addresses

List of Participants

Bob Bastasz
Phone: 510-294-2013
Fax: 510-294-3231

Sandia National Laboratories, MS9162
P. O. Box 969, Livermore, CA 94551
USA
e-mail: bastasz@ca.sandia.gov

Chuck Cadden
Phone: 510-294-3650
Fax: 510-294-3410

Sandia National Laboratories, MS9403
P. O. Box 969, Livermore, CA 94551
USA
e-mail: chcadde@sandia.gov

Rich Castro
Phone: 505-667-5191
Fax: 505-667-5266

Los Alamos National Laboratory, MSG-770
P. O. Box 1663, Los Alamos, NM 87545
USA
e-mail: rcastro@lanl.gov

Sam Cohen
Phone: 609-243-3185
Fax: 609-243-2160

Princeton Plasma Physics Laboratory
Princeton University, P. O. Box 451
Princeton, NJ 08543, USA
e-mail: scohen@pppl.gov

Jim Davis
Phone: 416-667-7868
Fax: 416-667-7799

Univ. of Toronto, Inst.for Aerospace Studies
4925 Dufferin Street, North York, Ontario
CANADA M3H 5T6
e-mail: jim@starfire.utias.utoronto.ca

John Davis
Phone: 314-233-6200
Fax: 314-234-4506

McDonnell Douglas
P. O. Box 516, St. Louis, MO 63166-0516
USA
e-mail: davis@lllsrv.mdc.com

Russ Doerner
Phone: 619-534-7830
Fax: 619-534-7716

University of California at San Diego
9500 Gilman Drive, Building 302
La Jolla, CA 92093-0035, USA
e-mail: rdoerner@fusion.ucsd.edu

Dave Dombrowski
Phone: 216-383-4007
Fax: 216-481-5480

Brush Wellman, Inc.
17876 St. Clair Ave., Cleveland, OH 44110
USA
e-mail: ddombrow@notes#@brush.geis.com

Dan Driemeyer
Phone: 314-232-7596
Fax: 314-234-4506

McDonnell Douglas
P. O. Box 516, St. Louis, MO 63166-0516
USA
e-mail: driemeyer@lllsrv.mdc.com

Ahmed Hassanein
Phone: 708-252-5889
Fax: 708-252-5287

Argonne National Laboratory
9700 S. Cass Avenue, Argonne, IL 60439
USA
e-mail: hassanein@anl.gov

List of Participants

Tomoaki Hino
Phone: 11-706-6660
Fax: 11-709-6413

Dept. of Nuclear Engineering, Hokkaido Univ.
Kita-13, Nishi-8, Kita-ku, Sapporo, 060
JAPAN
e-mail: tomhino@hune.hokudai.ac.jp

Yuko Hirohata
Phone: 11-706-7108
Fax: 11-747-7108

Dept. of Nuclear Engineering, Hokkaido Univ.
Kita-13, Nishi-8, Kita-ku, Sapporo, 060
JAPAN
e-mail: hirohata@hune.hokudai.ac.jp

Yoshi Hirooka
Phone: 619-534-9720
Fax: 619-534-7716

University of California at San Diego
9500 Gilman Drive, Bldg. 302
La Jolla, CA 92093-0035, USA
e-mail: yhirooka@fusion.ucsd.edu

Kendall Hollis
Phone: 505-665-8223
Fax: 505-667-5268

Los Alamos National Laboratory, MSG-770
P. O. Box 1663, Los Alamos, NM 87545
USA
e-mail: khollis@lanl.gov

Patricia Hubbard
Phone: 505-845-3306
Fax: 505-845-3130

Sandia National Laboratories, MS1129
P. O. Box 5800, Albuquerque, NM 87185-1129
USA
e-mail: pyhubba@sandia.gov

Keith Kahl
Phone: 423-574-0372
Fax: 423-574-9407

Oak Ridge National Laboratory, Eng. Tech. Div.
P. O. Box 2009, Oak Ridge, TN 37831
USA
e-mail: wwk@cosmail1.ctd.ornl.gov

Akio Komori
Phone: 572-57-5603
Fax: 572-57-5600

National Institute for Fusion Science
Shimoishi-cho-322-6, Toki-shi, 509-52
JAPAN
e-mail: komori@robin.nifs.ac.jp

Theron Marshall
Phone: 505-845-3136
Fax: 505-845-3130

Sandia National Laboratories, MS1129
P. O. Box 5800, Albuquerque, NM 87185-1129
USA
e-mail: tdmarsh@sandia.gov

Suguru Masuzaki
Phone: 572-57-5631
Fax: 572-57-5600

National Institute for Fusion Science
Shimoishi-cho-322-6, Toki-shi, 509-52
JAPAN
e-mail: masuzaki@roprint.nifs.ac.jp

Tomohiro Morisaki
Phone: 572-57-5622
Fax: 572-57-5600

National Institute for Fusion Science
Shimoishi-cho-322-6, Toki-shi, 509-52
JAPAN
e-mail: morisaki@roprint.nifs.ac.jp

List of Participants

Richard Nygren
Phone: 505-845-3135
Fax: 505-845-3130

Sandia National Laboratories, MS1129
P. O. Box 5800, Albuquerque, NM 87185-1129
USA
e-mail: renygre@sandia.gov

Ben Odegard
Phone: 510-294-2789
Fax: 510-294-3140

Sandia National Laboratories, MS9402
P. O. Box 969, Livermore, CA 94551
USA
e-mail: odegard@california.sandia.gov

Paul Rockett
Phone: 505-845-7466
Fax: 505-845-3130

Sandia National Laboratories, MS1129
P. O. Box 5800, Albuquerque, NM 87185-1129
USA
e-mail: pdrocke@sandia.gov

Akio Sagara
Phone: 572-57-5613
Fax: 572-57-5600

National Institute for Fusion Science
Shimoishi-cho-322-6, Toki-shi, 509-52
JAPAN
e-mail: sagara@rokudan.nifs.ac.jp

Masahiro Saidoh
Phone: 292-70-7430
Fax: 292-70-7449

JT-60 Group Japan Atomic Energy Research Inst.
Naka-machi, Naka-gun, Ibaraki-ken, 311-01
JAPAN
e-mail: saidoh@naka.jaeri.go.jp

Kazuyoshi Sato
Phone: 292-70-7552
Fax: 292-70-7558

NBI Group, Japan Atomic Energy Research Inst.
Naka-machi, Naka-gun, Ibaraki-ken, 311-01
JAPAN
e-mail: satohka@naka.jaeri.go.jp

Charles Skinner
Phone: 609-243-2214
Fax: 609-243-2418

Princeton Plasma Physics Laboratory
Princeton University, P. O. Box 451
Princeton, NJ 08543
USA
e-mail: cskinner@rax.pppl.gov

Peggy Stevens
Phone: 505-845-3133
Fax: 505-845-3130

Sandia National Laboratories, MS1129
P. O. Box 5800, Albuquerque, NM 87185-1129
USA
e-mail: plsteve@sandia.gov

Jyh-Ming Ting
Phone: 513-766-2020
Fax: 513-766-5886

Applied Sciences
P. O. Box 579, Cedarville, OH 45314-0579
USA
e-mail: jting@apsci.com

Kazutoshi Tokunaga
Phone: 92-573-9611
Ext. 517
Fax: 92-582-4210

Research Institute for Applied Mechanics
Kyushu Univ., Kasuga-Koen-6-1, Kasuga,
Fukuoka-ken, 816, JAPAN
e-mail: tokunaga@riam.kyushu-u.ac.jp

List of Participants

Mike Ulrickson
Phone: 505-845-3020
Fax: 505-845-3130

Sandia National Laboratories, MS1129
P. O. Box 5800, Albuquerque, NM 87185-1129
USA
e-mail: maulric@sandia.gov

Bob Watson
Phone: 505-845-3139
Fax: 505-845-3130

Sandia National Laboratories, MS1129
P. O. Box 5800, Albuquerque, NM 87185-1129
USA
e-mail: rdwatso@sandia.gov

Seiichi Yamazaki
Phone: 3-3615-5147
Fax: 3-3699-8587

Kawasaki Heavy Industries, Ltd.
Minamisuna-2-6-5, Koto-ku, Tokyo, 136
JAPAN
e-mail: net15289@asciinet.or.jp

Naoaki Yoshida
Phone: 92-573-9611
Ext. 516
Fax: 92-582-4210

Research Institute for Applied Mechanics
Kyushu Univ., Kasuga-Koen-6-1, Kasuga,
Fukuoka-ken, 816, JAPAN
e-mail: yoshida@riam.kyushu-u.ac.jp

Dennis Youchison
Phone: 505-845-3138
Fax: 505-845-3130

Sandia National Laboratories, MS1129
P. O. Box 5800, Albuquerque, NM 87185-1129
USA
e-mail: dlyouch@sandia.gov

Jim Yuen
Phone: 818-586-2820
Fax: 818-586-9481

Rockwell International, Rocketdyne Division
6633 Canoga Avenue, Canoga Park, CA 91303
USA
e-mail: jlyuen@rdyne.rockwell.com

Nelson Zhan
Phone: 412-256-1657
Fax: 412-256-2444

Westinghouse Electric Corporation
Science and Technology Center, 1310 Beulah Road
Pittsburgh, PA 15235, USA
e-mail: zhan.n.j@wec.com

DISTRIBUTION

3 Centre d'etudes de Cadarache
Attn: P. Chappuis M. Lipa
J. Schlosser
F-13108 Saint Paul lez Durance
Cedex FRANCE

2 D. F. Efremov Scientific Research Institute of Electrophysical Apparatus
Attn: R. Guiniatouline I. Mazul
P. O. Box 42
St. Petersburg 189631 RUSSIAN FEDERATION

1 ECN-Nuclear Energy
Attn: Jaap van der Laan
Technology Projects, Blg. U-53
1755 ZG Petten, THE NETHERLANDS

3 Hokkaido University
Department of Nuclear Engineering
Attn: I. Fujita M. Hashiba
T. Hino Y. Hirohata
Kita-13, Nishi-8, Kita-ku, Sapporo, 060 JAPAN

1 IAEA
Attn: R. K. Janev
Wagramerstrasse 5
P.O. Box 100, A-1400
Vienna, AUSTRIA

15 ITER Garching Joint Work Site
Max-Planck-Institut fur Plasmaphysik
Attn: V. Barabash R. Matera
A. Cardella R. Parker
S. Chiocchio R. Raffray
J. Dietz R. Santa
G. Federici S. Tanaka
Y. Gohar R. Tivey
K. Ioki C. Wu
G. Janeschitz
Boltzmannstrasse 2
D-85748 Garching bei Munchen GERMANY

8 JAERI
Attn: M. Akiba Y. Ohara
M. Araki M. Saidoh
T. Kunugi K. Sato
T. Kuroda S. Suzuki
801-1 Mukouyama
Naka-machi, Naka gun
Ibaraki-ken, JAPAN 311-01

DISTRIBUTION

2 JAERI
Attn: S. O'hira K. Okuno
Tritium Lab
Shirakata-shirane-2-4
Tokai-mura, Naka-gun
Ibaraki-ken, 319-11, JAPAN

3 JET Joint Undertaking
Attn: E. Deksuis M. Pick
Hans Dieter-Falter
Abingdon, Oxon OX14 3 EA
Abingdon, Oxfordshire, UNITED KINGDOM

1 Kawasaki Heavy Industries, Ltd.
Attn: S. Yamazaki
Minamisuna-2-6-5, Koto-ku, Tokyo, 136 JAPAN

3 Kernforschungsanlage (KFA) Juelich GmbH
Attn: R. Duwe M. Roedig
J. Linke
Postfach 1913
D-5170 Juelich 1, GERMANY

2 Kernforschungszentrum Karlsruhe (KFK) GmbH
Attn: M. Dalle-Donne F. Scaffidi-Argentina
Postfach 3640
D-7500 Karsruhe 1, GERMANY

2 Nagoya University
Attn: S. Amemiya H. Sugai
H. Toyodo
Furo-cho, Chikusa-ku, 464-01
Nagoya, JAPAN

5 National Institute for Fusion Science
Attn: A. Komori S. Masuzaki
T. Morisaki N. Noda
A. Sagara
Shimoishi-cho-322-6, Toki-shi, 509-52 JAPAN

2 NET Team
Attn: I. Smid G. Vieider
Max-Planck-Institut fur Plasmaphysik
Boltzmannstrasse 2
85748 Garching bei Munchen, GERMANY

1 Nippon Gaishi Co.
Attn: K. Nishida
NGK Insulators, Ltd.
Engineering & New Products Development
Maegata-cho, Handa, 475, JAPAN

DISTRIBUTION

1 Osaka University
Department of Nuclear Engineering
Attn: T. Tanabe
2-1 Yamada-Oka
Sulta-shi, Osaka 565 JAPAN

2 Research Institute for Applied Mechanics
Kyushu University
Attn: K. Tokunaga N. Yoshida
Kasuga-Koen-6-1, Kasuga,
Fukuoka-ken, 816 JAPAN

1 Toshiba Corporation
Heavy Apparatus Engineering Laboratory
Attn: M. Shibui
2-4, Suehiro-cho, Tsurumi-ku,
Yokohama 230 JAPAN

1 Tsukuba University
Attn: H. Nariai
Sakura-mura, Niihari-gun,
Ibaraki 305 JAPAN

1 University of Puerto Rico
Mayaguez Campus
Mechanical Engineering Department
Attn: Jorge Gonzales
P. O. Box 5000
Mayaguez, Puerto Rico 00681-5000

1 University of Tokyo
Department of Nuclear Engineering
Attn: S. Tanaka
7-3-1 Hongo, Bunkyo-Ku,
Tokyo 113 JAPAN

6 U.S. Department of Energy
Office of Fusion Energy
Attn: S. Berk S. Bryant
M. Cohen W. A. Marton
C. Sege F. W. Wiffen
ER-533, Germantown
Washington, DC 20585

3 U.S. ITER Home Team
U.S. ITER Project Office
Attn: C. Baker T. Davies
T. James
University of California at San Diego
9500 Gilman Drive, Building 302
La Jolla, CA 92093-0035

DISTRIBUTION

1	U.S. ITER Joint Central Team Attn: V. Tanchuk San Diego Joint Work Site 11025 N. Torrey Pines Road La Jolla, CA 92037	
2	Applied Sciences, Inc. Attn: J. Ming Ting P. O. Box 579 Cedarville, OH 45314-0579	M. Lake
10	Argonne National Laboratory Attn: H. Attaya J. Brooks T. Hua S. Majumdar D. Smith 9700 S. Cass Avenue Argonne, IL 60439	M. Billone A. Hassanein A. Hull R. Mattas D. Sze
3	Brush Wellman, Inc. Attn: D. Dombrowski J. Ratka 17876 St. Clair Ave. Cleveland, OH 44110	D. Krus
1	Ceracon, Inc. Attn: R. Raman 1101 N. Market B.vd., Suite #9 Sacramento, CA 95834	
2	Creare, Inc. Attn: M. Izenson P.O. Box 71 Hanover, NH 03755	J. Martin
1	Energy Sciences Labs, Inc. Attn: T. Knowles 6888 Nancy Ridge Dr. San Diego, CA 92121-2232	
1	Fiber Materials Attn: C. Baker 5 Morin Street Biddeford, ME 04005-4497	
1	Foster-Miller Attn: S. Khatri 303 Bear Hill Road Waltham, MA 02154-1196	

DISTRIBUTION

14 General Atomics
Advanced Materials Technology Division
Attn: S. Allen, P. Anderson, C. Baxi, T. Colleraine, D. Hill, K. Redler, E. Reis, L. Sevier, J. Smith, R. Stambaugh, P. Trestor, P. Valentine, P. West, C. Wong
P. O. Box 85608
San Diego, CA 92186

2 Karta Technology
Attn: J. Lee, S. Nair
1892 Grandstand
San Antonio, TX 78238

7 Lawrence Livermore National Laboratory
Attn: J. N. Doggett, MSL641, J. Hanafee, MSL352, R. Moir, D. Nilson, M. Rensink, T. Rognlien, G. Thomas, MSL352
P.O. Box 808
Livermore, CA 94550

4 Lockheed Martin Idaho Technologies
Attn: T. Dolan, G. Longhurst, K. McCarthy, D. Petti
765 Lindsay Blvd.
EROB E-3 N2
Idaho Falls, ID 83402-3815

4 Los Alamos National Laboratory
Attn: R. Castro, MSG770, K. Hollis, MSG770, L. Jacobson, P. Stanek
P. O. Box 1663
Los Alamos, NM 87545

11 McDonnell Douglas Aerospace
Attn: D. Bowers, J. Davis, D. Driemeyer, T. Hellwig, D. Kubik, V. D. Lee, H. Mantz, J. McAfee, D. Morgan, K. Slattery, G. Wille
Mail Code 1067220
P.O. Box 516
St. Louis, MO 63166-0516

DISTRIBUTION

2 Massachusetts Institute of Technology
Attn: B. Lipschultz G. McCracken
175 Albany Street
Cambridge, MA 02139

2 Materials and Electrochemical Research
Attn: S. Guha J. Withers
7960 South Kolb Road
Tucson, AZ 85706-9237

2 North Carolina State University
Department of Nuclear Engineering
Attn: M. Bourham G. E. Dale
Box 7909
Raleigh, NC 27695-7909

1 Northwest Technical Industries, Inc.
Attn: D. Butler
2249 Diamond Point Road
Sequim, WA 98382

10 Oak Ridge National Laboratory
Attn: T. D. Burchell, 6088 J. Haines
J. N. Herndon, 6376 C. Leitten
D. Lousteau W. Manly
A. F. Rowcliffe R. Seals
L. Snead, 6376 S. J. Zinkle, 6376
P. O. Box 2008
Oak Ridge, TN 37831

1 Oak Ridge National Laboratory
Engineering Technology Division
Attn: K. Kahl
P. O. Box 2009
Oak Ridge, TN 37831

2 Oak Ridge National Laboratory
Y-12 Plant
Attn: J. R. Haines, 8072 R. D. Seals, 8039
P. O. Box 2009
Oak Ridge, TN 38931

3 Pacific Northwest Laboratory/Battelle
Attn: D. Edwards D. Gelles
R. Kurtz
MS P8-15, P. O. Box 999
Richland, WA 99352

1 Plasma Processes, Inc.
Attn: T. McKechnie
4914D Moores Mill Road
Huntsville, AL 35811

DISTRIBUTION

1 Prairie View A&M University
Attn: R. Boyd
P. O. Drawer G
Prairie View, TX 77446

7 Princeton Plasma Physics Laboratory
Attn: S. Cohen, R. Hawryluk, P. Heitzenroeder, D. Mueller, H. Murray, K. Owens, C. Skinner
Princeton University
P. O. Box 451
Princeton, NJ 08543

1 Rennselaer Polytechnic Institute
Nuclear Engineering Department
Attn: Don Steiner
NES Building
Tibbits Avenue
Troy, NY 12181

3 Rockwell International
Rocketdyne Division
Attn: M. Dagher, M. Gabler, J. Yuen
6633 Canoga Avenue
Canoga Park, CA 91303

1 Saddleback Aerospace
Attn: G. Campbell
5318 East Second St., #154
Long Beach, CA 90803

1 SCM Metal Products, Inc.
Attn: J. Johnson, R. Solomon, J. Troxell
2601 Weck Drive
P.O. Box 12166
Research Triangle Park, NC 27709-2166

1 Sciences Research Laboratory
Attn: Dan Goodman
15 Ward Street
Somerville, MA 02143

1 Starfire Systems, Inc.
Attn: W. Sherwood
877 25th Street
Watervliet, NY 12189-1903

DISTRIBUTION

1 Surmet Corporation
Attn: S. Sastri
33B Street
Burlington, MA 01803-3406

2 Technical Research Associates
Attn: J. Sommer J. Weeks
2257 South 1100 East
Salt Lake City, UT 84106

2 Thermacore, Inc.
Attn: M. North J. Rosenfeld
780 Eden Road
Lancaster, PA 17601

1 Toyo Tanso
Attn: T. Matsuda
2575 NW Graham Circle
Troutdale, OR 97060

5 University of California at Los Angeles
Attn: M. Abdou N. Ghoniem
N. Morley L. Schmitz
M. Youssef
405 Hilgard Avenue
Los Angeles, CA 90024

7 University of California at San Diego
Attn: R. Boivin R. Doerner
Y. Hirooka J. Latchem
S. Luckhardt F. Najmabad
M. Tillack
9500 Gilman Drive, Building 302
La Jolla, CA 92093-0035

6 University of Illinois
Attn: D. Hayden B. Jones
K. Leedy D. Ruzic
J. Shang J. Stubbins
103 S. Goodwin Avenue
Urbana, IL 61801

1 University of New Mexico
Attn: J. Gahl
EECE Building
Albuquerque, NM 87108

2 University of Toronto
Institute for Aerospace Studies
Attn: J. W. Davis A. A. Haasz
4925 Dufferin Street, North York
Ontario, CANADA M3H 5T6

DISTRIBUTION

2	University of Wisconsin Attn: J. Blanchard M. Sawan Engineering Research Building 1500 Johnson Drive Madison, WI 53706-1687		
3	Westinghouse Electric Corporation Attn: M. Carelli L. Green N. Zhan Science and Technology Center 1310 Beulah Road Pittsburgh, PA 15235		
1	0736	N. R. Ortiz, 6400	
1	0827	A. J. Russo, 9114	
3	1056	Attn:	B. L. Doyle, 1111 D. S. Walsh W.R. Wampler
12	1129	Attn:	J. T. Ganley, 6428 P. Y. Hubbard T. J. Lutz T. D. Marshall R. E. Nygren P. D. Rockett P. L. Stevens M. A. Ulrickson J. G. Watkins R. D. Watson S. K. Willis D. L. Youchison
2	9162	Attn:	R. Bastasz, 8716 R. Causey
1	9163	K. L. Wilson, 8716	
1	9401	T. M. Dyer, 8700	
4	9403	W. D. Bonivert, 8230 C. H. Cadden, 8240 S. Goods, 8712 B. Odegard, 8712	
1	9407	S. L. Robinson, 8415	
1	9018	Central Technical Files, 8523-2	
5	0899	Technical Library, 13414	
1	0619	Print Media, 12615	
2	0100	Document Processing, 7613-2 (For DOE/OSTI)	